BIOPHYSICAL ASPECTS

OF

AUGER PROCESSES

Edited by

Roger W. Howell
Department of Radiology
UMDNJ - New Jersey Medical School
Newark, NJ, USA

Venkat R. Narra
Department of Radiology
UMDNJ - New Jersey Medical School
Newark, NJ, USA

Kandula S.R. Sastry
Department of Physics & Astronomy
University of Massachusetts
Amherst, MA, USA

Dandamudi V. Rao
Department of Radiology
UMDNJ - New Jersey Medical School
Newark, NJ, USA

These peer reviewed manuscripts were originally prepared for the 2nd International Symposium on Biophysical Aspects of Auger Processes held at the University of Massachusetts, Amherst, MA, July 5-6, 1991

Published for the
American Association of Physicists in Medicine
by the American Institute of Physics

DISCLAIMER: This publication is based on sources and information believed to be reliable, but the AAPM and editors disclaim any warranty or liability based on or relating to the contents of this publication.

The AAPM does not endorse any products, manufacturers, or suppliers. Nothing in this Monograph should be interpreted as implying such endorsement.

Library of Congress Catalog Card Number: 92-82921
International Standard Book Number: 1-56396-095-8

Published by the American Institute of Physics, Inc.
500 Sunnyside Blvd., Woodbury, NY 11797

Printed in the United States of America

PREFACE

Several radionuclides decaying by orbital electron capture (EC) and/or internal conversion (IC) are widely used in biology and medicine. These physical mechanisms (EC & IC) as well as external photoelectric effect entail the inner atomic shell of the atom. The complex atomic vacancy cascades involved in the de-excitation of the residual atom are dominated by non-radiative (Auger) processes. As a consequence, numerous electrons are ejected from the atomic orbitals. Inasmuch as a large fraction of these Auger electrons have very low energies (~ 20-500 eV) with extremely short ranges (~ 1-20 nm) in tissue equivalent matter, the biological implications of simultaneous and localized action of such electrons are of interest to basic science, diagnostic and therapeutic nuclear medicine, and to radiation protection. The interesting and intriguing effects of internal Auger emitters presented at the pioneering meeting organized by Ludwig Feinendegen at Jülich (1975) attracted a number of scientists to the interdisciplinary field of Radiobiology of Auger Emitters. A focal point of the intense activity was the International Workshop on Internal Auger Emitters, organized by Keith Baverstock and David Charlton in 1987 at Charney Bassett, England. The field has advanced significantly during the four years following the Charney Bassett meeting as evidenced by the publications. The 2nd International Symposium on Biophysical Aspects of Auger Processes held in July 1991, at the University of Massachusetts, Amherst attracted a large number of scientists from around the world. The scientific presentations and discussions of this Symposium are brought to the scientific community through this monograph.

This volume starts with an Opening Address by S. James Adelstein in which the developments in the field during 1987-1991 were reviewed with admirable clarity. The subsequent 23 papers presented in this meeting raise interesting new questions regarding the basic mechanism of action by which Auger processes effect biological damage, as well as the nature of the radiosensitive targets in the cell nucleus. In addition, new insight into the radiotoxicity of Auger processes arising from photon activation of atoms situated in the DNA were presented. Finally, novel approaches to implement agents radiolabeled with Auger electron emitters for cancer therapy were discussed. In view of this, the volume is organized into three sections: i) Biological effects of photon induced Auger processes, ii) Biological effects of Auger-electron emitting radionuclides, and iii) Therapeutic applications of

Auger electron emitters. The Closing Address by Kurt Hofer is an outstanding review of the key aspects of the papers presented in each section as well as his vision of the future of this growing field. In addition, there is a commentary by Keith Baverstock on the Panel Discussion, a special highlight of the Symposium. This insightful distillation of the highly interactive and incisive discussions may be of particular interest to the reader.

The articles presented in this volume highlight the present status and the future directions of the field of Auger emitters with a potential for new advances in medical applications. It is our hope that this volume will serve as a valuable reference for those already familiar with the field and as an introduction and a resource to those outside the field.

R.W. Howell
V.R. Narra
K.S.R. Sastry
D.V. Rao

ACKNOWLEDGMENTS

This Symposium was supported in part by United States Public Health Service - NIH Conference Grant No. CA-53064, College of Arts and Sciences, University of Massachusetts, and UMDNJ - New Jersey Medical School Department of Radiology. The Symposium was co-sponsored by the Radiation Research Society and the American Association of Physicists in Medicine. We would also like to express our appreciation to S. James Adelstein for his Opening Address, Kurt G. Hofer for his Closing Address, Keith F. Baverstock for moderating the Panel Discussion, and the Panel Discussion members S. James Adelstein, Dudley Goodhead, Alexander Halpern, and Dandamudi V. Rao. Finally, we would like to acknowledge the efforts of all those who served as session Chairs and Co-chairs, and those who peer reviewed the manuscripts.

CONTENTS

II. Biological Effects of Auger-Electron Emitting Radionuclides

III. Therapeutic Applications of Auger Electron Emitters

Biophysical Aspects of Auger Processes, AAPM Symposium Series No. 8 (1992) 001-013
Eds. RW Howell, VR Narra, KSR Sastry, DV Rao

BIOPHYSICAL ASPECTS OF AUGER PROCESSES: A REVIEW OF THE LITERATURE 1987-1991

S. JAMES ADELSTEIN

Department of Radiology
Harvard Medical School
Boston, MA 02115, USA

ABSTRACT

The workshop on Auger emitters held in Oxfordshire in 1987 produced papers on physical dosimetry, molecular damage, biologic effects, and therapeutic applications. These are briefly summarized. Since that time there has appeared in the literature a number of reports on Auger processes as they relate to microscopic and cellular dosimetry, DNA damage, biologic consequences, and therapeutic potential. A number of these are reviewed as background for the Second International Symposium.

THE WORKSHOP OF 1987

On opening this Second International Symposium, I thought it profitable to begin where we left off at Charney Bassett four years ago. As I had the honor of closing that first meeting, I was able to refer to my own notes as well as to the excellent volume of proceedings prepared by Keith Baverstock and David Charlton (1). The principal themes of that symposium can be divided into physical dosimetry, molecular damage, biologic effects, and therapeutic applications.

Physical Dosimetry

It had been realized for some time that conventional dosimetry significantly underestimates the energy deposited in radiosensitive targets when Auger emitters are affixed to DNA. Sastry showed that a better approximation is made by calculating the dose to the nucleus rather than averaging over all cells, cell compartments, and extracellular regions as in the MIRD and ICRU methodologies. Charlton presented a Monte Carlo approach to following each electron track so that a precise statistical estimate can be made of energy deposited per base in the DNA immediately surrounding the decay, and, by inference, of the number of single strand breaks (SSB) and double strand breaks (DSB) created. Humm extended this model to photoelectric interactions with inner shell electrons of incorporated nonradioactive bromine, concluding that the consequent Auger shower would only provide a small increment of damage above the usual sensitization. This last point, one of some contention, was on the verge of being settled by data from a new synchrotron source being applied to this problem in Japan by Ito, Ohara and Maezawa.

Molecular Damage

Molecular biologic approaches were employed by Martin who used a Hoechst dye (33258) labeled with ^{125}I that binds to certain A-T-rich regions of DNA. The labeled compound produces clusters of SSB and DSB at the binding site, while the unlabeled parent compound protects against DNAase degradation in the same regions, demonstrating again the "microsurgical" quality of DNA shattering produced by Auger emitters when brought into close proximity to the DNA. On the other hand, Baverstock presented an argument that certain experimental results in which ionizing energy is directly deposited in phage and plasmid DNA can be explained by long-range

(μm) transfer of excitation energy in DNA. He postulated a mechanism involving solitons and proposed that the hypothesis could be tested using the energy released on decay of ^{125}I incorporated at a specific site in a DNA molecule.

Biologic Effects

A number of biologic consequences were also elucidated. High-LET-like survival curves were seen not only with Auger emitters incorporated into DNA but also with ^{125}I brought into contact with DNA by way of thyroid hormone receptors as reported by Sundell-Bergman, by intercalators as discussed by Kassis and by dye-binding (*vide supra*). The importance of DSB as lethal lesions was stressed by Radford who pointed out that 60 DSB are found per lethal event with ^{125}I, while 83 DSB are found per lethal event with X rays. In his experiments, survival, chromosomal aberrations, and DSB were coincident. In addition, the site of labeling within the genome seemed of critical importance as determined from differential 5-[^{125}I]iodo-2'-deoxyuridine ($^{125}IUdR$) labeling within S phase by Kassis and aphidicolin-directed labeling by Yasui. The possibility that the function of the DNA that is damaged by an Auger cascade may be important in terms of the outcome at the cellular level was suggested by Apelgot. Other biologic end points being examined included mutagenesis by Fujiwara and gene amplification by Lucke-Huhle.

Therapeutic Applications

Lastly, a number of practical therapeutic applications were being tested. Bagshawe reported on the pharmacologic manipulation of $^{125}IUdR$ incorporation into the DNA of human tumors, and Brown on the use of tumor-targeting iodinated naphthoquinols, which also localize in the cell nucleus.

PUBLISHED REPORTS 1987-1991

I have taken as my further assignment a review of the literature published in the interval. There is no pretension that this review is complete or that the categories I have chosen would correspond with those of others.

Microscopic and Cellular Dosimetry

A number of papers on various aspects of dosimetry have appeared. Younis and Watt (2) have calculated the cross section for inactivation of ^{125}I, ^{77}Br, ^{3}H and ^{131}I from the slowing down charged particle fluence and published survival data. They conclude that ^{125}I, ^{77}Br, and ^{3}H have qualities approaching those of heavy particles. They infer from their results that the damage from ^{125}I and ^{77}Br is mostly direct and that from ^{3}H mostly indirect. All results are consistent with the interpretation that electron damage is caused predominantly at the end of the tracks. The Younis and Watt hypothesis stands in contrast to that of Goodhead (3) who has suggested "at all subcellular levels, even down to DNA, high linear-energy-transfer (LET) radiations can produce unique initial damage, different from that possible with low-LET radiations, and therefore may even, in principle, produce unique final biological effects."

Booz *et al.* (4) have tried to distinguish between ^{125}I specifically incorporated into DNA and the radionuclide homogeneously deposited in tissue. They have also tried to determine the importance of the charge transfer phenomenon. With reference to insights obtained from local dose profiles using electron ranges and stopping power, the Monte Carlo calculation of Auger-electron cascades, number distributions and energy spectra, the application of track-structure calculations to the disintegration of ^{125}I as well as the precise evaluation of local energy density produced by multiple charge on the atom after decay, they calculate total potential energy on "isolated" daughter atoms of ^{125}I after termination of the Auger-electron cascade. Since the energy potential due to multiple ionization is about equal to that due to the deposition of Auger electrons, they feel it is useless to separate these two effects by radiobiologic methods. They also estimate that for ^{125}I incorporated into specific biologic targets of 20 nm, most of the energy deposited is above 40 keV/μm and does not need to be subclassified. For the nonspecific, homogeneous incorporation of ^{125}I, about 20% of the energy deposited in 25 nm critical targets is made up from decays from those targets, while the remaining 80% of the dose is from low-LET radiation outside of the targets. Halpern (5) disagrees with their first conclusion. Evidence that the chemical nature of the component molecule or the solvent plays a role in the dissipation of charge (primarily through the presence or absence of π electron resonances) leads him to believe that the stacking of bases in DNA can be responsible for long-range effects due to this mechanism.

At the cellular level, there seems little doubt that the intranuclear localization of Auger-electron emitters is required to observe the biologic effect of the Auger process. Kassis *et al.* (6) have reported that with V79 cells mitochondrial-bound (cytoplasmic) ^{125}I produces a cytocidal survival curve having a distinct shoulder and a mean lethal dose (D_{37}) of 462 cGy, while ^{125}I incorporated into DNA produces a logarithmic survival curve with a D_{37} of 80 cGy. Link *et al.* (7) working with radiolabeled methylene blue, a dye that binds to the cytoplasmic melanin granules of melanoma cells, have shown that conspicuous cytocidal effects are obtained when the agent is labeled with the α particle emitter ^{211}At but not with the Auger-electron emitter ^{125}I.

A number of investigators have obtained similar results with ^{111}In. Rao *et al.* (8) have compared the ability of ^{111}In oxine, ^{111}In citrate, ^{114m}In citrate and X rays to reduce the spermhead population in mouse testes. The D_{37} of the four agents is 16 cGy, 34 cGy, 57 cGy and 67 cGy, respectively. The difference between ^{111}In oxine and ^{111}In citrate is ascribed to the higher nuclear fraction of the former (92% versus 30%). In the case of ^{114m}In, only 0.8% of the dose comes from Auger electrons, whereas in the case of ^{111}In, 20% comes from Auger electrons.

McLean and Wilkinson (9) have studied the survival of V79 cells *in vitro* after exposure to ^{111}In. They reckon that the dose to the cells from intranuclear decay is 3.5 mGy and from extracellular decay, 5.8 pGy, a considerable difference. McLean *et al.* (10) have demonstrated that ^{111}In oxine, some of which is tightly bound to chromosomal DNA, is a potent producer of chromosomal aberrations, while extracellular ^{111}In chloride is a much weaker one.

A number of investigators have been concerned that traditional dosimetry schemes (such as MIRD) underestimate the doses to specific population groups within tissues when Auger-electron emitting radionuclides are concentrated by cells and especially by the cell nucleus. Bialobrzeski *et al.* (11) have shown for ^{51}Cr-bleomycin that the doses calculated for cell nuclei and DNA in liver cells are higher than the cell-averaged values by factors of 2.5 and 5, respectively, and the corresponding dose equivalents (taking into account the quality factor for Auger showers) by factors of 9 and 24. Similar thinking has been applied to ^{51}Cr labeled lymphocytes by Vezza *et al.* (12), who calculate the actual dose to be twice the conventionally calculated one.

Makrigiorgos *et al.* (13) have also written about the limitations of conventional internal dosimetry at the cellular level. They have prepared a model that takes into account the intracellular-to-extracellular radionuclide concentration and the labeled cell density for radionuclides ^{99m}Tc, ^{201}Tl, ^{111}In and ^{123}I, all commonly used in the practice of nuclear medicine. They have shown that when selective intracellular uptake of a radiolabeled compound occurs in specific cells within a cell cluster, conventional dosimetry underestimates the radiation dose delivered to the labeled cells by two fold to more than 25-fold if the emitted electrons have ranges of a few micrometers or less. Under the same conditions, conventional dosimetry overestimates slightly the electron dose to the nonlabeled cells. This approach has been applied to the irradiation of liver and spleen macrophages by ^{99m}Tc labeled microaggregates (14) and of lung capillaries by ^{99m}Tc labeled macroaggregates (15). In the case of the lung, ascribed doses to some individual cells were found to be as high as 30,000 times the calculated average dose.

DNA Damage

The damage to DNA from Auger processes continues to fascinate a number of investigators, as indeed it should. Charlton and Humm (16) have refined the model presented at the Oxford meeting, which can be used to calculate initial DNA strand breakage following the decay of ^{125}I. DNA is again modeled as a 2.3 nm cylinder with a 1 nm base-pair core and the Paretzke electron track code is employed to calculate the energy deposited in the sugar-phosphate and base volumes. Two spectral sources are used, the original of Charlton and Booz and a newer one of Pomplun (*vide supra*), in which the charge energy is handled differently. Two types of SSB and three of DSB are recognized. The distribution of SSB fits the experimental results of Martin and Haseltine, while values between 0.82 to 1.07 DSB per decay are obtained depending on the electron spectra postulated.

Using their own method of calculating spatial energy distribution from low-energy electrons and the ^{125}I Auger-electron spectrum of Charlton and Humm (16), Unak and Unak (17) calculate that about one keV of energy is absorbed in regions of DNA 2 nm from the decay site in both directions. When they assume that 5 eV deposited in DNA produces a SSB, they reckon that local absorption of ^{125}I Auger electrons is able to produce at least one DSB without taking into account neutralization effects from the highly charged residual tellurium ion.

Some investigations have begun into the relative role of direct and indirect damage in DNA from Auger cascades. Wright *et al.* (18) have made Monte Carlo calculations for the physical and chemical interactions of Auger electrons with liquid water. They have illustrated the distribution of watery radicals in the vicinity of a DNA duplex and calculated the yields of each aqueous species from the decay of a number of radionuclides. For ^{125}I decaying on the surface of a DNA cylinder, they calculate 44 indirect and 21 direct interactions per disintegration, or an indirect/direct ratio of about 2/1.

Recently, Pomplun (19) has produced a new DNA target model for track structure calculations and applied it to the interaction of ^{125}I Auger electrons. He elaborates electron track interactions in a cylindrical model of DNA 14.3 nm long and 2.4 nm in diameter. (In contrast to the Wright model (18), he has the decay taking place within the cylinder.) In a series of histograms, he shows mean energy deposited by direct and indirect hits in phosphate-sugar strands and bases both on the ipsilateral and contralateral labeled filaments. As expected, the fraction of direct hits is greater on the contralateral strand. Assuming a minimum of 10 eV direct energy and 17 eV indirect energy to produce a strand break, Pomplun calculates 1.8 of a total 3.8 SSB per decay are caused by direct interactions. Of the 0.94 DSB produced per decay, about 40% are due to direct action.

Makrigiorgos *et al.* (20) have compared DNA damage produced in V79 cells by incorporated ^{123}I with that of ^{125}I. Using neutral elution, they have measured DSB production in frozen cells. They have also compared their experimental results with theoretical ones derived from the Charlton and Humm model (16). They have found ^{125}I to be 1.3 times as effective as ^{123}I in producing DSB, whereas theory has predicted it would be 1.6. If one assumes that each decay of ^{125}I produces one DSB, then each decay of ^{123}I produces, on average, 0.74 DSB.

Martin *et al.* (21) have measured the induction of double strand breaks in plasmid DNA following neutron capture by ^{157}Gd. The (n,γ) reaction results in ^{157}Gd and is accompanied by internal conversion. The DSB are thought to be generated by the resulting Auger cascade, as they are produced only when the ^{157}Gd is bound to DNA and not when the atom is sequestered by EDTA.

Biologic Consequences

At the biologic level, a number of observations have been made, the first group involving photon activation. Nath *et al.* (22) have studied survival of Chinese hamster cells exposed to low-energy photons after IUdR incorporation. The enhancement of IUdR sensitization is about 1.5 for 250 kVp X rays relative to 4 MV X rays and 1.4 and 2.7 for the 60 keV photons of ^{241}Am compared to the 860 keV photons of ^{226}Ra when IUdR replacement of thymidine is 5 and 25%, respectively. The authors ascribe the enhanced sensitization to the Auger effect. In comparison, Miller *et al.* (23) have examined the radiosensitization of V79 cells in which 16% of the thymidine residues have been replaced with IUdR. Enhancement ratios at the 1% survival level are 1.8 for 15 MV and 1.95 for 100 kVp radiation. This modest 10 to 15% additional enhancement with 100 kVp X rays is much less than that predicted by the proponents of photon activation therapy.

Larson and colleagues (24) have examined the Auger electron contribution to bromodeoxyuridine radiosensitization in V79 cells. When cells with 32% of thymidine residues replaced by BrUdR are exposed to monoenergetic X rays just below (13.450 keV) or above (13.490 keV) the K edge (13.475 keV) of bromine, enhancement ratios of 3 to 12% are obtained depending on the means of calculation; most values are between 5 and 7%. The authors conclude that Auger electrons produced following photoelectric absorption of X rays by the K shell of bromine contribute minimally to observed BrUdR cellular radiosensitization. In a simpler system, the radiolysis of bromodeoxyuridine-monophosphate, Takakura (25) has compared the effects of 13.49 and 13.43 keV X rays. The ratio of G values for the formation of the major product, dUMP (debrominated Br-dUMP), is 2.2, and for the conversion of dUMP to uracil, 1.0. The author believes the results confirm that Auger electrons stripped from the K shell of bromine play the major role in the radiolysis of the nucleotide.

Another set of experiments is concerned with the relative biologic effectiveness (RBE) of Auger emitters with themselves and other forms of radiation. Kassis *et al.* (26) have looked at the relative effectiveness of ^{125}I, ^{123}I and ^{77}Br on the survival of V79 cells. They find that the mean lethal dose (D_{37} survival) to the nucleus is about 80 cGy in all cases. However, the total number of decays needed to produce this D_{37} is about twice as much with ^{123}I as with ^{125}I, approximately equal to the ratio of the energy deposited in

microscopic volumes by ^{125}I and ^{123}I, respectively. When applied to 5 nm diameter spheres, all three radionuclides lie on the same line in an inverse plot of deposited energy versus decays required for 37% survival.

Pomplun *et al.* (27) have calculated the equivalence of ^{125}I decays to high-LET radiation. In sensitive biologic volumes of 20 nm, they reckon a mean lineal energy equivalent of 270 keV/μm. They have tabulated published RBE values for a number of biologic end points. For chromosomal aberrations, the values scatter between 6 and 77, for transformations between 32 and 38, and for mutations between 1 and 16. These values can be compared to the recommended ICRP quality factor of 20 for this level of LET, *i.e.*, 270 keV/μm.

Rao *et al.* (28) have examined the effects of radiations of different quality on spermhead survival and the induction of spermhead abnormalities. They find an RBE of 6.7 for ^{210}Po α particles and 7.9 for DNA-bound ^{125}I when compared with 60 or 120 kVp X rays for spermhead survival. For abnormalities, the corresponding values are 245 and 59. Using ^{7}Be, a monoenergetic photon emitter (477 keV), a dose rate effect is demonstrated which should be taken into account when comparing acute and chronic exposures.

Whaley and Little (29) have addressed the issue of mutation induction by incorporated radioiodine. They have examined the mutational frequencies at the hprt locus for cells proficient (TK6) and deficient (SE30) in thymidine kinase, an enzyme necessary for the incorporation of IUdR into DNA. For cells proficient in thymidine kinase, the D_0 values for $^{125}IUdR$, $^{131}IUdR$ and X rays are 5.9, 24 and 75 cGy, respectively. No cell death can be produced in the deficient cells with $^{125}IUdR$; for $^{131}IUdR$ and X rays the corresponding D_0 values are 54 and 77 cGy. The induced mutant fraction for $^{125}IUdR$ in the proficient cells is 3.3×10^{-6} per cGy, for $^{131}IUdR$, 0.45×10^{-6}, and for X rays, 0.05×10^{-6}. In deficient cells, no mutants are induced by $^{125}IUdR$; for both $^{131}IUdR$ and X rays the induced fraction is 0.04 to 0.05×10^{-6}. The results demonstrate clearly the extraordinary ability of incorporated ^{125}I to produce mutations as well as cytocidal effects. The RBE of ^{125}I relative to ^{131}I for survival is 4.0; for mutations, 7.3; the RBE of ^{125}I relative to X rays is 12.7 for survival and 66 for mutations. Whaley *et al.* (30) have also shown that the DNA intercalating agent ^{125}I-iodoacetylproflavine (^{125}IAP) can induce mutations at both the hprt and tk loci. When these results are compared with those observed with $^{125}IUdR$, ^{125}IAP shows a reduced effectiveness per decay; for survival the RBE is between 2 and 4, for mutations at the hprt locus

between 3.5 and 6. ^{125}IAP treatment induces large-scale genetic events at the hprt locus at high frequency in comparison to X rays, 90 versus 50%.

Therapeutic Potential

A keen interest in the potential use of Auger-electron emitters for targeted radionuclide therapy continues. Humm and Charlton (31) have developed a method to assess the therapeutic potential of Auger-electron emission. Their projection depends on electron track structure methods and the prediction of double strand breaks presented earlier (*vide supra*). According to their calculations, the DSB produced per decay of ^{125}I, ^{123}I and ^{77}Br incorporated into DNA are 1.10, 0.73 and 0.38, respectively. An advantage of ^{125}I with its 60 d half-life is that relatively few atoms need be incorporated into the genome for effective tumor sterilization. Humm *et al.* (32) have also focused on ^{123}I and ^{77}Br as alternatives to ^{125}I therapy based on results with experimental tumors using ^{125}IUdR. Baranowska-Kortylewicz *et al.* (33) have demonstrated that ^{123}IUdR can be used effectively for the diagnosis and therapy of ovarian ascites tumors in mice. The diagnostic capability stems from the 140 keV photon emitted by ^{123}I, which is suitable for imaging.

Anderson and Holt (34) and DeSombre *et al.* (35) have examined the potential of estrogens labeled with ^{125}I, ^{123}I and ^{80m}Br for the therapy of malignancies bearing estrogen receptors. Nuclear binding has been demonstrated in endometrium, granulosa cells and breast cancer cells. DNA-incorporated ^{80m}Br has been shown to be radiotoxic, while unbound ^{80m}Br is not (36).

Howell *et al.* (37) have compared dose rate profiles for potentially useful radionuclides to be used for radioimmunotherapy. As one might expect, high-energy beta emitters such as ^{90}Y would be most effective for treating large tumors (>1 cm), whereas for small tumors (~ 1 mm), medium energy beta emitters are more suitable, while micrometastases may be best handled with low-energy electron emitters.

Woo *et al.* (38) have examined the effects of ^{125}I labeled monoclonal antibodies on cultured cancer cells. They have found that one of the antibodies tested is internalized by the cells and produces cytotoxicity as well as chromosomal damage. They assume that the internalized ^{125}I interacts with the cell nucleus. This type of immunoglobulin might be suitable for radioimmunotherapy with Auger-electron emitters.

Hou and Maruyama (39) have developed a complex of ^{111}In-bleomycin which binds to DNA and have augmented its cytotoxicity to small-cell lung cancer cells with hyperthermia. Baranowska-Kortylewicz *et al.* (40) have conjugated IUdR to immunoglobulins. The pyrimidine nucleoside-protein bond is hydrolyzed by lysosomal enzymes. This complex could be used to deliver the radioiodinated compound to specific tumor cells. Lastly, Goodman *et al.* (41) have begun a treatment protocol for brain tumors that involves IUdR infusion and brachytherapy. They plan to treat below and above the K absorption edge of iodine to test the effectiveness of photon activation therapy.

REFERENCES

1. K.F. BAVERSTOCK and D.E. CHARLTON, Eds. *DNA Damage by Auger Emitters.* Taylor and Francis, London, 1988.
2. A.R.S. YOUNIS and D.E. WATT, The quality of ionising radiations emitted by radionuclides incorporated into mammalian cells. *Phys. Med. Biol.* **34**, 821-834 (1989).
3. D.T. GOODHEAD, Spatial and temporal distribution of energy. *Health Phys.* **55**, 231-240 (1988).
4. J. BOOZ, H.G. PARETZKE, E. POMPLUN, and P. OLKO, Auger-electron cascades, charge potential and microdosimetry of iodine-125. *Radiat. Environ. Biophys.* **26**, 151-162 (1987).
5. A. HALPERN, Intra- and intermolecular energy transfer and superexcitation in post-Auger processes. *Radiochim. Acta* **50**, 129-134 (1990).
6. A.I. KASSIS, F. FAYAD, B.M. KINSEY, K.S.R. SASTRY, R.A. TAUBE, and S.J. ADELSTEIN, Radiotoxicity of ^{125}I in mammalian cells. *Radiat. Res.* **111**, 305-318 (1987).
7. E.M. LINK, I. BROWN, R.N. CARPENTER, and J.S. MITCHELL, Uptake and therapeutic effectiveness of ^{125}I- and ^{211}At- methylene blue for pigmented melanoma in an animal model system. *Cancer Res.* **49**, 4332-4337 (1989).
8. D.V. RAO, K.S.R. SASTRY, H.E. GRIMMOND, R.W. HOWELL, G.F. GOVELITZ, V.K. LANKA, and V.B. MYLAVARAPU, Cytotoxicity of some indium radiopharmaceuticals in mouse testes. *J. Nucl. Med.* **29**, 375-384 (1988).
9. J.R.N. McLEAN and D. WILKINSON, The radiation dose to cells *in vitro* from intracellular indium-111. *Biochem. Cell Biol.* **67**, 661-665 (1989).
10. J.R. McLEAN, D.H. BLAKEY, G.R. DOUGLAS, and J. BAYLEY, The Auger electron dosimetry of indium-111 in mammalian cells *in vitro. Radiat. Res.* **119**, 205-218 (1989).
11. J. BIALOBRZESKI, J. LINIECKI, J. GREGER, D. BRYKALSKI, and A. ZADROZNA, Radiation doses from ^{51}Cr-bleomycin. *Nuklearmedizin* **26**, 97-104 (1987).
12. M. VEZZA, D. GIULIANI, D.V. RAO, and B.S. MORSE, Chromium-51 dosimetry of lymphocytes labeled incidentally during nuclear medicine procedures. *Nucl. Med. Biol.* **14**, 75-77 (1987).

13. G.M. MAKRIGIORGOS, S.J. ADELSTEIN, and A.I. KASSIS, Limitations of conventional internal dosimetry at the cellular level. *J. Nucl. Med.* **30**, 1856-1864 (1989).
14. G.M. MAKRIGIORGOS, S. ITO, J. BARANOWSKA-KORTYLEWICZ, D.W. VINTER, A. IQBAL, A.D. VAN DEN ABBEELE, S.J. ADELSTEIN, and A.I. KASSIS, Inhomogeneous deposition of radiopharmaceuticals at the cellular level: Experimental evidence and dosimetric implications. *J. Nucl. Med.* **31**, 1358-1363 (1990).
15. G.M. MAKRIGIORGOS, S.J. ADELSTEIN, and A.I. KASSIS, Cellular radiation dosimetry and its implications for estimation of radiation risks: Illustrative results with technetium 99m-labeled microspheres and macroaggregates. *JAMA* **264**, 592-595 (1990).
16. D.E. CHARLTON and J.L. HUMM, A method of calculating initial DNA strand breakage following the decay of incorporated ^{125}I. *Int. J. Radiat. Biol.* **53**, 353-365 (1988).
17. P. UNAK and T. UNAK, Microscopic energy absorption of the DNA molecules from Auger electrons of iodine-125. *Appl. Radiat. Isot.* **39**, 1037-1040 (1988).
18. H.A. WRIGHT, R.N. HAMM, J.E. TURNER, R.W. HOWELL, D.V. RAO, and K.S.R. SASTRY, Calculations of physical and chemical reactions with DNA in aqueous solution from Auger cascades. *Radiat. Prot. Dosim.* **31**, 59-62 (1990).
19. E. POMPLUN, A new DNA target model for track structure calculations and its first application to I-125 Auger electrons. *Int. J. Radiat. Biol.* **59**, 625-642 (1991).
20. G.M. MAKRIGIORGOS, R.M. BERMAN, J. BARANOWSKA-KORTYLEWICZ, E. BUMP, J.L. HUMM, S.J. ADELSTEIN, and A.I. KASSIS, DNA damage produced in V79 cells by DNA-incorporated iodine-123: A comparison with iodine-125. *Radiat. Res.* **129**, 309-314 (1992).
21. R.F. MARTIN, G. D'CUNHA, M. PARDEE, and B.J. ALLEN, Induction of double-strand breaks following neutron capture by DNA-bound ^{157}Gd. *Int. J. Radiat. Biol.* **54**, 205-208 (1988).
22. R. NATH, P. BONGIORNI, and S. ROCKWELL, Enhancement of IUdR radiosensitization by low energy photons. *Int. J. Radiat. Oncol. Biol. Phys.* **13**, 1071-1079 (1987).
23. R.W. MILLER, W. DeGRAFF, T.J. KINSELLA, and J.B. MITCHELL, Evaluation of incorporated iododeoxyuridine cellular radiosensitization by photon activation therapy. *Int. J. Radiat. Oncol. Biol. Phys.* **13**, 1193-1197 (1987).
24. D. LARSON, W.J. BODELL, C. LING, T.L. PHILLIPS, M. SCHELL, D. SHRIEVE, and T. TROXEL, Auger electron contribution to bromodeoxyuridine cellular radiosensitization. *Int. J. Radiat. Oncol. Biol. Phys.* **16**, 171-176 (1989).
25. K. TAKAKURA, Auger effects on bromo-deoxyuridine-monophosphate irradiated with monochromatic X-rays around bromine K-absorption edge. *Radiat. Environ. Biophys.* **28**, 177-184 (1989).
26. A.I. KASSIS, G.M. MAKRIGIORGOS, and S.J. ADELSTEIN, Implications of radiobiologic and dosimetric studies of DNA-incorporated ^{123}I: The use of the Auger effect as a biologic probe at the nanometre level. *Radiat. Prot. Dosim.* **31**, 333-338 (1990).
27. E. POMPLUN, J. BOOZ, A. DYDEJCZYK, and L.E. FEINENDEGEN, A microdosimetric interpretation of the radiobiologic effectiveness of ^{125}I and the problem of quality factor. *Radiat. Environ. Biophys.* **26**, 181-188 (1987).

28. D.V. RAO, V.R. NARRA, R.W. HOWELL, V.K. LANKA, and K.S.R. SASTRY, Induction of spermhead abnormalities by incorporated radionuclides: Dependence on subcellular distribution, type of radiation, dose rate, and presence of radioprotectors. *Radiat. Res.* **125**, 89-97 (1991).
29. J.M. WHALEY and J.B. LITTLE, Efficient mutation induction by ^{125}I and ^{131}I decays in DNA of human cells. *Radiat. Res.* **123**, 68-74 (1990).
30. J.M. WHALEY, A.I. KASSIS, B.M. KINSEY, S.J. ADELSTEIN, and J.B. LITTLE, Mutation induction by ^{125}Iodoacetylproflavine, a DNA-intercalating agent, in human cells. *Int. J. Radiat. Biol.* **57**, 1087-1103 (1990).
31. J.L. HUMM and D.E. CHARLTON, A new calculational method to assess the therapeutic potential of Auger electron emission. *Int. J. Radiat. Oncol. Biol. Phys.* **17**, 351-360 (1989).
32. J.L. HUMM, K.D. BAGSHAWE, S.K. SHARMA, and G. BOXER, Tissue dose estimates following the selective uptake of ^{125}IUdR and other radiolabelled thymidine precursors in resistant tumours. *Br. J. Radiol.* **64**, 45-49 (1991).
33. J. BARANOWSKA-KORTYLEWICZ, G.M. MAKRIGIORGOS, A.D. VAN DEN ABBEELE, R.M. BERMAN, S.J. ADELSTEIN, and A.I. KASSIS, 5-[^{123}I]Iodo-2'-deoxyuridine in the radiotherapy of an early ascites tumor model. *Int. J. Radiat. Oncol. Biol. Phys.* **21**, 1541-1551 (1991).
34. R.E. ANDERSON and J.A. HOLT, Binding of radiolabeled estrogens by human cells *in vitro*: Implications to the development of a new diagnostic and therapeutic modality in the treatment of malignancies with estrogen receptors. *Gynecol. Oncol.* **34**, 80-83 (1989).
35. E.R. DeSOMBRE, R.C. MEASE, A. HUGHES, P.V. HARPER, O.T. DeJESUS, and A.M. FRIEDMAN, Bromine-80m-labeled estrogens: Auger electron-emitting, estrogen receptor-directed ligands with potential for therapy of estrogen receptor-positive cancers. *Cancer Res.* **48**, 899-906 (1988).
36. E.R. DeSOMBRE, P.V. HARPER, A. HUGHES, R.C. MEASE, S.J. GATLEY, O.T. DeJESUS, and J.L. SCHWARTZ, Bromine-80m radiotoxicity and the potential for estrogen receptor-directed therapy with Auger electrons. *Cancer Res.* **48**, 5805-5809 (1988).
37. R.W. HOWELL, D.V. RAO, and K.S.R. SASTRY, Macroscopic dosimetry for radioimmunotherapy: Nonuniform activity distributions in solid tumors. *Med. Phys.* **16**, 66-74 (1989).
38. D.V. WOO, D. LI, L.W. BRADY, J. EMRICH, J. MATTIS, and Z. STEPLEWSKI, Auger electron damage induced by radioiodinated iodine-125 monoclonal antibodies. *Front. Radiat. Ther. Oncol.* **24**, 47-63 (1990).
39. D. HOU and Y. MARUYAMA, Enhanced killing of human small cell lung cancer by hyperthermia and indium-111-bleomycin complex. *J. Surg. Oncol.* **44**, 5-9 (1990).
40. J. BARANOWSKA-KORTYLEWICZ, S.J. ADELSTEIN, and A.I. KASSIS, 5-Iodo-2'-deoxyuridine-protein conjugates: Synthesis and enzymatic degradation. *Select. Cancer Ther.* **6**, 1-13 (1990).
41. J.H. GOODMAN, R.A. GAHBAUER, C. KANELLITSAS, N.R. CLENDENON, B.H. LASTER, and R.G. FAIRCHILD, Theoretical basis and clinical methodology for stereotactic interstitial brain tumor irradiation using iododeoxyuridine as a radiation sensitizer and ^{145}Sm as a brachytherapy source. *Stereotact. Funct. Neurosurg.* **54/55**, 531-534 (1990).

14 Biophysical Aspects of Auger Processes, AAPM Symposium Series No. 8 (1992) 014-023
Eds. RW Howell, VR Narra, KSR Sastry, DV Rao

FRAGMENTATION OF AMINO ACIDS DUE TO INNER SHELL X RAY ABSORPTION IN SULFUR ATOMS

KATSUMI KOBAYASHI, AKINARI YOKOYA[1],
NORIKO USAMI[1], and SHOZO ISHIZAKA[1]

Photon Factory, National Laboratory for High Energy Physics,
[1]Institute of Biological Sciences, University of Tsukuba, Tsukuba,
Ibaraki 305, Japan

ABSTRACT

In order to obtain evidence for damage specific to the Auger processes in biological molecules, sulfur containing amino acids (cystathionine and methionine) were irradiated with monochromatic synchrotron soft X rays around the K shell absorption edge of sulfur and phosphorus, and fragmentation products were analyzed with high performance liquid chromatography (HPLC). It was demonstrated that the fragmentation patten of methionine depends upon the X ray energy. Alanine was not observed among the products following irradiation of methionine. This may indicate that alanine observed in the products following irradiation of cystathionine is a result of S-C bond cleavage, not C-C bond cleavage in the molecule. Experiments with a mixed sample of cystathionine and phosphate salts showed that Auger electrons emitted by phosphorus atoms do not affect the degradation pattern of the amino acid.

INTRODUCTION

The high lethality of Auger cascades has attracted much attention not only from the therapeutic point of view, but also from the basic biophysical point. The Auger effect induces radiological effects via two mechanisms. One is through the many low-energy Auger electrons ejected from the atom. These electrons produce many ionizations in close vicinity of the atom. The other is the multiply-ionized atom itself as a result of release of the electrons, which may lead to fragmentation of the molecule. Biological effects caused by the Auger effect have been studied using certain types of radionuclides, *i.e.* ^{125}I (1) or ^{77}Br (2). Recently, with the advance of synchrotron radiation technology, external irradiation with monochromatic X rays became available to efficiently induce inner shell ionization of specific atoms constituting the cell. One typical such atom is phosphorus which constitutes the backbone of DNA in the form of phosphate. On the basis of exposure, monochromatic soft X rays which are absorbed efficiently by K shell electrons of phosphorus showed higher lethality on yeast cells than soft X rays which can not be absorbed by the K shell electrons of phosphorus (3). This biological enhancement can not be interpreted by the increase of absorbed dose in the cell nucleus, indicating that the Auger effect may produce specific types of molecular damage. In order to get evidence for molecular damage specific to the Auger effect, we chose an amino acid having a sulfur atom in the backbone and surveyed the products when irradiated with monochromatic soft X rays at energies which correspond to the K shell absorption edge of sulfur. It was demonstrated that the degradation pattern of the amino acid depends upon the site of photoabsorption in the molecule (4). In this paper, we will describe further studies on the degradation mechanisms of the amino acid using methionine and a mixture of cystathionine and phosphate salt as samples. Methionine has a part of cystathionine including a sulfur atom covalently binding a methyl group (see Fig. 1), and hence the number of amino acids expected is less than in the case of cystathionine. The latter sample was irradiated with phosphorus K edge X rays in order to estimate the effects of Auger electrons generated outside of the molecule. These results indicate that bond breakage can occur efficiently at the site of photoabsorption but the damage is not caused by Auger electrons. Multiply ionized atoms are considered to be responsible for the molecular damage specific to the Auger effect in sulfur containing amino acids.

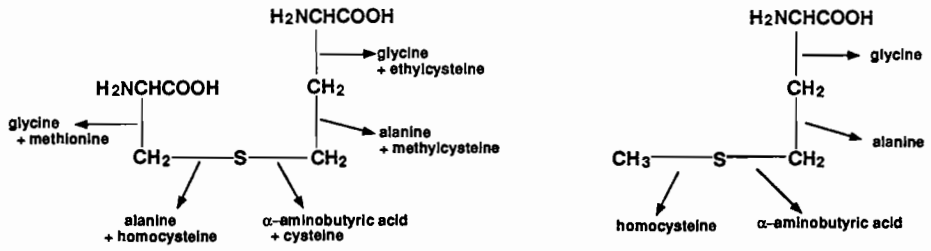

(a) Cystathionine (b) Methionine

FIG. 1. Molecular formula of the amino acids irradiated with monochromatic soft X rays. Arrows indicate the relation between the expected fragments (amino acids) and the cleaved bond.

MATERIALS AND METHODS

Methods of sample preparation, irradiation of monochromatic soft X rays and assay of degradation products, are the same as those described in our previous report (4). Briefly, sample molecules dissolved in double deionized ultrapure water were put and dried in an area of 4 mm(H) X 2 mm(V) on small aluminum plates. The sample weight was 50 μg. Mixed samples were prepared with Na_2HPO_4 and KH_2PO_4. Cystathionine was dissolved in the phosphate buffer instead of pure water and dried on the sample plates. The ratio of sulfur atoms to phosphorus in these samples was about one. These plates were set on a sample holder in a vacuum irradiation chamber. Synchrotron X rays, monochromatized with an InSb crystal, were used to irradiate the sample at the beamline 11B at the Photon Factory, National Laboratory for High Energy Physics, Tsukuba, Japan. The energies of monochromatic soft X rays used for irradiation were chosen after measuring the absorption spectra of the sample molecule. X ray energies for the irradiation of methionine were 2472 and 2466 eV, the former of which corresponds to the K shell resonance absorption of sulfur (4). Those for the mixed sample were 2153 and 2146 eV, which correspond to the resonance absorption of phosphorus and below the absorption edge of phosphorus, respectively (3). Exposure was determined by compensating the decrease of exposure in the sample due to the absorption of X ray by the sample

molecules. Irradiated samples were redissolved in water and injected into a high performance liquid chromatography (HPLC) system to analyze the products in combination with the OPA(o-phthal aldehyde) method to raise the detection sensitivity for amino acids (5). Quantities of the products were obtained from the peak areas on the HPLC chromatograms using the conversion factors previously determined. Production efficiencies were determined from the slope of the exposure-peak area relationship.

RESULTS

Products from Methionine

On the HPLC chromatograms, several peaks of the products were observed along with the remaining methionine, and the number of peaks was less than that in cystathionine (Fig. 2). The ratio of the peak height between α-aminobutyric acid and glycine was dependent upon the irradiation energy. Among the products, glycine and α-aminobutyric acid were identified. These same products were identified in the case of cystathionine. The peak areas were measured by an integrator. Peaks at the expected retention time of alanine could not be measured quantitatively at both irradiation energies, while the peak for alanine was observed in the irradiated cystathionine (4). Homocysteine can not be detected due to the HPLC condition adopted here. These results indicate that, in methionine, the C-C bond cleavage to produce alanine hardly occurs by the soft X ray irradiation irrespective of the photoabsorption site.

The production efficiencies of glycine and α-aminobutyric acid are obtained and listed in Table I. The production efficiency (41 pmol/MR) of α-aminobutyric acid per exposure at 2472 eV was 3.7 times the value (11 pmol/MR) at 2466 eV, while the production efficiency (1.9 pmol/MR) of glycine per exposure at 2472 eV was 2.5 times the value (0.77 pmol/MR) at 2466 eV. These efficiencies were close to the values obtained from cystathionine irradiated around the sulfur K edge (Table I). Energy dependence of the production efficiency of glycine from methionine was about twice that from cystathionine.

Products from Cystathionine-Phosphate Mixture

A mixed sample of cystathionine and phosphate was irradiated with phosphorus K edge X rays in order to estimate the effects of Auger electrons

generated outside of the molecule. Noticeable difference in the spectrum of the peak heights between the irradiation at 2153 eV and at 2146 eV was not observed (Fig. 3). The pattern of the degradation products on the HPLC chromatogram at 2146 eV were also very similar to that of cystathionine irradiated at the energy below the sulfur K edge (2466 eV). Production yields of the fragments were larger

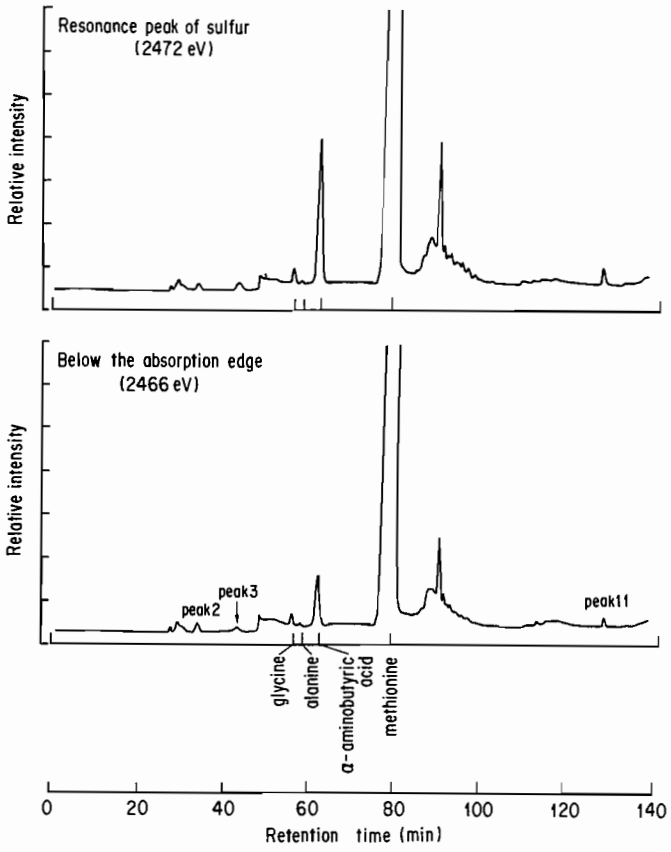

FIG. 2. HPLC chromatograms of irradiated methionine at 2472 eV and at 2466 eV. The names of the expected amino acids are inscribed on the abscissa. Exposures are 70 MR (1.8×10^4 C/kg) for the upper panel and 94 MR (2.4×10^4 C/kg) for the lower. Peaks for alanine were observed but were not large enough for quantitative analysis.

at 2153 eV than at 2146 eV due to the large absorption cross section of phosphorus at 2153 eV. The ratios of the production efficiencies of the products at the two energies were between 1.4 and 1.8, and did not vary much among the

products as seen in Table II. These results are clearly different from the case when irradiated with X rays at the sulfur K edge, where the ratios of the yield varied from 1.3 (glycine) to 4.1 (unidentified peak at the retention time of about 130 min), depending upon the products (4)).

TABLE I

Production Efficiencies† (pmol/MR) of α-Aminobutyric Acid and Glycine

Product	Methionine		Cystathionine*	
	2472 eV	2466 eV	2472 eV	2466 eV
α-Amino-butyric acid	41	11	38	13
Glycine	1.9	0.77	1.2	1.0
Alanine	n.d.	n.d.	75	28

†Efficiencies for alanine was calculated by assuming the peak of alanine and/or ethylcysteine contains alanine only.
*Data were taken from Yokoya et al. (4) for comparison
n.d.: not detected

DISCUSSION

Yield of C-C bond Cleavage Producing Alanine

Glycine and α-aminobutyric acid were identified on the chromatograms of irradiated methionine. However, the peak was not seen at the position of alanine on the HPLC chromatogram of the irradiated methionine at neither of the irradiation energies. In methionine, the C-C bond cleavage to produce alanine hardly occurred with the soft X ray irradiation. From these results, it might be suggested that alanine produced by the cleavage of the C-C bond in cystathionine did not contribute to the peak observed at the position of alanine on the HPLC chromatograms of the irradiated cystathionine; in other words, alanine was produced by the cleavage of S-C bond (see Fig. 1). Ethylcysteine, which might be produced from cystathionine as a counterpart fragment of

glycine, might be included in the alanine peak under the HPLC conditions used in this study (4). However, the amount of ethylcysteine can be considered very small upon estimation from the amount of glycine (about 1 pmol/MR at both irradiation energies). From these considerations, the large peak area observed at the position of alanine and/or ethylcysteine on the HPLC chromatograms of irradiated cystathionine could be considered as alanine produced by the S-C bond cleavage in cystathionine.

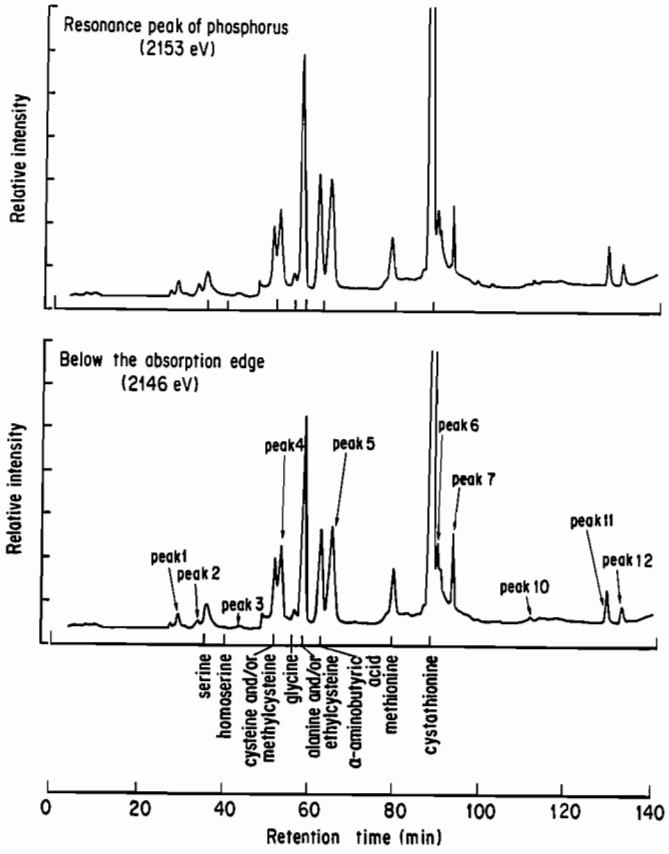

FIG. 3. HPLC chromatograms of the cystathionine-phosphate mixed sample irradiated with 2153 eV and at 2146 eV monochromatic soft X rays. Exposures are 57 MR (1.5×10^4 C/kg) for the upper panel and 82 MR (2.1×10^4 C/kg) for the lower. The names of the expected amino acids are inscribed on the abscissa. Peaks with numbers are unidentified ones.

The yield of alanine from cystathionine irradiated at the energy around the sulfur K edge was then calculated by assuming that the peak contains only alanine. The obtained yields are shown in Table I with the values of α-aminobutyric acid and glycine. Similar dependence of the yields of alanine and α-aminobutyric acid on the photoabsorption site may indicate that the production mechanisms have some part in common. Some role of the sulfur atom as the photoabsorption site can be suspected.

TABLE II

Production Efficiencies* of Irradiation Products Following Irradiation of a Mixed Sample of Cystathionine and Phosphate Salts

Product	Efficiency per unit exposure (pmol/MR)	
	2153 eV	2146 eV
α-Aminobutyric acid	47	26
Glycine	2.3	1.6
Alanine	108	63

*Irradiated at the resonance absorption peak of phosphorus (2153 eV) and at the energy below the peak (2146 eV)

Contribution of Auger electrons in the Degradation of the Amino Acids

The production efficiencies of α-aminobutyric acid and glycine at 2153 eV were larger than those at 2146 eV as shown in Table II, reflecting the large absorption cross section of phosphorus. From these results, it was confirmed that the Auger electrons from phosphorus did actually contribute to the degradation of cystathionine.

The ratio of the yields of three products; namely, α-aminobutyric acid, glycine and alanine, at the energy of 2153 eV was about 20:1:47. This ratio was

not so different from that at 2146 eV (16:1:39). At the energies around the sulfur K edge, on the other hand, the ratio clearly changed with the photoabsorption site from 13:1:28 to 32:1:62 (Table I). These results also indicate that the Auger electrons from phosphorus were not involved in the change of the degradation reactions of the amino acid. Inner shell excited atoms are multiply ionized after the Auger cascade. A multiply ionized sulfur atom in the amino acid, rather than the Auger electrons from the sulfur atom, is considered to play an important role in determining the degradation reaction of the molecule. These results may support the idea that the changes of the biological effects at the inner-shell absorption edges are due to the action of the multiple ionization of the atom after the Auger cascade rather than the action of the ejected secondary electrons. The Auger electrons are supposed to affect the chemical bonds non-specifically in the molecules in the sample.

CONCLUSION

Degradation pattern of amino acids depends much upon the photoabsorption site and the multiply ionized atom plays an important role in the degradation. These molecular changes (damage) could explain the enhancement of biological effect observed with irradiation of monochromatic soft X rays at the inner-shell absorption edge.

ACKNOWLEDGMENTS

This work has been performed under the approval of the Photon Factory Advisory Committee (Proposal No. 89-163).

REFERENCES

1. K.G. HOFER and W.L. HUGHES, Radiotoxicity of intranuclear tritium, ^{125}iodine and ^{131}iodine. *Radiat. Res.* **47**, 94-109 (1971).
2. A.I. KASSIS, S.J. ADELSTEIN, C. HAYDOCK, K.S.R. SASTRY, K.D. McELVANY, and M.J. WELCH, Lethality of Auger electrons from the decay of bromine-77 in the DNA of mammalian cells. *Radiat. Res.* **90**, 362-373 (1982).
3. K. KOBAYASHI, K. HIEDA, H. MAEZAWA, Y. FURUSAWA, M. SUZUKI, and T. ITO, Effects of K-shell X-ray absorption of intracellular phosphorus on yeast cells. *Int. J. Radiat. Biol.* **59**, 643-650 (1991).

4. A. YOKOYA, K. KOBAYASHI, N. USAMI, and S. ISHIZAKA, Radiolytic degradation of cystathionine irradiated with monochromatic soft X-rays at the K-shell resonance absorption of sulfur. *J. Radiat. Res.* **32**, 215-223 (1991).
5. M. ROTH, Fluorescence reaction for amino acid. *Anal. Chem.* **43**, 880-882 (1971).

DISCUSSION

Harapanhalli, R. S. 1) What reasons do you ascribe to the fact that S-C bond cleavage predominates at the absorption edge of the spectrum (2472 eV)? 2) What are the consequences on the sulfur containing residue after the S-C cleavage?

Kobayashi, K. 1) The reason for the increase of S-C bond breakage with 2472 eV irradiation is multiple ionization of sulfur atoms which absorbed an X ray photon and ejected several Auger electrons. Molecules having multiply charged atoms in it are known to break up in to small fragments. 2) Since the peak in HLPC for sulfur containing residues are observed as a mixture with other fragments, we cannot say decisively. However, we suggest that other S-C bonds are also cleaved and quantities of sulfur-containing residues become very small, mainly due to the same reason above when Auger effects occur.

Biophysical Aspects of Auger Processes, AAPM Symposium Series No. 8 (1992) 024-036
Eds. RW Howell, VR Narra, KSR Sastry, DV Rao

DAMAGE TO ADENOSINE-TRIPHOSPHATE INDUCED BY MONOCHROMATIC X RAYS AROUND THE K SHELL ABSORPTION EDGE OF PHOSPHORUS

RITSUKO WATANABE[1], MITSUO ISHIKAWA[1],
KATSUMI KOBAYASHI[2], and KAORU TAKAKURA[1]

[1]Department of Physics, International Christian University,
Tokyo 181, Japan
[2]Photon Factory, National Laboratory for High Energy Physics,
Ibaraki 305, Japan

ABSTRACT

Adenosine-triphosphate (ATP) is well known to have an important role in the energy metabolism in biological systems. The purpose of this study is to clarify the radiation effects on ATP specific to inner shell ionization. ATP, in concentrated aqueous solution, was irradiated with monochromatic X rays having energies of the resonance absorption peak of the phosphorus K shell, 2.153 keV, and slightly below and above the peak, 2.146 keV and 2.160 keV, selected from synchrotron radiation. Adenine, Adenosine 5'monophosphate (5'AMP) and Adenosine 5'diphosphate (5'ADP) were obtained as radioproducts by the method of high performance liquid chromatography

(HPLC). G values of these products were calculated on the basis of the absorbed energy. When the ATP solution of 0.282 mol/l was irradiated with 2.160 keV X rays which can ionize the K shell of phosphorus, G values of Adenine, 5'AMP and 5'ADP were estimated to be 1.4, 0.40 and 0.46, respectively. These values were respectively 1.3, 2.9 and 3.8 times higher than those obtained upon irradiation with 2.146 keV X rays which cannot ionize the K shell of phosphorus. These energy dependent enhancements may reflect the difference in energy absorption processes, especially the Auger cascade in phosphorus may be suspected to play an important role in these enhancements. With 2.153 keV X rays a stronger enhancement was obtained than for the irradiation with 2.160 keV. Radioproducts induced by the irradiation with ^{60}Co γ rays were also analyzed. In this case insignificant quantities of 5'AMP and 5'ADP were obtained and the G value of the Adenine produced was smaller than that for irradiation with X rays around the K absorption edge of phosphorus. This fact may suggest that the mechanism of radiation action on ATP induced by ^{60}Co γ rays is different from that by X rays around the K absorption edge of phosphorus.

INTRODUCTION

In order to determine the enhanced damage due to the Auger cascade initiated by the ionization of the K shell, the effects of irradiation on various systems with monochromatic X rays around an absorption edge of a selected component atom have been investigated. In particular, numerous studies which used bromine as a selected component atom have been tried. For example, the enhanced damage due to irradiation with monochromatic X rays having ionization energy of the K shell in bromine were examined in bromodeoxyuridine incorporated cells (1-6), plasmid DNA (4,7) or brominated synthetic DNA constituents (8,9). Referring to other selected component atoms, Shinohara *et al.* (10) have studied the sensitivity of HeLa cells with iododeoxyuridine incorporated into DNA to monochromatic X rays with energies slightly above the K shell absorption edge of iodine. In the situations of these experiments bromine and iodine are incorporated in the base moiety of DNA. On the other hand, phosphorus atoms are located at strategic positions as a constituent element of phosphodiester bonds of DNA. The irradiation with soft X rays around the K shell absorption edge of phosphorus in DNA may be considered to cause serious damage to DNA.

Recently some studies of the effects of irradiation with monochromatic X rays around the K shell absorption edge of phosphorous have been investigated using synchrotron radiation at the National Laboratory for High Energy Physics in Tsukuba, Japan. Plasmid DNA (11), chromosomes (12), T1 phage (13) and yeast cells (14) were irradiated with monochromatic X rays around the K shell absorption edge of phosphorus, and Auger enhancement effects induced via the ionization of the K shell of phosphorus were studied. In this report damage to ATP, especially the production of Adenine, 5'AMP and 5'ADP from ATP induced by monoenergetic X rays around the K shell absorption edge of phosphorus were studied by the method of HPLC.

MATERIALS AND METHODS

Preparation of Sample Solutions

Adenosine 5'-triphosphate (ATP) was purchased in powder form from Sigma Co. Ltd. It was dissolved in deionized triply distilled water without further purification and was used as a substance for irradiation. The concentration of ATP was 155 mg/ml (0.282 mol/l), and the pH of the ATP solution was 2.85. The ATP film for the measurements of the absorption spectrum was prepared by pressing the powder sample to 6.45 mg/cm^2 thickness between a pair of mylar films of 5 μm thickness. Adenine, Adenosine, 5'AMP and 5'ADP, purchased from Sigma Co. Ltd., were used as reference samples in the analysis of radioproducts.

Sources of Radiation

Synchrotron radiation from the 2.5 GeV electron storage (the Photon Factory, National Laboratory for High Energy Physics, Tsukuba, Japan) was used as the source of soft X rays. Details of the irradiation system, the characteristics of the X rays and their performance have been described elsewhere (15). White SR was deflected 2° upward in order to cut the high energy X ray components and was monochromatized with an InSb double-crystal monochromator. The full width at half maximum at 2 keV was about 1 eV. Irradiation with ^{60}Co γ rays was performed at the National Cancer Center Research Institute, Tokyo, Japan, using the irradiation apparatus with 24,000 Ci ^{60}Co γ source (Gamma-cell 220, AECL Industrial Irradiators).

Measurement of the Absorption Spectrum of ATP and Selection of X ray Photon Energy for Irradiation

As shown in Fig. 1, the absorption spectrum from the thin film of ATP was measured in the range of energy 2.10 - 2.25 keV, which is the soft X ray region around K absorption edge of phosphorus. For spectrum measurement, an ATP film was inserted between the monochromator and the ionization chamber installed downstream of the beamline. The absorption spectrum showed a stepwise change, going from below to above the edge with fine structure of a sharp peak at around 2.153 keV. A sharp absorption peak was found to be characteristic of the structure of P surrounded by O atoms in the form of PO_4^{3-} (14, 16). In the present study irradiations were carried out with monochromatic X rays of 2.153, 2.146 and 2.160 keV. The 2.153 keV X rays (K X ray (P_O)) energy corresponds to the resonance peak and 2.146 keV X rays (K X ray (P_-)) and 2.160 keV X rays (K X ray (P_+)) correspond to slightly below and above the peak energy, respectively.

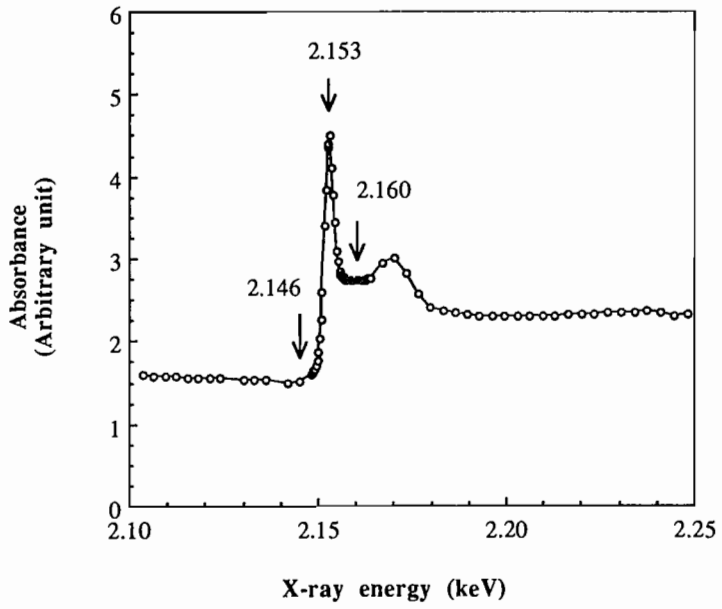

FIG. 1. Absorption spectrum of ATP film around the K absorption edge of phosphorus.

Irradiation Techniques

Monochromatic X rays were transported through a 5 μm mylar film into an atmospheric sample chamber installed at the end of the vacuum line (Beamline 11 B of Photon Factory). At the sample chamber a specially designed cell made of acrylic resin (Fig. 2) was used to hold the ATP solution for irradiation. The cell had a mylar film window of 5 μm thickness, through which the sample was exposed to X rays. The area of the window was 5 mm x 10 mm and the cell depth was 2 mm. The X ray beam size at the sample position was 4 mm x 8 mm. Under irradiation, ATP solutions were stirred with a glass-coated piece of iron. Irradiation was carried out under aerobic conditions at 23 ± 2°C. A free air parallel-plane ionization chamber was used for measurements of the exposure rate. The chamber was placed in front of the sample position. The exposure rate was 15.5 C/kg per min at a ring current of 250 mA. During the irradiation with ^{60}Co γ rays, 200 μl of the ATP solution was sealed in a 20 cm^3 glass ampoule under aerobic conditions. The exposure rate, measured with a Fricke actinometer, was 4.5 kGy/h.

Estimation of Absorbed Dose and Calculation of G value

When photons having energies around the K absorption edge of phosphorus are transmitted through water, the path length of water needed to reduce the intensity of photons to 1/e is very thin such as 20 μm (17). Therefore all the incident photons were absorbed completely by the ATP solution located in the cell with 2 mm depth. The estimation of the absorbed dose is rather simple for this situation. In this case all energies up to the maximum photon energies passing through the mylar film of the cell may be used to estimate the absorbed dose. The photon fluence Φ (photons/m^2) per 1 C/kg was calculated using:

$$\Phi = W \times 1/E \times 1 / (\mu_{en}/\rho)_{air} \quad (1)$$

where $(\mu_{en}/\rho)_{air}$ is the mass energy absorption coefficient of air, W the energy required to produce an ion pair in air at room temperature (33.7 J/C), and E the energy of an X ray photon. In the present study, G values, which are defined as the number of radioproducts in an irradiated solution per absorbed energy of 100 eV, were calculated on the basis of the absorbed dose estimated as described above.

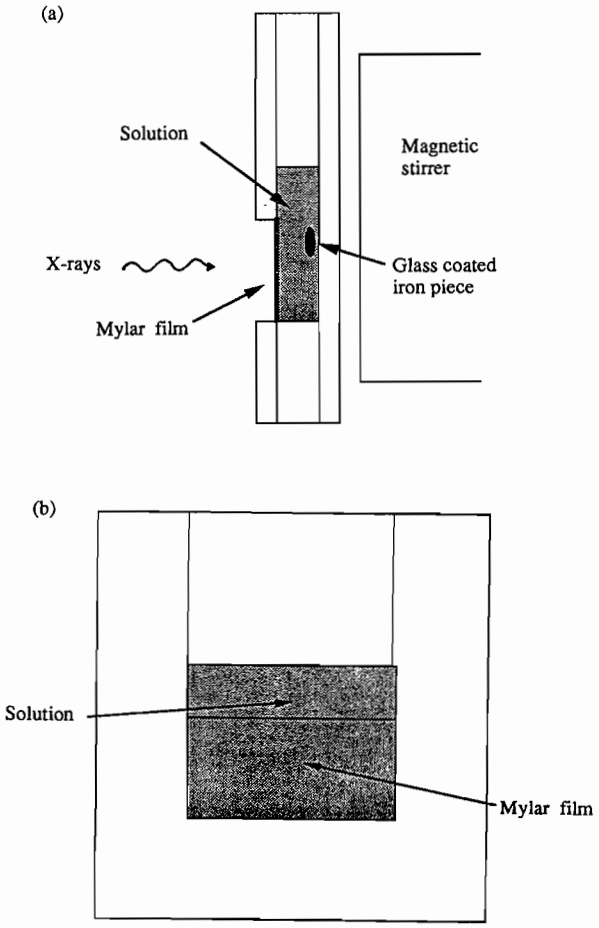

FIG. 2 A view of the cell prepared for irradiation with X rays around the K absorption edge of phosphorus. a) Side view of the cell. b) Front view of the cell. Scale (1 in = 8 mm).

Analysis of Radioproducts

The analyses of radioproducts were performed by HPLC using a Waters Model ALC/GPC 609G. An anion exchange column 10 mm in diameter by 100 mm in length (Partisil SAX) was employed. Two kinds of buffer solutions were used in the moving phase; A) a solution of 0.05 mol/l KH_2PO_4 (pH 4.5), B) a solution of 0.25 mol/l KH_2PO_4 with 0.5 mol/l KCl (pH 5.0). Buffer

solutions of A and B were delivered at linear gradient from 100% A to 100% B for 10 min and then 100% B was delivered for 40 min. The flow rate was 3 ml/min throughout the measurements. The reverse-phase column (μBondapak C_{18}) was used to get supplementary information and in this case a buffer solution of A was delivered at 3 ml/min. The spectra were monitored optically at 260 nm. The chromatograph was operated at a temperature of 21 ± 1°C. Adenine, Adenosine, 5'AMP and 5'ADP were used as reference samples. The retention times were 1.80 min for Adenine, 1.70 min for Adenosine, 2.95 min for 5'AMP and 9.30 min for 5'ADP during the ion exchange analysis.

RESULTS

HPLC elution profiles of ATP irradiated with K X rays ($P_{-,0,+}$) were observed (Figures are not shown). It was thus found that there were no qualitative differences among these HPLC patterns. The main radioproducts, Adenine, 5'AMP and 5'ADP, were identified among several fractions in the HPLC profiles, judging from the retention times of the reference samples described in the MATERIALS AND METHODS section above. By the method of reverse-phase HPLC it could be verified that Adenosine was not obtained as one of the radioproducts. The amount of each radioproduct was estimated from the peak area from each respective signal on the elution pattern and was plotted against absorbed dose. The amount of produced Adenine, 5'AMP and 5'ADP from ATP irradiated with K X ray (P_0), expressed in terms of the number of those radioproducts produced per unit volume of irradiated ATP solution of 1 cm^3, were plotted as a function of absorbed dose in Fig. 3. These were seen to increase linearly with increasing absorbed dose. Also during irradiation with K X rays (P_-) and (P_+), the amount of produced Adenine, 5'AMP and 5'ADP increased linearly with increasing absorbed dose (Figures not shown). G values of these radioproducts calculated on the basis of the absorbed dose, which was described in the MATERIALS AND METHODS section above, are shown in Table I for various cases. In Fig. 4, G values of Adenine, 5'AMP, and 5'ADP are shown as a function of the incident photon energy. As shown in Fig.4, the G values of these radioproducts upon irradiation with K X rays (P_0) and (P_+) were much larger than those from K X ray (P_-). Details about these enhancement effects will be described in the DISCUSSION.

The dependence of the amounts of produced Adenine, 5'AMP and 5'ADP on the absorbed dose in the case of irradiation with ^{60}Co γ rays are

TABLE I

G Values of Radioproducts from ATP Irradiated with X rays and ^{60}Co γ rays

Substrate	Radio-products	2.146 keV X rays	2.153 keV X rays	2.160 keV X rays	$G_{2.153\,keV}/G_{2.146\,keV}$	$G_{2.160\,keV}/G_{2.146\,keV}$	^{60}Co γ rays
ATP	Adenine	1.1	1.6	1.4	1.5	1.3	0.88
	5'AMP	0.14	0.48	0.40	3.4	2.9	0.00
	5'ADP	0.12	0.47	0.46	3.9	3.8	0.00

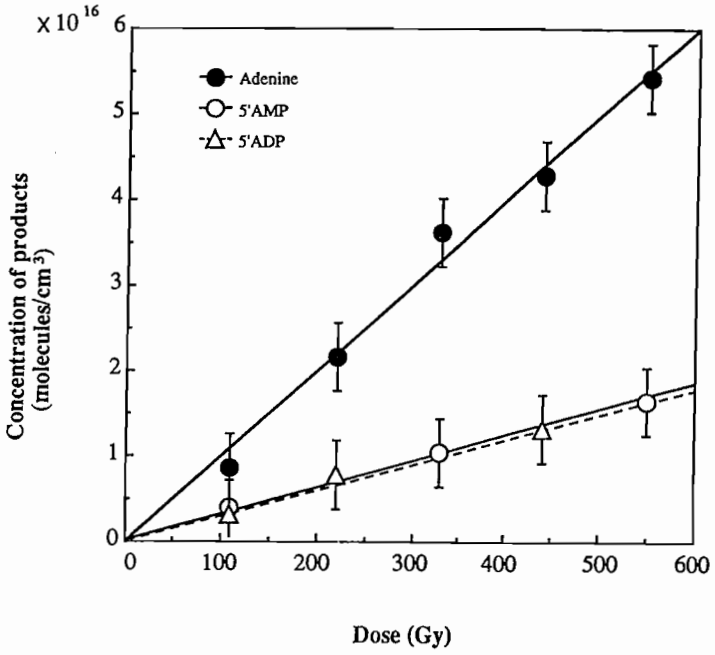

FIG. 3. Dose dependence of the concentrations of Adenine, 5'AMP and 5'ADP in the ATP solution following irradiation with 2.153 keV X rays (K X ray (P_o)).

shown in Fig. 5. Linear production of produced Adenine with increasing absorbed dose was obtained, however, 5'AMP and 5'ADP were not significantly produced. The G values of these products are shown also in Table I.

DISCUSSION

In this report only Adenine, 5'AMP and 5'ADP were analyzed as main radioproducts, although lesser amounts of other products were seen in the ion exchange liquid chromatogram. As shown in Table I, K X rays (P_0) and (P_+) effectively induced the production of Adenine, 5'AMP and 5'ADP, relative to K X ray (P_-). Irradiations with K X ray (P_+), which can ionize at the K shell in phosphorus atom, gave 1.3, 2.9 and 3.8 times higher G values for Adenine, 5'AMP and 5'ADP, respectively, compared with K X ray (P_-) which can not ionize the K shell of phosphorus. Upon irradiation with K X ray (P_0),

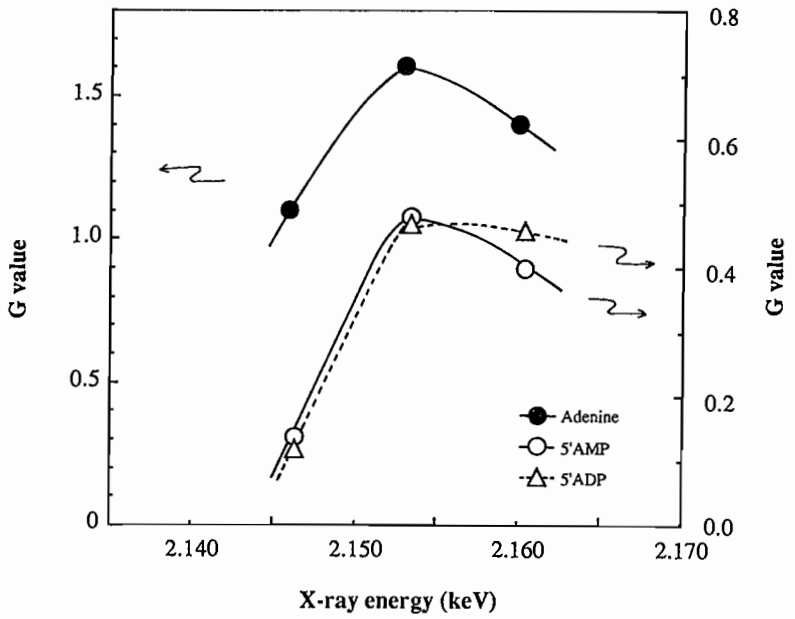

FIG. 4. The dependence of the G values of Adenine, 5'AMP and 5'ADP on the incident photon energy.

which is just the resonance energy of the K absorption edge of phosphorus, the maximum G values for these radioproducts were obtained for all three X ray energies. From this experiment it can be said that a slight increase in photon energy, for example only 0.3% increase {(2.153 - 2.146) / 2.146}, causes a greatly enhanced ratio of damage to ATP such as 45% (1.6 / 1.1 - 1) or 290% (0.47 / 0.12 - 1). The reason for this great enhancement in damage is suggested

to be as follows. The photoelectric absorption of photons having energies slightly above the K absorption edge is followed by the Auger cascade and leaves the atom highly ionized. Further, both the low energy Auger and Coster-Kronig electrons are set in motion, and the excitation energy released in charge neutralization is capable of producing extensive bond rupture and damage. The photons having energies slightly below the K edge do not induce these physical processes caused through the initiation of ionization at the K shell in phosphorus. The enhancement ratios for production of 5'AMP (3.4 for K X ray (P_0), 2.9 for K X ray (P_+)) and 5'ADP (3.9 for K X ray (P_0), 3.8 for K X ray (P_+)) were larger than those for Adenine (1.5 for K X ray (P_0), 1.3 for K

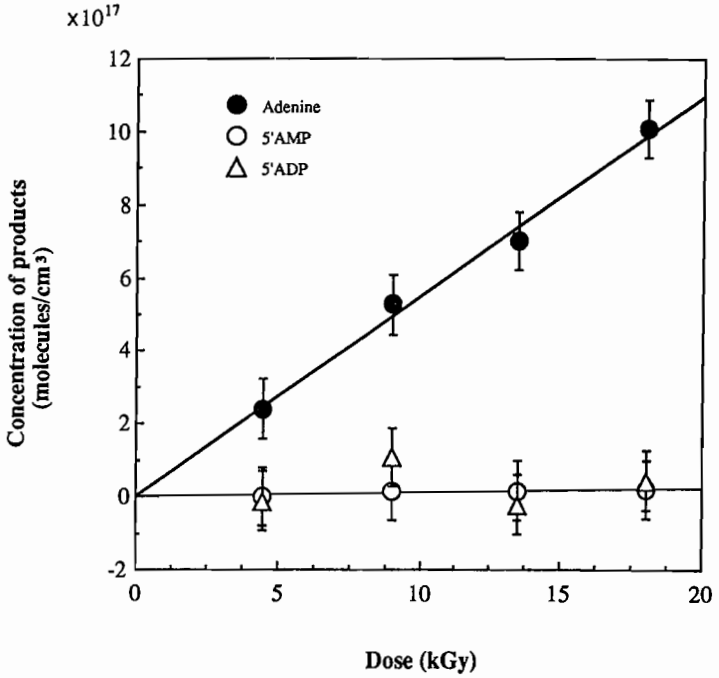

FIG. 5. Dose dependence of the concentrations of Adenine, 5'AMP and 5'ADP in the ATP solution irradiated with ^{60}Co γ rays.

X ray (P_+)) when comparing the G values upon irradiation with the K X rays (P_0) and (P_+) to that of K X ray (P_-). The reason for this phenomenon may be due to the release of electrons from the K shell followed by the positive ionization of the phosphorus atom. This then causes the production of inorganic phosphate which is more sensitive than the production of Adenine located at the base position because it is farther from the phosphorus atom.

The physical processes following the photoelectric absorption of photons having energies in the resonance region of the K edge should be carefully considered. In this experiment indirect effects from water should not be disregarded. From a simple calculation using the mass energy absorption coefficients (17), weight, and volume of water and ATP, it is estimated that about 85% of the total energy is absorbed by the water in the ATP solution during irradiation with K X ray (P_-), and 65% and 76% for K X rays (P_0) and (P_+), respectively. That is, the indirect contributions via water to the G values are reduced to about 80 or 90% during the irradiation with K X rays (P_0) and (P_+) compared with that of K X ray (P_-). This fact means that indirect effect via water has no essential role in the enhancement of G values of radioproducts during the irradiation with K X rays (P_0) and (P_+).

In this experiment irradiation of ATP solution with ^{60}Co γ rays was performed as a reference. Although the chromatogram pattern observed when ATP was irradiated with ^{60}Co γ rays was similar to that with K X rays ($P_{-,0,+}$), the corresponding G values of produced Adenine, 5'AMP and 5'ADP were very different. The G value of produced Adenine upon irradiation with ^{60}Co γ rays was 0.88 as shown in Table I. This value is much smaller than that obtained upon irradiation with K X rays ($P_{-,0,+}$). Another difference is that 5'AMP and 5'ADP were not significantly produced during irradiation with ^{60}Co γ rays, whereas they were clearly observed upon irradiation with K X rays ($P_{-,0,+}$). Thus the probability of production of intact Adenine, 5'AMP and 5'ADP is higher for irradiation with K X rays ($P_{-,0,+}$) than for ^{60}Co γ rays. It is suspected that during irradiation with ^{60}Co γ rays a higher possibility of degradation of sugar accompanying the production of Adenine, 5'AMP and 5'ADP is apparently found than during irradiation with X rays around the K absorption edge of phosphorus. Further studies to clarify the sugar damage to ATP induced by irradiation with X rays around the K absorption edge of phosphorus should be carried out.

ACKNOWLEDGMENTS

We would like to express our thanks to Dr. N. Munakata of the National Cancer Center Research Institute for his help in using the irradiation system with ^{60}Co γ rays. We greatly appreciate Mr. A. Yokoya and Ms. N. Usami for their technical instruction and assistance throughout the irradiation experiments. This work was performed under the approval of the Photon Factory Advisory Committee (Proposal No. 88-153)

REFERENCES

1. K. SHINOHARA, H. OHARA, K. KOBAYASHI, H. MAEZAWA, K. HIEDA, S. OKADA, and T. ITO, Enhanced killing of Hela cells pre-labelled with 5-Bromodeoxyuridine by monochromatic synchrotron radiation at 0.9 A; An evidence Auger enhancement in mammalian cells. *J. Radiat. Res.* **26**, 126-136 (1980).
2. H. OHARA, K. SHINOHARA, K. KOBAYASHI, and T. ITO, An additonal enhancement in BrdU-labelled cultured mammalian cells with monoenergetic synchrotron radiation at 0.09 nm; Auger effect in mammalian cells. In *DNA Damage by Auger Emitters* (K.F. BAVERSTOCK and D.E. CHARLTON, Eds.), pp.123-134. Taylor & Frances, London, 1988.
3. H. MAEZAWA, K. HIEDA, K. KOBAYASHI, *et al.*, Effects of monochromatic X-rays with resonance energy of bromine K-absorption edge on bromouracil-labelled E-coli cells. *Int. J. Radiat. Biol.* **53**, 301-308 (1988).
4. H. MAEZAWA, K. HIEDA, K. KOBAYASHI, and T. ITO, Effects of Auger cascades of bromine induced by K-shell photoionization on plasmid DNA, bacteriophages, E. coli and yeast cells. In *DNA Damage by Auger Emitters* (K.F. BAVERSTOCK and D.E. CHARLTON, Eds.), pp.135-146. Taylor & Frances, London, 1988.
5. D. LARSON, W. J. BODDEL, C. LING, T. L. PHILLIPS, M. SCHELL, D. SHRIEVE, and T. TROXEL, Auger electron contribution to bromodeoxyuridine cellular radiosensitization. *Int. J. Radiat. Oncol. Biol. Phys.* **16**, 171-176 (1989).
6. A. HALPERN and B. MÜTZE, Irradiation of micro-organisms with mono-energetic X-rays. Biological consequences of the Auger effect. *Int. J. Radiat. Biol.* **34**, 67-72 (1978).
7. H. MENKE, W. KÖHNLEIN, S. JOKSCH, and A. HALPERN, Strand breaks in plasmid DNA, natural and brominated, by low-energy X-rays. *Int. J. Radiat. Biol.* **59**, 85-96 (1991).
8. A. HALPERN and G. STÖCKLIN, A radiation chemical resonance effect in solid 5-bromodeoxyuridine. Chemical consequences of the Auger effect, *Radiat. Res.* **58**, 329-337 (1974).
9. K. TAKAKURA, Auger effects on bromodeoxyuridine-monophosphate irradiated with monochromatic X-rays around bromine K-absorption edge. *Radiat. Environ. Biophys.* **28**, 177-184 (1989).
10. K. SHINOHARA, A. ITO, and K. KOBAYASHI, Radiosensitization of 5-iododeoxyuridine in the soft X-ray region. In *Photon Factory Activity Report.* **7**, p.100, National Laboratory for High energy Physics, 1989.
11. K. HIEDA, A. AZAMI, M. SUZUKI, H. MAEZAWA, Y. FURUSAWA, and K. KOBAYASHI, Strand breaks in pBR322 DNA induced by monoenergetic X-rays around K-absorption edge of phosphorus. In *Photon Factory Activity Report.* **5**, p.286, National Laboratory for High Energy Physics, 1987.
12. M. WATANABE, M. SUZUKI, K. WATANABE, K. SUZUKI, N. USAMI, A. YOKOYA, and K. KOBAYASHI, Mutagenic and transforming effects of soft X-rays with resonance energy of phosphorus K-absorption edge. In *Photon Factory Activity Report.* **7**, p.99, National Laboratory for High Energy Physics, 1989.
13. H. MAEZAWA, Y. FURUSAWA, K. HIEDA, K. KOBAYASHI, T. MORI, K. SUZUKI, and T. ITO, Enhanced Killing on E. coli. and bacteriophage by X-rays at resonance energy of phosphorus K-absorption edge. In *Photon Factory Activity Report.* **5**, p.285, National Laboratory for High Energy Physics, 1987.

14. K. KOBAYASHI, K. HIEDA, H. MAEZAWA, Y. FURUSAWA, M. SUZUKI, and T. ITO, Effects of K-shell X-ray absorption of intracellular phosphorus on yeast cells. *Int. J. Radiat. Biol.* **59**, 643-650 (1991).
15. T. OHTA, P. M. STEFAN, M. NOMURA, and H. SEKIYAMA, Design and performance of the UHV compatible soft X-ray double crystal monochromator at the Photon Factory. *Nucl. Instr. and Meth.* **A246**, 373-376 (1986).
16. J. L. DEHMER, Evidence of effective potential barriers in the X-ray absorption spectra of molecules. *J. Chem. Phys.* **56**, 4496-4504 (1972).
17. J. H. HUBBELL, Photon mass attenuation and energy absorption coefficients from 1 keV to 20 MeV. *Int. J. Appl. Radiat. Isotopes* **33**, 1269-1290 (1974).

DISCUSSION

Adelstein, S. J. Were you able to measure G values for the destruction of ATP *i.e.* G(-ATP) as well as for the formation of adenine, AMP and ADP?

Takakura, K. It is difficult to detect the reduction in the amount of ATP because the ratio of the reduction must be between about 0.1% to 1%. On the other hand, small amounts of radioproducts such as adenine, AMP, and ADP can be detected if the amounts of these in the control are not so much. The corresponding signals in HPLC can be observed as newly produced signals.

Goodhead, D. It seems interesting that you find the two 5' products produced even below the phosphorus K edge but that they are not produced by ^{60}Co γ rays. Does this suggest even an L shell absorption in phosphorus (without a consequent Auger cascade) can produce a 5' product? Yet ^{60}Co γ rays do not even though secondary-electron ionization must take place (occasionally and randomly) in the phosphorus L-shell. Is this because there are so few such ionizations from ^{60}Co γ rays?

Takakura, K. I found that the two 5' products are produced even below the phosphorus K edge. However, in the case of irradiation with ^{60}Co, the γ rays produce the two 5' products but further degradation of the sugar attached to the 5' products apparently leads to nearly zero production of these products.

Martin, R. I presume that the ^{60}Co γ ray/ATP experiment is not new, and that there is established data on the radiation chemistry of DNA. What is known about the mechanism of adenine formation from ATP?

Takakura, K. I was looking for the publications concerning radiation effects on ATP using ^{60}Co γ rays but I didn't find them. Would you please tell me the references concerning this if you know of them? I am sorry, but I cannot tell you the exact mechanism of adenine formation from ATP. I think ESR would give the answer.

Biophysical Aspects of Auger Processes, AAPM Symposium Series No. 8 (1992) 037-050
Eds. RW Howell, VR Narra, KSR Sastry, DV Rao

INACTIVATION OF BACTERIOPHAGE T1 BY THE AUGER EFFECT FOLLOWING PHOSPHORUS RESONANCE ABSORPTION OF MONOENERGETIC SYNCHROTRON RADIATION

YOSHIYA FURUSAWA[1#], HIROSHI MAEZAWA[2], KENSHI SUZUKI[1], KATSUMI KOBAYASHI[3], MASAO SUZUKI[4*], and KOTARO HIEDA[4]

[1]Department of Molecular Biology,
[2]Department of Radiation Oncology,
Tokai University School of Medicine, Isehara,
Kanagawa 259-11, Japan

[3]Photon Factory, National Laboratory for High Energy Physics,
Tsukuba, Ibaraki 305, Japan

[4]Biophysics Laboratory, Department of Physics,
College of Science, Rikkyo University,
Toshima-ku, Tokyo 171, Japan

[#]Present address: Division of Radiation Hazards,
National Institute of Radiological Sciences, Inage-ku/263, Chiba, Japan

[*]Present address: Division of Radiation Biology,
School of Medicine, Yokohama City University, Yokohama, Kanagawa 236, Japan

ABSTRACT

Killing effect on bacteriophage T1 by the Auger cascade of phosphorus in DNA following K shell photoabsorption was studied with monoenergetic X rays obtained from synchrotron radiations. Phages embedded in nutrient

broth were irradiated under vacuum with X rays at the resonance peak (2153 eV), and below (2147 eV) and above (2159 eV) the peak. The corresponding mean lethal exposures (D_0) were 554, 332 and 434 kR, respectively. The Auger enhancements, as an energy dependent fractional increment of phage sensitivity, were 0.67 at 2153 eV and 0.28 at 2159 eV. Using the DNA absorption spectrum measured in this experiment, photoionization cross sections of Scofield (17), and the Auger yield after creation of a K shell vacancy, the number of phosphorus Auger cascades in one phage DNA at D_0 were calculated to be 0.00, 0.98 and 0.25 at 2147, 2153 and 2159 eV, respectively. Comparison between the Auger enhancement of phage killing and the number of Auger cascades indicated that one phosphorus Auger cascade in phage DNA caused about 0.41 (at 2153 eV) or 0.84 (at 2159 eV) lethal events.

INTRODUCTION

The Auger effect, characterized by a cascade of short-range electrons, leads to an intense local deposition of energy around the excited atom and correspondingly causes localized damage to the relevant molecule. Auger emitters, therefore, are an important tool in probing basic biological mechanisms. The effect of Auger cascades on several biological materials have been theoretically analyzed or experimentally tested with radioisotopes or quasi-monoenergetic fluorescent X rays (1). Excess damage was produced by X rays with energies above the K edge of the key atoms, leading to nearby DNA strand breaks. As a consequence, high relative biological effectiveness (RBE) was observed.

Several lines of study with nucleotides (2), DNA (3,4), phages (5), bacteria (6), and mammalian cells (7,8) have recently been performed to examine if an enhancement of the radiobiological effect of synchrotron X rays can be experimentally verified following their resonance absorption in brominated DNA. When bromouracil-labeled *E. coli* cells were irradiated with X rays, killing of cells was enhanced by 8% at energies above the absorption edge of bromine (13.49 keV) compared to below the edge (12.40 keV) (6). In the case of dried BrdU-labeled T1 phage, a larger (about 26%) enhancement was observed (5). This would partly be due to the associated suppression of radical mediated processes in *E. coli* cells.

Phosphorus, a constituent element of phosphodiester bonds of DNA, can be used to realize such an experimental situation. The results of the

experiment with K shell absorption of phosphorus atoms on yeast cells resulted in an enhancement factor of 1.4 (9). If one uses dry biological materials such as T1 phage for such an experiment, a larger enhancement could be expected because the indirect action of radiation can be completely suppressed. Therefore, an attempt was made in this study to investigate enhanced killing of bacteriophage T1 by Auger cascades following resonance absorption of X rays in the K shell of phosphorus atoms in the DNA. A large enhancement (about 67%) was obtained, as expected.

MATERIALS AND METHODS

Preparation of Bacteriophage T1

Host cells of *E. coli* strain B were cultured at 37°C with aeration in 400 ml of 3xD medium (4.5 g KH_2PO_4, 10.5 g Na_2HPO_4, 3.0 g NH_4Cl, 15 g casamino acid and 13 g glycerol per liter of distilled water with 1.2 mM $MgSO_4$, 0.15 mM $CaCl_2$ and 0.003% gelatin at the final concentrations). Phage T1 was added (multiplicity of infection, m.o.i. = 0.1) into the cell culture in logarithmic growth phase at 5×10^8 cells/ml, incubated at 37°C and phage lysate was obtained. After addition of 1 ml of chloroform and 1 μg/ml of both DNase and RNase, the lysate was incubated for 30 min at room temperature, and centrifuged (6,000 rpm, 30 min, 4°C) to remove cell debris. The supernatant was ultracentrifuged (100,000 X g, 2 hr, 4°C) and the phage pellet was saved. The pellet was resuspended in 1 ml of T1 absorption buffer (0.3 g KH_2PO_4 and 1.5 g Na_2HPO_4 per liter of distilled water with 40 μM $MgSO_4$, 50 μM $CaCl_2$ and 0.0025% gelatin at the final concentrations).

For calculation of a photoionization cross section of phage DNA, base composition of phage DNA was measured. Phage DNA was extracted, purified, hydrolyzed, and then analyzed with high performance liquid chromatography (HPLC) as reported previously (5). The GC content of T1 phage DNA was 0.49.

Source of Monoenergetic X rays

Irradiation was performed at the beam-line BL-1B and -11B of the 2.5 GeV storage ring at the Photon Factory, National Laboratory for High Energy Physics, Tsukuba, Japan. Details of the BL-11B system and the characteristics of the monoenergetic X rays were reported previously (10).

Briefly, white synchrotron radiation is focussed by a toroidal premirror, and monochromatized by an InSb double-crystal monochromator. The full width at half maximum of band width of the monoenergetic X rays around 2 keV was about 1 eV (10). The cross section of the X ray beam was about 2 X 5 mm. At BL-1B, the irradiation system consisted of a plane premirror and an InSb channel cut monochromator. The cross section of the beam was about 4 X 5 mm. X ray energy was chosen using the absorption spectrum of DNA film (see RESULTS).

Measurements of Exposure Rates and Calculation of Photon Fluences

Exposure rates in R were measured by a parallel-plate free air ionization chamber (11) in atmospheric air conditions. The monoenergetic X ray beam was transported from an irradiation chamber (~10^{-5} Pa) to the atmosphere through a Kapton (25 μm) window, a low pressure chamber (~10^{-1} Pa) and a Mylar (5 μm) window. Exposure rate at the sample position in the vacuum irradiation chamber was corrected by attenuation factors for the window materials and the air between Mylar window and the ionization chamber. The exposure rates at 100 mA of ring current at the sample position under a scanning condition (see below) were about 500 kR/min at BL-11B and 4 kR/min at BL-1B.

The photon fluences Φ (photons/m^2) per R were calculated by

$$\Phi = 2.58 \times 10^{-4} \times W \times 1/E \times 1/(\mu_{en}/\rho)_{air} \quad (1),$$

where $(\mu_{en}/\rho)_{air}$ is the mass energy absorption coefficient (m^2/kg) of air taken from Hubbell's data (12), W the energy required to produce an ion pair in normal room air (33.73 J/C), E the X ray photon energy in eV and 2.58 X 10^{-4} the conversion factor from R to C/kg.

Calculation of Absorbed Dose

Absorbed doses of X ray in Gy were calculated as the product of exposure in R and the Roentgen-Gray conversion factor (f-factor). The f-factor, given by equation 2, are listed in Table I.

$$f = 2.58 \times 10^{-4} \times W \times [(\mu_{en}/\rho)_s / (\mu_{en}/\rho)_{air}], \quad (2)$$

TABLE I

Mean Lethal Doses (D_0) for Bacteriophage T1			
	X ray energy		
	2147 eV	2153 eV	2159 eV
Mean lethal dose (kR)			
exp.1	525	389	461
exp.2	581	339	490
exp.3	556	268	351
Avg. ± se [a]	554 ± 20	332 ± 43	434 ± 52
f-factor [b]	0.00938	0.00938	0.00939
Mean lethal dose (kGy) [c]			
Avg. ± se [a]	5.21 ± 0.18	3.12 ± 0.40	4.07 ± 0.49
Relative sensitivity [d]	1.00	1.67	1.28

[a] Averaged value with standard error.

[b] Roentgen-Gray conversion factor; for calculation method, see text.

[c] D_0 (kGy) = D_0 (kR) x f-factor.

[d] Reciprocals of mean lethal doses (kGy) normalized at 2147 eV. Same values were obtained using the mean lethal doses in units of R.

where $(\mu_{en}/\rho)_s$ and $(\mu_{en}/\rho)_{air}$ are the mass energy absorption coefficients of the sample and the air, respectively. The mass energy absorption coefficient of the sample $(\mu_{en}/\rho)_s$ was calculated under the following assumptions. The sample (see below) consisted of 16 μg of dried nutrient broth containing about 100 pg of phage particles, which was assumed to be twice its DNA weight, 50 pg = $(1 \times 10^6) \times (3.1 \times 10^7) \times (1.66 \times 10^{-12})$, where 1×10^6 the number of phage particles in a sample, 3.1×10^7 the molecular weight of T1 DNA (13) and 1.66×10^{-12} the picogram per atomic mass unit. Thus the sample can be assumed as to be essentially pure NB, but its atomic composition is not known. Then the $(\mu_{en}/\rho)_s$ is assumed to be that of the solid components of striated muscle of ICRU, $(\mu_{en}/\rho)_m$ (12) and calculated by,

$$(\mu_{en}/\rho)_s = \{(\mu_{en}/\rho)_m - 0.6 \times (\mu_{en}/\rho)_w\} / 0.4, \quad (3)$$

where $(\mu_{en}/\rho)_w$ is the mass energy absorption coefficient of water and 0.6 the water content of the muscle which was assumed to be 60%. The mass energy absorption coefficients were taken from Hubbell's data (12).

Irradiation and Survival Assay of Phage

The stock suspension of bacteriophage T1 was diluted at 5×10^8 plaque forming units per 1 ml with 0.8% nutrient broth (Difco). Two µl of the phage suspension, which has 16 µg of dry weight, was placed on a small polypropylene sheet (2 X 10 mm with 0.2 mm of thickness) and dried in a silica-gel desiccator at room temperature (25°C). After being dried on the sheet, the shape of the phage sample was a disk with a diameter of about 1.5 mm and thickness of 9 µm ($= 16 \times 10^{-6}$ g / $(\pi \times 0.075^2)$ cm^2 / 1 g-cm^{-3}). Phage sample thickness was greater than the ranges of the photoelectrons, which have the maximum energy of about 2 keV corresponding to the range of 0.2 µm in unit density matter (14).

About 30 phage samples were attached to a sample holder in the vacuum irradiation chamber. These samples were sequentially and automatically irradiated under vacuum (about 10^{-5} Pa) with monoenergetic X rays at assigned doses with a computer aided program. Immediately after the last sample had been irradiated, each sample was resuspended in 0.5 ml of NB medium (0.8% NB and 0.5% NaCl, pH~7) and kept in the dark at 4°C. Phage survivals were determined by the usual agar layer method with indicator host cells of repair deficient *E. coli* B_{s-1}. After irradiated phage samples were adequately diluted with T1 absorption buffer, 100 µl of the diluted phage sample and 100 µl of the cell suspension cultured in NB medium overnight were added into 2.5 ml of pre-warmed (45°C) NB soft agar (0.75% agar). This mixture was quickly spread on an NB agar plate (1.5% agar). After the soft agar had hardened, the plate was incubated in the dark at 37°C for 16 h. Phage survivors were counted as numbers of phage plaques.

Measurement of DNA Absorption Spectrum

An absorption spectrum of a self-standing thin DNA film was measured. About one milliliter of calf thymus DNA (Sigma, Type I: Sodium Salt) solution dissolved at about 5 mg/ml in distilled water with sonication was dropped on a polypropylene sheet, and then dried in a silica-gel desiccator. After being dried, the DNA film was peeled off from the sheet.

This self-standing DNA film was inserted in front of the ionization chamber and the X ray intensity measured. The absorbance of the DNA film was calculated as $\log(I_0/I)$ from the output of the ionization chamber with (I) and without (I_0) the DNA film.

RESULTS

Confirmation of the Resonance Absorption of Phosphorus in DNA

The absorption spectrum of the DNA film (about 1 mg/cm^2) was measured around the K absorption edge of phosphorus (Fig. 1). The spectrum had a highly intense peak (resonance peak), the energy of which was defined as 2153 eV following the methods of Kobayashi *et al.* (9). This intense peak was assigned (15) to be the 1s to t_2* (3p-like) transition of phosphorus, and a next broad band in the higher energy region is the shape resonance (15,16).

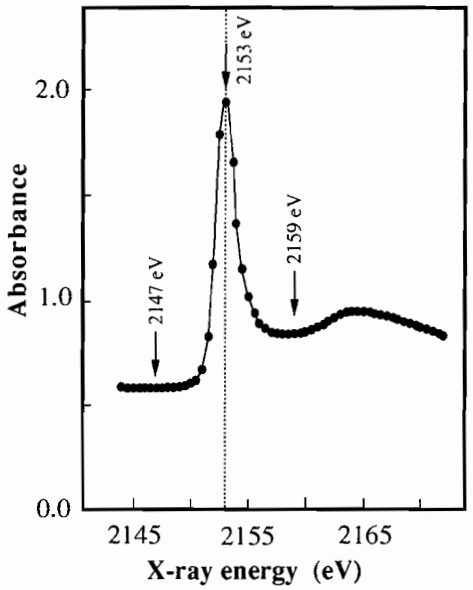

FIG. 1. Absorption spectrum of a thin film (about 1 mg/cm^2) of calf thymus DNA at energies around the K shell absorption edge of phosphorus. Arrows indicate the X ray energy used for irradiation experiments.

From this observation, three energies were chosen for phage irradiation: at the resonance peak (2153 eV), below (2147 eV) and above (2159 eV) the resonance peak.

Absorption Cross Section of Phage DNA at the Resonance Energy

Using the absorption spectrum, the absorption cross section of the phage DNA molecule was estimated as follows. Below the K absorption edge of phosphorus (2147 eV), the cross section was assumed to be the sum total of tabulated cross sections over atoms constituting the phage DNA molecule. For each constituent element, the number of atoms was calculated from the molecular weight (13) and the GC content (0.49) of the phage DNA molecule (see MATERIALS AND METHODS), and they were 1.13×10^6, 9.83×10^5, 3.77×10^5, 6.05×10^5, 1.01×10^5 and 1.01×10^5 for hydrogen, carbon, nitrogen, oxygen, sodium and phosphorus, respectively. The cross section at 2147 eV was obtained by extrapolation from the values at 1.5 and 2.0 keV of Scofield (17). The cross section of phage DNA at 2147 eV was calculated as 2.36×10^{10} barn, and thus those at 2153 eV (7.69×10^{10} barn) and 2159 eV (3.37×10^{10} barn) were the products of that at 2147 eV and the ratio of absorption spectrum, 3.26 at 2153 eV and 1.43 at 2159 eV. The cross section at 2159 eV calculated by extrapolation from the data of Scofield (17) at 3.0 and 4.0 keV agrees (3.47×10^{10} barn) with the result. The increments of the cross sections from 2147 eV must be the K shell cross section of phosphorus.

Enhanced Killing Effect at the Resonance Peak

Figure 2 shows survival curves of phages embedded in NB irradiated by monoenergetic X rays. The phage survivals were lowest at the peak energy (2153 eV, circles) and highest below the peak (2147 eV, inverted triangles). All of the survival data points collected at each X ray energy fell on a line on semi-logarithmic scale. Consequently, the experimental results can be conveniently expressed in terms of 37% exposure dose (D_0) calculated using an unweighted least squares method (Table I). The D_0 expressed in units of kR were converted into absorbed dose in units of kGy with the f-factors (Table I) for each X ray energy. The ratio of D_0 expressed in kR and kGy units were the same because the f-factors were not different for the different X ray energies. The sensitivity, as expressed by $1/D_0$, at the resonance peak (2153 eV) is clearly higher than both below and above the peak. The ratios of the averaged sensitivity normalized at 2147 eV were 1.68 at 2153 and 1.26 at 2159 eV (Table I).

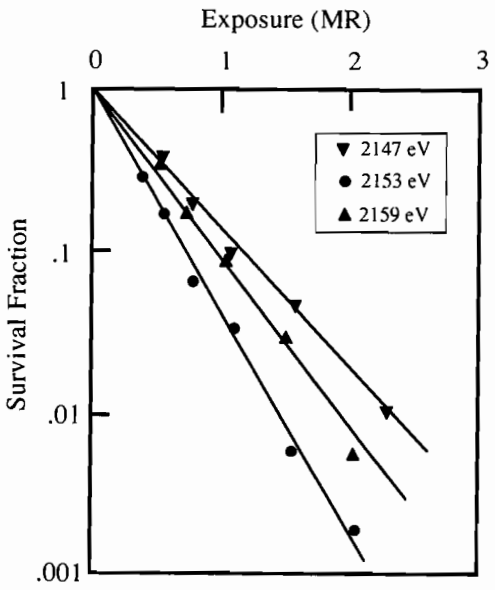

FIG. 2. Exposure-survival curves of bacteriophage T1 embedded in nutrient broth and irradiated with 2147, 2153 and 2159 eV monoenergetic X rays in vacuum condition.

DISCUSSION

Killing Efficiency of an Auger Cascade of Phosphorus

Absorbance of a DNA film (Fig. 1) sharply increased at 2153 eV by a factor of 3.26 (Table II) from 2147 eV. At the same energy, phage sensitivity increased by a factor of 1.67 (Table I). The enhanced sensitivity must be related to the K shell absorption of phosphorus, because the increment in absorbance was caused by K shell absorption of phosphorus in DNA. The number (N_P) of photoabsorption events by the K shell of phosphorus at the mean lethal dose (D_0) can be obtained as the products of three values: the number of phosphorus atoms in a phage DNA molecule, the photon fluence at D_0 from Eq. (1), and the photoionization cross section of the K shell of phosphorus. The number of phosphorus atoms and the cross sections were described in the RESULTS section. The calculated number of photoionizations of the K shell of phosphorus is shown in Table II. The number of Auger cascades per

D_0 in one phage (N_A in Table II) were calculated by $N_A = N_P \times 0.937$, where 0.937 is the Auger transition probability (18) for a K shell vacancy in phosphorus. Thus, 1.05 phosphorus K shell photoionizations, or 0.98 Auger cascades, occurred at 2153 eV in one phage DNA at one lethal hit (Table II). The 0.98 Auger cascades caused an increment in phage sensitivity of 1.20 MR^{-1} (= 3.01-1.81, Table II), or 0.40 (= 1.20/3.01) of fraction in total sensitivity. Thus, we suggest that the killing efficiency of Auger cascades induced at the resonance peak of the K shell of phosphorus is 0.41 (= 0.40/0.98).

At 2159 eV, the number of K shell photoabsorptions and the number of Auger cascades was calculated to be 0.27 and 0.25 per D_0 per phage DNA (Table II)

TABLE II

	X ray energy			Symbol
	2147 eV	2153 eV	2159 eV	
Normalized DNA absorbance	1.00 [f]	3.26	1.43	
Phage sensitivity (1/MR)				
total [a]	1.81	3.01	2.30	S_T
increased fraction [b]	-	1.20	0.49	S_I
Photoabsorption [c]				
1 / D_0 / phage	-	1.05	0.27	N_P
Auger enhancement				
1 / D_0 /phage [d]	0.00	0.98	0.25	N_A
efficiency [e]	-	0.41	0.84	E_A

[a] $S_T = 1 / D_0$. Data taken from Table I.

[b] $S_I = S_T$(at each energy) - S_T(at 2147 eV).

[c] For calculation method, see text.

[d] $N_A = N_P \times 0.937$, 0.937 is the transition probability (14) to Auger cascade from K-shell vacancy of phosphorus.

[e] $E_A = (S_I / S_T) / N_A$.

[f] 2.36×10^{10} barn (or 2.36×10^{-18} m^2) (for calculation method, see text).

using the same methods described above. The increment in the phage sensitivity was 0.49 MR^{-1} (Table II). A fraction of 0.21 (= 0.49/2.30) in total sensitivity was caused by the Auger cascades. Thus, the killing efficiency of an Auger cascade following K shell photoabsorption at 2159 eV was 0.84 (= 0.21/0.25). This result is twice that at the resonance peak. The reasons for this difference in the efficiency is not known at the present stage. It should be noted that very different mass-spectra (19) for fragmentation of simple molecules caused by a small difference in photon energy were shown around the K shell absorption edge. It may be possible that photolytic processes in DNA molecules are different at 2153 and 2159 eV, and the different photolytic processes may affect the killing efficiency of the Auger cascades.

Basal Sensitivity without the Auger Effect

For 2147 eV X rays, phosphorus atoms have no K shell photoionization cross section. Phages, however, were killed through photoabsorptions in outer-shells of phosphorus and in other elements in phage DNA, and through photoelectrons arising from phage and surrounding materials. Phage sensitivity at 2147 eV was 0.192 kGy^{-1} (= 1/5.21, Table I), which agrees with that (0.197 kGy^{-1}) obtained for monoenergetic synchrotron radiations at 12.4 keV under dry NB conditions (5) and that (0.235 kGy^{-1}) for ^{60}Co γ rays at high NB concentrations (13) at which the indirect effects is thought to be very small. The agreement of phage sensitivities over a wide range of energies of radiation indicates that phage sensitivities, except for the K shell photoabsorption of phosphorus, are determined by absorbed dose. We call this phage sensitivity the basal sensitivity.

At 2147 eV, the number of photoabsorptions by phage DNA, that is, photoabsorption at atoms except for phosphorus and outer-shells of phosphorus, could be superficially calculated by the same way described above: the number of photoabsorptions was 0.77 and the killing efficiency by the photoabsorption was 1.37 (= 1/0.77). The unexpected calculated result that the killing efficiency (1.37) of photoabsorptions other than in the K shell of phosphorus was higher than that (0.41 or 0.84) for Auger cascades of phosphorus is due to the fact that the basal sensitivity is due predominantly to the interactions in the phage DNA of secondary electrons originating from photoabsorption in the nutrient broth - as is the justification for the calculation of f-factors based on the nutrient broth (rather than DNA or phage) composition. These photoabsorptions, or their electrons, do not appear

at all in the above calculation and therefore the superficial, false result is obtained.

CONCLUSIONS

The absorption spectrum of a self-standing DNA film (calf thymus) at energies around resonance absorption energy of phosphorus showed a sharp peak at 2153 eV; the relative values were 1.00, 3.26 and 1.43 at 2147, 2153 and 2159 eV, respectively. Thus, bacteriophage T1 embedded in nutrient broth were irradiated under vacuum by monoenergetic X rays at energies of 2147, 2153 and 2159 eV and corresponding mean lethal doses of 553, 332 and 434 kR, respectively, were obtained. Fractional increments of the phage sensitivities due to Auger cascades following absorption in the K shell of phosphorus atoms in phage DNA were 0.67 at the resonance peak (2153 eV) and 0.28 above the resonance (2159 eV). The number of lethal events in phage per Auger cascade was 0.41 at 2153 eV and 0.84 at 2159 eV. The reason for lower efficiency at the resonance peak compared to above the resonance still remains to be studied. The basal sensitivity (Gy^{-1}), which was the sensitivity below the peak (2147 eV), was similar to the sensitivity at 12.4 keV previously reported, indicating that basal sensitivity was determined by absorbed dose.

ACKNOWLEDGMENTS

The authors are grateful to Dr. Takashi Ito and Dr. Shigefumi Okada for their valuable advice in the course of this work. We thank Dr. Akinori Yokoya and Noriko Usami of University of Tsukuba for their assistance in the operation of the irradiation system. This work was performed under the approval of the Photon Factory Program Advisory Committee (Proposal No. 86-098 and No. 86-101), and was partly supported by a Grant-in-Aid from the Ministry of Education, Science and Culture of Japan (59880014) and by a Tokai University School of Medicine Research Aid (1986,1987).

REFERENCES

1. K.F. BAVERSTOCK and D.E. CHARLTON, *DNA Damage by Auger Emitters*, Taylor and Francis (1988).
2. K. TAKAKURA, Auger effects on bromo-deoxyuridine-monophosphate irradiated with monochromatic X-rays around bromine K-absorption edge. *Radiat. Environ. Biophys.* **28**, 177-184 (1989).

3. H. MAEZAWA, K. HIEDA, K. KOBAYASHI,and T. ITO, Effects of Auger cascades of bromine induced by K-shell photoionization on plasmid DNA, bacteriophages, *E. coli* and yeast cells. In *DNA Damage by Auger Emitters* (K.F. Baverstock and D.E. Charlton, Eds.) pp. 135-146. Taylor and Francis, London (1988).
4. H. MENKE, W. KOHNLEIN, and A. HALPERN, Strand breaks in plasmid DNA, natural and brominated, by low-energy X-rays. *Int. J. Radiat. Res.* **59**, 85-96 (1991).
5. Y. FURUSAWA, H. MAEZAWA, and K. SUZUKI, Enhanced killing effect on 5-bromodeoxyuridine labelled bacteriophage T1 by monoenergetic synchrotron X-ray at the energy of bromine K-shell absorption edge. *J. Radiat. Res.* 32, 1-12 (1991).
6. H. MAEZAWA, K. HIEDA, K. KOBAYASHI, Y. FURUSAWA, T. MORI, K. SUZUKI, and T. ITO, Effects of monoenergetic X-rays at the resonance energy of bromine K-absorption edge on bromouracil-labelled *E. coli* cells. *Int. J. Radiat. Biol.* **53**, 301-308 (1988).
7. K. SHINOHARA, H. OHARA, K. KOBAYASHI, H. MAEZAWA, K. HIEDA, S. OKADA, and T. ITO, Enhanced killing of HeLa cells pre-labelled with 5-bromodeoxyuridine by monochromatic synchrotron radiation at 0.9 A: An evidence for Auger enhancement in mammalian cells. *J. Radiat. Res.* **26**, 334-338 (1985).
8. D. LARSON, W.J. BODELL, C. LING, T.L. PHILLIPS, M. SCHELL, D. SHRIEVE, and T. TROXEL, Auger electron contribution to bromodeoxyuridine cellular radiosensitization. *Int. J. Radiat. Oncol. Biol. Phys.* **16**, 171-176 (1989).
9. K. KOBAYASHI, K. HIEDA, H. MAEZAWA, Y. FURUSAWA, M. SUZUKI, and T. ITO, Effects of K-shell X-ray absorption of intracellular phosphorus on yeast cells. *Int. J. Radiat. Biol.* **59**, 643-650 (1991).
10. T. OHTA, P.M. STEFAN, M. NOMURA, and H. SEKIYAMA, Design and performance of a UHV compatible soft X-ray double crystal monochromator at the Photon Factory. *Nucl. Instr. Meth. Phys. Res.* **A246**, 373-376 (1986).
11. K. KOBAYASHI, K. HIEDA, H. MAEZAWA, M. ANDO, and T. ITO, Monochromatic X-ray irradiation system (0.08 nm-0.4 nm) for radiation biology studies using synchrotron radiation at the Photon Factory. *J. Radiat. Res.* **28**, 243-253 (1987).
12. J.H. HUBBELL, Photon mass attenuation and energy-absorption coefficients from 1 keV to 20 MeV. *Int. J. Appl. Radiat. Isot.* **33**, 1269-1290 (1982).
13. G. HOTZ, Infectious DNA from coliphage T1, IV. The action of radicals induced by ^{60}Co-gamma rays in the wet state. *Int. J. Radiat. Biol.* **24**, 1-13 (1973).
14. A. COLE, Absorption of 20-eV to 50,000-eV electron beams in air and plastic. *Radiat. Res.* **38**, 7-33 (1969).
15. H. SEKIYAMA, Y. KITAJIMA, N. KOSUGI, H. KURODA, and T. OHTA, P K absorption spectra of PO_4^{3-}, PHO_3^{2-}, PH_2O^{2-}, $P_2O_7^{4-}$ and $P_3O_{10}^{5-}$. Photon Factory Activity *Report* **3**, VI-126 (1985).
16. J.L. DEHMER, Molecular effects in inner-shell photoabsorption. K-shell spectrum of N_2. *J. Chem. Phys.* **65**, 5327-5334 (1976).
17. J.H. SCOFIELD, Theoretical Photoionization Cross Section from 1 to 1500 keV. *Research Report* **UCRL-51326**, Lawrence Livermore Laboratory, University of California. (1973).
18. M.O. KRAUSE, Atomic radiative and radiationless yields for K and L shell. *J. Phys.Chem. Ref. Data.* **8**, 307-327 (1979).
19. W. EBERHARDT, Core electron excitations and decay in molecules. *Physica Scripta* **T17**, 28-38 (1987).

DISCUSSION

Humm, J. The photon energies with which you are irradiating your specimens are extremely close to the K-absorption edge of phosphorus. You used the photoelectric cross section close to the edge. Did you consider the possibility of large errors in your estimated cross section and if so how?

Furusawa, Y. The cross section was experimentally measured as absorption spectrum. We found no special structure in the lower energy region than the highly intense resonance peak at 2153 eV. The cross section at 2147 eV (lower than the resonance peak) of 2.36×10^{10} barn/phage was obtained by extrapolation from Scofield's cross sections at 1.5 and 2.0 keV. Then we obtained the cross section at 2153 and 2159 eV with the value at 2147 eV and the measured absorption spectrum of DNA film normalized at 2147 eV. Also the cross section at 2159 eV was checked with extrapolated values from those at higher (3 & 4 keV) energies. The value calculated by the absorption spectrum 3.37×10^{10} barn/phage and the extrapolated value of 3.47×10^{10} barn/phage from the higher energy region showed good agreement.

Biophysical Aspects of Auger Processes, AAPM Symposium Series No. 8 (1992) 051-065
Eds. RW Howell, VR Narra, KSR Sastry, DV Rao

A CALCULATION OF THE PHYSICAL PARAMETERS RESPONSIBLE FOR THE ENHANCEMENT OF RADIATION DAMAGE DUE TO THE INCORPORATION OF Br/I ATOMS INTO THE DNA

DAVID E. CHARLTON[1] and HOOSHANG NIKJOO[2]

[1]Physics Department, Concordia University, Montreal H3G 1M8, Canada

[2]M. R. C. Radiobiology Unit, Chilton, Didcot, Oxon OX11 0RD England

ABSTRACT

It is well known that when analogs of thymidine containing iodine or bromine are incorporated into the DNA of irradiated cells there is a decrease of the D_o. Three mechanisms for this effect have been discussed; (a) Photoactivation of the Br/I atom and the production of Auger electrons, (b) Creation of highly reactive uracil radicals by the interaction of hydrated electrons with BrUdR/IUdR, leading to SSB, (c) Interference with repair or the fixation of the damage by the presence of the Br/I atoms. Experiments to investigate photoactivation of the Br/I atoms will include all three, so that knowledge of the relative size of each contribution is useful. The first process is reasonably well understood and here the second process is examined. It is assumed that the incorporated analogs only produce radicals if they are present in a region of DNA containing energy depositions. An SSB produced by this radical can combine with a nearby SSB produced by electron damage to give a DSB, thus increasing the yield of DSB compared to the yield without the analog present. The increased yields at various levels of Br/I incorporation are compared to experiment for different models of radical action.

INTRODUCTION

It is well known that incorporation of bromine or iodine atoms into DNA via halogenated thymine analogs increases the sensitivity of an irradiated system. Three mechanisms for this enhancement have been discussed in the literature. (i) The Auger effect. Here the photons interacting in the inner shells of the bromine or iodine atoms leads to the release of what has been called an Auger electron cascade. This flux of low energy electrons originating from one atom produces a high-LET-like effect in the DNA and is very efficient per unit dose at producing DNA double strand breakage (1). (ii) An increase in the damage to the DNA per unit dose as a result of the production of highly reactive uracilyl radicals by the action of hydrated electrons on the BrUdR or IUdR, adding to the number of single strand breaks (SSB) (2). The production of SSBs alone will not lead to significant radiation effects since these can readily be repaired by the cell, but in combination with SSB from other sources the more important DSB can be produced. (iii) A reduction of repair or a fixation of the damage (3) by the presence of the Br or I atom. It is likely that all three mechanisms are present in various degrees for a particular experimental procedure.

The enhancement of the radiation damage is not only of interest for radiation biology but is being actively pursued as a means of sensitizing tumor cells which are proliferating in the presence of slowly growing normal cells (4,5,6 for example). A summary of some experimental results is given in Table I and Fig. 1. No distinction is made between iodine and bromine data since they overlap and Miller *et al.* (4) obtained undistinguishable results from incorporation of the two atoms. Strictly the data are not comparable since different criteria for evaluating the increased sensitivity have been used. With non-linear survival curves the choice of level of cell survival greatly influences the calculated enhancement, thus the results of Ling and Ward (7) and Iliakis *et al.* (3 and 8) who use D_o, cannot be directly compared with those of Miller *et al.* (4) or Larson *et al.* (6) who use a 10% level of survival. Nath *et al.* (9) compare the slopes of the survival curves to obtain their enhancement ratios and in addition use a continuously growing cell population under constant low dose rate irradiation as distinct from the acute irradiation used in the other experiments.

Two of the experiments in the table (Maezawa *et al.* (10) and Larson *et al.* (6)) specifically examine the role of the Auger cascade by irradiating the

samples just below and just above the K edge of the target atom, in both cases, bromine. Here if the Auger cascade is important, irradiation just above the K edge of the target atom is expected to produce a lower D_o since these photons can remove the K shell electrons which have a higher photoelectric cross section and which produce a larger cascade originating in the K shell rather than the L shell. However, the increase in sensitization above the edge is less than 10%, suggesting that the contribution from the Auger effect is small. Later, a more detailed examination of the importance of the Auger effect will be presented showing that the results of Larson *et al.* (6) and Maezawa *et al.* (10) are not unexpected.

There is some evidence from the results of Nath *et al.* (9) that the Auger effect can produce significant damage in that ^{241}Am with a mean photon energy just above the iodine K edge yields a significantly greater sensitivity than the irradiation below or far above the edge. Here, since the cells are being damaged through several generations and little is known of the transport of damage through cell division, there may be circumstances in which the Auger effect can not be ignored. Certainly this is a most interesting finding.

For irradiation at photon energies well above the K edges of Br/I, where photoelectric interactions with the target atoms per unit dose are small in number, there is an increase of the radiosensitization which cannot be accounted for by the Auger electron damage. In part this can be due to the second mechanism mentioned above, the additional induction of single strand breaks. Iliakis *et al.* (8) investigated this using repair deficient cells in which repair fixation (the third proposed mechanism) would be small or not exist. Again an increase in sensitivity with incorporation of the thymine analog was observed.

In general, the increased sensitivity, irrespective of how it is measured, is less than three for a replacement of about half of the thymine molecules. Based on 6 pg of DNA in a mammalian cell, this requires an incorporation of about 10^9 molecules of the analog in the DNA of each cell. That such a small enhancement requires such a large incorporation is curious, suggesting that very few of the incorporated molecules participate in the radiation action. One way of explaining this is to require that the incorporated analog be at, or lie close to, the site of damage in the DNA. This is the basis of the calculation presented here.

TABLE I
Sensitization of Cells by the Incorporation of BrUdR or IUdR

Author(s)	Cell type	Radiation	Type of measure	Atom	% incorporation	Sensitization
Iliakis *et al.*(8)	xrs-5	250 kV X rays	D_o	Br	9	1.13
					14	1.17
					25	1.30
Nath *et al.* (9)	V79	$^{226}Ra^a$	α	I	22	1.35
					45	1.89
		$^{241}Am^b$	α	I	22	1.67
					45	3.04
		$^{125}I^c$	α	I	22	1.47
					45	2.48
Ling and Ward (7)	V79	^{137}Cs	D_o	Br	16	1.55
					32	1.88
Iliakis *et al.* (3)	CHO	250 kV X rays	D_o	Br	22	1.18
					50	1.71
Larson *et al.* (6)	V79	13.45 keV	10% surv	Br	32	2.25
		13.49 keV			32	2.31
Maezawa *et al.* (10)	*E. Coli*	12.4 keV	D_o	Br	87	2.32
		13.5 keV			87	2.52
Miller *et al.* (4)	V79	10 MeV	10% surv	I	16	2.0
		100 kVp X rays			16	2.2
Myers *et al.* (14)	T4	^{60}Co 14 keV	D_o	Br	100	2.29
					100	2.12

For further details of these experiments see text.

[a] Mean photon energy 830 keV

[b] Mean photon energy 60 keV

[c] Mean photon energy 28 keV

In this presentation an attempt is made to estimate the increased cell sensitivity by calculating the additional burden of DSB due to an additional SSB production. It will be assumed that the charges associated with ionization and excitation of the DNA in a section of DNA damaged by the electron flux can produce uracilyl radicals or that hydrated electrons generated away from the site of damage can drift into the already damaged region. By either mechanism there is an additional source of SSB at an already damaged site. The SSBs produced by the action of the uracilyl radical will be important only if they occur in conjunction with SSB produced by direct energy deposition in the DNA. It is also required that the ensemble of SSBs be close enough together with some on opposite strands to produce a DSB. In this way a fraction of the SSBs produced in a system irradiated without bromine or iodine incorporation are converted to DSB when irradiated in the presence of incorporated bromine or iodine. Implicit in this approach is the assumption that there is no significant clustering of SSB from uracilyl radicals alone.

A difficulty with the type of analysis which can be performed is that only the production of DSBs can be calculated, whereas a wide range of variables has been used as a measure of increased sensitivity (see Table I).

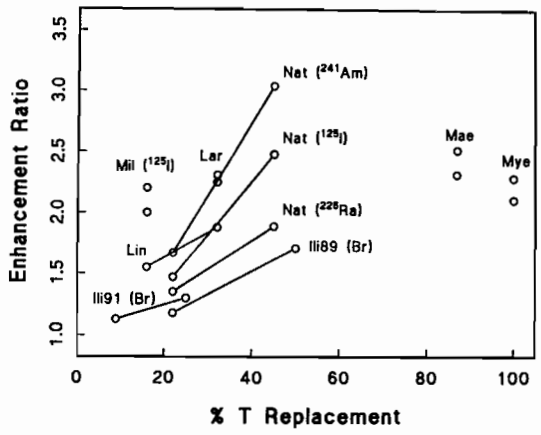

FIG. 1. Experimental results for the sensitization of cells by incorporated thymine analogues containing either bromine or iodine atoms. Key to authors: Ili(91)-Iliakis *et al.* (1991); Ili(89)-Iliakis *et al.* (1989); Lar-Larson *et al.* (1989); Lin-Ling and Ward (1990); Mae-Maezawa *et al.* (1987); Mil-Miller *et al.* (1987); Mye-Myers *et al.* (1977); Nat-Nath *et al.* (1990).

There is some evidence however which suggests that the increased production of DSB correlates with increased sensitivity (Ling and Ward (7), Iliakis *et al.* (8)). This does not necessarily imply that the increase in DSB alone is responsible for the increased effect since interference with repair or fixation of damage could also increase with increasing Br/I load.

METHODS

The Auger Effect in "Cold" Incorporated Atoms

The action of the Auger electrons in producing DNA damage is reasonably well understood and has been described for electrons originating both from radioactive decay (11,12) and from photoelectric interactions in "cold" atoms (13). The method for calculating the production of DSB in incorporated "cold" atoms is first to find the frequency of photoelectric interactions with the atom. This can be done using conventional radiation physics calculations of the photon fluence per Gy to the medium, photoelectric cross sections for the incorporated atom and the number of incorporated atoms per cell. Each photoelectric interaction leads to either the release of a fluorescence photon and/or an Auger cascade originating in the hit shell. Humm and Charlton (12) have evaluated the electron spectra produced by the inner-shell vacancies and, using electron track structure, estimated the number of DSB per interaction. For incorporated cold iodine they obtained 0.66 DSB per photoelectric interaction for photon energies just above the K edge. For incorporated bromine the result was 0.41 and 0.34 DSB per interaction for photon energies just above and just below the bromine K edge, respectively.

The yields of DSB produced by irradiation just above and just below the K edge of bromine which were examined in detail by Humm and Charlton (12) gave an enhancement of 6% for a 100% replacement of thymine by BrUdR. The reason for such a small increase is that while above the edge the bromine photoelectric cross section jumps by a factor of about 6, the yield of DSB produced by the electron flux in the irradiated medium is constant across the edge and considerably larger. Thus, the first mechanism is not important. This is also illustrated by the work of Meyers *et al.* (14) (and Table I) who have shown that with photons from ^{60}Co and 100% replacement of thymine by the bromine analog, the enhancement is about 2.3 even though interactions with

bromine atoms will be rare. Clearly DNA damage by the Auger cascade is not an important mechanism here.

Recently Kobayashi *et al.* (15) have considerably improved the possibility of hitting incorporated cold atoms by irradiating at the absorption edge which is possible using synchrotron irradiation. In this case there is a resonance absorption with a considerably increased cross section and the increase in sensitivity is above the background of effects produced by the normal damage due to the electron flux.

Single Strand Breaks Produced by Uracilyl Radicals

The approach used here was to calculate yields of strand breaks in the DNA using the method described by Charlton and Humm (11) and Humm and Charlton (12). Here the electron track code of Paretzke (16) is used to describe the radiation field for the appropriate source and a volume representing the DNA is superposed at random on it. This technique gives a description of the deposition of energy in the bases and sugar-phosphates of the DNA which can be analyzed for the production of single and double strand breaks using an empirical method based on work of Martin and Haseltine (17). Here if 17.5 eV or more is deposited in the sugar-phosphate moiety of the DNA a single strand break is assigned to that site. Single strand breaks on opposite strands, separated by less than 10 base pairs, are assumed to produce double strand breaks. The method has been reasonably successful in predicting absolute yields of single and double strand breaks for a wide range of radiations (18).

To include the sensitization due to incorporated Br/I atoms producing uracilyl radicals (and subsequent single strand breaks), each base in the portion of the hit section of the DNA is assigned as A, T, C, G by random in equal proportion. The T or the compliment to an A is replaced by the thymine analog carrying the Br/I atom, again by random according to the degree of substitution. In this way the number and positions of Br/I atoms in the hit region can be determined for bifilar incorporation of the analogs. This is illustrated in Table II. In the first example the final sequence of bases is "GATG" but the compliment of A has been replaced by an analog represented by the '+' in the table. In the third example in the sequence "GCCATCT", there is an analog replacing the T complimentary to the A and the first T has been replaced by an analog. These analog sites are the positions at which additional single strand breaks due to uracilyl radical action can occur and

they can combine with already existing breaks due to the ionizing radiation damage to increase the yield of double strand breaks. In particular, damage sites producing only single strand breaks can be converted to sites containing double strand breaks by this method.

Several models of the production of single strand breaks from uracilyl radicals were examined. In the first model it is assumed that an additional single strand break is produced if an energy deposition of any size occurs in a

TABLE II

Energy Depositions in the DNA and Base Sequences

	GCTGTCG+TG		CGA*CGGCAA
75 eV	...x.-....	93 eV	.....132..
	...4.....		..1.3.....
	....		....
	CAAC+ACACCCGCC+*CT*GGACAT		
124 eV	.1-...1..................		
	..........2x.............		
	.......-.-1..........1..		
	*CGAGACCC+CC+*AGACC*GCACC		
190 eV	-2-1.................-2..		
	.151.....................		
	..........-1............		

Key to symbols: Each column of four symbols is one nucleotide pair. The top row represents the base sequence of the segment, the lower three rows are the energy deposited in the sugar-phosphate backbone, the pair of bases and the other sugar-phosphate chain. The energy deposition greater than 17.5 eV in a sugar-phosphate is the condition for a SSB.

-The energy deposition symbols have the following form: no energy '.'; less than 10 eV '-'; less than 17.5 eV '1'; 17.5-20 eV 'x'; 20-30 eV '2'; 30-40 eV '3'; etc.

-The total energy deposited in the DNA is given at the left of each segment.

-The base symbols have their usual meaning and here * means an analog has replaced T and + means a T complimentary to an A is replaced.

-These data are for 50% substitution of thymine.

-Note that without the incorporated atoms these hits in the DNA would normally produce SSB.

base pair containing a Br/I atom. Br/I atoms in neighboring bases are assumed to be unaffected by this energy deposition, that is, there is no movement of charge or energy along the DNA. A second model in which any energy deposition produces SSB at all Br/I sites in the hit region gave very large enhancements (see Fig. 4 later) and showed very clearly that even within the length of DNA containing the energy depositions the probability of SSB production by Br/I action must be small. A third model based on this result was developed in which at least 15 eV (about the size of an ionization) had to be deposited in the DNA and this energy had only a 50% probability of producing one SSB by the action of the uracilyl radical. The activated Br/I atom could lie within ± 4 base pairs of the hit region. In this model even Br/I atoms lying very close to or in a region of damaged DNA did not necessarily participate in SSB production. Analysis will be presented in detail for this model although final results will be shown for all three models.

RESULTS

The calculation was carried out in two stages. Firstly, the relationship between the energy deposited in the DNA (hit size) and the probability that this energy deposition will produce a double strand break was determined. These data were then multiplied by the distribution of hit sizes for a unit dose of a particular radiation and summed to give absolute yields of breaks per Gray. These data give the yields of DSB without the additional effect of the incorporated atom. The calculation was carried out for irradiation by 20 keV electrons and 6 MeV α particles. This method has been fully described by Charlton *et al.* (18) and Charlton (19) and the hit size distribution for these two sources of radiation are given in Table III.

Next, each hit segment of DNA was assigned a sequence of bases and incorporated atoms and the effect of the incorporated analog was examined for each hit segment according to the three models discussed above. Examples of hits calculated from electron track structure and the assigned bases are given in Table II. Note that in the examples given no DSB will be produced by the damage caused by the energy deposited directly by the radiation.

For model 1, the first three examples have no hits in the base pair containing a replaced thymine and no additional breaks will be produced. In the last example (an energy deposition of 190 eV), an SSB will be produced at

TABLE III
Hit Size Distributions per Gy in a Segment of DNA 54 bp Long

Energy interval (eV)	20 keV electrons	6 MeV α particles
0-20	5.770×10^{-6}	2.103×10^{-6}
20-40	2.903×10^{-6}	1.444×10^{-6}
40-60	1.158×10^{-6}	0.970×10^{-6}
60-80	0.552×10^{-6}	0.687×10^{-6}
80-100	0.293×10^{-6}	0.548×10^{-6}
100-150	0.296×10^{-6}	0.804×10^{-6}
150-200	0.078×10^{-6}	0.374×10^{-6}
200-250	0.026×10^{-6}	0.188×10^{-6}
250-300	0.008×10^{-6}	0.084×10^{-6}
300-350		0.053×10^{-6}
350-400		0.020×10^{-6}
>400		0.024×10^{-6}

the second '+' on the lower strand in the figure and this will produce a DSB in the DNA by combining with one of the breaks on the upper strand. For model 2, in which all replaced bases are sources of SSB, examples 1, 3 and 4 will lead to DSB, example 2 will produce two SSB in one strand. In the third model in which any of the replaced bases may act as a source of SSB with a 50% probability, examples 1 and 4 may produce a DSB.

Several thousand hit segments were examined with and without the analogs. The additional SSB produced by the incorporated analogs was found for the three models above and a new yield of DSB determined. The enhancement of the radiation effect is the ratio of the yield of DSB with and without the incorporated Br/I atoms.

Figure 2 shows the probability of producing SSB and DSB as a function of the energy deposited in the DNA without an incorporated analog and for 50% replacement of thymine and calculated for the third model. The calculation without the sensitizer is shown for 20 keV electrons and 6 MeV α particles. These results, which have been reported previously for no

incorporation (18), show that this relationship is independent of type of particle both for SSB and DSB. There is a greater yield of DSB for the same energy deposited when the analog is present and this is greatest for smaller energy depositions where the efficiency of break production is the least. For larger energy depositions there is little change in the yield of DSB. This suggests that high-LET radiations will produce a smaller sensitization than low-LET radiations. This was tested and the results are shown later in Fig. 3.

Combining the data as in Fig. 2, but for different replacements of thymine, with that in Table III gives the relative yield of DSB as a function of the replacement of thymine, and this is taken as the degree of enhancement. The results for model 3 as a function of thymine replacement are shown in Fig. 3. The upper pair of curves are for 20 keV electrons and the higher of the pair includes the increased yield due to the Auger effect. The lower curve shows the calculated results for 6 MeV α particles. The results for model 3 indicate an enhancement of about 2.3 for a 50% replacement of thymine while the same substitution gives about 1.4 for 6 MeV α particles.

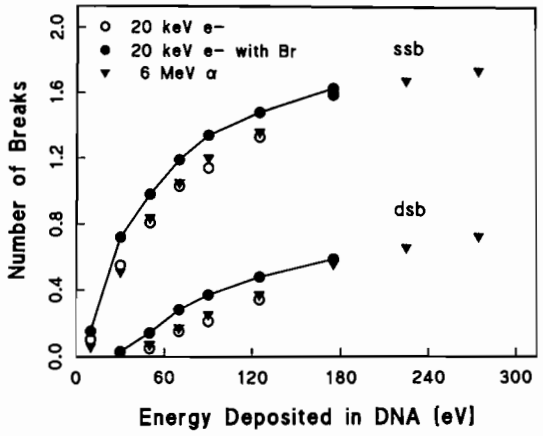

FIG. 2. Calculated yields of SSB and DSB as a function of the energy deposited in the DNA. The yields without sensitization are calculated for 20 keV electrons and 6 MeV α particles. The yields for sensitized DNA are given for 20 keV electrons and 50% incorporation.

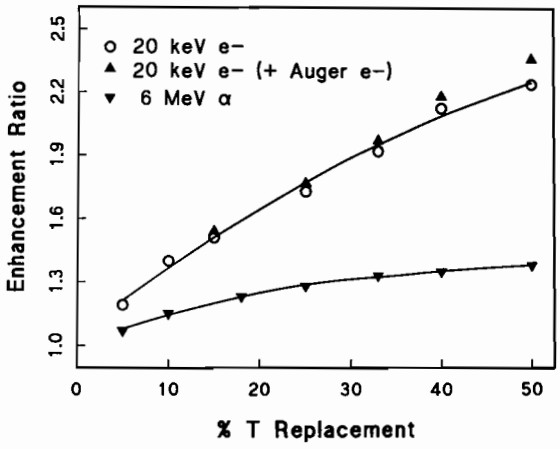

FIG. 3. The increase in yields of DSB as a function of thymine replacement for 20 keV electrons and 6 MeV α particles. These data were calculated for Model 3 in which at least 15 eV must be deposited in a hit region of DNA and only one of the Br/I atoms in this region has a 50% chance of producing an SSB at its location.

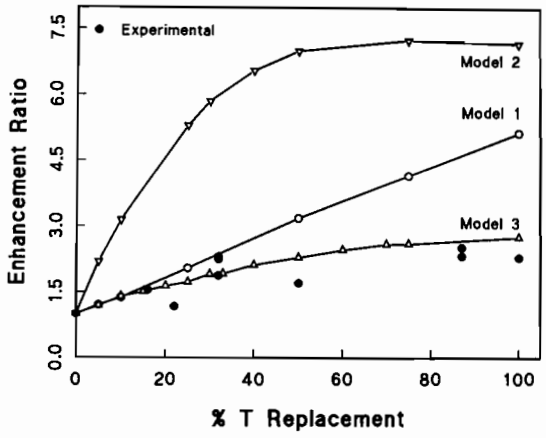

FIG. 4. Comparison of the models of damage with experiment.

In the final diagram (Fig. 4) the calculated results for all three models are compared to the experimental results shown in the first figure. Both models 1 and 3 give reasonable agreement with experiment at the smaller replacements. At higher levels of substitution model 3 is considerably better. In both of these models the number of substituted analogs which participate in producing additional damage is limited to one or less which suggests that even within a damaged region of DNA few of the incorporated Br/I participates in the enhancement. For model 2, where all incorporated Br/I atoms add to the burden of strand breaks, the calculated enhancement of the radiation effect due to the incorporation of thymine analogs is much larger than that measured. This supports the conclusion above that very few of the incorporated atoms play a role in producing enhancement of the radiation damage.

CONCLUSIONS

It has been possible for several years now to describe the initial damage to the DNA from the "direct" interaction of the radiation electron flux with the molecule. This description gives the energy deposited in the base pairs and the sugar-phosphate moieties hit by hit. This initial damage has been used to calculate the generation of single and double strand breaks for radiations of various LET. In this application the description of the initial damage is used to calculate the enhancement of radiation damage due to the action of hydrated electrons on incorporated 'cold' bromine or iodine atoms carried by thymine analogs.

As a measure of this enhancement, the increased yields of DSB have been calculated using techniques which have previously been shown to be in fair agreement with measured values. The method requires that the incorporated atom be present at the site of the DNA damage produced by the usual flux of electrons interacting with the DNA. This is a reasonable initial assumption in that an incorporated atom remote from any other damage producing an isolated single strand break will do little damage to a cell. In the introduction it was pointed out that about 10^9 incorporated atoms were needed to produce an enhancement of less than 3. Since in a mammalian cell there are about 1000 hits of any size in the DNA per Gray for 20 keV electrons (19), the upper limit of the number of the 10^9 incorporated atoms which can contribute to additional damage via SSB production can be estimated. Assuming an average hit length of 10 base pairs and 50% substitution gives

2500 atoms in the hit regions. This initial assumption therefore gives the result that about 2.5×10^{-6} of the incorporated atoms are not utilized in producing additional damage.

Further, in order to get reasonable agreement with experimental results, few of the bromine/iodine atoms lying within an already damaged region produce additional SSB to increase the sensitivity of the cell. These figures give some useful quantitative guidelines as to the maximum sensitivity which can be achieved by this method.

In the following paper in this volume (20) a new test of this model is described in which it becomes apparent that it is not sufficient to model the radiation damage alone but that the biological consequences of the incorporation play an important role.

REFERENCES

1. J.H. BURKI, R. ROOTS, L.E. FEINENDEGEN, and V.P. BOND, Inactivation of mammalian cells after disintegrations of ^{3}H or ^{125}I in cell DNA at -196°C. *Int. J. Radiat. Biol.* **24**, 363-375 (1973).
2. J.D. ZIMBRICK, J.F. WARD, and L.S. MYERS, Studies on the chemical basis of cellular radiosensitization by 5-bromouracil substitution in DNA. II. Pulse and steady-state radiolysis of bromouracil-substituted and unsubstituted DNA. *Int. J. Radiat. Biol.* **16**, 525-534 (1969).
3. G. ILIAKIS, S. KURTZMAN, G. PANTELIAS, and R. OKAYASU, Mechanism of radiosensitization by halogenated pyrimidines; Effect of BrdU on radiation induction of DNA and chromosome damage and its correlation with cell killing. *Radiat. Res.* **119**, 286-304 (1989).
4. R.W. MILLER, W. DeGRAFF, T.J. KINSELLA, and J.B. MITCHELL, Evaluation of incorporated iododeoxyuridine cellular radiosensitization by photon activation therapy. *Int. J. Oncol.* **13**, 1193-1197 (1987).
5. R. NATH, P. BONGIORNI, and S. ROCKWELL, Enhancement of IUdR radiosensitization by low energy photons. *Int. J. Radiat. Oncol.* **13**, 1071-1079 (1987).
6. D. LARSON, W.J. BODELL, C. LING, T.L. PHILLIPS, M. SCHELL, D. SHRIEVE, and T. TROXEL, Auger electron contribution to bromodeoxyuridine cellular radiosensitization. *Int. J. Radiat. Oncol.* **16**, 171-176 (1989).
7. L.L. LING, and J.F. WARD, Radiosensitization of Chinese hamster V79 cells by bromodeoxyuridine substitution of thymidine: Enhancement of radiation-induced toxicity and DNA strand break production by monofilar and bifilar substitution. *Radiat. Res.* **121**, 76-83 (1990).

8. G. ILIAKIS, G. PANTELIAS, and S. KURTZMAN, Mechanisms of radiosensitization by halogenated pyrimidines: Effect of BrdU on cell killing and interphase chromosome breakage in radiation-sensitive cells. *Radiat. Res.* **125**, 56-64 (1991).
9. R. NATH, P. BONGIORNI, and S. ROCKWELL, IUdR radio-sensitization by low and high energy photons for brachytherapy dose rates. *Radiat. Res.*, (submitted) (1990).
10. H. MAEZAWA, K. HIEDA, K. KOBAYASHI, and T. ITO, Effects of Auger cascades of bromine induced by K-shell photoionization on plasmid DNA, bacteriophages, E. coli and yeast cells. In *DNA Damage by Auger Emitters*, (K.F. BAVERSTOCK and D.E. CHARLTON, Eds), Taylor and Francis, London, pp 135-146, 1988.
11. D.E. CHARLTON and J.L. HUMM, A method of calculating initial DNA strand breakage following the decay of incorporated ^{125}I. *Int. J. Radiat. Biol.* **53**, 353-365 (1988).
12. J.L. HUMM and D.E. CHARLTON, A new calculational method to assess the therapeutic potential of Auger electron emission. *Int. J. Radiat. Oncol.* **17**, 351-360 (1989).
13. J.L. HUMM and D.E. CHARLTON, Double strand breakage in DNA produced by the photoelectric interaction with incorporated 'cold' bromine. In *DNA Damage by Auger Emitters*, (K.F. BAVERSTOCK and D.E. CHARLTON, Eds), Taylor and Francis, London, pp 111-122, 1988.
14. D.K. MEYERS, J.D. CHILDS, and A.R. JONES, Sensitization of bacteriophage T4 to ^{60}Co γ-radiation and to low-energy X radiation by bromouracil. *Radiat. Res.* **69**, 152-165 (1977).
15. K. KOBAYASHI, K. HIEDA, H. MAEZAWA, Y. FURUSAWA, M. SUZUKI, and T. ITO, Effects of K-shell absorption of intracellular phosphorus on yeast cells. *Int. J. Radiat. Biol.* **59**, 643-650 (1991).
16. H.G. PARETZKE, Radiation track structure theory. In *Kinetics of Nonhomogeneous Processes*, (G.R. Freeman, Ed.) Wiley, New York, pp 89-170, 1987.
17. R.F. MARTIN and W.A. HASELTINE, Range of radiochemical damage to DNA with decay of iodine-125. *Science* **213**, 896-898 (1981).
18. D.E. CHARLTON, H. NIKJOO, and J.L. HUMM, Calculation of yields of single- and double-strand breaks in cell nuclei from electrons, protons and alpha particles. *Int. J. Radiat. Biol.* **56**, 1-19 (1989).
19. D.E. CHARLTON, The application of biophysical models to cellular DNA damage. In *The Early Effects of Radiation on DNA*, (E.M. FIELDEN and P. O'NIELL, Eds), Springer-Verlag, London, pp 179-193, 1991.
20. H. NIKJOO, J.R.K. SAVAGE, D.E. CHARLTON, A. HARVEY, and S.Z. AGHAMOHAMMADI, Test of radiation damage enhancement due to incorporation of BrdU into DNA using chromatid aberrations. This volume.

 Biophysical Aspects of Auger Processes, AAPM Symposium Series No. 8 (1992) 066-079
Eds. RW Howell, VR Narra, KSR Sastry, DV Rao

TEST OF RADIATION DAMAGE ENHANCEMENT DUE TO INCORPORATION OF BrUdR INTO DNA USING CHROMATID ABERRATIONS

HOOSHANG NIKJOO, JOHN R.K. SAVAGE,
DAVID E. CHARLTON[1],
ALISON HARVEY, and S.Z. AGHAMOHAMMADI

MRC Radiobiology Unit Chilton Didcot, Oxon, OX11 0RD, U.K.

[1]Physics Department, Concordia University,
1455 de Maisonneuve Blvd. West, Montreal Quebec H3G 1M8
Canada

ABSTRACT

Monte Carlo track structure calculations, leading to an estimation of the magnitude of enhancement of radiation damage due to the incorporation of the halogenated pyrimidine, bromodeoxyuridine (BrUdR) a thymine analog, into DNA have been made. The increase in the yield of double strand breaks for various degrees of substitution in one (monofilarly) or both strands (bifilarly) have been calculated. To test these calculations, quantitative selected radiation-induced aberrations have been obtained in Chinese hamster (V79) fibroblast chromosomes having various patterns of BrUdR substitution following irradiation with 250 kV X rays. Free "breaks" and achromatic lesions "gaps" show no appreciable sensitizations, but breaks involved in chromatid interchanges show significant enhancement though of lower magnitude than theoretical predictions.

INTRODUCTION

This paper attempts to correlate the early biophysical effects of radiation induced-damage obtained using Monte Carlo track structure calculations with experimental data, chromosome aberrations being the biological end point.

When ionizing radiation interacts with living cells a long chain of events ensues which may lead to cell death, mutation or transformation. The quest toward an understanding of the mechanisms of damage caused by ionizing radiation has been pursued in the multidisciplinary field of radiobiology which combines knowledge of physics, chemistry and biology. Chromosomal structural change was one of the earliest systems for the quantitative study of the effects of radiation (1,2). These provide a visible and quantitative measure of the effect on the cell. Recent developments have made it possible to explain the chromosomal structural changes in terms of the molecular theory of radiation effect (3). A central theme of the molecular theory of radiation-induced chromosomal structural change is that the DNA double strand breaks correspond to the primary breaks that lead to aberrations (4,5).

The conceptual framework here is that the interaction of the ionizing particle results in deposition of energy at the target site and this subsequently can lead to the induction of many forms of damage (6-8). In spite of great advances made in the past two decades to further our basic understanding of the processes which lead to biological damage, there remain many questions as to the mechanisms linking the initial physico-chemical damage to the final cellular effect. The paper by Charlton and Nikjoo (this volume) presents a method and examines the complexity of attempting to model the very basic initial interactions at very short times ($< 10^{-12}$ s). We have used the same modelling technique to obtain the data for the theoretical calculations of this study. The physico-chemical stages of radiation can be envisaged as inducing a variety of types of damage, such as single strand breaks, double strand breaks, base damage and cross-links. Most single strand breaks and base damage are repaired very rapidly (9-14). Double strand breaks are thought to be the most important lesion participating in radiation-induced damage. As these are not repaired very efficiently, they lead to the induction of chromosomal aberrations (15-20).

Halogenated pyrimidines, such as BrUdR and IUdR, which are analogs of thymidine, incorporate into DNA and enhance the radiation effect (21-25).

This property has been explored both for clinical interest in certain tumor treatments and for identifying the mechanism(s) involved in radiation-induced damage (26-32). To understand the radiosensitization effect, a number of investigations have been reported on the loading effect of the DNA by bromine or iodine analogs (28,29,33-36). These studies which use either a cellular system, measuring radiosensitivity in terms of survival fraction, or chromosome aberrations, sometimes, but not always, show quantitative differences in sensitization between monofilarly and bifilarly substituted DNA. These differences have been attributed to the level of substitution and chromatin packing.

Because of the semi-conservative nature of DNA replication, chromosomes with contrasting forms of substitution can readily be obtained. Natural DNA contains thymine (T) in both strands and is therefore TT (Fig. 1a). If bromodeoxyuridine is present for one complete synthesis/replication period (S phase), both the chromatids will have DNA with thymine in one strand (T) and bromouracil replacing some thymines in the other (B). So the chromosome constitution is TB/TB (Fig. 1b).

If the bromodeoxyuridine is removed and a further round of replication permitted in the presence of thymidine, the chromosome constitution will be TT/TB. If, however, the bromodeoxyuridine remains for the second round, the chromosome constitution will be TB/BB (Fig. 1c). In either case, the chromatids can be differentially stained and aberrations produced in TT, TB or BB chromatids recorded.

Using these two protocols, it should be possible to produce experimental sensitization factors for TT/TB and TB/BB and, by inference (since TB is common to both protocols) TT/BB. This we have attempted, so that the factors can be compared with the theoretical predictions.

METHODS

Monte Carlo Track Structure Calculations

The approach is to first simulate the stochastic tracks of electrons and then calculate the energy deposited in the target volume. We have compiled a comprehensive set of data on energy deposition by ionizing radiations in cylindrical targets for use in biophysical models of the action of radiation on

biological targets (37-40). These data have been used to calculate the yield of single and double strand breaks in a model of DNA (41-44). Model number three of Charlton and Nikjoo (this volume) was used to calculate effects in bifilarly bromine-substituted DNA. A fifth model was developed, by modifying model number three, to calculate the enhancement when DNA was monofilarly substituted. Unlike the experimental protocol, the present simulation work does not distinguish on which template the substitution was made. In this calculation the sensitization effect was due to incorporated

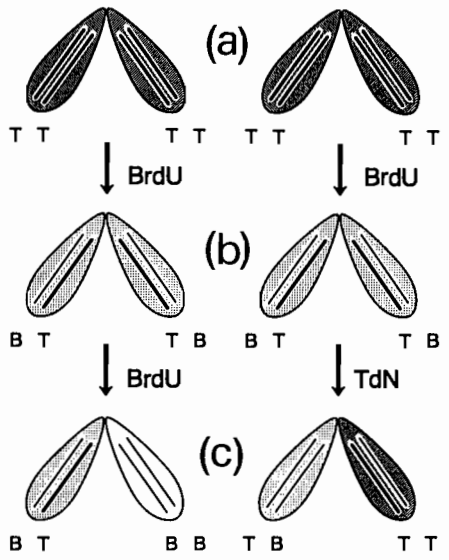

FIG. 1. Protocols for obtaining substituted chromatids. The group on the left of the Figure 1 is the protocol for producing the TB/BB chromatids where one chromatid (BB) is bifilarly substituted and the other (TB) monofilarly substituted. The BB chromatid is light (l) and the TB chromatid is dark (d). The group on the right of the figure shows the protocol for obtaining the TT/TB chromatids. In this case BrUdR (BrdU) was removed and normal thymidine medium was added for the second cycle replication. At the end of 2nd replication one chromatid is monofilarly substituted (TB) and the other unsubstituted (TT). The TB chromatid is light (l) and TT is dark (d). The heavy lines show the unsubstituted template. Fig. 1a shows the 1st generation, Fig. 1b the 2nd generation, and Fig. 1c the 3rd generation.

bromine inducing SSB and DSB calculated by replacing T's by the bromine analog with a 50% probability of filling on one strand of the DNA only, and assuming the threshold energy of 15 eV for bromine activation with a probability of 0.5 to produce an SSB. A suitable number of 20 keV monoenergetic electrons were simulated and subsequently were used to calculate the enhancement ratio when bromine was added monofilarly and bifilarly. Enhancement is the quotient of the effect after to that of the effect before the addition of the bromine.

A Biological Test

Cells of Chinese hamster, V79-379A, were grown in Falcon T75 culture flasks using Eagles MEM supplemented with 10% FCS, L-glutamine and antibiotics. Under these conditions, they have a modal cycle time of ≈ 8.5 h. The flasks were divided into two batches:

Batch A; (TB/BB protocol). BrUdR (final concentration, 10 μg/ml, 3.25×10^{-5} M) was given and 17 h later they received 0.9 or 1.5 Gy X ray irradiation (250 kV, 14 mA, HVL 1.2 mm Cu, 0.76 Gy/min). Cells were sampled at 3 h post-irradiation, following a 2 h colcemid accumulation (0.05 μg/ml).

Batch B; (TT/TB protocol). BrUdR (concentration as above) was given for 9 h. The medium was removed, the cells rinsed with Earle's BSS and complete medium containing added thymidine (10 μg/ml, 4.13×10^{-5} M) restored. At 17 h, they were irradiated along with the flasks of Batch A, receiving the same absorbed doses, and then sampled at 3 h following 2 h colcemid.

Air dried chromosome preparations were stained with fluorescence-plus-Giemsa methods to produce "harlequin" sister-chromatid differentiation. Care was taken to ensure that the pale chromatids (BB for batch A, TB for batch B) were not under-stained, for that could lead to under-scoring of achromatic lesions. Aberrations were scored in fully differentiated second-division chromosomes and chromosome groups. Only three of several types of chromatid-type aberrations were recorded and the following procedure was adopted: Slides were traversed until at least 400 unambiguous chromatid breaks ("discontinuities") were collected for each dose, and allocated to the light (l) or dark (d) chromatid. In about 12% of cases, the break

was accompanied by an exchange of sister-chromatids, seen as a color-jump at the point of breakage (c*).

Whilst searching for breaks, all achromatic lesions ("gaps") encountered were also recorded and l,d allocated. A "buffer" category of gap/break was provided for those aberrations where an unequivocal decision could not be made. For analysis, this buffer was merged with gaps. All chromatid interchanges observed during break search were classified for symmetry and completeness, and the presumptive break-points were assigned l/l, l/d, d/d. About 2-3% showed mixed breaks, having a color-jump break at one end.

Since we included isolated chromosomes and incomplete cells in our scoring, and only scored selected aberrations, absolute frequencies, expressed as aberrations per cell can not be given (not that such values mean very much in a situation where observed yield fluctuates with sample time). Instead, we scored for each dose treatment the total aberration involvement of a random sample of at least 200 large metacentric chromosomes (of which there are 4 per cell) and provide "aberrations per metacentric" for comparative purposes.

RESULTS

Table I is a summary of computational data showing the bifilar and monofilar enhancement ratios for various bromine loadings. The data show the ratios TT/BB for bifilarly and TT/TB for monofilarly substituted DNA strands. The bifilarly substituted ratio TT/BB was obtained from model number three of Charlton & Nikjoo (this volume) and the monofilarly substituted ratio TT/TB from model number five. The data in brackets show the effect plus the contribution due to Auger electrons.

Table II summarizes the experimental results. Only non-color jump lesions have been included in the calculations. It is seen that for the TB/BB situation (BB light), neither free breaks nor gaps show any evidence of excess BB involvement. Conversely, the breaks/lesions involved in interchanges show a highly significant excess, a factor exceeding 2. For the TT/TB situation (TB light), free breaks at 0.9 Gy show a significant excess in TB. This is absent at 1.5 Gy and absent for gaps at both doses. Interchanges show significant excess at both doses, though the factor is lower (about 1.5) than for TB/BB.

TABLE I
Enhancement Ratios Calculated for Various Bromine Loading in the DNA

Br %	Bifilar TT/BB	Monofilar TT/TB
10	1.40 (1.40)	1.19 (1.19)
20	1.64 (1.66)	1.34 (1.40)
30	1.85 (1.90)	1.51 (1.53)
40	2.12 (2.18)	1.65 (1.69)
50	2.25 (2.36)	1.73 (1.77)
60	2.46 (2.57)	1.84 (1.89)
70	2.69 (2.81)	2.00 (2.60)

Table III gives the absolute aberration yields. The chromosomes show hardly any sensitization for the TT/TB situation but a very obvious one for TB/BB.

DISCUSSION

Starting from a physical basis for radiation-induced DNA damage we have attempted to present a simple model for calculating the effect of monofilar substitution of the DNA strand and compare it with experimental chromosome aberration data. In calculating these data we have made the following assumptions for the sensitization effect:

1. Energy is deposited in the target volume discretely by individual tracks.
2. SSB are produced as a result of a threshold energy deposition of 17.5 eV by a single ionization or excitation.
3. SSB's interact to produce a DSB.
4. DSB is the primary damage.
5. Repair and other primary damage is not considered.
6. Energy for bromine activation is 15 eV.
7. All the biological damage is mediated via chromosome aberrations.

TABLE II
Dominance of Lesions in Light (l) Chromatids

Treatment	Dose (Gy)	l	d	l/d	Prob.
BREAKS TT/TB	0.9	202	153	1.32	0.009**
	1.5	143	120	1.19	0.16
TB/BB	0.9	236	214	1.10	0.30
	1.5	211	219	0.96	0.70
GAPS TT/TB	0.9	587	625	0.94	0.28
	1.5	288	329	0.88	0.10
TB/BB	0.9	350	324	1.08	0.32
	1.5	177	204	0.87	0.17
INTERCHANGES	0.9	214	150	1.43	0.0008***
TT/TB	1.5	147	91	1.62	0.0003***
TB/BB	0.9	216	101	2.14	1.1×10^{-10}***
	1.5	175	79	2.22	1.7×10^{-9}***

Breaks showing color-jumps have not been included in the table or the calculations.

The data from theoretical calculations show the increase in yield of DSB's for various degrees of substitution in one (monofilar) or both (bifilar) strands. Calculated data show a greater sensitization effect than the experimental data. For each experimental substitution situation, there are two quite different sensitization factors, dependent upon the particular aberration category chosen. We cannot be certain that either represents a relevant value.

If we accept the results for breaks and for achromatic lesions (gaps) then, with the sole exception of TT/TB breaks at 0.9 Gy, there is no evidence for any sensitization by either mono- or bifilar bromouracil incorporation. On the other hand, if we accept the results from interchange breaks/lesions then TB>TT $\approx$ 1.5 and BB>TB $\approx$ 2.2.

TABLE III
Absolute Aberration Yields

Substitution	Dose (Gy)	No. of metacentrics scored	Total aberrations	Abs. per metacentric
TT/TB	0.9	200	8	0.04
	1.5	600	62	0.10
TB/BB	0.9	200	29	0.15
	1.5	400	107	0.27
Control	0.9	200	9	0.05
	1.5	200	19	0.10

It is difficult to reconcile these differences between aberration categories with currently accepted ideas of aberration origin. If there is a common pool of breaks from which all structural changes are formed, then any sensitivity bias should affect all aberrations equally. Perhaps some kind of differential repair of BrUdR-enhanced breaks occurs between the formation of interchanges and the intrachange/break/gap categories.

A second worrying feature of this data appears when we consider the absolute aberration frequencies in relation to absorbed dose. We find consistently that, for a given dose, TT/TB chromosomes are, overall, much less sensitive to aberration production than TB/BB chromosomes by a factor 2 - 3. This tells us immediately that the monofilarly substituted chromatid (TB), common to both protocols, does not have a fixed sensitivity. Rather, its response in terms of aberration production/involvement is dependent in some way upon the constitution of its sister-chromatid. TB with a BB sister always has more aberrations than TB with a TT sister. From this it follows that the data do not support a model of sensitization based simply on the amount of BrUdR incorporated. We have to conclude that the TB aberration frequency is conditional upon the substitution condition present in its sister. This has interesting implications for the theory of aberration formation.

However, it is only fair to point out that the two TB chromatids are not identical with regard to their mode of formation. For TB/BB, bromouracil-containing DNA is built onto a template containing endogenous thymine, but for TT/TB, exogenous thymine-containing DNA is built onto a bromouracil-containing template. These differences could affect the packing and condensation of the chromatin, but whether this would produce aberration frequency disparities of the magnitude we observe is questionable. Because of this difference in absolute frequency of the common TB chromatid, we cannot use it to produce a common overlap value which will allow us to predict the sensitivity effect for TT→BB.

We have not measured the actual degree of substitution we obtained with an exposure concentration of 10 μg/ml for one or two cycles. Extrapolations from published measurements where Chinese hamster cells were used, indicate an expectation of about 60% thymine replacement (45).

ACKNOWLEDGMENTS

The authors would like to thank Adrian Ford, Kevin Glover and Elton Evans for assisting in the preparation of this manuscript. Part of the theoretical calculations were carried out on the Cray XMP at Rutherford Laboratory. This work was partially supported by the Commission of European Communities (contract numbers BI7-0032-C and BI7-039).

REFERENCES

1. K. SAX, Types and frequencies of chromosomal aberrations induced by X-rays. *Cold Spring Harb Symp. Quant Biol.* **9**, 93-103 (1941).
2. D.E. LEA, *Actions of Radiation on Living Cells.* Cambridge University Press, 1946.
3. M.A. BENDER, H.G. GRIGSS, and J.S. BEDFORD, Mechanisms of chromosomal aberration production. III. Chemicals and Ionizing Radiation. *Mutat. Res.* **23**, 197-212 (1974).
4. E.J. DUPRAW, *DNA and Chromosomes.* Holt, Rinehart and Winston Inc., New York, 1970.
5. A.T. NATARAJAN, G. OBE, A.A. VAN ZEELAND, F. PALITTI, M. MEIJERS, and E.A.M. VERDEGAAL-IMMERZEEL, Molecular mechanisms involved in the production of chromosomal aberrations. *Mutat. Res.* **69**, 293-305 (1980).
6. E.M. FIELDEN and P. O'NEILL, *The Early Effects of Radiation on DNA*, Springer-Verlag, Berlin, 1991.

7. G.R. FREEMAN, *Kinetics of Nonhomogeneous Processes.*, John Wiley & Sons, New York, 1987.
8. D.T. GOODHEAD, Relationship of microdosimetric techniques to applications in biological systems. In *Dosimetry of Ionizing Radiations*, Vol **2**, (K.R. Kase, B.E. Bjarngard and F.H. Attix, Eds.) Academic Press, New York, pp 1-89, 1987.
9. I.J. KORNER, K. GEUNTER, and W. MALTZ, Kinetics of single-strand break rejoining in X-ray and neutron-irradiated Chinese hamster cells. *Stud. Biophys.* **70**, 175-182 (1978).
10. P.E. BRYANT, Enzymatic restriction of mammalian cell DNA using PvuII and BamH1: Evidence for the double-strand break origin of chromosomal aberrations. *Int. J. Radiat. Biol.* **46**, 52-65 (1984).
11. P.A. CERUTTI, Effects of ionising radiation on mammalian cells. *Naturwissenchaften* **61**, 51-59 (1974).
12. F.T. GATES and S. LINN, Endonuclease from E. coli that acts specifically upon duplex DNA damaged by ultraviolet light, osomium tetroxide or X-rays. *I. Biol. Chem.* **252**, 2801-2807 (1977).
13. M.S. PATIL, S.E. LOCHER and P.V. HARIHAN, Radiation-induced thymine base damage and its excision-repair in inactive chromatin of HeLa cells. *Int. J. Radiat. Biol.* **48**, 691-700 (1985).
14. G.P. VAN DER SCHANS, H.B. CENTEN, and P.H.M. LOHMAN, Studies on the repair defects of ataxiatelagientasia cells, In *Proceedings of NATO Advanced Study Institute*, (E. Seeburg and K.K. Kleppe, Eds.) Bergen, Norway, pp 355-359, 1980.
15. P.E. BRYANT and D. BLOCHER, The effects of 9-D- arabinofuranosyladenine on the repair of DNA strand breaks in Ehrlich ascites tumor cells. *Int. J. Radiat. Biol.* **42**, 385-394 (1984).
16. F. KRASIN and F. HUTCHINSON, Repair of DNA double-strand breaks in Escherichia coli which require rec A function in the presence of a duplicate genome. *J. Mol. Biol.* **116**, 81-98 (1977).
17. M.N. CORNFORTH and J.S. BEDFORD, X-ray induced breakage and rejoining of human interphase chromosomes. *Science* **222**, 1141-1143 (1983).
18. D. WLODEK and W.N. HITTELMAN, The relationship of DNA and chromosome damage to survival of synchronized X-irradiated 5178Y cell. *Radiat. Res.* **115**, 550-575 (1988).
19. G. KLEIN and E. KLEIN, Oncogene activation and tumor progression. *Carcinogenesis* **5**, 429-435 (1984).
20. J.D. ROWLEY, Chromosome abnormalities in cancer. *Cancer Genet. Cytogenet.* **2**, 175-198 (1980).
21. T. BONURA and K.C. SMITH, The involvement of indirect effects in cell-killing and DNA double-strand breakage in γ-irradiated Escherichia coli K-12. *Int. J. Radiat. Biol.* **29**, 293-296 (1976).
22. W.C. DEWY and R.M. HUMPHREY, Increase in radiosensitivity to ionizing radiation related to replacement of thymidine in mammalian cells with 5-bromodeoxyuridine. *Radiat. Res.* **26**, 538-553 (1965).
23. S.H. KAPLAN, DNA strand scission and loss of viability after X irradiation of normal and sensitized bacterial cells. *Proc. Natl. Acad. Sci. USA* **55**, 1442-1446 (1966).

24. B. DJORDJEVIC and W. SZYBALSKI, Incorporation of 5-bromo- and 5-iododeoxyuridine into deoxyribonucleic acid of human cells and its effect on radiation sensitivity. *J. Exp. Med.* **12**, 509-531 (1960).
25. H. OHARA, K. SHINOHARA, K. KOBAYASHI, and T. ITO. An additional enhancement in BrdU-labelled cultured mammalian cells with monoenergetic synchrotron radiation at 0.09 nm: Auger effect in mammalian cells. In *DNA Damage by Auger Emitters*, (K.F. Baverstock and D.E. Charlton, Eds.) Taylor & Francis, London, pp 123-134, 1988.
26. R. NATH, P. BONGIORNI and S. ROCKWELL, Iododeoxyuridine radiosensitization by low- and high-energy photons for brachytherapy dose rates. *Radiat. Res.* **124**, 249-258 (1990).
27. T.J. KINSELLA, P.O. DOBSON, J.B. MITCHELL, and A.J. FORNACE, Enhancement of X ray induced DNA damage by pre-treatment of halogenated pyrimidine analogs. *Int. J. Radiat. Oncol. Biol. Phys.* **13**, 733-739 (1987).
28. J.B. MITCHELL, T.J. KINSELLA, and E. GLATSTEIN, The use of non-hypoxic cell sensitizers in radiobiology and radiotherapy. *Int. J. Radiat. Oncol. Biol. Phys.* **12**, 1513-1518 (1986).
29. L.L. LING and J.F. WARD, Radiosensitization of Chinese hamster cells by bromodeoxyuridine substitution of thymidine: Enhancement of radiation-induced toxicity and DNA strand break production by monofilar and bifilar substitution. *Radiat. Res.* **121**, 76-83 (1990).
30. T.S. LAWRENCE, M.A. DAVIS J. MAYBAUM, P.L. STETSON, and W.D. ENSMINGER, The effect of single versus double-strand substitution on halogenated pyrimidine-induced radiosensitization and DNA strand breakage in human tumor cells. *Radiat. Res.* **123**, 192-198 (1990).
31. G. ILIAKIS, S. KURTZMAN, G. PANTELIAS, and R. OKAYASU, Mechanism of radiosensitization by halogenated pyrimidines: Effect of BrdU on radiation induction of DNA and chromosome damage and its correlation with cell killing. *Radiat. Res.* **119**, 286-304 (1989).
32. G. ILIAKIS, G. PANTELIAS, and S. KURTZMAN, Mechanism of radiosensitization by halogenated pyrimidines: Effect of BrdU on cell killing and interphase chromosome breakage in radiation-sensitive cells. *Radiat. Res.* **125**, 56-64 (1991).
33. M. JACOB, Differential Radiosensitivity of the uni- and bi-filarly BrdUdr-substituted chromatids of mutajac chromosomes. *Mutat. Res.* **63**, 211-213 (1979).
34. S. WOLFF and J. BODYCOTE, The induction of chromatid deletions in accord with the breakage-and-reunion hypothesis. *Mutat. Res.* **29**, 85-91 (1975).
35. S. WOLFF and N. FIJTMAN, X-ray sensitization of chromatids with unifilarly and bifilarly substituted DNA. *Mutat. Res.* **80**, 133-140 (1981).
36. N.V. LUCHNICK, M.M. ANTOSHCHINA, and N.A. PORJADKOVA, On the radiosensitivity of uni- and bi-filarly BrdUrd-substituted chromatids. *Mutat. Res.* **91**, 463-465 (1981).
37. D.E. CHARLTON, D.T. GOODHEAD, W.E. WILSON, and H.G. PARETZKE, The deposition of energy in small cylindrical targets by high LET radiations. *Radiat. Prot. Dosim.* **13**, 123-125, (1985).

38. H. NIKJOO, D.T. GOODHEAD, D.E. CHARLTON, and H.G. PARETZKE, Energy deposition in small cylindrical targets by ultrasoft X-rays. *Physics in Medicine and Biology*, **34**, 691-705, (1989).
39. H. NIKJOO and D.T. GOODHEAD, The relative biological effectiveness (RBE) achievable by high and and low LET radiations, In *Low Dose Radiation*, (K.F. Baverstock and Stather, Eds.) Taylor & Francis, London, pp 491-502, 1989.
40. H. NIKJOO and D.T. GOODHEAD, Track structure analysis illustrating the prominent role of low-energy electrons in radiobiological effects of low-LET radiations. *Physics in Medicine and Biology* **36**, 229-238, (1991).
41. D.E. CHARLTON, The application of biophysical models to cellular DNA damage, In *The Early Effects of Radiation on DNA* (E.M. Fielden and P. O'Neil, Eds.) Springer-Verlag, London, pp 179-193, 1991.
42. D.E. CHARLTON, DNA breakage from incorporated ^{125}I. In *DNA Damage by Auger emitters*, (K.F. Baverstock and D.E. Charlton, Eds.) Taylor and Francis, London, pp 111-122, 1988.
43. D.E. CHARLTON, H. NIKJOO, and J.L. HUMM, Calculations of initial yields of single- and double strand breaks in cell nuclei from electrons, protons and alpha particles. *Int. J. Radiat. Biol.* **56**, 1-19, (1989).
44. J.L. HUMM and D.E. CHARLTON, Double strand breakage in DNA produced by the photoelectric interaction with incorporated 'cold' bromine. In *DNA Damage by Auger emitters*, (K.F. Baverstock and D.E. Charlton, Eds.) Taylor and Francis, London, pp 111-122, 1988.
45. T.S.B. ZWANENBURG, A.A. VAN ZEELAND, and A.T. NATARAJAN, Influence of incorporated bromodeoxyuridine on the induction of chromosomal alterations by ionizing radiation and long-wave UV in CHO cells. *Mutat. Res.* **150**, 283-292 (1985).

DISCUSSION

Schneiderman, M. The labeling protocol, irradiation, and subsequent measurements of strand breaks do not take account of cell cycle effects. Your protocol would allow you to look only at cells that can recover from radiation induced division delay.

Nikjoo, H. I do not think that cell cycle is a major factor influencing the observations for the following reasons: 1) We are not measuring strand breaks but structural chromatid-type aberrations which are not necessarily the same thing. 2) Obviously we can only observe and score these in cells that come to metaphase. 3) Mitotic delay is not, at these doses (up to 2.0 Gy), an "all or nothing" phenomenon. The mitotic index never reaches zero and cells continue to proceed, at varying rates, into the cycle, but obviously arrive at division in different order and different relative frequencies than they would have done if no dose was given. 4) In any case, we sample at intervals through G_2 in a multiple sample time regime up to 5 h post-irradiation. Immediately after irradiation we replace the medium with one containing

thymidine instead of BrUdR. This allows us to recognize S phase cells by virtue of the TT patches and bands which they carry. By 5 h post irradiation, the fraction of S cells is 50-60% at 1.5 Gy - higher (>80%) in controls. Thus post-S (G_2) and S-cells are progressing into metaphase to be scored. 5) Whilst we cannot claim to have sampled all of G_2, we obviously have cells from most, if not all, developmental stages (this, after all, is the principle of a multiple sampling regime). There is no variation in the frequency of true discontinuities or of achromatic lesions in the light or in the dark strand (BB or TB) at any sample time even though there are, as expected, differences in absolute yield of aberrations is, as expected, much lower in S-cells, so we do not have as much data. Mid-early S cells have much lower frequencies of chromatid aberrations and we have insufficient data to perform suitable tests. 6) There is, as far as I know, no evidence for interphase death in V79 fibroblasts at these dose levels for lower LET radiations (high-LET might be different). Therefore, all cells eventually "recover" from mitotic delay - but to sample the whole of G_2 would involve sampling up to probably 20 h and beyond (there are few very slow cells in V79). The period 0-6 h is the region most people sample for G_2 cells and chromatid-type aberrations. We have covered most of this - so I doubt that the few percent of G_2 cells missed are likely to make much difference.

Biophysical Aspects of Auger Processes, AAPM Symposium Series No. 8 (1992) 080-090
Eds. RW Howell, VR Narra, KSR Sastry, DV Rao

DNA STRAND BREAKS IN IUdR CONTAINING CELLS AFTER IRRADIATION WITH LOW-ENERGY X RAYS

SYNNÖVE SUNDELL-BERGMAN and KARL J. JOHANSON

Department of Radioecology,
The Swedish University of Agricultural Sciences
P.O. Box 7031, S-750 07 Uppsala, Sweden

ABSTRACT

The induction and repair of DNA strand breaks were studied in control and IUdR labeled CHO cells after irradiation with low-energy X rays. More DNA strand breaks were found in IUdR labeled compared to control cells. If the data were least square fitted, the slope ratios (IUdR/control) were 1.23 immediately after irradiation and 1.22 after 60 min of repair. Using the linear quadratic model, the ratio between the two α-terms was 1.43 after 60 min repair. After 120 min of repair, the number of DNA breaks in control cells was close to zero for doses below 4 Gy while for IUdR labeled cells the number was significantly higher than zero.

INTRODUCTION

It is well known that incorporation of halogenated thymidine analogs into cellular DNA increases the radiosensitivity of mammalian cells as measured by survival (1-4), and may affect the ability of cells to repair radiation damage (2,5). Several reports have shown that the degree of radiosensitization increases as the percentage of thymidine replacement increases (6,7). Although the mechanism of sensitization has not been fully elucidated, it is probably not related to secondary effects such as inhibition of DNA polymerase or inhibition of enzymes involved in thymidine synthesis (8,9).

Recently Fairchild *et al.* (10) reported theoretical calculations showing that IUdR radiosensitization might be enhanced substantially by the use of photon energies just above 33.2 keV, the K absorption edge of iodine (10). According to Fairchild *et al.* (10) the enhancement would result from the effects of the Auger electron cascade which follows the creation of vacancy in the K shell of iodine via the photoelectric effect. These Auger electrons are very effective in causing subcellular damage in critical cell structures in a manner similar to ^{125}I decay in DNA (11,12).

Cells which have incorporated IUdR into their DNA show significant reductions of both the slope and the shoulder of their radiation survival curves (13,14). The α-coefficient in the linear-quadratic model, $y = \alpha D + \beta D^2$, which is supposed to account for the formation of double-strand breaks in one single radiation event (15), has been reported to be significantly higher for X irradiated IUdR labeled cells compared to control cells (13). Radiosensitization by IUdR has also been correlated with increases in chromosomal aberrations and micronuclei formation (16). Few studies have been reported on the induction and repair of DNA strand breaks in mammalian cells after IUdR incorporation, although the enhancement in sensitivity suggests the involvement of DNA damage and repair (17,18).

The effect on induction and repair of DNA strand breaks after irradiation with low-energy X rays has been examined using the DNA unwinding technique with double-labeling (19). Incorporation of IUdR into CHO cells followed by irradiation resulted in an increased number of DNA strand breaks in IUdR labeled cells. Furthermore the repair of the induced strand breaks in IUdR containing cells was less efficient than in the controls.

MATERIAL AND METHODS

Culturing Conditions

Exponentially growing CHO cells were cultured in plastic flasks (Nunc, Roskilde, Denmark) containing Ham's F10 (SVA, Uppsala, Sweden), supplemented with 10% newborn calf serum (Gibco, N.Y. USA), 1.0 mM L-glutamine, 100 IU/ml penicillin and 100 μg/ml streptomycin and maintained in a 5% CO_2 atmosphere at 37°C.

Labeling of DNA

Iododeoxyuridine (IUdR) was added to cells to a final concentration of 10^{-6} M and the cells were incubated for three days in darkness. The IUdR solution was stored frozen in a weak alkaline stock solution of 1 mM. During the IUdR labeling, the cells were grown in medium prepared from thymidine depleted Ham's F10 medium. Cells were labeled with 7.4 kBq/ml of ^{3}H-thymidine (^{3}H-TdR) or 1.85 kBq/ml of ^{14}C-thymidine (^{14}C-TdR) (Amersham, U.K.) for 18 h before harvest. The cells were then washed 2-3 times in phosphate buffered saline (PBS) and, after the addition of new prewarmed medium, the incubation continued for an additional 3 h at 37°C.

Irradiation Conditions

The cells were irradiated at 0°C using a Siemens Stabilipan therapy X ray unit operating at 75 kV and 20 mA with a total filtration of 4 mm Al. The radiation dose and radiation quality were measured using an ionization chamber and thermoluminescence dosimeters. The half-value layer (HVL) for the 75 kV X rays was measured to be 4.3 mm Al corresponding to a mean photon energy of 38 keV (13). The dose rate was 0.16 Gy per min.

DNA Strand Break Analysis

The cells were detached from the flask with trypsin (0.25% in PBS). Prior to irradiation cells were mixed according to the following schedule: Cells which had incorporated IUdR and ^{3}H-TdR were mixed with only ^{14}C-TdR labeled cells. Furthermore ^{3}H-TdR labeled cells were mixed with IUdR and ^{14}C-TdR labeled cells (19,20). This implies that IUdR labeled and control cells were treated simultaneously during the DNA strand break analysis. The

number of DNA strand breaks was determined by the unwinding technique either directly after the irradiation or after a repair period of 60 or 120 min. Briefly, 100 µl of the cell suspension was added to 1 ml of a weak alkaline solution and left in the dark for 30 min. After neutralization the samples were sonicated and, after adding SDS, stored at -20°C until chromatography was performed. Single- and double-stranded DNA were separated on hydroxylapatite and the ^{3}H- and ^{14}C-activities were then determined in a liquid scintillation counter (Packard Instr. Co., USA) using Instagel (Packard Instr. Co., USA) as a scintillation solution. The number of DNA strand breaks, the sum of the single- and double-strand breaks, was calculated according to Rydberg (19).

RESULTS

In order to estimate the amount of cellular IUdR uptake, cells were incubated with ^{125}IUdR of known specific activity for 72 h. Following the incubation the DNA content and the incorporation of ^{125}IUdR per cell were determined. The replacement of thymidine with IUdR under these circumstances was estimated to be on average 10%.

Compared to control cells, some strand breaks were induced in IUdR labeled cells during the labeling period although care was taken to avoid light exposure to the cells. The experiments were repeated several times and the mean values based on 10 to 30 samples.

Figure 1 illustrates the induction of DNA strand breaks after irradiation with low-energy X rays. The number of DNA strand breaks increases in a dose-dependent manner up to 5 Gy where the curves approached saturation which probably is due to the limit of the method. The data were least-squares fitted and the slopes of the dose-response curves were found to be 0.32 ± 0.02 Gy^{-1} for IUdR labeled cells and 0.26 ± 0.02 Gy^{-1} for control cells. The relation between the slopes results in a ratio of 1.23 indicating a higher response for the IUdR labeled cells.

Figure 2 shows the DNA strand breaks that are remaining after 60 min of incubation at 37°C. The number of residual DNA strand breaks seems to be dose-dependent for both the control and the IUdR labeled cells. The slopes were found to be 0.037 ± 0.01 Gy^{-1} and 0.030 ± 0.007 Gy^{-1} for IUdR labeled and control cells, respectively, and the ratio between the two slopes was 1.23.

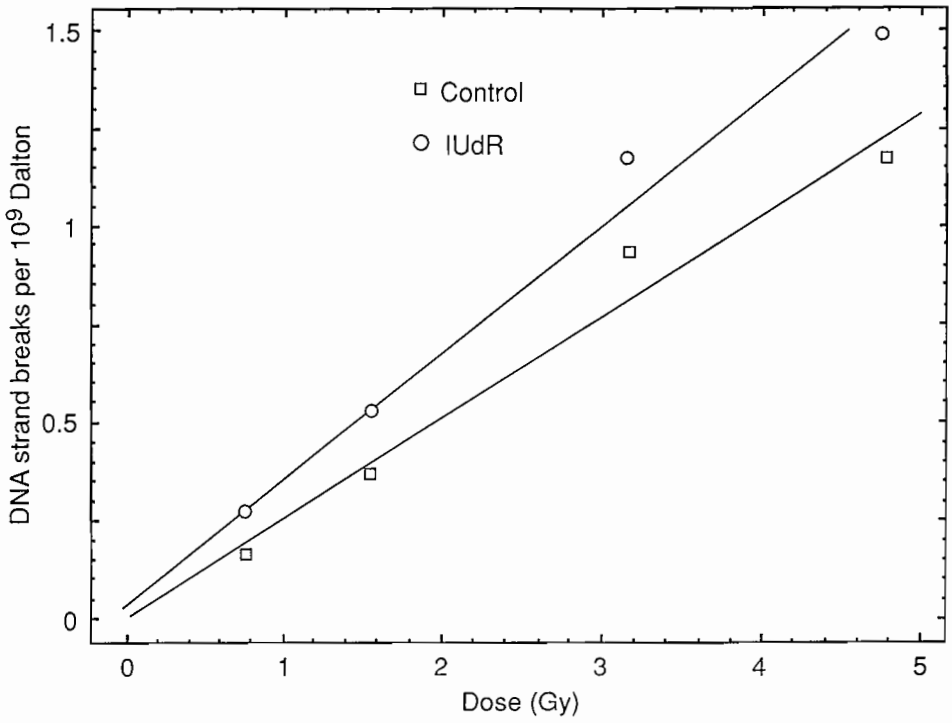

FIG. 1. The number of DNA strand breaks induced in control and IUdR labeled cells after irradiation with low-energy X rays. The dose rate was 0.16 Gy min^{-1}. The data were fitted by the least squares method.

The repair of DNA strand breaks was also fitted to the linear-quadratic relationship ($y = \alpha D + \beta D^2$) using an iterative least-square fit where D is the dose in Gy. The α-coefficients were $4 \times 10^{-3} \pm 0.4 \times 10^{-3}$ Gy^{-1} for IUdR and $2.8 \times 10^{-3} \pm 0.5 \times 10^{-3}$ Gy^{-1} for control cells which yields a ratio of 1.43. This indicated that the relative difference in the low dose range had increased during the 60 min repair phase.

The results obtained after 120 min of repair are presented in Fig. 3. In the low dose region (up to approximately 4 Gy), very few non-rejoined breaks were found in control and IUdR groups. For control cells the residual breaks in this region were not significantly different from zero, while for the IUdR labeled cells the number was significantly higher than zero. The difference

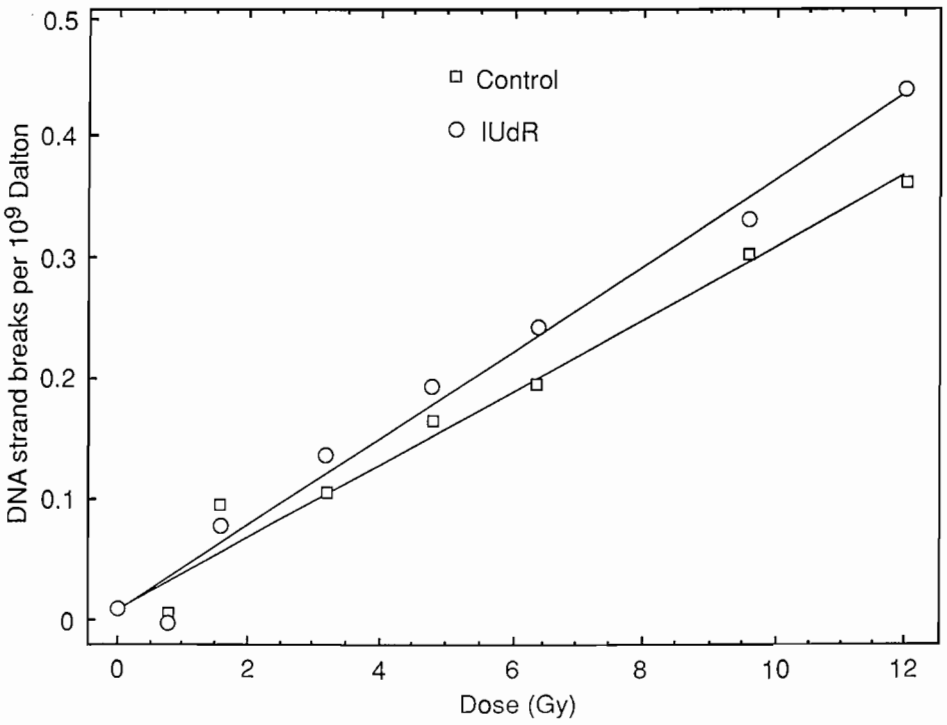

FIG. 2. Residual DNA strand breaks after 60 min of repair at 37°C in control and IUdR labeled cells as a function of radiation dose. The data were fitted by the least squares method.

between the two treatments after 120 min repair seems to be most pronounced in the low dose range.

DISCUSSION

The results show that replacement of thymidine by IUdR into cellular DNA sensitizes the cells to a subsequent exposure to low-energy X rays and this effect persisted after a prolonged incubation. The DNA strand breaks remaining after 60 min of incubation (repair phase) are assumed to be double-strand breaks or other severe DNA damage since the single strand breaks are repaired within 10 to 20 min of incubation (unpublished data). We therefore suggest that the observed increase in radiation damage per unit radiation dose

(A)

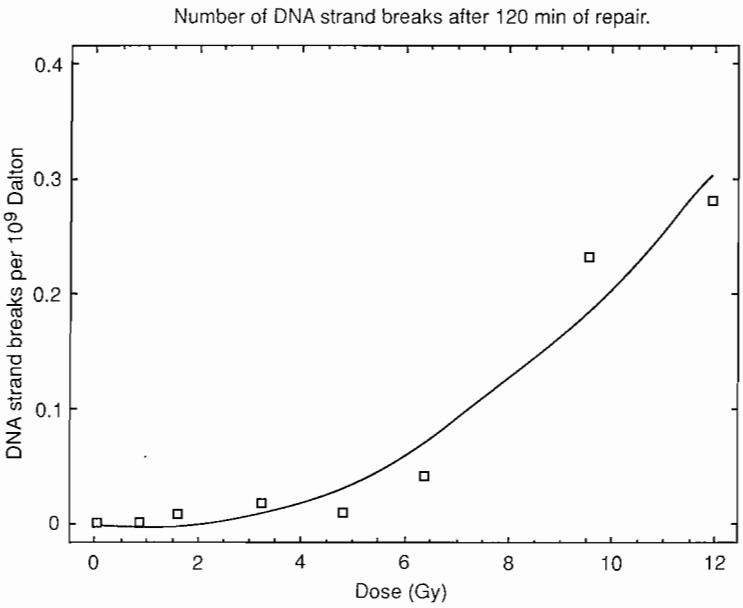

(B)

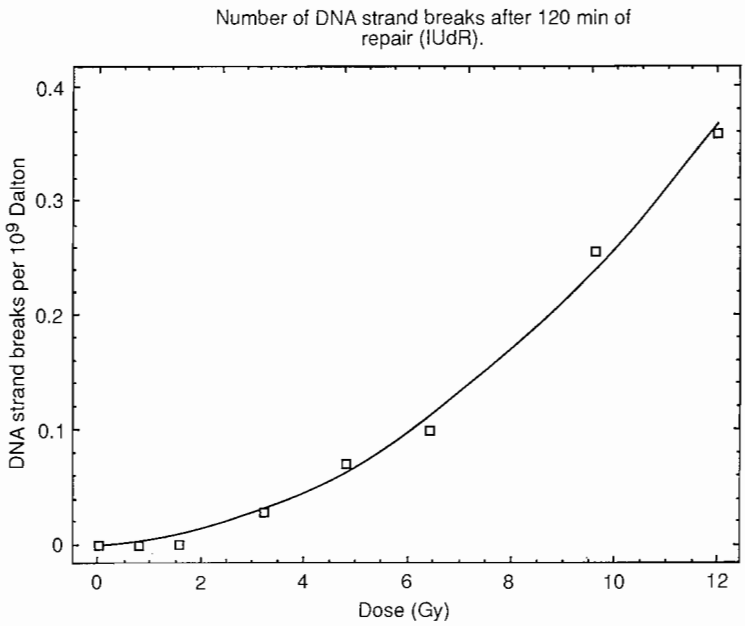

FIG. 3. Residual DNA strand breaks after 120 min of repair at 37°C in (A) control and (B) IUdR labeled cells as a function of radiation dose. The data were fitted to the linear quadratic model.

in IUdR labeled cells is an indication that more severe damage such as DNA double-strand breaks have been induced relative to the controls. This enhancement may be due to Auger processes, and previous survival studies support the possibility that a high-LET component might be involved in the radiation response of IUdR labeled cells (13). Our results are also consistent with findings by Shinohara *et al.* (21) who suggested that X irradiation of IUdR labeled HeLa cells induces critical DNA lesions for cell lethality.

Kinsella *et al.* (17,18) using the filter elution technique reported an enhancement factor of about 1.5 for double-strand break induction and repair in V79 cells after 23% replacement of thymidine bases. This ratio agrees fairly well with our results considering the differences in thymidine replacement. They also reported a higher enhancement factor for BrUdR than for IUdR which is not consistent with the photoactivation hypothesis proposed by Fairchild *et al.* (10).

There is growing evidence suggesting that double-strand breaks are the ultimate lesion involved in the formation of chromosome aberrations (22,23). In a previous study on micronuclei formation (16), a dose-modifying factor of 1.3 was obtained which is in agreement with the data from the DNA strand break studies. This similarity is particularly interesting because it suggests a cause-effect relationship between the two phenomena.

CONCLUSION

Irradiation with low-energy X rays was 1.2 times more efficient in inducing DNA strand breaks in IUdR labeled cells than in control cells. After repair, the corresponding value had increased and, according to the α/β model, more double-strand breaks seem to be induced in IUdR labeled cells. The results, however, give no ultimate answer to the possible involvement of Auger electrons in the radiation response after IUdR incorporation.

ACKNOWLEDGMENTS

We would like to thank Sven Richter for help with the dosimetry and irradiating of the cells, Ulla Johanson and Gertruda Ludwikow for performing the DNA strand break analysis. This work was supported by the Swedish Cancer Society.

REFERENCES

1. N. GELIHAS, M.A. RICH, and M.L. EIDINOFF, Radiosensitization of a mammalian cell line with 5-bromodeoxyuridine. *Radiat. Res.* **17**, 479-491 (1962).
2. J.T. LETT, G. PARKINS, and P. ALEXANDER, Mechanisms of sensitization to X rays of mammalian cells by 5-bromodeoxyuridine. *Nature* **203**, 593-596 (1964).
3. R.M. HUMPHREY and W.C. DEWEY, Radiosensitivity of normal and 5-bromodeoxyuridine treated mammalian cells during different phases of the cell cycle. *Exp. Cell Res.* **39**, 483-495 (1965).
4. W.C. DEWEY, L.E. STONE, H.H. MILLER, and R.E. GIBLAK, Radiosensitization with 5-bromodeoxyuridine of Chinese hamster cells x-irradiated during different phases of the cell cycle. *Radiat. Res.* **47**, 672-688 (1971).
5. W.U. SHIPLEY, M.M. ELKIND, and W.B. PRATHER, Potentiation of X ray killing by 5-bromodeoxyuridine in Chinese hamster cells: A reduction in capacity for sublethal damage accumulation. *Radiat. Res.* **47**, 437-449 (1971).
6. H.S. KAPLAN, K.C. SMITH, and P.A. TOMLIN, Effect of halogenated pyrimidines on radiosensitivity of *E. Coli*. *Radiat. Res.* **16**, 98-113 (1962).
7. T.L. PHILLIPS, W.J. BODELL, V. UHL, G.Y. ROSS, J. RASMUSSEN, and J.B. MITCHELL, Correlation of exposure time, concentrations and incorporation of IdUrd in V79 cells with radiation response. *Int. J. Radiat. Oncol. Biol. Phys.* **16**, 1251-1255 (1989).
8. B. GOZ, The effects of incorporation of 5-halogenated deoxyuridines into the DNA of eukaryotic cells. *Pharmacol. Rev.* **29**, 249-272 (1985).
9. W. SZYBALSKI, X ray sensitization by halopyrimidines. *Cancer Chemother. Rep.* **58**, 539-557 (1974).
10. R.G. FAIRCHILD and V.P. BOND, Photon activation therapy. *Strahlentherapie* **160**, 758-763, (1984).
11. S. SUNDELL-BERGMAN, R. BERGMAN, and K.J. JOHANSON, Chromosome damage induced by decay of ^{3}H and ^{125}I incorporated into DNA of Chinese hamster cells. *Mutat. Res.* **149**, 257-263 (1985).
12. K.G. HOFER and W.L. HUGHES, Radiotoxicity of intranuclear tritium, iodine-125 and iodine-131. *Radiat. Res.* **47**, 94-109 (1971).
13. S. SUNDELL-BERGMAN, K.J. JOHANSON, R. RICHTER, and P. ÖSTBERGH, Enhancement of radiation sensitivity in iododeoxyuridine labeled cells exposed to low energy X rays. *Acta Oncol.* **29**, 623-626 (1990).
14. R. NATH, P. BONGIORNI, and S. ROCKWELL, Enhancement of IUdR radiosensitization by low-energy photons. *Int. J. Radiat. Oncol. Biol. Phys.* **13**, 1071-1079 (1987).
15. K.H. CHADWICK and H.P. LEENHOUTS, The molecular theory of radiation biology. *Monographs on Theoretical and Applied Genetics* 5. Berlin, Springer Verlag, 1981.
16. G. LUDWIKOW, C.G. STALNACKE, K.J. JOHANSON, S. SUNDELL-BERGMAN, and S. RICHTER, Microscopic and flow cytometric study of micronuclei in iododeoxyuridine labeled cells irradiated with soft X rays. *Acta Oncol.* **29**, 761-767, (1990).

17. T.J. KINSELLA, P.P. DOBSON, J.B. MITCHELL, and A.J. FORNACE Jr., Enhancement of x ray induced DNA damage by pretreatment with halogenated pyrimidine analogs. *Int. J. Radiat. Oncol. Biol. Phys.* **13**, 733-739 (1987).
18. A.J. FORNACE Jr., P.P. DOBSON, and T.J. KINSELLA, Enhancement of radiation damage in cellular DNA following unifilar substitution with iododeoxyuridine. *Int. J. Radiat. Oncol. Biol. Phys.* **18**, 873-878 (1990)
19. B. RYDBERG, Detection of induced DNA strand breaks with improved sensitivity in human cell. *Radiat. Res.* **81**, 492-494 (1980).
20. B. SANDSTROM and K.J. JOHANSON, A direct assay for detection of chemically induced changes in the rejoining kinetics of radiation induced DNA strand breaks. *J. Biochem. Biophys. Methods* **14**, 183-190 (1987).
21. K. SHINOHARA, H. NAKANO, and H. OHARA, Estimation of protectable fraction by cysteamine in 5-iododeoxyuridine labeled HeLa cells irradiated with X rays or Co-60-gamma-rays. *Abstr. Proc. of the 8th Intern. Congr. of Radiat. Res.* July, 1987.
22. G. OBE, A.T. NATARAJAN, and F. PALITTI, Role of doublestrand breaks in the formation of radiation-induced chromosomal aberrations. *Progress in Mutat. Res.* **4**, 1-9 (1982).
23. P.E. BRYANT, Enzymatic restriction of mammalian cell DNA using Pvu II and Bam H1: Evidence for the double-strand break origin of chromosomal aberrations. *Int. J. Radiat. Biol.* **46**, 75-65 (1984).

DISCUSSION

Martin, R. Have you compared OER for the two cell populations (re ± IUdR)?

Johanson, K. J. No. In order to study possible high-LET effects we have performed some studies using low dose rate.

Baverstock, K. F. What was the dose rate?

Johanson K. J. 0.16 Gy/min.

Halpern, A. It is customary to use the term "double labeling" for cases where the molecule contains two isotopes, not for the mixture of two singly-labeled molecules.

Johanson, K. J. When using liquid scintillation techniques for detection of radionuclides, the term double (or dual) labeling is often used when two radionuclides are mixed in the scintillation vials.

Goodhead, D. T. What do you suggest might be the reason for the curvature in the dose response for strand breaks after 120 min repair? Is this not surprising if you are measuring ssb?

Johanson, K. J. The unwinding technique measures both single strand breaks and double strand breaks. After 120 min of repair, there are mostly double strand breaks left unrepaired. I have no good suggestion which can explain the reason for the curvature. In the control cells it seems to be a

threshold and then a linear increase. In IUdR containing cells, the threshold seems to disappear but the linear part has a rather similar shape to the control. Thus, it seems that a more serious DNA damage is induced in IUdR containing cells.

Biophysical Aspects of Auger Processes, AAPM Symposium Series No. 8 (1992) 091-105
Eds. RW Howell, VR Narra, KSR Sastry, DV Rao

THE BIOLOGICAL EFFICACY OF INDUCED AUGER CASCADES: COMPARISON OF IODINE AND BROMINE AS TARGET ATOMS

BRENDA H. LASTER[1,5], WILLIAM C. THOMLINSON[1,2], JOHN KALEF-EZRA[1,3], VILI BENARY[1,4], EDWIN A. POPENOE[1], VICTOR P. BOND[1], CHRIS GORDON[1], LYNNE WARKENTIEN[1], NICHOLAS GMÜR[2], NANCY LAZARZ[2], and RALPH G. FAIRCHILD[1]

[1]Medical Department, [2]National Synchrotron Light Source
Brookhaven National Laboratory, Upton, NY 11973

[3]University of Ioannina, Ioannina, 451.10 Greece

[4]Tel Aviv University, Tel Aviv, Israel

[5]Department of Radiation Oncology
University Hospital at Stony Brook, Stony Brook, NY 11794

ABSTRACT

Photon Activation Therapy (PAT) has been postulated as a binary system for the treatment of malignant brain tumors. PAT proposes the clinical administration of iododeoxyuridine (IUdR) followed by irradiation with radioactive sources (^{145}Sm, 40 keV γ rays) interstitially implanted via brachytherapy techniques. The radiosensitizing properties of halogenated pyrimidines are well known (1-3). This study was undertaken to compare the biological efficacy of the Auger cascades following an induced photoelectric effect in iodine or bromine target atoms using synchrotron radiation.

To document if Auger electron emission would increase the effectiveness of a dose (in addition to the enhancement from sensitization) delivered to mammalian cells, a series of experiments were conducted at the Brookhaven National Laboratory (BNL). Either iodine (K absorption edge = 33.17 keV) or bromine (K edge = 13.47 keV) was introduced into the DNA of exponentially growing V79 Chinese hamster cells during cell replication through the analog nucleosides, iododeoxyuridine (IUdR) or bromodeoxyuridine (BrUdR), replacing the DNA precursor thymidine. The percent replacement of thymidine by the substituted halogenated pyrimidines was determined by neutron activation analysis of digested cell samples. Control cells, without incorporated halogen, and halogenated cells irradiated below the K absorption edge of the halogen, were used to separate the radiosensitization enhancement component as distinct and apart from any observable enhancement attributable to the induced Auger cascades. An Auger effectiveness factor (AEF) resulting from the combined effect of the X rays and the Auger electron emission, was obtained by comparing the ratios of the D_{10} and D_0 values for the halogenated cells irradiated above and below their respective absorption edges. Monochromatic photons above and below the K absorption edge of each halogen were obtained at the National Synchrotron Light Source (NSLS) at the Brookhaven National Laboratory. Cells were irradiated at a dose rate of 0.65 Gy/min. Data analyses were based on curve fits using both the linear-quadratic and single-hit multi-target models.

An Auger Effectiveness Factor of 1.4 was observed for iodinated cells when comparing irradiations with 33.4 and 32.9 keV photons. However, brominated cells, irradiated at 13.5 and 13.4 keV failed to show a similar response. The AEF observed for bromine was 1.0. Sensitization enhancement due to the incorporated halogen was 2.2 for both iodine and bromine. The total therapeutic gain factor for iodinated cells was, therefore, 1.4 X 2.2 = 3.1, and for brominated cells, 2.2. These results indicate that IUdR is the better of these two halogens for both demonstrating the Auger effectiveness in biological experiments, and for providing a clinical therapeutic advantage for PAT.

INTRODUCTION

The halogenated pyrimidines, 5-bromo-2'-deoxyuridine (BrUdR) and 5-iodo-2'-deoxyuridine (IUdR), are incorporated in cellular DNA during cell

replication as analog nucleosides replacing the natural DNA precursor, thymidine (Thd). Having demonstrated radiosensitizing properties (1,2), it was anticipated that ^{125}IUdR would serve as an endoradiotherapeutic agent, seeking and being taken up by malignant tumor cells during cell replication, thus, providing radiation directly to the DNA, the presumed critical target of cells. However, uptake of the analogs was not restricted to tumor cells alone, since all rapidly proliferating tissue competed for IUdR uptake as avidly as did the tumor. Normal proliferative tissue accrued severe biological damage due to the incorporation of the ^{125}I label. This was attributed to the emission of Auger electrons as an inherent part of the photoelectric process initiated by the electron capture and internal conversion events during the radioactive decay of the iodine-125 (3). While the use of the radiolabeled analog nucleoside was precluded due to its severe biological toxicity, it was postulated that irradiation with photons above the K absorption edge of stable halogens could induce a photoelectric effect and concommitant Auger cascades (4). To propose a feasible radiotherapeutic modality, it was necessary to consider a means of delivering the radiation locally to avoid the problem of poor penetration associated with the low energy of the photons required for inducing a photoelectric effect.

Photon Activation Therapy was proposed by Fairchild *et al.* (5) as a radiotherapeutic technique for the treatment of malignant brain tumors. Stable IUdR, in addition to radiosensitizing tumor cells, would be activated by photons above the K absorption edge of iodine (33.2 keV); samarium-145, emitting 40 keV photons, would be interstitially implanted into the tumor via brachytherapy techniques.

The present work was undertaken to document the therapeutic gain which might be achieved from the high-LET type damage in DNA resulting from the induction of a photoelectric effect and the release of Auger electrons. It was designed to separate the contribution to cellular damage from radiosensitization alone and from any increased effectiveness resulting from the combined effect of the X rays and the Auger electrons. V79 Chinese hamster cells, with either BrUdR or IUdR incorporated in DNA, were irradiated with monochromatic photons obtained from the National Synchrotron Light Source at the BNL. Irradiations were carried out at energies above and below the respective edges of the halogens, 33.4 and 32.9 keV for iodine, and 13.5 and 13.4 keV for bromine. The cell preparation, irradiation procedure and geometry was identical in both cases. The plating efficiency was similar. The data were analyzed and fit using the same software (6).

MATERIALS AND METHODS

Incorporation of Halogenated Pyrimidines in Cellular DNA

V79 Chinese hamster cells in exponential growth were incubated with Dulbecco's Modified Eagle's growth medium[1], consisting of 10% dialyzed fetal bovine serum[1], 0.1 mM hypoxanthine[2], 1.0 μM aminopterin[2], 2.0 μM L-glutamine[1], 6.0 μM IUdR or BrUdR[2], and 4.0 μM thymidine[2], for one cell cycle (~14 h) at 37°C in a humidified environment, 95% air, 5% CO_2. After this "pulsing" period, cell monolayers were washed 3X with 1% PBS[1], trypsinized[1], harvested and counted. Control cells were treated similarly, receiving 10 μM thymidine, and no halogen. Aliquots corresponding to a cell density of 3.0×10^5 cells/ml were prepared and 120 μl of this cell suspension were placed in 250 μl polypropylene tubes for irradiation. Cells from the same iodinated or brominated dish were taken for the above and below K edge irradiations to assure identical uptake of the halogen. All cell processing, including the irradiation, was carried out under amber light to minimize any effects of photosensitization. Replicate dishes were harvested similarly and processed for neutron activation analysis to determine the amount of halogen present. This procedure is described below.

Cell Digestion Procedure for Neutron Activation Analysis

After counting the cells in suspension, cells were centrifuged at 1500 RPM and pelletized 3X, following their resuspension in TCA (5% w/v) and EtOH, then finally digested in 2.5 ml formic acid (88%) for 10 min in a 60°C hot water bath. A 1.2 ml aliquot of this TCA-insoluble fraction was placed in a 1.8 ml cryogenic vial for activation. Following activation, 1 ml of the sample was transferred to a new, non-activated 1.5 ml Eppendorf tube to increase the signal-to-noise ratio.

Neutron Activation Analysis (NAA) for Quantifying Halogen Uptake

The 1.8 ml cryogenic vial was placed in a transporting sleeve or "rabbit" for pneumatic passage through a tangential tube to a position adjacent to the core of the reactor. A 2 μg/ml iodine or bromine standard was treated

---

[1]Gibco
[2]Sigma

similarly and activated simultaneously. Subjected to a thermal neutron fluence of 3.0×10^{12} thermal neutrons cm^{-2} at a reactor power level of 1 Megawatt for 10 minutes (iodine) and 1.25 Megawatt for 30 minutes (bromine), ^{127}I atoms were converted to ^{128}I ($\tau_{1/2}$ = 25 min). The 443 keV γ ray from ^{128}I was counted with a sodium iodide detector. The stable isotopes of bromine (^{79}Br = 50.6% abundance and ^{81}Br = 49.4% abundance) produced ^{80}Br and ^{82m}Br upon activation. The two peaks (554.3 and 776.5 keV) were counted 18.5 h post-activation to allow for the decay of radionuclides having interfering energies.

Calculation of Percent Uptake of Halogen

Assuming that an asynchronously growing population of cells has 8×10^{-12} g of DNA/cell (personal communication, S.L. Commerford), the average molecular weight of all DNA bases is 309, the molar amount of all DNA bases is 2.8×10^{-14} moles/cell and that Thd constitutes 29.4 mole percent of all DNA, the thymidine content is 7.51×10^{-15} moles/cell. The molar concentration of iodine in the cell sample was established by taking the ratio of counts in the sample and in the standard, and converting the mass of halogen in grams to a molar concentration. The ratio between the molar concentration of halogen and the molar concentration of Thd calculated to be present in the sample determined the percent incorporation in DNA.

Irradiation Procedure

The 250 µl tapered tube containing the cell suspension was positioned horizontally in a vertically oscillating scanner, designed for these experiments, with a stroke of 0.96 cm at 4.73 sec intervals. This stroke assured that the cells oscillated completely through the collimated beam, thus providing a uniform dose to all cells. For the bromine experiments, the cells were rotated about the horizontal axis at 330 rpm to assure uniform penetration of the photons. The photon source for the iodine experiments was the X17B1 wiggler magnet operating at a magnetic field of 4.9 Tesla; the X18B bending magnet (1.2 T) beam line was used for the bromine experiments. A bent Laue geometry Si (111) monochromator selected the above and below K edge X rays for the iodine experiments. A Si (220) double crystal monochromator was used for the bromine. The beam dimensions at the position of the cells were 0.8 mm X 27 mm, and 2 mm X 25 mm for iodine and bromine, respectively. The cell scanner was positioned downstream of a fast computer-activated shutter, slits which collimated the monochromatic

beam, and a 10 cm long ion chamber. The ion chamber was filled with 1 atmosphere of argon and an accelerating voltage of 300 V was used. The samples and the cell scanner were inside a Pb shielding enclosure in the beamline hutch. The energy of the monochromator was calibrated by scanning the monochromator through the absorption edge of an iodine or bromine sample. The inflection points of the absorption curves were defined to be exactly 33169 and 13474 eV for iodine and bromine, respectively.

All the experiments were performed in the mode in which dose was delivered for a predetermined number of ion chamber scaler counts. The ion chamber signal was amplified by a Keithley 427 Current Amplifier at a gain of 10^7, and converted to scalar counts by a Voltage/Frequency at 1 volt/103 Hz. This mode of operation automatically compensated for the effect of the decreasing storage ring current.

The number of scalar counts at each energy necessary for delivery of a predetermined dose to the cells was calculated from measured coefficients. With the monochromator set at an energy, LiF thermoluminescent dosimeters (TLDs) were put inside a sample tube and oscillated through the beam for a predetermined number of scalar counts. The TLDs were then read and the dose/count coefficient was thereby determined. The accuracy of the coefficient was improved by repeating this procedure many times at both energies. The TLDs were distributed inside the tubes to measure any variation in dose with position. No such variations were found. Dosimetry calibration runs were conducted before and after each experiment to verify consistency of experimental parameters. Dosimetry runs in which the monochromatic beam was prevented from impinging on the TLDs showed no dose delivered from scattered radiation in the hutch. The maximum error in the dose delivered due to the indeterminate starting point of oscillation was less than 2% for the lowest doses and less than 0.25% for the highest. Closure time for the fast shutter was less than 0.1 s, so the maximum additional dose delivered after the closure command was less than 0.8%.

Irradiation Dosimetry

Dose measurements were performed with thermoluminescent dosimeters (TLD-700, 1 mm X 1 mm X 6 mm) inserted in the same irradiation tubes and irradiated under the same conditions as the cell suspensions.

The average absorbed dose to water was calculated using the following relation:

$$D_{H_2O} = \left(\frac{\mu_{en}}{\rho}\right)_{H_2O/TLD} \bullet \frac{S(H_2O)}{S(TLD)} \bullet \frac{f^{\gamma}(D)}{f^{x}(D)} \bullet D_{TLD}$$

where $(\mu_{en}/\rho)_{H_2O/TLD}$, or the ratio of the mass energy absorption coefficient of the photons in water and in the TLD,

$S(H_2O)$, the self-shielding factor $1\text{-}e^{-\mu d}/\mu d$ for the water in the tube

S(TLD), the self-shielding factor $1\text{-}e^{-\mu d'}/\mu d'$ for the TLD
$f^{x}(D)$ and $f^{\gamma}(D)$ the supralinearity factor for the X and γ field, respectively, and

D(TLD), the absorbed dose for the calibration ^{60}Co field that is required to produce the same TL-signal as the X ray field, corrected for energy dependence.

Since the photon beam is plane parallel, the average path length d' of the photon in the dosimeter was assumed to be 82% of the thickness of the dosimeter (*i.e.*, 0.82 mm), and d is $2^{-1/2}$ times the diameter of the water in the tube. The dosimeters were calibrated individually by irradiation in a known field (^{60}Co source) both before and after the measurements. Pre-irradiation annealing was carried out at 400°C for one hour, post-irradiation annealing at 100°C for 15 min. A one-hour cooling time was used in both procedures. Twenty eight TLD dosimeters were irradiated before and in between cell irradiations.

Colony Assay for Cell Survival

After irradiation, cells were plated in 60 mm petri dishes with DME complete growth medium (FBS[3] , pen-strep-fungizone[1]), and permitted undisturbed colony growth for 5 days. After washing with PBS, colonies were fixed with EtOH, and stained with Giemsa. Colonies were counted opto-electronically on an Artec counter, adjusted to exclude colonies consisting of

[3] Hyclone

fewer than fifty cells. Survival curves were fit using an iteratively-weighted least squares analysis program as described in Ref. 6. Both the linear quadratic (LQ) and single-hit-multi-target (SHMT) models were used.

RESULTS

Cell survival curves obtained after irradiation with monochromatic photons (33.4 and 32.9 keV for above and below the K absorption edge of iodine, respectively) with a ~16% IUdR replacement in DNA are shown in Fig. 1 (LQ) and Fig. 2 (SHMT). Table I summarizes the data obtained from three experiments in composite form. The AEF is 1.4 when comparing iodinated cells irradiated above and below the K edge using the ratio of doses

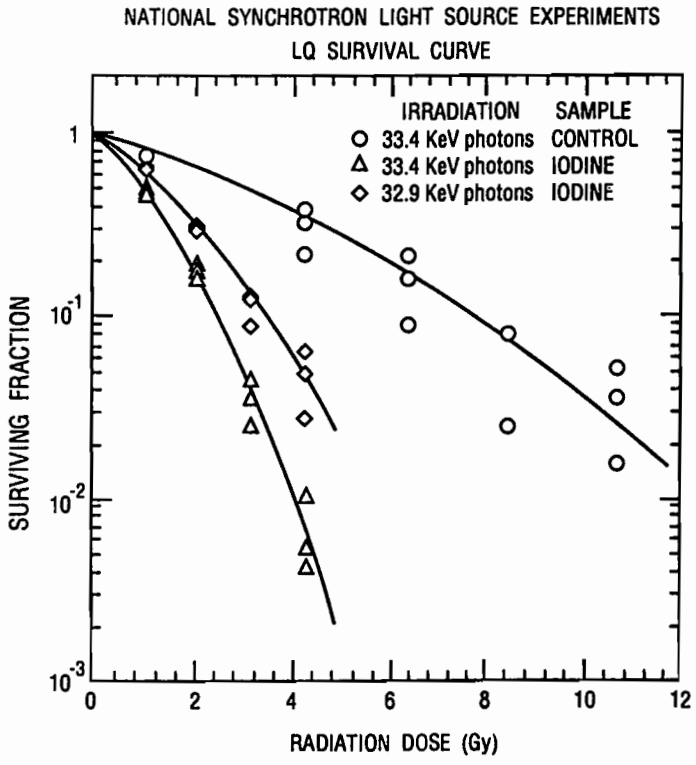

FIG. 1. V79 Chinese hamster cell survival assay post irradiation with monochromatic photons above and below the K absorption edge of iodine. Curves were least squares fit with the linear-quadratic model as in Ref. 6. IUdR incorporation ~16%.

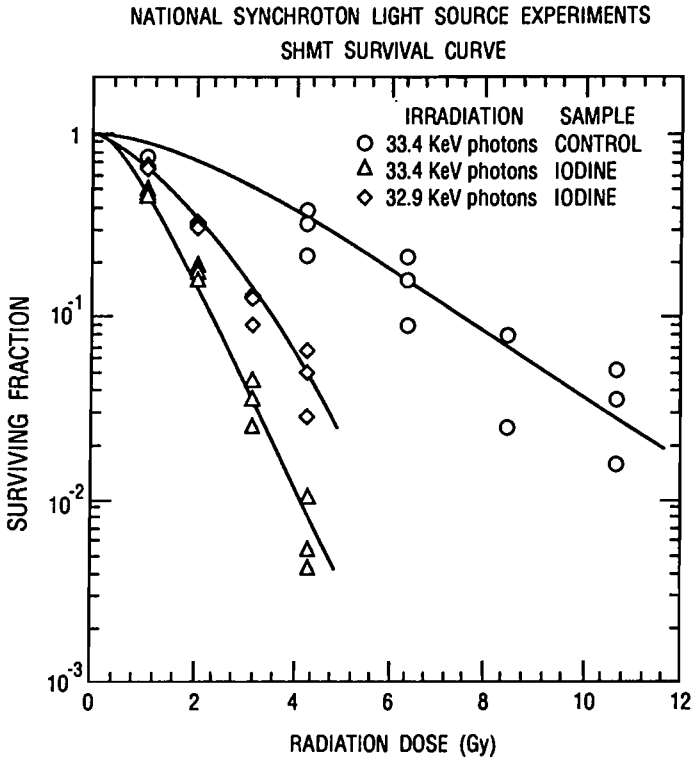

FIG. 2. V79 Chinese hamster cell survival following irradiation with monochromatic photons above and below the K absorption edge of iodine. Curves were fit with single-hit multi-target model as in Ref. 6. IUdR incorporation ~16%.

at a 10% level of survival (LQ). Using the ratio of doses at the D_0 values the factor is ~1.5. The sensitization enhancement ratio (SER) compares the ratio of doses between non-iodinated control cells and iodinated cells irradiated below the K absorption edge. At 10% survival, the SER is 2.2. Thus, the total therapeutic gain factor is the product of the SER and the AEF, 1.4 X 2.2 = 3.1.

Survival curves from cells with a ~60% BrUdR replacement in DNA are shown in Figs. 3 (LQ) and Fig. 4 (SHMT) after irradiation with monochromatic photons. Table II is a summary of these experiments. Photon energies of 13.5 and 13.4 keV were used for the above and below K edge

TABLE I
Monochromatic X ray Irradiation of IUdR Labeled V79 Cells

Sample	Dose (Gy) @ 10% Survival		D_o[a]	Therapeutic Enhancement @ 10% Survival		Gain Enhancement from Ratio of D_o Values	Auger Effectiveness Factor[b]	
	LQ	SHMT		LQ	SHMT		@ D_{10}	D_o[a]
Control	7.63	7.49	2.39					
Iodinated, above K[c]	2.53	2.46	0.74	3.02 ± 0.23	3.05 ± 0.49	3.20 ± 0.51	1.38	1.51
Iodinated, below K[d]	3.49	3.46	1.1	2.19 ± 0.16	2.17 ± 0.33	2.13 ± 0.32		

[a]SHMT only
[b]Ratio of doses or slopes (iodine below: iodine above)
[c]at energy above K edge
[d]at energy below K edge

irradiations, respectively. The SER determined at 10% survival is 2.2, or 1.94 if based on the ratio of the D_0 values. The total therapeutic gain factor is 2.2 (SER) X 1.0 (AEF) = 2.2.

DISCUSSION

While the IUdR showed a significant and demonstrable enhancement of the dose effectiveness resulting from the release of the Auger electrons, the results with the BrUdR were rather tenuous. The bromine data fell within the statistical error which interferes with the ability to distinguish an effect. However, the observed sensitization enhancement comparing unhalogenated control cells with their iodinated or brominated counterparts at 10% survival, when irradiated below their respective K edges, is 2.2 for both. This value was obtained despite a difference in halogen uptake, the bromine uptake being a factor of 4 greater than the iodine. Sensitization has

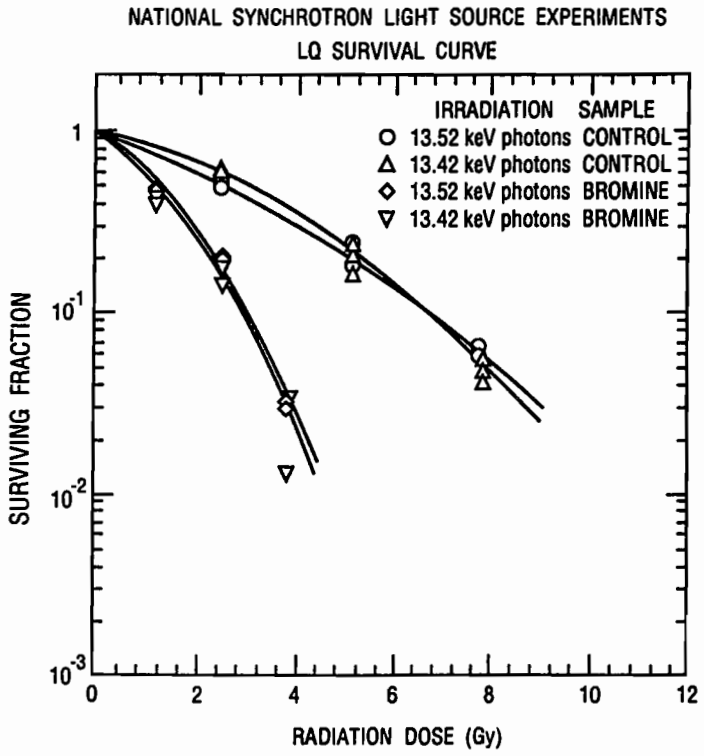

FIG. 3. V79 Chinese hamster cell survival assay post irradiation with monochromatic photons above and below the K absorption edge of bromine. Curves were fit with the linear-quadratic model as in Ref. 6. BrUdR incorporation ~60%.

been shown to increase with increased incorporation of the halogen (1). Our results show neither increased sensitization with bromine, nor any increased effectiveness attributable to Auger electron emission. This result will have to be investigated further.

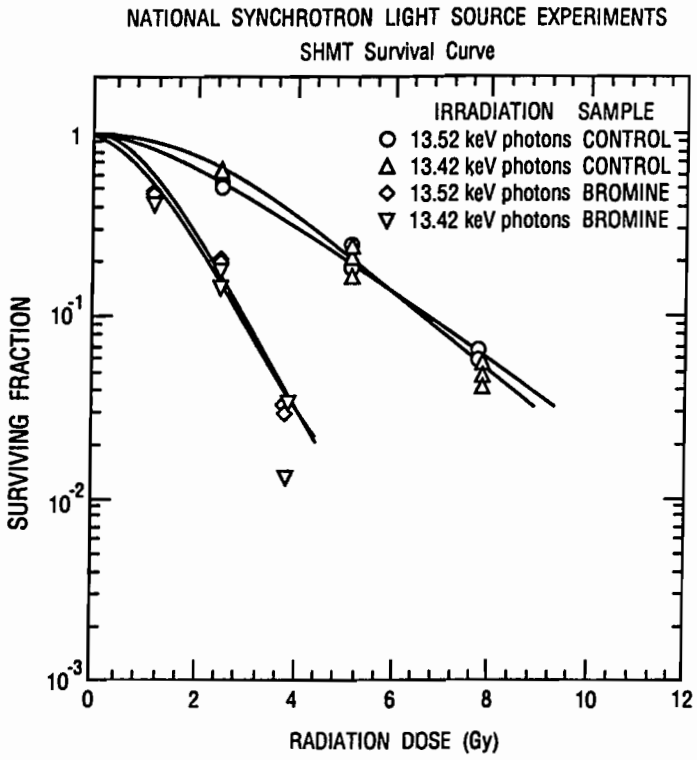

FIG. 4. V79 Chinese hamster cell survival after irradiation with monochromatic photons above and below the K absorption edge of bromine. Curves were fit with the single-hit multi-target model as in Ref. 6. BrUdR incorporation ~60%.

TABLE II
Monochromatic X ray Irradiation of BrUdR Labeled V79 Cells

Sample	Dose (Gy) @ 10% Survival		D_o[a]	Therapeutic Enhancement @ 10% Survival		Gain Enhancement from Ratio of D_o Values	Auger Effectiveness Factor[b]	
	LQ	SHMT		LQ	SHMT		@ D_{10}	D_o[a]
Control	6.83	6.74	2.23					
Iodinated above K[c]	3.13	3.08	0.89	2.18 ± 0.09	2.19 ± 0.38	2.51 ± 0.44	0.99	1.1
Iodinated below K[d]	3.09	3.04	0.98	2.21 ± 0.11	2.21 ± 0.41	1.94 ± 0.36		

[a]SHMT only
[b]Ratio of doses or slopes (bromine below: bromine above)
[c]at energy above K edge
[d]at energy below K edge

CONCLUSION

IUdR, demonstrating a 40-50% increased effectiveness of the dose from the combined effect of X rays above the K absorption edge of the iodine and the concommitant Auger electron emission, appears to be superior to BrUdR for use in PAT.

ACKNOWLEDGMENTS

The authors are very grateful to Dr. L. Wielopolski for his advice and assistance in developing the NAA technique, and to Ms. A. Ruggiero for preparing this manuscript.

REFERENCES

1. R.L. ERIKSON and W. SZYBALSKI, Molecular radiobiology of human cell lines III. Radiation-sensitizing properties of 5- iododeoxyuridine. *Cancer Res.* **23**, 122-130 (1963).
2. R.L. ERIKSON and W. SZYBALSKI, Molecular radiobiology of human cell lines V. Comparative radiosensitizing properties of 5-halodeoxycytidines and 5-halodeoxyuridines. *Radiat. Res.* **20**, 252-262 (1963).
3. L.E. FEINENDEGEN, Biological damage from the Auger effect, possible benefits. *Radiat. Envir. Biophys.* **12**, 85-99 (1975).
4. G. TISLJAR-LENTULIS, L.E. FEINENDEGEN, and V.P. BOND, Biological radiation effects on the incorporation of moderately heavy nuclei in the tissue and the use of soft X-rays. *Strahlentherapie* **145**, 656-662 (1977).
5. R.G. FAIRCHILD, A.B. BRILL, and K.V. ETTINGER, Radiation enhancement with iodinated deoxyuridine. *Invest. Radiol* **17**, 407-415 (1982).
6. N. ALBRIGHT, Computer programs for the analysis of cellular survival data. *Radiat. Res.* **112**, 331-340 (1987).
7. W. THOMLINSON, D. CHAPMAN, N. GMÜR, and N LAZARZ, The superconducting wiggler beamport at the National Synchrotron Light Source. *Nucl. Inst. Meth. Phys. Res.* **A266**, 226-233 (1988).

DISCUSSION

Goodhead, D. T. Have you calculated the number of photons absorbed in incorporated iodine per cell (above the K shell edge) and compared this with the amount of extra killing that you see? I am surprised that there are sufficient absorptions to cause such an effect.

Laster, B. H. No, we have not. However, I would welcome someone more experienced to assist in this approach.

Halpern, A. What is the dose you are talking about? Exposure or absorbed dose? How do you determine it?

Laster, B. H. TLD's were inserted in to lucite holders and placed in the irradiation vessel (250 µl polypropylene tube). Calculating the average absorbed dose to H_2O:

$$[(\mu_{en}/\rho)_{H_2O/TLD}]\,[S_{H_2O}/S_{TLD}]\,[f^{\gamma}(D)/F^{x}(D)]\,[D_{TLD}]\,,$$

where, $(\mu_{en}/\rho)_{H_2O/TLD}$ = ratio of mass energy absorption coefficient of the photons in water and in the TLD, S_{H_2O} = self-shielding factor $(1-e^{-\mu d})/(\mu d)$ for the water in the tube, S_{TLD} = self-shielding factor $(1-e^{-\mu d'})/(\mu d')$ for the TLD, $f^{x}(D)$ and $f^{\gamma}(D)$ = supralinearity factor for x and γ field, D_{TLD} = the absorbed

dose for the calibration in the ^{60}Co that is required to produce the same TL signal as the X ray field. The average path length d' of photons in the dosimeter was assumed to be 0.82 mm, and d is 2.5 times the diameter of the tube in H_2O. The X ray energy is 13.424 keV. D_{H_2O} = 208.6 ± 6% for 1.324353×10^6 counts from ionization chamber = 157.5 rad/10^6 counts at 13.54 keV. D_{H_2O} = 213.9 ± 6% = 161.5 rad/10^6 counts.

106 Biophysical Aspects of Auger Processes, AAPM Symposium Series No. 8 (1992) 106-120
Eds. RW Howell, VR Narra, KSR Sastry, DV Rao

ELECTRON CAPTURE DECAY OF INDIUM-111 HUMAN CARBONIC ANHYDRASE I: A TIME DIFFERENTIAL K X RAY COINCIDENCE PERTURBED ANGULAR CORRELATION STUDY

CHRISTOPHER HAYDOCK

Research Computing Facility
Mayo Foundation, Rochester, MN, USA

ABSTRACT

The relaxation effects in the perturbed angular correlation spectra of ^{111}In human carbonic anhydrase I (HCA I) are the result of chemical transmutation and/or the complex Auger cascades that follow the electron capture decay of ^{111}In. Time differential K X ray coincidence perturbed angular correlation (PAC) spectroscopy shows that these relaxation effects are independent of the Auger cascade intensity. This suggests that chemical transmutation is responsible for the relaxation effects, and that bond breaking and damage product formation around the decay site resulting from localized energy deposition by Auger and Coster-Kronig electrons probably occur in the microsecond time regime. Numerical simulations of chemical transmutation relaxation effects in the time differential PAC spectrum of ^{111}In HCA I are also presented.

INTRODUCTION

Perturbed angular correlation spectroscopy (PAC) is a potential technique for investigating hot atom chemistry following electron capture decay of a radionuclide probe (1,2). As is the case with Mössbauer emission spectroscopy, it may be possible to identify the chemical form of the probe nuclide coordination complex during the nuclear lifetime (3,4). The average Auger and Coster-Kronig electron yield is significantly diminished when the vacancy cascade following electron capture includes the emission of a K X ray as compared to when it does not. It is in principle possible to study the dependence of hot atom chemistry on the intensity of Auger and Coster-Kronig emissions by detecting the nuclear radiations of perturbed angular correlation or Mössbauer emission spectroscopy in coincidence with K shell X rays (5,6). Given the very limited knowledge of hot atom chemistry of electron capture nuclides that are possible perturbed angular correlation probes, one may ask only a yes or no question. Does or does not the hot atom chemistry depend on electron emission intensity? To answer this, a chemical transmutation model, and a dose dependent damage model are constructed for the perturbed angular correlation spectra following electron capture. Both models encompass several alternative pictures of the hot atom chemistry. The simplest hot atom chemistry of the chemical transmutation model is very similar to β^+ decay on the nanosecond time scale. Note that β^+ decay is energetically forbidden for ^{111}In. The multiple Auger ionization processes are followed by complete electron recombination that leaves the daughter nuclide in a metastable state with both the atomic number and valence decreased by one unit from the parent. The metastable state is the result of the change in charge rather than charge neutralization or Auger electron irradiation. The metastable state of the daughter nuclide decays within tens of nanoseconds to the ground state coordination complex of the daughter and ligands. However, any hot atom chemistry involving an excited state of the daughter that decays thereafter into the ground state complex is equally consistent with the chemical transmutation model. The only requirement is that the excited state be independent of Auger emission intensity. The dose dependent damage model pictures radiolytic fragmentation of probe coordination complex ligands. The amplitudes and rates of ligand fluctuations increase with the intensity of the Auger emissions. Though uncertain about the details of hot atom chemistry, both models predict perturbed angular correlation spectra. The comparison of these spectra with experimental data indicates whether or not the hot atom chemistry during

the nanoseconds following electron capture depends on Auger emission intensity.

A partial decay scheme for ^{111}In and ^{111m}Cd is shown in Fig. 1. Perturbed angular correlation spectra of the isomeric ^{111m}Cd decay provide the quadrupole interaction parameters of the ground state coordination complex in the chemical transmutation model and the ligand relaxation parameters at zero dose in the dose dependent damage model. Following ^{111}In electron capture decay the ^{111}Cd daughter is in a 120 picosecond nuclear excited state that initiates the 171 - 245 keV gamma cascade. Processes occurring faster than the life time of this initial nuclear state, including dissipation of thermal hotspots (3,7), do not influence perturbed angular correlation spectra. The spectra reflect the hot atom chemistry occurring during the lifetime of the intermediate state. Indirect effects involving the diffusion of water radicals are not observed. A great variety of radiochemical and radiobiological experiments show that direct and indirect processes together result in damage

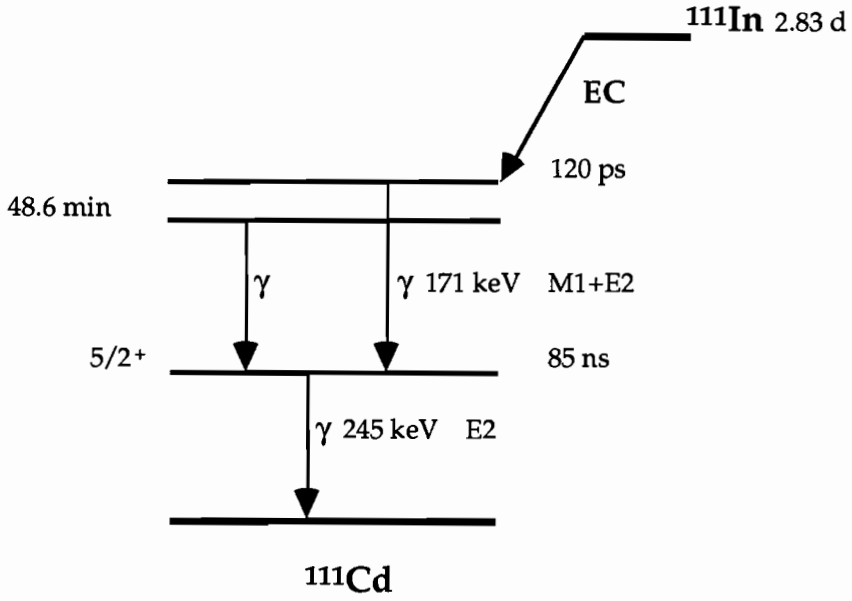

FIG. 1. Partial decay scheme for ^{111}In and ^{111m}Cd (9). The half-life of each level is labeled. The 171 - 245 keV gamma cascade follows the electron capture decay of ^{111}In; the 48.6 min ^{111m}Cd state decays by the 151 - 245 keV gamma cascade. Both cascades share the same 245 keV $5/2^+$ ^{111}Cd intermediate nuclear state.

that is proportional to the Auger emission intensity. For example, when zinc bovine carbonic anhydrase is X ray irradiated just above the zinc K edge, enzyme activity and zinc release assays indicate significant Auger inactivation (8). The more intense Auger emissions accompanying ^{111}In decay can be expected to inactivate HCA I even more effectively. The combined direct and indirect effects are Auger emission intensity dependent. An Auger dependent effect on the nanosecond time scale can be detected with K X ray coincidence perturbed angular correlation spectroscopy.

MATERIALS AND METHODS

Human carbonic anhydrase I was isolated from freshly outdated erythrocytes (10). The apoenzyme was obtained by dialysis at 4°C against pyridine-2,6-dicarboxylic acid (11). HCA I activity was assayed spectrophotometrically with p-nitrophenyl acetate (Sigma Chemical Co., St. Louis, Missouri) as substrate (12). Conventional time differential gamma-gamma perturbed angular correlation spectra of ^{111}In labeled HCA I were measured on a movable two detector perturbed angular correlation spectrometer (13). A 2 X 2 inch cylindrical BC-404 plastic scintillator with 0.25 inch centered side bore for internal sample mounting and RCA 8575 phototube detected the K X rays. Coincidence gating electronics, including a time to pulse height converter for coincidence timing of K X rays and the gamma-gamma cascade, selected either K X ray coincidence or anti-coincidence spectra for storage and analysis. Carrier free ^{111}In in 0.05 M HCl (Du Pont de Nemours & Co. Inc., Wilmington, Delaware) was ordered at two week intervals. ApoHCA I was incubated for 48 h with ^{111}In in 100 mM HEPES buffer (Research Organics Inc., Cleveland, Ohio) at pH 7.7 with sodium citrate acting as carrier for indium. In order to hold constant both the volume and total indium concentration, the specific activity of the ^{111}In stock was adjusted with cold indium chloride. After labeling with indium, the effects of HCA I rotational motions on the perturbed angular correlation spectrum were diminished by adding sucrose to a final concentration by weight of 50%. Seven labeled protein samples were prepared from each shipment of ^{111}In. A perturbed angular correlation spectrum was accumulated for 46 h from each sample. The first and last sample were run as incubation controls. These samples were measured for an initial twelve hours as indium-111 citrate; HCA I was added, and the measurement was continued for another 34 h. The time integral perturbation factors accumulated for 20 min intervals monitored the HCA I labeling reaction. All spectra from shipments that did

not give excellent labeling were discarded. Three of the five non-control samples per shipment were measured in K X ray coincidence mode and two in K X ray anti-coincidence mode. A total of 52 coincidence mode samples and 36 anti-coincidence mode samples were combined for analysis. All sample preparations and measurements were done at 21 ± 1°C.

Electron capture gamma-gamma perturbed angular correlation spectra measure the ensemble average electric quadrupole relaxation of the daughter nucleus spin. Magnetic dipole interactions are assumed to be negligible. The measurable parameters are model dependent. All models must contain one or more rate constants that characterize the time dependence of the quadrupole interactions. In the chemical transmutation model, spin relaxation is the result of the decay of a metastable state of the daughter nucleus coordination complex. This metastable state might be a valence electron, coordination geometry, or ligand conformation state. In any case, the quadrupole interaction parameters of the initial metastable state are the frequency mean, frequency standard deviation, asymmetry and the mean lifetime of the state. The initial state decays into the ground state coordination complex. The interaction parameters of the ground state are the frequency mean, frequency standard deviation, asymmetry, and Euler rotation angles relative to the initial state. The initial and ground state interaction frequencies are independent Gaussian distributions. Each individual daughter nucleus interacts with the initial and ground state coordination complexes at fixed quadrupole frequencies that are randomly and independently sampled from the respective Gaussian distributions. The lifetimes of the initial interactions are given by an exponential distribution. In addition to relaxation from coordination complex decay, the chemical transmutation model includes relaxation from overall molecular tumbling by multiplying the spectrum with an exponential factor.

The dose dependent damage model ascribes the spin relaxation to ligand reorientation in the coordination complex. The quadrupole interaction parameters of the coordination complex are the mean frequency, frequency standard deviation, asymmetry, rotation angle standard deviation, and jump rate. These five parameters depend linearly on dose to the coordination complex and have a baseline value for the zero dose coordination complex. The electric field gradient orientation distribution is defined by rotations from a reference orientation, where the rotation angle distribution is Gaussian and the rotation axis distribution is isotropic. Note that though there is a single reference orientation in this interaction model, the perturbed angular

correlation spectrum is for an isotropic source because the interactions of each daughter nucleus are averaged over random orientations when the spectrum is computed. The interaction frequency distribution is a Gaussian. Both the interaction frequency and orientation are sampled after every jump. The time intervals between jumps are exponentially distributed.

In both the chemical transmutation and dose dependent damage models, the interaction of each individual daughter nucleus is piecewise static and each set of model parameters specifies a probability distribution function for piecewise static interactions. The perturbation factor (which is loosely referred to as the perturbed angular correlation spectrum), is the average over this probability distribution of the perturbation factor of each piecewise static interaction. For a piecewise static interaction averaged over random source orientations, the perturbation factors are (13),

$$G_{kk}(t) = \sum_{m_a m_b N} (-1)^{2I+m_a+m_b} \begin{pmatrix} I & I & k \\ m'_a & -m_a & N \end{pmatrix} \begin{pmatrix} I & I & k \\ m'_b & -m_b & N \end{pmatrix}$$

$$\times \langle m_b|\Lambda(t)|m_a\rangle \langle m'_b|\Lambda(t)|m'_a\rangle^*, \qquad (1)$$

where k is an even index, t is the delay time between emission of the two gamma rays from the daughter nucleus gamma-gamma cascade, I is the spin of the intermediate nuclear state, m_a, m'_a, m_b, and m'_b index magnetic substates of the intermediate state, the matrix element coefficients are the Wigner 3-j symbols, and $\Lambda(t)$ is the piecewise static time evolution operator. Since only $G_{22}(t)$ is usually measurable, it is referred to as the perturbation factor. The index N takes all integer values with absolute value less than or equal to k and the primed magnetic substate indices are given by $m'_a - m_a + N = 0$ and $m'_b - m_b + N = 0$. Since the perturbation factor is always computed at a series of time points, it is appropriate to express the piecewise static time evolution operator as a series operator product of interval evolution operators. The interval evolution operator for the time interval (t',t) is a series operator product of static evolution operators,

$$\Lambda(t',t) = \prod_{j=J'}^{J} e^{-iH_j t_j/\hbar}, \qquad (2)$$

where H_j is the j^{th} time independent interaction Hamiltonian, J is the index of the first Hamiltonian with active interval overlapping (t',t), J' is the index

of the last Hamiltonian with active interval overlapping (t',t), and t_j is the time overlap of (t',t) and the active time interval of the j^{th} Hamiltonian. Matthias *et al.* (14) give the electric quadrupole Hamiltonian matrix elements for arbitrary intermediate spin, interaction frequency, asymmetry parameter, and y convention (15) orientation. The quadrupole interaction frequency is specified by the angular frequency ω_0. By definition, ω_0 equals 3 times the quadrupole interaction frequency for integer spin and 6 times the quadrupole interaction frequency for half integer spin. When the electric quadrupole Hamiltonian is axially symmetric $\omega_0\hbar$ equals the smallest nonvanishing eigenvalue difference. The angular frequency ω_0 is frequently reported with correct numerical value but with the erroneous dimension of Hertz (16).

The piecewise static perturbation factors were evaluated by repeated extension of the time evolution operators in increments of $0.025(2\pi/\omega_0)$, where ω_0 was the mean angular frequency of the ground state or zero dose coordination complex. The evolution operator at each time point was extended to the next time point by matrix multiplication with a time interval evolution operator. Each time interval evolution operator was a product of static evolution operators with the Hamiltonian indices and overlap intervals indicated in Eq. 2. The interaction Hamiltonians were diagonalized (17); the static evolution operators were expressed in diagonal form with the eigenvalues, transformed back into the magnetic substate representation with the eigenvectors, and multiplied together to give the time interval evolution operators. Since in the parameter domain of interest the perturbation factor time intervals were an order of magnitude smaller than the typical static Hamiltonian active time interval, most interval evolution operators were a single static evolution operator and each Hamiltonian diagonalization generated many interval evolution operators. The time interval evolution operators were repeatedly multiplied to give the evolution operators at a series of 160 time points. The matrix elements of the evolution operators were inserted in Eq. 1 to give the piecewise static perturbation factors at these time points.

The piecewise static perturbation factor probability distribution function was averaged by Monte Carlo integration (18). Perturbation factor error estimates were calculated from the deviation of subaverages around the overall average as a function of the spectrum delay time. Gaussian interaction frequency and rotation angle distributions were generated by summing uniform random variates. Excited state and orientation lifetimes were generated by logarithmic transform of uniform random numbers on the unit

interval. Isotropic rotation directions were generated by an acceptance-rejection technique (19). Random numbers uniform on the unit interval were generated by a 32-bit linear congruential pseudo-random generator with divisor 2^{31}-1 and multiplier 7^5.

Initially the qualitative dependence of the perturbation factor on parameter space of the chemical transmutation and the dose dependent damage models was coarsely surveyed. The chemical transmutation model metastable state lifetime, ground state rotation angle, and relative magnitude of the metastable and ground state mean interaction frequency parameters were varied. Based on the preliminary survey and known ground state coordination complex parameters, a crude estimate was made of the parameter point that fit the data. This fit was refined by varying the unknown parameters one at a time until the residuals were about the same magnitude as the experimental error. The chemical transmutation model ground state frequency mean, frequency standard deviation, and asymmetry and the overall tumbling relaxation time constant were fixed at the known values. The Euler rotation angles relative to the initial state were fixed at values found in the preliminary survey to give strong spin relaxation. The initial metastable state was assumed to be axially symmetric, and the frequency mean and frequency standard deviation were varied.

The preliminary dose dependent damage model parameter survey fixed the mean frequency, frequency standard deviation, and asymmetry parameters at the known zero dose coordination complex values, and varied the rotation angle standard deviation and jump rate parameters. By comparing the results of this search and the perturbation factor measured by Bauer *et al.* (20) with the assumption that spin relaxation is due to molecular tumbling, values were identified for the rotation angle standard deviation and jump rate parameters approximately equivalent to the molecular tumbling time constant of the zero dose coordination complex. The preliminary search also yielded the initial parameter point for fitting the dose dependent damage model to the data. The mean frequency, frequency standard deviation, asymmetry, rotation angle standard deviation and jump rate parameters were all varied.

During the preliminary parameter space searches and parameter refinement, the perturbation factors were computed by averaging 10^3 piecewise static interactions. The standard deviations of these perturbation factors were fairly independent of spectrum delay time and typically about

0.01. The displayed perturbation factors were averaged over 10^4 interactions to give a standard deviation of about 0.003. All calculations were done on a DEC VAX 3600 or Silicon Graphics 4D workstation.

RESULTS AND DISCUSSION

The measured K X ray coincidence and anti-coincidence perturbed angular correlation spectra for ^{111}In HCA I in 50% sucrose are shown in both Figs. 2 & 3. Figure 2 shows theoretical spectra for the chemical transmutation model at parameter values listed in Table I and Fig. 3 shows theoretical spectra for the dose dependent damage model at parameter values listed in

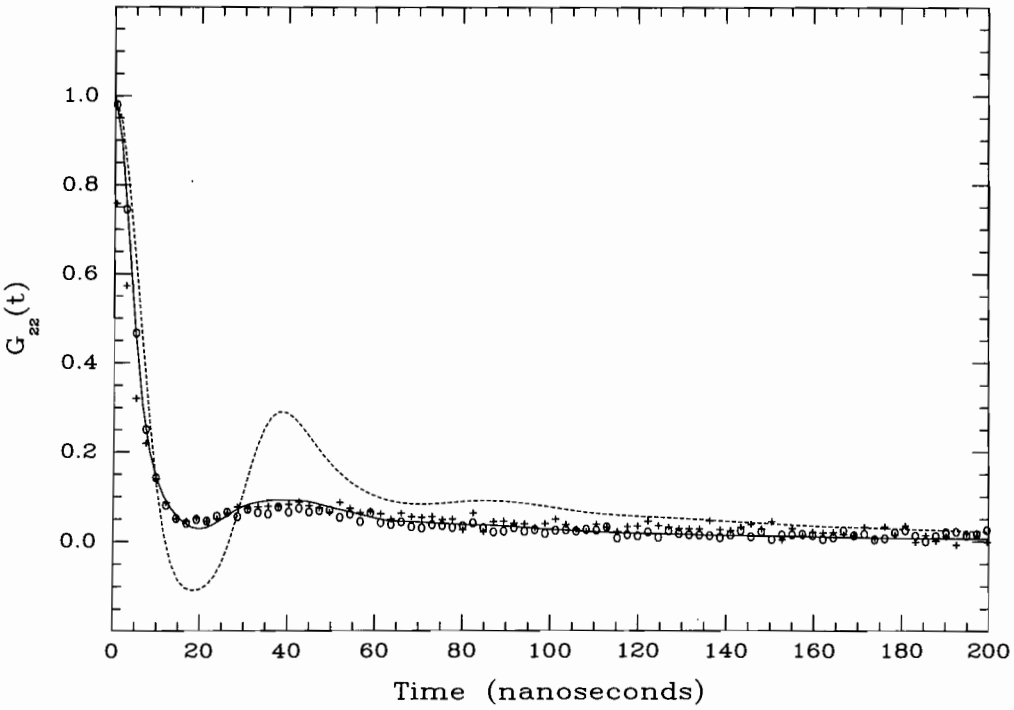

FIG. 2. Chemical transmutation model for HCA I perturbed angular correlation spectra. The open circles are the K X ray anti-coincidence spectrum and the crosses are the K X ray coincidence spectrum. Standard error bar heights vary from slightly smaller than to slightly larger than the markers over the displayed range of delay times. The solid curve is an approximate fit of the chemical transmutation model to the data. The dashed curve is the least squares fit of Bauer *et al.* (20) to the ^{111m}Cd HCA I perturbed angular correlation spectrum.

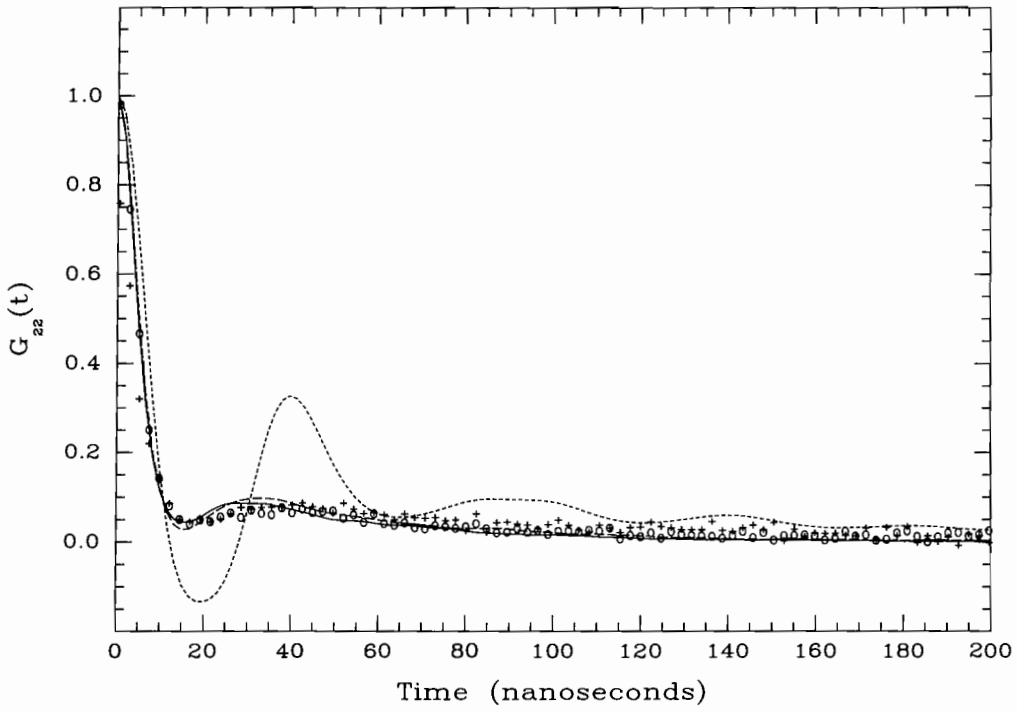

FIG. 3. Dose dependent damage model for HCA I perturbed angular correlation spectra. The experimental data is identical to that displayed in Fig. 2. The solid curve is an approximate fit of the dose dependent damage model to the data. The short dashed curve is an approximate fit to the ^{111m}Cd HCA I perturbed angular correlation spectrum with relaxation from ligand reorientation rather than molecular tumbling. The long dashed curve is the dose dependent damage model for the K X ray coincidence HCA I perturbed angular correlation spectrum derived by linear interpolation of the model parameters for the ^{111m}Cd and K X ray anti-coincidence spectra.

Table II. The procedure for approximately fitting the models is given in the methods section. Relaxation in the chemical transmutation model spectra results from metastable coordination complex decay and molecular tumbling. Evidently these mechanisms can account for all relaxation experimentally observed in ^{111}In HCA I perturbed angular correlation spectra. Since the coordination complex initial metastable state is assumed to be independent of the Auger emission intensity, the chemical transmutation model predicts equality of the K X ray coincidence and anti-coincidence spectra.

TABLE I

Chemical Transmutation Model Quadrupole Interaction Parameters for Perturbed Angular Correlation Spectra of HCA I

	^{111m}Cd	^{111}In
Metastable State		
Frequency mean (s^{-1})	-	133×10^6
Frequency SD	-	50%
Asymmetry	-	0.0
Lifetime (ns)	0.0	66
Ground State		
Frequency mean (s^{-1})	95×10^6	95×10^6
Frequency SD	18%	18%
Asymmetry	0.68	0.68
Euler angles (ϕ,θ,ψ)	-	$0, \pi/2, 0$
Tumbling lifetime (ns)	81	81

TABLE II

Dose Dependent Damage Model Quadrupole Interaction Parameters

	^{111m}Cd	^{111}In (k^+)	^{111}In (k^-)
Frequency mean (s^{-1})	95×10^6	127×10^6	133×10^6
Frequency SD	18%	47.6%	53%
Asymmetry	0.68	0.468	0.43
Rotation SD	25°	37.7°	40°
Jump lifetime (ns)	26.5	18.1	16.5

Relaxation in the dose dependent damage model spectra results from ligand reorientation. The absence of molecular tumbling relaxation in this model is a matter of convenience. Additional high precision ^{111m}Cd HCAB I spectra would be required to establish the correct balance of relaxation due to internal and overall motion. The theoretical K X ray coincidence and anti-coincidence spectra for the dose dependent damage model depend upon the relative Auger emission intensities. The electron capture decay of ^{111}In in coincidence with a cadmium K X ray yields on average 11.0 Auger and Coster-Kronig electrons and in anti-coincidence yields on average 16.8 electrons (R.W. Howell, private communication). The anti-coincidence yield must be corrected for the efficiency of detection for K X rays. The corrected anti-coincidence yield,

$$Y'_{k-} = \frac{(1 - \omega)}{1 - \varepsilon\omega} Y_{k-} + \frac{\omega (1 - \varepsilon)}{1 - \varepsilon\omega} Y_{k+} , \qquad (3)$$

where ε is the K X ray detection efficiency, ω is the probability per decay of K X ray emission, Y_{k-} is the perfect anti-coincidence yield, and Y_{k+} the K X ray coincidence yield. At the estimated detection efficiency for cadmium K X rays of 23%, the corrected anti-coincidence Auger electron yield is 13.0. The ratio $Y_{k+}/Y'_{k-} = 11/13$ interpolates the K Xray coincidence parameters between the zero dose and K X ray anti-coincidence parameters in the dose dependent damage model. The ratio of the difference between the K X ray coincidence and zero dose parameters to the difference between the K X ray anti-coincidence and zero dose parameters is 11/13, see Table II. The experimental ^{111}In HCA I K X ray coincidence and anti-coincidence spectra are identical. However, since the difference in the theoretical K X ray coincidence and anti-coincidence spectra is small enough relative to the experimental error, the dose dependent damage model may not be confidently rejected.

CONCLUSIONS

The indistinguishability of the experimental ^{111}In HCA I K X ray coincidence and anti-coincidence spectra suggests that during the first 10^{-8} s following electron capture decay the hot atom chemistry is independent of the Auger and Coster-Kronig electron emission intensity. As demonstrated by the dose dependent damage model, the experimental data do not conclusively rule out dependence of hot atom chemistry on emission intensity. The difference between the HCA I K X ray coincidence and anti-coincidence

spectra could be significantly increased by detecting K_β X rays for the coincidence spectrum, increasing the detection efficiency of all K X rays for the anti-coincidence spectrum, and possibly by measuring at liquid nitrogen temperature.

ACKNOWLEDGMENTS

Special thanks are due to Kandula S.R. Sastry and Franklyn G. Prendergast for their continued encouragement and support of this project. Lynda McDowell purified HCA I and helped with indium binding assays. Heiner Winkler introduced me to the Monte Carlo procedure (21) for computing a perturbation factor by averaging over the probability distribution of piecewise static interactions. Roger Howell provided electron yields. Alexander Halpern has called to my attention Refs. (1-3,8). This work was supported in part by National Institutes of Health grant 1 R03 RR02219-01.

REFERENCES

1. J.P. ADLOFF, Application to chemistry of electric quadrupole perturbation of γ-γ angular correlations. *Radiochim. Acta* **25**, 57-74 (1978).
2. P. BOYER and A. BAUDRY, Perturbed angular correlation of gamma rays. In *Hot Atom Chemistry* (T. Matsuura, Ed.) Elsevier, Amsterdam, pp 315-347, 1984.
3. H. SANO and P. GÜTLICH, Hot atom chemistry in relation to Mössbauer emission spectroscopy. In *Hot Atom Chemistry* (T. Matsuura, Ed.) Elsevier, Amsterdam, pp 265-302, 1984.
4. M. ALFLEN, C. HENNEN, F. TUCZEK, H. SPIERING, P. GÜTLICH, and Zs. KAJCSOS, Time-differential Mössbauer emission spectroscopy: Development of a new spectrometer and first results. *Hyperfine Interact.* **47**, 115-126 (1989).
5. C. HAYDOCK and K.S.R. SASTRY, Auger cascades following indium-111 decay: Effects on PAC spectroscopy. In *Proceedings of the 8th International Congress of Radiation Research* **1**, 67 (1987).
6. T. KOBAYASHI, K. FUKUMURA, T. KITAHARA, and S. SHIMIZU, Gamma - x ray coincidence Mössbauer spectroscopy with cobalt chloride. *J. Phys. Colloq.* **40**, C28-29 (1979).
7. H. KIM and D.D. DLOTT, Molecular dynamics simulation of nanoscale thermal conduction and vibrational cooling in a crystalline naphthalene cluster. *J. Chem. Phys.* **94**, 8203-8209 (1991).
8. B. DIEHN, A. HALPERN, and G. STÖCKLIN, Specific inactivation of solid carbonic anhydrase upon x-ray resonance absorption in the constituent zinc atom. *J. Am. Chem. Soc.* **98**, 1077-1079 (1976).

9. C.M. LEDERER and V.S. SHIRLEY, Eds., *Table of Isotopes*, 7th ed. John Wiley, New York, 1978.
10. R.G. KHALIFAH, D.J. STRADER, S.H. BRYANT, and S.M. GIBSON, Carbon-13 nuclear magnetic resonance probe of active-site ionizations in human carbonic anhydrase B. *Biochemistry* **16**, 2241-2247 (1977).
11. J.B. HUNT, M.-J. RHEE, and C.B. STORM, A rapid and convenient preparation of apocarbonic anhydrase. *Anal. Biochem.* **79**, 614-617 (1977).
12. Y. POCKER and J.T. STONE, The catalytic versatility of erythrocyte carbonic anhydrase. III. Kinetics studies of the enzyme-catalyzed hydrolysis of p-nitrophenyl acetate. *Biochemistry* **6**, 668-678 (1967).
13. H. FRAUENFELDER and R.M. STEFFEN, Angular correlations. In *Alpha-, Beta- and Gamma- Ray Spectroscopy* (K. Siegbahn, Ed.) North-Holland, Amsterdam, pp 997-1198, 1965.
14. E. MATTHAIS, W. SCHNEIDER, and R.M. STEFFEN, Nuclear level splitting caused by a combined magnetic dipole and non-axially symmetric electric quadrupole interaction. *Ark. Fys.* **24**, 97-111 (1963).
15. H. GOLDSTEIN, Euler angles in alternate conventions. In *Classical Mechanics*, 2nd ed. Addison-Wesley, Massachusetts, pp 606-610, 1980.
16. R. BAUER, Perturbed angular correlation spectroscopy and its application to metal sites in proteins: possibilities and limitations. *Q. Rev. Biophys.* **18**, 1-64 (1985).
17. B.T. SMITH, J.M. BOYLE, J.J. DONGARRA, B.S. GARBOW, Y. IKEBE, V.C. KLEMA, and C.B. MOLER, *Matrix Eigensystem Routines - EISPACK Guide*, 2nd ed. Springer-Verlag, Berlin, 1976.
18. F. JAMES, Monte Carlo theory and practice. *Rep. Prog. Phys.* **43**, 1145-1189 (1980).
19. M.P. ALLEN and D.J. TILDESLEY, Random numbers. In *Computer Simulation of Liquids*. Clarendon Press, Oxford, pp 345-351, 1989.
20. R. BAUER, P. LIMKILDE, and J.T. JOHANSEN, Low and high pH form of cadmium carbonic anhydrase determined by nuclear quadrupole interaction. *Biochemistry* **15**, 334-342 (1976).
21. E. GERDAU, H. WINKLER, B. GIESE, W. GEBERT, and J. BRAUNSFURTH, Time-dependent hyperfine interactions in moderately diluted Ni(Hf). *Hyperfine Interact.* **1**, 469-483 (1976).

DISCUSSION

HUMM, J. L. Using PAC techniques you have time resolution within the nanosecond realm. If I understood you correctly, you concluded that your major finding by this technique was chemical damage to the ^{111}In appended molecule resulting from transmutation. Since the Auger cascade is all over within about 10^{-13} s, I find it confusing as to why the effects of the Auger electron emission and charge neutralization have not produced a more noticeable effect on the observed spectra?

HAYDOCK, C. The half-life of the ^{111}Cd daughter nuclear excited state initiating the gamma-gamma cascade is 120 ps. Thus the electric and magnetic fields generated at the ^{111}Cd daughter nucleus during the Auger cascade and charge neutralization are not observed. However, the molecular damage should be observed in the spectra in proportion to the number of Auger electrons emitted. The indistinguishability of the K X ray coincidence and anti-coincidence spectra indicates that chemical transmutation effects dominate over direct Auger and charge transfer effects, and that the molecular damage is due to the indirect action of free radical ions.

Biophysical Aspects of Auger Processes, AAPM Symposium Series No. 8 (1992) 121-136
Eds. RW Howell, VR Narra, KSR Sastry, DV Rao

^{123}I: CALCULATION OF THE AUGER ELECTRON SPECTRUM AND ASSESSMENT OF THE STRAND BREAKAGE EFFICIENCY

EKKEHARD POMPLUN

Abteilung Sicherheit und Strahlenschutz,
Forschungszentrum Jülich GmbH, Postfach 1913, D-5170 Jülich,
Germany

ABSTRACT

Auger cascades induced by electron capture in ^{123}I have been simulated by the Monte Carlo technique with special emphasis on the determination of the electron kinetic energies. By using an approach which considers the individual electron population of all electronic shells before and after a transition, errors in the electron energy normally introduced when applying the so-called (Z+1)-approximation are avoided. Thus, the energy of the electrons released in transitions between higher shells were found to be about half the value mentioned in the literature. An average total number of 7.6 electrons (6.4 Auger-, and 1.2 shake-off electrons) has been determined to be emitted per decay, a number which is considerably lower than those reported in similar studies. The efficiency of strand break induction has been assessed to be 0.4 DSB and 1.1 additional SSB per decay of DNA bound ^{123}I. A comparison with the corresponding DSB values of ^{125}I reveals that ^{125}I is 2.5 times more effective than ^{123}I. This is about the same ratio as that determined by Makrigiorgos (1) on the basis of cell killing experiments.

INTRODUCTION

Auger electron emitting nuclides incorporated into sensitive biological structures like DNA have been demonstrated to be of extremely high effectiveness in inducing radiobiological damage (2-5). Furthermore, it has been shown experimentally by Martin and Haseltine (6) and theoretically by Charlton (7) that the initial damage is restricted to the immediate region surrounding the decay site. Although different mechanisms are believed to be involved in the damage process, the electron radiation is expected to be the most important one. To understand the underlying physical and biochemical mechanisms leading to the expression of the biological effects, an accurate description of the radiation source emissions is required.

Since Auger electron emitters decay by a complex process of electronic deexcitation, an evaluation of mean numbers of emitted electrons and their kinetic energies may be sufficient for radiation protection purposes but they are of limited significance for an interpretation of radiation induced biological damage (8). To obtain detailed information about the emitted electrons, a Monte Carlo technique can be used to simulate Auger cascades on the computer. An essential feature of these simulations is the kinetic energy calculation of the electrons released by individual Auger and Coster-Kronig transitions inside the electronic shells of the nuclide.

The first Monte Carlo code simulating an electron capture induced decay and the subsequent electron cascades was written by Charlton and Booz (9) for ^{125}I. In this code the so-called (Z+1)-approximation was used to determine the electron energies. Charge neutralization was considered by filling O-shell vacancies during the cascade process, although, as the authors stated, 'this is difficult to understand physically, since it assumes a very rapid charge transfer'. Applying these two conditions ((Z+1)-approximation and rapid and complete neutralization) results in a broad distribution for the number of electrons emitted (up to more than 40 electrons) with an average number of 21 electrons per decay (9).

It was shown later (10) that the (Z+1)-approximation leads to discrepancies in the total electron energy emitted. As an example, the summation of the kinetic electron energies released after photo-induced Auger cascades in iodine yields, for most deexcitation pathways, more energy than that having been transferred to the nuclide by the incident photon (see Fig. 1). Therefore, the code of Charlton and Booz (9) has been further developed with special emphasis on the calculation of the electron kinetic energies (11). By introducing Dirac-Fock methods that consider the individual

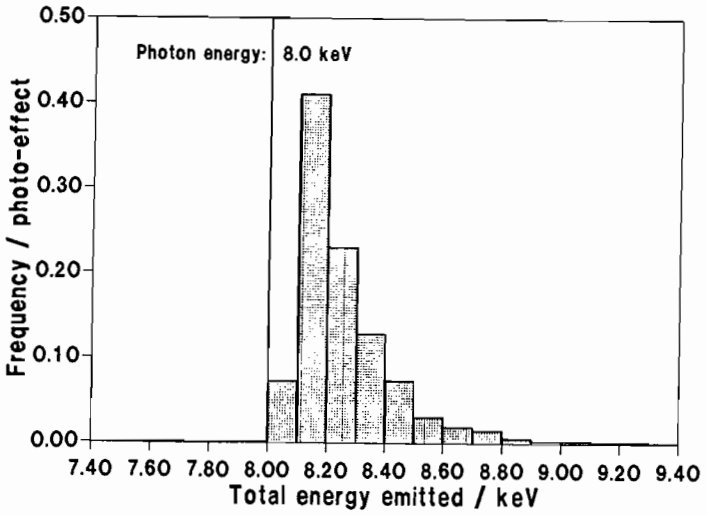

FIG. 1. Energy balance for simulated photon induced (E_{phot} = 8.0 keV) Auger cascades in cold iodine using the (Z+1)-approximation (frequency values are normalized to unity).

electronic configuration of the different shells before and after the Auger transition, an accurate determination of the electron kinetic energy is possible. The emitted energy can be assumed to result from the kinetic energy of the released Auger electrons and from an ionization potential build-up on the daughter atom during the electron cascade. Neutralization of vacancies during the very fast Auger cascade (10^{-16} - 10^{-14} s) is not possible. Vacancies will become neutralized during the comparably long-lived metastable state between two cascades such as the 0.035 MeV state of ^{125}Te (1.6 ns). The electron number distribution calculated for ^{125}I by this approach (11) is much smaller (only up to less than 30 electrons) than the one of Charlton and Booz (9) and the mean number of electrons emitted per ^{125}I decay has been evaluated to be about 13 instead of 21 (see above). This number approximates the number calculated by Charlton and Booz (9) and by Humm (16) for an isolated ^{125}I atom. Detailed comparison of both codes by tracing single cascades showed that the kinetic energies evaluated by the (Z+1)-approximation will be considerably overestimated, particularly for those electrons from higher shells that are mainly emitted when the shells already have been significantly depleted.

In further investigations with ^{125}I, track structures of the emitted Auger electrons generated by the code of Paretzke (12) were superimposed on DNA volume models of different geometrical resolutions (13,14). Again the locally restricted effectiveness of the Auger electrons could be demonstrated as well as the fact that the Auger electrons with a kinetic energy of less than 500 eV play the dominant role in the induction of single- and double strand breaks (14). Mostly originating from higher shell transitions, these electrons are the ones which are most strongly affected by an uncertain energy determination.

Until now the technique of energy calculation by the Dirac-Fock method has been applied to ^{125}I only. Another possibly useful nuclide in radiation biology is ^{123}I. This isotope has a 13.2 h half-life, compared to 60.1 d for ^{125}I, and is routinely used as an imaging isotope in nuclear medicine. Its decay scheme (see Fig. 2) is much more complex than that of ^{125}I insofar as the

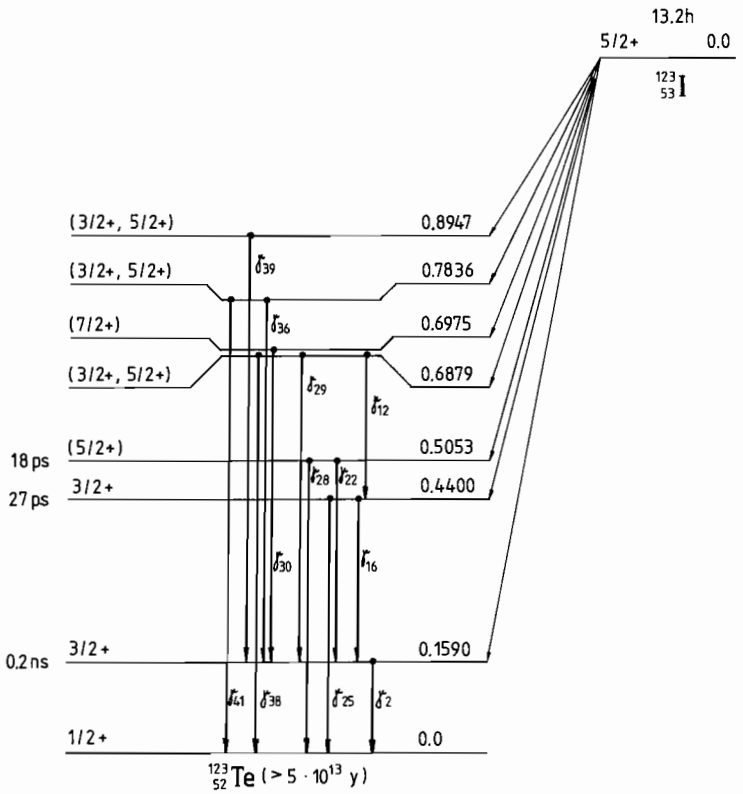

FIG. 2. Decay scheme of ^{123}I.

EC process (100%) may lead to different excited ^{123}Te states depending on the branching ratios (see legend of Table I). Most frequently (> 97%) the decay goes to the 159 keV level and subsequently, either by γ emission (84%) or by internal conversion (IC), to the ground state of ^{123}Te. Since only 16% of the ^{123}I decays result in internal conversion, only this percentage of decays give rise to two Auger cascades compared to 93% for ^{125}I. Recent radiobiological measurements performed with ^{123}I refer to the end point of cell survival (1) and reveal that 2.2 ± 0.3 times more ^{123}I decays are necessary to induce the same degree of cell death as with ^{125}I, whereas the mean lethal dose (D_{37}) to the nucleus is about the same for both nuclides. Because their Auger electron cascades are identical but the numbers of cascades are different, a comparison of the biological efficiencies of these nuclides will be of interest since - if the electron irradiation is mainly responsible for the biological effect - it should be possible to compare the different biological effectiveness in relation to the differences in the electron tracks and their energy deposition in the DNA.

TABLE I

Electron Capture and Internal Conversion Probabilities for the 0.159 MeV Level of ^{123}Te.

Shell	EC	IC
K	0.797	0.135
L_1	0.104	0.016
L_2	0.003	0.0011
L_3	0.007	0.0004
M_1	0.022	0.0035
M_2	0.001	0.0
M_3	0.038	0.0
M_4	0.0	0.0
M_5	0.0	0.0
N_1	0.005	0.0008
N_2	0.0	
N_3	0.0	

For other energy levels the following EC values have been used: 0.44 MeV: 0.004 (K shell), 0.506 MeV: 0.003 (K shell), 0.6975 MeV: 0.014 (K shell) and 0.002 (L_1 shell). IC values for other levels than 0.159 MeV were neglected. The EC data were taken from Humm (16), the IC data from ICRP (17).

In this work the number distribution of Auger electrons emitted by ^{123}I decays will be calculated and compared with results from the literature obtained by application of the (Z+1)-approximation. The presentation of the mean ^{123}I Auger electron spectrum together with the one of ^{125}I illustrates the characteristic differences between these two radiation sources. The effectiveness of strand break induction by DNA-incorporated ^{123}I will be assessed by superimposing electron track structures on a DNA target model of atomic scale resolution (14).

METHODS

A detailed description of the applied Monte Carlo program for the simulation of Auger cascades is given by Pomplun et al. (11) for the case of ^{125}I decay. Therefore, only a very brief description of the characteristics of this code and the necessary alterations for ^{123}I will be summarized. The code traces the different steps of the nuclide decay starting with the selection of the ^{123}Te energy level resulting from the EC transition and the shell from which the electron will be captured (in about 80% from the K shell; see Table I). Individual Auger- and Coster-Kronig transitions are chosen by the weighted probability distribution of all transitions energetically allowed in the single ionized atom. Each transition is tested by a special algorithm which calculates quite accurately by a relativistic Dirac-Fock approach (15) the total energy of the nuclide with the actual individual electron configuration at any step during the cascade. An Auger transition suggested by the random numbers will be checked with regard to the energy difference between the configurations before and after the transition. If a positive amount is evaluated it will be assigned to the kinetic energy of the emitted Auger electron. In case of a negative energy value the transition will be considered as energetically not possible at that stage of the cascade. The probabilities of the remaining transitions will be renormalized. Furthermore, whenever a transition is selected, the possibility of shake-off electron emission is tested and - when outer shells are involved in the transition - double Auger processes are also taken into account. The cascade comes to an end if no more transitions are energetically possible. The sources for the required input data are given in Ref. (9) and (11). To get sufficient statistics the calculations reported here have been performed for 10000 ^{123}I decays.

The kinetic energies of the individual Auger and conversion electrons for each decay provided by the cascade program were recorded as input data for the MOCA8 code of Paretzke (12). This code generates track structures of electrons in water vapor, a medium which poses some limitations to the comparability with real biological tissue. Those limitations are discussed in

detail by Charlton and Humm (13) and by Pomplun (14). The application of water vapor cross-sections in this work, therefore, means that the sizes of the energy transfer events and their positions relative to the site of decay can be seen as an approximation only.

The employed DNA target model (Fig. 3) is characterized by its high geometrical resolution which became possible by using the coordinates of the single atoms of the double helix molecule (18,19). Due to this atomic scale, a distinction has been made between the direct and the indirect hit mode of radiation action - according to the definition given by Dertinger and Jung (20) - when the interaction of electrons with the DNA were simulated. After shifting the starting point of the electrons to the assumed position of the incorporated iodine (the methyl group of a thymine base), then, for each energy transfer event from the electron tracks, the program DNAMOD (14) looks for the nearest atom, and the event is considered to be a direct hit if its position lies within the van der Waals radius of that atom. If the event's position is outside of the atomic volumes but inside a virtual straight cylinder - representing a DNA segment including the structural water molecules - then an indirect hit is assumed. The program registers these events separately from those recognized as direct events.

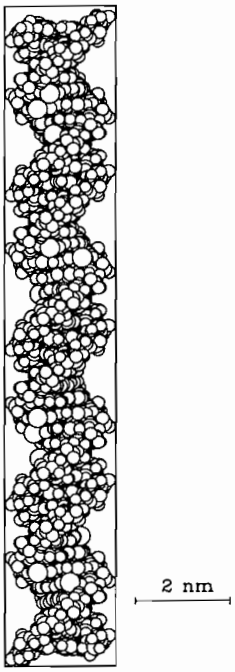

FIG. 3. DNA target model; the straight cylinder indicates the total DNA segment including structural water molecules located preferably in the grooves.

Different energy threshold values have been applied for the assessment of strand break induction by direct and indirect hits. For the direct hit mode, an energy deposition of $E \geq 10$ eV inside the phosphate/sugar chain was assumed to be necessary to induce a SSB due to the fact that ionization potentials of biomolecules are below this value (21). According to Chatterjee and Magee (22) a radical pair requires an energy of $E \geq 17$ eV in the surrounding water to be created; this value has been taken as the threshold for indirect hits. In a very simple approximation a strand break by radical attack is assumed if the nearest atom of the DNA molecule to an indirect hit position belongs to the phosphate or sugar group. A DSB will be recorded if there are two SSB on complementary strands less than 20 base pairs apart from each other (for details see Ref. (14)). Whereas SSB can be induced by direct or indirect hits, compound hits have to be considered for DSB, *i.e.* one strand is broken by a direct, the other by an indirect hit. This implies that the total number of DSB might be greater than the sum of DSB induced by direct or indirect hits only. Other mechanisms of strand breaks, *e.g.* via base damage, have been neglected here.

RESULTS AND DISCUSSION

The calculated numbers of the emitted electrons are given in Table II (mean values per decay) and in Fig. 4 (frequency distribution). Following the approach developed by Pomplun *et al.* (11) the term 'condensed phase', as it is used in this work, implies boundary conditions in the application of the Monte Carlo code different from those used by Humm (16) and by Sastry and Rao (23) (see Introduction). Because of the assumptions made in Ref. (16) and (23) for the charge transfer velocity, the values reported in these investigations can be seen as an upper limit. However, a rough comparison might be reasonable between the 'isolated atom' case in Ref. (16) yielding 8.9 electrons and the 'condensed phase' situation of this work (one cascade only in 84% of the decays and also no neutralization during the cascade) yielding 6.4 electrons. The additional 1.2 shake-off electrons found here result from a different mechanism which was not taken into account by Humm (16). Thus, the difference in the energy determination leads to a difference in the mean value of emitted Auger electrons of about 2.5 per decay. A similar difference in the mean number of emitted electrons can be found for ^{125}I. For the case of a completely isolated atom (even during the metastable state with a half-life of 1.6 ns no neutralization has been assumed) 13.2 electrons have been calculated with the (Z+1)-approximation but only 10.1 electrons using the Dirac-Fock approach (11). The present frequency distribution for the number of emitted electrons (Fig. 4) compared with that of Humm (16) covers the same range but the maximum is shifted to a smaller value.

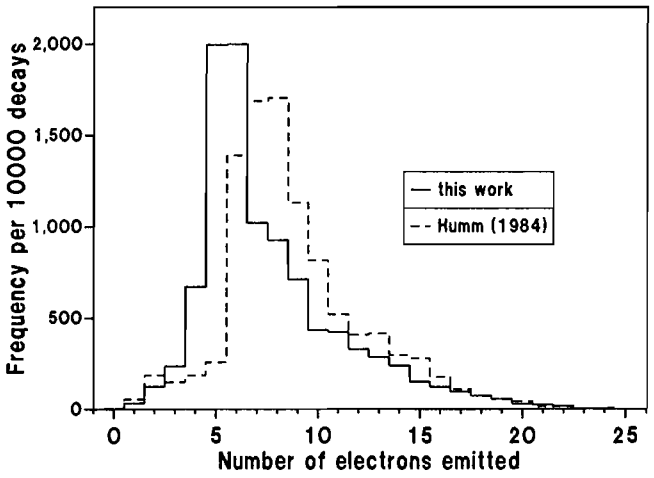

FIG. 4. Distribution of the number of emitted electrons, comparison with results obtained by (Z+1)-approximation (16).

TABLE II

Electron Yield per ^{123}I decay: Comparison with (Z+1)-Approximation

Radiation	This work	Humm (16)		Sastry and Rao (23)
	Cond. Phase	Isol. Atom	Cond. Phase	Cond. Phase
Auger Coster-Kronig Electrons	6.4	8.9	12.3	11
Shake-off Electrons	1.2	-	-	-

The term 'condensed phase' in this work means that charge transfer took place only during the metastable states of ^{123}Te whereas in the work of Humm (16) and Sastry & Rao (23) a permanent neutralization of O shells is assumed.

The mean values for frequencies and energies of the emitted radiation per ^{123}I decay are listed in Table III. These values are compared with the corresponding ones determined by ICRP (17) on the basis of a (Z+1)-approximation. Whereas the energy differences for Auger electrons resulting from transitions to the K shell are less than 1%, and those to the L shells are less than 5%, for transitions to higher shells the Auger electron kinetic energy is about 55% of the corresponding ICRP value (MXY-transitions). Coster-Kronig electrons as well as N shell Auger electrons and shake-off electrons are not mentioned by ICRP (17). The mean ionization potential at the end of the ^{123}I Auger cascade has been evaluated here to be 0.577 keV, as expected, about one half of the corresponding value (1.07 keV) for ^{125}I (11).

A comparison of the energy spectra between ^{123}I and ^{125}I (Fig. 5) shows that - as expected - all ^{123}I Auger- and Coster-Kronig electrons have identical energy values but reduced frequencies. The qualitative differences between these two spectra result from the conversion electrons which lie for ^{123}I in the energy range above 100 keV with frequencies comparable to most Auger electrons. In contrast, the conversion electron from the K shell represents the most prominent line in the ^{125}I spectrum, appearing in nearly each (83%) decay.

The results for the strand break efficiency are presented in Table IV. The total, as well as the corrected, numbers of SSB are given for both mechanisms (direct and indirect) and for all hits separately. Due to compound hits (see METHODS) the total number of DSB is greater than the sum of DSB induced by direct and indirect hits only. Therefore, the corrected numbers for 'all hit' SSB are not necessarily the sum of the corresponding direct and indirect hit values (see also Ref. (14)). The number of total SSB induced by ^{123}I yields nearly 2 per decay, just half the number of ^{125}I induced breaks. This value seems to be reasonable due to the fact of having, in most decays, one electron cascade in the tellurium daughter atom instead of two like in the great majority of ^{125}I decays. But for DSB the situation is different. About 40% of the ^{123}I decays produce a DSB whereas the corresponding efficiency of ^{125}I is 100%, *i.e.* on average each ^{125}I decay induces one DSB. To assess the influence of the conversion electrons which are responsible for the qualitative difference in the electron spectra of ^{123}I and ^{125}I, separate calculations (data not shown here) have been performed for ^{125}I electron spectra without the conversion electrons (which appears in 93% of all decays). The contribution to strand break induction by these electrons was found to be negligibly small (less than 3% of all SSB).

TABLE III. ^{123}I Radiation Spectrum

Radiation	Frequency per decay		Mean energy (keV)	
	this work	ICRP (17)	this work	ICRP (17)
γ_2	0.8391	0.828	159.0	159.0
γ_{12}	0.0004	0.0007	248.0	248.0
γ_{16}	0.0011	0.0008	281.0	281.0
γ_{22}	0.0009	0.0013	346.3	346.3
γ_{25}	0.0033	0.0043	440.0	440.0
γ_{28}	0.0020	0.0031	505.3	505.3
γ_{29}	0.0115	0.0138	529.0	529.0
γ_{30}	0.0038	0.0038	538.5	538.5
γ_{36}	0.0003	0.0008	624.6	624.6
γ_{38}	0.0002	0.0003	687.9	687.9
γ_{39}	0.0006	0.0006	735.8	735.8
γ_{41}	0.0003	0.0006	783.6	783.6
ce-K	0.1341	0.135	127.123	127.2
ce-L_1	0.0151	0.016	154.028	154.0
ce-L_2	0.0008	0.0011	154.371	154.4
ce-L_3	0.0004	0.0004	154.647	154.6
ce-M_1	0.0037	0.0035	157.973	158.2
ce-N_1	0.0010	0.0008	158.811	159.0
$K_{\alpha 1}$	0.4452	0.458	27.444	27.47
$K_{\alpha 2}$	0.2466	0.246	27.214	27.20
$K_{\beta 1}$	0.0814	0.0866	30.984	31.0
$K_{\beta 2}$	0.0222	0.0266	31.688	31.71
$K_{\beta 3}$	0.0415	0.0446	30.935	30.94
$K_{\beta 5}$	0.0008	-	31.235	-
$L_{X\text{-ray}}$	0.0837	-	3.935	-
AUG KLL	0.0751	0.0815	22.499	22.54
AUG KLX	0.0367	0.0369	26.418	26.35
AUG KXY	0.0029	0.0049	30.179	30.13
C-K LLX	0.1432	-	0.279	-
AUG LMM	0.7187	0.606	3.018	3.080
AUG LMX	0.2003	0.311	3.650	3.849
AUG LXY	0.0116	0.044	4.265	4.380
C-K MMX	0.8587	-	0.095	-
AUG MXY	1.9473	1.80	0.383	0.699
AUG NXY	2.2614	-	0.031	-

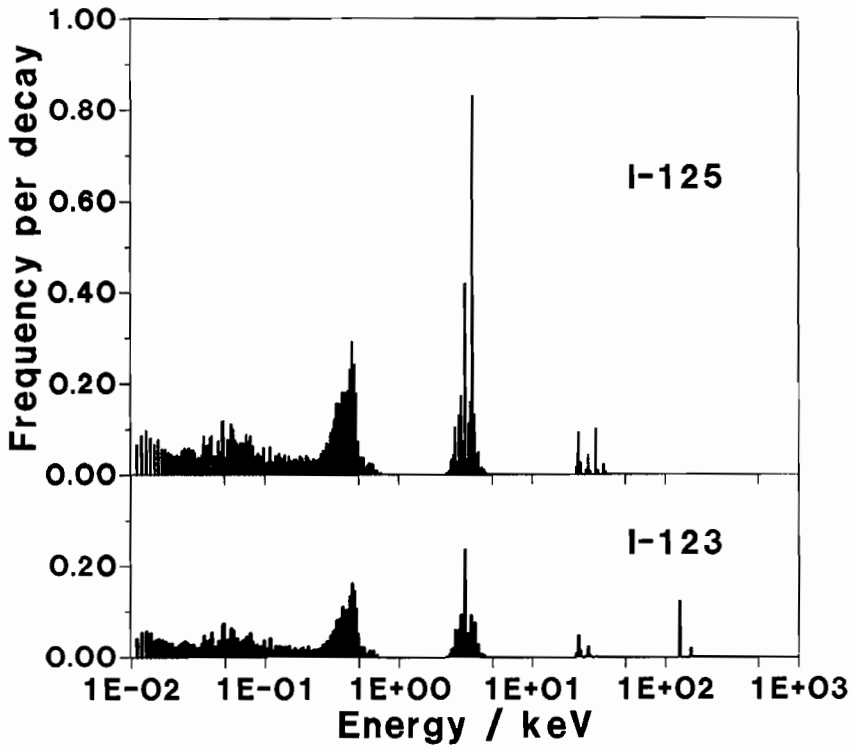

FIG. 5. Mean electron spectra of ^{123}I and ^{125}I.

A direct comparison with experimental results is not possible due to the lack of data for strand break induction. However, since there is strong indication that cell death is directly related to the number of DSB (24-26) it seems justified to compare the ratio between the numbers of ^{125}I (14) and ^{123}I (this work) induced DSB with the ratio of 2.2 ± 0.3 obtained experimentally by Makrigiorgos *et al.* (1) for the total number of ^{123}I decays versus ^{125}I decays to find the same level of cell survival. The calculated values for DSB induction per decay by ^{125}I, 1.0, and by ^{123}I, 0.4, (see Table IV) result in a corresponding ratio of 2.5 which is inside the uncertainty range of the experimentally found value. Strand break induction, as it is considered here, is due to electron radiation only; *i.e.* if the underlying assumptions are correct, then the Auger electrons are responsible for the biological effects discussed here. This is also supported by the finding of Makrigiorgos *et al.* (1) that Auger electron irradiation is the predominant reason for the observed biological toxicity.

Under these implications the ionization potential built up during the Auger cascade on the Te-daughter atom and the subsequent charge transfer processes would be of minor significance.

TABLE IV
Number of DNA Strand Breaks per Decay Induced by Direct and Indirect Hits

	Direct Hits		Indirect Hits		All Hits	
	^{123}I	^{125}I	^{123}I	^{125}I	^{123}I	^{125}I
SSB (tot.)	1.1	1.9	0.8	2.1	1.9	4.0
SSB (corr.)	0.7	1.1	0.6	1.2	1.1	2.0
DSB	0.2	0.4	0.1	0.5	0.4	1.0

The ^{125}I data had been slightly changed against the values reported in Ref. (14) because of a revision to eliminate a minor program error. In the last column ('all hits') no distinction was made between the hit modes, so that for total SSB the values are just the sum of the breaks from direct and indirect hits, whereas in case of DSB compound hits also contributed to the figure.

CONCLUSIONS

The electron capture induced decay of ^{123}I has been simulated by a Monte Carlo technique to calculate the electron emission spectrum and to assess the biological efficiency when this nuclide is incorporated into the DNA molecule. Since the Auger electrons with $E \leq 500$ eV are the main contributors to strand break induction subsequent to electron capture decay, the determination of the electron kinetic energies is of particular interest. By application of an approach using Dirac-Fock methods it has been possible to take into account the influence of complex electron configurations on the binding energies of those electrons involved in the individual Auger transitions. The calculations performed here reveal a mean total number of 7.6 emitted electrons per decay (6.4 Auger and Coster-Kronig electrons and 1.2 additional shake-off electrons). This number is about 30% less than that obtained by Humm (16) for a comparable situation with the (Z+1)-approximation although the broadness of the distribution is about the same. The electron kinetic energies are smaller than those previously reported *e.g.* by ICRP (17), in particular those in the energy range below 500 eV. Specifically, for the MXY transition electrons (Table III), the kinetic energies were reduced by 45% compared with the ICRP energies.

The effectiveness of DNA-incorporated ^{123}I to induce SSB by electron irradiation has been found to be about 0.5 of the corresponding ^{125}I value due to the reduced intensity of the Auger electron spectrum by about one half according to its decay characteristics. If one compares the evaluated numbers of DSB produced by these two nuclides, ^{125}I appears to be 2.5 times more effective than ^{123}I. Nearly the same relation (2.2 ± 0.3) was found by Makrigiorgos *et al.* (1) for cell survival in an experimental investigation. Since here in this work only electron interaction with DNA has been considered, the similarity of both values could be an indication that neutralization processes do not significantly contribute to the induction of strand breaks. However, to further elucidate the different possible mechanisms of radiation action, experimental measurements of strand break induction by ^{123}I would be most desirable.

ACKNOWLEDGMENTS

The author thanks Dr. H.G. Paretzke, GSF Neuherberg, for use of the MOCA8 code for the generation of track structures.

REFERENCES

1. G.M. MAKRIGIORGOS, A.I. KASSIS, J. BARANOWSKA-KORTYLEWICZ, K.D. McELVANY, M.J. WELCH, K.S.R. SASTRY, and S.J. ADELSTEIN, Radiotoxicity of 5-[^{123}I]Iodo-2'-deoxyuridine in V79 cells: A comparison with 5-[^{125}I]Iodo-2'-deoxyuridine. *Radiat. Res.* **118**, 532-544 (1989).
2. L.E. FEINENDEGEN, H.H. ERTL, V.P. BOND, Biological toxicity associated with the Auger effect. *Proc. Symposium Biological Aspects of Radiation Quality*, p. 419-429, International Atomic Energy Agency, Vienna, SM-145-22, 1971.
3. R. ROOTS, L.E. FEINENDEGEN, and V.P. BOND, Comparative radiotoxicity of ^{3}H-IUdR and ^{125}IUdR after incorporation into DNA of cultured mammalian cells. In *Proc. Third Symposium on Microdosimetry*, pp. 371-388, Report EUR 4810, (H.G. Ebert, Ed), Commission of the European Communities, Luxembourg, 1971.
4. K.G. HOFER, C.R. HARRIS and J.M. SMITH, Radiotoxicity of intracellular ^{67}Ga and ^{125}I and ^{3}H. Nuclear versus cytoplasmic radiation effects in murine L1210 leukemia. *Int. J. Radiat. Biol.* **28**, 225-241 (1975).
5. A.I. KASSIS, F. FAYAD, B.M. KINSEY, K.S.R. SASTRY, and S.J. ADELSTEIN, Radiotoxicity of an ^{125}I-labelled DNA intercalator in mammalian cells. *Radiat. Res.* **118**, 283-294 (1989).
6. R.F. MARTIN and W.A. HASELTINE, Range of radiochemical damage to DNA with decay of iodine-125. *Science* **213**, 896-898 (1981).
7. D.E. CHARLTON, The range of high-LET effects from ^{125}I decays. *Radiat. Res.* **107**, 163-171 (1986).
8. D.E. CHARLTON, Comments on strand breaks calculated from average doses to the DNA from incorporated isotopes. *Radiat. Res.* **114**, 192-197 (1988).
9. D.E. CHARLTON and J. BOOZ, A Monte Carlo treatment of the decay of ^{125}I. *Radiat. Res.* **87**, 10-23 (1981).

10. E. POMPLUN, Mikrodosimetrische Berechnung der Energiedeposition und des Dosisgrenzwertes nach Zerfall von Radionukliden in biologischen Systemen. *Ph.D. Dissertation*, Universität Düsseldorf, 1987.
11. E. POMPLUN, J. BOOZ, and D.E. CHARLTON, A Monte Carlo simulation of Auger cascades. *Radiat. Res.* **111**, 533-552 (1987).
12. H.G. PARETZKE, Radiation track structure theory. In *Kinetics of Nonhomogeneous Processes*, (G.R. Freeman, Ed.) Wiley, New York, pp. 89-170, 1987.
13. D.E. CHARLTON and J.L. HUMM, A method of calculating initial DNA strand breakage following the decay of incorporated ^{125}I. *Int. J. Radiat. Biol.* **53**, 353-365 (1988).
14. E. POMPLUN, A new DNA target model for track structure calculations and its first application to I-125 Auger electrons. *Int. J. Radiat. Biol.* **59**, 625-642 (1991).
15. J.P. DESCLAUX, A multiconfiguration relativistic Dirac-Fock program. *Comput. Phys. Commun.* **9**, 31-45 (1975).
16. J.L. HUMM, The analysis of Auger electrons released following the decay of radioisotopes and photoelectric interactions and their contribution to energy deposition. *Bericht der Kernforschungsanlage Jülich*, Jül-1932, 1984.
17. ICRP, *Radionuclide Transformations*, Publication 38, International Commission on Radiation Protection and Standards, Pergamon Press, Oxford.
18. S. ARNOTT and D.W.L. HUKINS, Refinement of the structure of B-DNA and implications for the analysis of X-ray diffraction data from fibers of biopolymers. *J. Mol. Biol.* **81**, 93-105 (1973).
19. R. CHANDRASEKARAN and S. ARNOTT, The structures of DNA and RNA helices in oriented fibers. *Landolt-Börnstein, New Series* VII, 1b, Springer-Verlag, Berlin, 1989.
20. H. DERTINGER and H. JUNG, *Molekulare Strahlenbiologie*, Springer Verlag Berlin, 1969.
21. M. INOKUTI, Atomic processes pertinent to radiation physics. *Electronic and Atomic Collisions*, (N. Oda and K. Takayanagi, Eds.), North-Holland Publishing Company, Amsterdam-London, pp. 31-45, 1980.
22. A. CHATTERJEE and J.L. MAGEE, Theoretical investigation of the production of strand breaks in DNA by water radicals. *Radiat. Prot. Dosim.* **13**, 137-140 (1985).
23. K.S.R. SASTRY and D.V. RAO, Dosimetry of low energy electrons. In *Physics of nuclear medicine: Recent advances.* (D.V. RAO, R. CHANDRA, and M.C. GRAHAM, Eds.) American Association of Physicists in Medicine, Medical Physics Monograph No 10, American Institute of Physics, New York, pp. 169-208, 1984.
24. I.R. RADFORD, The level of induced DNA double-strand breakage correlates with cell killing after X irradiation. *Int. J. Radiat. Biol.* **48**, 45-54 (1985).
25. P.E. BRYANT, Enzymatic restriction of mammalian cell DNA: Evidence for double strand breaks as potentially lethal lesions. *Int. J. Radiat. Biol.* **48**, 55-60 (1985).
26. M. FRANKENBERG-SCHWAGER, Induction, repair and biological relevance of radiation induced DNA lesions in eukaryotic cells. *Radiat. Environ. Biophys.* **29**, 273-292 (1990).

DISCUSSION

Kassis, A. I. What are the assumptions of > 10 keV and > 17 keV needed for direct and indirect effects based on?

Pomplun, E. They were taken from the literature.

Halpern, A. What do you mean when you say indirect effects?

Pomplun, E. Effects mediated by vehicles, *e.g.* radicals.

Halpern, A. Water radicals?

Pomplun, E. Yes.

Halpern, A. DNA structural water is not vapor. It changes the physical properties of DNA (*e.g.* its conductivity).

Pomplun, E. The calculations presented here have been performed for a DNA model. It is obvious that such a model has its restrictions. Of course, this model - compared with real DNA - is a very simple one because it neglects a number of physical, chemical, and biological DNA properties (*e.g.* the conductivity). These properties can be incorporated into the model step by step as far as appropriate data for the different properties are available. Furthermore, in the special case of this paper, although the calculated absolute values of strand breaks might be of less reliability due to the incomplete DNA model, the relation between ^{123}I and ^{125}I induced strand breaks gives a reasonable value.

Biophysical Aspects of Auger Processes, AAPM Symposium Series No. 8 (1992) 137-152
Eds. RW Howell, VR Narra, KSR Sastry, DV Rao

SIMULATION OF STRAND BREAK INDUCTION BY DNA INCORPORATED ^{125}I

EKKEHARD POMPLUN[1], MARTINE ROCH[2], and MICHEL TERRISSOL[2]

[1]Abteilung Sicherheit und Strahlenschutz, Forschungszentrum Jülich GmbH, Postfach 1913, 5170 Jülich, Germany

[2]Centre de Physique Atomique, Universite Paul Sabatier, 118 route de Narbonne, 31062 Toulouse Cedex, France

ABSTRACT

Monte Carlo calculation of ^{125}I Auger cascades has provided electron spectra for individual decays with kinetic energies determined by Dirac-Fock methods. For these Auger electrons, track structures in liquid water have been generated and superimposed on a straight DNA plasmid model with atomic coordinates taken from X ray diffraction studies. Due to its high geometrical resolution, this DNA model makes it possible to localize the energy deposition or/and radical production events relative to the sub-molecular units of the DNA strands (base, sugar, phosphate). Furthermore, it is possible to distinguish between events inside (direct) and outside (indirect, radical production) of the atomic volumes of the DNA. On the basis of different assumptions for the effectiveness of strand break induction by direct hits and by OH· and H· radicals, the yields for single- and double strand breaks, as well as the strand break distribution as a function of the distance from the decay site, has been evaluated and compared with experimental and theoretical results from the literature.

INTRODUCTION

It is well known that Monte Carlo simulation represents a very good way of investigation for the understanding of radiation damage at the molecular level. A source of radiation which induces a specific pattern of damage within a distance of a few molecules only can be seen with DNA-incorporated Auger electron emitters, *e.g.* ^{125}I. This nuclide has been demonstrated to possess high-LET-like biological effectiveness when it is incorporated in the DNA molecule. A decay site only a few nanometers apart from this critical target will drastically reduce its efficiency (1). Due to this particular character of damage, the Auger electrons released by ^{125}I represent a most useful tool in radiation biology. The Monte Carlo codes that simulate the electron spectra of individual decays (2,3) and that generate track structures (4,5), in combination with superimposing the tracks on an atomic DNA target model (6), are expected to provide information about the radiation action mechanism.

Since the details of these mechanisms are still unknown, one has to introduce different assumptions for the relationship between energy deposition events and the resulting biological effects in order to simulate the radiation damage. To validate these assumptions, a comparison with experimental results is necessary. A pioneering experiment for the determination of the spatial distribution of biological damage on the DNA scale was performed by Martin and Haseltine (7). These authors labeled a linear segment of plasmid DNA with ^{32}P at a position 58 base pairs away from the site of a decaying ^{125}I nuclide. By measuring the length of the phosphorus-labeled DNA-fragments, a distribution of those strand breaks could be derived which are most distant from the ^{125}I position.

Charlton and Humm (8) made use of this experimental data when they introduced a method to calculate the number of DNA strand breaks. They generated water vapor track structures for the ^{125}I Auger electrons and compared these tracks with a geometrical DNA model. This model is described by a straight cylinder consisting of three parts, an inner core representing the base pairs, and around this core semi-annuli representing the phosphate/sugar chain. All the energy transfer events taking place inside the phosphate/sugar volumes were counted to be effective in terms of strand break induction when the amount of energy deposited was above a certain threshold (17.5 eV). Without any further assumptions the authors found a surprisingly good coincidence with the experimental results of Martin and

Haseltine (7). In another recent paper, Pomplun (6) assessed by principally the same technique the energy deposition in and near the different submolecules of the DNA and estimated the number of strand breaks caused by direct and indirect effects. The target model used allowed a geometric atomic scale resolution based on the coordinates of the individual DNA atoms (9,10). In particular, the importance of those Auger electrons with a kinetic energy of $E \leq 500$ eV could be revealed, thereby demonstrating the necessity to determine these energies as accurate as possible. The calculation of the Auger electron kinetic energies by the empirical (Z+1)-approximation, normally sufficient in the case of single charged atoms, leads to a more or less strong energy imbalance when applied for cascade released electrons (11).

Another important aspect of these two papers must be seen in the application of water vapor track structures which may induce significant uncertainties in the localization of energy deposition events with regard to the nanometer scale of the DNA target models. There are two main reasons to use liquid water conditions for the particle transport code rather than those for water vapor: 1) The production of secondary electrons is not always localized at the site of initial energy transfer (12,13). In liquid water, inelastic collisions may involve thousands, even 10^6 or more electrons, and the collective excitations can produce H_2O^+ or H_2O^* at sites situated up to several nanometers from the primary trajectory. It is the reason we use liquid water cross-sections derived from dielectric theory in which liquid water is assumed to respond to the passage of charged particles as any dielectric medium responds to an electromagnetic disturbance (12). 2) The physico-chemical step (10^{-15} s to 10^{-12} s) must not be neglected. During this step subexcitation electrons may recombine and/or thermalize, early physico-chemical events arise and then the chemical stage begins with diffusion and chemical reactions of all species created: e^-_{aq}, $OH\cdot$, $H\cdot$, H_3O^+, H_2O_2, OH^-, H_2, HO_2. Furthermore, the liquid water code identifies the chemical species created by the energy deposition events of the tracks. This opens the possibility to trace individual radicals or *e.g.* to exclude all those species from further consideration which are supposed not to react efficiently with the DNA (see METHODS).

In this paper we try to utilize these advantages in the simulation of strand break induction by DNA incorporated ^{125}I on the basis of liquid water track structures. To have accurate Auger electron kinetic energies, the initial electron spectrum was calculated with a Dirac-Fock approach (3). By introducing specific assumptions for the damaging effectiveness of individual

chemical species, the numbers of SSB and DSB as well as the local distribution of the breaks will be evaluated and compared with experimental results. The fractions of direct and indirect hit modes contributing to the total number of breaks will also be given.

METHODS

The Auger electron spectrum of ^{125}I has been generated by Monte Carlo simulation of the Auger cascades produced by electron capture which is the first step in the decay of ^{125}I. To determine the electron kinetic energy the difference between the total energy of the (multiple) ionized atom before and after the Auger electron emission was calculated. For details see Ref. (3).

For track structure generation we used three Monte Carlo type codes chained together as described in Ref. (26) to obtain the space and time evolution of each chemical species created during the slowing-down of electrons in liquid water. Input data for the physical step (up to 10^{-15} s) are cross-sections derived from the dielectric response function (13) from electron scattering in gases (14) or theory. During the physico-chemical step (10^{-15} s to 10^{-12} s), the subexcitation electrons are transported with the use of cross-sections measured in amorphous ice (15,16), while recombination and thermalization follow the Onsager-Debye theories, and dissociation semi-empirical ones. Finally, in the chemical step (10^{-12} s to seconds), about twenty-five reactions are considered and species diffuse according to the Smoluchowski law.

The DNA target model used here (see Fig. 1) has been described in detail elsewhere (6). It is based on the geometric coordinates of the individual DNA atoms allowing a very high geometric resolution. Only those energy deposition events were considered which take place inside a volume of interest represented by a virtual cylinder enveloping all nucleotides of the straight DNA segment. This includes also the structural water molecules in the major and minor grooves for which individual coordinates are not available. Due to the lack in knowledge of the species and radicals created by electron-DNA direct interactions, we have only used the chemical species from the physical stage in this third part of this study, and it has been assumed that no radical from the environmental regions will diffuse into this volume of interest nor any radical will escape from this volume. Such a situation reflects a frozen state condition. Therefore, the numbers of SSB and

DSB calculated here have been compared with the experimentally derived data reported by LeMotte and Little (17) for human cells at -90°C.

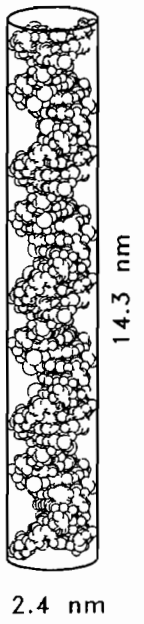

FIG. 1. DNA target model (inclined by 15°); the ^{125}I is positioned at the site of the methyl group of the 41st base (out of 82) which has been assumed here to be thymine. This position is 0.56 nm distant from the central helix axis. The volume of interest is indicated by the virtual cylinder.

The strand break induction has been simulated here in the following way: all the energy deposition events located inside the van der Waals radius of a phosphate-group or sugar atom were counted as SSB caused by direct hits if the amount of deposited energy in the phosphate/sugar molecule was greater than a threshold value of 18 eV (see next chapter). For the indirect effects from all the radicals evaluated by the track structure code, only the primary water radicals OH·, H· and e^-_{aq} have been assumed here to react with the DNA (see *e.g.* Refs. 18,19). However, e^-_{aq} was neglected for strand

break induction due to the studies of Lemaire *et al.* (20) for poly U and of Nabben *et al.* (21) for the inactivation of double-stranded DNA, whereas the effectiveness of OH· and H· were supposed to be equal (21). As possible mechanisms for strand break induction by the OH· radicals the hydrogen abstraction from deoxyribose and the hydroxyl addition to bases are discussed (22), the H· radical is supposed to act also via base radicals (20). All other radicals have been excluded from further consideration. Two SSB on opposite strands within a distance of less than 20 base pairs have been detected as one DSB (for a more detailed discussion see Ref. 6). For the simulation of the Martin and Haseltine (7) experiment only those strand breaks have been considered which - according to the experimental design - are furthest from ^{125}I.

RESULTS AND DISCUSSION

For all particles belonging to each ^{125}I decay, a data set in a four coordinate system (t, x, y, z) is obtained for each species: e^-_{aq}, OH·, H·, H_3O^+, H_2O_2, OH^-, H_2, HO_2 between 10^{-15} s and 1 second. In Fig. 2 (a-d) are represented three-D space and time evolutions (all species together) for one randomly chosen ^{125}I decay in liquid water. Figs. 3 and 4 are zooms near the initial ^{125}I decay point, assumed at axes origin. On all axes, the distance unit is nanometers. No interaction with any atom from the target model has been considered here.

In Fig. 5 we have plotted the average number of chemical species produced in 10^{-12} s in spherical shells of thickness one nanometer centered at the site of ^{125}I decay. The shapes for OH·, H· and H_3O^+ species are very close to the initial (10^{-15} s) dose point kernel obtained for ^{125}I decays. The hydrated electron smooth curve is due to the recombination, diffusion and thermalization of subexcitation electrons created at 10^{-15} s with energies up to 7.4 eV. If we compare this result with same found in literature (23), the shapes are very similar except for hydrated electrons and absolute values. There are two reasons for the discrepancies: first, the absolute number of species per decay is strongly dependent on the ^{125}I cascade electron spectra. Secondly, for hydrated electrons, the travel distance depends on elastic and inelastic cross-sections, diffusion coefficient and the recombination model used between 10^{-15} s and 10^{-12} s, the physico-chemical step.

a

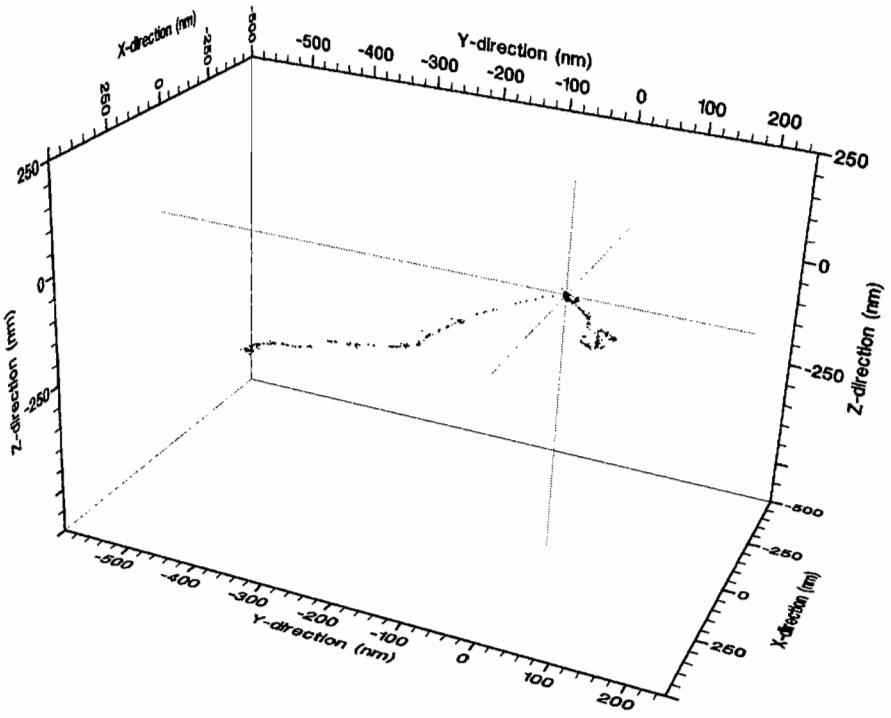
X-direction (nm)
Y-direction (nm)
Z-direction (nm)
Z-direction (nm)
X-direction (nm)
Y-direction (nm)

b

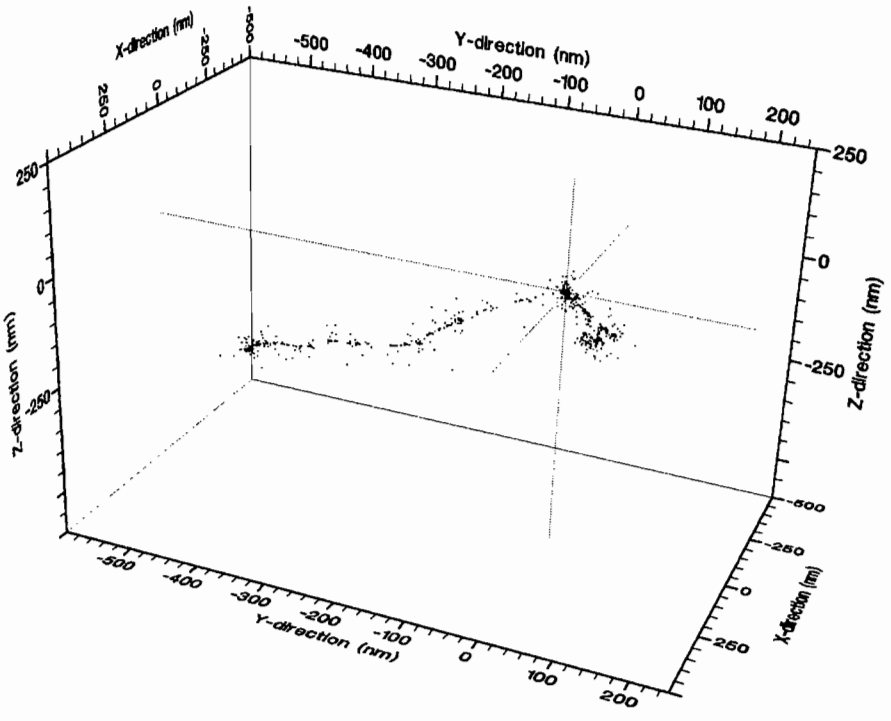
X-direction (nm)
Y-direction (nm)
Z-direction (nm)
Z-direction (nm)
X-direction (nm)
Y-direction (nm)

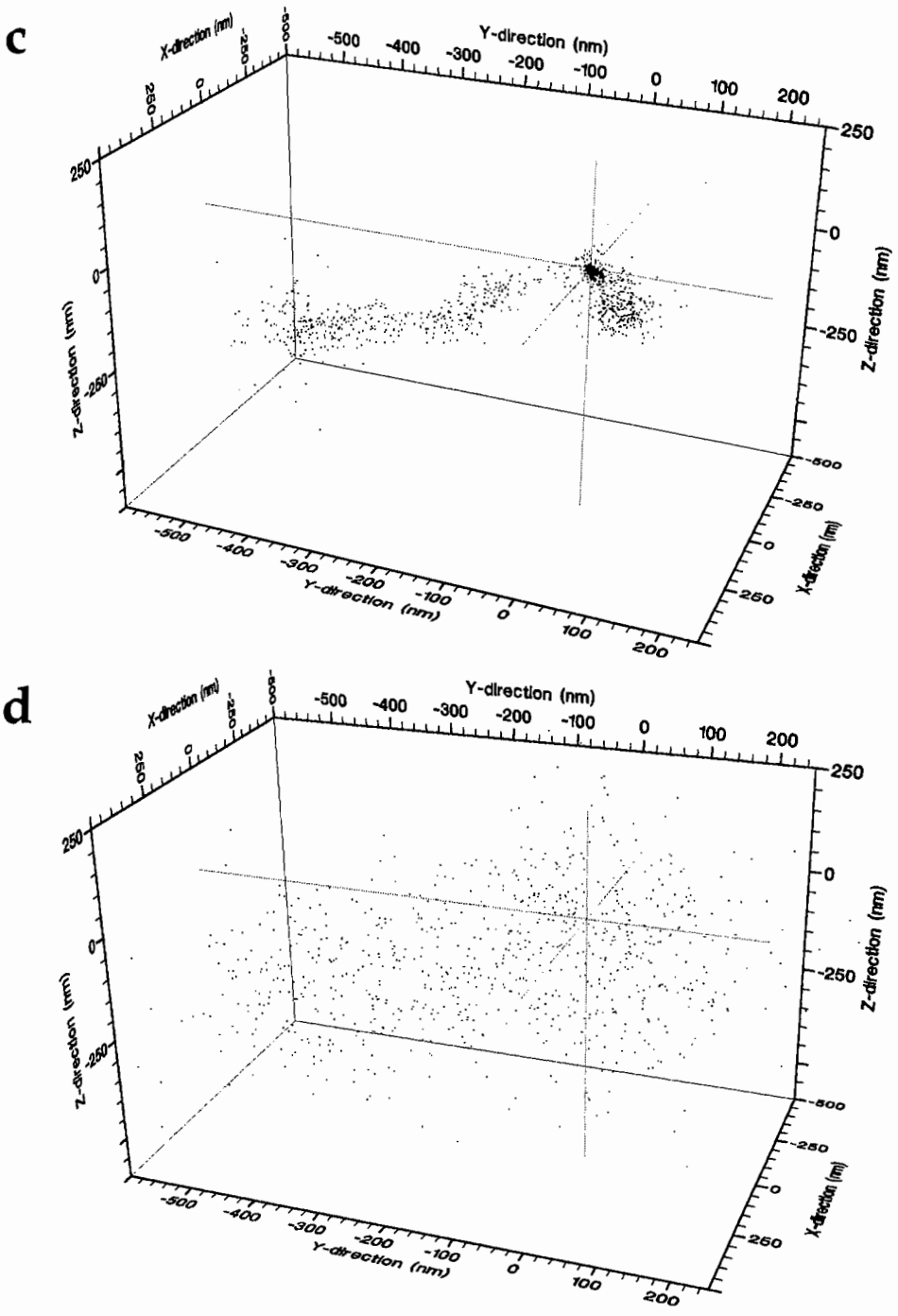

FIG. 2. Complete track of one randomly chosen ^{125}I-decay for (a) 10^{-15} s, (b) 10^{-12} s, (c) 10^{-9} s, (d) 10^{-8} s.

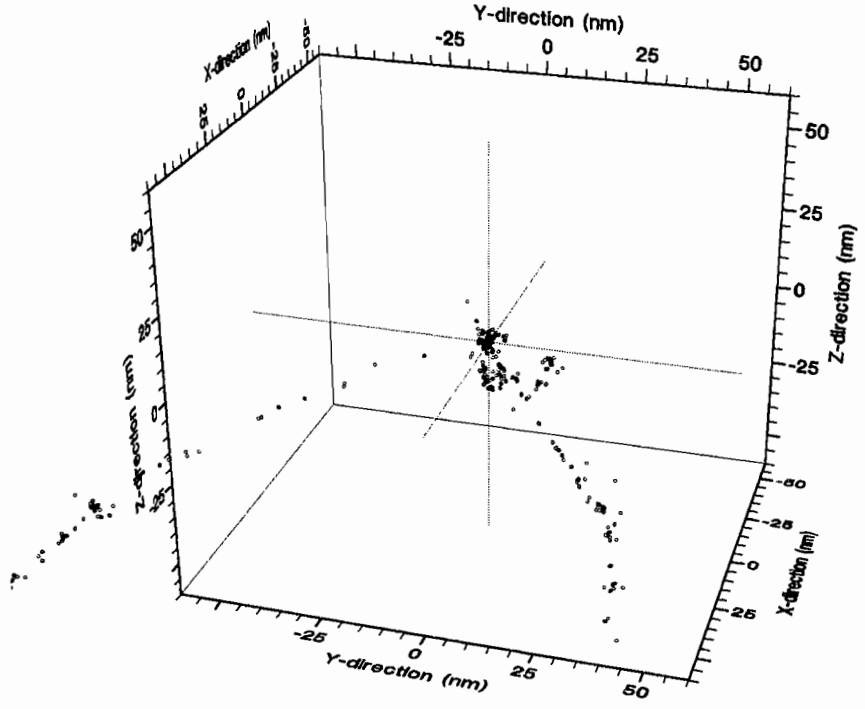

FIG. 3. Zoom from Fig. 2a.

The best agreement with the experimental data of Martin and Haseltine (7) for the spatial distribution of those strand breaks furthest from ^{125}I were obtained by using a threshold energy of 18 eV for direct hits. Charlton and Humm (8) found nearly the same value (17.5 eV). Until now only the labeled strand could be considered (Fig. 6) demonstrating that in the immediate vicinity of the decay site - where the overwhelming number of breaks have been found experimentally - the calculated values fit very well. For comparison the water vapor tracks generated by the MOCA8 code (4) for the same electron spectrum have been used to simulate the Martin and Haseltine (7) experiment. In this case, energy deposition events of $E > 18$ eV inside an atom of the phosphate/sugar group (direct hit) or near to these submolecules (indirect hits) were assumed to be effective in strand break induction. The results of this simulation are shown in Fig. 6. Whereas for distances of three and more base pairs from the decay site there are only small differences between the liquid water and the water vapor data. The latter ones

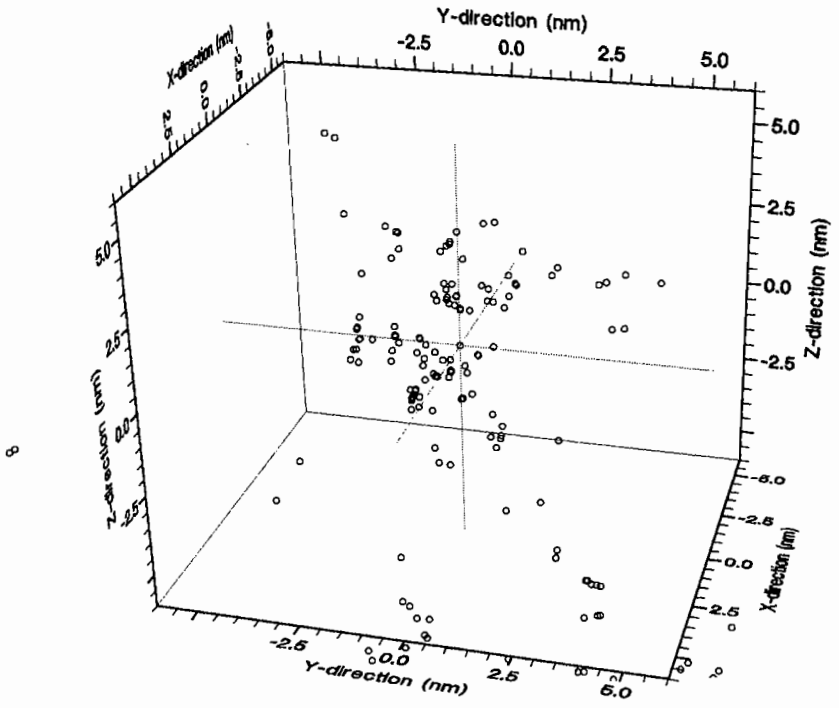

FIG. 4. Zoom from Fig. 2a.

significantly disagree with the experimental distribution by revealing less breaks at the site of decay and too many at distances of one and two base pairs apart from the labeled base. Due to the satisfactory results obtained by the liquid water tracks, the contribution of each of the two hit modes has been assessed. As can be seen from Fig. 7, the characteristic shape of the curve for all hits (taken from Fig. 6) is determined by the direct hit pattern in the region from '0' to '5' base pairs distance. The number of radical-induced breaks (indirect hits) falls more or less continuously with a steep decline (parallel to the direct hits) between the second and third base pair from the site of decay. It should be noted here that there is an inherent bias in these curves due to the experimental condition of measuring the farthest breaks only; additional breaks at positions nearer to the decaying ^{125}I are masked.

The results for the total numbers of strand breaks per ^{125}I decay are summarized in Table I. The water vapor values additionally shown here were obtained by recalculation of data from Ref. (6) by increasing the

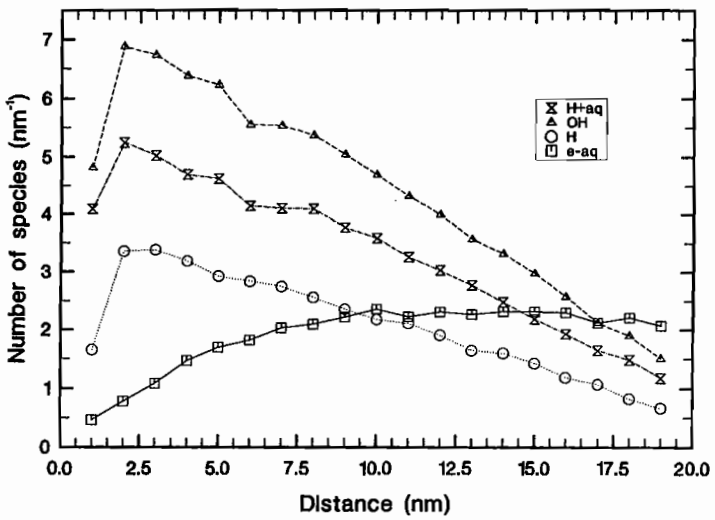

FIG. 5. Number of different species inside spherical shells around the decay.

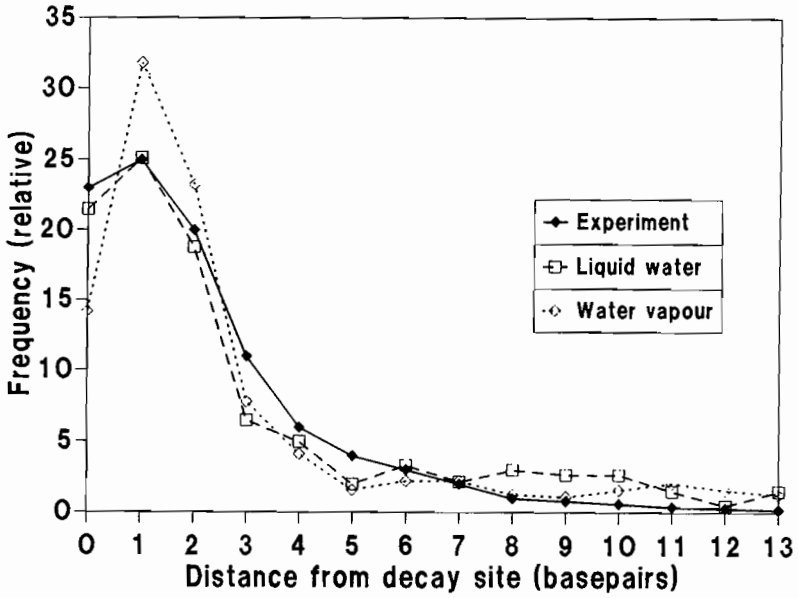

FIG. 6. Spatial distribution of ^{125}I induced DNA strand breaks; comparison of liquid water and water vapor calculations with experimental results from Martin and Haseltine (7).

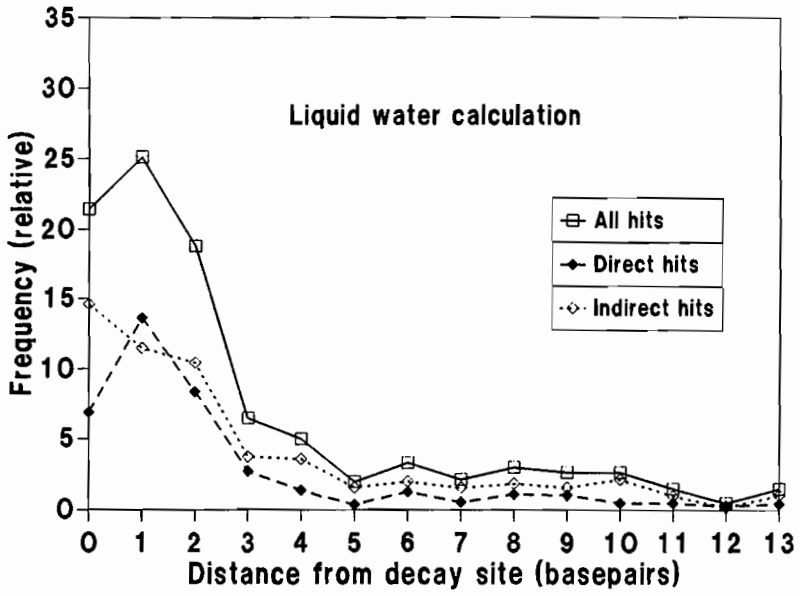

FIG. 7. Calculated direct and indirect hit mode fractions in the distribution of DNA strand breaks for liquid water conditions.

TABLE I
Number of SSB and DSB per ^{125}I Decay

Kind of Break	DNA-Helix Model		Experiment
	Liquid Water	Water Vapor	Human Diploid cells -90°C
SSB (total)	2.9	2.9	3.0 (4.3±1.2)
SSB (corr.)	1.7	1.6	1.7 (2.4)
DSB	0.6	0.7	0.6 (0.86±0.3)

Due to the best fit values obtained in this work (energy threshold for direct hits E > 18 eV) the values published in Ref. (6) have been recalculated using this threshold instead of E > 10 eV, the original experimental results from Ref. (17) (in brackets) have been reduced by 30% due to the alkaline elution technique (see Ref. (25)).

threshold values for direct hits (see above) from 10 eV to 18 eV. For indirect hits a threshold of 17 eV was taken according to Chatterjee and Magee (24). For the comparability of the experimental conditions with the data calculated here see Ref. (6). Due to the alkali elution technique used by LeMotte and Little (17), these values have been reduced by 30% (25). On first view it might be surprising that considerably less than 1 DSB per decay - the expected value from many studies - is found here. However, in the frozen state situation simulated here, the radicals will become relatively immobile so that only those species produced in the water sheaths of the DNA may react efficiently. On the other hand, possible repair processes are suppressed at these temperatures. With regard to the number of breaks both of these effects (immobilization of radicals outside the volume of interest and inhibition of repair) would have opposite directions (with an unknown net effect) but for this high-LET Auger electron radiation it seems to be reasonable to expect for room temperature conditions a stronger influence of the radicals than of the repair so that by the elimination of both effects due to frozen state the number of breaks should be lower than under room temperature. In general, there is a good agreement between all three sets of data without any significant difference between the water vapor and the liquid water data. The advantage, however, which can be taken from the liquid water data is given by the more detailed information about the involved radiation action mechanisms which had been incorporated into the DNAMOD code (6) controlling the interaction of the tracks with the target model. In particular only OH· and H· radicals attacking the sugar and bases are responsible for strand breaks by indirect effects (see METHODS).

This sophisticated model (^{125}I decay + track generation + DNA model) will be a very useful tool when more precise electron-DNA cross-sections and physico-chemical data on the electron diffusion and reactions with water species are known.

CONCLUSIONS

Track structures of Auger electrons released by ^{125}I decay have been generated for liquid water conditions. By superimposing these tracks onto a DNA target model, the strand break induction by direct hits as well as by radical attack were simulated. A satisfactory agreement with experimentally determined spatial distribution of the breaks could be achieved by introducing an energy threshold of $E > 18$ eV for direct hits and by considering only OH·

and H· radicals out of all the chemical species. Whereas about two thirds of the strand breaks at the site of decay (labeled nucleotide) seem to be induced by radical attack, the direct hits by Auger electrons are responsible for the peak in the distribution at the neighboring nucleotide position (Fig. 7). The total number of SSB and DSB calculated here also agree very well with experimental findings. These results support radical-behavior mechanisms suggested in the literature.

REFERENCES

1. D.E. CHARLTON, The range of high-LET effects from ^{125}I decays. *Radiat. Res.* **107**, 163-171 (1986).
2. D.E. CHARLTON and J. BOOZ, A Monte Carlo treatment of the decay of ^{125}I. *Radiat. Res.* **87**, 10-23 (1981).
3. E. POMPLUN, J. BOOZ, and D.E. CHARLTON, A Monte Carlo simulation of Auger cascades. *Radiat. Res.* **111**, 533-552 (1987).
4. H.G. PARETZKE, Radiation track structure theory. In *Kinetics of Nonhomogeneous Processes*, (G.R. FREEMAN, Ed.), Wiley, New York, pp. 89-170, 1987.
5. M. TERRISSOL and A. BEAUDRE, Simulation of space and time evolution of radiolytic species induced by electrons in water. *Radiat. Prot. Dosim.* **31**, 171-175 (1990).
6. E. POMPLUN, A new DNA target model for track structure calculations and its first application to I-125 Auger electrons. *Int. J. Radiat. Biol.* **59**, 625-642 (1991).
7. R.F. MARTIN and W.A. HASELTINE, Range of radiochemical damage to DNA with decay of iodine-125. *Science*, **213**, 896-898 (1981).
8. D.E. CHARLTON and J.L. HUMM, A method of calculating initial DNA strand breakage following the decay of incorporated ^{125}I. *Int. J. Radiat. Biol.* **53**, 353-365 (1988).
9. S. ARNOTT and D.W.L. HUKINS, Refinement of the structure of B-DNA and implications for the analysis of X ray diffraction data from fibers of biopolymers. *J. Mol. Biol.* **81**, 93-105 (1973).
10. R. CHANDRASEKARAN and S. ARNOTT, *The structures of DNA and RNA helices in oriented fibers*. Landolt-Börnstein, New Series VII, 1b, Springer-Verlag, Berlin, 1989.
11. E. POMPLUN, ^{123}I: Calculation of the Auger electron spectrum and assessment of the strand breakage efficiency. (this volume).
12. R.H. RITCHIE, R.N. HAMM, J.E. TURNER, and H.A. WRIGHT, The interaction of swift electrons with liquid water. In *Proceedings of the Sixth Symposium on Microdosimetry*, Brussels, Belgium, EUR 6064, London: Harwood Academic, pp. 345-354, 1978.
13. J.M. HELLER, R.N. HAMM, R.D. BIRKHOFF, and L.R. PAINTER, Collective oscillation in liquid water. *J. Chem. Phys.*. **60**, 3483-3486 (1974).
14. G.J. KUTCHER and A.E.S. GREEN, A model for energy deposition in liquid water. *Radiat. Res.* **67**, 408-425 (1976).
15. M. MICHAUD and L. SANCHE, Total cross-section for slow electron (1-20 eV) scattering in solid H_2O. *Phys. Rev.* **A36**, 4672-4683 (1987).
16. M. MICHAUD and L. SANCHE, Absolute vibrational excitation cross-sections for slow electron (1-18 eV) scattering in solid H_2O. *Phys. Rev.* **A36**, 4684-4699 (1987).
17. P.K. LEMOTTE and J.B. LITTLE, DNA damage induced in human diploid cells by decay of incorporated radionuclides. *Cancer Res.* **44**, 1337-1342 (1984).

18. D. SCHULTE-FROHLINDE, Comparison of mechanisms for DNA strand break formation by the direct and indirect effect of radiation, In *Mechanisms of DNA damage and repair*, (G.M. SIMIC *et al.*, Eds.) pp. 19-27, Plenum Press, New York, 1986.
19. M.V.M. LAFLEUR and H. LOMAN, Radiation damage to ϕX174 DNA and biological effects. *Radiat. Environ. Biophys.* **25**, 159-173 (1986).
20. D.G.E. LEMAIRE, E. BOTHE, and D. SCHULTE-FROHLINDE, Yields of radiation-induced main chain scission of poly U in aqueous solution: strand break formation via base radicals. *Int. J. Radiat. Biol.* **45**, 351-358 (1984).
21. F.J. NABBEN, M.V.M. LAFLEUR, J.C.M. SIKKERS, A.C. LOMAN, J. RETEL, and H. LOMAN, Repair of damage in double-stranded ϕX174 (RF) DNA due to radiation-induced water radicals. *Int. J. Radiat. Biol.* **45**, 379-388 (1984).
22. D. SCHULTE-FROHLINDE, Mechanisms of strand breaks in DNA induced by OH radicals in aqueous solution. In *Proc. 6th Int. Congr. Radiat. Res.* (S. OKADA *et al.*, Eds.), pp. 407-422, Mazuren, Tokyo, 1979.
23. H.A. WRIGHT, R.N. HAMM, J.E. TURNER, R.W. HOWELL, D.V. RAO, and K.S.R. SASTRY, Calculation of physical and chemical reactions with DNA in aqueous solution from Auger cascades. *Radiat. Prot. Dosim.* **31**, 59-62 (1990).
24. A. CHATTERJEE and J.L. MAGEE, Theoretical investigation of the production of strand breaks in DNA by water radicals. *Radiat. Prot. Dosim.* **13**, 137-140 (1985).
25. R. ROOTS, G. KRAFT, and E. GOSSCHALK, The formation of radiation-induced DNA breaks: the ratio of double-strand breaks to single-strand breaks. *Int. J. Radiat. Oncol. Biol. Phys.* **11**, 259-265 (1985).
26. A. BEAUDRE, Simulation spatio-temporelle des processus radiolytiques induits dans l'eau par des électrons. Thèse de l'Université Paul Sabatier, Toulouse, France, No. 371, 1988.

DISCUSSION

Hofer, K. G. According to early work by Burki, the oxygen effect for ^{125}I damage is quite small. Here you claim that indirect effects are quite prominent. How do you reconcile this apparent discrepancy?

Pomplun, E. The approach used here considers only the DNA itself, including the structural water in the grooves, so that the terms direct and indirect effects also refer to this volume only. Effects like the oxygen effect which depend on the conditions in the environment of the DNA are not taken into account here. In this sense, the calculations simulate a frozen state situation with an assumed immobilization of radicals. Only those radicals which are produced in the nearest surroundings of the DNA molecule, namely inside the 2.4 nm diameter cylinder, are expected here to attack the DNA strands.

Nikjoo, J. We need to move from the concepts of direct and indirect effect to mechanisms of SSB production.

Pomplun, E. By the classical terms direct effects and indirect effects, a clear distinction between two different mechanisms is made. As long as no more precise mechanisms are fully understood, I think we should retain these terms.

Humm, J. L. You showed (6) that 90% of the strand break contributing energy deposition arises from electrons of energies < 500 eV (*i.e.* M & N

Auger and Coster-Kronig electrons). Accurate DNA dose specification therefore depends on the accurate evaluation of these electrons. The current Auger electron Monte Carlo calculations agree on the K and L Auger series, but deviations become more significant for the lowest energy electrons. You showed differences of nearly a factor of two in the low energy electron yields and energies for the different methods. Yet the DNA strand break yields you showed using your Auger cascade code and the simpler code of Charlton & Booz were in close agreement. Do you think that this is due to the enormous magnitude of ^{125}I decay, making it an unsuitable isotope as the basis for different Monte Carlo simulation code comparison? Perhaps such comparisons should be made with an isotope emitting a small number of Auger electrons such as ^{55}Fe. Do you agree?

Pomplun, E. Both strand break calculations have been performed not only with different electron spectra but also with different DNA models and, what could be of special importance, different ^{125}I positions relative to the central DNA axis. Therefore, it would be very interesting, first, to repeat the calculations for both electron spectra on the basis of equal models and ^{125}I positions. If the close agreement in the strand break remains, the enormous magnitude of ^{125}I decay could be an explanation for masking differences in the electron spectra. In that case one should indeed use an isotope like ^{55}Fe to demonstrate the differences in the electron spectra as being responsible for differences in strand break yields.

Biophysical Aspects of Auger Processes, AAPM Symposium Series No. 8 (1992) 153-163
Eds. RW Howell, VR Narra, KSR Sastry, DV Rao

^{125}I DECAY IN SYNTHETIC OLIGODEOXYNUCLEOTIDES

ROGER F. MARTIN and GLENN D'CUNHA

Peter MacCallum Cancer Institute
481 Little Lonsdale Street
Melbourne, Victoria 300, Australia

ABSTRACT

The availability of synthetic oligodeoxynucleotides provides the opportunity to study the effects of ^{125}I in DNA with added precision and detail, compared to an earlier study (Martin and Haseltine, *Science* **214**, 296, 1981). We have designed a template/primer system which enables incorporation of ^{125}IdC into a defined location in a 31mer. The main advantage of this approach is that relatively large amounts (a few μCi) of DNA with both ^{32}P and ^{125}I can be produced quite easily. Consequently, when ^{125}I-induced DNA damage is analyzed on DNA sequencing gels, the distribution of ^{32}P-labeled cleavage products can be determined more accurately, following accumulation of decay events under various conditions (*e.g.* temperature, buffer components, free radical scavengers). The results of preliminary experiments suggest that the yield of DNA strand breaks per decay approaches one, at least for the ^{125}I labeled strand. Extension of this experimental approach will also enable investigation of the nature of the terminii (*e.g.* phophoryl - *versus* phophorylglycollate) at either side of ^{125}I decay-induced DNA strand breaks. The question of energy migration is also being investigated in the oligodeoxynucleotide system, by studying the effects of inclusion of BrUdR nucleotides at various distances from the ^{125}IdC.

INTRODUCTION

The biological effectiveness of ^{125}I decay in DNA stems from the intensely focussed radiochemical damage that arises from two successive Auger cascades. The appreciation of the microdosimetry involved was underlined in studies involving Monte Carlo analysis of the ^{125}I decay event (1), and track structure analysis of each of the electrons emitted in simulated decays (2). The molecular analysis of DNA damage resulting from DNA-associated ^{125}I decay began with quantitation of strand breakage by sedimentation analysis of DNA from bacteriophages (3,4), *E. coli* (5) and eukaryote cells (6), in which ^{125}I decays had been accumulated. From such studies emerged the finding that on average, each ^{125}I decay yielded approximately 1 DNA double strand break.

The advent of restriction endonucleases and DNA sequencing techniques provided the opportunity to produce DNA molecules with a single ^{125}I atom in a defined location, and to analyze the location of DNA strand breaks resulting from accumulated ^{125}I decay events. These studies showed that DNA-associated ^{125}I decay resulted in the induction of single-strand breaks in both ^{125}I-containing strand, and the opposite strand. Most of this strand breakage occurred within four to five base pairs of the ^{125}I-labeled nucleotide (7).

These two approaches, microdosimetry and DNA damage analysis, eventually converged in an important study in which the energy deposition patterns from simulated ^{125}I decays were superimposed on a model of the B-DNA helix (8). This study actually utilized the distribution of DNA damage reported from the DNA sequencing study (7). In fact one of the parameters of the microdosimetry model, namely the amount of energy required to be deposited in a DNA strand to yield a single-strand break, was set at a value of 17.5 eV to give optimal concurrence of the model with the experimental data from DNA sequencing analysis. These studies, which were later refined (9), enabled an extension of this microdosimetric approach to other forms of radiation (10). More importantly, in the current context, the studies provided an explanation for the observation that the number of ^{125}I decays per lethal event in the eukaryote genome could be as high as 100. The potential explanation for this resides in the fact that the dosimetric studies demonstrated a wide variation amongst different decay events, in the nature

of the ^{125}I decay induced DNA double strand breaks. In short, some DNA double stranded breaks involved a lot more extensive damage, than others.

Regardless of the relationship between ^{125}I decays and lethal events, all the above studies, when taken together, indicated a picture in which most of the induced DNA double stranded breaks were in the close vicinity to the site of ^{125}I decay in DNA. This view was contradicted by an electron-microscopy study which reported strand breakage at sites distant from ^{125}I decay (11). Furthermore, there have been a number of proposals for energy transfer in DNA (12,13). These ideas have underlined the fact that in the earlier DNA sequencing studies (7), the efficiency of strand breaks induced per decay, was not actually measured, due to limitations in the technology available at that time. The assumption that the one double strand break per ^{125}I decay refers to a DNA double strand breaks induced at the site of decay, is clearly an important issue to verify. In the earlier studies of measuring DNA double strand induction per ^{125}I decay event (3-6), the observation of an average of about one DNA double strand break per decay was not inconsistent with the idea that not all these breaks are at the site of ^{125}I decay. The availability of the means to easily produce synthetic oligodeoxynucleotides provides the opportunity to revisit the application of DNA sequencing techniques to study DNA damage from ^{125}I decay. In particular it provides a possibility of measuring the absolute efficiency of strand break induction in the vicinity of the ^{125}I decay event. This communication reports our progress in this endeavor.

MATERIALS AND METHODS

The design strategy for the experiments is illustrated in Fig. 1. Briefly, oligodeoxynucleotides are synthesized (Applied Biosystems, Model 26A), and annealed to yield a template/primer configuration. Hybridization was monitored by electrophoresis in native polyacrylamide gels, after 5'-^{32}P-end labeling (4) of the primer oligoDNA. Carrier-free ^{125}I-dCTP (NEN-Dupont) is then incorporated by T4 DNA polymerase (Promega), and the primer extension completed by the addition of excess dCTP and other dNTPs. The extended primer strand is then isolated from a (denaturing) DNA sequencing gel, by excision of a gel slice and extraction in the presence of excess 31mer template strand. The extracted, full length "target" DNA, migrates as double-stranded hybrid on native polyacrylamide gel electrophoresis. Minor

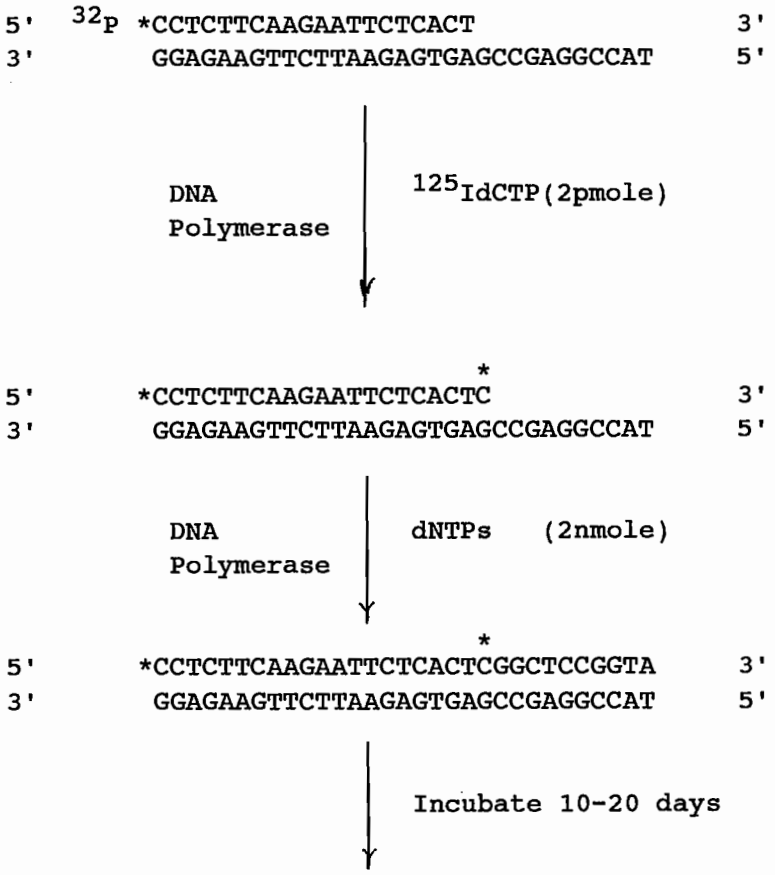

FIG. 1. ^{125}I decay in oligoDNA; outline of basic experimental design.

modifications to this strategy allow labeling of the ^{125}I-containing strand at the 3'-end, and then opposite (template) strand at either end.

At this juncture it is worthwhile to note the flexibility of the design strategy. For example, Br-dUTP can be included in the dNTP mixture. This enables investigation of energy transfer, as ^{125}I decay-induced strand cleavage adjacent to the Br-U sites. This feature is illustrated in Fig. 2. Furthermore, it will be noted that the target DNA in Figs. 1 & 2 comprises a binding site (AATT) for Hoechst 33258 and similar analogs. This provides the opportunity

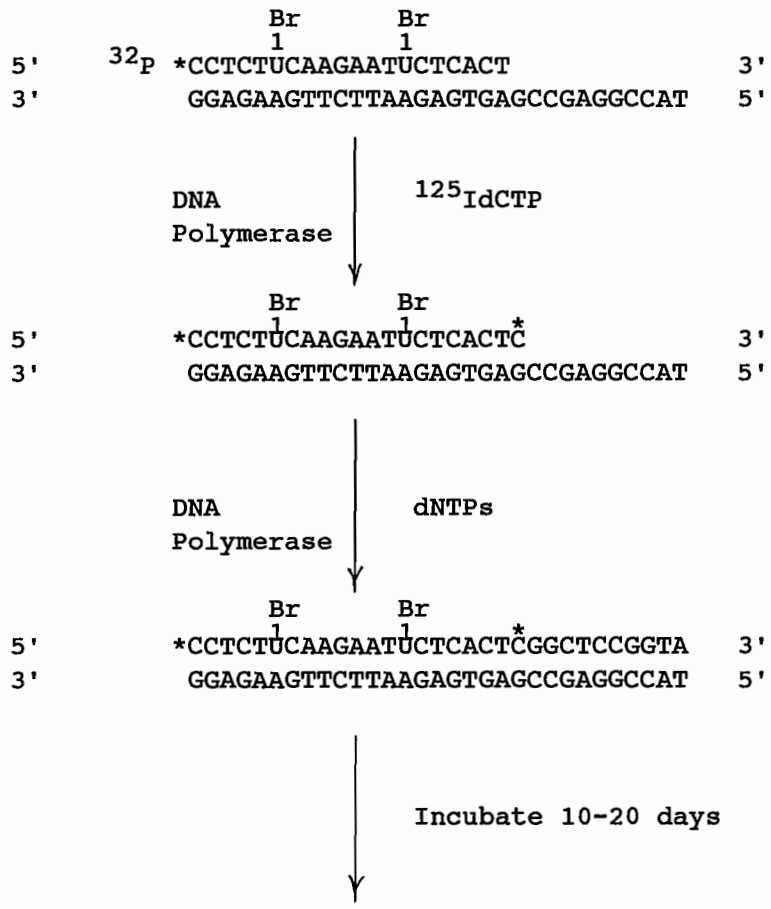

FIG. 2. ^{125}I decay in oligoDNA; experimental design to investigate energy transfer (*i.e.* induction of strand breaks at BrU sites, by ^{125}I-decay.

to investigate the effects of these radioprotecting ligands (15) on ^{125}I-induced DNA strand breakage. A further opportunity presented by this strategy is to use the DNA sequencing technology to investigate the nature of the terminii produced by ^{125}I-decay-induced DNA-strand breaks. Irradiation of 5'-end labeled DNA reveals the presence of doublets in DNA sequencing gels, first described by Henner *et al.* (16). The slower of these doublets corresponds to 3'-phosphoryl terminii, and the faster, 3'-phosphorylglycollate (15,16). The latter

is indicative of strand breakage initiated by abstraction of 4'-deoxyribosyl C-Hs (17), but are not observed under conditions of direct action (18).

The use of short primers maximizes the resolution of the DNA sequencing gel analysis and hence of detection of 3'-phosphorylglycollate species. A strategy is outlined in Fig. 3. After synthesis and isolation of the ^{125}I-oligoDNA, the sample is allowed to accumulate ^{125}I- decays under various conditions, such as:

(i) 0.5 M NaCl in 25 mM Tris HCl (pH 7.5) /5 mM EDTA/2 mM KI, at 4°C or at -20°C.
(ii) as in (i) except that 10% glycerol is included.
(iii) as in (i) except that 100 mM mannitol is included.

Given the relative half-lives of ^{125}I and ^{32}P (the "indicator" isotope), the optimal storage time is 15-20 days. At this time, the samples were denatured and analyzed on DNA sequencing gels (14,16). When required, an X ray film autoradiograph was used to locate the ^{32}P-labeled DNA fragments, and the individual bands excised from the gel. In this preliminary study, the amount of ^{32}P in the product DNA bands, and the parent full-length bands, was quantitated by Cerenkov counting. The fraction of ^{32}P in fragment bands compared to the total of parent and fragment bands was then calculated, and taken to indicate the average numbers of breaks per parent molecule. This calculated value was then compared with the number of ^{125}I decays accumulated over the incubation period.

RESULTS

The results of one experiment are shown in Fig. 4. The autoradiograph shows the resolution obtained between successive bands of ^{125}I-decay induced fragments; sufficient for excission and quantitation of individual bands. Since the load of ^{32}P-DNA varies between the different lanes, it is not possible to compare the various storage conditions by direct inspection. Some preliminary results, obtained from gels such as that shown in Fig. 4, suggest that the yield of DNA strand breaks per decay approaches one, at least for the ^{125}I-labeled strand. More data is required to evaluate the effect of storage conditions. Moreover, the quantitation of ^{32}P in gel slices by Cerenkov counting has been found to be sub-optimal, and alternative methods (*viz* use of scintillants) are being investigated.

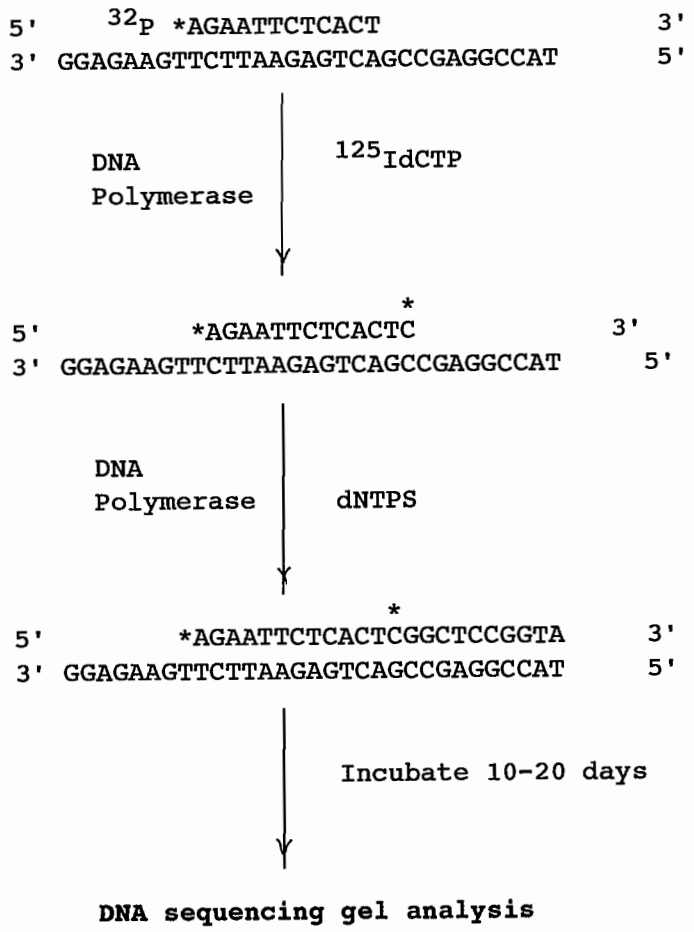

FIG. 3. ^{125}I-decay in oligoDNA; experimental design to investigate chemical nature of the terminii left by ^{125}I-decay-induced strand breaks. The short 5'-end-labeled primer maximizes the resolution obtained on DNA sequencing gel analysis.

DISCUSSION AND CONCLUSIONS

In order to evaluate the results reported here, it is important to appreciate the limitations of the earlier DNA sequencing study (7). That was done at a time when DNA sequencing was in its infancy, and obtaining sufficient ^{32}P-labeled material was a major problem. The ^{125}I-dCTP was

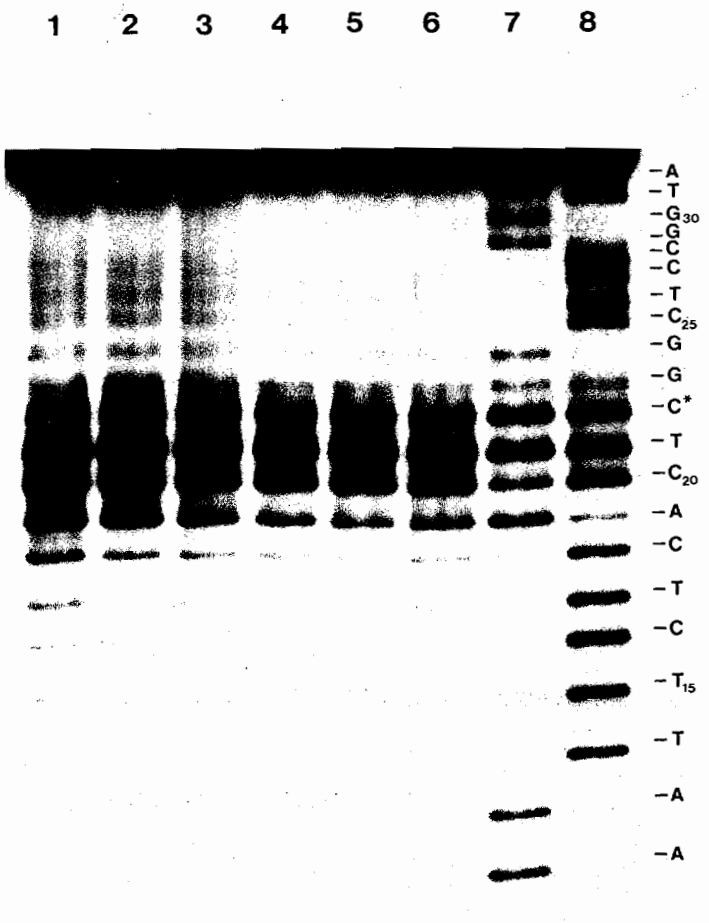

FIG. 4. DNA sequencing gel analysis of ^{125}I-decay-induced damage in oligoDNA. The ^{125}I/^{32}P double-labeled oligoDNA samples (Fig. 1), were stored for 12 days prior to DNA sequencing gel analysis, either at 4°C (lanes 1-3) or -20°C (lanes 4-6). Prior to storage, glycerol was added to the level of 10% in some samples (lanes 2 and 5), and mannitol to 100 mM in others (lanes 3 and 4). The asterisk in the sequence at right indicates the site of incorporation of ^{125}IdC.

introduced by 3'-end labeling of plasmid DNA restriction fragments, after 5'-^{32}P end labeling. The required labeled fragment was purified by preparative gel electrophoresis, denatured and reannealed to template strand. The procedure required successive rounds of preparative gel electrophoresis, and recovery of ^{32}P-DNA was generally low. Indeed it proved impossible to obtain

adequate yields of extended ^{125}I-labeled primer. When the appropriate ^{32}P/^{125}I double-labeled DNA species for the experiment were obtained, and then allowed to accumulate ^{125}I decays, the yield of the resulting ^{32}P-labeled fragments was only sufficient to yield images on X ray film after exposure for several days. In other words, there was not enough ^{32}P-labeled DNA to actually quantitate by counting gel slices. Densitometry was used to quantitate the relative yields of the ^{32}P-labeled fragmentation products. It was not possible to calculate the yields of DNA strand breaks per ^{125}I-decay. In contrast, the availability of synthetic oligoDNA enables preparation of the required double-labeled DNA in large amounts.

The potential of the approach is clear from the autoradiograph in Fig. 4. The bands are well separated and easily excised from the gel for counting. However, the results of the quantitation experiments must be taken as preliminary at this stage. The important conclusions from the results to date are that the use of ^{125}I-oligodeoxynucleotides should provide more precise data on the yield of strand breaks from ^{125}I decay in DNA, as well as information on the chemical nature of the terminii in ^{125}I-decay-induced DNA strand breaks, and the extent of energy transfer to BrU sites.

REFERENCES

1. D.E. CHARLTON and J. BOOZ, A Monte Carlo treatment of the decay of ^{125}I. *Radiat. Res.* **107**, 163-171 (1986).
2. D.E. CHARLTON, The range of high LET effects from ^{125}I-decays. *Radiat. Res.* **107**, 163-171 (1986).
3. A. SCHMIDT and G. HOTZ, The occurrence of double strand breaks in coliphage T1-DNA by iodine-125 decays. *Int. J. Radiat. Biol.* **24**, 307-313 (1973).
4. R.E. KRISCH and C.J. SAURI, Further studies of DNA damage and lethality from the decay of iodine-125 in bacteriophages. *Int. J. Radiat. Biol.* **27**, 553-560 (1975).
5. R.E. KRISCH, F. KRASIN, and C.J. SAURI, DNA breakage, repair and lethality after ^{125}I-decay in rec$^+$ and recA strains of Escherichia col. *Int. J. Radiat. Biol.* **29**, 37-50 (1976).
6. H.J. BURKI, R. ROOTS, L.E. FEINENDEGEN, and V.P. BOND, Inactivation of mammalian cells after disintegrations of ^{3}H or ^{125}I in cell DNA at -196°C. *Int. J. Radiat. Biol.* **24**, 363-375 (1973).
7. R.F. MARTIN and W.A. HASELTINE, Range of radiochemical damage to DNA with decay or iodine-125. *Science*, **213**, 896-898 (1981).
8. D.E. CHARLTON and J.L. HUMM, A method of calculating initial DNA strand breakage following the decay of incorporated ^{125}I. *Int. Radiat. J. Biol.* **53**, 353-365 (1988).

9. E. POMPLUN, A new DNA target model for track structure calculations and its first application to I-125 Auger electrons. *Int. J. Radiat. Biol.* **59**, 625-642 (1991).
10. D.E. CHARLTON, H. NIKJOO, and J.L. HUMM, Calculation of initial yields of single and double-strand breaks in cell nuclei from electrons, protons and alpha particles. *Int. J. Radiat. Biol.* **56**, 1-20 (1989).
11. U. LINZ and A. STÖCKLIN, Chemical and biological consequences of the radioactive decay of iodine-125 in plasmid DNA. *Rad. Res.* **101**, 262-278 (1986).
12. A. HALPERN, Intra - and intermolecular energy transfer and super excitation in post-Auger processes. *Radiochim. Acta*, **50**, 129-134 (1990).
13. K.F. BAVERSTOCK and R.B. CUNDALL, Solitons and energy transfer in DNA. *Nature* **332**, 312-313 (1988).
14. R.F. MARTIN, V. MURRAY, G. D'CUNHA, M. PARDEE, E. KAMPOURIS, A. HAIGH, D.P. KELLY, and G.S. HODGSON, Radiation sensitisation by an iodine-labelled DNA ligand. *Int. J. Radiat. Biol.* **57**, 939-946 (1990).
15. L. DENISON, A. HAIGH, G. D'CUNHA, and R.F. MARTIN, DNA ligands as radioprotectors: Molecular studies with Hoechst 33342 and Hoechst 33258. *Int. J. Radiat. Biol.* **61**, 69-81 (1992).
16. W.D. HENNER, S.M. GRUNBERG, and W.A. HASELTINE, Sites and structures of gamma-radiation-induced DNA strand breaks. *J. Biol. Chem.* **257**, 11750-11754 (1982).
17. J. STUBBE and J.W. KOZARICH, Mechanisms of Bleomcyin-Induced DNA Degradation. *Chem. Reviews* **87**, 1107-1136 (1987).
18. P.M. CULLIS, G.D.D. JONES, M.C. SWEENEY, M.C.R. SYMONS, and B.W. WREN, DNA damage in frozen aqueous solution: Sequence dependence and end groups. *Free Radical Research Communications* **6**, 149-152 (1989).

DISCUSSION

Adelstein, S. J. Before we write off indirect effects (mediated by watery radicals) two matters should be taken into account: 1) Mannitol is a less than ideal OH radical scavenger, and 2) Although strand breaks may not be mediated through these radicals, base damage may be.

Martin, R. Yes, I agree that mannitol is not an ideal scavenger (in fact we have learned that by experience), and we plan to use others, but 100 mM mannitol in the frozen state should restrict "indirect" effects. The other relevant point, which I did allude to briefly, is the investigation of strand break terminii; 3-phosphorylglycollate terminii might be an indicator of indirect action.

Baverstock, K. Have you checked to see whether you find preferential strand breakage close to cold bromine in DNA when you use γ radiation?

Martin, R. No, but of course we plan to do such experiments.

Hofer, K. G. From your presentation I am not quite certain about the existence of energy transfer. Are you saying that energy transfer exists, does not exist, or you do not know?

Martin, R. Our preliminary results suggest that energy transfer is limited, on the basis of two points: 1) Since the yield of SSB at the site of decay seems to approach unity, there is no need to invoke energy transfer to explain the established experimental findings of an average of 1 DSB/decay (an observation of substantially less than 1 SSB/decay at the site of decay would have come to the opposite conclusion). 2) In our experiment, measuring energy transfer in terms of excitation of BrUdR (and hence strand cleavage) by ^{125}I decay we could not observe any evidence of transfer over a distance of 8 base pairs.

Biophysical Aspects of Auger Processes, AAPM Symposium Series No. 8 (1992) 164-179
Eds. RW Howell, VR Narra, KSR Sastry, DV Rao

DNA STRAND BREAKAGE BY ^{125}I DECAY: PLASMID DNA IN DILUTE AQUEOUS SOLUTION

CINDY L. McINTYRE[#] and KEITH F. BAVERSTOCK[*]

M.R.C. Radiobiology Unit,
Chilton, Didcot, Oxon OX11 0RD, U.K.

Present Address: [#]Viridian Bio Ltd., Chestfield, Whitstable, Kent, UK.

Present Address: [*]Who European Centre for Environment and Health, Rome, Italy

ABSTRACT

The question of the extent of damage to DNA, in particular double strand breaks, that can be caused by the decay of the Auger emitter ^{125}I when it is covalently incorporated into the DNA requires resolution. In particular, experiments with plasmid DNA reported by Linz and Stöcklin (1) would seem to indicate that the range of effect extends over the whole length of the molecule (a few 1000's base pairs (bp)) in contrast to the generally accepted view that the decay is very localized (*i.e.* effect over a few 10's bp). This raises the question of whether a long range energy migration process is operative in DNA or whether the fragmentation can be accounted for by free radical diffusion. We report here experiments to help resolve this issue by investigating and trying to eliminate the possible effects of free radicals. Our results which are broadly consistent with the findings of Linz and Stöcklin (1) indicate that long-range damage in labeled DNA in aqueous solution is due to effects of free radicals. We confirm the high-LET nature of the ^{125}I decay.

INTRODUCTION

The role of Auger emitters in biology is of both practical and fundamental interest. The high energy densities produced in the local regions surrounding the nuclide upon radioactive decay possibly lead to effects similar to those produced by high-LET particles (2). However, the relevance of this damage may depend on the spatial relationship of the nuclide to critical biological targets which in the case of high-LET particles would be a stochastic relationship.

One critical biological target is DNA and it is of fundamental interest to know the extent of damage resulting from Auger decays that take place within or close to the DNA duplex. Iodine-125 has traditionally been chosen for such studies because of the ease with which it can be covalently bonded to DNA. ^{125}I introduced into cells in the form of a labeled base that becomes incorporated into the cell nucleus is very much more cytotoxic than ^{125}I introduced in a form that excludes it from the nucleus (3). If it is assumed that each decay results in at least a double strand break in the nuclear DNA at the site of decay (not unreasonable considering the combined effects of electron release, charge build-up and transmutation involved in the decay), then for many normally sensitive cell lines some 60 such decays would appear, on average, to be lethal to a mammalian cell.

Early studies with DNA species specifically labeled with ^{125}I indicated that multiple single strand breaks could be formed up to the order of 20 base pairs (~ 10 nm) from the site of decay (4). Calculations, based upon track structures for the electron emission upon Auger decay, confirm these conclusions (5). It may then be concluded that ^{125}I decay within a DNA molecule is a highly localized event with damage confined to within a few DNA diameters of the site of the decay, but with the likelihood of considerable damage within that region leading to the loss of genetic information.

Subsequent experiments (1) seemed to indicate that the above picture was incomplete. Plasmid DNA, linear pBR322 labeled at both ends with ^{125}I, was stored either in phosphate buffer or sodium chloride solution to allow radioactive decay and then analyzed for double strand breakage using electron microscopic imaging. These studies revealed that double strand breaks could occur at positions remote (several hundreds of bp) from the sites of

radioactive decay. The conditions under which these studies were made did not prevent the possibility that free radicals resulting from the radioactive decay might cause damage after migration through the aqueous medium, although experiments in which ^{125}I was present in the solution, but not incorporated into the DNA, did not suggest that radical migration would be effective in causing damage. Alternatively it has been suggested that a long range energy migration process might be operative in DNA stimulated by the 'far from equilibrium' condition created by the Auger decay (6).

The purpose of the experiments described in this paper is to resolve the question of whether the fragmentation observed by Linz and Stöcklin (1) is due to free radical effects or energy migration. It is stressed that breaks formed in close proximity to the site of the label can not be measured by the techniques employed here, and so these experiments shed no light on the mechanism by which the local effects of ^{125}I decay occur.

MATERIALS AND METHODS

^{125}IdCTP was purchased from Dupont New England Nuclear at a specific activity of 81.4 TBq/mmole and a radioactive concentration of 37 MBq/ml. The radiolabeled base was supplied in an ethanol:water mixture of 3:1, the majority of which was removed under vacuum immediately prior to use to give a radioactive concentration of approximately 370 MBq/ml. Enzymes were purchased from Life Science Technologies (Gibco BRL), the Klenow enzyme at a concentration of 2 units per pmol. pSVL plasmid DNA in pure vector form, Sephacryl S-1000 and S-400 gel filtration media, and cold dNTPs were obtained from LKB Pharmacia. Agarose and Sephadex gel filtration media were obtained from Sigma, and all other general laboratory chemicals either from Sigma or BDH.

Isolation of pSVL Plasmid DNA

The vector form of pSVL plasmid was multiplied in *Eshericia coli* HB101 from in house supplies, isolated and purified by base/acid extraction and Sephacryl S-1000 gel filtration following the protocol of Bywater *et al.* (7). This method routinely produced DNA preparations with a high percentage of supercoiled molecules.

Preparation of Plasmid for 3'- Endlabeling

The plasmid was initially linearized by digestion at 37°C with the restriction endonuclease EcoR V, which produces blunt ends, at a concentration of 3 units of enzyme per microgram of plasmid. A second digestion at 37°C with the enzyme Xba 1 at a concentration of 5 units per microgram of plasmid produced a sample containing a mixture of 4.2 kb and 700 base pair plasmid, each possessing one blunt and one cohesive end. After each digestion the reaction was terminated with EDTA to a final concentration of 20 mM, heated to 65°C for 5 min, and then immediately incubated on ice to dissociate any annealed cohesive ends.

Separation of Restriction Fragments

Restriction fragments were separated using a Sephacryl S-1000 gel filtration column, the dimensions of which were 2.5 X 50 cm. The gel was initially equilibrated in 0.5 M NTEB (0.5 M NaCl, 10 mM Tris pH 7.5 and 1 mM EDTA) and a sample of 200 µg in a volume of < 500 µl was loaded onto the column and eluted at a flow rate of 25 ml per hour.

3'-Endlabeling

The Klenow fragment of DNA polymerase 1 was employed for this purpose in a reaction mixture containing 260 nM of DNA cohesive ends, 260 nM Klenow enzyme and 4 µM ^{125}I dCTP in 12.5 mM NaCl, 5 mM magnesium chloride and 50 mM Tris-HCl pH 7.4 polymerase buffer adapted from Kuchta *et al.* (8). Initially the plasmid and ^{125}I dCTP in the polymerase buffer were incubated at 20°C for 5 min independently of the enzyme which was then added to initiate the reaction. The reaction was terminated with EDTA to a final concentration of 20 mM after an incubation time of 40 min.

Spun column chromatography as described by Maniatis *et al.* (9) was used to remove the excess labeled deoxynucleotides. All gel filtration media employed during this stage had first been equilibrated in 10 mM NaCl except for the sample that was to be stored in 10 mM phosphate buffer pH 7.0 which was treated independently in columns prepared under phosphate conditions. The first column was packed with Sephacryl S-400 to simultaneously remove excess nucleotides and any contaminating protein. This was followed by at least one more elution down a Sephadex G-50 spun column to remove the

last traces of labeled nucleotides. Using the Klenow enzyme we have found that there is inevitably some extraneous incorporation. Indeed, we have noticed that the enzyme is capable of blunt end labeling, the extent of which is dependent upon the recognition site. This is, however, to a much lesser degree than with cohesive ends. Therefore, to determine to what extent this had occurred, an aliquot of the plasmid was further digested with Sal 1 under conditions of 5 units of enzyme per microgram of DNA at 37°C. The digest was analyzed by agarose gel electrophoresis and revealed a 3% extraneous incorporation probably at the blunt ends.

Sample Preparation, Storage, and Analysis

All samples were prepared for storage immediately after labeling. The DNA was already present both in the 10 mM NaCl pH 7.0 and independently in the 10 mM phosphate buffer pH 7.0. The volume of both these samples were thus adjusted to give a final DNA concentration of 20 μg/ml. A portion of the DNA sample in 10 mM NaCl was taken before dilution and glucose added to a final concentration of both 50 and 500 mM. This also applies to the 10 mM and 100 mM Tris pH 7.5. Control samples were prepared under identical conditions using cold dCTP and the effect of unincorporated ^{125}I studied by the addition of free labeled base to samples of cold labeled plasmid. All solution experiments were stored in heat sterile screw cap vials at 4°C in a moist environment. In the labeled samples the molar ratio of ^{125}I:DNA was 0.5, while for the unlabeled samples the ratio was 2. Samples were imaged using electron microscopy and analyzed by methods described in Baverstock *et al.* (10).

Estimation of Strand Break Yields

Due to measurement errors the means of the distributions of DNA fragments vary from one sample to another. This complicates the estimation of break yields on the basis of the fractions of DNA remaining unbroken. An alternative method, and arguably a better one when fragment length information is available, is to estimate the mean length of the unbroken fragments. This is essentially a simple task when break yields are low. By dividing the total length in the distribution by this length estimate, the number of fragments of unbroken DNA that would constitute the sample are obtained.

If n DNA molecules each have p breaks per molecule (on average), then there will be $(n+pn)$ fragments in the sample. Thus, for a sample exposed to radiation which was found to have f fragments,

$$p = (f - n) / n$$

Breaks caused in the handling and preparation of the DNA, or spontaneous breaks formed during storage of the samples, can be estimated from yields observed in the control samples.

RESULTS

Figure 1 shows double strand breakage in DNA labeled at one end with ^{125}I and stored in phosphate buffer solution. Samples were analyzed at intervals to observe the dependence of breakage on the fraction of ^{125}I decayed. Also shown in the figure are the break yields for solutions in which the ^{125}I was not incorporated in the DNA but present in solution as the labeled base. In both cases the breakage observed in DNA subjected to the same procedures, but without exposure to radioactive iodine, has been subtracted. Fifty percent of the molecules in the sample are labeled with iodine so the molar ratio of ^{125}I to DNA was 1:2. In the non-incorporated sample it was 2:1. Fig. 2 shows a similar plot for DNA stored in sodium chloride (pH 7).

In both these cases the extent of breakage observed was very small but somewhat greater in the experiments where the ^{125}I was incorporated in spite of the higher ^{125}I ratio. Indeed the breakage observed was markedly less than that observed by Linz and Stöcklin (1), but in common with them we observed an indication of slightly higher yields in the sodium chloride solution. As indicated by the fitted lines (see DISCUSSION) the results from the labeled samples are consistent with breakage being related to the square of the dose, as would be expected if the effect were due to free radical attack on the DNA. However, because of the low levels of breakage, a linear fit would be equally acceptable.

Figures 3 and 4 show the effect of added glucose at 50 and 500 mM. Glucose acts to scavenge free radicals generated from the radiolysis of water. The reduced yields of breaks observed in these experiments (virtually undetectable even when 90% of the activity had decayed) and absence of any

detectable trend of breakage with fractional decay would suggest that such breakage as is observed in the salt and buffered solutions is generated by free radical attack. This conclusion is confirmed by the absence of breakage in similarly labeled DNA stored in Tris buffer at 10 and 100 M as shown in Figs. 5 and 6.

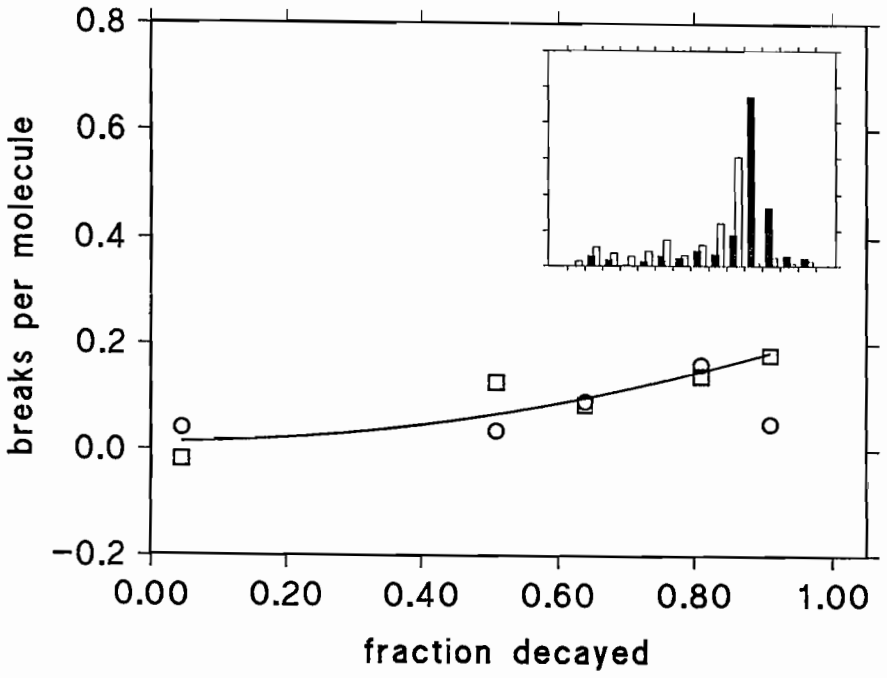

FIG. 1. Measured numbers of double strand breaks in linearized pSVL plasmid DNA molecules either labeled with ^{125}I (open squares) or with labeled base in solution (open circles) stored in 10mM phosphate buffer (pH 7) at 4°C. Break yields were determined as described in the text. Typically between 100 and 200 μm of DNA fragments (initially 1.05 μm in length) were measured per sample. Labeling efficiency in the labeled experiments was about 50%. In the unincorporated samples four times as much ^{125}I was present in solution. The fitted line is to the points for the labeled samples only and is of the form $y = m\,x^2 + b$. The inset diagram shows the fragmentation pattern (number of fragments of DNA on the y axis vs length (x axis)) for the sample at 91% decay (fifth point) (open squares) compared to unlabeled DNA stored under the same conditions. Each bin (x axis) corresponds to 0.1 μm length of DNA. The solid bars refer to the unlabeled sample and the open bars to the labeled sample.

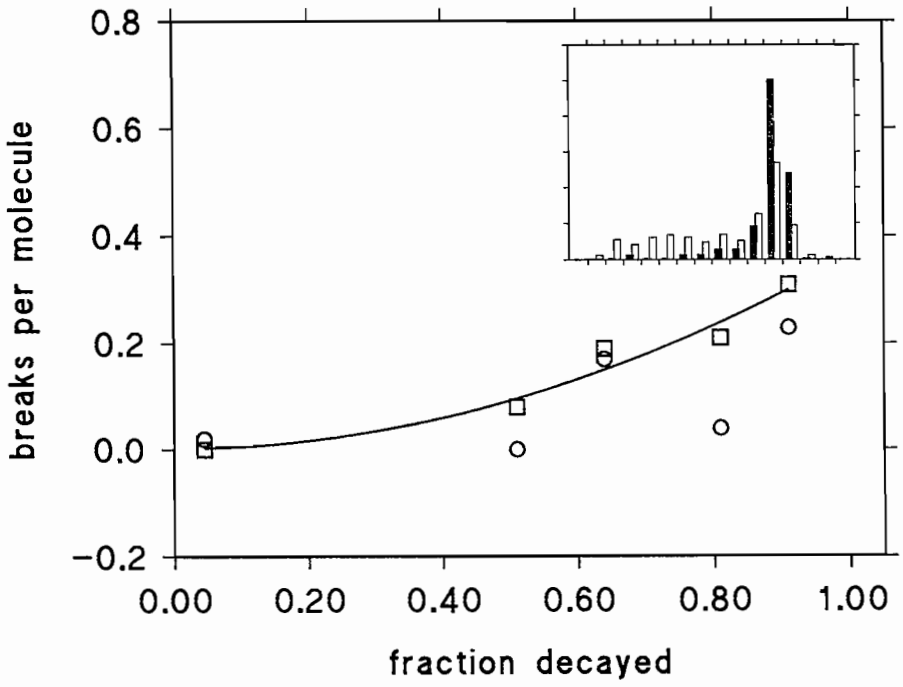

FIG. 2. As for Fig. 1 but samples stored in 10 mM sodium chloride.

To assess the relationship between strand breakage and radiation dose under the experimental conditions (*i.e.* DNA at 20 μg/ml in either sodium chloride solution or phosphate buffer) similar solutions were irradiated with gamma rays. Full decay of the ^{125}I in the incorporated samples would be equivalent to a dose of 6 Gy. At such a dose ~ 0.05 double strand breaks per molecule are observed. In solutions containing glucose no damage is observed at such doses. In the experiments with non-incorporated ^{125}I, where the ratio of iodine to DNA is four times greater, the expected number of double strand breaks per molecule is about 4.5.

DISCUSSION

The experiments reported above were designed to determine whether the extensive fragmentation of the labeled DNA observed by Linz and

Stöcklin (1) was due to a long range energy migration process in the DNA or to free radical migration following ionization of the aqueous medium. In addition to this fragmentation, localized effects in the DNA within 10-20 bp of the site of the label are also expected, but the techniques employed here can not detect damage at this resolution.

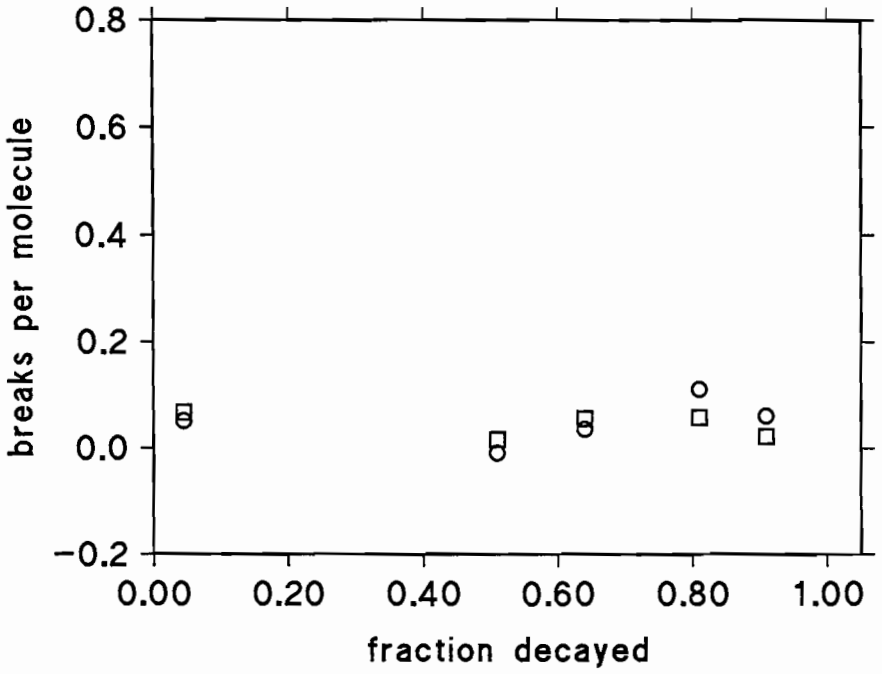

FIG. 3. As for Fig. 2 but with 50 mM glucose added.

Linz and Stöcklin (1) used a plasmid linearized by cutting with the enzyme Sal 1 and labeled with ^{125}I at each end. The labeled plasmid was stored in sodium chloride solution (10 mM) or phosphate buffer (10 mM) with and without the presence of oxygen for up to 6 months. Upon imaging with electron microscopy the DNA was seen to be fragmented, especially in the samples stored in sodium chloride. Two possible explanations were offered, namely, that free radicals generated from water radiolysis had caused single strand breaks to be formed, the combined effects of which was to fragment the DNA, or that the π-electron structure of DNA had enabled energy migration to points on the DNA molecule remote from the site of decay. In support of

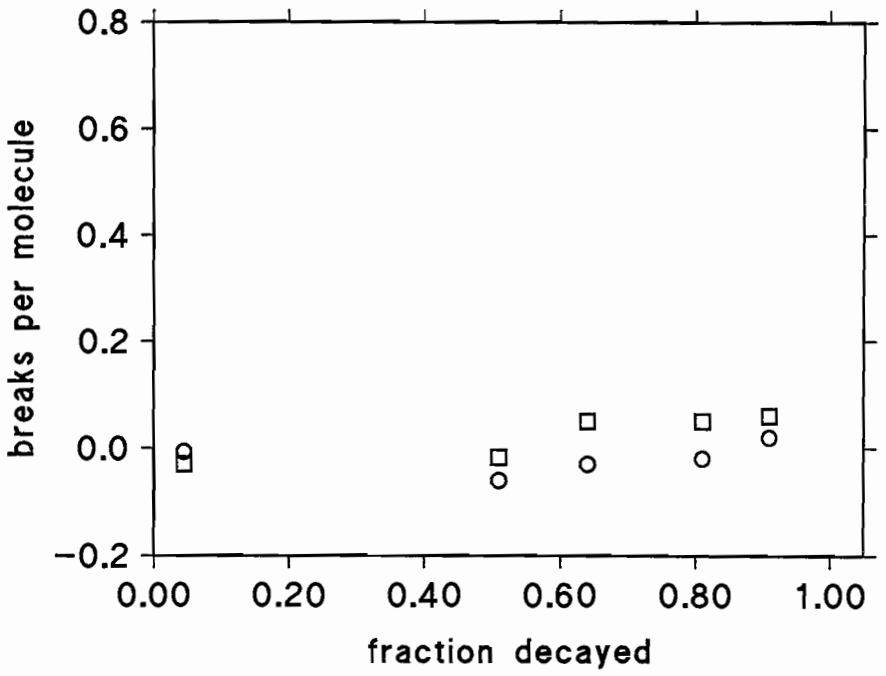

FIG. 4. As for Fig. 2 but with 500 mM glucose added.

this latter contention the authors noted that the size of fragments generated in sodium chloride solutions corresponded to the intervals between regions of the plasmid DNA rich in the base thymine which might act as a trap for migrating energy. In experiments in which the ^{125}I was not incorporated into the DNA, but free in solution, no significant breakage was observed. When the doubly labeled plasmid was recircularized through ligation of the ends linearization of the circle was observed on decay but fragmentation was much less severe than in the case of the molecules originally stored in the linear state.

Our experiments differed from those of Linz and Stöcklin (1) in the following ways:

a) only a single ^{125}I labeled base was incorporated;
b) only half the DNA molecules contained a label;

c) labeling was carried out with the Klenow fragment of DNA polymerase I, which lacks the 5 to 3' exonuclease activity of DNA polymerase I used by Linz and Stöcklin (1);
d) samples were taken at intervals during the decay of the radionuclide to obtain the relationship between decay of the label and breakage in the DNA.

These departures from the Linz and Stöcklin (1) protocol were not deemed to change the essential nature of the experiment, but rather to simplify the interpretation of the results. For example, in molecules labeled at both ends, the state of the DNA when the second decay occurred would not be known. By leaving half the molecules unlabeled we would expect, if the energy migration was intramolecular, to see half the molecules intact at 100% decay but not if the mechanism was intermolecular. In none of the experiments, including those with no radical scavenger present, was fragmentation on the scale reported by Linz and Stöcklin (1) observed.

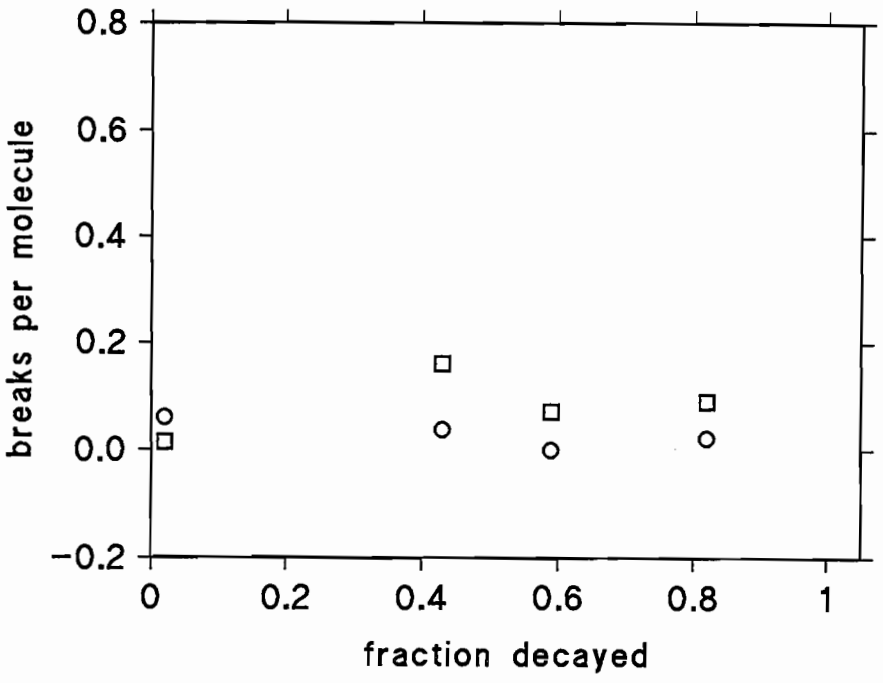

FIG. 5. As for Fig. 1 but stored in 50 mM NaCl with 10 mM Tris buffer at pH 7 .

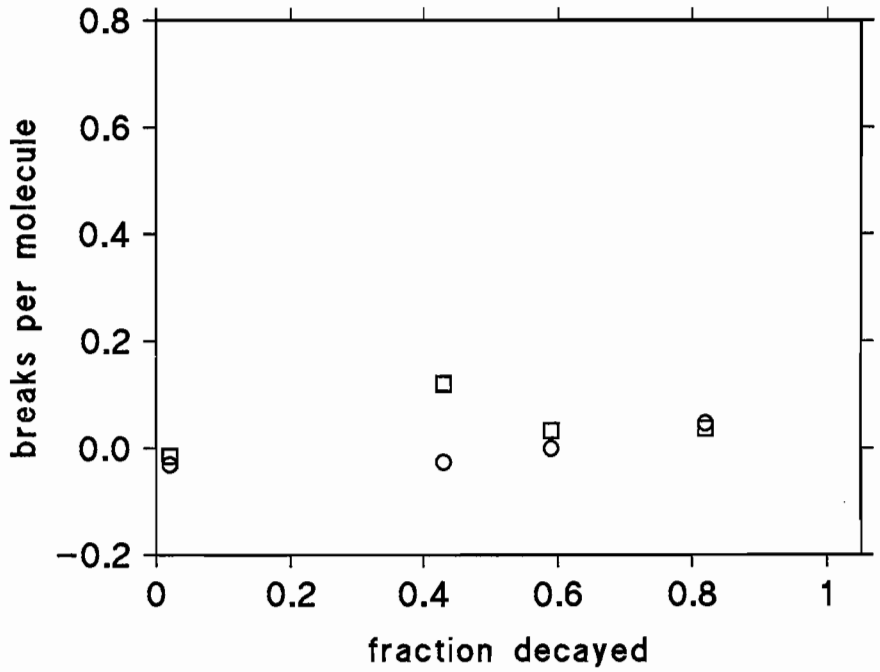

FIG. 6. As for Fig. 5 but with 100 mM Tris buffer.

We observed some degree of breakage of DNA in sodium chloride solutions, about half this amount in phosphate buffer, but apparently no significant breakage in the presence of 50 mM and 500 mM glucose or with 10 and 100 mM Tris buffer. Both the glucose and the Tris buffer would be expected to scavenge free radicals, thus suggesting that any breakage we did observe might be due to radical damage. However, in common with Linz and Stöcklin (1), we did not observe significant damage when the ^{125}I was not incorporated into the DNA even though in our experiments the concentration of ^{125}I was four times greater than for the incorporated samples.

On the basis that radical damage was indicated by those findings we fitted the results for DNA with incorporated ^{125}I in sodium chloride and phosphate buffer to the following relationship:

$$p = mD^2 + b,$$

where p is the number of breaks per molecule and D is the dose in terms of fraction of decay of ^{125}I. This is based on the assumption that double strand breaks in DNA subject to radical attack result from two single strand breaks formed on opposite strands of the DNA, but in close proximity. Assuming this relationship and a random distribution of single strand breaks, we can extrapolate the conditions of our experiment (*i.e.* one ^{125}I per molecule, 50% of the molecules labeled) to the assumed conditions of Linz and Stöcklin's experiment (*i.e.* two ^{125}I atoms per molecule, all molecules labeled). When this is done we estimate that Linz and Stöcklin (1) would observe about 5 breaks per molecule in sodium chloride solution and about 2 breaks per molecule in phosphate buffer. These estimates are in reasonable agreement with the results of Linz and Stöcklin (1), given that the extrapolation is quite substantial and therefore bound to be somewhat uncertain.

We also compared the effects, on similar DNA solutions, of external gamma irradiation. For a dose equivalent to 100% decay of the ^{125}I in the incorporated samples (~ 6 Gy) we found about 0.05 double strand breaks per molecule in both sodium chloride solutions, and phosphate buffer; significantly less than expected on the basis of the experiments with incorporated DNA.

We rationalize these results in the following way. The very localized nature of the energy deposition following the decay of ^{125}I leads to a high concentration of free radicals around the site of decay. If there are no reactive solute molecules (in this case DNA) in the immediate vicinity, the dominant reaction is recombination of radicals to form non-reactive molecular products, H_2O_2, H_2 and of course H_2O. However, if a reactive solute molecule is close by, there will be a competition between the reaction of free radicals with that molecule and recombination. These are precisely the circumstances one would expect in the case of a high-LET radiation and would lead to the results we observe. Namely, damage to DNA where the decay of the ^{125}I occurs close to it, but not where there is no correlation between the sites of decay and the DNA molecules, as is the case in the experiments where the ^{125}I is not incorporated. Thus, we conclude that the fragmentation observed by Linz and Stöcklin (1) was due to free radical effects and not energy migration within the molecule and that, in spite of the lower yields of fragmentation we observed, our results are broadly compatible with theirs.

The first decay in a doubly labeled molecule leads to little double strand breakage, but provides latent damage in the form of single strand breaks. The

second decay adds to the single strand damage causing a dramatic increase in double strand breaks and thus extensive fragmentation.

This interpretation is not apparently fully consonant with the observation of Martin and Haseltine (4) which has subsequently been confirmed (see paper by Martin; this volume) and supported by theoretical calculation (5) in so far as single strand breaks seem to be confined to the bases within 15 bp of the site of decay. Martin and Haseltine (4) stored their samples in 50 mM Tris-borate buffer and so molecules capable of scavenging free radicals were present. However, this level of scavenger would not be expected to remove all free radicals but a small background yield of single strand breaks distributed evenly along the DNA molecule might be difficult to detect. In our experiments 10 mM Tris buffer was sufficiently effective to prevent double strand breaks from forming, and we suggest that the much longer DNA (4300 bp compared to between 50 and 75 bp used by Martin *et al.* (4)) molecule is capable of forming a random coil in the solution so creating a reactive 'cage' environment around the iodine giving a locally very high effective scavenging cross section that can compete with recombination at early times (10^{-8} - 10^{-6} s) after decay of the ^{125}I. The much shorter molecules used by Martin and Haseltine (4) would not be capable of this.

The calculation by Charlton (5) only considered direct excitation of the DNA and it is probable that the breaks close to the site of decay in our experiments were caused by this mechanism rather than radical attack.

The biological implications of this result are that under circumstances where DNA is 'packed' such as in chromatin, some degree of indirect effect might be expected, but that the damage caused is unlikely to lead to double strand breakage by this mechanism unless more than one decay occurs in the same local region.

As for other observations by Linz and Stöcklin (1), namely that when the doubly labeled molecule is recircularized fragmentation was reduced; we suggest this can be explained if it is assumed that the effect of the Auger decay is to excise bases in the immediate vicinity of the decay. Upon recircularization the two labels are located within six base pairs apart. When the first iodine decays, there would seem to be a high probability of excising the remaining label and thus separating the largely intact DNA molecule for the remaining ^{125}I. This would seem to confirm that the decay of ^{125}I in an isolated molecule of DNA does not form a clean double strand break but

rather that there is a high probability of loss of genetic information even if the lesions can be repaired in a mechanical sense (see paper by Yasui; this volume).

That intramolecular energy migration has not been observed in this instance, does not rule out the possibility in other circumstances - for example solid state DNA.

REFERENCES

1. U. LINZ and G. STÖCKLIN, Chemical and biological consequences of the radioactive decay of ^{125}I in plasmid DNA. *Radiat. Res.* **101**, 262-278 (1985).
2. D.E. CHARLTON, The range of high LET effects from ^{125}I decays. *Radiat. Res.* **107**,163-171 (1986).
3. K.G. HOFER, C.R. HARRIS, and J.M. SMITH, Radiotoxicity of intracellular Ga-67, I-125, and H-3. Nuclear versus cytoplasmic radiation effects in murine L1210 leukaemia. *Inter. J. Radiat. Biol.* **28**, 225-241 (1975).
4. R.F. MARTIN and W.A. HASELTINE, Range of radiochemical damage to DNA with decay of iodine-125. *Science* **213**, 896-898 (1981).
5. D.E. CHARLTON, Calculation of single and double strand DNA breakage. In *DNA damage by Auger emitters.* (K.F. Baverstock, and D.E. Charlton, Eds.) Taylor and Francis :London, pp 89-100, 1988.
6. K.F. BAVERSTOCK and R.B. CUNDALL, Long range energy transfer in DNA. *Radiat. Phys. Chem.* **32**, 553-556 (1988).
7. M. BYWATER, R. BYWATER, and L. HELLMAN, A novel chromatographic procedure for purification of bacterial plasmids. *Analyt. Biochemistry.***132**, 79 1983.
8. R.D. KUCHTA, V. MIZRAHI, P.A. BENKOVIC, K.A. JOHNSON, and S.J. BENKOVIC, Kinetic mechanism of DNA polymerase 1 (Klenow). *Biochemistry* **26**,8410 (1987).
9. T. MANIATIS, E.F. FRISH, and J. SAMBROOK,.*Molecular Cloning - A Laboratory Manual*, Cold Water Spring Harbour p464, 1982.
10. K.F. BAVERSTOCK, J. BERRIMAN, T. PARKER, and M.A. STEPHENS, An improved technique of strand break analysis for isodisperse DNA. *Radiat. Environ. Biophys.* **21**, 81-96 (1982).

DISCUSSION

Halpern, A. 1) Which radical scavengers did you use? 2) It is highly questionable whether the results reported by Linz and Stöcklin can be interpreted in terms of the usual concepts of radiation chemistry. The most

plausible explanation of their results to be suggested is long-range energy transfer in DNA.

Baverstock, K. F. 1) Tris buffer (pH 7) and glucose. 2) I think the presence of scavengers which seem to protect against DNA fragmentation must strongly suggest that it is not an intramolecular energy migration process that is responsible. We seem then to be left with a radical mediated effect. This explains most, but not all, of the observations of Linz and Stöcklin. There is probably room for further experiments designed to resolve these issues.

Adelstein, S. J. The role of hydrated (solvated) electrons could be classified by using H_2O in the absence of oxygen.

Baverstock, K. F. I think the main damaging agent for DNA is overwhelmingly the OH radical. Solvated electrons are comparatively unreactive. I do, however, think that some basic radiation chemistry of the ^{125}I decay would be beneficial and they of course should include the influence of H_2O and other selective scavengers. This would help to characterize the competition between radical combination and reaction with solutes such as DNA.

 Biophysical Aspects of Auger Processes, AAPM Symposium Series No. 8 (1992) 180-193
Eds. RW Howell, VR Narra, KSR Sastry, DV Rao

INDUCTION OF MICRONUCLEI BY ^{125}IUDR AND ^{125}I-T_3 IN TWO MAMMALIAN CELL LINES

GERTRUDA LUDWIKOW[1], FRANCISZEK LUDWIKOW[2], and KARL J. JOHANSON[1]

[1]Department of Radioecology
The Swedish University of Agricultural Sciences
P.O. 7031, S-75007 Uppsala, Sweden

[2]Department of Radiation Physics
Karolinska Institute and University of Stockholm
P.O. Box 60211, S-104 01 Stockholm, Sweden

ABSTRACT

The high effectiveness of ^{125}I Auger electrons in inducing damage to DNA has two practical aspects. The first aspect involves their use in cancer therapy as a modality with desirable radiobiological properties. The second introduces an undesirable, but highly specific, risk associated with the thyroid hormone (T_3) specific metabolic pathways and its target tissues and cells. In the target cells, the ^{125}I carrying thyroid hormone will be directed to the defined DNA sequences within the thyroid hormone regulated genes through the specific thyroid hormone nuclear receptors. Accordingly, ^{125}I will be localized there within the nanometer range of action and cause damage tantamount to high-LET-like effects. In this work an *in vitro* comparison of the damaging effectiveness of ^{125}I labeled to two different molecules is investigated: IUdR, the classical molecule used in experiments on the radiobiology of ^{125}I, and T_3.

Published by American Institute of Physics, Inc., Woodbury, NY 11797

Two cell lines were employed that differ in responsiveness to T_3: GC, responsive and CHO, non-responsive. The kinetics of micronuclei formation served as a measure of the biological effectiveness of the radiochemical. It was found that ^{125}I-T_3 elicited significant damage to DNA at physiological concentrations in the hormone responsive cells and that its effectiveness for inducing micronuclei was 9 times lower than that of $^{125}IUdR$. The possibility of using Auger emitters bound to transcription regulating factors in fundamental research and therapy is discussed.

INTRODUCTION

The *in vivo* use of ^{125}I for diagnostic purposes (1) and attempts to utilize its severely damaging effect (observed *in vitro* and *in vivo*) in tumor therapy (2-4) implies the introduction of this radionuclide to organisms.

Iodine belongs to the class of biologically important trace elements. It is an indispensable constituent of thyroid hormone molecules. Insufficiency in this element leads to iodine deficiency diseases including cretinism, goiter, myxedema, Hashimoto's and Gull's diseases. To maintain a constant level of this element in organisms, vertebrates have adopted selective and highly effective mechanisms aimed at accumulating and preventing iodine excretion. Thus iodine nuclides, once introduced into the body of vertebrates by any means (food, air, medical treatment), become included into the iodine pools: the large thyroid compartment (8 - 10 mg for a 70 kg man), and a small extra-thyroid compartment (40 - 60 μg for a 70 kg man).

The nanometer range (5) of the large number of low-energy Auger electrons (6) emitted from decaying ^{125}I atoms poses a threat to DNA only when the decay occurs inside or in close proximity to the DNA molecule (7,8). When ^{125}I enters the thyroid compartment, which serves to accomplish the synthesis, storage, and secretion of the thyroid hormones - thyroxin and triiodothyronine - it is concentrated in the extracellular space of the follicular colloid. On the molecular scale this is far away from the cell nuclei of the thyroid gland. Thus, the risk to the thyroid gland can mainly be ascribed to the sparsely ionizing γ radiation from ^{125}I.

On the other hand, the risk from ^{125}I in the extra-thyroid compartment is inseparably connected with the regulating functions of thyroid hormones elicited in several genes in responsive tissues (9-11). These functions are

realized at the cellular level within the nanometer range of DNA-hormone interaction mediated by the thyroid hormone nuclear receptor (12-14). The interaction between these three components occurs in the following sequence: 1) activation of the receptor by its ligand, the thyroid hormone, 2) binding of the receptor-hormone complex to specific DNA base pairs, and finally 3) regulation of the transcription of responsive genes (14,15).

In order to probe the position of ^{125}I in the thyroid hormone receptor-thyroid hormone complex after binding to DNA, the damaging effect of ^{125}I measured by micronuclei formation in two cell lines (responsive and non-responsive to thyroid hormone) was determined. As a reference probe for DNA damage, the thymidine analog, ^{125}IUdR, was applied.

MATERIALS AND METHODS

Cells and their Growth Conditions

The number of thyroid hormone nuclear receptors is different in different tissues (16). Two cell lines were employed as the *in vitro* models: 1) Chinese hamster ovary (CHO) cells, originating from the reproductive organ known to have a very low number of thyroid hormone nuclear receptors, and 2) GC, a cell line originating from the anterior pituitary gland, the tissue richest in thyroid hormone nuclear receptors (16). The cells were grown as monolayers in plastic flasks or petri dishes (Nunc, Nunclon, Denmark) at 37°C in a humidified atmosphere of 5% CO_2 and 95% air. The standard medium for CHO cells consisted of Ham's F-10 medium, 10% newborn calf serum, glutamine (0.02 M), penicillin (50 units/ml) and streptomycin (50 µg/ml). For GC cells Dulbecco's medium supplemented with 10% donor horse serum, 5% foetal bovine serum, and glutamine and antibiotics as above, was used. The doubling time (t_d) of the cells was 13 - 15 h and 28 - 30 h for CHO and GC cell lines, respectively.

Labeling with ^{125}IUdR or ^{125}I-T_3

When experiments with ^{125}I-labeled triiodothyronine (L- 3,5,3'[^{125}I]-T_3, of specific activity of 81.4 TBq/mM, Dupont De Nemours GMBH NEN Products, Germany) were set up, the cells were seeded into T_3-depleted media. Depletion of T_3 from the standard sera was performed by repeated incubation of the commercially purchased standard sera with resin (AG 1-X 8, Bio-Rad

Laboratories, Richmond, California, USA; 5 mg resin/100 ml of serum during 5 and 18 h) (17). After a lag period and about one t_d in the T_3-depleted medium, the cells were labeled with ^{125}I-T_3 at an activity concentration of 74 kBq/ml medium, which was 2 to 3 times higher than the molar T_3 concentration of the euthyroid serum. The cells were incubated in ^{125}I-T_3 medium either 1) For one t_d (pulse labeling mode) and thereafter the cells continued to grow in their proper standard culture medium, or 2) The cells were cultured in the radioactive medium up to 6 t_d (continuous mode of labeling). For the dose-response curve (only GC cells), the cells were cultured with ^{125}I-T_3 activity concentrations ranging from 0 up to 74 kBq/ml during 4 t_d.

Labeling with $^{125}IUdR$ (^{125}I-5-iodo-2'-deoxyuridine with specific activity of 74 TBq/mM, Amersham, England) was performed by substitution of the proper standard medium with $^{125}IUdR$ containing medium at various ^{125}I-activity concentrations during one t_d incorporation period. Afterwards the cells were cultured in the proper standard medium up to 5 t_d.

The experiments were performed in replicate sets of petri dishes for various ^{125}I-T_3 concentrations and incubation times. The initial number of cells was constant and was 3×10^4 (CHO) and 5×10^4 (GC) per dish. The control cells were cultured in their proper standard medium except for the ^{125}I-T_3 dose-response study where the control cells were cultured in T_3-depleted medium supplemented with 1 nM of cold T_3.

^{125}I Activity Measurements

As 95% of $^{125}IUdR$ is found to be incorporated into nuclear DNA of labeled cells (18), the measurement of ^{125}I activity was performed on whole cells. The T_3 concentration in nuclei depends on the nuclear receptor density which varies considerably from tissue to tissue (16). However, T_3 can be bound specifically or non-specifically to cytoplasmic proteins (19,20). Therefore we measured ^{125}I-T_3 activity in both intact cells as well as in nuclei. Preparation of the nuclei is described elsewhere (21).

After harvesting by trypsinization (0.25% trypsin in EDTA) the cells were suspended in culture medium and counted with a Coulter electronic particle counter. One ml of the cell suspension was taken for both $^{125}IUdR$ and ^{125}I-T_3 activity measurements. The ^{125}I activity measurement in the suspension of cell nuclei (in 1 ml of buffer B (21)) using a Packard NaI Auto-

Gamma counter with a 15-80 keV window. To obtain the kinetics of the labeled compounds, the activity determination was done after every doubling time over 5-6 t_d.

Micronuclei Assay

Micronuclei (MN) are observed in interphase cells and are formed from chromosome and/or chromatid acentric fragments arising in the preceding mitoses (22). The acentric fragments reflect damage of chromosomes caused by clastogenic agents, in particular by ionizing radiation. The formation of micronuclei depends on cell division and thus the scoring of MN should be restricted only to the proliferating cells in order to get reliable results. Practically, this restriction was obtained by using cytochalasin B (CB) which arrests cytokinesis of the post-mitotic cells (23). Cells which divided once in the presence of CB appear as binuclear (BN), *i.e.*, as containing two nuclei.

CB (3 μg/ml) (23) was added to the culture medium at the beginning of n_{th} t_d and the cells were harvested at the end of the n_{th} t_d, n = 1,2,...6 (this time interval will subsequently be denoted as t_{dn}). In this way we could follow the kinetics of appearance of micronucleated binuclear cells throughout the investigated time period. After incubation with CB for one t_d the cells were trypsinized, ^{125}I activity measured, and the cells were prepared for scoring micronucleated binuclear cells. The trypsinized, suspended cells were centrifuged for 2 min at 1500 rpm, the cell pellet was gently resuspended in about 1 ml of 1% sodium citrate, and the cells were immediately centrifuged (1-2 min, 1500 rpm). The pellet of hypotonically treated cells was resuspended in about 1 ml of fixative (ethanol:acetic acid - 3:1). An improvement in preservation of the cytoplasm around the nuclei was obtained when the fixative was added directly to the suspension of cells in the 1% sodium citrate before centrifugation, and then centrifuged and resuspended again in fixative. The fixed cells were dropped on a clean glass slide, air-dried and stained in 5% Giemsa solution in Sorensen's buffer for 20 min (GC cells) or 30 min (CHO cells). Slides were scored under a light microscope (Zeiss-Axioplan) at 1000 X magnification. An average of 500 binuclear cells were scored per slide. It should be noted that the term micronucleation has been used to denote the frequency of binuclear cells with micronuclei regardless of the number of micronuclei per cell and has constantly been applied throughout the paper.

RESULTS

Cellular Uptake of the ^{125}I-labeled Molecules

The ^{125}IUdR and ^{125}I-T_3 cellular uptake is presented in Fig. 1 (A and B). M_1, the exponent of the power fit $y = M_0 x^{M_1}$), where y is the activity per cell and x is the concentration of activity in the medium, was 0.95 for CHO cells and 0.97 for GC cells indicating a linear uptake of ^{125}IUdR in both cell lines. For ^{125}I-T_3, the exponent was 0.76, which indicates a saturation of the uptake of this compound in GC cells. The CHO cells showed a very low uptake of ^{125}I-T_3 at 74 kBq/ml (2 to 3 times higher than the physiological T_3 concentration) and therefore the concentration dependence was not investigated.

Cellular Retention of the Radiochemicals

The ^{125}IUdR activity concentration decreased with every doubling time in both cell lines (Fig. 2A and 2B). In contrast, the level of ^{125}I-T_3 in GC cells in the continuous mode of labeling decreased during the first three t_d and then a steady state was established. The diminishing of ^{125}I could be ascribed to the down-regulation of the T_3 receptors by an excess of its ligand (24,25). In CHO cells, the ^{125}I-T_3 activity concentration was, on average, one order of magnitude lower than in GC cells, but increased with incubation time.

Micronuclei

Comparison of ^{125}I-T_3 and ^{125}IUdR using the same experimental conditions was not possible. After labeling for one doubling time there was a rapid decrease of ^{125}I-T_3 when the radioactive medium was removed, whereas ^{125}IUdR decreased more slowly with cell divisions (Fig. 2A and 2B). Therefore, to construct the dose-response curve for ^{125}I-T_3, we chose the continuous labeling mode which was more comparable with the dilution of ^{125}IUdR due to the down-regulation of receptors (and thus ^{125}I activity per nucleus) at the first three t_d. The micronuclei were scored at t_{d4} when a steady state of ^{125}I-T_3 in the nuclei was obtained. For ^{125}IUdR, the dose-response curve was constructed as an average of micronucleated cells observed at four consecutive doubling times after labeling.

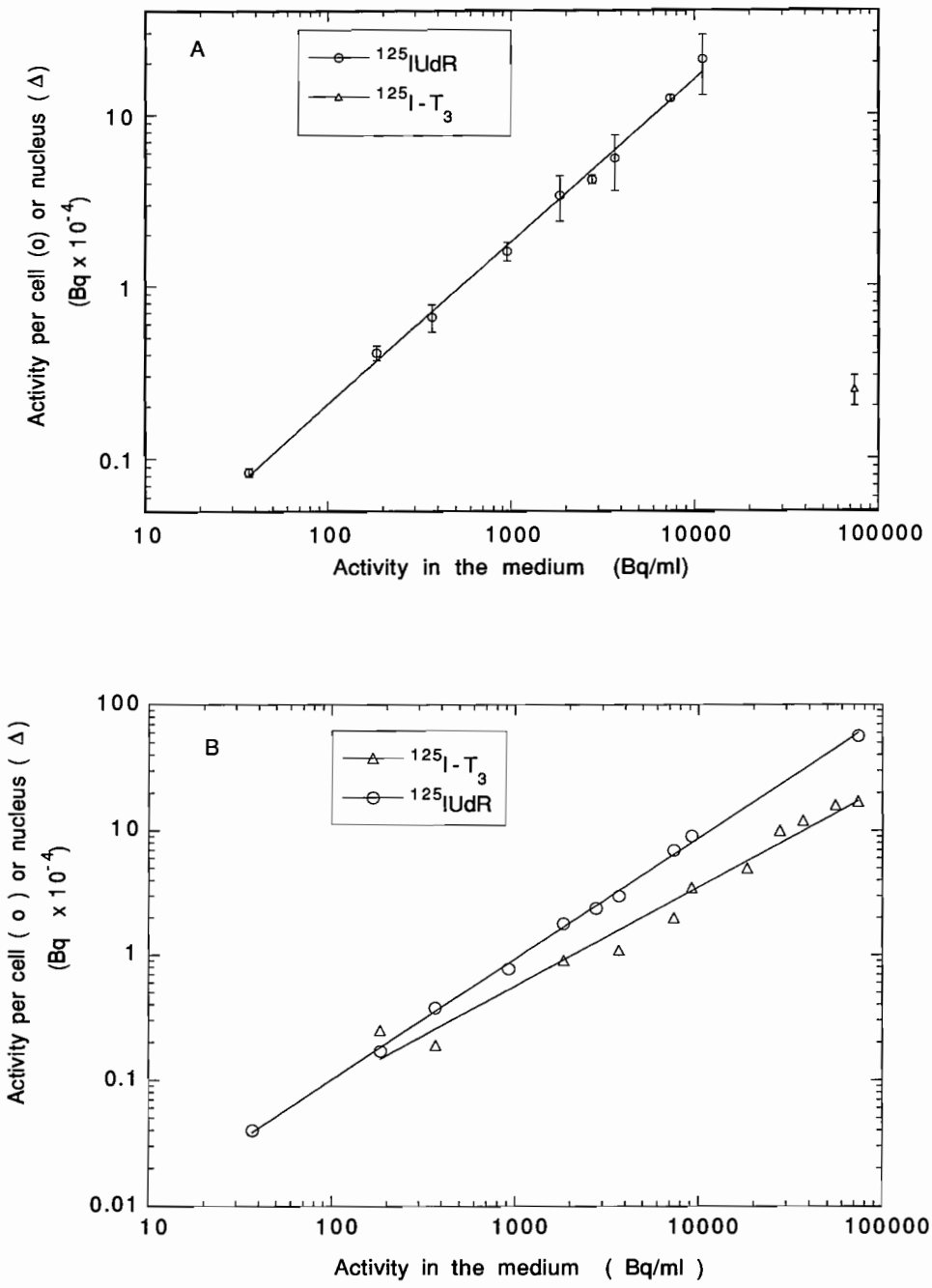

FIG. 1. Cellular uptake of ^{125}IUdR (open circles) and ^{125}I-T$_3$ (open triangles) in CHO cells (A) and GC cells (B).

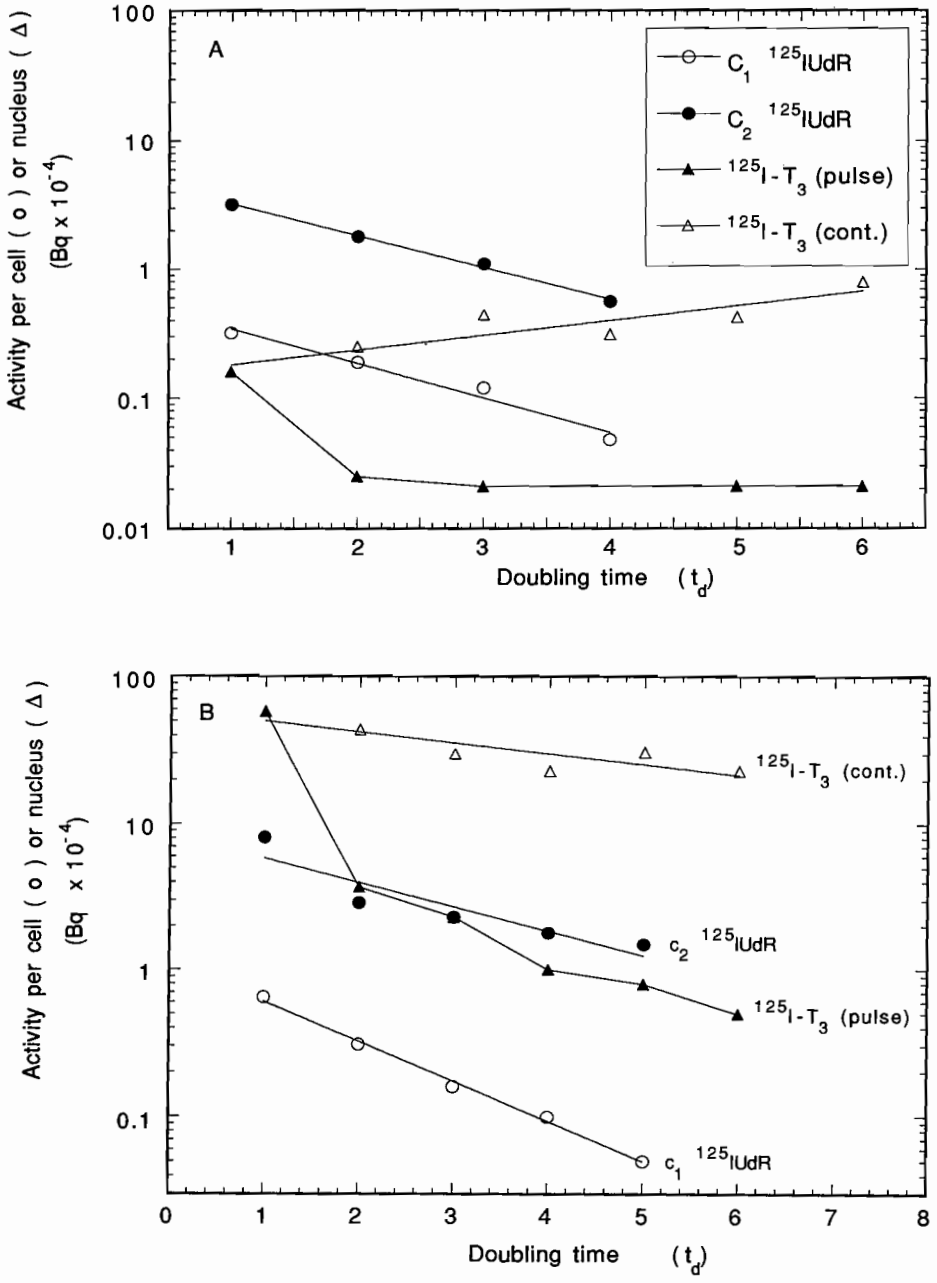

FIG. 2. Kinetics of ^{125}IUdR (open circles, solid circles) incorporated during one t_d, and of ^{125}I-T_3 permanently present in the medium (open triangles) or for one t_d (solid triangles): A) - CHO cells, B) - GC cells; initial ^{125}IUdR is taken at two different concentrations.

In GC cells the micronucleation was linear along the whole range of ^{125}I activity in the nucleus. The micronucleation induced by $^{125}IUdR$ increased linearly with ^{125}I activity up to 0.3 - 0.4 mBq/cell and then reached a plateau. The ratio of the slopes was 9 (Fig. 3B).

The uptake of ^{125}I-T_3 in the nuclei of CHO cells was very low at the high external activity concentrations used in the experiment (about 40 μBq/nucleus at 74 kBq/ml medium). The micronucleation induced by this ^{125}I activity did not significantly differ from the control (3 ± 1 vs 3.1 ± 0.8) and therefore the dose-response curve for lower activity concentrations (comparable with the physiological T_3 concentration) was not performed. The micronucleation induced by $^{125}IUdR$ was linear up to about 0.8 mBq/cell, where a deviation from linearity was seen (Fig. 3A).

DISCUSSION

The results obtained in this study show that the ^{125}I-labeled thyroid hormone induces a significant number of micronucleated cells in hormone-responsive cells but with lower efficiency than the reference compound, $^{125}IUdR$. In the non-responsive cells, ^{125}I-T_3 at physiological T_3 concentrations did not significantly increase micronucleation. The reasons for the observed differences in efficacy of inducing micronuclei may be of geometrical, biochemical or dosimetric nature.

The proximity of ^{125}I to the DNA molecule is considered to be crucial for the magnitude (7) and severity (6) of damage imparted. $^{125}IUdR$ is unspecifically incorporated into dividing cells. When incorporated into the DNA molecule, $^{125}IUdR$ is retained in it until the end of G_2 phase. During division the ^{125}I-activity per cell is halved (7). However, the distance of ^{125}I to the DNA constituents is close and remains unchanged. Hence, the activity measurements carried out with whole cells actually reflects the ^{125}I-activity in DNA. Thus, for $^{125}IUdR$, the position of ^{125}I in the DNA molecule is constant and independent of the particular phase of the cell cycle.

The intracellular concentration of ^{125}I-T_3 is governed by the abundance of the thyroid hormone nuclear (TR) receptors in a given cell type (16), and the regulation of the number of receptors by the ligand itself within this cell type (24,25). The limited number of nuclear receptors, therefore, gives a cell-

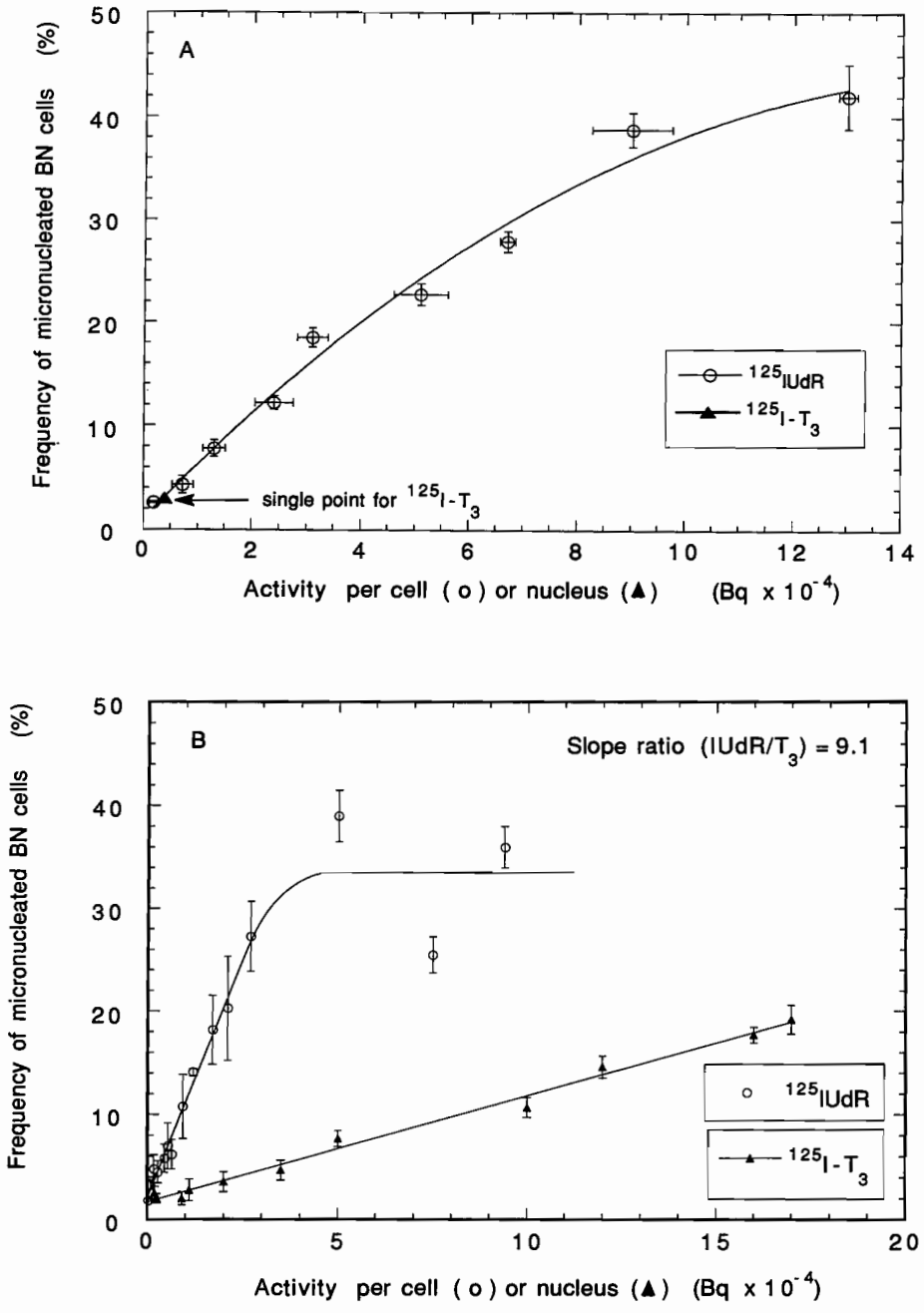

FIG. 3. Micronucleation of CHO cells (A) and GC cells (B) after one t_d labeling with ^{125}IUdR (open circles) or after continuous incubation with ^{125}I-T$_3$ (solid triangles) for 4 t_d.

specific upper limit for the dose delivered to the nucleus. TR belongs to ligand-dependent transcription regulating proteins of specific genes. This protein consists of three distinct structural and functional domains: ligand-, DNA- and histone- binding domains (26). When the ligand-receptor complex is formed the binding of the complex to DNA is enabled. The receptor binds to DNA in the form of a dimer. Each DNA-binding domain of the receptor creates two finger-like structures coordinated by zinc atoms (14,32). These zinc fingers recognize and interact with specific DNA sequences through the major groove at a distance of about 200 base pairs in the 5' flanking DNA from the transcription starting point of the regulated genes (12,15).

The nuclear receptors regulate the duration of association of ^{125}I-T_3 with DNA. The mean half-life of the receptors is approximately 4 h (13), and thus the mean time of association of ^{125}I-T_3 to the receptor is shorter than the cell cycle (30 h). Moreover, the action of the receptor on regulated genes is exerted during a limited time of the cell cycle, for instance during the G_1 phase (10). In the S phase the receptors probably dissociate from the DNA and move to a nuclear subcompartment distant from DNA (*i.e.*, from the nuclear matrix) (27). Thus, the measurement of ^{125}I activity in the nucleus is not tantamount to the ^{125}I activity measurement in DNA.

This study indicates that ^{125}I-T_3, which is not incorporated into the DNA, interacts with DNA indirectly through its nuclear receptor and induces concentration dependent damage at physiological concentrations of the hormone (below 0.5 nM of T_3). This implies that the mediator itself, the thyroid hormone nuclear receptor, can be used as a targeting molecule for ^{125}I to investigate distance-related damage to the DNA helix and/or can be applied for therapeutic purposes owing to the receptor's tissue and gene specificity.

The thyroid hormone nuclear receptor and functionally related proteins from the large steroid- and thyroid-hormone receptor superfamily show structural similarities with other transcription regulating proteins (28,29). The structural similarities can be seen in their three-domain construction, zinc-finger feature in the DNA-binding domain, and the dimerization of the COOH terminal domain. ^{125}I labeling of the zinc finger amino acids involved in interaction with DNA should damage the specific nucleotide sequences (6,30). The expected specificity and efficacy of damage caused by this, and other Auger emitters, might be useful for therapeutic purposes. The use of ^{125}I in therapy was suggested by Martin *et al.* (31) and

applied by Adelstein *et al.* (2). However, the compounds proposed by Martin *et al.* (31) as well as IUdR used by Adelstein *et al.* (2) did not have cell and/or tissue specific DNA affinity.

The carboxy-terminal end of the zinc finger transcription regulation proteins/nuclear receptors participate in dimer formation. It was shown (20) for C/EBP (CAT/Enhancer-Binding Protein) that two homo- and hetero-molecules are pieced together by a characteristic arrangement of leucine residues in the COOH-domain. A mode for the association of hormone receptor molecules has not yet been reported, but it has been suggested that binding of the hormone to this domain seems to be necessary for the receptor dimerization (14,32). The superfamily of the leucine-zipper transcription factors can offer a new tool for experimental elucidation of the distance-dependence of damage caused by ^{125}I and other Auger emitters. Labeling of the seven leucine residues of the transcription factors with ^{125}I, which probably are at different distances from the DNA molecule, should create a molecular scale of distances of ^{125}I from the DNA, which could be used to investigate the damage-distance relationship.

CONCLUSIONS

The ^{125}I labeled thyroid hormone places ^{125}I nanometers from the DNA where a high-LET-like effect is exerted and the dose-related damage is linear. This effect is specific for cells with large numbers of nuclear receptors for the thyroid hormone. The relative ^{125}I-T_3 toxicity is about one order of magnitude lower than ^{125}IUdR. Because the effect of ^{125}I bound to the thyroid hormone depends on the thyroid hormone nuclear receptor, we suggest an application of structurally related molecules, *i.e.* zinc finger proteins, labeled with Auger emitters for tumor therapy and fundamental research of Auger-electron emitting radionuclides.

REFERENCES

1. E.E. CAMERGO, G.S. JOHNSTONE, S.M. LARSON, and H.N. WAGNER, In *Textbook of Nuclear Medicine: Clinical Applications*, (A.F.G. ROCHA and J.C. HARBERT, Eds.) Philadelphia: Lea & Febiger, 440-455, 1979.
2. S.J. ADELSTEIN, A.I. KASSIS, J. BARANOWSKA-KORTYLEWICZ, A.D. VAN DEN ABBEELE, G. MARIANI, and S. ITO, Potential for tumor therapy with iodine-125 labeled immunoglobulins. *Nucl. Med. Biol.* **18**, 43-44 (1991).

3. K.D. BAGSHAWE, S.K. SHARMA, P.J. SOUTHALL, J.A. BODEN, G.M. BOXER, T.A. PATRIDGE, P. ANTONIW, and R.B. PEDLEY, Selective uptake of toxic nucleoside (^{125}IUdR) by resistant cancer. *Brit. J. Radiol.* **64**, 37-44 (1991).
4. D.V. WOO, D. LI, J.A. MATTIS, and Z. STEPLEWSKI, Selective chromosomal damage and cytotoxicity of ^{125}I-labeled monoclonal antibody 17-1a in human cancer cells. *Cancer Res.* **49**, 2952-2958 (1989).
5. A.I. KASSIS, F. FAYAD, B.M. KINSEY, K.S.R. SASTRY, R.A. TAUBE, and S.J. ADELSTEIN, Radiotoxicity of ^{125}I in mammalian cells. *Radiat. Res.* **111**, 305-318 (1987).
6. D.E. CHARLTON and J. BOOZ, A Monte Carlo treatment of the decay of ^{125}I. *Radiat. Res.* **87**, 10-23 (1981).
7. A.I. KASSIS, K.S.R. SASTRY, and S.J. ADELSTEIN, Kinetics of uptake, retention and radiotoxicity of ^{125}IUdR in mammalian cells: implications of localized energy deposition by Auger processes. *Radiat. Res.* **109**, 78-89 (1987).
8. D.E. CHARLTON, The range of high LET effects from ^{125}I decays. *Radiat. Res.* **107**, 163-171 (1986).
9. C.R. DEFESI and M.I. SURKS, 3,5,3'-triiodothyronine effects on the growth rate and cell cycle of cultured GC cells. *Endocrinology* **108**, 259-267 (1981).
10. C.R. DEFESI, E.C. FELS, and M.I. SURKS, Triiodothyronine stimulates growth of cultured GC cells by action in the G_1 period. *Endocrinology* **114**, 293-295 (1984).
11. M.H. KUMARA-SIRI and M.I. SURKS, Regulation of growth hormone mRNA synthesis by 3,5,3'-triiodo-L-thyronine in cultured growth hormone-producing rat pituitary tumor cells (GC cells). *J. Biol. Chem.* **260**, 14529-14537 (1985).
12. J.W. APRILETTI, J.D. BAXTER, and T.N. LAVIN, Large scale purification of the nuclear thyroid hormone receptor from rat liver and sequence-specific binding of the receptor to DNA. *J. Biol. Chem.* **263**, 9409-9417 (1988).
13. J. CASANOVA, Z.D. HOROVITZ, R.P. COPP, W.R. MCINTYRE, A.PASCUAL, and H.H. SAMUELS, Photoaffinity labeling of thyroid hormone nuclear receptors. *J. Biol. Chem.* **259**, 12084-12091 (1984).
14. R.M. EVANS, The steroid and thyroid hormone receptor superfamily. *Science* **240**, 889-895 (1988).
15. R.P. LARSEN, J.W. HARNEY, and D.D. MOORE, Sequences required for cell-type specific thyroid hormone regulation of rat growth hormone promoter activity. *J. Biol. Chem.* **261**, 14373-14376 (1986).
16. J.H. OPPENHEIMER, H.L. SCHWARTZ, and M.I. SURKS, Tissue differences in the concentration of triiodothyronine nuclear binding sites in the rat: Liver, kidney, pituitary, heart, brain, spleen and testis. *Endocrinology* **95**, 897-903 (1974).
17. H.H. SAMUELS, F. STANLEY, and J. CASANOVA, Depletion of L-3,5,3'-triiodothyronine and L-thyroxine in euthyroid calf serum for use in cell culture studies of the action of thyroid hormone. *Endocrinology* **105**, 80-85 (1979).
18. E.W. BRADLEY, P.C. CHAN, and S.J. ADELSTEIN, The radiotoxicity of iodine-125 in mammalian cells. *Radiat. Res.* **64**, 555-563 (1975).
19. K. ICHIKAWA, K. HASHIZUME, M. KOBAYASHI, and T. YAMADA, Evidence for induction by thyroid hormone of cytosolic proteins which control mitochondrial protein synthesis. *Endocrinology* **117**, 1749-1758 (1985).

20. N.B. PLIAM and I.D. GOLDFINE, High affinity thyroid hormone binding sites on purified rat liver plasma membranes. *Biochem. Biophys. Res. Commun.* **79**, 166-172 (1977).
21. S. SUNDELL-BERGMAN, K.J. JOHANSON, and G. LUDWIKOW, Radiotoxic effect of ^{125}I-labeled thyroid hormones with affinity to cellular chromatin. In *DNA damage by Auger Emitters*, (K.F. BAVERSTOCK and D.E. CHARLTON, Eds.) London: Taylor & Francis, pp. 147-157, 1988.
22. P.I. COUNTRYMAN and J.A. HEDDLE, The production of micronuclei from chromosome aberrations in irradiated cultures of human lymphocytes. *Mutation Res.* **41**, 321-332 (1976).
23. M. FENECH and A.A. MORLEY, Measurement of micronuclei in lymphocytes. *Mutation Res.* **147**, 29-36 (1985).
24. H.H. SAMUELS, F. STANLEY, and L.E. SHAPIRO, Dose-dependent depletion of nuclear receptors by L-triiodothyronine: Evidence for a role in induction of growth hormone synthesis in cultured GH1 cells. *Proc. Nat. Acad. Sci. USA* **73**, 3877-3881 (1976).
25. B.M. RAAKA and H.H. SAMUELS, Regulation of thyroid hormone nuclear receptors levels in GH1 cells by 3,5,3'-triiodo-L-thyronine. *J. Biol. Chem.* **256**, 6883-6889 (1981).
26. K. ICHIKAWA and L.J. DEGROOT, Separation of DNA binding domain from hormone and core histone binding domains by trypsin digestion of rat liver nuclear thyroid hormone receptor. *J. Biol. Chem.* **261**, 16540-16546 (1986).
27. M.H. KUMARASIRI, L.E. SHAPIRO, and M.I. SURKS, Cell cycle dependence of thyroid hormone nuclear receptors in cultured GC cells: Relationship to nuclear matrix. *Endocrinology* **122**, 1897-1904 (1988).
28. N.P. PAVLETICH and C.O. PABO, Zinc finger-DNA recognition: Crystal structure of a Zif268-DNA complex at 2.1 Å. *Science* **252**, 809-817 (1991).
29. S.L. MCKNIGHT, Molecular zippers in gene regulation. *Sci. Am.*, **264**, 32-39 (1991).
30. V. MURRAY and R.F. MARTIN, Sequence specificity of ^{125}I-labeled Hoechst 33258 in intact human cells. *J. Mol. Biol.* **201**, 437-442 (1988).
31. R.F. MARTIN, T.R. BRADLEY, and G.S. HODGSON, Cytotoxicity of ^{125}I-labeled DNA-binding compound that induces double-stranded DNA breaks. *Cancer Res.* **39**, 3244-3247 (1979).
32. M. BEATO, Gene regulation by steroid hormones. *Cell* **56**, 335-344 (1989).

194 Biophysical Aspects of Auger Processes, AAPM Symposium Series No. 8 (1992) 194-209
Eds. RW Howell, VR Narra, KSR Sastry, DV Rao

COMPARISON OF MUTATION INDUCTION BY EXTERNAL AND INTERNAL RADIATION SOURCES IN SYNCHRONIZED CHINESE HAMSTER OVARY (CHO) CELLS

HATSUMI NAGASAWA,[1] AMIN I. KASSIS,[2]
ROBERT M. BERMAN,[2] SHAILENDRA K. SAHU,[2]
JAC A. NICKOLOFF,[1] RICHARD T. OKINAKA,[3]
S. JAMES ADELSTEIN,[2] and JOHN B. LITTLE[1]

[1]Laboratory of Radiobiology,
Harvard School of Public Health, Boston, MA 02115, USA

[2]Department of Radiology, Harvard Medical School,
Boston, MA 02115, USA

[3]Genetics Group, Los Alamos National Laboratory,
Los Alamos, NM 80545, USA

ABSTRACT

Synchronized CHO cells were either X irradiated or pulse-labeled with ^{3}H-TdR or ^{125}IUdR at 5 h (early S phase, ES), 8 h (mid S phase, MS) and 12 h (late S phase, LS) after mitotic selection. Radiation-induced hprt gene mutation frequencies were determined and mutants were isolated for further molecular analysis. Mutation frequencies of X irradiated ES cell populations increased linearly with dose, reaching 30 times the spontaneous level at 600 cGy. However, mutation frequencies of MS and LS cell populations increased at doses up to 200 cGy and then reached a plateau at doses up to 600 cGy. Although the same mutation frequencies were observed in ES and LS cell populations following X irradiation at 200 cGy, the cell survival

fractions were 0.6 and 0.98, respectively. Cells with DNA-incorporated ^{3}H-TdR had similar patterns of induced mutations. The results suggest that the most susceptible period for the induction of hprt mutations occurs while the gene is replicating in early S phase. Compared with X rays, DNA-incorporated ^{3}H-TdR and ^{125}IUdR produced D_0 doses with RBE values of 2.1 and 8.6, respectively, and hprt mutation frequencies with RBE values of 6.9 and >60, respectively. The structures of mutant hprt genes in radiation-induced mutant clones were analyzed by Southern hybridization. Seventeen to twenty-eight percent of hprt mutant clones had no detectable structural changes (point mutations). For X irradiation, 56% of mutant clones had complete hprt gene deletion, while for both internal radiation emitters (^{3}H-TdR and ^{125}IUdR), nearly 50% showed partial deletions at the hprt locus.

INTRODUCTION

Induction of 6-thioguanine resistance ($6TG^{r}$) mutations at the hypoxanthine-guanine-phosphoribosyl-transferase (hprt) gene locus has been widely studied with low- and high-LET radiation in the Chinese hamster ovary (CHO) cell system (1-7). The hprt gene product is one of the enzymes responsible for the salvage of preformed purine bases during normal nucleic acid turnover in mammalian cells (8). The Chinese hamster hprt gene is located at the distal end of the short arm of the X chromosome where DNA replication occurs in early S phase (9,10). High frequency X ray-induced hprt mutation has been reported at the G_1/S phase border of synchronized CHO cells (7,11). These studies suggest that DNA replication may influence the induction of mutations at the hprt locus.

The induction of hprt mutations with radioactive nucleic acid precursors (tritiated thymidine [^{3}H-TdR] and 5-[^{125}I]iodo-2'-deoxyuridine [^{125}IUdR]) has been studied in mammalian cells (12-15). Although beta rays from tritium are classified as low-LET particles, the ionizing radiation from ^{3}H-TdR incorporated in DNA may produce greater injury to cells than that from an equivalent amount of more generally distributed energy from internal (such as ^{3}HOH and ^{3}H-amino acid) (16) and external (such as X ray and γ ray) low-LET radiation sources.

Many studies have shown that the emission of a shower of low energy Auger electrons results in a highly localized biological effect similar to high-LET radiation (17-35). Nearly 30% of the electron tracks emitted from a single

decay of the Auger emitter ^{125}I incorporated into DNA as $^{125}IUdR$ interact as a direct hit with the atoms of DNA (36). The base most affected is the labeled base and in roughly 1% of all decays more than 100 eV is deposited here (37). Pomplun (37) calculated that ^{125}I incorporated in DNA produced 0.9 double strand breaks (DSB) per decay plus 1.9 additional single strand breaks (SSB) or a total of 3.7 SSB per decay. These findings are in agreement with those of LeMotte and Little (38).

In this paper, we discuss the mutation frequencies and molecular structural changes of the hprt locus in synchronized CHO cells induced by external (X ray) and internal (^{3}H-TdR and $^{125}IUdR$) radiation sources.

MATERIALS AND METHODS

Cell Culture

Chinese hamster ovary (CHO) cells were grown at 37°C in a humidified 95% CO_2 - 5% air atmosphere with McCoy 5a medium supplemented with 10% heat-inactivated bovine calf serum (56°C for 30 min), penicillin (50 units/ml), and streptomycin (50 μg/ml). To reduce the level of spontaneous hprt mutants, the cells were grown in HAT medium (2×10^{-4} M hypoxanthine, 2×10^{-7} M aminopterin, and 1.75×10^{-5} M thymidine) for 3 days. Synchronous cells (mitotic indices above 95%) were obtained by shaking loose the mitotic cells from asynchronous cultures as described previously (39). The mitotic cells ($1\text{-}3 \times 10^{8}$ cells) were pooled in an ice bath and frozen in dimethylsulfoxide (DMSO) freezing medium (40).[1] Prior to use, the cells were defrosted, seeded into plastic tissue culture flasks/tubes/petri dishes and returned to an incubator at 37°C.

X Irradiation

Synchronized cells were irradiated aerobically with a GE Maximar X ray generator operating at 190 kV and 15 mA with 1 mm/Al added filtration, yielding a dose rate of 80 cGy/min.

---

[1]The progression of cells through the cell cycle is not affected by the freezing-defrosting procedure.

Incorporation of ^{3}H-TdR and ^{125}IUdR

Synchronized CHO cells were incubated at 37°C. At 1 to 2 h intervals, the cultures were pulse-labeled for 15 min with 3.7×10^{4} Bq/ml of ^{3}H-TdR (approximately 7.4×10^{11} Bq/mmol) or ^{125}IUdR (approximately 7.4×10^{13} Bq/mmol, Du Pont) to obtain labeling indices throughout the cell cycle. The cells were fixed with 100% methanol and Kodak nuclear emulsion NTB type 2 was applied to the dishes for autoradiography. The autoradiograms were stained with 0.1% crystal violet. Two hundred cells were scored from each dish to determine the pulse-labeling indices (41).

To investigate other biological endpoints (cytotoxicity and mutation, see below), various radioactive concentrations of ^{3}H-TdR or ^{125}IUdR were incorporated into early S (ES), mid S (MS), or late S (LS) cell populations for 15 to 30 min at 37°C. The labeled cells were washed twice with warm medium containing nonradioactive thymidine (final concentration 10^{-5} M). The cells were then stored at 2 to 4°C for 15 to 24 h to accumulate radiation doses from the decay of the DNA-incorporated ^{125}I or ^{3}H.

Cytotoxicity and Mutation Assays

Cytotoxicity was determined by the colony forming assay. The treated cells were seeded at low densities and incubated for 8 days to allow colony formation. Plating efficiencies were determined by a similar procedure. To determine mutation frequencies, each treated culture, containing at least 10^{6} surviving cells, was incubated with nonselective medium for 7 to 9 days to allow phenotypic expression. The cells (2×10^{5}) were then added to each of 20 P-100 petri dishes containing 5 μg/ml of 6-thioguanine and incubated for 10 days to select mutant clones. For further molecular analysis (see below), one mutant clone was isolated from one petri dish per treatment (to avoid sibling problems) and these clonal mutant cells were cultured in P-100 dishes containing 6-thioguanine medium until the cells reached the near confluence level.

Molecular Analysis

High molecular weight DNA was isolated from mutant clones by a standard method (42). Samples (10 μg) were digested (37°C, overnight) with 20 units of Pst-I (New England Biolabs), electrophoresed on 0.8% agarose gels, and transferred to Nytran membranes (pore size 0.2 μm, Schleicher and

Schuell) for ≥14 h according to the recommendations of the manufacturer. Membranes were hybridized with a PCR-amplified hprt probe labeled by a random primer labeling procedure (43). The PCR primers (5'- GGCTTCCTCC TCACACCGCT-3' and 5'-GGACTCCTCG TGTTTGCAGA-3') were used to amplify a 496 bp fragment from a Chinese hamster hprt cDNA. The Southern blot banding patterns were analyzed and assorted into three categories as reported previously (44): (i) full deletions: all hprt-specific bands are missing; (ii) alterations: partial deletions and rearrangements are seen; and (iii) no change: indistinguishable from control (including point mutations).

Dose Determination

Radiation doses (cGy) were calculated from the DNA-incorporated ^{3}H-TdR or ^{125}IUdR activity per cell as described by Kassis and co-workers (26,31,32,34,35). Basically, the cumulative mean lethal dose (D) to the cell nucleus during these *in vitro* experiments is given by $D = E/V_N$, where V_N is the nuclear volume of CHO cells and E, the total amount of energy deposited in the nucleus. E is given by $E = (N_{37})\varepsilon$, N_{37} being the cumulated number of decays of the radionuclide (during the 15 to 24 h 4°C and the subsequent 8 day 37°C incubation periods) in the nucleus at 37% survival, and ε the average energy deposited in the nucleus (for ^{125}I, ε = 10.8 keV; for ^{3}H, ε = 4.3 keV) per decay in the nucleus.

RESULTS

The progression of pooled, previously frozen, mitotic cells through the cell cycle was followed by obtaining pulse-labeling indices (Fig. 1). The synchronized cells entered S phase 4 h after mitosis at 37°C, with nearly 95% of cells in S phase during mid S phase (8-10 h after mitosis). Labeling indices rapidly declined when cells entered G_2 phase.

With X irradiation, the early S phase (5 h) cell population showed the highest sensitivity to induced cell lethality (Table I) and the late S phase population the greatest radioresistance. Hprt mutation frequencies increased linearly with dose up to 600 cGy in early S phase cells (Fig. 2A). The relationship of cell survival and mutation frequencies of early S phase cells was nearly linear to the 5% survival level (Fig. 2B). X irradiation induced 1.3×10^{-7} mutants/cGy and the mutation frequencies increased linearly as a

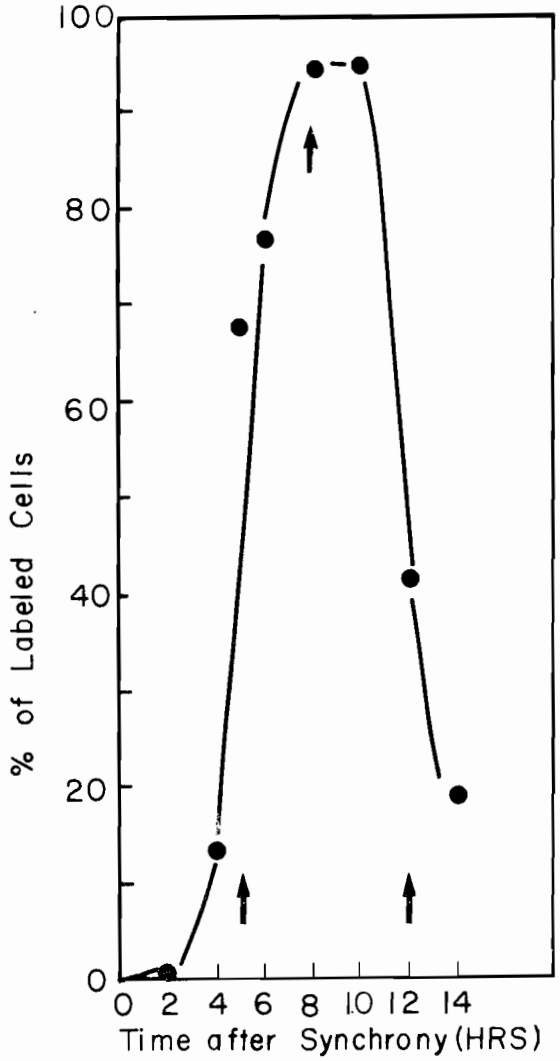

FIG. 1. Pulse-labeling indices of synchronized CHO cells after mitosis. Arrows indicate time when cell population was studied.

function of dose. Although mid and late S phase cells were more X ray resistant than early S phase cells (Table I), X ray-induced mutation frequencies increased at the same rate as in early S phase cells up to 200 cGy, with no increase between 200 cGy and 600 cGy (Fig. 2A). With mid S phase (Fig. 2A)

and late S phase (Fig. 2B) cell populations, X ray-induced hprt mutations increased only in the shoulder region of the cell survival curve (up to 200 cGy).

TABLE I
Radiosensitivities of Synchronized CHO Cells to X Ray, ^{3}H-TdR, and ^{125}IUdR

Radiation Source	Time after Mitosis (h)	N[a]	D_0 (cGy)	RBE[b]
X ray	5 (ES)	3	170	1.0
	8 (MS)	2	180	1.0
	12 (LS)	4	190	1.0
^{3}H-TdR	5 (ES)	1	20	8.5
	8 (MS)	~1	88	2.1
	12 (LS)	1	65	2.9
^{125}IUdR	5 (ES)	1	0.6-2.0	85-288
	8 (MS)	1	5.6	32.1
	12 (LS)	1	35.8 (1.6)[c]	5.3 (11.8)[c]

[a] extrapolation number
[b] RBE = D_0 (^{3}H-TdR or ^{125}IUdR)/D_0 (X ray)
[c] Parentheses show D_0 dose and RBE from sensitive cell populations

The cell survival curves of CHO cells pulse-labeled with ^{3}H-TdR at 5, 8, or 12 h after mitosis had no shoulder. There were no clear cell cycle effects on cellular lethality in MS and LS cell populations (Table I). Early S phase cell populations had mutation frequencies that increased linearly with dose to nearly 100 cGy of ^{3}H-TdR (9×10^{-7} mutants/cGy, RBE = 6.9), while mid and late S phase cell populations demonstrated increased mutation frequencies at doses from 5 to 10 cGy, with no further increase between 10 and 270 cGy (Fig. 3). With ^{125}IUdR incorporation, there were no dose-response or cell cycle effects when the mutation frequencies were calculated on the total cell populations. Only early S phase cell populations showed slightly higher mutations frequencies (Fig. 4).

In order to study the molecular structural changes at the hprt locus, genomic DNA isolated from independent mutant clones was examined by Southern hybridization analysis. Fifty-eight percent of spontaneously arising

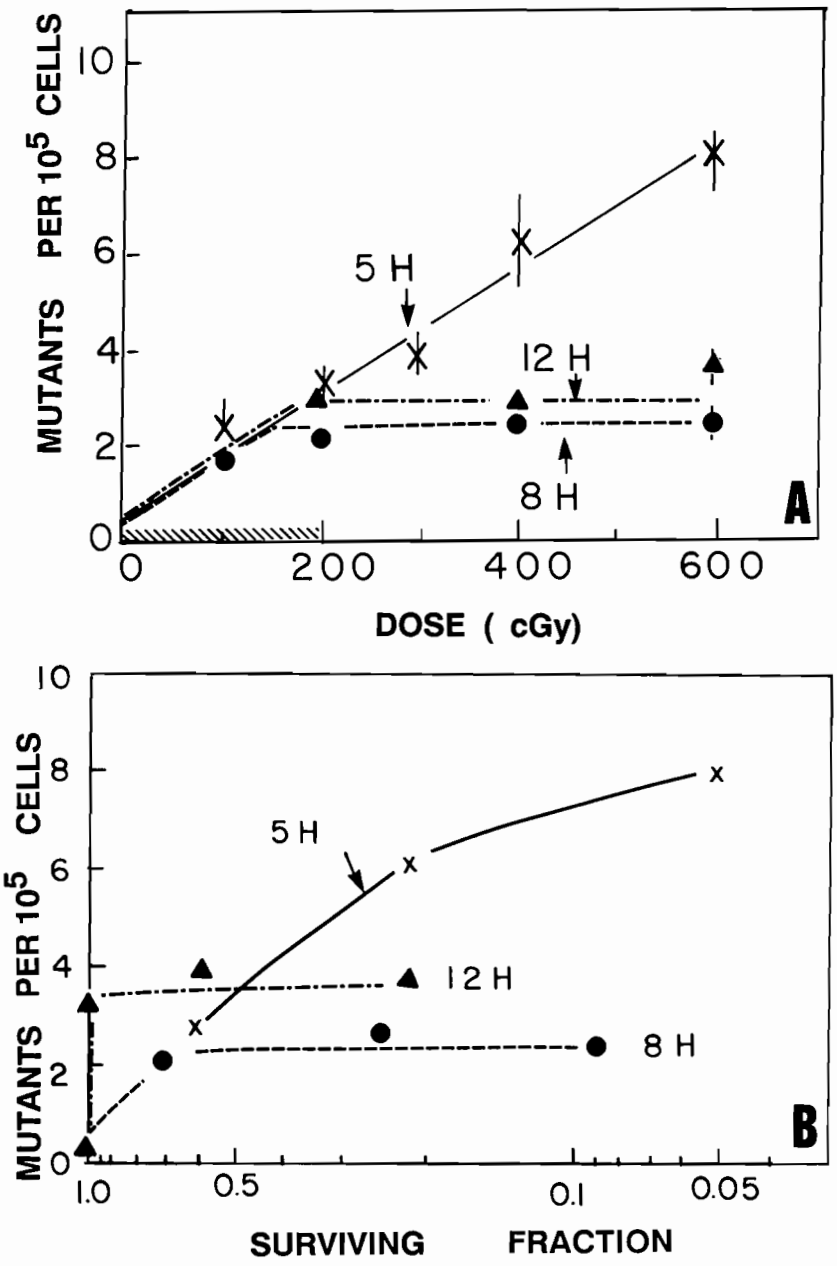

FIG. 2. A. Mutation frequencies at hprt locus in synchronized CHO cells following X irradiation. Early S (ES): X; Mid S (MS): solid circles; Late S (LS): solid triangles. Spontaneous background frequencies ([0.27 ± 0.12] X 10^{-5}) shown as shaded area. B. Relationship of cell survival and X ray-induced mutation frequencies at hprt locus in synchronized CHO cells. Early S : X; Mid S : solid circles; Late S : solid triangles.

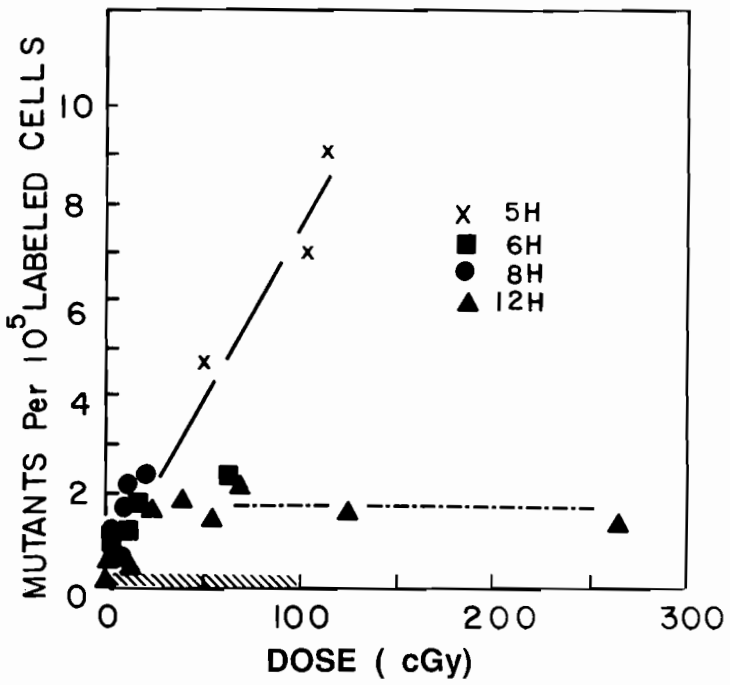

FIG. 3. Mutation frequencies at hprt locus in synchronized CHO cell populations following ^{3}H-TdR pulse-labeling. Early S (ES): X, solid squares; Mid S (MS): solid circles; Late S (LS): solid triangles. Spontaneous background frequencies ([0.50 ± 0.12] X 10^{-5}) shown as shaded area.

mutants had no detectable structural changes, while 56% of 600 cGy X ray-induced mutant clones had total gene deletions and 27% partial gene deletions. In contrast, half the mutant clones obtained after ^{3}H-TdR or ^{125}IUdR incorporation had partial gene deletions. Seventeen to twenty-eight percent of mutant clones were point mutations after both external and internal radiation (Table II).

DISCUSSION

The hprt gene of CHO cells is functionally hemizygous in pseudodiploid cells, since one X chromosome is inactivated in female cells during embryonic development (45). Farrell and Worton (9) localized the

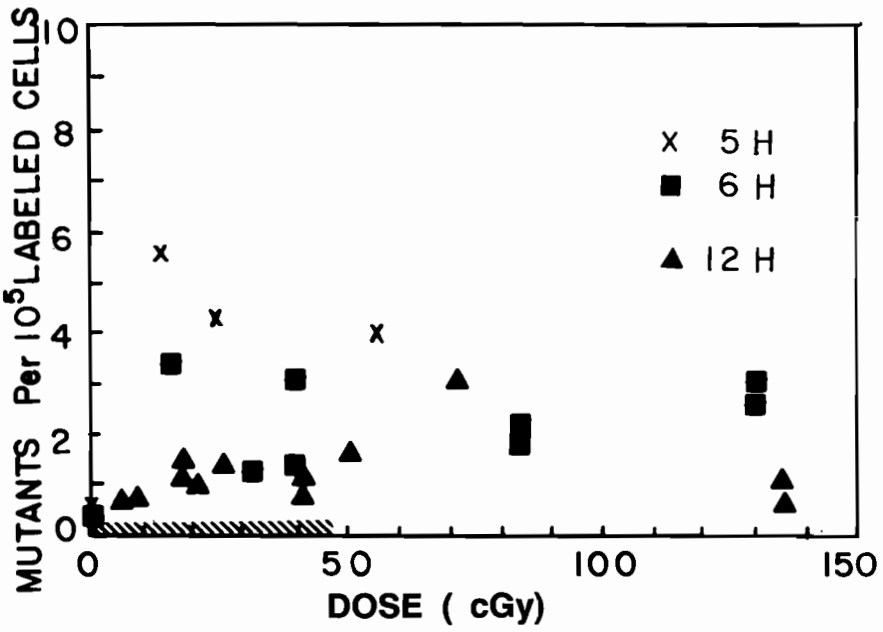

FIG. 4. Mutation frequencies at hprt locus in synchronized CHO cell populations following ^{125}IUdR pulse-labeling. Early S (ES): X, closed squares; Late S (LS): solid triangles. Spontaneous background frequencies ($[0.60 \pm 0.13] \times 10^{-5}$) shown as shaded area.

hprt gene to the distal end of the short arm on the Chinese hamster X chromosome. DNA replication in these cells occurs intensively at the short and long arm of the X chromosome during early and late S phase, respectively (10). At early, mid, and late S phase, the survival fractions of X irradiated CHO cells showed the same age responses as demonstrated previously (39,46-48) (Table I).

It has been reported that in many mutation systems in eukaryotic cells, plots of radiation-induced mutation frequencies (mutants/survivors) against the logarithm of the surviving fraction often give a straight line with low- and high-LET radiation (7,29,49-51). In this study, only early S phase cell populations showed a linear increase in the induction of hprt mutants following X irradiation to 600 cGy and cell survival levels of about 5% (Fig. 2B). This suggests that a close relationship between cell killing and

TABLE II
Molecular Analysis of the HPRT Mutant Clones

Radiation Source	Number of Clones	Structural changes at hprt locus: Total Deletion	Partial Deletion	Point Mutation
Control	29	4 (14%)	8 (28%)	17 (58%)
X ray (600 cGy)	48	27 (56%)	13 (27%)	8 (17%)
^{3}H-TdR (1-265 cGy)	36	9 (26%)	16 (46%)	11 (28%)
^{125}IUdR (7-137 cGy)	57	15 (26%)	31 (54%)	11 (22%)

induction of hprt mutants in early S phase cells exists. On the other hand, late S phase cells were the most radioresistant (Fig. 2A) (39,46-48). When hprt mutants were induced with nonlethal doses (up to 200 cGy), however, the mutation frequency level remained constant (Fig. 2A).

The same effects of X ray-induced hprt mutational patterns through the cell cycle have been reported in synchronous CHO cells by others (7,11). This phenomenon may be related to the order of gene replication in the cell cycle. Housekeeping genes are located in the euchromatin area and tend to replicate in early S phase, whereas tissue-specific genes (transcriptionally inactive genes located in heterochromatin) tend to replicate in late S phase (52). The hprt locus might be highly susceptible to radiation during the replication period when cells escape from lethal radiation damage. Once the hprt gene has finished replicating, however, it may become more resistant to radiation-induced mutation while other essential genes may be more sensitive to damage in mid and late S phase.

Since ^{3}H-TdR and ^{125}IUdR are incorporated into nuclear DNA, they pass into daughter nuclei after cell division. In addition, G-C-rich DNA (euchromatin) is synthesized in early S phase and low G-C DNA (heterochromatin) in late S phase (52). The same mutation frequencies in early S phase CHO cells with ^{3}H-TdR incorporated into DNA required nearly a sixfold lower radiation dose than with X ray (Fig. 2B and 3). This RBE value

correlates well with that of 5.9 reported in a previous study in which ^{3}H-TdR incorporation was compared to chronic gamma ray induction of hprt mutations in mouse L5178Y lymphoblastoid cells (13). When ^{3}HOH and ^{3}H-amino acids were incorporated into cells, the radioactivity was homogeneously distributed throughout the cells and RBE values of 1 to 3 were reported for cell killing, chromosomal aberrations and mutations (16). Since ^{3}H-TdR is incorporated into thymine-rich DNA, these areas received more radiation than expected, and the RBE values observed were higher.

It has been reported that ^{125}IUdR incorporated into the DNA of cells generates highly localized, low energy, Auger electrons resulting in extremely high RBE values for cell lethality, mutations and malignant transformations (7,15,17-35,38). In the present studies, the RBE (at D_0 doses) of ^{3}H-TdR and ^{125}IUdR treated cells were extremely high in ES phase (85-288) as compared to MS and LS phase cells (Table I). These results and those published earlier (29), in which an RBE value of 49 for ^{125}IUdR-induced hprt mutations in human lymphoblast cells had been reported, suggest that very low doses of internal emitters (especially ^{125}IUdR) are efficient inducers of mutations in the absence of cell killing. While significantly high rates of hprt mutations were induced at low DNA-incorporated ^{125}IUdR levels, we were unable to measure a dose response in the present studies (Fig. 4). It is possible that the decay of DNA-incorporated ^{125}IUdR and the subsequent shower of Auger electrons could have led to nonrepairable DNA damage and death of the irradiated cells. In such a scenario, the surviving cells are those in which (a) the decay of ^{125}I occurred within nonlethal genes, or (b) DNA damage had been repaired.

As determined by Southern hybridization analysis, 58% of the spontaneous hprt mutants were shown to have undetectable changes (Table II). These findings are in agreement with results from other cell systems (14,15,53). Fifty-six percent of 600 cGy X ray-induced mutant clones were total gene deletions (Table II). This value was higher than that in 100 cGy X ray-induced TK-6 cells, where 30% of mutant clones were reported as total gene deletions (14,15). However, other studies with CHO, V79, and TK-6 cells indicated over 50% of X ray-induced mutant clones were total hprt gene deletions (12,44,53,54).

Similar molecular structural changes were observed after DNA incorporation of both internal emitters (^{3}H-TdR and ^{125}IUdR) (Table II). Forty-six and fifty-four percent of the mutant clones were partial gene deletions after exposure to ^{3}H-TdR and ^{125}IUdR, respectively. Twenty-six percent of the

mutant clones were missing a total gene with both of these radionuclides. It is possible that ^{3}H-TdR and ^{125}IUdR incorporated within, or in close proximity to, the hprt gene damage local regions. In the presence of high radioactive concentrations within the hprt gene, total deletions might result. In the present study, however, nearly half the molecular structural changes appeared as partial gene deletions. Whaley and Little (14,15) reported that the molecular structural changes were dependent on the dose of ^{125}IUdR incorporated. Currently, mutant clones are being analyzed to determine the relationship between DNA replication patterns and molecular structural changes of the hprt gene in different phases of the cell cycle with X, ^{3}H-TdR, and ^{125}IUdR irradiation.

In conclusion, our data suggest that the most susceptible period for the induction of hprt mutation occurs while the gene is replicating in early S phase. Compared with X rays, the RBE values for ^{125}I incorporated into DNA for cell killing and induction of hprt mutations were much higher than those of tritium. With these internal emitters, approximately 50% of the mutant clones exhibited partial gene deletions and 25% were missing a total gene.

ACKNOWLEDGMENTS

This research was supported by NIH grants CA 47542 (JBL, HN) and CA 15523 (AIK, SJA) , NIEHS grant ES 00002 (JBL, HN), ACS grant ACS-PDT-440 (HN, JBL) and US DOE contract W-7405-ENG-36 (RTO).

REFERENCES

1. C.F. ARLETT and J. POTTER, Mutation to 8-azaguanine resistance induced by gamma-radiation in a Chinese hamster cell line. *Mutat. Res.* **13**, 59-65 (1971).
2. J. MORROW, J. COLOFIORE, and D. RINTOUL, Azaguanine resistant hamster cell lines not deficient in hypoxanthine-guanine phosphoribosyl transferase. *J. Cell. Physiol.* **81**, 97-100 (1973).
3. B.C. MYHR and J.A. DIPAOLO, Requirement for cell dispersion prior to selection of induced azaguanine-resistant colonies of Chinese hamster cells. *Genetics* **80**, 157-169 (1975).
4. J.H. CARVER, W.C. DEWEY, and L.E. HOPWOOD, X-ray induced mutants resistant to 8-azaguanine. II. Cell cycle dose response. *Mutat. Res.* **34**, 465-480 (1976).

5. M. WATANABE and M. HORIKAWA, Analyses of differential sensitivities of synchronized HeLa S3 cells to radiation and chemical carcinogens during the cell cycle. IV. X- rays. *Mutat. Res.* **44**, 413-426 (1977).
6. R.F. JOSTES, L.E. HOPWOOD, W.C. DEWEY, and G.R. BLACKBURN, The dependence of mutation frequency on 8-azaguanine concentration in control and irradiated CHO cells. *Mutat. Res.* **50**, 433-440 (1978).
7. H.J. BURKI, Ionizing radiation-induced 6-thioguanine-resistant clones in synchronous CHO cells. *Radiat. Res.* **81**, 76-84 (1980).
8. C.T. CASKEY and G.D. KRUH, The HPRT locus. *Cell* **16**, 1-9 (1979).
9. S.A. FARRELL and R.G. WORTON, Chromosome loss is responsible for segregation at the hprt locus in Chinese hamster cell hybrids. *Somat. Cell Genet.* **3**, 539-551 (1977).
10. E. STUBBLEFIELD, Analysis of replication pattern of Chinese hamster chromosomes using 5-bromodeoxyuridine suppression of 33258 Hoechst fluorescence. *Chromosoma* **53**, 209-221 (1975).
11. R.F. JOSTES, K.M. BUSHNELL, and W.C. DEWEY, X-ray induction of 8-azaguanine-resistant mutants in synchronous Chinese hamster ovary cells. *Radiat. Res.* **83**, 146-161 (1980).
12. R.A. GIBBS, J. CAMAKARIS, G.S. HODGSON, and R.F. MARTIN, Molecular characterization of ^{125}I decay and X- ray-induced hprt mutants in CHO cells. *Int. J. Radiat. Biol.* **51**, 193-199 (1987).
13. A.M. UENO, I. FURUNO-FUKUSHI, and H. MATSUDAIRA, Cell killing and mutation to 6-thioguanine resistance after exposure to tritiated amino acids and tritiated thymidine in cultured mammalian cells. In *Proceedings Third Japan- US Workshop on Tritium Radiobiology and Health Physics*, November 8-10, 1988, (S. Okada, Ed.) IPPJ-REV-3, pp. 200-210. Institute of Plasma Physics, Nagoya University, Nagoya, Japan, 1989.
14. J.M. WHALEY and J.B. LITTLE, Molecular characterization of hprt mutants induced by low- and high-LET radiations in human cells. *Mutat. Res.* **243**, 35-45 (1990).
15. J.M. WHALEY and J.B. LITTLE, Efficient mutation induction by ^{125}I and ^{131}I decays in DNA of human cells. *Radiat. Res.* **123**, 68-74 (1990).
16. T. STRAUME, Health Risks from Exposure to Tritium. *Lawrence Livermore National Laboratory Manuscript* (Dist. Category 702) pp. 1-32. Lawrence Livermore National Laboratory, Livermore, CA, 1991.
17. C. AHNSTROM, L.E. EHRENBERG, S. HUSSAIN, and A.T. NATAJARAN, On the killing and mutagenic action in E. coli associated with the Auger effect during ^{125}I decay. *Mutat. Res.* **10**, 247-250 (1970).
18. K.G. HOFER and W.L. HUGHES, Radiotoxicity of intracellular tritium, ^{125}iodine and ^{131}iodine. *Radiat. Res.* **47**, 94-104 (1971).
19. E.W. BRADLEY, P.C. CHAN, and S.J. ADELSTEIN, The radiotoxicity of iodine-125 in mammalian cells. I. Effects on the survival curve of radioiodine incorporated into DNA. *Radiat. Res.* **64**, 555-563 (1975).
20. K.G. HOFER, C.R. HARRIS, and J.M. SMITH, Radiotoxicity of intracellular ^{67}Ga, ^{125}I, and ^{3}H. Nuclear versus cytoplasmic radiation effects in murine L1210 leukemia. *Int. J. Radiat. Biol.* **28**, 225-241 (1975).
21. R.E. KRISCH, F. KRASIN, and C.J. SAURI, DNA breakage, repair and lethality after ^{125}I decay in rec+ and recA strains of E. coli. *Int. J. Radiat. Biol.* **29**, 37-50 (1975).

22. P.C. CHAN, E. LISCO, H. LISCO, and S.J. ADELSTEIN, The radiotoxicity of iodine-125 in mammalian cells, II. A comparative study on cell survival and cytogenic responses to ^{125}IUdR, ^{131}IUdR and ^{3}HTdR. *Radiat. Res.* **67**, 332-343 (1976).
23. R.L. WARTERS, K.G. HOFER, C.R. HARRIS, and J.M. SMITH, Radionuclide toxicity in cultured mammalian cells: Cytoplasmic radiation effects in murine L1210 leukemia. *Curr. Top. Radiat. Res. Q.* **12**, 389-407 (1977).
24. W.D. BLOOMER, W.H. McLAUGHLIN, R.R. WEICHSELBAUM, R.N. HANSON, S.J. ADELSTEIN, and D.E. SEITZ, The role of subcellular localization in assessing the cytotoxicity of iodine-125 labeled iododeoxyuridine, iodotamoxifen and iodoantipyrine. *J. Radioanal. Chem.* **65**, 209-221 (1981).
25. N. MIYAZAKI and Y. FUJIWARA, Mutagenic and lethal effects of [5-^{125}I]iodo-2'-deoxyuridine incorporated into DNA of mammalian cells, and their RBEs. *Radiat. Res.* **88**, 456- 465 (1981).
26. A.I. KASSIS, S.J. ADELSTEIN, C. HAYDOCK, K.S.R. SASTRY, K.D. McELVANY, and M.J. WELCH, Lethality of Auger electrons from the decay of bromine-77 in the DNA of mammalian cells. *Radiat. Res.* **90**, 362-373 (1982).
27. P.K. LeMOTTE, S.J. ADELSTEIN, and J.B. LITTLE, Malignant transformation induced by incorporated radionuclides in BALB/3T3 mouse embryo fibroblasts. *Proc. Natl. Acad. Sci. USA* **79**, 7763-7767 (1982).
28. P.K. LeMOTTE and J.B. LITTLE, A comparison of the lethal effects of intracellular radionuclides in human and rodent cells. *Radiat. Res.* **95**, 359-369 (1983).
29. H.L. LIBER, P.K. LeMOTTE, and J.B. LITTLE, Toxicity and mutagenicity of X-rays and [^{125}I]dUrd or [^{3}H]TdR incorporated in the DNA of human lymphoblast cells. *Mutat. Res.* **111**, 387-404 (1983).
30. A.I. KASSIS, K.S.R. SASTRY, and S.J. ADELSTEIN, Intracellular localization of Auger electron emitters: Biophysical dosimetry. *Radiat. Prot. Dosim.* **13**, 233-236 (1985).
31. A.I. KASSIS, F. FAYAD, B.M. KINSEY, K.S.R. SASTRY, R.A. TAUBE, and S.J. ADELSTEIN, Radiotoxicity of ^{125}I in mammalian cells. *Radiat. Res.* **111**, 305-318 (1987).
32. A.I. KASSIS, K.S.R. SASTRY, and S.J. ADELSTEIN, Kinetics of uptake, retention and radiotoxicity of ^{125}IUdR in mammalian cells: Implications of localized energy deposition by Auger processes. *Radiat. Res.* **109**, 78-89 (1987).
33. A.I. KASSIS, R.W. HOWELL, K.S.R. SASTRY, and S.J. ADELSTEIN, Positional effects of Auger emitters in mammalian cells. In *DNA Damage by Auger Emitters* (K.F. Baverstock and D.E. Charlton, Eds.) pp. 1-13. Taylor & Francis, Ltd., London, 1988.
34. A.I. KASSIS, F. FAYAD, B.M. KINSEY, K.S.R. SASTRY, and S.J. ADELSTEIN, Radiotoxicity of an ^{125}I-labeled DNA intercalator in mammalian cells. *Radiat. Res.* **118**, 283- 294 (1989).
35. G.M. MAKRIGIORGOS, A.I. KASSIS, J. BARANOWSKA-KORTYLEWICZ, K.D. McELVANY, M.J. WELCH, K.S.R. SASTRY, and S.J. ADELSTEIN, Radiotoxicity of 5-[^{123}I]iodo-2'-deoxyuridine in V79 cells: A comparison with 5-[^{125}I]iodo-2'-deoxyuridine. *Radiat. Res.* **118**, 532-544 (1989).
36. E. POMPLUN, J. BOOZ, and D.E. CHARLTON, A Monte Carlo simulation of Auger cascades. *Radiat. Res.* **111**, 533-552 (1987).

37. E. POMPLUN, A new DNA target model for track structure calculations and its first application to I-125 Auger electrons. *Int. J. Radiat. Biol.* **59**, 625-642 (1991).
38. P.K. LeMOTTE and J.B. LITTLE, DNA damage induced in human diploid cells by decay of incorporated radionuclides. *Cancer Res.* **44**, 1337-1342 (1984).
39. T. TERASIMA and L.J. TOLMACH, Changes in X-ray sensitivity of HeLa cells during the division cycle. *Nature* **190**, 1210-1211 (1961).
40. M.J. BORRELLI, M.A. MACKEY, and W.C. DEWEY, A method for freezing synchronous mitotic and G_1 cells. *Exptl. Cell Res.* **170**, 363-368 (1987).
41. H. NAGASAWA, J.B. ROBERTSON, C.S. ARUNDEL, and J.B. LITTLE, The effect of X irradiation on the progression of mouse 10T1/2 cells released from density-inhibited cultures. *Radiat. Res.* **97**, 537-545 (1984).
42. J. SAMBROOK, E.F. FRITSCH, and T. MANIATIS, *Molecular Cloning: A Laboratory Manual*, second edition. Cold Spring Harbor Laboratory Press, Cold Spring Harbor, NY, 1989.
43. A.P. FEINBERG and B. VOGELSTEIN, A technique for radiolabeling DNA restriction endonuclease fragments to high specific activity. *Anal. Biochem.* **132**, 6-13 (1983).
44. T.L. MORGAN, E.W. FLECK, K.A. POSTON, B.A. DONOVAN, E.N. NEWMAN, J.F. ROSSITER, and J.H. MILLER, Molecular characterization of X-ray-induced mutations at the hprt locus in plateau-phase Chinese hamster ovary cells. *Mutat. Res.* **232**, 171-182 (1991).
45. M.F. LYON, X-chromosome inactivation and developmental patterns in mammals. *Biol. Rev.* **47**, 1-35 (1973).
46. W.C. DEWEY and R.M. HUMPHREY, Relative radiosensitivity of different phases in the life cycle of Lp59 mouse fibroblasts and ascites tumor cells. *Radiat. Res.* **16**, 503-530 (1962).
47. W.K. SINCLAIR, Cyclic X-ray responses in mammalian cells *in vitro*. *Radiat. Res.* **33**, 620-643 (1968).
48. H. NAGASAWA, A.B. COX, and J.T. LETT, The radiation response of synchronous L5178Y S/S cells and their significance for radiological theory. *Proc. R. Soc. Lond.* **B211**, 25-49 (1980).
49. J. THACKER and R. COX, Mutation induction and inactivation in mammalian cells exposed to ionizing radiation. *Nature* **258**, 429-431 (1975).
50. R.J. MUNSON and D.T. GOODHEAD, The relation between induced mutation frequency and cell survival a theoretical approach and an examination of experimental data for eukaryotes. *Mutat. Res.* **42**, 145-159 (1977).
51. D.T. GOODHEAD, R.J. MUNSON, J. THACKER, and R. COX, Mutation and inactivation of cultured mammalian cells exposed to beams of accelerated heavy ions IV. Biophysical interpretation. *Int. J. Radiat. Biol.* **37**, 135-167 (1980).
52. A. TOBIA, C.L. SCHILDKRAUT, and J.J. MAIO, Deoxyribonucleic acid replication in synchronized cultured mammalian cells. J. Mol. Biol. **54**, 499-515 (1970).
53. H.L. LIBER, D.W. YANDELL, and J.B. LITTLE, A comparison of mutation induction at the tk and hprt loci in human lymphoblastoid cells; quantitative differences are due to an additional class of mutations at the autosomal tk locus. *Mutat. Res.* **216**, 9-17 (1989).
54. J. THACKER, The nature of mutants induced by ionizing radiation in cultured hamster cells. *Mutat. Res.* **160**, 267-275 (1986).

210 Biophysical Aspects of Auger Processes, AAPM Symposium Series No. 8 (1992) 210-226
Eds. RW Howell, VR Narra, KSR Sastry, DV Rao

NUCLEAR LESIONS PRODUCED BY ^{125}I DECAY

LINDA S. YASUI

Department of Biological Sciences
Northern Illinois University
DeKalb, IL 60115, USA

ABSTRACT

^{125}I decay induced DNA damage was investigated in Chinese hamster ovary (CHO) cells which had incorporated ^{125}I-iododeoxyuridine (^{125}IUdR) into their DNA. ^{125}I decays were accumulated in frozen cells. DNA strand breaks produced by low numbers (0-1200 decays per cell) of ^{125}I decays were assayed using the alkaline unwinding technique and the alkaline filter elution technique. Approximately 300 ^{125}I decays reduced the relative damage to 50%. DNA protein cross links were not detected after accumulation of ^{125}I decay. The production of DNA double strand breaks by ^{125}I decay was assayed by the neutral filter elution technique at pH 9.6 and 7.2 after accumulating 100-5000 decays per cell. No alkali labile lesions were detected. Approximately 3000 ^{125}I decays were required to reduce the mean value of the fractions to 50%. In all the assays, DNA damage induction data was fit to a straight line by regression analysis except at very low numbers of accumulated ^{125}I decays where an initial drop in the fraction of DNA retained on the filter was observed. This drop suggests multiple chromatin fragmentation is produced by ^{125}I decay.

INTRODUCTION

^{125}I decay has been used as a tool to calibrate the neutral filter elution assay (1-3) and pulsed field gel electrophoresis (4,5). ^{125}I decay is also extremely effective in cell killing (for example, see Refs. 6-14). This is likely due to the extremely dense energy deposition of Auger electrons emitted from ^{125}I decay in a volume of 30 nm diameter (14), and because of the residual positive charge on the ^{125}Te daughter nuclide (which could produce extensive local ionizations and excitations as the charge is shared with neighboring atoms) (15) resulting in a DNA double strand break (DSB).

Recently it has been shown that cell survival changes depending on when in the cell cycle ^{125}I is incorporated into the DNA (1,13). This indicates that some lesions produced by ^{125}I decay are more lethal to the cell than other lesions produced by ^{125}I decay, *i.e.*, and not all ^{125}I decay produced DNA DSBs have the same biological effect. These data suggest that further understanding of the lesions produced by ^{125}I decay is required.

One factor that may modify the impact of energy deposition from ^{125}I decay is chromatin conformation. A computer graphics model of the energy deposition for ^{125}I decay (17) illustrates that the ^{125}I M-XY Auger electrons have a range of energy deposition that corresponds to the diameter of a solenoid fiber in chromatin structure (17). Local ionizations and excitations from ^{125}I decay could be shared with the numerous DNA strands in the solenoid fiber. Computer decay simulations (16) predict that a portion of the energy deposition from ^{125}I decay is sensitive to DNA conformation (approximately 0.17 out of the 0.82 to 1.07 DNA DSBs produced per decay of ^{125}I).

Another factor affecting DNA damage induction and cell killing could be nuclear organization. The calibration studies are based on ^{125}I damage induction studies in prokaryotes. The energy deposition event from ^{125}I decay produces 1 DNA DSB with very high probability when ^{125}I is incorporated into prokaryotic DNA (18-20). Extrapolation of the DNA DSB induction data as a result of ^{125}I decay in prokaryotes to eukaryotic cells is problematic because a phage or plasmid DNA system (a two dimensional DNA structure) is a completely different radiation target compared to the highly compacted, three dimensional mammalian cell genome. Also, a mammalian cell nucleus (a three dimensional sphere having an approximately 5 μm diameter) provides a much larger and more chemically complex "target" that could act as an "energy

sink" for the transition events from ^{125}I decay compared to a plasmid or phage DNA. Therefore, to more fully understand the role of ^{125}I decay produced lesions in mammalian cells, we initiated a study to identify the nature of lesions produced by ^{125}I decay.

MATERIALS AND METHODS

Cell Culture

Chinese hamster ovary (CHO) cells (originally obtained from Dr. R.A. Tobey) were maintained in monolayer culture using Ham's F10 medium supplemented with 5% fetal bovine serum and 5% bovine serum in a 37°C incubator continuously gassed with 5% CO_2.

DNA Damage Induced by ^{125}I Decay

CHO cells were trypsinized off of their plates and then 10^6 cells were seeded onto a tissue culture flask containing 5 ml of medium. ^{125}I-iododeoxyuridine ($^{125}IUdR$) was added to the cells to a final concentration of 0.37 to 3.7 X 10^4 Bq/ml (0.1 to 1.0 μCi/ml) (specific activity = 8.14 X 10^{10} Bq/mmol or 2.2 X 10^6 mCi/mM; ICN). After the cells had incorporated $^{125}IUdR$ during 16 h, the cells were collected by trypsinization. Before freezing the labeled cells, an aliquot of cells was removed for microscopic examination to determine cell number and the general cellular appearance. The cell radionuclide content and labeling index (L.I.) were also determined. The L.I. was greater than or equal to 97%.

The radionuclide content per cell was determined by precipitating a known number of labeled cells with approximately 10^6 unlabeled carrier cells with 10% ice-cold trichloroacetic acid (TCA) and the number of ^{125}I decays per cell per unit time was determined in a calibrated well-type crystal scintillation counter as previously described (13).

The labeled cells were suspended in cryoprotectant medium (F10 medium supplemented with 10% fetal bovine serum and 15% dimethylsulfoxide) to freeze the cells to -70°C. After the appropriate number of ^{125}I decays were accumulated, the cells were quickly thawed by immersion of the vial in a 37°C water bath. The cell samples were immediately assayed for DNA damage. The freezing and thawing procedure itself did not

introduce DNA strand breaks (also see Refs. 3,21) or change the plating efficiency from that for cells, or cell generation time, or cell cycle progression, from cells that had never been frozen.

X irradiation

CHO cells (10^6 cells/ml) were irradiated with increasing doses of X rays in medium in a 15 ml plastic centrifuge tube at 4°C. Irradiation of the cells was performed with a Phillips X ray machine operated at 250 kVp, 15 mA and the beam filtered with 3 mm Al (HVL 0.2 mm Cu). The dose rate employed was 2.5 Gy per minute as measured by a Victoreen ionization chamber.

DNA Damage Detection

The alkaline filter elution technique (22) was used to measure DNA damage induction by assaying the rate of elution of single-stranded DNA through a filter at an alkaline pH (pH 12.2). Cells (5×10^5) prelabeled with ^{14}C-TdR or ^{125}IUdR were loaded onto a polycarbonate filter (1 μm pore size) and assayed as previously described (23). Each elution profile from the ^{125}I decay irradiated cells was curvilinear and had a different Y-intercept, so did not lend itself to analysis by a strand scission factor. Instead, a mean value was calculated for the fractions collected from one column (24).

The neutral filter elution technique (25) was used to detect DNA DSBs in cells labeled with ^{125}IUdR as previously described (26). No difference in the elution profiles were observed when cells were lysed at pH 10 versus pH 9.6 versus pH 7.2. The mean value of the fractions was calculated for the neutral elution profiles (24).

The alkaline unwinding technique followed by hydroxyapatite chromatography (27) was also used to detect DNA damage produced by ^{125}I decay. Labeled cells (2×10^5) were lysed under alkaline conditions (1 M NaCl, 0.03 M NaOH) at 4°C for 1 hour in the dark. After cell lysis, the samples were neutralized and immediately sonicated (10 s) before application to hydroxyapatite chromatography at 65°C. The columns were washed with 0.012 M phosphate buffer. The single stranded (SS) fraction was eluted from the columns with 0.12 M phosphate buffer and then the double stranded (DS) fraction was eluted with 0.4 M phosphate buffer. Each eluant was collected directly into scintillation vials. Optifluor scintillation fluid was added to each

vial and the samples were counted. The percentage of double stranded DNA was calculated as described by Olive *et al.* (28).

RESULTS

DNA Damage Assayed by the Alkaline Filter Elution Technique

The induction of DNA-protein cross links was investigated after accumulation of ^{125}I decays. As shown by the data in Fig. 1, DNA protein cross links can be detected with the alkaline filter elution technique after X-irradiation. Cells irradiated with increasing doses of X rays were treated with 0.5 mg/ml proteinase K during the 45-60 min cell lysis, or no proteinase K was applied to a replicate column. The DNA from cell samples not treated with proteinase K eluted at a slower rate compared to the DNA from cell samples that were treated with proteinase K indicating DNA protein cross links were present.

Representative elution profiles from cells damaged by ^{125}I decay and then treated, or not treated, with proteinase K can be seen in Fig. 2. No consistent difference between proteinase K treated samples and samples not treated with proteinase K was detected (Fig. 2). However, to confirm this observation a dose response curve was generated (Fig. 3). The mean values of the fractions from all the experiments that were performed can be seen in Fig. 3. Regression analysis was performed to determine the slope of the best-fit line for the data. The calculated values for the slopes were not statistically different. The slopes equaled -0.0002 for both the proteinase K treated samples and the samples not treated with proteinase K. Therefore, no ^{125}I decay induced DNA protein cross links were detected by this assay.

The data in Fig. 3 also represents the overall damage induction measured by the alkaline filter elution technique. Approximately 300 ^{125}I decays were required to reduce the mean value of the fractions to 50%. The alkaline filter elution data (Fig. 3 panel A and B) were analyzed by regression analysis ($r = -0.62$). The Y-intercept = 68.70%.

DNA Damage Assayed by the Alkaline Unwinding Assay

The alkaline unwinding assay was also performed to estimate DNA damage induced by 0-1000 ^{125}I decay in CHO cells (Fig. 4). For this assay, the DS

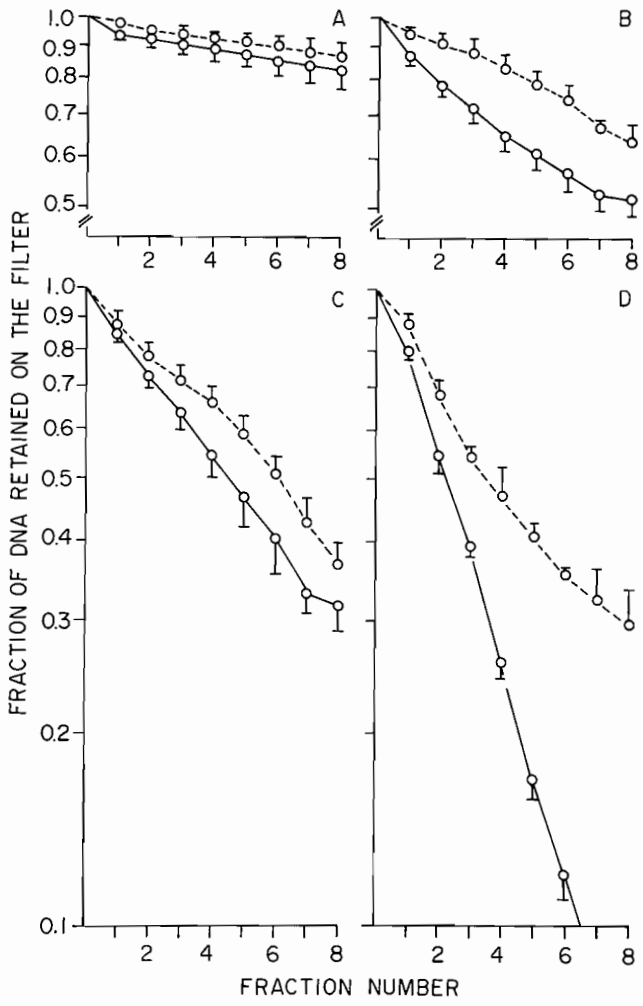

FIG. 1. DNA protein cross-links induced by X rays as determined by the alkaline filter elution technique. The lysed DNA was treated with proteinase K (solid line) or not treated with proteinase K (dashed line) after irradiation with 0 Gy (panel A), 2.5 Gy (panel B), 5.0 Gy (panel C) or 10 Gy (panel D) of X rays. The mean value for each fraction obtained from 3-5 separate experiments ± 1 standard error of the mean are plotted.

fraction is calculated as a proportion of the sum of the SS fraction plus the DS fraction. Three hundred ^{125}I decays were required to reduce the DS fraction

to 50%. The data were fit to a straight line (r = -0.92). The Y intercept = 66.49%. No constraints to unwinding (28) were apparent from the data in Fig. 4.

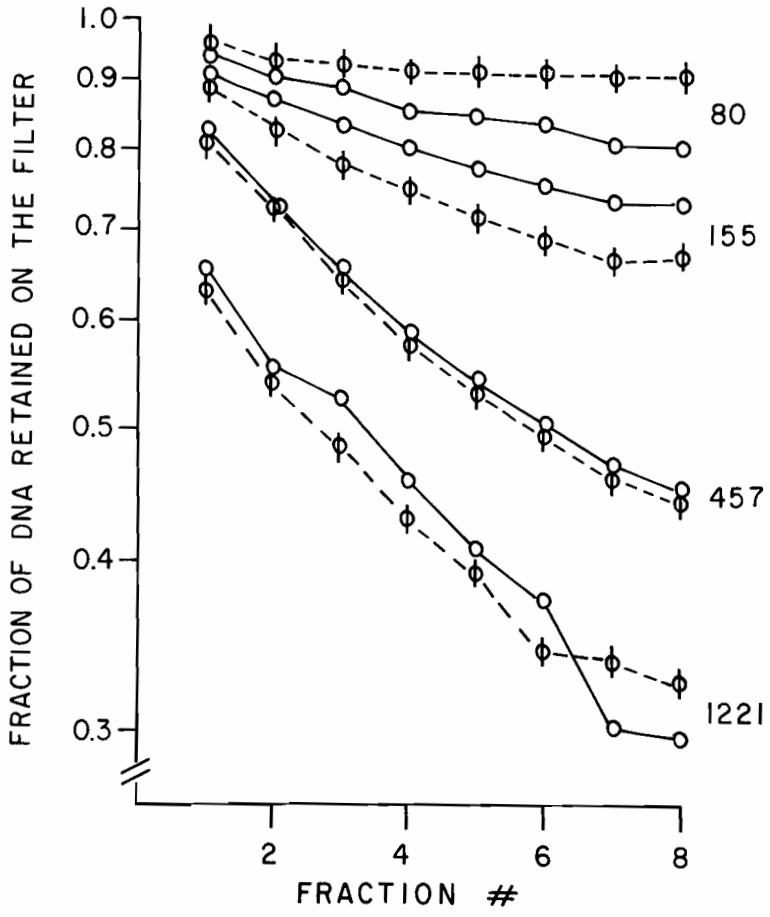

FIG. 2. DNA protein cross link induction by ^{125}I decay. DNA damage induced by ^{125}I decay was measured by the alkaline filter elution technique in samples that were treated with proteinase K (open circles) or not treated with proteinase K (dashed lines and hatched circles) in the lysis step of the elution technique. The number of ^{125}I decays accumulated are indicated to the right of the elution profiles.

DNA Damage Assayed by the Neutral Filter Elution Technique

DNA DSBs can be assayed using the neutral filter elution technique (25). Representative elution profiles for cells that had accumulated ^{125}I decays can be

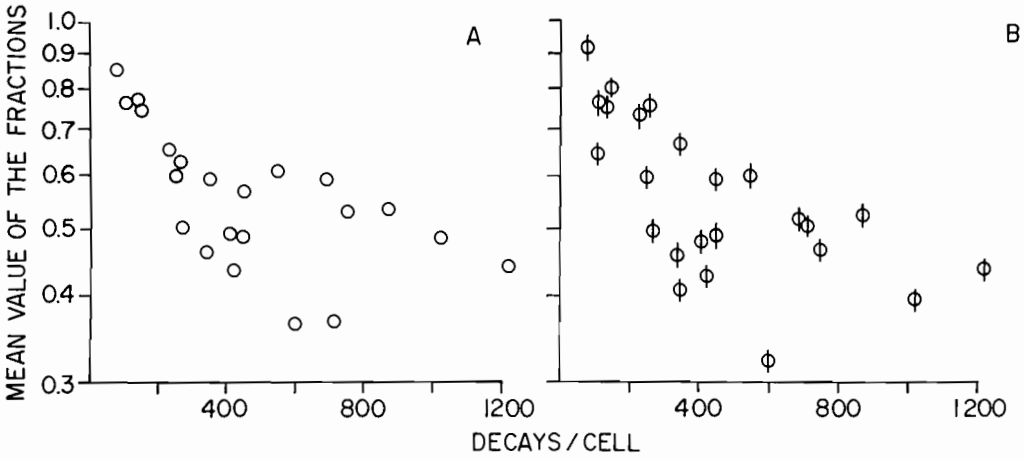

FIG. 3. Dose response curves obtained using data in Fig. 2. The mean values of the fractions for each elution profile is plotted versus the number of accumulated ^{125}I decays per cell treated with proteinase K (panel A) or not treated with proteinase K (Panel B). The slopes of the lines calculated by linear regression for the data shown in panel A and B were the same.

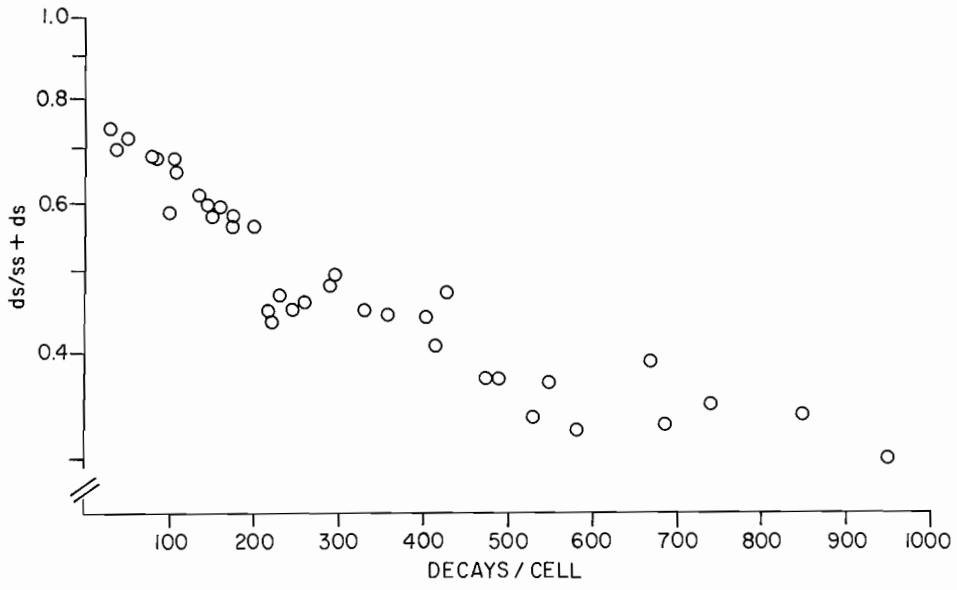

FIG. 4. DNA damage induction by ^{125}I decay as measured by the alkaline unwinding assay followed by hydroxyapatite chromatography. The double stranded (DS) fraction divided by the single stranded (SS) fraction were plotted versus the total number of accumulated ^{125}I decays per cell.

seen in Fig. 5. Figure 6 shows a dose response curve for cells that were damaged by 0 to 5,000 accumulated ^{125}I decays. As seen in Figs. 5 and 6, no difference in damage induction is observed for samples assayed at pH 7.2 versus 9.6 as also reported previously by Flick *et al.* (26). Approximately 3000 ^{125}I decays were required to reduce the mean values to 50%. The data were fit to a straight line (r = -0.94). The Y-intercept = 83.44%.

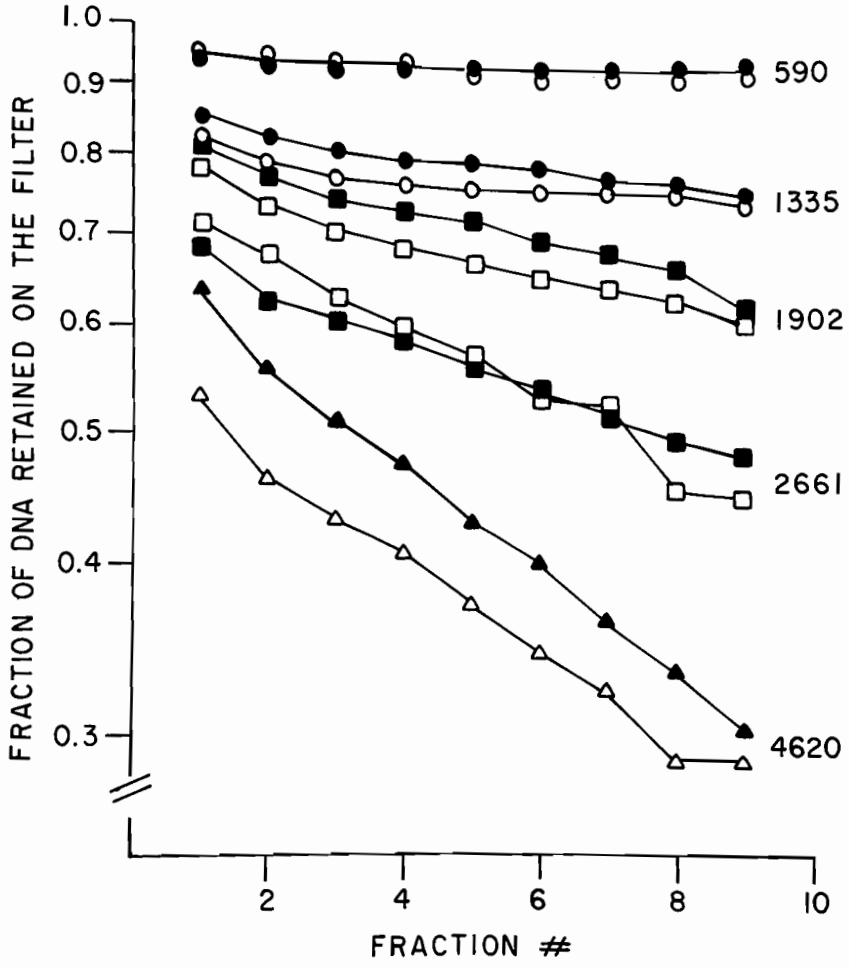

FIG. 5. Representative elution profiles of DNA damaged by ^{125}I decay and assayed by the neutral filter elution technique at pH 7.2 (open symbols) versus pH 9.6 (closed symbols). The number of accumulated ^{125}I decays is indicated to the right of each elution profile.

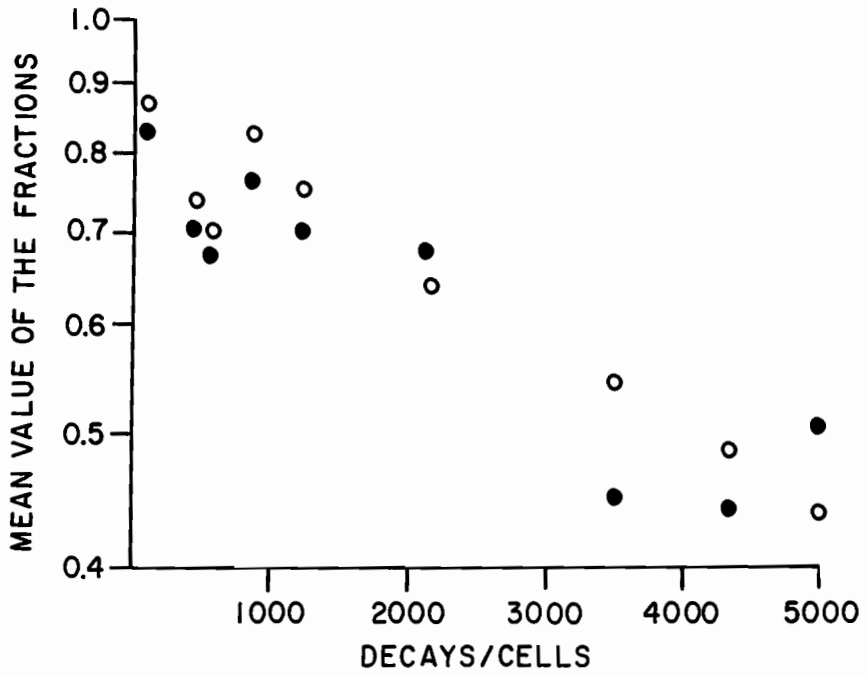

FIG. 6. A dose response curve for the neutral filter elution data. The mean value of the fractions for each elution profile was plotted versus the total number of accumulated ^{125}I decays per cell assayed at pH 7.2 (open symbols) or pH 9.6 (closed symbols). Approximately 3000 ^{125}I decays were required to reduce the mean value of the fractions to 50%. The slopes of the lines were calculated by linear regression analysis of the pH 7.2 data and the pH 9.6 data were the same.

The relative efficiency of the neutral filter elution assay compared to the alkaline filter elution assay can be calculated from the 50% values. The neutral filter elution assay was 10 times less sensitive in detecting ^{125}I decay induced DNA damage compared to the alkaline filter elution assay. As previously stated, 300 ^{125}I decays were required to reduce the fraction of retained DNA to 50% in the alkaline filter elution technique, and 300 ^{125}I decays required to reduce the double stranded fraction to 50% using the alkaline unwinding technique, whereas 3000 ^{125}I decays were required to reduce the fraction of retained DNA to 50% in the neutral filter elution technique.

DISCUSSION

The yield of DNA lesions produced by ^{125}I decay in mammalian cells has been calculated by measuring the molecular weight of DNA in alkaline (29) and both alkaline and neutral sucrose gradients (30). ^{125}I decay produces about 4-5 SSBs per decay (29,30) and about 1.4 to 2.7 DSBs per decay (30). Ward (31) discusses the following 4 temporally distinct stages for the production of chemically stable damage:

1. Physical deposition of energy (10^{-18} s).
2. Production of primary radicals on the target molecule and in molecules surrounding the target-direct and indirect effect (10^{-12} s).
3. Reaction of radicals on surrounding molecules with target molecule (10^{-8} s).
4. Reactions of unstable target radicals leading to chemically stable damage.

Step 1 is the first event involved in DNA damage induction by ^{125}I decay. The time required for the vacancy cascade associated with ^{125}I decay is less than 10^{-15} seconds (32). Steps 2-4 are likely swamped out by the range of energy deposition from ^{125}I decay (approximately 30 nm) (14) relative to the range of migration of OH· radicals (only about 6.8 nm) (33). In fact, indirect DNA damage produced by ^{125}I decay may be biologically inconsequential. LeMotte and Little (21) measure approximately a 5 fold increase in DNA DSBs produced by ^{125}I decay after decays were accumulated at 0°C in medium compared to when accumulation occurred at -90°C in medium containing 10% glycerol (radical scavenger). However, no change in cell survival is detected when decays are accumulated with or without the scavenger present (21). The chemically stable DNA lesion mentioned in step #4 above, should be fundamentally different for those lesions produced by ^{125}I decay compared to X or γ rays. This conclusion is an extrapolation of our simple microdosimetric calculations (17). The above conclusion is in contrast to conclusions by Iliakis *et al.* (1). They compared repair kinetics after ^{125}I decay and X irradiation and find that the rates are the same. Based on these results, the authors suggest that the DNA lesions produced by these two radiations are identical. However, the authors (1) do not state whether equitoxic levels of radiations were used or whether DNA damage induction levels were the same for the two radiations used. Indeed, the authors do not state the number of decays of ^{125}I that were used for their experiments. Much more work needs to be performed before such conclusions can be made.

DNA damage induction by ^{125}I decay was investigated by the alkaline (Figs. 2 and 3) and neutral filter elution (Figs. 5 and 6) assays and the alkaline unwinding assay (Fig. 4). In this investigation, no DNA protein cross links (Figs. 2 and 3) are detected. Also, no pH 9.6 labile lesions (Figs. 5 and 6) (see also Ref. 26) are detected suggesting that these assays are measuring frank DNA DSBs produced by ^{125}I decay. It is found that 300 ^{125}I decays per cell are required to reach the 50% damage level for both the alkaline unwinding (Fig. 4) and the alkaline filter elution assays (Fig. 3). Approximately 10 times greater number of accumulated ^{125}I decays are required to reach the 50% damage level for the neutral filter elution technique (Fig. 6).

The three different methods of measuring DNA damage (alkaline and neutral filter elution and alkaline unwinding) all indicate that damage induction relative to the number of accumulated ^{125}I decays can be fit to a straight line (no shoulder) except at very low numbers of ^{125}I decays where there is an initial increase in damage induction rate, *i.e.*, Y-intercept is significantly less than 100% (also see Ref. 21). Linear ^{125}I decay induced DNA damage curves are also found by Peak *et al.* (2), Radford and Hodgson (3), and LeMotte and Little (21).

All of the alkaline and neutral elution profiles show a marked drop in the fraction of retained DNA in the first fraction collected (Figs. 2 and 5). This large drop is attributed to ^{125}I decay induced clusters of lesions or multiply fragmented DNA released from genomic DNA under the elution conditions. The formation of multiple chromatin breaks or clusters of lesions in DNA has previously been suggested in connection with the strand breaking effectiveness of high-LET radiations (34). Martin and Haseltine (35) detected multiple chromatin breaks produced by ^{125}I decay in a small region of DNA in a synthetic linear piece of DNA when using DNA sequencing methodology. Turner *et al.* (36) also measured fragmentation of chromatin by ^{125}I decay into much smaller pieces of DNA than by ^{3}H decay using neutral sucrose gradient methods. It is predicted that conventional assays that measure DNA damage provide an underestimate of the numbers of strand breaks produced by ^{125}I decay. This prediction is supported by: 1) data presented here using the filter elution techniques and alkaline unwinding where an initial drop is observed in the damage induction curves (Figs. 3, 4 and 6), and 2) physical calculations (38). Calculations indicate that ^{125}I decay deposits a mean energy of 1.6 keV in a spherical volume of 10 nm (38) and this could lead to energy deposition that either has no impact on DNA (energy misses target and is "wasted") or causes

the induction of more than 1 DNA DSB (energy "hits" target) (30,37). In comparison, 600 eV from external γ irradiation can produce a DNA DSB (30,37).

In conclusion, these data indicate no DNA protein cross links or pH 9.6 labile lesions are produced by ^{125}I decay. Frank breaks are assayed by the neutral filter elution assay. Clusters of lesions or multiple chromatin breaks are detected after ^{125}I decay. Such multiple fragmentation of DNA may be modified by local chromatin compaction and in some cases may represent a devastating lesion with little or no chance for "repair". Based on these data and previous work with ^{125}I decay, we conclude that the consequences of ^{125}I decay in DNA and chromatin are not yet fully understood and, therefore, care should be exercised in the use of ^{125}I decay as a tool in calibrating assays to measure DNA damage in mammalian cells.

ACKNOWLEDGMENTS

This work was supported by USPHS grant CA 45011.

REFERENCES

1. G. ILIAKIS, G.E. PANTELIAS, R. OKAYASU, and R. SEANER, ^{125}IUrd-induced chromosome fragments, assayed by premature chromosome condensation, and DNA double-strand breaks have similar repair kinetics in G_1-phase CHO cells. *Int. J. Radiat. Biol.* **52**, 705-722 (1987).
2. J.G. PEAK, E.R. BLAZEK, C.K. HILL, and M.J. PEAK, Measurement of double strand breaks in Chinese hamster cells DNA by neutral filter elution: Calibration by ^{125}I decay. *Radiat. Res.* **115**, 624-629 (1989).
3. I.R. RADFORD and G.S. HODGSON, ^{125}I-induced DNA double strand breaks: Use in calibration of the neutral filter elution technique and comparison with X-ray induced breaks. *Int. J. Radiat. Biol.* **48**, 555-566 (1985).
4. D.D. AGER and W.C. DEWEY, Calibration of pulsed-field gel electrophoresis for measurement of DNA double-strand breaks. *Int. J. Radiat. Biol.* **58**, 249-260 (1990).
5. G.E. ILIAKIS, O. CICILIONI, and L. METZGER, Measurement of DNA double-strand breaks in CHO cells at various stages of the cell cycle using pulsed field gel electrophoresis: Calibration by means of ^{125}I decay. *Int. J. Radiat. Biol.* **59**, 343-357 (1991).
6. H.J. BURKI, R. ROOTS, L.E. FEINENDEGEN, and V.P BOND, Inactivation of mammalian cells after disintegrations of ^{3}H or ^{125}I in cell DNA at -196°C. *Int. J. Radiat. Biol.* **24**, 363-376 (1973).

7. P.C. CHAN, E. LISCO, and S.J. ADELSTEIN, The radiotoxicity of iodine-125 in mammalian cells. II. A comparative study on cell survival and cytogenetic responses to ^{125}IUdR, ^{131}IUdR and ^{3}HTdR. *Radiat. Res.* **67**, 332-343 (1976).
8. K.G. HOFER and W.L. HUGHES, Radiotoxicity of intranuclear tritium, ^{125}Iodine and ^{131}Iodine. *Radiat. Res.* **47**, 94-109 (1971).
9. A.I. KASSIS, S.J. ADELSTEIN, and K.S.R. SASTRY, Kinetics of uptake, retention and radiotoxicity of ^{125}IUdR in mammalian cells: Implications of localized energy deposition by Auger processes. *Radiat. Res.* **109**, 78-89 (1987).
10. A.I. KASSIS, F. FAYAD, B.M. KINSEY, K.S.R. SASTRY, R.A. TAUBE, and S.J. ADELSTEIN, Radiotoxicity of ^{125}I in mammalian cells. *Radiat. Res.* **111**, 305-318 (1987).
11. H.L. LIBER, P.K. LeMOTTE, and J.B. LITTLE, Toxicity and mutagenicity of X-rays and [^{125}I]dUrd or [^{3}H]TdR incorporated into the DNA of human lymphoblast cells. *Mutat. Res.* **111**, 387-404 (1983).
12. R.L. WARTERS, K.G. HOFER, C.R. HARRIS, and J.M. SMITH, Radionuclide toxicity in cultured mammalian cells: Elucidation of the primary site of radiation damage. *Cur. Top. Radiat. Res. Q.* **12**, 389-407 (1977).
13. L.S. YASUI, K.G. HOFER, and R.L. WARTERS, Inhomogeneity of the nucleus to ^{125}IUdR cytotoxicity. *Radiat. Res.* **102**, 106-118 (1985).
14. K.G. HOFER, G. KEOUGH, and J.M. SMITH, Biological toxicity of Auger emitters: Molecular fragmentation versus electron irradiation. *Cur. Topics Radiat. Res. Q.* **12**, 335-354 (1977).
15. D.E. CHARLTON, E. POMPLUN, and J. BOOZ, Some consequences of the Auger effect: Fluorescence yield, charge potential and energy imparted. *Radiat. Res.* **111**, 553-564 (1987).
16. D.E. CHARLTON, Calculation of single and double strand DNA breakage from incorporated ^{125}I. In *DNA Damage by Auger Emitters* (K.F. Baverstock and D.E. Charlton, Eds) pp. 89-100. Taylor and Francis, London, 1988.
17. L.S. YASUI, A.S. PASCHOA, R.L. WARTERS, and K.G. HOFER, Cytotoxicity of ^{125}I decay produced lesions in chromatin. In *DNA Damage by Auger Emitters* (K.F. Baverstock and D.E. Charlton, Eds.), Taylor and Francis, London, pp. 181-189 1988.
18. R.E. KRISCH, Lethal effects of iodine-125 decay by electron capture in Escherichia coli and bacteriophage T4. *Int. J. Radiat. Biol.* **21**, 167-189 (1972).
19. R.E. KRISCH and R.D. LEY, Introduction of lethality and DNA breakage by the decay of iodine-125 in bacteriophage T4. *Int. J. Radiat. Biol.* **25**, 21-30 (1974).
20. R.E. KRISCH and C.J. SAURI, Further studies on DNA damage and lethality from the decay of iodine-125 in bacteriophages. *Int. J. Radiat. Biol.* **27**, 535-560 (1975).
21. P.K. LeMOTTE and J.B. LITTLE, DNA damage induced in human diploid cells by decay of incorporated radionuclides. *Cancer Res.* **44**, 1337-1342 (1984).
22. K.W. KOHN, R.A.G. EWIG, L.C. ERICKSON, and L.A. ZWELLING, In *DNA Repair: A Laboratory Manual of Research Procedures* (E.C. Friedberg and P.C. Hanawalt, Eds.) vol 1, part. B. Marcel Dekker, Inc. N.Y., 1981
23. L.S. YASUI, R. HIGASHIKUBO, and R.L. WARTERS, The effect of chromatin decondensation on DNA damage and repair. *Radiat. Res.* **112**, 318-330 (1987).

24. T.M. COQUERELLE, K.R. WEIBEZAHN, and C. LUHKE-HUHLE, Rejoining of double strand breaks in normal and Ataxia telangiectasia fibroblasts after exposure to ^{60}Co gamma rays, ^{241}Am-alpha particles or bleomycin. *Int. J. Radiat. Biol.* **51**, 209-218 (1987).
25. M.O. BRADLEY and K.W. KOHN, X-ray induced DNA strand break production and repair in mammalian cells as measured by neutral filter elution. *Nuc. Acids Res.* **7**, 793-804 (1979).
26. M.B. FLICK, R.L. WARTERS, L.S. YASUI, and R.E. KRISCH, Measurement of radiation induced DNA damage using gel electrophoresis or neutral filter elution shows an increased frequency of DNA strand breaks after exposure to pH 9.6. *Radiat. Res.* **119**, 452-465 (1989).
27. G. AHNSTROM and K. ERIXON, Radiation induced strand breakage in DNA from mammalian cells. Strand separation in alkaline solution. *Int. J. Radiat. Biol.* **23**, 285-289 (1973).
28. P.L. OLIVE, J. HILTON, and R.E. DURAND, DNA conformation of Chinese hamster V79 cells and sensitivity to ionizing radiation. *Radiat. Res.* **107**, 115-124 (1986).
29. R.B. PAINTER, B.R. YOUNG, and H.J. BURKI, Non-repairable strand breaks induced by ^{125}I incorporated into mammalian DNA. *Proc. Nat. Acad. Sci, U.S.A.* **71**, 4836-4838 (1974).
30. G. TISLJAR-LENTULIS, P. HENNEBERG, Th. MIELKE, and L.E. FEINENDEGEN, DNA strand breaks induced by ^{125}I in cultured human kidney cells and their repair. In (J. Booz and H.G. Ebert, Eds.) *Sixth Symposium on Microdosimetry*, Brussels, Harwood, pp. 111-120, 1978.
31. J.F. WARD, The yield of DNA double-strand breaks produced intracellularly by ionizing radiation: A review. *Int. J. Radiat. Biol.* **57**, 1141-1150 (1990).
32. S. WEXLER, Destruction of molecules by nuclear transformations. *Science*, **156**, 901-907 (1967).
33. R. ROOTS and S. OKADA. Estimation of life times and diffusion distances of radicals involved in X-ray-induced DNA strand breaks or killing of mammalian cells. *Radiat. Res.* **64**, 306-320 (1975).
34. M.A. RITTER, J.E. CLEAVER, and C.A. TOBIAS, High LET radiations induce a large proportion of non-rejoining DNA breaks. *Nature.* **266**, 653-655 (1977).
35. R.F. MARTIN and W.A. HASELTINE, Range of radiochemical damage to DNA with decay of iodine-125. *Science*, **213**, 896-898 (1981).
36. G.N. TURNER, P. NOBIS, and W.C. DEWEY, Fragmentation of chromatin with ^{125}I radioactive disintegrations. *Biophys. J.* **16**, 1003-1012 (1976).
37. G. TISLJAR-LENTULIS, F.H.A. SCHNEEWEISS, and L.E. FEINENDEGEN, $^{125}Iodine$ decay in DNA: A discussion of its effectiveness for the breaking of DNA strands. *Radiat. Environ. Biophys.* **26**, 189-195 (1987).
38. D.E. CHARLTON, J. BOOZ, J. FIDORRA, Th. SMIT, and L.E. FEINENDEGEN, Microdosimetry of radioactive nuclei incorporated into the DNA of mammalian cells. In *6th Symposium on Microdosimetry, Brussels*, Belgium, Harwood Academic Publishers Ltd. for the Commission of the European Communities. Vol. 1: 91-110 (1978).

DISCUSSION

Schneiderman, M. If you get a number of breaks clustered around the ^{125}I decay, then on pulsed field gel electrophoresis you should have a large number of small DNA pieces. Have you used PFGE?

Yasui, L. No, I have not used PFGE. We are currently thinking of pushing the alkaline unwinding technique with lower concentrations of phosphate buffer to pick up the fragments produced by ^{125}I decay at the clustered lesion site.

Martin, R. 1) Linda, the 30 nm range figure you quoted seems very high to me, but there are other people in the audience who can comment on that better than I. In short, I am trying to draw a comment from the microdosimetry people.

Humm, J. L. 2) If you look at the DNA doughnut model of Charlton, presented at the last Auger Symposium, you will find that the dose deposition in adjacent strands in supercoiled DNA is between one tenth and one hundredth of the dose to the strands within which the ^{125}I is located.

Yasui, L. S. 1) The 30 nm range was taken from our studies using older Auger spectra. I am aware of newer data that also lists N-shell Auger electrons from ^{125}I decay - these have much shorter ranges. However, the main point I wanted to make with our model was that the range of energy deposition in DNA is much larger for ^{125}I decay than for X ray energy deposition. 2) If ^{125}I decay deposits 1.6 keV in a 10 nm target size (Tisljar-Lentulis *et al., Radiat. Environ. Biophys.* **26**: 189-195, 1987), then adjacent fibers could receive 16 to 160 eV. Assuming 100 eV is sufficient energy to produce a single strand break, there could certainly be enough energy to cause a single strand break in adjacent DNA. In addition, the residual positive charge on the ^{125}Te daughter nuclide could produce extensive local ionizations and excitations as the charge is shared with neighboring atoms producing DNA single strand and double strand breaks in adjacent DNA molecules.

Goodhead, D. You suggested looking specifically for clustered damage extending over about 30 nm, based on the estimated average size of the dense-ionization region around the Auger decay. Because of the large statistical variations in individual decays in the tracks of the emitted electrons, would it not be more reasonable to expect a wide spectrum of different clustered damages?

Yasui, L. I think it is reasonable to expect a wide spectrum of different clustered damages produced by ^{125}I decay in the DNA. One possible explanation for the differential cell survival data from ^{125}I decay is that local

chromatin or nuclear conformation modifies the DNA damage induction pattern and these different lesions are handled differently in the cells.

Rao, D. V. Linda, are you suggesting that when ^{125}I decay occurs on the coiled or folded DNA, there is more than one double strand break, but they all show up as one double strand break in your measurement?

Yasui, L. Yes, the model we propose would have highly localized multiple fragmentation of DNA. By the assays used in our investigation this cluster of lesions would fall through the filters and not be bound by hydroxyapatite. Thus, the assay measures these clusters of lesions as frank DNA double strand breaks.

Nagasawa, H. N. What are the different cell killing mechanisms for α particle and ^{125}IUdR irradiation of CHO K-1 and XRS-5? I found that the D_0 doses were nearly 1 for Il-treated, G_1-phase, CHO K-1 and XRS-5 after α particle irradiation.

Yasui, L. There does appear to be a different mechanisms of killing by ^{125}I decay and α particle irradiation. The RBE calculated for the K-1 and XRS-5 cells relative to ^{137}Cs γ radiation at 10% survival is about 8 and 10.3, respectively. The RBE values after α particle irradiation (depending upon the lab where studies were performed) have a reversed or equivalent relationship. Perhaps the spectrum of lesions produced by these radiations are handled differently by cells.

Biophysical Aspects of Auger Processes, AAPM Symposium Series No. 8 (1992) 227-248
Eds. RW Howell, VR Narra, KSR Sastry, DV Rao

HIGH AND LOW-LET CYTOCIDAL EFFECTS OF DNA-ASSOCIATED IODINE-125

KURT G. HOFER[1], NANETTE VAN LOON[2]
MARTIN H. SCHNEIDERMAN[3], and DAVID E. CHARLTON[4]

[1]Institute of Molecular Biophysics, Florida State University, Tallahassee, FL 32306
[2]Laboratory of Radiobiology, University of California, San Francisco, CA 94143
[3]Department of Radiology, University of Nebraska Medical Center, Omaha, NE 68198
[4]Department of Physics, Concordia University, Montreal, Quebec, Canada H3G 1M8

ABSTRACT

Chinese hamster ovary (CHO) cells synchronized by mitotic selection were plated and resynchronized with aphidicolin at the G_1/S boundary of the cell cycle. Thirty minutes after release from the aphidicolin block the cells were pulse-labeled for 10 min with ^{125}I-iododeoxyuridine and cell samples were harvested for freezing and ^{125}I-decay accumulation at time intervals ranging from 15 min to 8 h after termination of labeling. Control studies were carried out on X irradiated cells and on cells labeled continuously throughout the S phase or pulse-labeled during different stages of the S phase. Cell survival was evaluated by the standard colony forming assay.

The survival data demonstrated a striking shift from a low-LET to a high-LET mode of action for ^{125}I-induced cell killing with increasing time intervals between DNA pulse-labeling and decay accumulation. Cells harvested and frozen within 1 h after pulse-labeling exhibited a low-LET dose-survival response with a pronounced shoulder and a large D_0 of up to 0.9 Gy. With longer post-labeling chase periods, the shoulder and the D_0 decreased progressively and cells harvested 5 h after pulse-labeling or later yielded the high-LET dose-survival response that is usually encountered with DNA-associated ^{125}I (D_0: 0.13 Gy).

Two alternative interpretations for these findings can be envisioned. (1) If it is assumed that DNA is the sole target for radiation death, the results indicate that DNA maturation increases radiation damage to DNA or reduces damage repair. (2) If radiation death involves damage to higher-order genome structures and/or associated nuclear matrix elements, the findings would suggest that newly replicated DNA is not attached to these structures during the initial low-LET period, but ^{125}I starts to induce high-LET effects as labeled DNA segments become associated with the target structure(s). On balance, our data favor the second of these alternatives.

INTRODUCTION

Biological damage from the decay of internal Auger emitters such as ^{125}I, ^{67}Ga, ^{77}Br, or ^{75}Se has been the subject of numerous investigations for more than 20 years (1-7). Due to their unique decay pattern, these radionuclides provide information on the fundamental mechanisms of radiation action not easily duplicated by other modes of cellular irradiation. The most widely used Auger emitter, ^{125}I, decays by electron capture and emits a shower of up to 50 electrons with energies ranging from a few eV to several tens of keV (8). Thus, unlike external radiation sources which usually irradiate the entire cell volume, Auger emitters decaying in any particular cell compartment cause highly differential radiation exposure to the labeled site, with only minor irradiation of distant subcellular regions (5,8,9).

It is believed that radiation-induced cell death in mammalian cells results primarily from damage to a target (or targets) located within the cell nucleus (10,11). Support for this notion is derived from studies where Auger emitters are incorporated into different cell compartments such as the plasma membrane (12), lysosomes (5), mitochondria (13), the general cytoplasm (6), or

nuclear DNA (1-5,7,9,12). The results prove that even massive radiation doses to the plasma membrane or cytoplasmic organelles are relatively nontoxic, but when ^{125}I is incorporated into nuclear DNA via the thymidine analogue ^{125}I-iododeoxyuridine ($^{125}IUdR$), the high local energy deposition within the genome results in extreme, high-LET like, radiation lethality.

In this report we present evidence that the radiobiological consequences of ^{125}I can be variable even if the radionuclide is incorporated into DNA. When cells are pulse-labeled with $^{125}IUdR$ and harvested for decay accumulation at different time intervals after labeling, ^{125}I-decays in the DNA can result in biological effects that resemble either low-LET or high-LET radiation damage. These unexpected findings suggest that ^{125}I toxicity may be related to changes in chromatin organization and/or variations in distance between decay events and potential critical targets within the cell at different times after DNA replication.

MATERIALS AND METHODS

Cell Synchronization

Chinese hamster ovary (CHO) cells were grown as monolayers on 25 cm^2 or 75 cm^2 Falcon plastic flasks, at 37°C, in a humidified atmosphere of 5% CO_2 in air. The growth medium was modified McCoy's 5a supplemented with 5% calf bovine serum, 100 units/ml penicillin-G and 100 μg/ml streptomycin. Under these conditions the population doubling time during exponential growth was 12-13 h (14) with a 3-4 h G_1 phase (15), 7 h S phase, 1.25 h G_2 phase (16), and 0.75 h M phase (17). To avoid genetic drift, new cultures were initiated from frozen stocks every 6 weeks. The stock cultures, carried without antibiotics, were used only if they tested free of mycoplasma using the Gibco Myco Tect test.

Prior to synchronization by mitotic cell selection, 4.5×10^6 CHO cells were plated into each of ten 75 cm^2 flasks. At the start of selection (about 18 h after plating) each flask contained $1.3\text{-}1.7 \times 10^7$ cells in exponential growth. Mitotic cells were selectively detached from this population during a 15 s selection shake as previously described (16,17). The mitotic cells were harvested and immediately cooled to 4°C. The cells remaining on the flask were refed with temperature and pH adjusted medium. The entire procedure (selection, harvesting, and refeeding) took less than 30 s and was carried out

aseptically in a portable selection apparatus specifically designed to maintain the temperature and pH of the medium. The apparatus basically consisted of a large, custom-made 37°C CO_2 incubator outfitted with a reciprocal shaker and a complex pumping system that permitted simultaneous semi-automatic cell harvest from up to 10 flasks by vacuum suction and subsequent refeeding of the flasks by a motor-driven multiple syringe system. The mitotic cell selection procedure was repeated every 10 min for up to 8 h. With repeated harvests, up to 5×10^7 mitotic cells with a mitotic index of 98% or higher were collected in a single experiment.

After harvesting, the mitotic cells were pooled, pelleted by centrifugation at 4°C, and resuspended in "cryoprotectant medium" (Ham's F10 supplemented with 15% bovine calf serum and 10% DMSO). Aliquots of the cell suspension (1 ml) were pipetted into 2 ml Nalgene Cryovials, and the tightly closed vials were placed into a rack and immersed in upright position into 100 ml of ethanol in a flat-bottom glass container with a screw-cap top. The container was then placed into a -90°C deep-freezer for 60 min. This procedure resulted in slow freezing of the cell suspension at a rate of 1.5-2.0°C/min as monitored on cell samples frozen in modified Cryovials outfitted with a low temperature thermometer (heavily insulated except for bulb region). After 60 min the vials were removed from the ethanol bath and transferred to liquid nitrogen storage for future use. The freezing and thawing procedure did not affect cell viability as determined by the standard colony forming assay and did not induce any detectable changes in cell cycle traverse after replating.

^{125}I Toxicity Studies

Carrier-free ^{125}IUdR (specific activity: 82.14 PBq/mol) was synthesized in this laboratory as described previously (18). Before use, the ^{125}IUdR was purified by HPLC on a Beckman Ultrasphere reverse phase column (5 µm spherical 80 A pore, 250 X 4.6 mm). The purification procedure involved an initial elution step (15 min at 1 ml/min) with a buffer containing 4.75 mM KH_2PO_4 dissolved in 1.5% ethanol/water and adjusted to pH 4.0 with concentrated H_3PO_4, followed by elution of ^{125}IUdR with a buffer containing 4mM KH_2PO_4 in 6% ethanol/water, adjusted to pH 4.0 with concentrated H_3PO_4. In this second elution step (also at 1 ml/min) the ^{125}IUdR peak eluted with fraction 17 or 18.

For ^{125}IUdR labeling, samples of frozen mitotic cells were thawed by immersion in a 37°C water bath. The cells were then pelleted by centrifugation, suspended in fresh temperature and pH adjusted McCoy's 5a, and plated in 25 cm^2 flasks. After 1 h incubation at 37°C, when the cells had completed mitosis and had become attached to the flask, aphidicolin (APC, 5 μg/ml) was added to the medium for 7 h to block the cells at the G_1/S boundary of the cell cycle (19). Exposure to APC did not affect the viability of the cells, but did shorten the subsequent S phase from the usual 7 h to about 5.5 h.

After removal of APC, cells were subjected to 10 min pulse-labeling with ^{125}IUdR (12-25 kBq/ml in McCoy's 5a with no added thymidine) during different stages of the S phase. For comparison, other groups of cells were labeled continually throughout the S phase (1.25 kBq/ml, with 1×10^{-6} M thymidine added to the medium). Labeling was terminated by discarding the labeling medium and rinsing the cells three times with 5 ml of temperature and pH adjusted medium. After refeeding, the cells were returned to the 37°C incubator. Depending on the requirements of the experiment, cells from individual flasks were harvested at time intervals ranging from 15 min to 8 h after termination of labeling. The number of cells harvested from each flask was evaluated by counting on a Coulter Model B particle counter.

The radionuclide content per cell was evaluated by precipitating known numbers of labeled cells (in some cases with approximately 10^6 "carrier" cells) with ice-cold 10% TCA. The ^{125}I content of the cell pellet was determined in a calibrated well-type crystal scintillation counter. Additional cell samples were retained for autoradiographic examination of the labeling index (98% or higher in all experimental groups). To permit accumulation of ^{125}I damage under controlled conditions, the remaining labeled cells were suspended in cryoprotectant medium and cell aliquots were frozen and stored in liquid nitrogen as described above.

At the time of freezing the cells sustained ^{125}I-decays at a rate of 0.4 to 0.8 decays/cell/h. Depending on the required number of decays/cell, the storage time in liquid nitrogen ranged from 1 h to 5 weeks. The 1 h group served as the "zero decay" control group, *i.e.*, the 1-6 ^{125}I-decays that had occurred in the cells up to this point were disregarded and accumulation of decays in all experimental groups was assumed to start 1 h after the onset of liquid nitrogen storage. This procedure produced a significant underestimate of the actual number of ^{125}I decays experienced by cells removed from storage

after short accumulation periods but did not significantly affect the dose calculations for cells stored in liquid nitrogen for prolonged periods of time.

After the frozen cells had accumulated the desired number of ^{125}I-decays, cell samples were removed from cold storage, thawed, and diluted in McCoy's 5a medium supplemented with 5% calf bovine serum and 10% fetal bovine serum. Three replicate plates (60 mm Petri dishes) were prepared for each experimental group. The dishes were incubated at 37°C for 7 days until the colonies were large enough for fixation and staining with 0.25% crystal violet. Unlabeled control cells subjected to all these procedures (including labeling with nonradioactive IUdR) exhibited a plating efficiency of between 70-80%.

X ray Studies

Cells synchronized by mitotic selection and subsequent treatment with APC (but not labeled with ^{125}IUdR) were harvested either during early-S phase (1 h after removal of APC) or in late-S/G_2 phase (6 h after removal of APC). The cells were suspended in cryoprotectant medium and irradiated with an X ray beam generated by a General Electric Maxitron 300 therapy machine operated at 250 kVp and 20 mA. The X ray beam was filtered with 1 mm copper (HVL 20 mm Al). The dose rate was 1 Gy/min as measured by a Victoreen ionization chamber. All irradiations were performed at 4°C and the cell samples were rotated at 18 rpm to ensure uniform dose distribution.

Microdosimetry Calculations

Microdosimetry calculations were performed for early-S phase cells (15 min chase group) and for late-S/G_2 cells (5 h chase group). The geometry and dimensions of the cell nuclei were evaluated by microscopic observation on a Nikon Microphot-FX microscope on cells fixed in 3:1 methanol:acetic acid. To account for possible shrinkage in the volume of the cell nucleus during freezing (20), the nuclear size measurements were performed on unfrozen and frozen cell samples. In the latter case, aliquots of the frozen cell suspensions were transferred directly from liquid nitrogen storage into 3:1 methanol:acetic acid and allowed to thaw in the presence of the fixative to preserve the nuclear morphology of frozen cells. It was found that in all cases tested the nuclear volume of frozen cells was about 30-35% lower than that of corresponding unfrozen control cells. For our dosimetry calculations the nuclei of frozen CHO cells were assumed to be ellipsoids with axial

dimensions of 4.95 μm X 3.55 μm X 3.55 μm (volume 261 μm^3) for cells in early-S phase and 6.95 μm X 4.68 μm X 4.68 μm (volume 637 μm^3) for cells in late-S/G_2.

Based on a method described by Charlton and Booz (8), the mean dose per decay to cell nuclei was calculated from a file of 1,000 individual ^{125}I electron spectra. The origins of the decays were chosen at random within the ellipsoids, and the electron tracks from each decay spectrum were examined using the electron track code MOCA7B of Paretzke (21). Each electron was followed to the end of its track or until the primary electron had left the ellipsoid and its distance from the nearest surface was sufficiently large to minimize the chance of back-scattering into the ellipsoid. From the sum of energy deposited inside the ellipsoid by all interactions (averaged over 914 decays for early-S phase nuclei and over 800 decays for late-S/G_2 phase nuclei), the average intranuclear energy deposition per ^{125}I-decay was calculated to be 11.2 keV (0.00687 Gy) for early-S phase nuclei and 11.8 keV (0.00296 Gy) for late-S/G_2 nuclei. The similarity in total energy deposition (11.2 versus 11.8 keV) was not unexpected because the dimensions of both early-S and late-S nuclei are sufficiently large to ensure that most Auger electrons deposit all of their energy within the nuclear volume.

To facilitate a comparison between DNA double-strand breaks (DSB) and cell survival, DSB/decay values were calculated for early-S phase cells (15 min chase group) and late-S/G_2 phase cells (5 h chase group). According to previous calculations (22,23), each ^{125}I-decay in the DNA produces approximately 0.8 DSB at the site of decay. A lesser number of additional breaks are produced by high-energy Auger electrons at sites distant from the decay event. Assuming a DNA content of 3.6×10^{12} daltons/cell at the beginning of the S phase (twice this amount at the end of the S), and using 1×10^{-11} DSB/Gy/dalton as an estimate for the yield of breaks from low-LET radiations, it can be calculated that 0.247 DSB/decay are produced in early-S phase cells and 0.213 DSB/decay in late-S/G_2 cells due to low-LET radiation exposure contributed by the high-energy Auger electrons. Thus, the total DSB yield/^{125}I-decay amounts to 1.047 DSB/decay for early-S phase cells and 1.013 DSB/decay for late-S/G_2 cells.

RESULTS

Figure 1 presents the results of an experiment where mitotic CHO cells were plated and resynchronized at the G_1/S boundary of the cell cycle with

APC. The cells were then allowed to progress through the S phase and subjected to 10 min pulse-labeling with ^{125}IUdR starting 0.5, 1.5, 2.5, 3.5, or 4.5 h after removal of APC. This labeling schedule resulted in selective incorporation of ^{125}IUdR into five different subfractions of the genome, *i.e.*, in each experimental group a different 10 min segment of DNA (about 2-5% of the entire DNA) was labeled, the remaining 95-98% of the DNA remained unlabeled. To achieve random labeling of the entire genome, groups of identically pretreated CHO cells were labeled with ^{125}IUdR throughout the S phase. After labeling, the cells were chased in ^{125}IUdR-free medium and harvested in the G_1/early-S phase of the next cell cycle for freezing and accumulation of ^{125}I-decays. As shown in Fig. 1, the dose-survival curves for all six labeling groups were identical. This indicates that DNA-associated ^{125}I produces equal cytocidal effects regardless of whether the decays are randomly distributed over the entire DNA or are restricted to different 2-5% subfractions of the genome.

Figure 2 shows survival values for CHO cells pulse-labeled with ^{125}IUdR for 10 min starting 0.5 h after release from APC. The cells were then chased in nonradioactive medium and cell aliquots were harvested for freezing and decay accumulation after chase periods ranging from 15 min to 8 h. In other words, THE SAME 10 MIN SEGMENT OF DNA WAS LABELED IN ALL EXPERIMENTAL GROUPS, ONLY THE DURATION OF THE POST-LABELING CHASE WAS VARIED. Nevertheless, there was a striking change in the survival response of different groups. Cells harvested for decay accumulation within 1 h of labeling showed greatly enhanced resistance to ^{125}I-decays, yielding low-LET dose-survival curves with a pronounced shoulder and a large D_0 of about 135 decays/cell. With longer post-labeling chase periods the shoulder and the D_0 progressively declined and cells harvested 5 h after labeling or later were as sensitive to ^{125}I damage as cells labeled uniformly throughout the S phase (D_0: 42 decays/cell). The chase experiment shown in Fig. 2 was repeated five times, including twice on cells that had not been resynchronized with APC at the G_1/S boundary, always with similar results.

It should be noted that during the post-labeling chase the cells continued to progress through the cell cycle. To determine whether the shift from low-LET to high-LET action shown in Fig. 2 might be related to cell cycle position at the time of harvest, the chase experiment was repeated on cells pulse-labeled in late-S phase, 4.5 h after release from APC. The results were

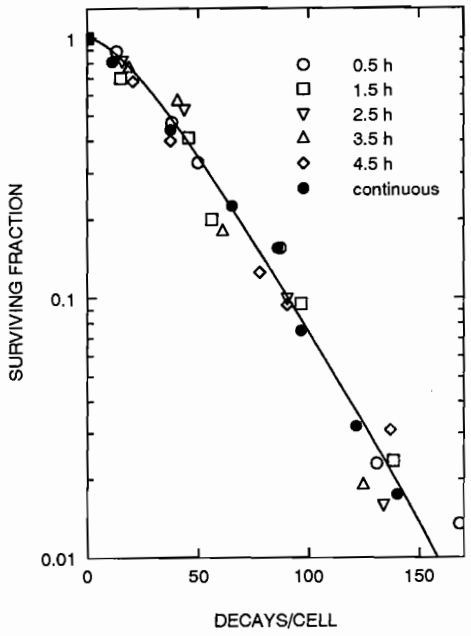

FIG. 1. Fractional survival of CHO cells ^{125}IUdR-labeled for 10 min at different times during the S phase (0.5, 1.5, 2.5, 3.5, 4.5 h after release from APC), and frozen for decay accumulation in the G_1/early-S phase of the next cell cycle. To compensate for increased ^{125}IUdR uptake during mid and late-S phase, the labeling dose was 28 kBq/ml, 22 kBq/ml, 14 kBq/ml, 12 kBq/ml, and 10 kBq/ml for the 0.5, 1.5, 2.5, 3.5 and 4.5 h groups, respectively. At the time of cell harvest in the G_1/early-S phase (after completion of one cell division), the exposure rate was 0.6-0.9 decays/cell/h. Using ^{125}I uptake ratios (pulse-labeled cells/continuously labeled cells) as a measure of fractional DNA replication during the 10 min labeling pulse indicates that about 1.8%, 2.3%, 4.2%, 4.7%, and 5.4% of the entire DNA was labeled in the 0.5, 1.5, 2.5, 3.5, and 4.5 h labeling groups, respectively.

similar to those shown in Fig. 2, that is, cells harvested for freezing and dose accumulation shortly after pulse-labeling exhibited a low-LET pattern of radiation death and cells harvested after prolonged post-labeling chase periods demonstrated a high-LET pattern of ^{125}I-induced radiation death (data

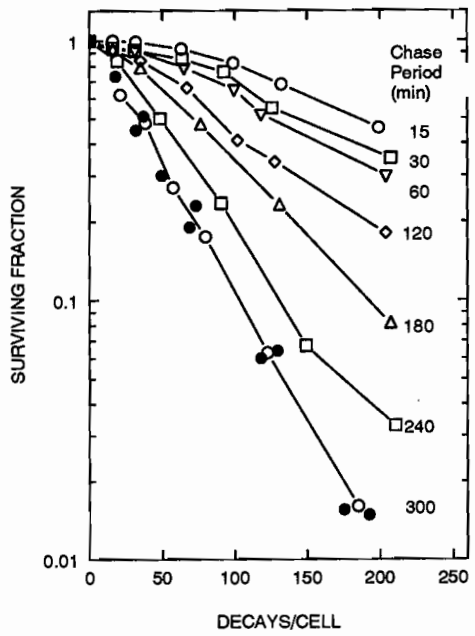

FIG. 2. Fractional survival of CHO cells pulse-labeled with ^{125}IUdR for 10 min starting 0.5 h after release from APC. The labeled cells were harvested for freezing and decay accumulation after post-labeling chase periods ranging from 15-480 min, but only values for up to 300 min are shown (open symbols). For comparison, survival values for cells labeled continuously through the S phase and harvested 3 h after termination of labeling are included (solid circles).

not shown). Expressed in terms of cell cycle position at the time of harvest, in experiments where cells were labeled 0.5 h after release from APC (Fig. 2), the 15 min chase group was located in early-S phase and the 5 h chase group in late-S/G_2 phase. In the second set of experiments, where cells were labeled 4.5 h after release from APC, the 15 min chase group was located in late-S phase and the 5 h chase group in the G_1 phase of the next cell cycle. Yet in both cases, regardless of cell cycle position, the 15 min chase group exhibited a low-LET pattern of ^{125}I-induced cell death and the 5 h chase group experienced high-LET type radiation lethality.

In another control experiment, mitotic CHO cells were plated and blocked at the G_1/S boundary with APC as described above and then X irradiated 1 h or 6 h after removal of APC. These two time points were chosen for X irradiation because they corresponded to the cell cycle positions occupied by the 15 min and 5 h ^{125}I chase groups at the time of harvesting and freezing. The results shown in Fig. 3 indicate a small difference in the X ray response of early-S phase cells (narrow shoulder, D_0 of 1.4 Gy) and late-S/G_2 cells (more pronounced shoulder, D_0 of 1.6 Gy), but this difference could not be responsible for the enhanced ^{125}I resistance of early-S phase cells shown in Fig. 2 because early-S phase cells exhibit enhanced (rather than reduced) sensitivity to X irradiation.

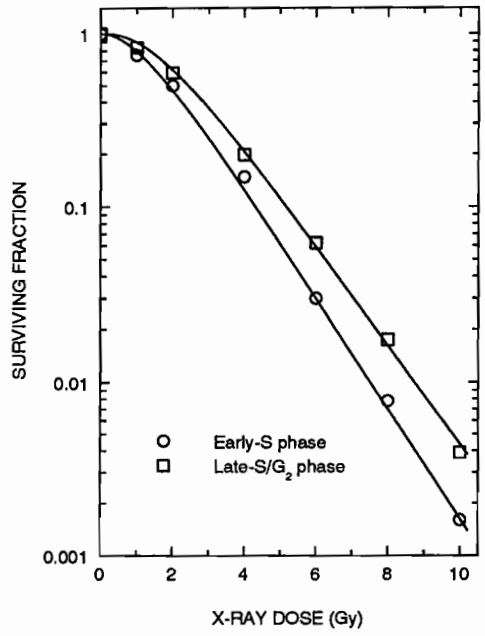

FIG. 3. Dose-survival curves for CHO cells subjected to X irradiation 1 h or 6 h after removal of APC.

To provide a more meaningful comparison between X ray and ^{125}I survival data, the ^{125}I-decay/cell values from Fig. 2 were converted to absorbed dose in Gy. Figure 4 shows the survival curves for the 15 min and

5 h chase groups as a function of dose to the cell nucleus. Using this method of presentation reveals that the ^{125}I response of the 15 min chase group is similar to that of the corresponding 1 h X ray group. In contrast, the ^{125}I survival curve for the 5 h chase shows a high-LET pattern with a D_0 of only 0.13 Gy, which is 12 times smaller than the D_0 of the corresponding 6 h X ray group. This comparison confirms the notion that depending on the time interval between $^{125}IUdR$ incorporation and decay accumulation, DNA-associated ^{125}I can produce either low-LET or high-LET radiation effects.

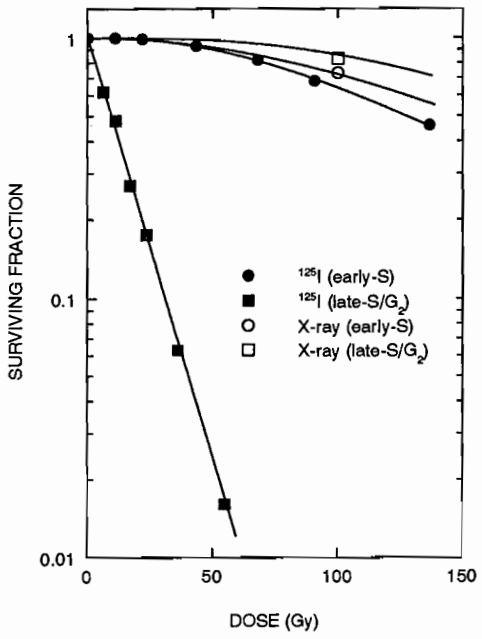

FIG. 4. ^{125}I dose-survival curves for CHO cells (15 min and 300 min chase groups from Fig. 2), plotted as a function of radiation dose to the cell nucleus (solid symbols). The values for CHO cells subjected to X irradiation at equivalent points in the cell cycle are indicated by the open symbols.

It is widely believed that a causative (or at least quantitative) link exists between DNA double-strand breaks (DSB) and radiation death (24,25). To test this hypothesis, the number of DNA DSB per ^{125}I-decay was calculated (22) for

early-S phase cells (15 min chase group) and late-S/G_2 phase cells (5 h chase group). According to these calculations about 1 DNA DSB/decay should be produced in both groups. This value agrees well with literature values for both naked oligonucleotide chains (26) and DNA in intact mammalian cells exposed to ^{125}I-decays under frozen conditions (27-29). Figure 5 shows the ^{125}I and X ray survival data from Figs. 2 and 3 plotted as a function of calculated DNA DSB/cell rather than absorbed dose in Gy. From this comparison it is clear that no obvious correlation between DNA DSB and cell lethality can be inferred from our data.

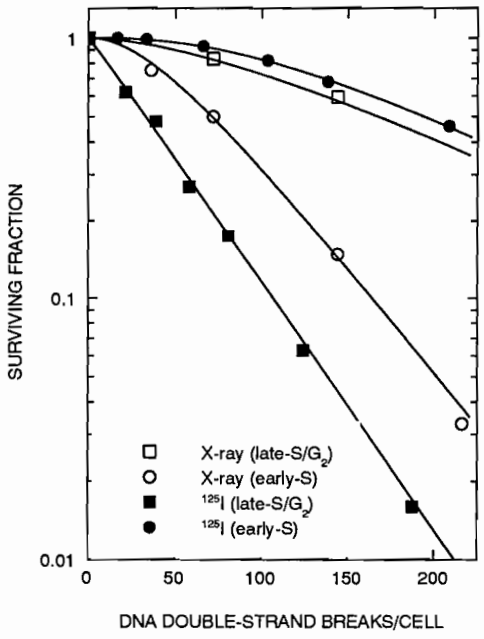

FIG. 5. ^{125}I dose-survival curves for CHO cells (15 min and 300 min chase groups from Fig. 2), plotted as a function of calculated DNA double-strand breaks/cell (solid symbols). The values for cells X irradiated at equivalent points in the cell cycle are indicated by the open symbols.

DISCUSSION

^{125}I Toxicity Studies

Previous radionuclide suicide studies on mammalian cells indicate that ^{125}I-decays in the DNA produce high-LET type radiation damage, but identical decay events at the plasma membrane, the cytoplasm, or specific cytoplasmic structures such as lysosomes or mitochondria yield low-LET dose survival curves with a shoulder and a large D_0 (1-9). Microdosimetric calculations suggest that these differences in biological action can be attributed to the unique decay and dose distribution characteristics of ^{125}I. The emission of a dense shower of low-energy Auger electrons results in highly localized deposition of radiation energy at the site of decay, with distant sites receiving only minor radiation doses from the few high-energy electrons emitted during ^{125}I-decay (5,8,9). Expressed differently, ^{125}I induces high-LET damage when the decay event takes place directly at the primary target site responsible for radiation death, but decays at sites distant from the primary target produce low-LET radiation effects. Although low-LET effects have been reported only for Auger emitters located outside the cell nucleus, similar low-LET cell killing can be expected for intranuclear decays if the decay site is sufficiently distant from the primary target to place the target outside the high-LET region around the site of ^{125}I decay.

The results reported here indicate that ^{125}I-decays at the DNA do not always result in high-LET radiation damage. Synchronized CHO cells pulse-labeled with ^{125}IUdR and frozen for decay accumulation within 1 h after labeling yield a low-LET survival response (Figs. 2 and 4) even though the ^{125}I-decays occur in close association with DNA. However, when cell harvesting and freezing are delayed for several hours, the cells exhibit the typical high-LET pattern of ^{125}I-induced radiation death. This marked shift in radiation action cannot be attributed to drug effects from cell synchronization because similar changes in the survival response can be observed on pulse-labeled cells that had not been resynchronized at the G_1/S boundary with aphidicolin. The shift is also not related to cell cycle progression during the chase period because the effect is observable regardless of whether cells are pulse-labeled in early-S phase or in late-S phase. It appears, therefore, that the low-LET to high-LET shift in the ^{125}I response represents a true shift in the cellular mechanism of ^{125}I-induced radiation death.

DNA Double-Strand Breaks and Cell Lethality

Several different hypotheses can be advanced to explain the findings described above. If it is assumed that DNA is the primary (or sole) target responsible for radiation death, the results indicate that DNA maturation increases the radiosensitivity of DNA, either by changing the type or amount of damage induced, or by decreasing damage repair. If radiation death involves damage to higher-order structures within the cell nucleus (*e.g.*, solenoid, DNA loop domain, nuclear matrix, nuclear envelope), the findings would suggest that ^{125}I is able to induce high-LET effects only after the labeled DNA segments have become part of (or attached to) the higher order target.

The first of these alternatives, enhanced radiation damage to mature DNA, appears to be the least likely explanation. There is no evidence that mature DNA is more radiosensitive than newly replicated DNA; it may in fact be more resistant to damage from low-LET radiations (30). However, even without invoking the prospect that mature DNA might show similarly enhanced resistance to ^{125}I effects, our results do not suggest any direct correlation between DNA DSB and cell lethality. ^{125}I administered in the form of ^{125}IUdR is covalently bound to DNA. Thus, regardless of the length of the post-labeling chase period, each ^{125}I-decay would be expected to produce DNA DSB with high efficiency (22,23,26-29), and the dose-survival curves for early and late harvested cells should become superimposed when fractional survival is plotted as a function of DSB/cell. No such correlation is apparent from the data shown in Fig. 5, *i.e.*, our findings argue against the widely held view that DNA DSB are directly linked to radiation death.

It might be postulated that even if the induction of DNA DSB is not linked to cell death, DNA repair may be more efficient in newly replicated DNA, resulting in enhanced cell survival after short post-labeling chase periods. However, preliminary repair studies using the neutral filter elution assay and gel electrophoresis do not support this interpretation (unpublished data). The repair hypothesis also conflicts with the finding that for the 15 min chase group (where ^{125}I-decays occur in newly replicated DNA) the low-LET dose component is sufficient to fully account for the observed radiation lethality (Fig. 4). If DNA DSB are assumed to be the primary lethal lesion, and if cell death in the 15 min chase group can be attributed to the relatively few DNA DSB produced by the low-LET dose component, it follows that the much more numerous (and probably also more severe) local breaks at the site

of ^{125}I-decay in newly replicated DNA do not contribute to radiation death. Such breaks must therefore be completely repaired. This is contrary to the conventional view that local damage at the site of ^{125}I decay is difficult to repair. Even if we were to grant the possibility that all the local DNA DSB at the decay site could be fully repaired, the existence of such total repair would merely confirm that there is no direct quantitative correlation between DNA DSB and subsequent cell death.

This conclusion is supported by a different line of reasoning. As pointed out above, a low-LET pattern of ^{125}I-induced cell death indicates that the ^{125}I-decays had occurred at a site distant from the primary target for radiation death. From the data shown in Figs. 2 and 4, it is apparent that ^{125}I-decays in newly synthesized DNA (15 min chase group) do not induce high-LET type cell death. It would be difficult to reconcile this finding with the notion that DNA is the sole target for radiation death. Labeled DNA obviously is always located within the high-LET region around the site of ^{125}I-decay and thus invariably sustains high-LET type damage. This suggests that the primary radiation target in mammalian cells is a higher-order structure that is closely associated with DNA in the cell nucleus. This structure may or may not sustain high-LET damage from ^{125}I-decays in the DNA, depending on whether or not the labeled DNA is directly associated with the structure. Viewed from this perspective, our findings in conjunction with similar discrepancies between DNA damage and cell death reported earlier (28,29,31-33), contradict the widely held view that DNA DSB are directly linked to cellular radiation death.

Alternative Target Structures for Cell Death

The suggestion that damage to DNA may not be the sole mechanism for radiation death, although startling, is not novel. Alper (34) has long maintained that two types of damage may contribute to radiation death in mammalian cells, type O damage to membranes and type N damage to DNA. Elkind and coworkers have repeatedly interpreted their data as indicating that DNA may be closely associated with a non-DNA target capable of accumulating sublethal damage (35,36). Cole (37) suggested that toxic products from radiation-induced peroxidation of lipids may induce configurational damage in chromatin and/or supporting structures in the nuclear matrix. Recent findings by Yasui *et al.* (31) support this view and suggest that damage to higher-order chromatin structures may be responsible for radiation death.

The notion that higher-order structures within the cell nucleus may play a decisive role in the genesis of cellular radiation death is in accord with current knowledge on the organization of the genome (38). At least three higher levels of DNA organization (nucleosome, solenoid, DNA loop domain) have been identified and found to interact with the nuclear matrix in a dynamic structural arrangement. Various components of the nuclear matrix appear to be intimately involved in DNA synthesis, RNA transcription, DNA processing and transport, and possibly also DNA repair. Other attachment points of the DNA at the nuclear matrix are believed to be involved in chromosome condensation during mitosis and meiosis. In short, proper functioning of the genome appears to demand a spatial and temporal precision that would be unattainable in the absence of structural order. Given the complexity of genome organization it would not be surprising if damage to this structural order were the ultimate cause of radiation death. In fact, it is conceivable that disruption of the structural hierarchy within the cell nucleus may in itself be sufficient to cause cell death without any accompanying damage to the linear sequence of DNA.

The hypothesis that DNA damage *per se* may not be the sole mechanism for radiation death provides a cohesive and internally consistent interpretation for our results. It explains the finding that the cytocidal effects of ^{125}I increase as the length of the post-labeling chase period is increased (Fig. 2), whereas no such effect is observed with X ray exposures (Fig. 3). Most of the nucleoprotein would be associated with other nuclear structures such as the nuclear matrix throughout the cell cycle and external X irradiation would disrupt this structural arrangement whether or not any particular DNA segment is attached to it. In contrast, ^{125}I incorporated into newly replicated segments of DNA would initially not be directly associated with the target structure. Thus, ^{125}I-decays in newly replicated DNA would not be expected to reach full toxic potential until the labeled DNA segments had established close contact with (or become part of) higher-order structures. At that stage, Auger electrons originating from ^{125}I-decays in the DNA would be able to induce high-LET damage not only in DNA, but also in the DNA-containing superstructure, causing greatly enhanced cell death.

It should be noted that the chase experiments described above could not be duplicated with any external radiation source, high-LET or low-LET, because external radiations would not permit selective irradiation of newly replicated portions of the genome. This demonstrates again the unique features of ^{125}I-decay and its utility for dissecting the molecular mechanisms

of radiation damage. In many ways, the difference between ^{125}I and external radiations is analogous to the difference between smart bombs and conventional bombs. ^{125}I acts like a smart bomb that destroys individual components of the system, with only minor collateral damage to distant sites. Exposure to external radiations is comparable to large-area carpet bombing that indiscriminately damages the system as a whole.

CONCLUSIONS

The data reported here indicate that, depending on the labeling conditions and the duration of the post-labeling chase, ^{125}I incorporated into DNA can act either as a low-LET or high-LET radiation source. If a sufficient time interval (about 5 h) is allowed to elapse between ^{125}I incorporation and decay accumulation, DNA-bound ^{125}I induces high-LET like cytocidal effects regardless of whether decays are randomly distributed over the entire genome (continuous labeling) or restricted to different 2-5% subfractions of the genome (10 min pulse-labeling). However, if pulse-labeled cells are harvested for decay accumulation within 1 h of labeling, ^{125}I-decays in the DNA yield a low-LET dose-survival curve comparable to that obtained with external X ray exposures. This paradox can be explained by postulating that damage to high-level structures within the cell nucleus (*e.g.*, solenoids, DNA loop domains and/or associated nuclear matrix elements) constitutes the primary mechanism for radiation-induced cell death.

REFERENCES

1. K.G. HOFER, W. PRESNKY, and W.L. HUGHES, Death and metastatic distribution of tumor cells in mice monitored with ^{125}I-iododeoxyuridine. *J. Nat. Cancer Inst.* **43**, 763-773 (1969).
2. H.H. ERTL, L.E. FEINENDEGEN, and J. HEINIGER, ^{125}I, a tracer in cell biology: Physical properties and biological aspects. *Phys. Med. Biol.* **15**, 447-456 (1970).
3. K.G. HOFER and W.L. HUGHES, Radiotoxicity of intranuclear tritium, 125-iodine and 131-iodine. *Radiat. Res.* **47**, 94-109 (1971).
4. L.E. FEINENDEGEN, H.H. ERTL, and V.P. BOND, Biological toxicity associated with the Auger effect. In *Biophysical Aspects of Radiation Quality*, pp. 419-430. IAEA, Vienna, 1971.
5. K.G. HOFER, C.R. HARRIS, and J.M. SMITH, Radiotoxicity of intracellular ^{67}Ga, ^{125}I and ^{3}H: Nuclear versus cytoplasmic radiation effects in murine L1210 leukemia. *Int. J. Radiat. Biol.* **28**, 225-241 (1975).

6. A.I. KASSIS and S.J. ADELSTEIN, Radiotoxicity of ^{75}Se and ^{35}S: Theory and application to a cellular model. *Radiat. Res.* **84**, 407-425 (1980).
7. A.I. KASSIS, S.J. ADELSTEIN, C. HAYDOCK, K.S.R. SASTRY, K.D. McELVANY, and M.J. WELCH, Lethality of Auger electrons from the decay of bromine-77 in the DNA of mammalian cells. *Radiat. Res.* **91**, 362-373 (1982).
8. D.E. CHARLTON and J. BOOZ, A Monte Carlo treatment of the decay of ^{125}I. *Radiat. Res.* **87**, 10-23 (1981).
9. K.G. HOFER, G. KEOUGH, and J.M. SMITH, Biological toxicity of Auger emitters: Molecular fragmentation versus electron irradiation. *Cur. Top. Radiat. Res. Q.* **12**, 335-354 (1977).
10. R.E. ZIRKLE and W. BLOOM, Irradiation of parts of individual cells. *Science* **117**, 487-493 (1953).
11. T.R. MUNRO, The relative radiosensitivity of the nucleus and cytoplasm of Chinese hamster fibroblasts. *Radiat. Res.* **42**, 451-470 (1970).
12. R.L. WARTERS, K.G. HOFER, C.R. HARRIS, and J.M. SMITH, Radionuclide toxicity in cultured mammalian cells: Elucidation of the primary site for radiation damage. *Cur. Top. Radiat. Res. Q.* **12**, 389-407 (1977).
13. L.S. YASUI and K.G. HOFER, Role of mitochondrial DNA in cell death induced by ^{125}I decay. *Int. J. Radiat. Biol.* **49**, 601-610 (1986).
14. M.H. SCHNEIDERMAN, K.G. HOFER, and G.S. SCHNEIDERMAN, An in vitro ^{125}IUdR-release assay for measuring the kinetics of cell death. *Int. J. Radiat. Biol.* **59**, 397-408 (1991).
15. M.H. SCHNEIDERMAN, K.G. HOFER, and G.S. SCHNEIDERMAN, Cell cycle progression after selective irradiation of DNA during the cell cycle. *Radiat. Res.* **116**, 283-291 (1988).
16. M.H. SCHNEIDERMAN and K.G. HOFER, The target for radiation-induced division delay. *Radiat. Res.* **84**, 462-476 (1980).
17. M.H. SCHNEIDERMAN, W.C. DEWEY, D.B. LEEPER, and H. NAGASAWA, Use of the mitotic selection procedure for cell cycle analysis. Comparison between the X ray and cyclohexamide G_2 markers. *Exp. Cell Res.* **74**, 430-438 (1972).
18. W.G. KEOUGH and K.G. HOFER, An improved method for synthesis and purification of ^{125}I or ^{131}I labeled carrier-free 5-iodo-2'-deoxyuridine. *J. Lab. Comp. Radiopharm.* **14**, 83-90, (1978).
19. G. PEDRALI-NOY, S. SPADARI, A. MILLER-FAURES, A.O.A. MILLER, J. KRUPPA, and G. KOCH, Synchronization of HeLa cell cultures by inhibition of DNA polymerase alpha with aphidicolin. *Nucl. Acid Res.* **8**, 377-387 (1980).
20. S.L. COMMERFORD, V.P. CRONKITE, and U. REINCKE, The effect of changes in cell geometry associated with freezing on the radiation dose from decay of internal isotopes. *Int. J. Radiat. Biol.* **41**, 99-103 (1982).
21. H.G. PARETZKE, Radiation track structure theory. In *Kinetics of Nonhomogenesis Processes* (G.R. FREEMAN, Ed.), pp. 89-170, Wiley, New York, 1987.
22. D.E. CHARLTON and J.L. HUMM, A method of calculating initial DNA strand breakage following the decay of incorporated ^{125}I. *Int. J. Radiat. Biol.* **53**, 353-365 (1988).
23. E. POMPLUN, A new DNA target model for track structure calculations and its first application to I-125 Auger electrons. *Int. J. Radiat. Biol.* **59**, 625-642 (1991).

24. R.B. PAINTER, The role of DNA damage and repair in cell killing induced by ionizing radiation. In *Radiation Biology in Cancer Research* (R.E. MEYN and H.R. WITHERS, Eds.), pp. 59-68, New York, Raven Press, 1980.
25. I.R. RADFORD, G.S. HODGSON, and J.P. MATTHEWS, Critical DNA target size model of ionizing radiation-induced mammalian cell death. *Int. J. Radiat. Biol.* **54**, 63-79 (1988).
26. R.F. MARTIN and W.A. HASELTINE, Range of radiochemical damage to DNA with decay of iodine-125. *Science* **213**, 896-898 (1981).
27. I.R. RADFORD and G.S. HODGSON, ^{125}I-induced DNA double strand breaks: Use in calibration of the neutral filter elution technique and comparison with X ray induced breaks. *Int. J. Radiat. Biol.* **48**, 555-566 (1985).
28. H.L. LIBER, P.K. LeMOTTE, and J.B. LITTLE, Toxicity and mutagenicity of X rays and [^{125}I]dUrD or [^{3}H]TdR incorporated in the DNA of human lymphoblast cells. *Mutat. Res.* **111**, 387-404 (1983).
29. P.K. LEMOTTE and J.B. LITTLE, DNA damage induced in human diploid cells by decay of incorporated radionuclides. *Cancer Res.* **44**, 1337-1342 (1984).
30. M. LJUNGMAN, The influence of chromatin structure on the frequency of radiation-induced DNA strand breaks: a study using nuclear and nucleoid monolayers. *Radiat. Res.* **126**, 58-64 (1991).
31. L.S. YASUI, A.S. PASCHOA, R.L. WARTERS, and K.G. HOFER, Cytotoxicity of ^{125}I decay produced lesions in chromatin. In *DNA Damage by Auger Emitters* (K.F. BAVERSTOCK and D.E. CHARLTON, Eds.), pp. 181-189, Taylor and Francis, London, 1988.
32. I.R. RADFORD and S. BROADHURST, Aphidicolin synchronization of mouse L cells perturbs the relationship between cell killing and DNA double-strand breakage after X-irradiation. *Int. J. Radiat. Biol.* **53**, 205 -215 (1988).
33. G. ILIAKIS, L. METZGER, R.J. MUSCHEL, and W. GILLIES McKENNA, Induction and repair of DNA double strand breaks in radiation-resistant cells obtained by transformation of primary rat embryo cells with the oncogenes H-ras and v-myc. *Cancer Res.* **50**, 6575-6579 (1990).
34. T. ALPER, *Cellular Radiobiology*, Cambridge University Press, Cambridge, 1979.
35. E. BEN-HUR and M.M. ELKIND, Thermally enhanced radioresponse of cultured Chinese hamster cells: Damage and repair of single-strand DNA and a DNA complex. *Radiat. Res.* **59**, 484-495 (1974).
36. M.M. ELKIND and J.I. REDPATH, Molecular and cellular biology of radiation lethality. In *Cancer, A Comprehensive Treatise*, Vol. 6 (F. F. BECKER, Ed.), pp. 51-99, Plenum Publishing Company, New York, 1977.
37. A. COLE, Radiation effects on DNA and membranes. In *Proc. 7th Int. Cong. Radiat. Res.* (J.J. BROERSE, G.W. BARENDSEN, H.B. KAL, and A.J. VAN DER VOGEL, Eds.), pp. 225-230, Martinus Nijhoff, Amsterdam, 1983.
38. W.G. NELSON, K.J. PIENTA, E.R. BARRACK, and D.S. COFFEY, The role of the nuclear matrix in the organization and function of DNA. *Ann. Rev. Biophys. Chem.* **15**, 457-475 (1986).

DISCUSSION

Nagasawa, H. N. 1) What concentration of ^{125}IUdR did you apply for the 10 min pulse label? 2) What percent of cells did you recover after the aphidicolin block? 3) Did all labeled cells moving into the next cell cycle have a normal chromosome component? Were there any ploidy changes and chromosomal aberrations in the nucleus for different labeling times?

Hofer, K. G. 1) For 10 min pulse-labeling we used 10-28 kBq/ml of ^{125}IUdR, giving us an exposure rate of about 0.5-1.0 ^{125}I decays/cell/h at the time of cell harvest and freezing. 2) We used an aphidicolin dose of 5 μg/ml administered to G_1 cells for 7 hours. This treatment regimen did not reduce the survival fraction of cells as compared to control cells that had not been treated with aphidicolin. 3) We have not yet done any studies on chromosome damage or ploidy changes after aphidicolin treatment. As far as the labeling pattern is concerned, we had exceedingly good cell synchrony and our labeling index for pulse-labeled cells was close to one.

DeSombre, E. R. If different organizational forms are involved would you not expect to see different morphological effects (*i.e.* chromosomal damage)?

Hofer, K. G. This is one of the long-range goals of our work. We have shown here that one type of genome damage - DNA DSB - is apparently not quantitatively linked to radiation death. It is conceivable that chromosome breaks will turn out to be directly proportional to cell death. If so, this would be a strong argument that chromosome breaks, rather than DNA DSB, are the ultimate cause of radiation death.

Rao, D. V. Dr. Hofer, I would like your opinion about the nature of the radiosensitive targets. Dudley Goodhead several years ago suggested that the size of the radiosensitive target is about 5 nm in radius based on his soft X ray work. Several years ago our group postulated that these targets may be nucleosome units. Do you think that nucleosomes might be the targets based on your work?

Hofer, K. G. I agree with you that the sensitive target for radiation death is not DNA *per se*, but a higher-order DNA-protein structure. The nucleosome is a potential candidate, but the kinetics of nucleosome formation argues against this possibility. Nucleosome formation is complete within minutes after DNA replication, whereas in our experiments it takes several hours before nearly replicated DNA becomes fully associated with the higher-order target structure. For this reason I believe that the sensitive structure must be a more central structure such as, for example, the DNA-

protein subunit that forms the backbone of the chromosomes. However, this is still speculation and we cannot at this stage exclude the nucleosome or any other higher-order structure closely associated with DNA.

Biophysical Aspects of Auger Processes, AAPM Symposium Series No. 8 (1992) 249-272
Eds. RW Howell, VR Narra, KSR Sastry, DV Rao

TISSUE, CELLULAR, AND SUBCELLULAR DISTRIBUTION OF INDIUM RADIONUCLIDES IN THE RAT

BO-ANDERS JÖNSSON, SVEN-ERIK STRAND, HADAR EMANUELSSON[1], and BENGT LARSSON[2]

Departments of Radiation Physics and Zoophysiology[1]
University of Lund, Sweden

Department of Toxicology[2]
University of Uppsala, Sweden

ABSTRACT

The tissue distribution of ^{111}In-activity in rat organs after intravenous injections of different ^{111}In-radiopharmaceuticals have been studied by autoradiography. Quantitation was performed utilizing an image analyzing system designed for local measurements on whole-body autoradiographs. Additional studies of the cellular and subcellular localization in testes and bone marrow were performed by light and electron microscopy autoradiography after injection of ^{114m}In. The whole-body autoradiographs demonstrated a marked inhomogeneous radionuclide distribution in various tissues (*e.g.* kidneys, spleen, liver, bone marrow, lymph nodes and testes). In the testes it was observed by light microscopy autoradiography that the activity was localized in a significant concentration in the interstitial tissue, and to a minor amount in the periphery of the seminiferous tubules, coincident with the location of the radiosensitive spermatogenic cell lineage. In electron microscope autoradiographs subcellular localization sites appeared near and within the cell nucleus of spermatogonial cells, and also close to mitochondria. Similar results were found in the bone marrow. Our experiments show that the distribution pattern may have a significant impact

Published by American Institute of Physics, Inc., Woodbury, NY 11797

on calculation of the local absorbed dose to organs or individual cells when conventional dosimetry is employed. In the light of the increased interest in energy deposition at the cellular level, the present investigation suggests that autoradiographic techniques are excellent for acquiring localization data necessary for cell-level dosimetry calculations.

INTRODUCTION

The average absorbed dose to a tissue or organ in the body comprises the basic data necessary for risk estimates. The procedures outlined by MIRD, ICRU and ICRP (1-3) assume that the radionuclide, as well as the total energy imparted[a] (4), are uniformly distributed in organs or tissues. Thus, the absorbed dose to all cells in the organ is the same as the calculated mean absorbed dose to the organ. Heterogeneously distributed activity within an organ is not considered. In the case of radionuclides emitting low energy electrons (*i.e.* conversion-, Auger-, and Coster-Kronig electrons), special attention should be paid to the cellular distribution and subcellular decay sites (5-8). In addition to the two γ-rays with energies of 171 and 245 keV, and X ray photons of approximately 24 keV, ^{111}In emits numerous low energy electrons as given in Table I (9), which deposit their energy in small volumes ranging from a few nm for Auger electrons (10) to several cell diameters for the conversion electrons (11).

Many radiopharmaceuticals have, during the two last decades, been labeled with ^{111}In. In the early 1970's, efforts using ^{111}In-chloride for diagnosis of tumors (12-15) and for erythroid marrow scintigraphy (16,17) were performed. Later, different ^{111}In-chelates (*i.e.* oxine[b], tropolone[c], and MERC[d]) were introduced for labeling of different blood cells *in vitro* (18-27). During the 1980's tumor-imaging using labeled monoclonal antibodies expanded considerably, and ^{111}In is still the radionuclide of choice (28-34). Recently blood cell specific monoclonal antibodies labeled with ^{111}In for non-tumor imaging have also been developed (35-40).

---

[a]For radiation protection purposes, the tissue- or organ-average absorbed dose, D_T, is defined as $D_T = \varepsilon_T / m_T$ where ε_T is the total energy imparted in tissue or organ and m_T is the mass of that tissue or organ. The SI unit for absorbed dose is J/kg or Gy.

[b]In-111-TRIS-8-hydroxyquinoline

[c]In-111-2-hydroxy-2,4,6-cycloheptatrenine

[d]In-111-2-Mercaptopyridine-N-Oxide

TABLE I

^{111}In Average Radiation Spectrum[e]

Radiations	Average Energy (keV)	Yield per decay	Range[f] (μm)
Photons			
γ_1	171.3	0.902	
γ_2	245.3	0.940	
K_α X rays	23.1	0.680	
K_β X rays	26.2	0.146	
Conversion electrons			
K-shell, γ_1	114.6	0.0841	194
L,M,N-shells, γ_1	168.0	0.0130	254
K-shell, γ_2	218.6	0.0503	386
L,M,N-shells, γ_2	242.1	0.0097	445
Auger electron groups			
KLL	19.17	0.1059	8
KLX	22.32	0.0455	10
KXY	25.44	0.0059	13
LXY	2.81	1.0178	0.33
MXY	0.51	1.91	0.03
NXY	0.12	1.13	0.005
Coster-Kronig electron groups[g]			
L-shell	0.182	0.149	0.008
M-shell	0.039	0.925	< 0.002
N-shell	0.012	2.54	<0.001

[e]In-111 decays by electron capture with a half-life of 2.83 d. For a complete decay scheme see Ref. 9.

[f]Ranges for conversion electrons are taken from Ref. 11 and is the x_{90} value (*i.e.* the radius of a sphere in which 90% of the electron energy is absorbed) Ranges for Auger- and Coster Kronig electrons are calculated from Ref. 10.

[g]Data taken from Ref. 48.

Although it is likely that many radiopharmaceuticals are not distributed homogeneously and concentrate in parts of an organ, and in or adjacent to specific cells, only few studies have dealt with tissue and cellular localization studies after intravenously injected radiopharmaceuticals (41-43). For radiosensitive cells in organs such as the reproductive systems or the red bone marrow, localization studies are of prime importance. Recent radiobiological *in vivo* experiments have demonstrated that ^{111}In may have severe radiotoxicity to cells. The deleterious effect of ^{111}In was first noticed after ^{111}In-oxine labeling of lymphocytes (44-46). The radionuclide was found to bind firmly to cellular components and to some extent to DNA (47). The first experiment showing the enhanced biological effect of ^{111}In *in vivo* was reported by Rao *et al.* (48,49) where the cytotoxicity of ^{111}In-oxine, ^{111}In-citrate, and ^{114m}In-citrate were studied using mouse spermatogenesis and oogenesis as the models. They reported a significant decrease in survival of sperm heads and loss in the testes weight after intratesticular injection of ^{111}In-oxine. Similar results have been found in rat testes after intratesticular injection of oxine labeled with either ^{111}In (50) or ^{110}In (51). Later it has also been reported that internalized ^{111}In induced sperm head abnormalities (52). Few published studies, however, have demonstrated activity in the testicular cells after intravenously administered ^{111}In-radiopharmaceuticals. After intravenous injections of ^{111}In labeled compounds, a small portion (~ 0.5%) of the injected activity localizes in the testes and clears with a prolonged effective half-life (53,54). Jackson *et al.* (55) found that after injection of ^{114m}In labeled leukemia cells, minute amounts of ^{114m}In deposited in the testes and entirely destroyed the seminiferous tubules by 120 days. They also reported that ^{114m}In-oxine in plasma damaged the stem cell spermatogonia.

Consequently, there may be good reasons to suspect an inhomogeneous distribution and long term accumulation of indium isotopes in the testes, and that the indium atoms can be internalized by various cells. To date, no studies have reported data relevant to nuclear medicine practice (*i.e.* on the cellular distribution in the testes or other organs after intravenous injection of ^{111}In labeled radiopharmaceuticals).

The structure of the mammalian testes is characterized by the seminiferous tubules and the interstitial tissue (56). The epithelium consists of supporting Sertoli cells and cells that constitute the spermatogenic lineage (*i.e.* spermatogonial stem cells, differentiating spermatogonia, spermatocytes, spermatids and spermatozoa). The spermatogonia represent the proliferative stage of spermatogenesis and are identified as very radiosensitive cells (57,58).

The Sertoli cells are found in the basal membrane of the seminiferous tubules extending towards the lumen. These cells maintain a microenvironment suitable for the spermatogenic cells. The space between the seminiferous tubules is occupied by interstitial cells (*i.e.* Leydig cells and tissue macrophages, as well as connective tissue, nerves, blood and lymphatic vessels).

The International Commission on Radiological Protection (ICRP) (59,60), approximates the uptake of ionic indium as being divided between four major organs; kidneys (0.07), liver (0.2), red bone marrow (0.3) and spleen (0.01). The remaining fraction is assumed to be uniformly distributed through all other organs and tissues in the body. The red bone marrow is of significant importance for radiation protection. The bone marrow is, after the blood itself, the largest and most widely dispersed tissue in the body. The two components recognized in the bone marrow are hematopoietic cords that comprise the majority of the cellular elements, and the stroma cells that support the proliferation of hematopoietic cells. Different cells, including erythrocytes, granular leukocytes, monocytes, and platelets, are derived from stem cells in the red bone marrow, which are known to be very radiosensitive (61,62). Since ^{111}In, now recognized as radiotoxic when accumulated in the testes, is also taken up in a considerable amount in the red bone marrow, more detailed studies of the tissue and cellular localization after intravenous injections of ^{111}In-labeled agents are extremely important.

Here we report results from investigations of the activity distribution in various organ after intravenous administration of ^{111}In-radiopharmaceuticals into rats. Whole-body autoradiography (WBARG) as well as studies of the cellular and subcellular localization using light- and electron microscope autoradiography (LMARG and EMARG) were performed on testes and red bone marrow. In the cellular case we used ^{114m}In because of its longer half-life.

MATERIALS AND METHODS

Macro-autoradiography

Male Wistar rats (MOELLEGAARD Breeding Centre, Denmark) weighing approximately 220 g were used in this study. The animals had free

access to food and water *ad libitum*. Animals were sacrificed by inhalation of carbon dioxide.

The animals were given intravenous injections (0.2 ml) of either 18.5 MBq ^{111}In-chloride (pH 2), ^{111}In-oxine, or ^{111}In-tropolone (Mallinckrodt Diagnostica, Petten, Holland), or 25 MBq of ^{111}In-CEA-F(ab')$_2$ BW431/31 (Scintimun®, Behringwerke, Marburg, Germany). The method used for whole-body autoradiography (WBARG) has been given in detail elsewhere (63) and is only described briefly. Five days after injection the rats were killed and immediately immersed in a -70°C freezing mixture of liquid hexane and solid carbon dioxide for 5 min. The animal was then horizontally attached to a cryomicrotome stage surrounded by a metal frame and embedded in carboxymethyl cellulose (CMC) by freezing in hexane. From the animals 25 sections each 20 and 60 µm thick were cut with a cryomicrotome (LKB PMV 2250) and picked-up on an adhesive tape (Scotch 3M No. 810). After freeze-drying the sections were attached to X-ray films (Structurix D7, Agfa-Geavert, Germany) and put into cassettes. After an exposure time of 2 weeks the films were developed and fixed.

The autoradiographs from the WBARG-rats were analyzed with a digital image analyzing system especially adapted for whole-body autoradiography (64). The image sampling device was a video-camera (Phillips LDH 400/61) on an adjustable mounting above a light box (Novalux A4E, Photron, Sweden). The video signal was transferred to a microcomputer (Cromemco System 2-HD) via an image digitizer (384 X 241 pixels and 256 gray levels). Using a digitizer pad, regions of interest (ROI) were indicated on a stored autoradiographic image, and the gray-level distribution displayed as a pixel histogram (y-axis) as a function of the gray-levels (x-axis).

All autoradiographs were examined qualitatively, searching for activity uptakes and distribution patterns in various tissues and organs. Selected autoradiographs were examined in detail quantitatively using the digital imaging system. After a software controlled calibration for accurate measurements of the optical density, several consecutive autoradiographs were digitized and images stored in the computer. The contrast of the image was enhanced and regions of interest (ROI) were chosen over a specific organ to generate a histogram representing the gray-scale distribution (*i.e.* the number of pixels as a function of optical density). The histogram was scanned with different selected "windows" and detailed information about the location, mean optical density and its standard deviation, and the number of

pixels within the selected window were displayed. The optical density of consecutive small selected windows was, after correction for background density, divided by the mean optical density for the whole ROI area. Thus, an estimate of the activity concentration ratios in different parts of the organ was obtained. The activity distribution was then expressed as the fraction of a tissue area with a specific activity concentration ratio (65).

Micro-autoradiography

One rat was intravenously injected with 18.5 MBq ^{114m}In-chloride in 0.5 M HCl (DuPont de Nemours & Co. Inc., Wilmington, Delaware, USA) in a volume of 0.2 ml. Twenty four hours after injection the rat was killed and small samples (1-2 mm^3) from the testes and from the bone marrow of the femur were rapidly removed and immediately fixed in 2.5% glutaraldehyde in 0.1 M sodium cacodylate buffer (pH 7.2, 1 h, 4°C). Post-fixation was done in 1% osmium tetroxide in the same buffer (1 h, 4°C). After rinsing, the tissue fragments were dehydrated in graded series of acetone, embedded in Epon overnight, and finally sectioned for light and electron microscope autoradiography.

For light microscope autoradiography 1 μm sections were covered with in ILFORD K2 liquid nuclear emulsion according to the dipping method, and the autoradiographs were exposed for 2-4 weeks at 4°C. They were developed in Kodak D-19 (5 min, 18°C), briefly rinsed in distilled water, and fixed in Kodak F-24 (6 min, 18°C). After a final rinsing, they were stained through the film with Richardson's azure II and methylene blue, and mounted in DePeX.

The ultrathin sections for electron microscope autoradiography were first coated with a monolayer of ILFORD L4 liquid nuclear emulsion according to the loop method and exposed for 1-3 months at 4°C. The autoradiographs were developed in Kodak D-19 (2 min, 20°C), rinsed in distilled water (30 s, 20°C), fixed in newly made 15% $Na_2S_2O_3$ (3 min, 20°C), and finally washed in distilled water. They were examined with a JEOL 100CX electron microscope at the Unit of Electron Microscopy, Department of Zoology, University of Lund. Control samples from an unlabeled animal were fixed and prepared for autoradiography in exactly the same manner as the radiolabeled samples. The background level of silver grains in these autoradiographs was insignificant.

A total of 20 autoradiographs of germ cells from different parts of the seminiferous tubule and from the red bone marrow were documented in a systematic random manner.

RESULTS

The patterns of activity distribution for ^{111}In after intravenous injections into rats are almost the same after a few days regardless of the radiopharmaceutical injected. In general, numerous tissues contain significant uptake of ^{111}In which can be seen in Fig. 1A. The whole-body autoradiograph in panel A shows the activity distribution after injection of ^{111}In-chloride, and is also representative for the other substances injected. ^{111}In is strongly accumulated in rapidly proliferating tissues such as bone marrow, intestinal walls, testes, skin, and the pulp cavity of the incisor teeth. High concentrations of activity are also found in the liver and spleen. No blackening at all is seen over the brain or in the intestines. The major difference between the different radiochemicals is the rate of blood elimination which is relatively slow after injection of ^{111}In-oxine (54). This is because ^{111}In-oxine very rapidly labels circulating erythrocytes, resulting in a longer retention time. For the other substances, however, the blood elimination is fast and no activity can be seen in the blood (see heart chamber in Fig. 1).

The autoradiographic results are confirmed by biokinetic studies (53,54) with the same substances used in the present study. Almost the same activity concentrations were found in various organs at day 5 regardless of the compound injected (Table II). A large difference was found, however, for the uptake in liver and spleen in the case of ^{111}In-oxine which was due to the labeled erythrocytes as mentioned above. In other autoradiographic experiments we also found a considerable accumulation in the liver and spleen after injection of ^{111}In-labeled leukocytes and platelets (data not presented).

A marked heterogeneous distribution of ^{111}In-activity is found in some organs. The distribution in the testes is complex (Fig. 1, panel B). In the bone marrow (Fig. 1, panel C) several hot spots were found, while in the spleen (Fig. 1, panel D) activity is mainly localized in the red pulp. Histograms from quantitatively examined autoradiographs of saggital sections of the testes, bone marrow, and spleen are presented in Figs. 2A-2I for the ^{111}In-

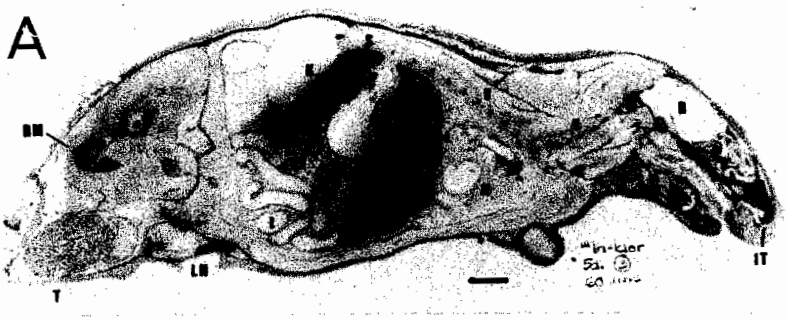

FIG. 1A. Representative whole-body autoradiograph of a rat 5 days after I.V. injection of ^{111}In-chloride. Significant concentrations of activity are seen in numerous organs. It should be noted that many of the organs that accumulated ^{111}In are characterized by areas of rapid cell proliferation. Abbreviations are; T=testes, BM=bone marrow, K=kidney, LN=lymph nodes, L=liver, V=vertebrae (bone marrow) S=spleen, I=intestines, H=heart, B=brain, and IT= incisor teeth (pulp cavity). Bar=10mm.

FIG. 1B. Illustration of the marked heterogeneous distribution of activity in the testes. The activity which has been transported into the testes as ^{111}In-transferrin is mainly localized in a network pattern, apparently representing the tubule of the testes. The image is contrast enhanced for clarity.

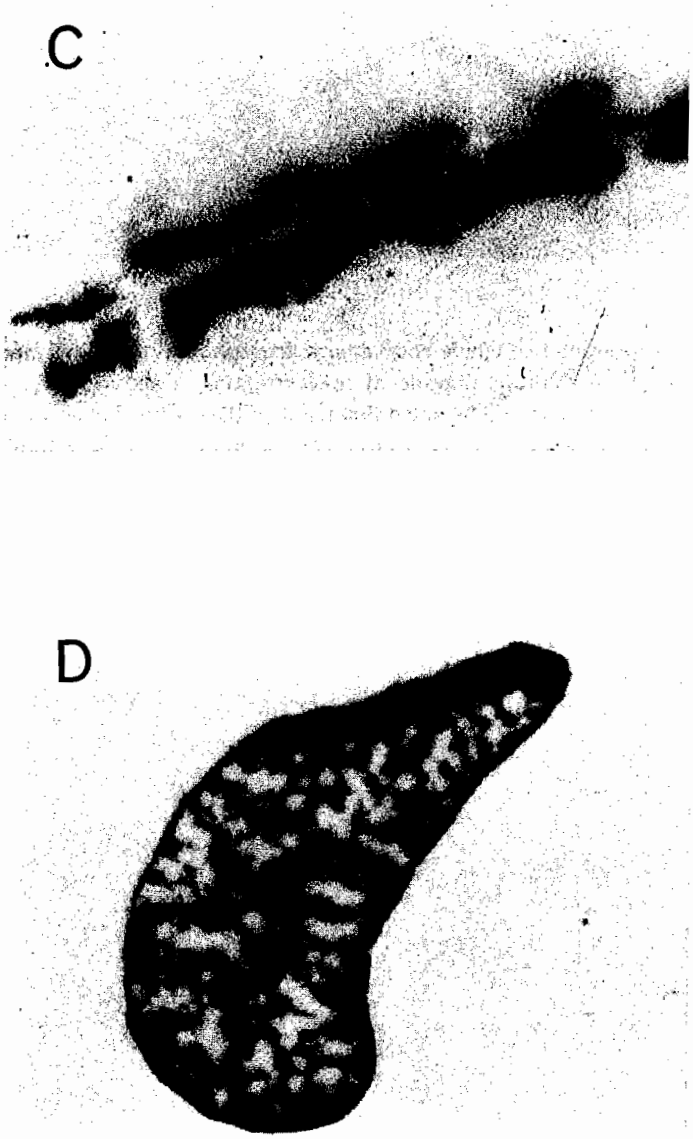

FIGS. 1C-1D. Illustrations above show the marked heterogeneous distribution of activity in the bone marrow in vertebral column (panel C), and spleen (panel D). The red and white pulp in the spleen are easily distinguished. Images are contrast enhanced for clarity.

radiopharmaceuticals. The diagrams illustrate the fraction of pixels in an ROI with a specific optical density, normalized to the mean optical density of the whole ROI-area (typically the whole tissue area of the autoradiograph). The width of the bars is approximately one standard deviation. In this manner, an estimation of the heterogeneity in the organ may be made at a macroscopic level. It should be noted that a similar pattern was found regardless of the radiocompound. In the testes (Figs. 2A-2C) at least half of the area has an optical density equal to that of the mean, although there were areas with significantly greater or lesser optical density. In the bone marrow (Figs. 2D-2F) about one third of the area corresponds to the mean optical density and several hot or cold spots are located irregularly in the tissue. The optical

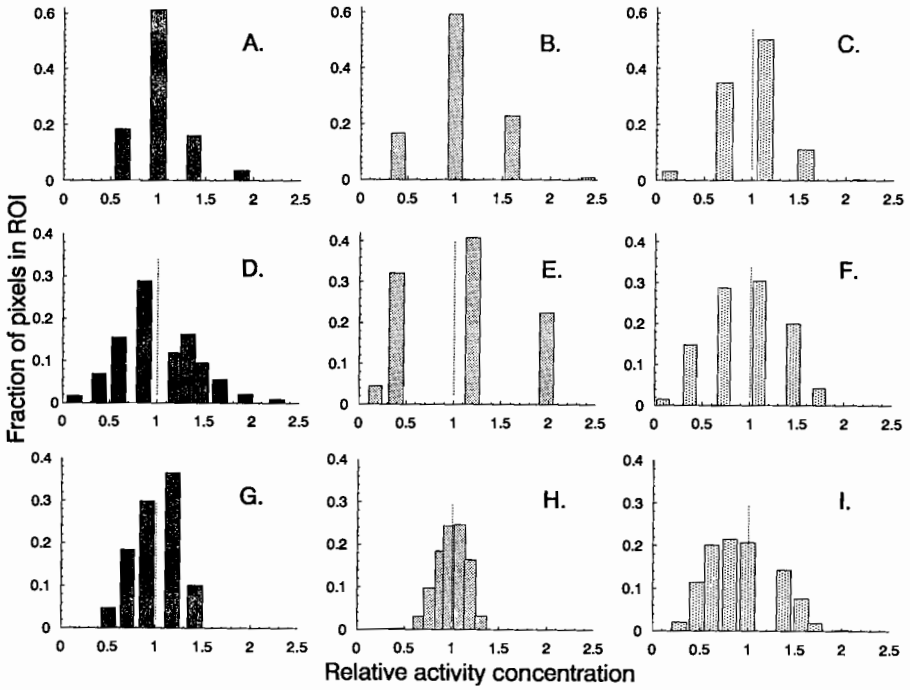

FIG. 2. Diagrams showing the fraction of pixels in an ROI with a measured optical density (specific activity) normalized to the mean optical density of the whole ROI. Left column: ^{111}In-chloride; middle column: ^{111}In-oxine; and right column: ^{111}In-CEA-F(ab')$_2$. Histograms A-C testes, D-F red bone marrow, and G-I spleen. The width of the bars is one standard deviation.

density of the spleen image (Figs. 2G-2H) is symmetrically scattered around the mean optical density, meaning that the organ contains either black or white areas that correspond to either abundant or deficit activity relative to the mean.

Representative autoradiographs of the activity uptake and distribution at the cellular level in the testes and bone marrow are shown in Figs. 3A and 3B, respectively. High concentrations of silver grains can be seen over and around the interstitial cells in the testes, but also over cells in the seminiferous tubule. Cells in the bone marrow are accumulating an extensive amount of indium (Fig. 3B), but in these cells the grains seem relatively uniformly distributed.

The electron microscope autoradiographs confirmed the suspicions that indium isotopes are internalized and retained in tissue cells. The results show that ^{114m}In accumulated in spermatogonia and in bone marrow cells as shown in Figs. 4A and 4B, respectively. In the spermatogonia, grains were found over the cell nucleus and in its immediate vicinity, as well as close to mitochondria.

DISCUSSION

The results in the present study represent situations in which the absorbed dose calculation based on conventional methods may underestimate or overestimate the absorbed dose to a fraction of cells in a specific organ. This may be particularly important if the cells to which the absorbed doses are underestimated are radiosensitive cells such as the hematopoietic stem cells in the red bone marrow or germ cells in the reproductive system. In light of the results in this paper, attention should be paid especially in situations where radionuclides emitting low-energy electrons are internalized by the cell.

Many physiologic and biochemical factors influence the *in vivo* localization and retention of a radiolabeled compound. In parallel studies we have found that the elimination of ^{111}In from tissues that have accumulated ^{111}In is slow (53,54). It has previously been established that ionic indium, like iron and gallium isotopes, binds to transferrin (Trf) in the plasma (66-68), and later is trans-chelated to this glycoprotein from different radiochelates and antibodies (69-71). It is likely that ^{111}In-transferrin identifies cells expressing

TABLE II
Percent Injected Activity in Rat Organs 5 Days Post-injection

Organ	^{111}In-Radiopharmaceutical				
	Chloride (n=7)	Oxine (n=3)	Tropolone (n=3)	CEA-F(ab')$_2$ (n=7)	
Testes	0.27±0.04	0.16±0.04	0.20±0.04	0.30±0.06	%/g
	(0.36±0.02)	(0.22±0.01)	(0.29±0.04)	(0.43±0.06)	%
Bone Marrow	1.00±0.05	0.91±0.04	0.85±0.04	0.93±0.095	%/g
	(7.38±0.35)	(6.78±0.29)	(5.89±0.71)	(7.42±0.74)	%
Spleen	1.18±0.04	4.76±0.04	1.68±0.04	1.62±0.06	%/g
	(1.00±0.04)	(2.24±0.10)	(1.02±0.10)	(1.05±0.10)	%
Liver	1.18±0.04	5.27±0.04	0.92±0.04	0.56±0.06	%/g
	(12.44±0.42)	(35.69±1.52)	(9.79±0.31)	(6.81±1.02)	%

transferrin receptors, TrfR, (72,73) and is taken up by receptor-mediated endocytosis (74-76). It is interesting to note that significant accumulation of indium takes place in tissues with cells expressing a large number of transferrin receptors, thus making them potential targets for ^{111}In-transferrin.

Notable tissues expressing transferrin receptors are the spleen and hematopoietic tissue, especially precursors to erythrocytes (77-79), basal epidermis, germ cells in the seminiferous tubules of the testis, Kupffer cells and hepatocytes. Macrophages in several tissues also appear to express receptors for transferrin (72). Presence of high affinity TrfRs on both murine and human macrophages has recently been confirmed, and it is assumed that TrfR expression may reflect macrophage immune activation (80). Monocyte-macrophages, together with other cells of the reticuloendothelial system, play a key role in the storage of iron, which is mostly derived from the breakdown of senescent red blood cells. This may explain the higher accumulation in the case of administered ^{111}In-oxine as described above. Transferrin receptors

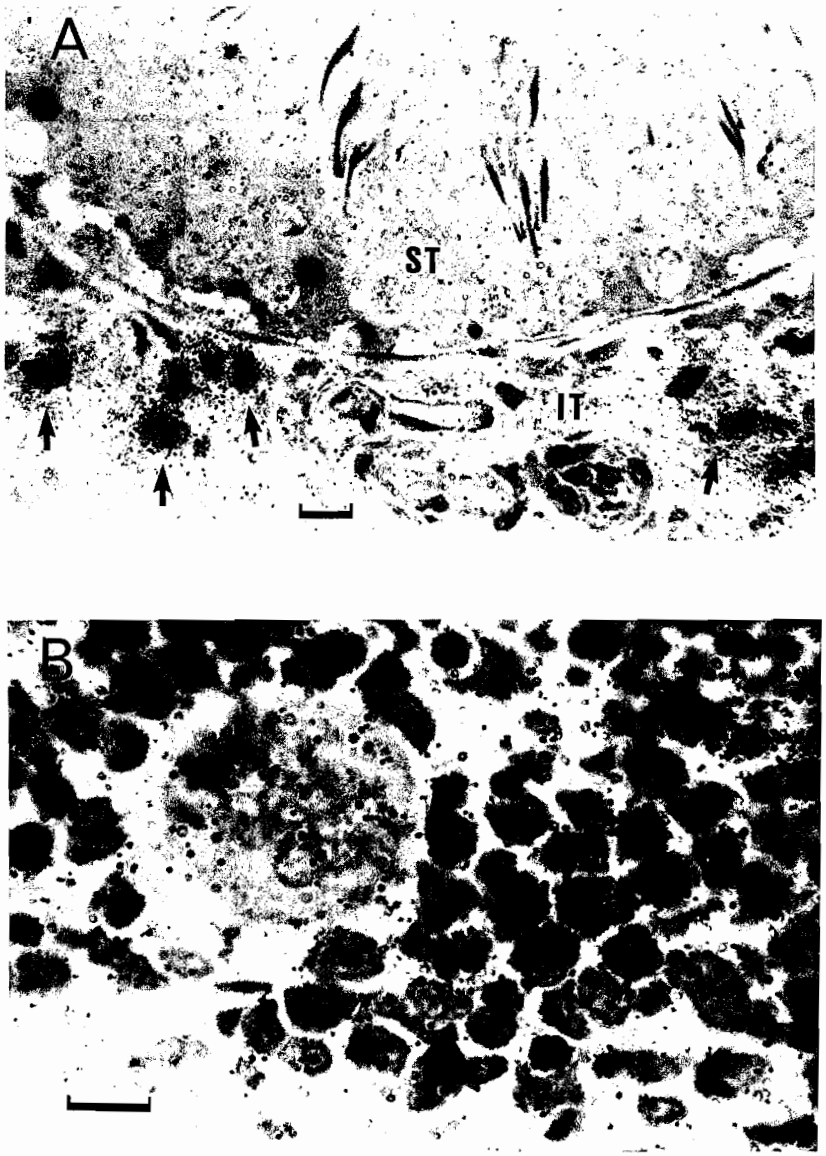

FIG. 3. Light-microscope autoradiographs illustrating the cellular localization of ^{114m}In in rat testes (A) and in a part of the red bone marrow (B). Several heavily labeled macrophages (arrows) are apparent in the interstitial tissue (IT) of the testes. Silver grains are also overlying cells in the seminiferous tubule (ST). The grains over the bone marrow cells seem to be relatively uniform, but some cells have a more intense accumulation. The large cell to the left is a megakaryocyte. Epon sections are stained with Richardson's azure II and methylene blue. Bars=10 μm.

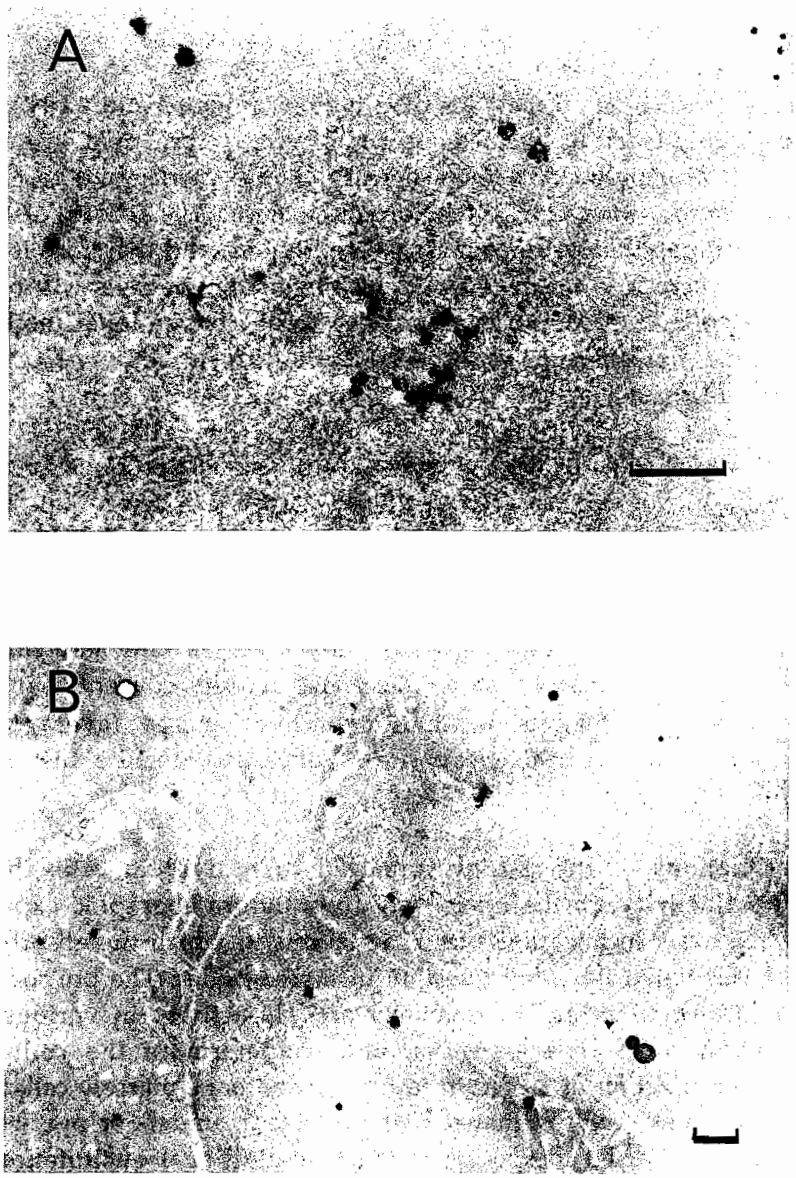

FIG. 4. Electron microscope autoradiographs showing uptake of ^{114m}In activity in a spermatogonial cell nucleus (A), and in bone marrow cells (B). In the spermatogonia silver grains were frequently found in the cell nucleus and its immediate vicinity. Bars=1 μm.

have also been identified in ovarian follicular cells (81). In the testes, Sertoli cells in the seminiferous tubules synthesize transferrin for delivery of iron to the developing germ cells (82), and may also be responsible for the transport of indium across the blood/testis barrier.

In our investigation the ^{111}In distribution in organs and parts of organs was measured in terms of the mean optical density. In principle, if the activity is uniformly distributed, the mean density should correspond to the mean absorbed dose to the organ or subregion of the organ. The activity distribution is, however, highly heterogeneous in several organs, and therefore it is likely that the absorbed dose to several cell clusters and single cells will be higher than the calculated average absorbed dose using conventional methods. At the same time, however, the absorbed dose to cells in "activity-free" regions will be overestimated.

It is possible to convert the measured optical density to cumulated activity (kBq-h) per unit area or, as in Fig. 5, per unit mass (65). Then the activity concentration for specific regions may be calculated and used as basic data for calculation of macroscopic absorbed doses to large cell clusters with an appropriate cell-to-cell calculation method (83-85). It is also possible to count grains in the micro-autoradiographs, however we did not make any estimation of the intracellular-to-extracellular activity concentration in this study because ^{114m}In emits β-radiation of high energy (average energy 777 keV) and therefore the decay site is uncertain despite the thin film emulsion.

Estimations of the energy imparted to individual cells that have accumulated activity can be made only from autoradiographic experiments showing the exact localization sites. The targets to which the absorbed dose should be calculated is a vital question in these studies. The purpose of this study was to examine the heterogeneity of ^{111}In-activity in various organs after injections of ^{111}In-substances, and to determine the cellular and subcellular localization of ^{114m}In in testes and red bone marrow cells. We did not, however, make any estimates of the degree of under- or over-estimates of the energy imparted to specific cells since additional quantitation of the cellular uptake should be done first with both microscopic autoradiography and subcellular fractionation before reliable and accurate calculations can be done.

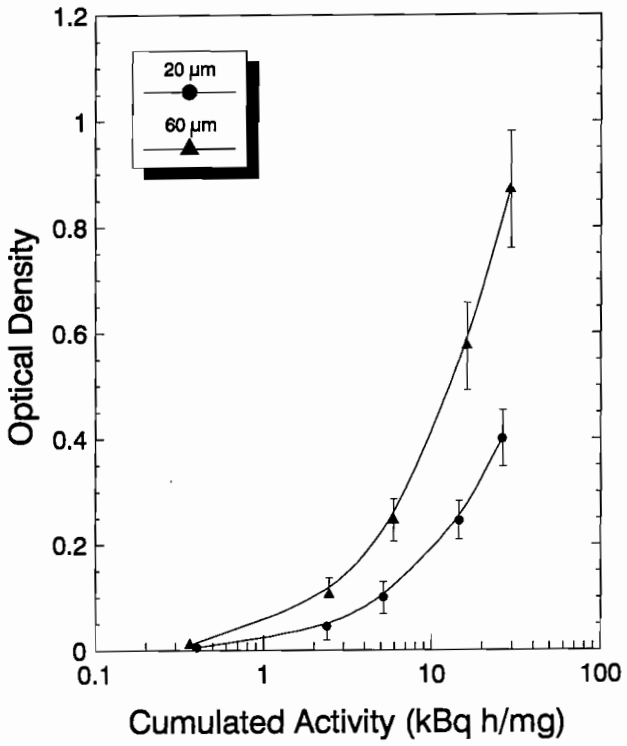

FIG. 5. Calibration curve for the autoradiographic film (Structurix D7) plotting optical density vs. cumulated ^{111}In-activity (*i.e.* exposure). Sectioned liver-homogenates with activities ranging from 3 to 300 Bq/mg, and of 20 µm and 60 µm were used for the calibration (65).

We found significant amounts of activity in interstitial cells, identified as macrophages. Very little is known about their differential radiosensitivity, although they are thought to be less radiosensitive than other hematopoietic cells (62). Spermatogonia are, however, known to be very radiosensitive, and it is interesting to note that besides activity in spermatogonia, the intense accumulation of indium in testicular interstitial cells may irradiate not only themselves, but also continuously expose stem cells and other cells in the spermatogenic cell lineage that are in the seminiferous tubule. Numerous cells in the bone marrow have been shown to accumulate large amounts of activity in both the cytoplasm and nucleus. In this study the cellular activity was not quantified, nor was the identity of the cells determined, but such investigations are presently under way.

CONCLUSIONS

In this new era of radiation protection (*i.e.* cell-level dosimetry) we must perform careful investigations of the cellular distribution of radioactivity and try to understand the biological behavior of different compounds at a microscopic level. In some cases it may be possible to use such data to introduce a dose-enhancement factor (5) specific for the radiopharmaceutical in question. In other cases, the high activity concentration in certain cells may need to be considered more harmful than we earlier thought it to be.

In conclusion, this study was the first attempt to examine the tissue distribution and cellular and subcellular localization after intravenously injected ^{111}In-radiopharmaceuticals. It was found that the activity was accumulated in a strikingly heterogeneous fashion in numerous organs and tissues. Thus, our experiments demonstrate that the distribution pattern may have a significant impact on calculation of the average absorbed dose to organs or individual cells, using conventional dosimetry. Finally, we suggest that autoradiographic techniques are excellent methods for acquiring localization data necessary for small scale dosimetry.

ACKNOWLEDGMENTS

The authors gratefully acknowledge the assistance of Mrs. Marianne Palmegren, at the Unit of Electron Microscopy, Department of Oncology, University of Lund. This work was in part supported by grants from the John and Augusta Persson Foundation for Medical Research, Lund, The Royal Physiographic Society, Lund, the Mrs. Berta Kamprad Foundation for Cancer Research, Lund, the Medical Faculty of Lund, and the Swedish Cancer Foundation, grant no. 2353-B91-05XAB and 3010-B91-01X.

REFERENCES

1. R. LOEVINGER and M. BERMAN, A revised schema for calculation of the absorbed dose from biologically distributed radionuclides. *MIRD Phamplet No. 1*, Revised. New York, Society of Nuclear Medicine, March 1976.

2. ICRU, *Methods of Assessment of Absorbed Dose in Clinical Use of Radionuclides*, Report 32, International Commission on Radiation Units and Measurements, Washington, D.C., 1979.
3. ICRP, *Radiation Dose to Patients from Radiopharmaceuticals*, Publication 53, The International Commission on Radiological protection Oxford, England: Pergamon Press, 1987.
4. ICRU, *Microdosimetry*, Report 36, International Commission on Radiation Units and Measurements Bethesda, MD, 1983.
5. D.V. RAO, G.F. GOVELITZ, and K.S.R. SASTRY, Radiotoxicity of thallium-201 in mouse testes: Inadequacy of conventional dosimetry. *J. Nucl. Med.* **24**, 145-153 (1983).
6. A.I. KASSIS, S.J. ADELSTEIN, C. HAYDOCK, and K.S.R. SASTRY, Thallium-201: an experimental and theoretical radiobiological approach to dosimetry. *J. Nucl. Med.* **24**, 1164-1175 (1983).
7. S.J. ADELSTEIN, A.I. KASSIS, and K.S.R. SASTRY, Cellular versus organ approaches to dose estimates. In *Proceedings of the Fourth Intenational Radiopharmaceutical Dosimetry Symposium* (A.T. Schlafke-Stelson and E.E. Watson, Eds.) Oak Ridge, TN, November 5-8, 1985; Oak Ridge: Oak Ridge Associated Universities, 1986:13-25. [CONF-851113-(DE86010102)].
8. G. MAKRIGIORGOS, S.J. ADELSTEIN, and A.I. KASSIS, Auger electron emitters: Insights gained from *in vitro* experiments. *Radiat. Environ. Biophys.* **29**, 75-91 (1990).
9. D.A. WEBER, K.F. ECKERMAN, L.T. DILLMAN, and J.C. RYMAN, *MIRD: Radionuclide data and decay schemes*. The Society of Nuclear Medicine, Inc. New York, 1989.
10. A. COLE, Absorption of 20-eV to 50,000-eV electron beams in air and plastic. *Radiat. Res.* **38**, 7-33 (1969).
11. M.J. BERGER, Distribution of absorbed dose around point sources and beta-particles in water and other media. *J. Nucl. Med.* (Suppl. No. 5), MIRD Pamphlet No. 7, 5-23 (1971).
12. W.W. HUNTER and X.J. RICCOBONO, Clinical evaluation of ^{111}In for localization of recognized neoplastic disease. *J. Nucl. Med.* **11**, 328 (1970).
13. D.A. GOODWIN, C.J. IMBORNE, and C.H. SONG, Comparative study of tumor and organ distribution of ^{111}In- and ^{67}Ga-labeled compounds in mice. *J. Nucl. Med.* **12**, 434 (1971).
14. D.A. GOODWIN, R. GOODE, L. BROWN, and C.J. IMBORNE, Indium-111-labeled transferrin for the detection of tumors. *Radiology*. **100**, 175-179 (1971).
15. P.A. FARRER, G.B. SAHA, and H.N. SHIBITA, Evaluation of ^{111}In-transferrin as a tumor scanning agent in humans. *J. Nucl. Med.* **13**, 429 (1972).
16. D.L. LILLIEN, H.G. BERGER, D.P. ANDERSON, and L.R. BENNETT, Indium-111-chloride: a new agent for bone marrow imaging. *J. Nucl. Med.* **14**, 184-186 (1973).
17. E.H. GILBERT, J.D. EARLE, M.L. GORIS, H.S. KAPLAN, and J.P. KRISS, The accuracy of ^{111}In-Cl3 as a bone marrow scanning agent. *Radiology*. **119**, 167-168 (1976).
18. M.L. THAKUR, J.P. LAVENDER, R.N. ARNOT, D.J. SILVESTER, and A.W. SEGAL, Indium-111-labeled autologous leukocytes in man. *J. Nucl. Med.* **18**, 1012-1019 (1977).
19 U. SCHEFFEL, P.A. MCINTYRE, B. EVATT, J.A. DVORNICKY, T.K. NATARAJAN, D.R. BOLLING, and E.A. MURPHY, Evaluation of Indium-111 as a new high photon

yield gamma-emitting "physiological" platelet label. *John Hopkins Med. J.* **140**, 285-293 (1977).

20. U. SCHEFFEL, M-F. TSAN, and PA. MCINTYRE, Labeling of human platelets with (111-In) 8-Hydroxyquinoline. *J. Nucl. Med.* **20**, 524-531 (1979).
21. M.K. DEWANJEE, S.A. RAO, and P. DISISHEIM, Indium-111 tropolone, a new high-affinity platelet label: Preparation and evaluation of labeling parameters. *J. Nucl. Med.* **22**, 981-987 (1981).
22. M.L. THAKUR, L. WALSH, H.L. MALECH, and A. GOTTSCHALK, Indium-111-labeled human platelets: improved method, efficacy and evaluation. *J. Nucl. Med.* **22**, 381-385 (1981).
23. J.E.T. BURKE, S. ROATH, D. ACKERY, and P. WYETH, The comparison of 8-hydroxyquinoline, tropolone, and acetylacetone as mediators in the labelling of polymorphonuclear leukocytes with Indium-111: A functional study. *Eur. J. Nucl. Med.* **7**, 73-76 (1982).
24. G.L. DETTMAN, B.L. VANDENBURG, R.D. JOHNSON, and G.W. MEYER, Indium-111-oxine labeled mouse spleen cells. *Int. J. Nucl. Med. Biol.* **8**, 137-144 (1981).
25. R.J.M. TENBERGE, A.T. NATARAJAN, S.L. YONG, M.R. HARDEMAN, E.A. VAN ROYEN, and P.Th.A. SCHELLEKENS, Labelling of human lymphocytes with 111-In-oxine. *Nuclear Geneeskundig Bullentin.* **4** (suppl), 18-20 (1982).
26. M.L. THAKUR, Radioisotopic labeling of platelets: A historical perspective. *Sem. Thromb. Hemost.* **9**, 79-85 (1983).
27. A.G. DESAI and M.L. THAKUR, Radiolabeled blood cells: Techniques and applications. *CRC Critical Reviews in Clinical Laboratory Sciences.* **24**, 95-122 (1986).
28. D.S. FAIRWEATHER, A.R. BRADWELL, P.W. DYKES, A.T. VAUGHAN, S.F. WATSON-JAMES, and S. CHANDLER, Improved tumour localization using indium-111 labeled antibodies. *Br. Med. J.* **287**, 167-170 (1983).
29. S.E. HALPERN, P.L. HAGAN, P.R. GARVER, J.A. KOZIOL, A.W.N. CHEN, J.M. FRINCKE, R.M. BARTHOLOMEW, G.S. DAVID, and T.H. ADAMS, Stability, characterization, and kinetics of 111-In-labeled monoclonal antitumor antibodies in normal animals and nude mouse-human tumor models. *Cancer Res.* **43**, 5347-5355 (1983).
30. S.E. HALPERN, The advantages and limits of Indium-111 labeling of antibodies Experimental studies and clinical applications. *Nucl. Med. Biol.* **13**, 195-201 (1986).
31. C.F. MEARES, Chelating agents for the binding of metal ions to antibodies. *Nucl. Med. Biol.* **13**, 311-318 (1986).
32. G.H. HINKLE, J.A. LOESCH, T.L. HILL, S.R. LEFEVRE and J.O. OLSEN, Indium-111-monoclonal antibodies in radioimmunoscintigraphy. *J. Nucl. Med. Tech.* **18**, 16-28 (1990).
33. D.J. HNATOWICH, Antibody radiolabeling, problems and promises. *Nucl. Med. Biol.* **17**, 49-55 (1990).
34. D.M. GOLDENBERG, In-vivo antibody imaging for detection of human tumors. In *Cancer Imaging with Radiolabeled Antibodies.* (D.M. Goldenberg, Eds.) pp. 293-312. Kluwer Academic Publishers, Norwell, MA, 1990.
35. Z.H. OSTER, S.C. SRIVASTAVA, P. SOM, G.E. MEINKEN, L.E. SCUDDER, K. YAMAMOTO, H.L. ATKINS, A.B. BRILL, and B.S. COLLER, Thrombus radioimmunoscintigraphy: An approach using monoclonal antiplatelet antibody. *Proc. Natl. Acad. Sci. USA.* **82**, 3465-3468 (1985).

36. A.M. PETERS, J.P. LAVENDER, S.G. NEEDHAM, I. LOUTFI, D. SNOOK, A.A. EPENETOS, P. LUMLEY, R.J. KEERY, and N. HOGG, Imaging thrombus with radiolabeled monoclonal antibody to platelets. *Br. Med. J.* **293**, 1525-1527 (1986).
37. M.L. THAKUR, P. THIAGARAJAN, F. WHITE III, C.H. PARK, and P.H. MAURER, Monoclonal antibodies for specific cell labeling: considerations, preparations and preliminary evaluation. *Nucl. Med. Biol.* **14**, 51-58 (1987).
38. M.L. THAKUR, M.D. RICHARD, and F.W. WHITE III, Monoclonal antibodies as agents for selective radiolabelling of human neutrophils. *J. Nucl. Med.* **29**, 1817-1825 (1988).
39. I. LOUTFI, J.R. BATCHELOR, J.P. LAVENDER, and A.A. EPENETOS, Lymphocyte targeting with 111-In-labeled monoclonal antiobodies. *Int. J. Cancer.* **2**, 45-49 (1988).
40. I. LOUTFI, P.M. CHISHOLM, D. BEVAN, and J.P. LAVENDER, *In vivo* imaging of rat lymphocytes with an indium 111-labeled anti-T cell monoclonal antibody: A comparison with indium 111-labeled lymphocytes. *Eur. J. Nucl. Med.* **16**, 69-76 (1990).
41. E. HINDIE, N. COLAS-LINHART, A. PETIET, and B. BOK, Microautoradiographic study of Technetium-99m colloid uptake by the rat liver. *J. Nucl. Med.* **29**, 1118-1121 (1988).
42. G.M. MAKRIGIORGOS, S. ITO, J. BARANOWSKA-KORTYLEWICZ, D.W. VINTER, A. IQBAL, A.D. VAN DEN ABBEELE, S.J. ADELSTEIN, and A.I. KASSIS, Inhomogeneous deposition of radiopharmaceuticals at the cellular level: Experimental evidence and dosimetric implications. *J. Nucl. Med.* **31**, 1358-1363 (1990).
43. B.A. JÖNSSON and S.E. STRAND, Biokinetics and tissue uptake of Indium-111 radiopharmaceuticals evaluated in the rat approaching radiation dosimetry at the cellular level [abstract]. *Eur. J. Nucl. Med. (suppl.)* **16**, S160, (1990).
44. A.W. SEGAL, P. DETEIX, R. GARCIA, P. TOOTH, G.D. ZANELLI, and A.C. ALLISON, Indium-111 labeling of leukocytes: a detrimental effect on neutrophil and lymphocyte function and an improved method of cell labeling. *J. Nucl. Med.* **19**, 1238-1244 (1978).
45. R.J.M. TENBERGE, A.T. NATARAJAN, M.R. HARDEMAN, E.A. VANROYEN, and P.TH.A. SCHELLEKENS, Labeling with Indium-111 has detrimental effects on human lymphocytes: concise communication. *J. Nucl. Med.* **24**, 615-620 (1983).
46. M. MEIGNAN and E. WIRQUIN, Lymphocyte radiolabeling: A challenge to their survival (letters to the editor). *J. Nucl. Med.* **28**, 1228-1229 (1987).
47. M.L. THAKUR, A.W. SEGAL, L. WELCH, M.J. LOUIS, J. HOPKINS, and T.J. PETERS, Indium-111-labeled cellular blood components: Mechanism of labeling and intracellular location in human neutrophils. *J. Nucl. Med.* **18**, 1020-1024 (1977).
48. D.V. RAO, K.S.R. SASTRY, H.E. GRIMMOND, R.W. HOWELL, G. GOVELITZ, V.K. LANKA, and V.B. MYLAVARAPU, Cytotoxicity of some indium radiopharmaceuticals in mouse testes. *J. Nucl. Med.* **29**, 375-384 (1988).
49. D.V. RAO, V.B. MYLAVARAPU, K.S.R. SASTRY. Internal Auger emitters: Effects on spermatogenesis and oogenesis in mice. In *DNA Damage by Auger Emitters* (K.F. Baverstock and D.E. Charlton, Eds), pp. 15-26. Taylor & Francis, London, 1988.
50. G. GRAFSTRÖM, A.M. EL HASSAN, B.A. JÖNSSON, S.E. STRAND, and J. TENNVALL, Rat testes as a radiobiological *in vivo* model for Auger electron emitting radionuclides. (Submitted).

51. G. GRAFSTRÖM, S.E. STRAND, J. TENNVALL, B.A. JÖNSSON, and H. LUNDGVIST, Radiobiological effects of ^{110}In versus ^{111}In in the rat testes. This volume.
52. D.V. RAO, V.R. NARRA, R.W. HOWELL, V.K. LANKA, and K.S.R. SASTRY. Induction of sperm head abnormalities by incorporated radionuclides: Dependence on subcellular distribution, type of radiation, dose rate, and presence of radioprotectors. *Radiat. Res.* **125**, 89-97 (1991).
53. B.A. JÖNSSON, S.E. STRAND, and L. ANDERSSON. Radiation dosimetry for ^{111}In-labeled F(ab')$_2$ fragments evaluated from tissue distribution in rats. *J. Nucl. Med.* (In press).
54. B.A. JÖNSSON and S.E. STRAND, Absorbed doses of ^{111}In and ^{114m}In after administration of ^{111}In-complexes with different biokinetics. J. Nucl. Med. (submitted).
55. H. JACKSON, N.C. JACKSON, I.D. MORRIS, and H.L. SHARMA. Intratesticular radionuclide and spermatogenic damage. *Br. Med. J.* **300** (1990).
56. L.C. JUNQUEIRA, J. CARNEIRO, and R.O. KELLEY, In *Basic Histology*, 6th ed. Appleton & Lange, Prentice-Hall International Inc., St. Mateo, CA, 1989.
57. M.L. MEISTRICH, N.R. HUNTER, N. SUZUKI, P.K. TROSTLE, and H.R. WITHERS, Gradual regeneration of mouse testicular stem cells after exposure to ionizing radiation. *Radiat. Res.* **74**, 349-362 (1978).
58. M. BIANCHI, Cytotoxic insult to germinal tissue. Part I. The Testes. In *Cytotoxic Insult to Tissue - Effects on Cell Lineages* (C.S. Potten and J.H. Hendry, Eds.) pp. 258-328, Churchill Livingstone, Edinburgh-London-Melbourne-New York, 1983.
59. ICRP, *Limits for Intakes of Radionuclides by Workers*, Report 30, Part 2, The International Commission on Radiological Protection, Oxford, England:Pergamon Press, 1980.
60. ICRP, *Radiation Dose to Patients from Radiopharmaceuticals*, Report 53, The International Commission on Radiological Protection. Oxford, England: Pergamon Press, 1987.
61. M. TAVASSOLI and J.M. YOFFEY, In *Bone Marrow: Structure and Function*, Alan R. Liss, Inc., New York, 1983.
62. J.H. HENDRY and B.I. LORD, The analysis of early and late response to cytotoxic insults in the haemopoietic cell hiearchy. In *Cytotoxic Insult to Tissue. Effects on cell lineages* (C.S. Potten and J.H. Hendry, Eds.), pp. 1-66, Churchill Livingstone, Edinburgh-London-Melbourne-New York, 1983.
63. S. ULLBERG, B. LARSSON, and H. TJÄVLE, Autoradiography. In *Biological Applications of Radiotracers* (H.J. Glenn and L.G. Colombetti, Eds.), part I, pp. 55-108. CRC Press Inc., Boca Raton, FL, 1982.
64. R. D'ARGY, G.O. SPERBER, B.S. LARSON, and S. ULLBERG. Computer-assisted quantification and image processing of whole body autoradiograms. *J. Pharmacol. Meth.* **24**, 165-181 (1990).
65. B.A. JÖNSSON, S.E. STRAND, and B.S. LARSSON. A quantitative autoradiographic study of the heterogeneous activity distribution of different Indium-111-labeled radiopharmaceuticals. *J. Nucl. Med.* (In press).
66. F. HOSAIN, P.A. McINTYRE, K. POULOSE, H.S. STERN, and H.N. WAGNER JR, Binding of trace amounts of ionic Indium-113m to plasma transferrin. *Clin. Chim. Acta*, **24**, 69-75 (1969).

67. R.D. WOCHNER, M. ADATEPE, A. VAN AMBERG, and E.J. POTCHEN, A new method for estimation of plasma volume with the use of the distribution space of indium-113m-transferrin. *J. Lab. Clin. Med.* **75**, 711-720 (1970).
68. R.W. EVANS and W. OGWANG, Interaction of indium with transferrin. *Biochem. Soc. Trans.* **16**, 833-823 (1988).
69. S.M. YEH, C.F. MEARES, and D.A. GOODWIN, Decomposition rates of radiopharmaceutical indium chelates in serum. *J. Radioanalyt. Chemistry.* **53**, 327-336 (1979).
70. W.C. COLE, S.J. DENARDO, C.F. MEARES, M.J. MCCALL, G.L. DENARDO, A.L. EPSTEIN, H.A. O'BRIEN, and M.K. MOI, Comparative serum stability of radiochelates for antibody radiopharmaceuticals. *J. Nucl. Med.* **28**, 83-90 (1987).
71. D.J. HNATOWICH, Biodistribution of 111-In-Labeled Monoclonal Antibodies - Letters to the Editor. *J. Nucl. Med.* **28**, 1924-1925 (1987).
72. K.C. GATTER, G. BROWN, I.S. TROWBRIDGE, R.E. WOOLSTON, and D.Y. MASON, Transferrin receptors in human tissues: their distribution and possible clinical relevance. *J Clin Pathol.* **36**, 539-545 (1983).
73. H.A. HUEBERS and C.A. FINCH, The physiology of transferrin and transferrin receptors. *Physiol Reviews.* **67**, 520-582 (1987).
74. S.M. LARSON, Z. GRUNBAUM, and J.S. RASEY, The role of transferrins in gallium uptake. *Int. J. Nucl. Med. Biol.* **8**, 257-266 (1981).
75. J.N. OCTAVE, Y.J. SCHNEIDER, A. TROUET, and R.R. CRICHTON, Iron uptake and utilization by mammalian cells. I: Cellular uptake of transferrin and iron. *Trend. Biochem. Sci. (TIBS).* **8**, 217-220 (1983).
76. R. WEINER, The role of transferrin and other receptors in the mechanism of Ga-67 localization. *Nucl. Med. Biol.* **17**, 141-149 (1990).
77. F.M. VAN BOCKXMEER and E.H. MORGAN, Identification of transferrin receptors in reticulocytes. *Biochim. Biophys. Acta.* **468**, 437-450 (1977).
78. S. DE ABREW, Assays for transferrin and transferrin receptors in tumour and other mouse tissues. *J. Nucl. Med. Biol.* **8**, 217-221 (1981).
79. J.N. OCTAVE, Y.J. SCHNEIDER, R.R. CRICHTON, and A. TROUET, Transferrin protein and iron uptake by isolated rat erythroblasts. *FEBS lett.* **137**, 119-123 (1982).
80. U. TESTA, M. PETRINI, M.T. QUARANTA, E. PELOSI-TESTA, G. MASTROBERARDINO, A. CAMAGNA, G. BOCCOLI, M. SARGIACOMO, G. ISACCHI, A. COZZI, P. AROSIO, and C. PESCHE, Iron up-modulates the expression of transferrin receptors during monocyte-macrophage maturation. *J. Biol. Chem.* **264**, 13181-13187 (1989).
81. S.L. ALESHIRE, K.G. OSTEEN, W.S. MAXSON, S.S. ENTMAN, C.A. BRADLEY, and F.F. PARL, Localization of transferrin and its receptor in ovarian follicular cells: morphologic studies in relation to follicular development. *Fertil. Steril.* **51**, 444-449 (1989).
82. C. MORALES, S.R. SYLVESTER, and M.D. GRISWOLD, Transport of iron and transferrin synthesis by seminiferous epithelium of the rat *in vivo*. *Biol. Reprod.* **37**, 995-1005 (1987).
83. K.S.R. SASTRY, C. HAYDOCK, A.M. BASHA, and D.V. RAO, Electron dosimetry for radioimmunotherapy: Optimal electron energy. *Radiat. Prot. Dosim.* **13**, 249-252 (1985).

84. M. MAKRIGIORGOS, S.J. ADELSTEIN, and A.I. KASSIS, Limitations of conventional internal dosimetry at the cellular level. *J. Nucl. Med.* 30, 1856-1864 (1989).

85. R.W. HOWELL, D.V. RAO, and K.S.R. SASTRY, Macroscopic dosimetry for radioimmunotherapy: Nonuniform activity distributions in solid tumors. *Med. Phys.* 16, 66-74 (1989).

DISCUSSION

Laster, B. H. Have you ever observed increased localization of the radiolabel in the adrenal gland? Your autoradiograph shows uptake in nasal epithelium and interstitium of testis which are associated with benzodiapapene receptors.

Strand, S. E. No, But perhaps we should.

Van den Abbeele, A. D. Which chelator did you use to label the monoclonal antibody? Did you see any nuclear localization of activity following injection of the antibody? Which of the ^{111}In labeled compounds showed intranuclear localization? In the case of DTPA, it has been reported that following metabolism in the liver, radiolabeled metabolites remain bound to cytoplasmic components.

Strand, S. E. We obtained our antibodies commercially (Scinhimum, Behringerwerhe, Marberg, Germany) with antibody conjugated with DTPA. So far in our experiments we believe that there is an intracellular and also a nuclear localization, although much smaller than compared to the other results due to the stronger bond between indium and antibody, and thus a much smaller transfer to transferrin.

Kassis, A. I. Being on the MIRD Committee, we have been aware of the possibility of dose nonuniformity for some radiopharmaceuticals. The problem is how to translate these expectations into humans undergoing diagnostic imaging. How will the nonuniform distribution you have seen in the animals be established in patients?

Strand, S. E. I think that we should, as much as possible, obtain tissue biopsies from patients (as we right now are doing for radiolabeled monoclonal antibodies) at the time of surgery. Detailed animal experimental studies must be done in order to extrapolate to the human situation with confirmation with biopsy data if possible.

Biophysical Aspects of Auger Processes, AAPM Symposium Series No. 8 (1992) 273-289
Eds. RW Howell, VR Narra, KSR Sastry, DV Rao

RADIOBIOLOGICAL EFFECTS OF ^{110}In VERSUS ^{111}In IN RAT TESTIS

GUSTAV GRAFSTRÖM[1], SVEN-ERIK STRAND[1], J. TENNVALL[2], BO-ANDERS JÖNSSON[1], and H. LUNDQUIST[3]

Departments of Radiation Physics[1] and Oncology[2]
University Hospital, Lund, Sweden

The Svedberg Laboratory[3]
Uppsala University, Uppsala, Sweden

ABSTRACT

Induction of radiobiological effects after intratesticular (IT) injection of ^{110}In-oxine or ^{111}In-oxine in Wistar rats were evaluated in the present report. These two radionuclides were chosen because of their different energy deposition patterns. ^{110}In is almost a pure β emitter with no Auger electron emission, whereas ^{111}In emits conversion electrons and Auger electrons. The retention of ^{111}In activity in the testis was measured with a scintillation camera and ^{110}In with a collimated HpGe detector. Measurements were performed immediately after IT injection and repeated over several half-lives. Time-activity curves were generated for each animal and these were used for absorbed dose calculations. The resulting D_{37} values for spermhead survival were approximately 1.9 Gy for ^{110}In-oxine, and 2.2 Gy for ^{111}In-oxine.

INTRODUCTION

Various radionuclides decay by electron capture and/or internal conversion. These events are followed by cascades of Auger and Coster-Kronig electrons. Such cascades involve emission of numerous low-energy electrons, which are of very short range. If these radionuclides are incorporated into the cell nucleus, the short-range electrons locally deposit their energy causing high absorbed doses in the proximity to the DNA (2-4).

The rationale for utilizing mammalian testis as an *in vivo* model to study the effects of these radionuclides is the extreme radiosensitivity of the spermatogonial cells compared to other testicular cells (5-7). Rao *et al.* (8-13) have, in various reports, evaluated the radiobiological effects of Auger electron emitters in the mouse testis. A similar model has been established by our group in rat testis (14). The rodent testis model seems appropriate for further investigation of basic phenomenon (such as geometry, intracellular biokinetics and heterogeneity of radioactivity) crucial for understanding the biological effects of Auger electron emitters (14).

A straightforward way of assessing the radiobiological effects of Auger emitters is to compare their effects with radionuclides of the same element having various energy deposition patterns. Our project consequently aims to use the indium isotopes: ^{110}In, ^{111}In, ^{113m}In, ^{114m}In and ^{115m}In. Indium radioisotopes are of great interest in diagnostic and therapeutic nuclear medicine. In the present report we compare the radiobiological effects induced by intratesticularly (IT) injected ^{110}In-oxine and ^{111}In-oxine.

Earlier, electron microscopy studies of our group indicate that intravenously injected indium radiopharmaceuticals localize in the cell nuclei of the testicular cells (15). Similarly, cell fractionation studies show that the fraction of IT injected indium activity found within the cell nuclei was about 60% 6-24 h post-injection (14). Because ^{111}In has a half-life of 2.8 d it has sufficient time to become intracellularly incorporated and therefore the short-ranged Auger electrons (Table I) should exert the major influence on spermatogonial cell killing. Conversely IT-injected ^{110}In, an almost pure β emitter with a half-life of only 69 min (Tables I,II), mostly decays outside the nucleus.

TABLE I

Absorbed Energy from ^{110}In in Rat Testis

Radiation	Energy (MeV)	Yield per decay	ϕ	E_{emit} (MeV)	E_{abs} (MeV)	% E_{tot}
γ_1	0.511	1.23	0.12	0.6285	0.00774	1.2645
γ_2	0.6577	0.978	0.12	0.6432	0.0079	1.2942
γ_3	0.8153	0.0028	0.12	0.0023	0.000028	0.00455
γ_4	0.818	0.0079	0.012	0.00648	0.000078	0.01274
γ_{11}	1.126	0.0102	0.011	0.01149	0.000132	0.02154
γ_{13}	1.236	0.0026	0.012	0.003263	0.000038	0.006131
γ_{16}	1.421	0.0042	0.011	0.005982	0.000065	0.0107
γ_{17}	1.476	0.0047	0.011	0.006922	0.000075	0.01227
γ_{19}	1.103	0.0013	0.011	0.002036	0.000022	0.003544
γ_{23}	1.698	0.0027	0.011	0.004653	0.000049	0.007987
γ_{25}	1.783	0.0028	0.01	0.005064	0.000053	0.008584
γ_{26}	1.975	0.0015	0.01	0.002903	0.000029	0.00478
γ_{27}	2.003	0.0013	0.01	0.002544	0.000025	0.004156
γ_{29}	2.129	0.0213	0.01	0.04535	0.000446	0.07290
γ_{30}	2.211	0.0176	0.01	0.03891	0.000378	0.06174
γ_{31}	2.318	0.0131	0.01	0.03037	0.000029	0.04736
γ_{32}	2.2421	0.0054	0.009	0.01302	0.000122	0.01997
γ_{33}	2.444	0.003	0.009	0.007405	0.000069	0.01131
γ_{34}	2.536	0.0024	0.009	0.00596	0.000055	0.00897
γ_{36}	2.746	0.0009	0.009	0.002337	0.000021	0.003391
γ_{37}	2.787	0.0009	0.009	0.002425	0.000021	0.003486
γ_{38}	2.808	0.0055	0.009	0.01539	0.000135	0.02212
γ_{39}	2.818	0.0006	0.009	0.001818	0.000016	0.002584
γ_{41}	2.975	0.0014	0.009	0.004046	0.000035	0.005685
γ_{42}	3.044	0.0013	0.009	0.003988	0.000034	0.005538
γ_{43}	3.078	0.003	0.009	0.009326	0.000079	0.01295
γ_{48}	3.475	0.0065	0.008	0.002241	0.000188	0.03076
γ_{49}	3.597	0.0013	0.008	0.004496	0.000037	0.006098
γ_{50}	3.772	0.0007	0.008	0.002508	0.000021	0.003361
$K_{\alpha 1}$	0.02317	0.15	0.112	0.003476	0.000388	0.06333
$K_{\alpha 2}$	0.02298	0.08	0.114	0.001838	0.000209	0.03410
β_5^+	0.5056	0.0024	1.0	0.001203	0.001203	0.1966
$\beta_{8,9}^+$	0.6426	0.0038	1.0	0.002435	0.002435	0.3979
β_{10}^+	1.015	0.609	0.95	0.6181	0.5872	95.94
$CK_{1,2}$	0.631	0.0027	1.0	0.001678	0.001678	0.2742
A-KLL	0.01917	0.0359	1.0	0.000688	0.000688	0.1124

Energy and yield data taken from Refs. 17-18.

ϕ = absorbed fraction

$\%E_{tot}$ = percent of the total energy absorbed in the rat testis.

E_{emit} = Yield X Energy

$E_{abs} = \phi E_{emit}$

TABLE II
Breakdown of Absorbed Energy in Rat Testis from ^{110}In and ^{111}In

	% of Total Energy Absorbed in the Testis	
Radiation	^{110}In	^{111}In
Photons, X rays	3.1	55.4
β particles	96.5	-
Conversion Electrons	0.3	35.5
Auger Electron	0.1	9.1

By employing radioactive isotopes of the same element (indium), labeled to the same compound (oxine), this model should be able to distinguish between the biological effects of different types of radiation with different energy deposition patterns. In this study, the radiobiological effects of IT injected ^{110}In and ^{111}In were investigated and compared with external X irradiation of the rat testis.

MATERIALS AND METHODS

Animals

Adult male Wistar rats of 7-8 weeks age, weighing 200-250 g, were used (M llegaard Breeding Center Ltd., Denmark). The animals had free access to commercial pellet food and tap water. They were kept under controlled light (12 h light and 12 h darkness) and constant temperature (22°C). Light ether anesthesia was employed during the invasive procedures, *i.e.* IT injections. The rats were maintained in groups of three.

Production of ^{110}In

^{110}In, not commercially available, was cyclotron produced at the Svedberg Laboratory, Uppsala, Sweden. The mother radionuclide ^{110}Sn ($T_{1/2}$ = 4.15 h) is produced by the reaction In (p,xn) ^{110}Sn which has a maximum cross-section of 110 mb at approximately 70 MeV and a practical

yield of 400 MBq/μA-h (16). The ^{110}In produced was eluted in 0.5 ml fractions with 0.05 N HCl. Impurities produced during irradiation of the In target were separated from ^{110}In by the ion exchange column in the generator. The radioimpurity ^{111}Sn ($T_{1/2}$ = 35 min) which decays to ^{111}In ($T_{1/2}$ = 2.81 d) was avoided by waiting 4-5 h between the end of the bombardment and preparation of the generator. Gamma spectroscopy with an HpGe detector was performed to assure radionuclide purity.

Rat Testis Model

Details regarding the evaluation of the rat testis model, as well as the procedures for intratesticular injection of ^{111}In and testicular X ray irradiation, have previously been described in detail (14) and are only briefly described below. The minimum time necessary for spermatogonial cells to become spermheads has been established to be 7 wk after exposure to ^{111}In-oxine and X rays. Hence, the minimum spermhead count is observed at this time and therefore all spermhead counts were performed 7 wk after the injection of radionuclides or exposure to external irradiation.

The study design is presented in Table III. Seven series were analyzed. All rats were sacrificed and assayed at the 7th wk post-injection. Series 1 and 2 were IT injected with ^{110}In-oxine and ^{111}In-oxine, respectively. The testes of the rats in series 7 were exposed to external X rays (250 kVp). Four series served as controls, *viz.* series 3 (decayed ^{110}In-oxine), series 4 (oxine IT), series 5 (NaCl IT), and series 6 (sham irradiated).

Intratesticular Injections

A series of 12 rats were IT injected with an ^{110}In-oxine activity concentration of 0.02-0.34 MBq/μl (series 1). These results were compared with a previous investigation of 25 animals IT injected with ^{111}In-oxine activity concentrations of 0.17-1.58 MBq/μl (series 2) (14). The injection technique was as follows: A small incision was made distally in the scrotum, and the testis was manipulated to the opening and partly externalized during the injection. The incision was sutured after injection. All radiolabeled and unlabeled compounds were injected centrally into the testis in a volume of 1 X 10 μl or 2 X 10 μl using a microsyringe equipped with a newly grinded 27 gauge (diameter 0.41 mm) needle. During the injection, the syringe was drawn backwards to form an initial "line source" of the injected

radionuclides. The volume injected was approximately 1% of the rat testis mass (1.4 g).

TABLE III
Rat Testis Study Design[a]

Series	Absorbed Dose (Gy)	No. of Animals[b]
1. ^{110}In-oxine, IT[c]	0.15 - 2.6	12
2. ^{111}In-oxine, IT[c]	0.4 - 7.7	25
3. Decayed ^{110}In-oxine, IT[c]	-	4
4. Oxine, IT[c]	-	2
5. NaCl, IT[c]	-	7
6. Sham-irradiated	-	5
7. X ray, 250 kVp	0.48-9.45	28

[a]Series 2 & 4-7 are described in detail elsewhere (14).
[b]All the animals sacrificed the 7th week after exposure, when the minimum number of spermheads is attained.
[c]IT=Intratesticular injection.

External Irradiation with 250 kVp X rays

Local external testicular X ray irradiation was performed with a commercial X ray unit (Siemens, 250 kVp, HVL 2.59 mm Cu) with a dose rate of 0.46 Gy/min. To assure only irradiation of the scrotum, a field of 28 X 38 mm^2 was applied (14). The 28 animals irradiated received a testis dose between 0.48 and 9.45 Gy (series 7). These animals, as well as a series of sham irradiated controls (series 6), were sacrificed after 7 wk.

Production of ^{110}In-oxine

^{110}In has a half-life of 69.1 min and decays to stable cadmium. The mother nuclide ^{110}Sn (in the ^{110}Sn/^{110}In generator) decays to ^{110}In with a half-life of 4.15 h (17,18). As indicated in Fig. 1 and Table I, ^{110}In decays mainly by

β^+ (61%) with an average energy of 1 MeV. Photons of 658 keV (98%) and 511 keV (123%) are also emitted.

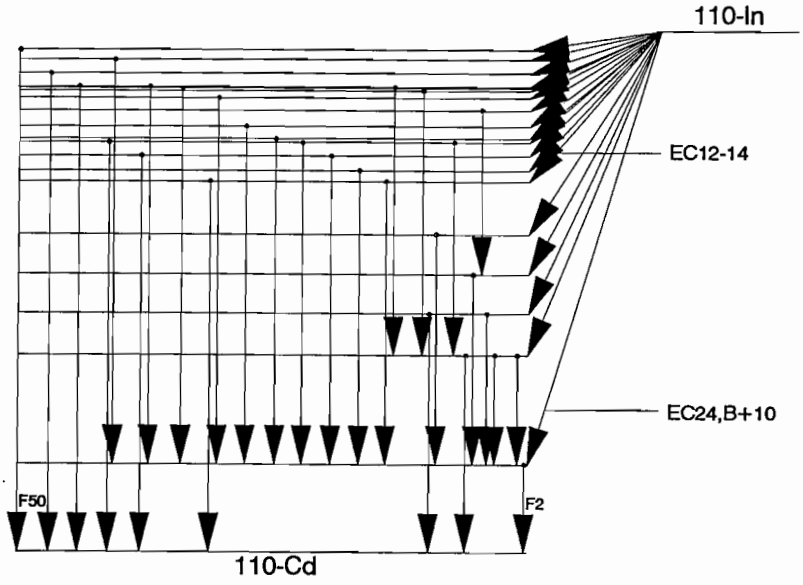

FIG. 1. Decay scheme for ^{110}In (half-life = 69.1 min). Main transition lines are indicated (β^+10 - 61%, EC24 - 27%, EC12-14 - 6%). Transitions with probabilities less than 1% are not indicated in the figure.

Absorbed Energy in the Rat Testes from ^{110}In

Table II gives the main contributions to the absorbed dose to the rat testes. The organ is assumed to have a mass of 1.438 g, a shape averaged of 1:2:4 ellipsoid and sphere, and uniform distribution of ^{110}In.

Labeling Procedure and Quality Control for ^{110}In-oxine

The procedures in Ref. 1 were employed. ^{110}In was eluted from the generator as a chloride solution in 0.05 N HCl. The activity was eluted in 0.5 ml fractions, which were separately measured for activity content. Fractions containing the main part of the activity were pooled in a polypropylene centrifuge tube (15 ml). The chloride solution was neutralized with an appropriate volume of 0.1 N NaOH. A buffer of 0.3 N sodium acetate,

pH 5.5, was added (0.2 ml) to the solution and mixed. A volume of 50 µl of oxine dissolved in ethanol, with a concentration of 1 mg/ml, was added and mixed. The labeled ^{110}In-oxine is lipophilic, while unlabeled ^{110}In chloride is not. By adding chloroform and mixing it well, the labeled part may be extracted in the chloroform. The chloroform phase was transferred to a new tube and evaporated to dryness. The ^{110}In-oxine was dissolved in ethanol, measured for activity, and evaporated to a quarter of the desired final volume. Physiological saline was added to form a 25% ethanol solution. Activity concentrations of 19-335 MBq/ml were thus achieved. The fraction of ^{110}In not labeled to oxine was negligible.

Retention of ^{110}In-oxine in Rat Testis

Because we have previously demonstrated a great variability of the indium elimination from the rat testis (14), the retention of ^{110}In in the testis for each animal was measured with a collimated HpGe detector. After IT injection, the slightly anesthetized animal was placed in a horizontal Perspex tube and the root of the tail fixed in a slot. After adjustment of the front end of the tube, the animal was unable to move. The animal was placed 2 m away from the detector. Apart from the testes, the rat was collimated with a 40 mm thick lead shield. ^{110}In emits high energy photons (658 keV) which are faintly attenuated in the animal. Repeated measurements were performed without anesthesia. Between the measurements, the animal was free to move in its cage. The fraction of injected radioactivity retained in the testis was followed over a period of up to eight hours post-injection. Using efficiency calibrations for the detector geometry, the activity in the testis was calculated. After correction for physical decay of the nuclide, the biological retention of activity was calculated.

Retention of ^{111}In-oxine in Rat Testis

The radiopharmaceutical employed was ^{111}In-oxine ($T_{1/2}$ = 2.8 d) (Mallinckrodt Diagnostica, Peten, Holland) dissolved in sodium chloride with a specific activity of 1.58 MBq/µl (30 mCi/ml) (14). A stock solution of 8-hydroxyquinoline (Sigma Chemical Co., St. Louis, MO) for the control (series 4) was prepared in the same manner.

The retention of ^{111}In in each testis for each animal was measured with a scintillation camera (Maxi Camera I, General Electric, equipped with a medium energy parallel hole collimator). The retention of ^{111}In in the testis

was followed by performing 2 min accumulations to obtain images during the early hours after the IT injection, and then regularly (1-4 times per day) up to 13 days. For each animal, a region of interest (ROI) was selected over the scrotum, and the area was corrected for the background and the dead-time of the detector. The activity content in each testis could then be calculated employing a calibration constant of 194 s^{-1} MBq^{-1}. Time-activity curves were generated for each testis. The biological clearance for all the testes in all the animals are plotted during the time interval used for the absorbed dose assessment. An enlarged plot for the first 6 h is given in Fig. 3.

Determination of Spermhead Count

The spermhead count was performed according to the technique introduced by Meistrich *et al.* (5) and further elaborated by Rao *et al.* (8). The elongated nuclei of late spermatids of the mouse and rat are resistant to sonication, whereas spermatogonial and other cells in testicular homogenates are disrupted. Consequently, the method is appropriate for isolation and counting of spermheads. After the animal was sacrificed, both the testes were removed, weighed, homogenized (Ultra-Turrax TP18/2) in 10 ml deionized water for 20 s, and sonicated for 60 s (Ultrasonicator 4712-2, 40W, Cole-Parmer Instrument Co., Chicago). The spermheads from each testis were counted (200-500) in a hemocytometer (Bürker chamber) using a phase contrast microscope. The term "relative spermhead survival" implies a quotient between the number of spermheads exposed to radiation and the corresponding series of controls, *viz.* ^{110}In-oxine/decayed ^{110}In-oxine; ^{111}In-oxine/oxine; and X ray 250 kVp/the sham irradiated group, respectively.

Activity Distribution in the Testis

The distribution of the activity in the testis after the IT injection was checked with autoradiographic techniques. Briefly, after IT injection the testes were embedded in carboxymethyl cellulose, frozen and sectioned with a microtome (14). The freeze-dried sections containing radioactivity were placed on X ray film to produce autoradiographic grains. To investigate the influence on the distribution of the injected volume, controls were made with a staining agent. Fifteen minutes after IT injection of 10 µl, 20 µl, or 50 µl of Evans Blue, testes were dissected and frozen. After sectioning, photographs were taken.

RESULTS

Biokinetics of the Radiochemicals

The rat testicular time-activity curves for ^{110}In-oxine demonstrated a biological elimination of almost 10% within the first hour after IT injection (Fig. 2), but subsequently the clearance became much slower. After 4-5 h post-IT injection, almost 90% of the activity was retained in the testis with almost negligible elimination. These results were further confirmed by measuring alternatively the testes and the rest of the animal with the collimated HpGe detector. Less than 10% of the IT injected activity was found in the rest of the body during the time of investigation.

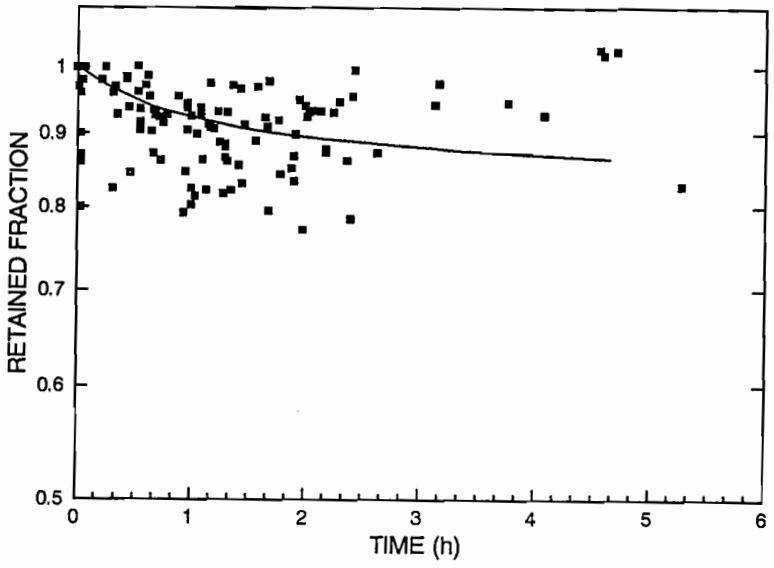

FIG. 2. Biological elimination during the first 6 h after intratesticular injection of ^{110}In-oxine. Activity is corrected for physical decay.

The retention of ^{111}In-oxine activity in the testes for each animal was measured up to 34 times throughout the time used for assessment of the absorbed dose to the testis (Fig. 3). The decrease of activity was rapid during

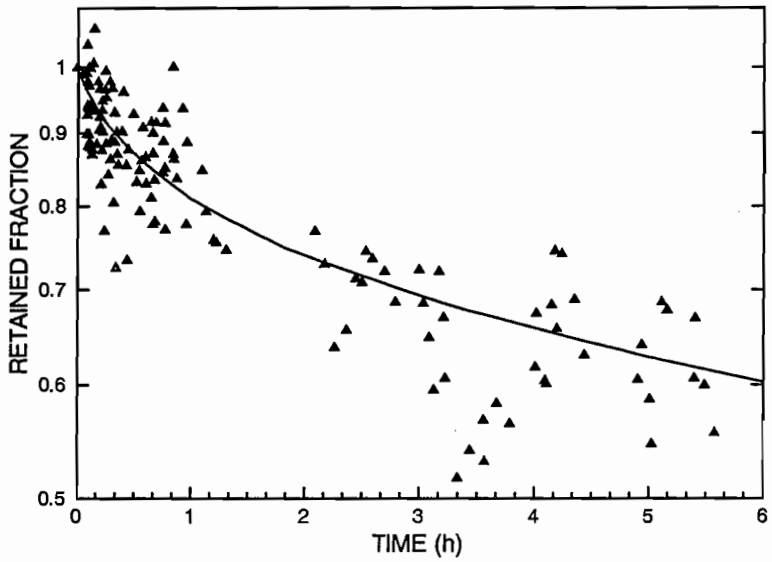

FIG. 3. Biological elimination during the first 6 h after an intratesticular injection of ^{111}In-oxine. Activity is corrected for physical decay.

the first 6 h, but became much slower. At the end of the time interval for the absorbed dose calculation (13 d), the retention was approximately 50%.

Activity Distribution in the Rat Testes

As can be seen in Fig. 4a, the activity is heterogeneously distributed. The distribution of Evans Blue is similar to the autoradiograph (Fig. 4a) at low injection volumes (Fig. 4b), but becomes more homogeneous the larger the injected volume (Figs. 4b-d).

Radiobiological Effects: Spermhead Survival

The spermhead count in the controls, series 3 (decayed ^{110}In-oxine), series 4 (oxine) , series 5 (NaCl) and series 6 (sham irradiated) showed 279, 294, 281 and 264 million per testis respectively, which revealed no significant difference. The relative spermhead survival count assessed at the 7th wk post-exposure, as a function of absorbed dose to the testis subsequent to local external irradiation or IT injection of the radiochemical, showed (Figs. 5-7) a

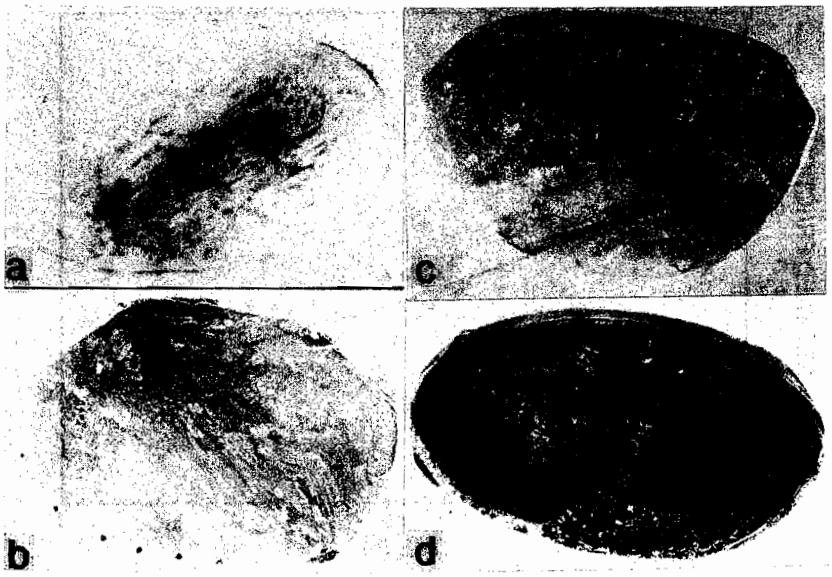

FIG. 4. a) Activity distribution in the testis, 30 min post-injection of 10 µl ^{111}In-oxine. Distribution of Evans Blue in rat testis 15 min after IT injection of b) 10 µl, c) 20 µl, and d) 50 µl.

dose dependent response curve. The relative spermhead survival for all the series exposed to ^{110}In-oxine, ^{111}In-oxine and the X ray irradiation showed a two-component exponential decline. Based on these curves, the D_{37} (*i.e.* the absorbed dose, where 37% of the initial number of spermheads remained) was established. Analyses of the survival data gave a D_{37} of approximately 1.9 Gy for ^{110}In-oxine, 2.2 Gy for ^{111}In-oxine, and 1.2 Gy for 250 kVp X rays. In addition, the decrease in relative testis weight showed a dose related response curve with corresponding D_{37} values of 5.8 Gy, 5.3 Gy and 6.5 Gy, respectively.

DISCUSSION

In the mouse testis model, Rao *et al.* (8-10,12) have established the radiobiological effects of low-energy electron emitting radionuclides. Besides measuring the spermatogonial survival, Rao *et al.* (11,13) also have examined other radiobiological models in the mouse, *e.g.* measuring spermhead abnormalities (13) and oogenesis (11). The results of all three radiobiological

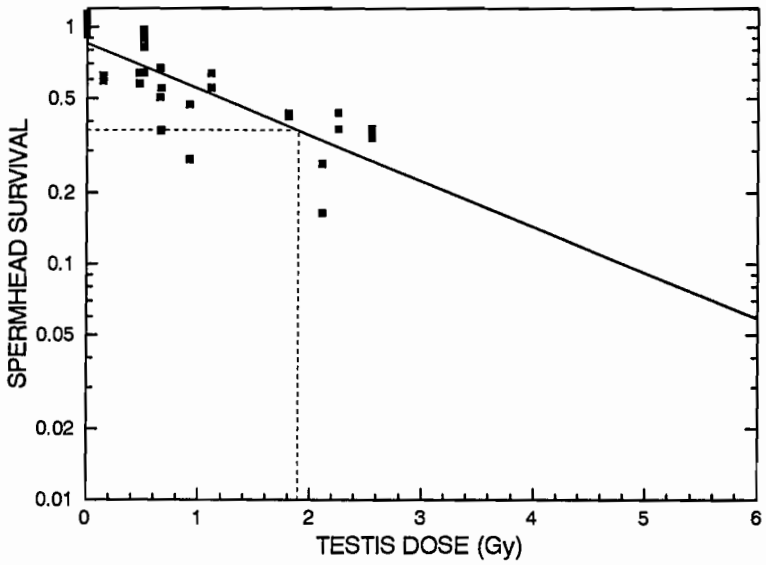

FIG. 5. Relative spermhead count as a function of absorbed dose to rat testis from intratesticularly injected ^{110}In-oxine.

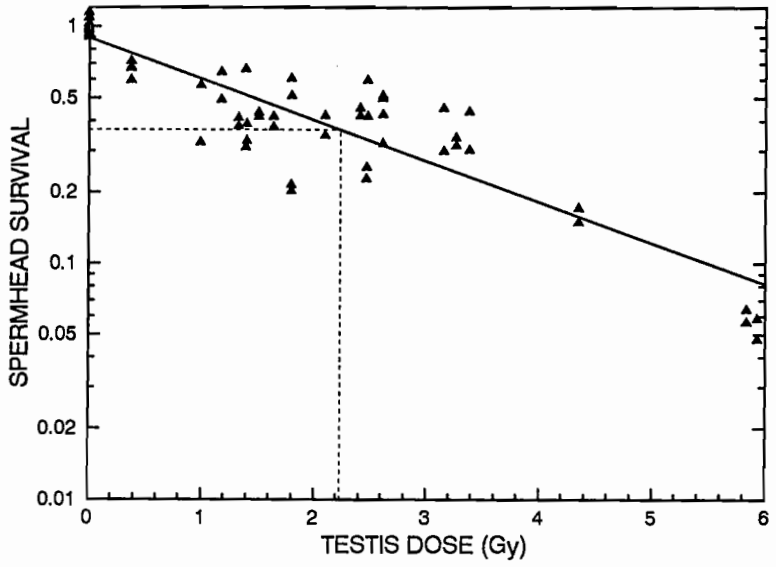

FIG. 6. Relative spermhead count as a function of absorbed dose to rat testis from intratesticularly injected ^{111}In-oxine.

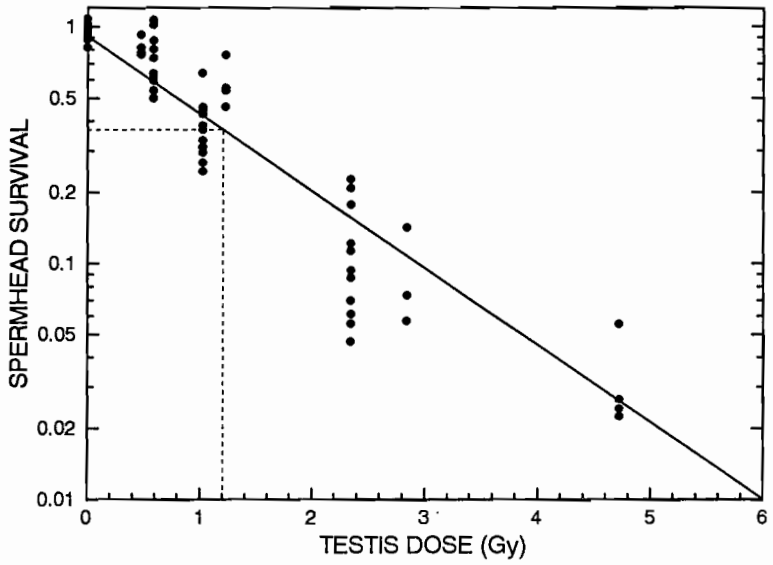

FIG. 7. Relative spermhead count as a function of absorbed dose to testis subsequent to local external irradiation with 250 kVp X rays.

models have been consistent with each other. The investigations have shown great differences in D_{37} values between the various radiopharmaceuticals employed.

By employing two different radioactive isotopes of the same element *viz.* ^{110}In and ^{111}In, labeled to the same chemical (oxine), the rat testis model might discern the biological effects of different types of radiation with different patterns of energy deposition. In all of our experiments, the spermhead survival showed a dose-dependent response curve. The data also suggests that spermhead survival is a much more sensitive radiobiological model than decrease of the testis weight.

The absorbed energy distribution in the testis from the relatively high-energy charged particle radiation of ^{110}In is much more homogeneous than that of ^{111}In which only exposes the region in close proximity to the injection channel (14). Although only a minor part of the testis was exposed to ^{111}In, the biological effect was almost equivalent to the effect of ^{110}In. This is

perhaps due to the nonuniform distribution of the radiochemicals in the testis (Fig. 4a) which only results in local irradiation of the testis along the line injection for ^{111}In. Whereas the energetic β particles emitted by ^{110}In irradiate the testis somewhat uniformly. In that event, the biological effects of the ^{111}In Auger electrons may have been underestimated in spite of similar experimental results for both radionuclides. The Evans Blue stain studies with different injection volumes (Figs. 4b-d) suggest that an injection volume of 50 µl would provide a more uniform distribution of radioactivity in the rat testis. This injection volume for the rat testis (1.4 g in weight) would be more consistent with the 3 µl injection for the mouse testis (0.1 g in weight) used by Rao *et al.* (8-10). Although our present studies involve only a 10 µl injection volume, our future studies will employ 50 µl volumes. This technique should provide better delineation between the radiobiological effects of Auger and β emitters and also help establish reliable RBE values compared to external X ray values.

It should also be pointed out that, in contrast to the mouse testis (10), a large fraction (55.4%) of the energy deposited in the rat testis by ^{111}In is from photons and X rays. This low-LET component, in conjunction with the conversion electron component (35.5%), may contribute to masking the high-LET type effects of the Auger electrons observed by others (10).

Finally, we believe that the larger rat testis model might be a useful supplement to the more radiosensitive, but smaller, mouse testis model for scrutinizing different patterns of energy deposition by incorporated radionuclides.

ACKNOWLEDGMENTS

This study was supported by grants from the Swedish Cancer Society, the Swedish Natural Science Research Council, the Swedish Society of Medicine, Mrs. Berta Kamprad's Foundation for Cancer Research, John and Augusta Persson's Foundation for Scientific Medical Research, Gunnar-, Arvid-, Elisabeth Nilsson's Foundation for Cancer Research, the Medical Faculty of the University of Lund, and the Donation Funds at Lund University Hospital.

REFERENCES

1. M.L. THAKUR, J.P. LAVENDER, R.N. ARNOT, D.J. SILVESTER, and A.W. SEGAL, Indium-111-labeled autologous leukocytes in man. *J. Nucl. Med.* **18** 1014-1021 (1977).
2. K.S.R. SASTRY and D.V. RAO, Dosimetry of low energy electrons. In *Physics of Nuclear Medicine: Recent Advances.* (D.V. Rao R. Chandra, and M. Graham, Eds.) American Association of Physics in Medicine. Medical Physics Monograph No 10. American Institute of Physics, New York, pp. 169-208, 1984.
3. B.A. JÖNSSON and S.E. STRAND, Auger electron emitters as therapeutic agents or sources of hazards in diagnosis - A review. In *Radionuclides for Therapy* (P.A. Schubiger and P.H. Hasler, Eds.) Basle, Switzerland, pp. 92-104, 1986.
4. K.S.R. SASTRY, R.W. HOWELL, V.B. MYLAVARAPU, A.I. KASSIS, S.J. ADELSTEIN, H.A. WRIGHT, R.N. HAMM, and J.E. TURNER, Dosimetry of Auger emitters: Physical and phenomenological approaches In *DNA Damage by Auger Emitters* (K.F. Baverstock and D.E. Charlton, Eds.) Taylor and Francis, London, pp. 27-38, 1988.
5. M.L. MEISTRICH, B.O. REID, and W.J. BARCELLONA, Changes in sperm nuclei during spermiogenesis and epididymal maturation. *Exp. Cell. Res.* **99**, 72-78 (1976).
6. BIANCHI -The Testis. Part I In *Cytotoxic Insult to Germinal Tissue - Effect on Cell Lineages.* (C.S. Potten and J.H. Hendry, Eds.) Churchill Livingstone, Edinburgh-London-Melbourne-New York 7: pp. 258-328, 1983.
7. J.H. HENDRY, Survival of cells in mammalian tissues after low doses of irradiation: A short review. *Int. J. Radiat. Biol.* **53**, 89-94 (1988).
8. D.V. RAO, G.F. GOVELITZ, and K.S.R. SASTRY, Radiotoxicity of thallium-201 in mouse testes: Inadequacy of conventional dosimetry. *J. Nucl. Med.* **24**, 145-153 (1983) .
9. D.V. RAO, K.S.R. SASTRY, G.F. GOVELITZ, H.E. GRIMMOND, and H.Z. HILL, In vivo effects of Iron-55 and Iron-59 on mouse testes. Biophysical Dosimetry of Auger Electrons. *J. Nucl. Med.* **26**, 1456-1465 (1985).
10. D.V. RAO, K.S.R. SASTRY, H.E. GRIMMOND, R.W. HOWELL, G. GOVELITZ, V.K. LANKA, and V.B. MYLAVARAPU, Cytotoxicity of some indium radiopharmaceuticals in mouse testes. *J. Nucl. Med.* **29**, 375-384 (1988).
11. D.V. RAO, V.B. MYLAVARAPU, K.S.R. SASTRY, and R.W. HOWELL, Internal Auger emitters: Effects on spermatogenesis and oogenesis in mice. In *DNA Damage by Auger emitters* (K.F. Baverstock and D.E. Charlton, Eds.) Taylor and Francis, London, pp.15-26, 1988.
12. D.V. RAO, V.R. NARRA, R.W. HOWELL, G.F. GOVELITZ, and K.S.R. SASTRY, DNA-incorporated I-125 is as radiotoxic as densely ionizing alpha-particles. *Lancet* **II**, 650-653 (1989).
13. D.V. RAO, V.R. NARRA, R.W. HOWELL, V.K. LANKA, and K.S.R. SASTRY, Induction of spermhead abnormalities by incorporated radionuclides: Dependence on subcellular distribution, type of radiation, dose rate, and presence of radioprotectors. *Radiat. Res.* **125**, 89-87 (1991).
14. G. GRAFSTRÖM, A.M. EL HASSAN, B.A. JÖNSSON, S.E. STRAND, and J. TENNVALL, Rat testis as a radiobiological in vivo model for Auger electron emitting radionuclides. Submitted (1992).
15. B.A. JÖNSSON, H. EMANUELSSON, and S.E. STRAND, Autoradiographic demonstration of the biodistribution in rat testes of intravenously administered indium. *Radiat. Res.* (submitted).
16. H. LUNDQUIST, S.S. ROBSON, and P. MALMBORG, $^{110}Sn/^{110}In$ - A new generator system for positron emission tomography. *Appl. Radiat. Isot.* **42**, 447-450 (1991).
17. P. DeGELDER, E. JACOBS, and D. DeFRANCE, Nuclear data sheets for A=110. *Nucl. Data Sheets* **38**, 545-627 (1983).

18. ICRP, *Radionuclide Transformations, Energy and Intensity of Emission*, ICRP Publication 38, International Commission of Radiation Units and Measurements, Pergamon Press, pp. 338-356 (1983).

290 Biophysical Aspects of Auger Processes, AAPM Symposium Series No. 8 (1992) 290-318
Eds. RW Howell, VR Narra, KSR Sastry, DV Rao

RELATIVE BIOLOGICAL EFFECTIVENESS OF AUGER EMITTERS FOR CELL INACTIVATION: *IN VITRO* VERSUS *IN VIVO*

ROGER W. HOWELL, VENKAT R. NARRA, DE-YAN HOU, DOM A. TERRONE, RAVI S. HARAPANHALLI, KANDULA S.R. SASTRY[1], and DANDAMUDI V. RAO

Department of Radiology
University of Medicine & Dentistry of New Jersey
Newark, NJ 07103, USA

[1]Department of Physics & Astronomy
University of Massachusetts, Amherst, MA 01003, USA

ABSTRACT

Clonogenic survival of Chinese hamster V79 cells and spermhead survival in mouse testes have over the years provided a wealth of data concerning quantification of the lethality of Auger electron emitters *in vitro* and *in vivo*. The radiotoxicity of Auger emitting radiopharmaceuticals has been expressed in terms of the relative biological effectiveness (RBE) compared to reference acute external photon beams, with D_{37} serving as the point of comparison. Under these conditions, RBE values as high as 7 have been observed for DNA-bound Auger emitters. Since the ultimate utility of the RBE is for radiation protection, and perhaps radiation therapy, knowledge of the magnitude of the RBE value is essential. In this work, the techniques and assumptions used to obtain these RBE values both *in vitro* and *in vivo* are reviewed. In addition, the magnitude of the RBE values obtained in each model will be compared and critically examined in terms of: 1) reference radiation (*e.g.* type and dose rate), 2) comparison with α emitters, 3) importance of the site of decay, and 4) possible artifacts. The results indicate that reference radiation plays a key role in the V79 cell model, however, no

such observance was found in the mouse testis model. Experimental results in both models show that DNA-bound ^{125}I is as effective as incorporated α emitters in causing cell death, and that ^{125}I decays on thymine or cytosine bases are equally effective. Finally, the concept of quality factor (or radiation weighting factor) for Auger emitters is explored and a means of calculating the dose equivalent is advanced.

INTRODUCTION

The extreme lethality of Auger electron emitting radionuclides is well established both *in vivo* and *in vitro*. Their effectiveness is greatest when the Auger emitter is covalently bound to the DNA as in the case of the thymidine analogs ^{77}BrUdR (bromodeoxyuridine), ^{123}IUdR (iododeoxyuridine), and ^{125}IUdR (1-3). For clonogenic survival, values of relative biological effectiveness (RBE) of 6.4 (1), 7.3 (2), and 7.2 (3), respectively, were reported for cultured Chinese hamster V79 cells. *In vivo* studies of Rao *et al.* (4,5) with ^{125}IUdR gave a similar RBE value (7.9) for spermhead survival in mouse testes. When radionuclides decaying by EC and IC are non-covalently bound to the DNA of mammalian cells, high-LET (linear energy transfer) type effects are observed, albeit with a lower value of RBE (RBE ~ 4) (6-9). It has also been shown that, for covalent binding of ^{125}IUdR to the DNA, not all sites are equally radiosensitive to the ^{125}I Auger cascades (10).

The high RBE values reported for Auger emitters have prompted discussion regarding the notion of establishing a quality factor Q for this class of radionuclides. Pomplun *et al.* (11) have proposed $Q = 1$ for ^{125}I disintegrations "outside" the DNA and the high-LET Q for disintegrations "inside" the DNA, the high-LET Q being that for multiply charged particles (*e.g.* $Q = 20$ for α particles) (12). Before definite Q factors are assigned to Auger emitters such as ^{125}I, several questions need to be addressed regarding experimental RBE values for Auger emitters: 1) In view of the chronic nature of the irradiation from incorporated Auger emitters, how appropriate is use of acute X or γ rays as the reference radiation? This question has been raised recently by Rao *et al.* (13). 2) Can the high RBE values observed for Auger emitters be substantiated by parallel experiments with α emitters (4,14,15)? 3) The RBE of Auger emitters is highly dependent on cellular localization and subcellular distribution of the radionuclide (7,9,13,16), which are governed, in turn, by the chemical form (5,9). Is there a clear relationship between the RBE of the radiochemical and its subcellular distribution? 4) Does the DNA base

site where the Auger emitter binds play any role in the expression of the biological effect? These questions concerning RBE are of importance not only in recommending Q (or w_R) for ^{125}I and other Auger emitters, but also in calculating the dose equivalent H (17). In this work, experimental studies carried out *in vivo* with the mouse testis model (18,19) and *in vitro* with cultured Chinese hamster V79 cells are reviewed and new data are provided in an attempt to answer some of the above questions concerning the RBE of Auger emitters incorporated into proliferating mammalian cells. In addition, the quality factor for Auger emitters is discussed, and suggestions for incorporating subcellular distribution into the dose equivalent are advanced.

BIOLOGICAL MODELS AND EXPERIMENTAL METHODS

I. *In Vivo* Model: Spermatogenesis in Mouse Testis

The mouse testis model is a highly sensitive and quantitative model used to study the biological effects of radiation *in vivo* (20,21). The process of spermatogenesis in the mouse and man are very similar except for their time scales: about 5 wk for mouse and 10 wk for man. As indicated in Fig. 1 (20), the process is complex, yet tractable. The stem cell (A_s) differentiates to form a pair of cells which further divide to give type A_1 spermatogonial cells. The type A_1 cells in turn divide repeatedly through several spermatogonial cell

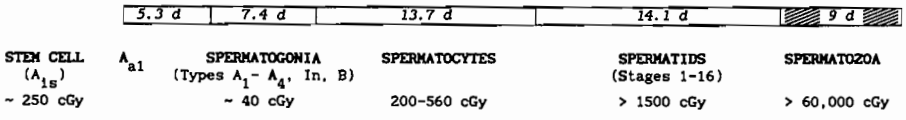

FIG. 1. The process of spermatogenesis in mouse testis is described by Meistrich *et al.* (53). There are five major populations of cells in the cycle: stem, spermatogonia, spermatocytes, spermatids, and spermatozoa. The relative radiosensitivity of the different groups to external beams of X rays is indicated by the LD_{50} values given above, the spermatogonial cells being the most radiosensitive. Timing of the spermatogenesis process as reported by Meistrich *et al.* (53) is indicated by the scale above. Approximately 29 days are required for the spermatogonia to become sonication resistant spermatids of Stages 12-16. Hence, after an initial acute radiation insult, the spermhead population in the testis reaches a minimum about 29 days later.

stages designated as A_2, A_3, A_4, In, and B. The type B spermatogonia divide to become secondary spermatocytes which mature into spermatids. Finally, the spermatids pass through 16 stages before they become functional sperm. The radiation sensitivity of these different subpopulations is markedly different (Fig. 1). When mouse testes are irradiated with external X rays, the differentiated spermatogonia (A_1-A_4, In, and B types) are found to be most sensitive $LD_{50} \sim 40$ cGy, whereas their precursors (A_{is}, A_{a1}) as well as the postgonial cells are relatively radioresistant with LD_{50} values of 100-300 cGy and 200-60,000 cGy, respectively (20). Because of this differential radiosensitivity, irradiation of the testis with low doses from external beams of X rays or from incorporated radionuclides results in a reduced testicular spermatid count 29-36 days later (see METHODS - Optimal Day Post-Administration to Assay Spermhead Survival), the time required for the spermatogonia to become sonication resistant spermatids of stages 12-16 (see below: Optimal Day) (9,18,19). Thus spermatogenesis may be used to study the effects of radiation *in vivo*.

General Procedures

Swiss Webster mice (Taconic Farms, Germantown, NY) aged 9-10 weeks were used in these studies. External irradiation of the testis with X rays was carried out by selective exposure of the organ with 60 kVp or 120 kVp X rays produced by an overhead fluoroscopy unit (9). Internal irradiation of the testis with incorporated radionuclides was achieved by intratesticular (i.t.) injection of radiochemicals in standard 3 µl volumes. This route of administration was selected over intravenous and intraperitoneal routes because essentially the entire testicular dose is attributed to energy deposited from decays occurring in the organ itself (self-dose). In the other modes of administration, the testicular dose is largely from the non-target to target dose from penetrating X and γ rays, thereby masking the effects of the low energy electrons (4,9,18,19). Intratesticular injection of the radiochemicals was performed following a minor surgical procedure to partially exteriorize the right testis (18). Using a microsyringe fitted with a 27-gauge needle, 3 µl of a solution containing the radiochemical was slowly injected along the long axis of the ellipsoidal testis as the needle was retracted. In this manner, a fairly uniform line injection was achieved. Controls were similarly injected with either saline or solutions containing the nonradioactive compounds at the same chemical concentration (18). Animals were maintained under anaesthesia throughout the procedure. The macroscopic uniformity of the resulting radionuclide distribution in the testis was confirmed by the

following method. At various times post-administration, the testes were removed, frozen with CRYOkwik™, sliced into sections, weighed, and the radioactivity per gram of tissue determined (19). The average subcellular distribution (cytoplasm, nucleus, DNA) of the radioactivity in the entire population of testicular cells was obtained 24 h postinjection using the cell fractionation methods outlined in Ref. 19.

Testicular Clearance of the Radiochemicals

The pattern of biological clearance of the radiopharmaceuticals following i.t. administration was monitored. Animals were injected with a fixed amount (~ nCi amounts) of radioactivity and sacrificed, in groups of four, at various times post-administration (18). The testes were removed immediately and the percent activity retained was determined using γ ray spectroscopy or liquid scintillation techniques. The amount of radiochemical injected did not influence the pattern of biological elimination over the range investigated.

Spermhead Count

The testicular spermhead count was determined immediately after sacrificing the animals. The testes were surgically removed (epididymis discarded), homogenized in 1 ml deionized water, and sonicated for 30 s. The sonication resistant spermheads of spermatids in Stages 12-16 were counted under a microscope to a minimum of 200.

Optimal Day Post-Administration to Assay Spermhead Survival

The optimal day post-administration to assay the spermhead survival is the day the spermhead count reaches a minimum (Fig. 2). Selective irradiation with acute external X rays yields a minimum spermhead count on the 29th day. This time scale is consistent with the spermatogenesis process (Fig. 1) in that it takes about 29 days for the radiosensitive spermatogonia to mature to spermatids of Stages 12-16. For intratesticularly injected radiochemicals, the optimal day varies between 29 and 36 days post-injection (4,9,18,19). Since this optimal day depends on the nature of the exposure (*e.g.* chronic versus acute), and perhaps on the cellular incorporation of radionuclides, it must be determined experimentally in each case (4,9,18,19).

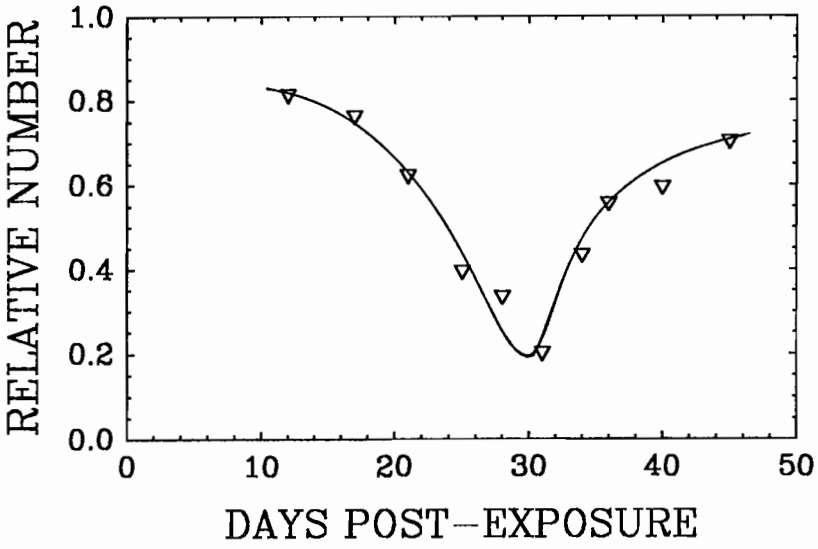

FIG. 2. Time dependence of sperm-head count in mouse testes exposed to external 120 kVp X rays (9). The spermhead count relative to unirradiated controls is plotted as a function of time post-exposure. The minimum spermhead count was observed on the 29th day post-irradiation.

Differential Radiosensitivity of Types A_1-A_4, In, and B Spermatogonia

Additional experiments were performed in order to prove that the two-component nature of the spermhead survival curves (see RESULTS) is not an artifact of the procedure, rather due to the differential radiosensitivity of the spermatogonial cells. In the spermhead survival assay described above, the killing of spermatogonial cells is measured indirectly by determining the testicular spermatid (spermhead) population 29-36 d post-injection of the radiochemical. To explore the differential radiosensitivity of the various types of spermatogonial cells (A_1-A_4, In, B), the spermatogonial cell survival was measured directly using standard histological techniques (22). Briefly, ten twelve-week old mice were sedated with sodium pentobarbital and the testes irradiated externally with 120 kVp X rays. The dose rate (9 cGy/min) was measured with a Victoreen rate meter. External X rays were employed to insure uniform irradiation of the testis and that intratesticular injections play no role in the shape of the survival curves. Mice, in groups of two, were

irradiated with 5, 25, 75, or 100 cGy. Two unirradiated mice, otherwise treated identically, served as controls. Forty-eight hours post-irradiation, the mice were sacrificed by cervical dislocation, and the testes removed. After removal of the tunica, the tubules were teased free *in toto* as they were bathed in Bouin's fixative. The tubules were kept in the fixative for 5 h and then allowed to decolorize overnight in a solution of 70% ethanol - 30% water. They were then stained in a dilute solution of Harris' hematoxylin for 5-6 min and immediately washed in tap water ten times at 30 min per wash. The sightly basic pH of the tap water facilitated removal of the excess stain. This was followed by five 30 min washes in distilled water and then a step-wise dehydration beginning at 20% ethanol up to 100%. A second wash with 100% ethanol was performed and the tubules allowed to soak overnight. Two successive washes with a 50% xylene - 50% ethanol solution and an overnight wash in 100% xylene were then performed. The tubules thus treated were mounted on glass slides with Permount and allowed to dry 3 d. With the aid of an ocular grid, the various types of spermatogonial cells were counted individually and normalized to the number per 100 Sertoli cells. At least 4 continuous grid-lengths per tubule were counted and 4 tubules were counted per animal. The entire procedure was repeated a second time with the addition of three dose points: 10, 50, and 100 cGy.

II. *In Vitro* Model: Clonogenicity of Cultured V79 Cells

Cultured mammalian cells have been widely used as a biological model to study the radiotoxicity of incorporated Auger emitters. Clonogenic survival of Chinese hamster V79 lung fibroblasts provides a simple, yet highly effective, model to examine the lethality of radionuclides in mammalian cells. Accordingly, this model has been used extensively by Kassis *et al.* (1,3,23), and is used in the present work.

Cell Culture

Chinese hamster V79-513 cells (kindly provided by Dr. Athwal, UMDNJ) are maintained as monolayers under standard conditions (37°C, 5%CO_2 - 95% air). Cells are cultured in minimum essential medium (MEM) supplemented with 10% fetal calf serum, 50 units/ml penicillin, 50 µg/ml streptomycin, and 2mM L-glutamine. Twice weekly, the cells are subcultured.

Clonogenic Survival

Cells in exponential growth are removed from the culture flask with trypsin, suspended in calcium-free MEM (for suspension culture), and diluted to 400,000 cells/ml. One ml aliquots of cell suspension are transferred to 15 ml culture tubes and placed on a rocker-roller for 3-4 h under standard conditions. Subsequently, an additional 1 ml of MEM containing the radiochemical is added and the tubes further rolled for a predetermined period to allow the radioactivity to incorporate into the cells. Aliquots of the cells are removed and the radioactivity per cell determined according to the method of Kassis *et al.* (24). The remaining cells are washed 3 times with fresh MEM, serially diluted, and seeded in triplicate into 25 cm^2 flasks for colony formation. Aliquots of these washed cells are also assayed for intracellular radioactivity content to determine the amount of unbound radioactivity lost during the washing process. After 1 wk the colonies are washed with saline, fixed with methanol, stained with crystal violet, scored, and the survival compared to controls. Untreated cells and cells treated with the non-radioactive chemicals serve as controls.

Cellular Uptake and Clearance of Radioactivity

The cellular uptake of radioactivity is monitored as a function of time. Aliquots of cell suspension are removed at various times and the radioactivity per cell determined (25). The uptake kinetics are essential for determining the cellular self absorbed dose during the period the cells are incubated in MEM containing radioactivity.

After the cells are washed free of extracellular radioactivity and seeded for colony formation, the radioactivity per cell typically decreases exponentially in time. The effective half-life of the cellular activity is determined by seeding a large number of labeled cells into several flasks, removing the cells from the flasks with trypsin at various times later, and determining the radioactivity per cell. The clearance kinetics thus obtained are used to determine the cellular self absorbed dose during the colony forming period (25).

Subcellular Distribution of the Radiochemicals

Subcellular distribution of the radionuclide plays a critical role in dosimetry. Accordingly, using the techniques outlined in Ref. 23, the fraction

of intracellular radioactivity in the cytoplasm versus nucleus is determined as well as the fraction bound to nuclear DNA.

III. Radiochemicals and External Radiation Sources

It is well known that in some radiobiological models the effects of acute radiation are substantially greater than those of a chronic nature. According to the International Commission on Radiation Protection (ICRP), the relative biological effectiveness of radiation A with respect to reference radiation R is defined as the ratio of absorbed dose D_R in a tissue to the dose D_A that causes a qualitatively and quantitatively equal effect. Each RBE derived from a set of observations for tissue cultures or for responses of tissues, in animals or in man, refers to a defined end point produced under a specified set of exposure conditions (26). Hence, because the definition requires that the test and reference radiations be delivered under the essentially the same conditions, it is important to carefully select the reference radiation. Conventionally, photons of low-LET in the form of acute 250 kVp X rays have served as the reference radiation. However, in view of the chronic nature of the exposure from incorporated radionuclides, the conventional reference may not be adequate.

In order to establish the appropriate reference radiation for the spermhead survival assay, several sources of radiation were examined. First, two different sources of photon radiation were examined: acute external X rays (60 kVp and 120 kVp), and the radiochemical ^{7}Be chloride. The X rays were delivered over a period of only a few minutes. ^{7}Be is essentially a pure γ emitter (also emits a single 40 eV electron) which chronically irradiates the testis following i.t. injection. Secondly, the effects of the low-LET β emitter ^{131}I, localized in the cytoplasm of the testicular cells with the radiochemical H^{131}IPDM (5), was studied as a further source of low-LET chronic irradiation. Finally, the effects of H^{125}IPDM and ^{123}IMP (Spectamine™) were also examined.

In the *in vitro* model, acute and chronic irradiation of the V79 cells with photons was accomplished with external ^{137}Cs and ^{99m}Tc γ rays, respectively. The acute irradiation with ^{137}Cs γ rays was accomplished over a period of a few minutes (2.6 Gy/min). ^{99m}Tc (140.5 keV γ ray) decays with a physical half-life of 6 h and was therefore used to irradiate the cells externally over a period of hours with a dose rate which decreases exponentially in time

(initially ~ 1.2 Gy/h for a final cumulated dose of 10 Gy). This pattern is consistent with the manner in which the dose is delivered to the V79 cells from incorporated radionuclides. The details of the irradiation with a ^{99m}Tc "disk" source are given elsewhere (25).

The extreme toxicity of the Auger emitter ^{125}I, when incorporated into the DNA in the form of iododeoxyuridine (IUdR), is well known. Values of RBE as high as about 7 have been reported for cell killing both *in vivo* and *in vitro* (3,4). To confirm these high values we have compared the lethality of ^{125}IUdR with the α emitting radiochemical ^{210}Po-citrate (4,14,25). ^{210}Po emits a single 5.3 MeV α particle and is therefore an excellent source of high-LET radiation for comparison with Auger emitters in both biological models.

Auger emitters are most lethal when incorporated into DNA in the cell nucleus. Are all sites on the DNA equally radiosensitive? The highly localized action of Auger electron emitters provides a unique opportunity to examine the differential radiosensitivity of various locations on the genome through selective targeting with specific radiochemicals. Such precise delivery of the radiation insult is unattainable with external beams of radiation. We have compared the radiotoxicity of ^{125}I labeled iododeoxyuridine and iododeoxycytidine (IdC) to explore possible differential radiosensitivity of the thymine and cytosine base sites.

Finally, the dependence of the RBE of intracellularly incorporated ^{125}I on the fraction of radioactivity bound to DNA is investigated. This is accomplished by administering mixtures of two radiochemicals: 1) ^{125}IUdR which binds almost exclusively to the DNA, and 2) H^{125}IPDM which localizes in the cytoplasm of the cells. By varying the ratio of these two radiochemicals in the injectate, the fraction of radioactivity bound to nuclear DNA may be controlled.

RESULTS

I. *In Vivo* Model: Spermatogenesis in Mouse Testis

Optimal Day to Perform Spermhead Survival Assay

The testicular spermhead count is shown in Fig. 2 as a function of time post-irradiation. Acute 120 kVp X rays were employed. The minimum

spermhead count occurs on the 29th day post-irradiation (9). Hence, this is the optimal day to perform the spermhead survival assay. This same optimal day was found for all of the radiochemicals with the exception of ^{210}Po where the 36th day post-administration was the optimal day (4,5). It should be noted that this value is similar to those found in our earlier work (9) where optimal assay days for ^{111}In-oxine and ^{111}In-citrate were the 36th and 34th day, respectively.

Kinetics of the Radiochemicals in the Testis and Calculation of the Testicular Absorbed Dose

The testicular clearance patterns of the radiochemicals following intratesticular injection are shown in Fig. 3. The data were least squares fitted to a two-component exponential expression (19). Conventional dosimetry, as prescribed by the Medical Internal Radiation Dose (MIRD) Committee (27), was used to determine the absorbed dose to the testis following intratesticular injection of the radiochemical. The absorbed dose is given by $D = \tilde{A}\phi_i\Delta_i/m$, where $\tilde{A}$ is the cumulated activity, ϕ_i the absorbed fraction for the i_{th} radiation component, and Δ_i the equilibrium dose constant. Absorbed fractions were obtained using the computer code of Howell *et al.* (28) while Δ_i were obtained from Ref. 29. The cumulated activity was obtained by integrating the two-component time-activity relationships according to the provisions described in Refs. 18, 19, and 30, and the testicular dose determined (18,19,30).

Spermhead Survival Curves

Figure 4 shows the fraction of surviving spermheads as a function of the testicular absorbed dose for ^{125}IUdR (4), ^{125}IdC, ^{210}Po-citrate (4), ^{7}Be chloride, H^{131}IPDM, H^{125}IPDM (5), ^{123}IMP, and X rays (9). A least squares fit to the data using a two-component exponential expression yields the following relationships where S is the survival fraction and D is the absorbed dose in cGy:

$$S(\text{X rays}) = 0.27 \exp(-D/6.5) + 0.73 \exp(-D/98)$$

$$S(^{210}\text{Po}) = 0.30 \exp(-D/0.20) + 0.70 \exp(-D/15.6)$$

$$S(^{125}\text{IUdR}) = 0.46 \exp(-D/0.41) + 0.54 \exp(-D/22.1)$$

$$S(^{7}\text{Be}) = 0.13 \exp(-D/0.70) + 0.87 \exp(-D/76.2)$$

$$S(\text{H}^{125}\text{IPDM}) = 0.21 \exp(-D/1.8) + 0.79 \exp(-D/89.2)$$

$S(^{125}\text{IdC}) = 0.45 \exp(-D/0.56) + 0.55 \exp(-D/19.3)$

$S(\text{H}^{131}\text{IPDM}) = 0.22 \exp(-D/0.67) + 0.78 \exp(-D/81.6)$

$S(^{123}\text{IMP}) = 0.12 \exp(-D/0.68) + 0.88 \exp(-D/71.3)$

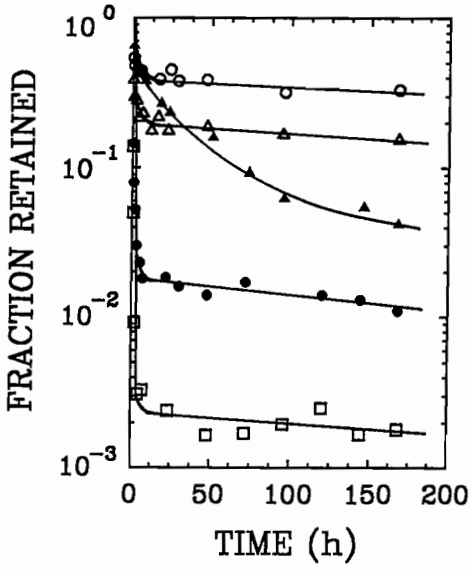

FIG. 3. Testicular clearance patterns of the radiochemicals following intratesticular injection. The fraction of injected activity retained by the testis is shown as a function of time post-injection for ^{210}Po-citrate (open circles) (4), ^{125}IUdR (solid circles) (4), ^{125}IdC (open squares), ^{7}Be chloride (open triangles) (13), H^{125}I(^{131}I)PDM (solid triangles) (5).

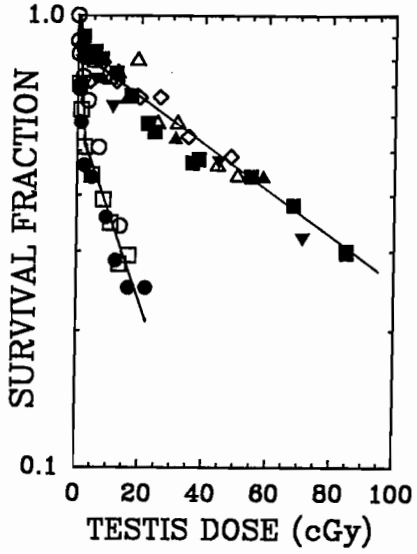

FIG. 4. Spermhead survival as a function of testicular absorbed dose following external and internal irradiation. Survival curves are shown for ^{210}Po-citrate (open circles) (4), ^{125}IUdR (solid circles) (4), ^{125}IdC (open squares), ^{7}Be chloride (open triangles), H^{125}IPDM (solid triangles) (5), H^{131}IPDM (solid inverse triangles), ^{123}IMP (open diamonds), and external X rays (solid squares) (49).

The low-LET sources of radiation (^{7}Be chloride, H^{131}IPDM, H^{125}IPDM, ^{123}IMP, X rays) all lead to comparable cell killing with similar D_{37} values (65 ± 10, 61 ± 6, 68 ± 6, 62 ± 6 and 67 ± 3 cGy, respectively). Iodine-125 labeled IUdR and IdC both bind to the DNA in the cell nucleus and yield the same 37% survival values of 8.5 ± 2.1 and 7.7 ± 1.2 cGy, respectively. This may be compared to the 37% survival value of 10 ± 1 cGy for the high-LET α particle emitter ^{210}Po (4).

Spermatogonial Cell Survival Curves

The individual survival curves for X irradiated spermatogonial cell types (A_1-A_4,In,B) are shown in Fig. 5. Each of these curves follows essentially a single-component exponential response. The large discrepancy in the slopes of the curves, particular between spermatogonial cell types A_1-A_2 and the remaining types, suggests that the first component of the spermhead survival curves (Fig. 4) is due to killing of the sensitive spermatogonial cell stages at low doses, while the second component is due to killing of the less sensitive types.

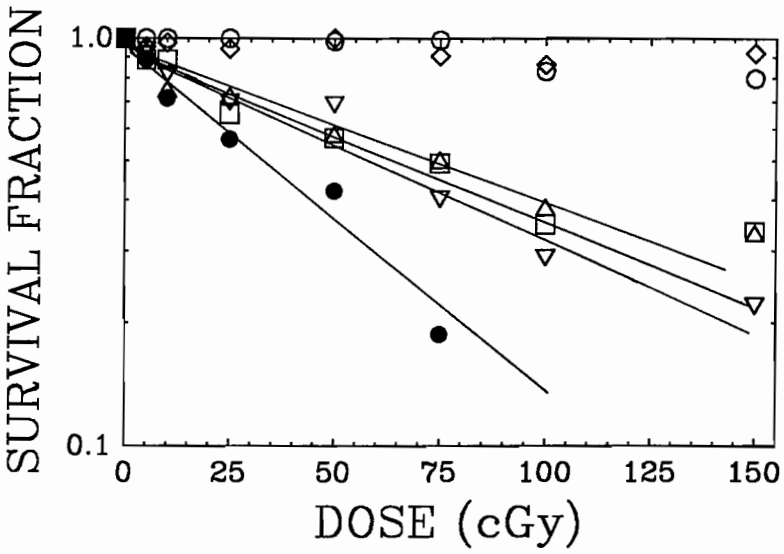

FIG. 5. Survival of spermatogonial cells as a function of testicular dose delivered externally by 120 kVp X rays. The survival curves for spermatogonial cell types A_1, A_2, A_3, A_4, In, and B, are represented by the open diamonds, open circles, open triangles, open squares, open inverse triangles, and filled circles, respectively. A least squares fit to the data yields D_o values of 103 ± 8, 96 ± 7, 86 ± 5, and 46 ± 3 cGy for types A_3, A_4, In, and B, respectively. Insufficient data was collected at high doses for types A_1 and A_2, hence, it was not possible to fit the data.

Dependence of RBE on Fraction of Cellular Activity Bound to DNA

Survival curves were obtained using various binary mixtures of $H^{125}IPDM$ (cytoplasmic localization) and $^{125}IUdR$ (binds to DNA in nucleus) (25). The 37% survival values and subcellular distribution for each mixture were determined. The RBE compared to external 120 kVp X rays is plotted as a function of the fraction f of ^{125}I which is bound to DNA in the testicular cells (Fig. 6). A linear relationship is observed with RBE = 1 + 7.4 f. (25)

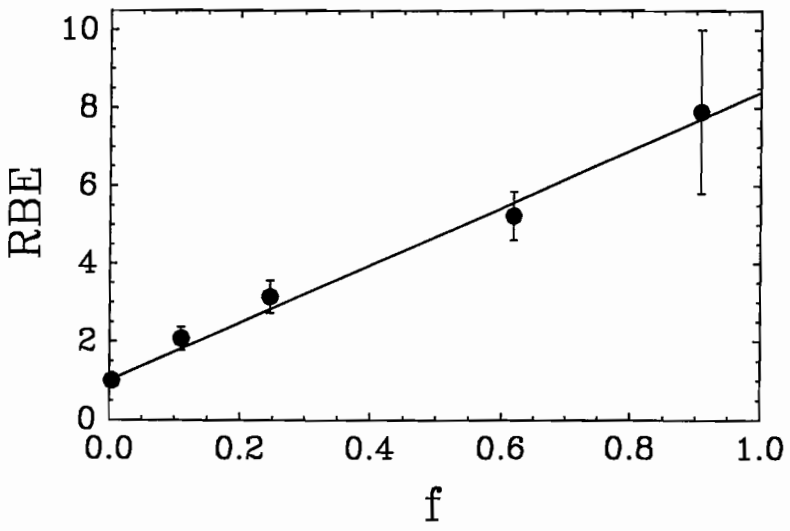

FIG. 6. Spermhead survival in the mouse testis model (5,9,18): RBE as a function of the fraction f of intracellular ^{125}I bound to DNA. The fraction of ^{125}I bound to DNA was adjusted by administering mixtures of the brain perfusion imaging agent $H^{125}IPDM$ (54) and $^{125}IUdR$ which localize in the cytoplasm (5) and nuclear DNA, respectively. The RBE is related to the DNA-bound fraction according to the relationship RBE = 1 + 7.4 f.

II. In Vitro Model: Clonogenicity of Cultured V79 Cells

Kinetics of Cellular Uptake of Radioactivity

Cellular incorporation of $^{125}IUdR$ (IdC) was directly proportional to both incubation time (up to 18 h) and radiochemical concentration κ (kBq/ml) in the extracellular medium. Based on these data, the average

cellular uptake of radioactivity in mBq/cell is given by $A(t) = \omega \kappa t$, where the constant $\omega = 0.037$ mBq/cell per h-kBq/ml and 0.0053 mBq/cell per h-kBq/ml for ^{125}IUdR and ^{125}IdC, respectively. The incorporation of these radioiodine compounds is cell cycle dependent. Therefore, since the doubling time of V79 cells is 9-12 h (23), an 18 h incubation time (T_I) was used in the survival studies with the ^{125}I radiochemicals to insure uniform labeling of the cells. The average uptake of radioactivity per cell A_I (mBq/cell) for $T_I = 18$ h is therefore given by $A_I = 0.67 \kappa$ and 0.1κ for ^{125}IUdR and ^{125}IdC, respectively. The cellular uptake of ^{210}Po-citrate was also linearly dependent on the extracellular radiochemical concentration κ, however, it was rapidly incorporated into the V79 cells, achieving saturation in only 0.5 h (14). Accordingly, cell survival studies with ^{210}Po-citrate called for only a 0.5 h exposure to the radiochemical before washing the cells and seeding them for colony formation. In this instance, the average uptake of radioactivity per cell A_I (mBq/cell) at $T_I = 0.5$ h is given by $A_I = 0.04 \kappa$.

Clonogenic Survival

The survival fraction S is related to the cellular uptake A_I (at T_I) according to the expression $S = \exp(-A_I / A_o)$, where A_o is the mean lethal uptake. A least squares fit to the data (data not shown, see Fig. 8 for dose-response curve) yielded A_o values of 0.13 ± 0.01 mBq/cell and 0.72 ± 0.05 mBq/cell for ^{210}Po-citrate, and ^{125}IUdR and ^{125}IdC, respectively. Characteristic of high-LET radiation effects, these curves had no initial shoulder.

Cellular Retention of Radioactivity During the Colony Forming Period

The radioactivity per cell during the colony forming period decreased exponentially with time for all three radiochemicals (Fig. 7). The effective half-lives (τ_e) were 13.8 h and 12 h, for ^{210}Po-citrate and the radioiodines, respectively. These values were independent of the cellular uptake of radioactivity for the range of uptakes studied.

Subcellular Distribution of Radioactivity

The subcellular distribution of the radiochemicals following incorporation into V79 cells is given in Table II. In all cases, the relative subcellular distributions remained the same during the uptake and colony forming period.

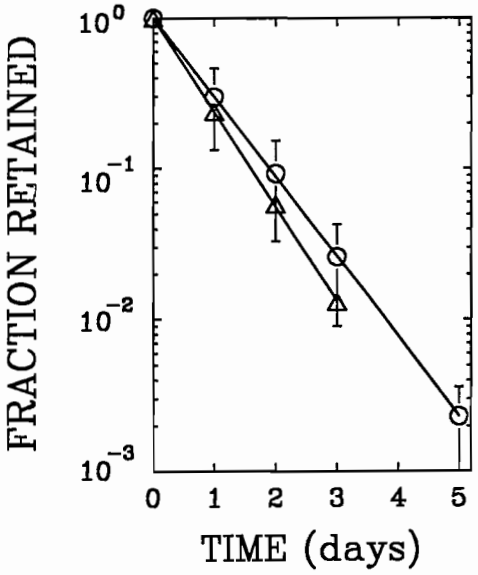

FIG. 7. Elimination of the radiochemicals from exponentially growing V79 cells during the one week colony forming period. The average amount of radioactivity per cell decreases with an effective half-life of 12 h for ^{125}IUdR and ^{125}IdC (solid circles), and 13.8 h for ^{210}Po-citrate (open circles) (Data taken from Ref. 25). Three experiments were averaged, the error bars representing the SDM.

Dosimetry for Internal Irradiation with Incorporated Radionuclides

Because the cell nucleus is widely believed to contain the radiosensitive targets, the absorbed dose to the nucleus is determined (3,16,23,25). There are four contributions to the average dose to the cell nucleus: 1) non-target to target dose from decays occurring in the extracellular medium during the incubation period T_I, 2) self-dose from decays within the target cell during the incubation period T_I, 3) self-dose from decays within the target cell during the colony forming period, and 4) cross irradiation from decays in neighboring cells of the colony. Since κ is small in these studies, contribution (1) is negligible (< 1% of the total dose). Calculation of contributions (2) - (4) requires determination of the cumulated cellular activity during the uptake ($\tilde{A}_I$) and colony forming periods ($\tilde{A}_{CF}$). Details of this calculation are

given in Ref. 25. For ^{125}IUdR (IdC) $\tilde{A}_I = 9\ A_I$ mBq-h, while for ^{210}Po-citrate $\tilde{A}_I$ is negligible compared to the cumulated cellular activity during the colony forming period $\tilde{A}_{CF}$. The values of $\tilde{A}_{CF}$ are 19.9 A_I mBq-h and 17.3 A_I mBq-h for ^{210}Po-citrate and the radioiodines, respectively. The cumulated intracellular disintegrations N are correspondingly 71.6 A_I and 94.6 A_I.

The average dose D to the V79 cell nucleus is given by $D = \xi/v_N$, where v_N is the volume of the nucleus, and ξ is the total energy deposited in the nucleus. If the cross irradiation component of the dose is ignored (see later), then $\xi = N\ (f_N\varepsilon_{NN} + f_{CY}\varepsilon_{NCY})$, where f_N and f_{CY} are the fraction of cellular radioactivity in the nucleus and cytoplasm, respectively. The parameters e_{NN} and e_{NCY} are the average energy deposited in the nucleus per decay in the cell nucleus and cytoplasm, respectively (31). The quantity e_{NN} is 10.9 keV for ^{125}I in V79 cells where the average diameter of the cell and cell nucleus are 10 μm and 8 μm, respectively (25,31). Since $f_N \sim 1$ for ^{125}IUdR and ^{125}IdC, $\xi = 1030\ A_I$ keV. For ^{210}Po $e_{NN} = 216$ keV and $e_{NCY} = 93$ keV. With $f_N = 0.28$ and $f_{CY} = 0.72$, $\xi = 9120\ A_I$ keV for ^{210}Po (25). With $v_N = 270\ \mu m^3$, the average dose to the V79 cell nucleus is 5.4 A_I Gy and 0.61 A_I Gy, for ^{210}Po-citrate and ^{125}IUdR (IdC), respectively. The corresponding dose response curves for cell survival are shown as a function of absorbed dose to the cell nucleus in Fig. 8. Fitting the data to $S = \exp(-\alpha D)$ yields $\alpha = 1.4 \pm 0.5$ Gy^{-1} for ^{210}Po-citrate, and 2.3 ± 0.8 Gy^{-1} for ^{125}IUdR (IdC). The corresponding D_{37} are 0.70 ± 0.25 Gy and 0.44 ± 0.15 Gy, respectively. For ^{210}Po, this corresponds to about 9 intracellular disintegrations. When the subcellular radionuclide distribution is taken into account, this is equivalent to about 2 α particle traversals across the cell nucleus. This number (9 disintegrations) is substantially fewer than the 66 disintegrations required for the ^{125}I compounds.

External Irradiation with γ rays

Dose response curves for V79 cells irradiated either acutely with a single exposure to 662 keV ^{137}Cs γ rays (2.6 Gy/min), or chronically with 140.5 keV ^{99m}Tc γ rays (initially ~ 1.2 Gy/h for final cumulated dose of 10 Gy), are shown in Fig. 8. The data were least squares fitted to the linear-quadratic model $S = \exp -(\alpha D + \beta D^2)$ (25). The resulting D_{37} values were 400 cGy and 880 cGy for ^{137}Cs and ^{99m}Tc γ rays, respectively. Based on these data, it is clear that the chronic irradiation, delivered in a manner somewhat similar to that for incorporated radionuclides, is significantly less effective than acute irradiation.

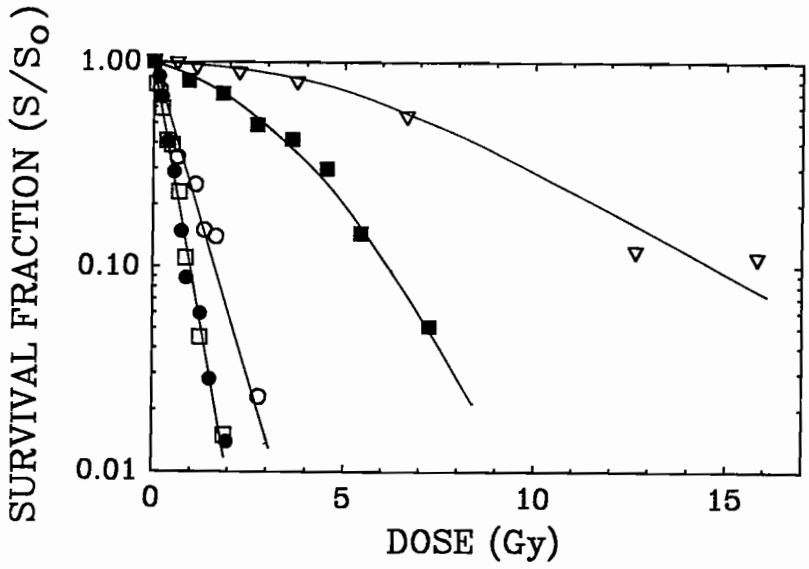

FIG. 8. Dose response curves for cultured V79 cells following incorporation of ^{210}Po-citrate (open circles), ^{125}IUdR (solid circles), and ^{125}IdC (open squares). The survival of Chinese hamster V79 cells following external irradiation with acute or chronic γ rays is also shown. The solid squares represent the cell survival fraction as a function of absorbed dose from ^{137}Cs γ rays delivered acutely (2.6 Gy/min). The open inverse triangles are for ^{99m}Tc γ rays delivered chronically with the dose rate decreasing exponentially over several days according to the 6 h physical half-life of ^{99m}Tc (initial dose rate ~ 1.2 Gy/h for final cumulative dose of 10 Gy). The SDM is indicated by the error bars. Data taken from Ref. 25.

DISCUSSION

Delineation of the biological effects of incorporated Auger electron emitters is complicated indeed. Therefore, the parallel *in vivo* and *in vitro* experiments presented in this work, namely spermhead survival in mouse testis and clonogenic survival of cultured V79 cells, provide valuable complementary data regarding the lethality of these radionuclides. These parallel data address several aspects including: 1) role of reference radiation for determining RBE values - dependence on dose rate, 2) RBE of DNA incorporated Auger emitters compared to α emitters, 3) dependence of RBE on decay site in DNA, 4) dependence of RBE on absorbed dose at which

comparison is made, and 5) calculation of the dose equivalent. In addition, experimental data are provided to support the validity of using the mouse testis model as a unique assay to study the effects of incorporated radionuclides *in vivo* at low doses.

Survival Curves

Before discussing the issue of reference radiation, it is perhaps useful to critically examine the dose-response (survival) curves obtained with the *in vivo* and *in vitro* models. As expected, the survival curves obtained following external irradiation of V79 cells with γ rays, delivered chronically or acutely, have a distinct shoulder (Fig. 8). Similarly, the exponential response of V79 cells (Fig. 8) to doses delivered by internal α and DNA-bound Auger emitters is also expected based on the observations of others (3,32). These shouldered and non-shouldered curves are classic radiobiological cell-survival curves for low- and high-LET radiations, respectively. In contrast, the spermhead survival curves obtained *in vivo* with the mouse testis model are strikingly different in their functional form (Fig. 4). The observed two-component exponential dose-response curves are not due to artifacts caused by intratesticular injection. Indeed, the same two-component nature is seen when the testis are uniformly irradiated with external X rays as shown in Fig. 4. Similar two-component curves were also observed by Oakberg (33), Gasinska (34), Hacker *et al.* (35), and Spano *et al.* (36) when spermhead survival was measured following exposure to external X rays. Furthermore, the data in Fig. 5, which show the response of spermatogonial cell types A_1-A_4, In, and B to external X irradiation, strongly suggest that the two-component nature of the spermhead survival curves is due to differential radiosensitivity of the spermatogonia. Perhaps even more important is the equivalence of survival curves for external X rays and internally administered radionuclides which impart low-LET type damage (Fig 4). Among these radiochemicals are ^{7}Be chloride (γ emitter), H^{131}IPDM (β emitter), and H^{125}IPDM & ^{123}IMP (cytoplasmically localized Auger emitters). The essentially identical nature of these curves (Fig. 4), which encompass the effects of intratesticular injection of extremely short range electron emitters (^{125}I) to very long range γ emitters (^{7}Be), clearly demonstrates that intratesticular injection of the radiochemicals does not lead to macroscopic inhomogeneities in activity distribution which in turn influence the shape of the survival curves. Even further support for this conclusion is provided by our studies with intraperitoneally administered ^{210}Po-citrate (data not shown) which result in the same mean lethal dose as

intratesticular administration. Finally, it should be noted that the sharply different slopes (compared to X rays) of the individual components of the curves for the high-LET radiations (^{210}Po-citrate and ^{125}IUdR & ^{125}IdC) are expected based on similar curves given by Spano *et al.* (36) and Oakberg (33) for neutron irradiation of mouse testes.

Reference Radiation

The issue of selecting a reference radiation for the purpose of calculating RBE values takes on very different degrees of importance for the *in vitro* and *in vivo* models utilized in this work. We established above for the mouse testis model that chronic internal irradiation from radionuclides which impart low-LET type damage are just as lethal as acute external X rays. Hence, selection of the reference radiation is not critical for the *in vivo* survival assay and therefore external X rays perhaps are the best choice in view of the conventional 250 kVp X rays. Conversely, the acute versus chronic nature of the irradiation plays a major role in the response of cultured V79 cells. As shown in Fig. 8, acute ^{137}Cs γ rays are more than twice as effective in killing V79 cells than ^{99m}Tc γ rays delivered chronically in a manner consistent with incorporated radionuclides. Therefore, ^{99m}Tc γ rays are perhaps the more relevant reference radiation for the *in vitro* model.

Relative Biological Effectiveness of the Radiochemicals

As indicated earlier, the relative biological effectiveness is defined as $RBE = D_R/D_A$ for radiation A relative to the reference radiation R for equal biological effect (26). With 120 kVp X rays serving as the reference radiation for the mouse testis model, the RBE at 37% survival for the radiochemicals ^{7}Be chloride, H^{131}IPDM, H^{125}IPDM, and ^{123}IMP is ~ 1.0 (Table I). The RBE values for ^{210}Po-citrate and ^{125}IUdR & ^{125}IdC are 6.7 and 7.9, respectively (4). Similarly, if we use ^{99m}Tc γ rays as the reference radiation (chronic) for Chinese hamster V79 cells (25), the RBE at 37% survival is 13 ± 5 for ^{210}Po-citrate and 20 ± 7 for ^{125}IUdR and ^{125}IdC (Table II). Although these values may be quite high for cell killing, we note that our data give RBE = 6 ± 2 and 9 ± 3 for the respective radiochemicals when acute γ ray exposure is used as the reference (Table II). These results are in good agreement with other published work with V79 cells (3,14,32,37,38). Similarly, a value of 12 was reported for mouse embryos (39). It is important to note that these RBE values also depend strongly on the end point. This is emphasized in Figs. 9A & 9B where the RBE is plotted as a function of the absorbed dose. For both the *in vivo* and *in vitro*

models, the RBE is greatest in the low-dose region and substantially smaller (4-6 times) in the high-dose region. Therefore, caution is needed when interpreting reported RBE values for incorporated Auger emitters.

TABLE I

RBE Values Obtained with Spermhead Survival Assay

Radiochemical	*In vivo* Subcellular Distribution	RBE Spermhead Survival
120 kVp X rays	-	-
^{7}Be chloride (9)	46% Cy, 54% N	1.0
H^{131}IPDM (5)	100% Cy	1.1
H^{125}IPDM (5)	100% Cy	1.0
^{123}IMP	100% Cy	1.1
^{125}IdC	100% N; 100% D	8.7
^{125}IUdR (4)	100% N; 100% D	7.9
^{210}Po-citrate (4)	80% Cy, 20% N; 45% D	6.7

TABLE II

RBE Values Obtained with Clonogenic Survival of V79 Cells

Radiochemical	*In vitro* Subcellular Distribution	RBE Compared Acute ^{137}Cs γ rays	RBE Compared to chronic ^{99m}Tc γ rays
^{125}IUdR (25)	100% N; 100% D	9	20
^{125}IdC (25)	100% N; 100% D	9	20
^{210}Po-citrate (25)	72% Cy, 28% N	6	13

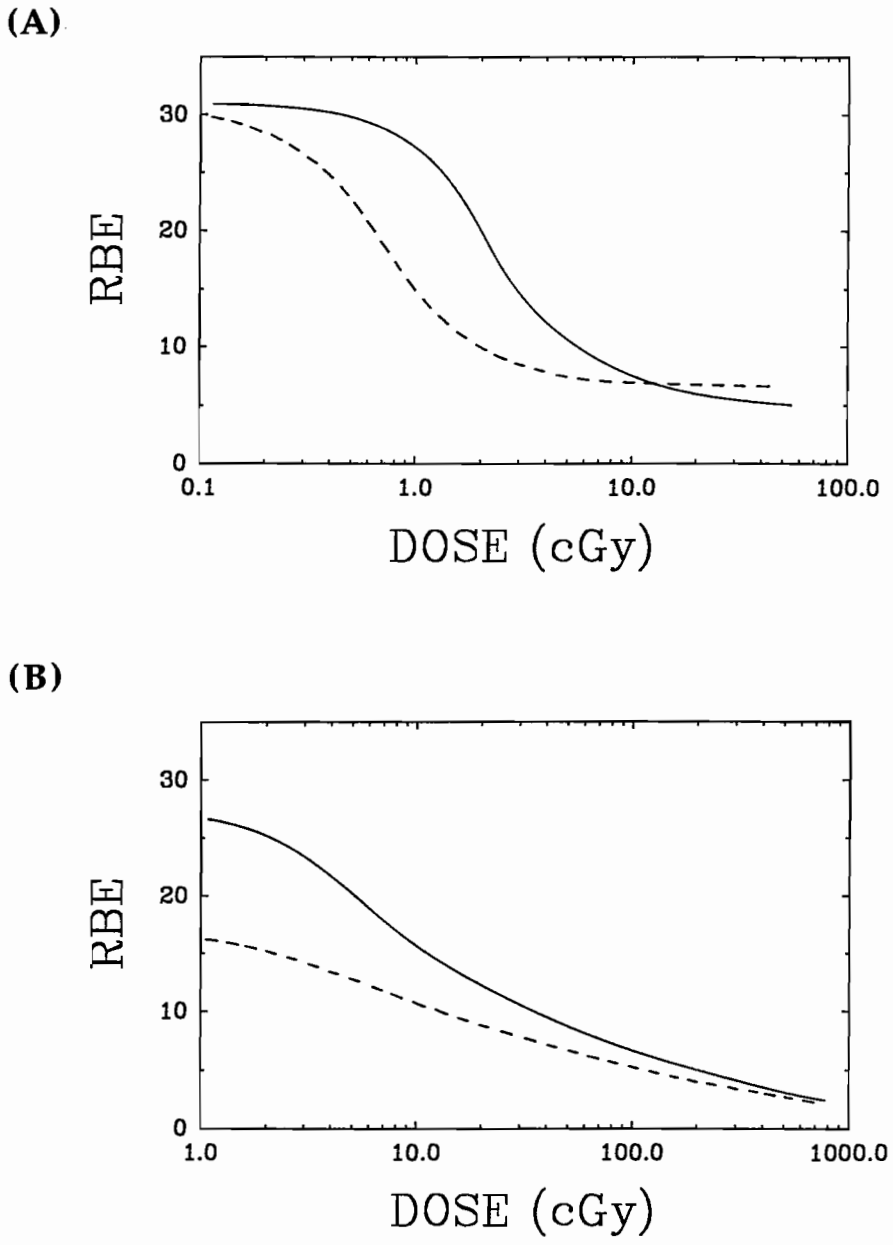

FIG. 9. Dependence of RBE on absorbed dose. The RBE for ^{210}Po-citrate (dashed line) and ^{125}IUdR (solid line) is plotted as a function of the absorbed dose for A) spermhead survival in mouse testis, and B) clonogenic survival of cultured V79 cells. For each assay and each radiochemical, the RBE is maximum (~ 20-30) at low doses and minimum (~ 5) in the high dose region.

Lethality of Auger Cascades Compared to High-LET α Particles

The data shown in Figs. 4 & 8 and Tables I & II allow a direct comparison between the lethality of incorporated high-LET α emitters and the Auger emitter ^{125}I covalently bound to the DNA in the form of ^{125}IUdR and ^{125}IdC. Both the *in vivo* and *in vitro* data indicate that ^{125}I Auger cascades are at least as lethal as 5.3 MeV α particles from ^{210}Po when compared on the basis of absorbed dose to the testis or V79 cell nucleus. This is consistent with theoretical expectations based on the very large energy densities (40-44) and number of chemical species ($OH\cdot$, H_3O^+, *etc.*) produced in the immediate vicinity of the decay site of ^{125}I in comparison with those along the track of a 5.3 MeV α particle (45).

Radiosensitivity of Different DNA Base Sites

The biological effects of Auger emitters are most severe when the radionuclide is covalently bound to the nuclear DNA (*e.g.* ^{125}IUdR) (1-5,13,46,47). However, Yasui *et al.* (10) have demonstrated that not all sites to which ^{125}IUdR binds are equally radiosensitive with some sites being over 3 times more sensitive than others. This suggests that thymine sites are not equally sensitive to radiation. One may ask, then, whether the different DNA base sites (*e.g.* adenine, thymine, guanine, cytosine) are differentially radiosensitive to Auger cascades. Inasmuch as ^{125}IUdR and ^{125}IdC covalently bind to DNA at the thymine and cytosine base sites, respectively, our experimental results for these radiochemicals (Figs. 4, 8; Tables I, II) suggest that thymine and cytosine sites are equivalent in terms of their radiosensitivity. This finding highlights the potential of Auger electron emitters to probe the radiosensitive targets in the DNA by directing them to particular sites with radiochemicals which damage only a highly localized region. This remarkable capacity for differential and site-specific damage, unattainable by conventional beams of external radiation, may have a significant impact on ultimately elucidating the radiosensitive targets in the mammalian cell.

The Quality Factor *Q* for Auger Electron Emitting Radiochemicals

The question of assigning quality factors Q (or radiation weighting factors w_R) to Auger-electron emitters is a complex issue. Unlike external beams of radiation where the variables which govern the biological response

of the system are easily controlled (*i.e.* type of radiation, dose rate, *etc.*), the effects of radiations from incorporated radionuclides are complicated by additional factors. These include the macroscopic and subcellular distribution of the radionuclide (40,41,48-52), as well as the patterns of biological clearance. These additional factors may affect the radiotoxicity of Auger emitters, and therefore must be considered when addressing the issue of quality factor and calculation of dose equivalent H. Such factors were considered by Pomplun *et al.* (11) who proposed a quality factor equal to that of high-LET radiations when "inside" the DNA. They have further suggested $Q = 1$ when the ^{125}I decay occurs "outside" the DNA. These suggestions are supported by our *in vivo* and *in vitro* data comparing the biological effects of ^{125}IUdR and ^{210}Po-citrate (Tables I and II). However, since the quality factor is intended to reflect the nature of the radiation (17), the value of Q for Auger emitters should not depend on where the decay occurs relative to the radiosensitive targets. Hence, the Q for Auger emitters should simply be equal to Q for high-LET radiations regardless of the decay site. With Q a constant, subcellular distribution of Auger emitters may in turn be built into the dose equivalent. The dose equivalent H has been defined by the ICRU (17) as $H = D\,Q\,N$, where D is the absorbed dose, and N is the product of any other factors influencing the dose equivalent. Since subcellular distribution of Auger emitters is clearly the primary determinant of their effects (5,7,9,16), the quantity H must also depend on their subcellular distribution. The data shown in Fig. 6 shows that the RBE is directly proportional to the fraction f of intracellular ^{125}I bound to DNA ($RBE = 1 + 7.4\,f$). Therefore, it is not unreasonable to suggest that H for ^{125}I, or other Auger emitters for that matter, might also be directly proportional to f. Insofar as H is linear in f, the relation $H = D\,(1 + f\,(Q - 1))$ may be a reasonable first step toward establishing meaningful radiation protection guidelines for Auger-electron emitters (25). This of course would be subject to confirmation of these conclusions with respect to experimental end points more pertinent to carcinogenesis.

ACKNOWLEDGMENTS

The authors would like to thank Dr. H. Huang (UMDNJ - Dept. of Anatomy) for his assistance and useful discussions regarding the spermatogonial cell killing assay. This work was supported in part by USPHS Grant No. CA-32877 (DVR) and NJ Cancer Commission Grants 688-009 (RWH) and 689-042 (DVR) and NJ Cancer Commission Fellowship Grant No. 689-080 (VRN).

REFERENCES

1. A.I. Kassis, S.J. Adelstein, C. Haydock, K.S.R. Sastry, K.D. McElvany, and M.J. Welch, Lethality of Auger electrons from the decay of bromine-77 in the DNA of mammalian cells. *Radiat. Res.* **90**, 362-373 (1982).
2. G.M. Makrigiorgos, A.I. Kassis, J. Baranowska-Kortylewicz, K.D. McElvany, M.J. Welch, K.S.R. Sastry, and S.J. Adelstein, Radiotoxicity of 5-[I-123]Iodo-2'-deoxyuridine in V79 cells: A comparison with 5-[I-125]Iodo-2'-deoxyuridine. *Radiat. Res.* **118**, 532-544 (1989).
3. A.I. Kassis, K.S.R. Sastry, and S.J.Adelstein, Kinetics of uptake, retention, and radiotoxicity of ^{125}IUdR in mammalian cells: Implications of localized energy deposition by Auger processes. *Radiat. Res.* **109**, 78-89 (1987).
4. D.V. Rao, V.R. Narra, R.W. Howell, G.F. Govelitz, and K.S.R. Sastry, In-vivo radiotoxicity of DNA-incorporated I-125 compared with that of densely ionising alpha-particles. *The Lancet* Vol **II**, No 8664, 650-653 (1989).
5. D.V. Rao, V.R. Narra, R.W. Howell, and K.S.R. Sastry, Biological consequence of nuclear versus cytoplasmic decays of I-125: Cysteamine as a radioprotector against Auger cascades in vivo. *Radiat. Res.* **124**, 188-193 (1990).
6. R.W. Howell, Radiobiological effects of Auger electrons in the decay of Pt-195m. *Ph.D. Dissertation, Department of Physics & Astronomy*, University of Massachusetts, Amherst, MA, USA 01003 (1987).
7. A.I. Kassis, R.W. Howell, K.S.R. Sastry, and S.J. Adelstein, Positional effects of Auger decays in mammalian cells in culture. In *DNA Damage by Auger Emitters*, (K.F. Baverstock and D.E. Charlton, Eds.) Taylor & Francis, London. pp 1-14, 1988.
8. A.I. Kassis, F. Fayad, B.M. Kinsey, K.S.R. Sastry, and S.J. Adelstein, Radiotoxicity of an I-125-labeled DNA intercalator in mammalian cells. *Radiat. Res.* **118**, 283-294 (1989).
9. D.V. Rao, K.S.R. Sastry, H.E. Grimmond, R.W. Howell, G.F. Govelitz, V.K. Lanka, and V.B. Mylavarapu, Cytotoxicity of some indium radiopharmaceuticals in mouse testes. *J. Nucl. Med.* **29**, 375-384 (1988).
10. L.S. Yasui, K.G. Hofer, and R.L. Warters, Inhomogeneity of the nucleus to ^{125}IUdR cytotoxicity. *Radiat. Res.* **102**, 106-118 (1985).
11. E. Pomplun, J. Booz, A. Dydejczyk, and L.E. Feinendegen, A microdosimetric interpretation of the radiobiological effectiveness of ^{125}I and the problem of quality factor. *Radiat. Environ. Biophys.* **26**, 181-188 (1987).
12. ICRP, *Recommendations of the ICRP*. Publication 26, Pergamon Press, New York, 1977.
13. D.V. Rao, V.R. Narra, R.W. Howell, V.K. Lanka, and K.S.R. Sastry, Induction of spermhead abnormalities by incorporated radionuclides: Dependence on subcellular distribution, type of radiation, dose rate, and presence of radioprotectors. *Radiat. Res.* **125**, 89-97 (1991).
14. R.W. Howell, V.R. Narra, D.V. Rao, and K.S.R. Sastry, Radiobiological effects of intracellular polonium-210 alpha emissions: A comparison with Auger-emitters. *Radiat. Prot. Dosim.* **31**, 325-328 (1990).

15. D.V. Rao, V.R. Narra, G.F. Govelitz, V.K. Lanka, R.W. Howell, and K.S.R. Sastry, In vivo effects of 5.3 MeV alpha particles from Po-210 in mouse testes: Comparison with internal Auger emitters. *Radiat. Prot. Dosim.* **31**, 329-332 (1990).
16. K.G. Hofer, C.R. Harris, and J.M. Smith, Radiotoxicity of intracellular Ga-67, I-125, H-3. Nuclear versus cytoplasmic radiation effects in murine L1210 leukaemia. *Int. J. Radiat. Biol.* **28**, 225-241 (1975).
17. ICRU, *Conceptual Basis for Determination of the Dose Equivalent.* Report 25, International Commission on Radiation Units and Measurements, Bethesda, MD, 1976.
ICRP, 1990 Recommendations of the International Commission on Radiological Protection, Publication 60, Pergamon Press, New York, NY, 1990.
18. D.V. Rao, G.F. Govelitz, and K.S.R. Sastry, Radiotoxicity of thallium-201 in mouse testes: Inadequacy of conventional dosimetry. *J. Nucl. Med.* **24**, 145-153 (1983).
19. D.V. Rao, K.S.R. Sastry, G.F. Govelitz, and H.E. Grimmond, In vivo effects of iron-55 and iron-59 on mouse testis: Biophysical dosimetry of Auger electrons. *J. Nucl. Med.* **26**, 1456-1465 (1985).
20. M.L. Meistrich, Critical components of testicular function and sensitivity to disruption. *Biol. Rep.* **34**, 17-28 (1986).
21. E.F. Oakberg, Spermatogonial stem-cell renewal in the mouse. *Anat. Rec.* **169**, 515-532 (1971).
22. C. Huckins and E.F. Oakberg, Morphological and quantitative analysis of spermatogonia in mouse testes using whole mounted seminiferous tubules: II. The Irradiated Testes. *Anat. Rec.* **192**, 529-542 (1978).
23. A.I. Kassis, K.S.R.Sastry, and S.J.Adelstein, Intracellular distribution and radiotoxicity of Chromium-51 in mammalian cells: Auger-electron dosimetry. *J. Nucl. Med.* **26**, 59-67 (1985).
24. A.I. Kassis and S.J. Adelstein, A rapid and reproducible method for the separation of cells from radioactive media. *J. Nucl. Med.* **21**, 88-90 (1980).
25. R.W. Howell, D.V. Rao, D.Y. Hou, V.R. Narra, and K.S.R. Sastry, The question of relative biological effectiveness and quality factor for Auger emitters incorporated into proliferating mammalian cells. *Radiat. Res.* **128**, 282-292 (1991).
26. ICRP, *RBE for Deterministic Effects.* Publication 58, International Commission of Radiation Units and Measurements, Pergamon Press, New York (1990).
27. R. Loevinger and M. Berman, A revised schema for calculating the absorbed dose from biologically distributed radionuclides. *MIRD Pamphlet No. 1*, Revised. Society of Nuclear Medicine, New York, 1976.
28. R.W. Howell, D.V. Rao, and K.S.R. Sastry, Macroscopic dosimetry for radioimmunotherapy: Nonuniform activity distributions in solid tumors. *Med. Phys.* **16**, 66-74 (1989).
29. D.A. Weber, K.F. Eckerman, L.T. Dillman, and J.C. Ryman, *MIRD: Radionuclide Data and Decay Schemes.* Society of Nuclear Medicine, New York, 1989.
30. T.A. Mian, H.J. Glenn, T.P. Haynie, and M.L. Meistrich, Radiation dose and biological effects to mouse testis from sodium P-32 phosphate. *Health Phys.* **42**, 657-664 (1982).
31. A.I. Kassis, S.J. Adelstein, C. Haydock, and K.S.R. Sastry, Radiotoxicity of Se-75 and S-35: Theory and application to a cellular model. *Radiat. Res.* **84**, 407-425 (1980).
32. A.I. Kassis, C.R. Harris, S.J. Adelstein, T.J. Ruth, R. Lambrecht, and A.P. Wolf, The in vitro radiobiology of astatine-211 decay. *Radiat. Res.* **105**, 27-36 (1986).

33. E.F. Oakberg, Effects of radiation on the testis. In *Hand Book of Physiology*, Section 7, Volume 5, (D.W. Hamilton and R.O. Greep, Eds.) American Physiological Society, Washington, D.C. pp 233-243, 1960.
34. A. Gasinska, Mouse testis weight loss and survival of differentiated spermatogonia following irradiation with 250 kV and 5.5 MeV fast neutrons. *Neoplasma* **32**, 443-449 (1985).
35. U. Hacker, W. Gohde, and J. Schumann, Mammalian spermatogenesis as a biological dosimeter for ionizing radiation. In *Symposium on Biological Dosimetry*, pp 2-12, 1982.
36. M. Spano, F. Pacchierotti, F. Mauro, S. Quaggia, and R. Uccelli, Flow cytometric analysis of the effects of 0.4 MeV fission neutrons on mouse spermatogenesis. *Int. J. Radiat. Biol.* **51**, 401-419 (1987).
37. R. Cox, J. Thacker, D.T. Goodhead, and R.J. Munson, Mutation and inactivation of mammalian cells by various ionising radiations. *Nature* **267**, 425-427 (1977).
38. B.J. Barnhart and S.H. Cox, Mutagenicity and cytotoxicity of 4.4-MeV alpha particles emitted by plutonium-238. *Radiat. Res.* **80**, 542-548 (1979).
39. V.R. Narra, R.W. Howell, K.L. Thanki, and D.V. Rao, Radiotoxicity of ^{125}I-iododeoxyuridine in preimplantation mouse embryos. *Int. J. Radiat. Biol.* **60**, 525-532 (1991).
40. K.S.R. Sastry and D.V. Rao, Dosimetry of low energy electrons. In *Physics of Nuclear Medicine: Recent Advances*, (D.V. Rao, R. Chandra, and M. Graham, Eds.), Medical Physics Monograph No. 10, American Institute of Physics. pp 169-208, 1984.
41. G.M. Makrigiorgos, S.J. Adelstein, and A.I. Kassis, Limitations of conventional internal dosimetry at the cellular level. *J. Nucl. Med.* **30**, 1856-1864 (1989).
42. D.E. Charlton and J. Booz, A Monte Carlo treatment of the decay of ^{125}I. *Radiat. Res.* **87**, 10-23 (1981).
43. E. Pomplun, J. Booz, and D.E. Charlton, A Monte Carlo simulation of Auger cascades. *Radiat. Res.* **111**, 533-552 (1987).
44. D.E. Charlton, H. Nikjoo, and J.L. Humm, Calculation of initial yields of single-and double-strand breaks in cell nuclei from electrons, protons, and alpha particles. *Int. J. Radiat. Biol.* **56**, 1-19 (1989).
45. H.A. Wright, R.N. Hamm, J.E. Turner, R.W. Howell, D.V. Rao, and K.S.R. Sastry, Calculations of physical and chemical reactions with DNA in aqueous solution from Auger cascades. *Radiat. Prot. Dosim.* **31**, 59-62 (1990).
46. A.I. Kassis, G.M. Makrigiorgos, and S.J. Adelstein, Implications of radiobiological and dosimetric studies of DNA-incorporated I-123: The use of the Auger effect as a biological probe at the nanometre level. *Radiat. Prot. Dosim.* **31**, 333-338 (1990).
47. L.S. Yasui, and K.G. Hofer, Role of mitochondrial DNA in cell death induced by I-125 decay. *Int. J. Radiat. Biol.* **49**, 601-610 (1986).
48. K.S.R. Sastry, R.W. Howell, D.V. Rao, V.B. Mylavarapu, A.I. Kassis, S.J. Adelstein, H.A. Wright, R.N. Hamm, and J.E. Turner, Dosimetry of Auger-emitters: Physical and phenomenological approaches. In *DNA Damage by Auger Emitters*, (K.F. Baverstock and D.E. Charlton, Eds.) Taylor & Francis, London. pp 27-38, 1988.
49. D.V. Rao, V.B. Mylavarapu, G.F. Govelitz, V.K. Lanka, K.S.R. Sastry, and R.W. Howell, Biological and biophysical dosimetry of Auger-emitters in vivo: A Review. In *Selected Topics in Physics of Radiotherapy and Imaging*, (U. Madhvanath,

K.S. Parthasarathy, and T.V. Venkateswaran, Eds.) Tata McGraw-Hill, New Delhi. pp. 232-258, 1988.

50. J.L. Humm, Dosimetric aspects of radiolabeled antibodies for tumor therapy. *J. Nucl. Med.* **27**, 1490-1497 (1986).
51. J.L. Humm, L.M. Chin, L. Cobb, and R. Begent, Microdosimetry in radioimmunotherapy. *Radiat. Prot. Dosim.* **31**, 433-436 (1990).
52. R.W. Howell, D.V. Rao, and C. Haydock, Dosimetry techniques for therapeutic applications of incorporated radionuclides. In *Dosimetry of Incorporated Radionuclides*. (S.J. Adelstein, A.I. Kassis, and R.W. Burt, Eds.) American College of Nuclear Physicians, Washington D.C. pp 215-256, 1990.
53. M.L. Meistrich, N.R. Hunter, N. Suzuki, P.K. Trostle, and H.R. Withers, Gradual regeneration of mouse testicular stem cells after exposure to ionizing radiation. *Radiat. Res.* **74**, 349-362 (1978).
54. B. Lui, J. Chang, J.S. Sun, J. Billings, A. Steves, R. Ackerhalt, M. Molanar, and H.F. Kung, Radioactive iodine exchange reaction of HIPDM: Kinetics and mechanism. *J. Nucl. Med.* **28**, 360-365 (1987).

DISCUSSION

Schneiderman, M. From the kinetics of cell production can you tell if the stem cells are being affected by your ^{125}IUdR treatment?

Howell, R. W. It is unlikely that the stem cells are being affected significantly because they are 5-10 times less radiosensitive than the rapidly dividing spermatogonial cells which actively incorporate the radiochemical. Furthermore, we assay the effects on the 29th day which is well before the time necessary for stem cells to become sonication resistant spermatids.

Humm, J. L. The use of RBE with an *in vivo* study can be dangerous in particular when one injects an isotope releasing short range particles directly into the testes. Did you perform autoradiography to investigate the degree of heterogeneity in the testes, and what influence do you think any heterogeneity will have on your determination of RBE's?

Howell, R. W. This question has been addressed extensively in our manuscript. Yes, we do perform autoradiographic studies and macroscopic distribution studies, but our survival curves perhaps yield more information in this regard. Testicular injection of various "low-LET radiochemicals", including those labeled with short-range electron emitters such as ^{125}I, invariably results in a survival curve that closely matches that obtained following external irradiation with 120 kVp X rays. Therefore, any heterogeneity caused by intratesticular injection of the radiochemicals does not lead to any appreciable effect on the shape of the survival curve and correspondingly no effect on the RBE.

Adelstein, S. J. For radiation protection purposes, it is the RBE for carcinogenesis that is most important, hence, one should look at such biological end points as transformations, mutagenesis, in defining the value of Q or, more lately, w_R.

Howell, R. W. I agree. Because of this, we took care not to specifically assign a Q value for Auger emitters, although we did suggest that a value of the order of that for α emitters may be appropriate based on the survival data. It also remains to be seen if a linear relationship between RBE and fraction of DNA-bound activity (Auger emitter) holds true when transformations and mutations are taken as the biological end points.

Biophysical Aspects of Auger Processes, AAPM Symposium Series No. 8 (1992) 319-335
Eds. RW Howell, VR Narra, KSR Sastry, DV Rao

CHEMICAL PROTECTION AGAINST RADIONUCLIDES *IN VIVO*: IMPLICATIONS TO THE MECHANISM OF THE AUGER EFFECT

VENKAT R. NARRA, RAVI S. HARAPANHALLI,
ROGER W. HOWELL,
[1]KANDULA S.R. SASTRY, and DANDAMUDI V. RAO

Division of Radiation Research
Department of Radiology
University of Medicine and Dentistry of New Jersey
Newark, NJ 07103, USA

[1]Department of Physics and Astronomy
University of Massachusetts, Amherst, MA 01003, USA

ABSTRACT

It is well known that chemical radioprotectors such as thiols are capable of mitigating acute radiation effects *in vitro*. If the effects of acute irradiation are reduced by the presence of radioprotectors, can we expect a similar response for chronic irradiation from incorporated radionuclides? Our present *in vivo* studies with the protector cysteamine (MEA), in the mouse testis model, suggest that this is indeed the case for a variety of radionuclides including α emitters. A number of mechanisms by which MEA provides protection against radiation damage have been suggested including radical scavenging, hydrogen atom donation, and induction of hypoxia. Therefore, cysteamine and similar compounds may provide an opportunity to elucidate the basic

mechanism (*i.e.* direct versus indirect interactions) of radiation damage from Auger emitters. Our results for the α emitter ^{210}Po, and the Auger emitter ^{125}I localized in the cell nucleus and bound to DNA, show that cysteamine provides considerably more protection against Auger emitters than 5.3 MeV α particles. This suggests that Auger effects may be largely due to the indirect action of radical species. Additional data for a variety of other radiopharmaceuticals and external X rays, administered in the presence and absence of cysteamine, are presented.

INTRODUCTION

For several years we have been investigating the radiotoxicity of different Auger-electron emitting radiopharmaceuticals using spermatogenesis in mouse testis as the biological model, spermhead survival and induction of sperm-shape abnormalities being the experimental end points (1-8). The extreme radiosensitivity of spermatogonial cells makes the mouse testis an effective *in vivo* experimental model to study the effects of low doses. Recently, using the same biological models, our emphasis has been to study the capacity of chemical radioprotectors to mitigate the biological effects of various incorporated radionuclides including Auger emitters (5). Such data may be helpful in elucidating the basic mechanism of radiation action by Auger electron cascades.

In order to understand how radioprotection against Auger cascades may provide basic mechanistic information, some background information concerning the biological effects of Auger emitters is necessary. Over the years it has been well documented that the effectiveness of Auger emitters depends on the subcellular localization of the radionuclide (*e.g.* 6,8-10). Specifically, our earlier *in vivo* studies showed that when the Auger emitter ^{125}I was localized in the DNA of the cell nucleus, the observed effects were much more severe when compared to ^{125}I localized in the cytoplasm (5). In fact, the biological effectiveness of ^{125}IUdR, which localizes in DNA, was observed to be as effective as 5.3 MeV α particles emitted by incorporated ^{210}Po (4). These *in vivo* results, which are consistent with several *in vitro* experiments (10-14), clearly demonstrate the high-LET type radiotoxicity of DNA incorporated Auger emitters and support the generally accepted notion that the severe biological damage caused by these radionuclides is mainly due to the direct action of Auger electrons.

Thiol compounds were first shown to protect against the effects of acute low-LET radiations by Patt *et al.* (15). Since then, many chemicals have been tested *in vitro* for their radioprotective properties against external beams of ionizing radiations. Bird (16) has shown that cysteamine (MEA) provides better protection against acute exposure to low-LET radiation compared to high-LET radiations. This suggests that MEA provides better protection against indirect effects than direct effects. Therefore, one would expect enhanced protection against cytoplasmically localized ^{125}I compared to that against DNA-bound ^{125}I. However, using the mouse testis model and MEA, Rao *et al.* (5) recently reported dose modification factors (DRF) of 3.6 for DNA incorporated $^{125}IUdR$ and 3.8 for cytoplasmically localized $H^{125}IPDM$. The fact that the both cytoplasmically and DNA incorporated ^{125}I were similarly protected against suggests that the indirect mechanism of radiation action is involved, at least in part.

This paper is an attempt to further understand the basic mechanism of radiation action of Auger electron emitters through a systematic examination of the radioprotective abilities of MEA against radionuclides which have very different radiation properties, as well as against external X rays. As before, the mouse testis model is employed, and results for intratesticular administration of MEA will be presented. In addition, the capacity of radioprotectors to mitigate the effects of chronic, versus acute, exposure will be explored. Finally, in an attempt to understand the mechanism of radioprotection, the pharmacokinetics of MEA were studied with ^{35}S labeled compound.

MATERIALS AND METHODS

Experimental Model

Of all the cell stages in the spermatogenic cycle of mouse testis, spermatogonial cells are the most sensitive to radiation. In contrast, the pre- and post-gonial cells are relatively radioresistent (17,18). This differential radiosensitivity provides the rationale for the mouse testis model as a means to investigate the effects of low doses of ionizing radiations. When testes are exposed to radiations externally, or with incorporated radionuclides, the initial damage to the spermatogonial cells results in a reduced spermhead population when counted after the time necessary (4 to 5 weeks) for spermatogonia to become spermatids of stages 12 to 16. It takes about 9 days for mature spermtids (spermatozoa) to migrate from the testis to the

epididymis. The epididymal sperm morphology is another sensitive indicator of radiation damage (19). The normal sperm have a hook-like head and a long tail. It is important that sperm shape abnormalities in epididymal sperm are assayed 9 days after the minimum spermhead count is reached following the radiation exposure. Since this optimal day depends on the nature of the exposure, and perhaps on cellular incorporation of the radionuclides, it must be determined experimentally in each case.

Radiochemicals

The radionuclides ^{125}I and ^{131}I were obtained from New England Nuclear (Billerica, MA) and labeled to stable HIPDM using procedures described by Lui *et al.* (20). Polonium-210 citrate was prepared according to the directions in Ref. 4. Iodine-125 iododeoxyuridine was obtained commercially from ICN Radiochemicals (Irvine, CA). Nonradioactive cysteamine was obtained from Sigma Chemical Company (St. Louis, MO). The radiolabeling of cysteamine with ^{35}S was accomplished using the methods described by Harapanhalli *et al.* (21).

Experimental Methods

Male Swiss Webster mice (8-9 weeks old) were used in the present studies. The animals (Taconic Farms, Germantown, NY) were maintained in the University animal care facility with standard food and water. The mice were anesthetized under ether and injected intratesticularly (i.t.) with known amounts of radionuclide in a suitable chemical form using a microsyringe. In the case of radioprotectors, the chemicals were also administered intratesticularly. The injected mice were sacrificed under ether after a predetermined number of days depending on the study undertaken.

Retention of the Radiochemicals

To determine the biological clearance of the injected activity from the testis, the radiochemical was administered into the right testis and the mice were sacrificed in groups of five at various times post-injection. The testis were removed and assayed for radioactivity using either a NaI well counter (^{125}I and ^{131}I) or liquid scintillation counter (^{35}S and ^{210}Po). The radionuclide clearance was checked in the presence of radioprotector.

Determination of Optimal Day for Assay

Mice, in groups of 5, were injected with the same amount of radiochemical. The animals were sacrificed at different times post-injection, and the injected testis removed and processed (see below for details) to determine the spermhead population. The day on which the spermhead count reaches a minimum is the optimal day to determine the spermhead survival. The optimal day to assay the abnormal sperm is 9 days after the minimum testicular count is reached. The optimal days for the spermtid survival assay and abnormal spermhead assay remained the same in the presence of MEA (see Table I in Ref. 6).

Determination of Spermhead Survival

The mice were intratesticularly injected with different amounts of the radionuclide of interest. In each case, a group of control mice were injected with the cold drug in amounts equal to the highest dose group. Animals injected with normal saline served as further controls. The animals were sacrificed at the predetermined optimal day. The injected testis were removed, placed in 1 ml of deionized water, homogenized for 15 s, and sonicated for 30 s. The spermheads, which are resistant to sonication, were counted in a hemocytometer using a microscope at 400X magnification.

In the case of radioprotectors, a predetermined non-toxic level of cysteamine (0.75 μg) was injected i.t. and mice were kept aside for 4 h to allow the agent to spread uniformly throughout the testis. After this time the radionuclide was administered i.t.

Abnormal Spermhead Assay

The optimal day to study the induction of sperm abnormalities was established as described above. Several groups of mice were injected i.t. with different amounts of the radiochemicals. On the predetermined optimal day, the animals were sacrificed and the epididymides removed. The epididymides of the mice in same group were pooled in 1 ml of 0.9% saline, minced with fine scissors, and pipetted vigorously (19). The solution was then filtered through four layers of gauze to separate the sperm from tissue fragments. About 20 μl of 2% eosin-Y was added to the suspension, smeared on the slide, air dried, and a cover slip mounted with Permount. At least 2000 sperm (normal + abnormal) were scored under a light microscope. The

abnormal fraction of the epididymal sperm was determined and corrected for spontaneously occurring abnormalities (~ 2%).

Macroscopic Distribution

Mice were injected i.t. with the radiochemical and the testes removed 24 h later, frozen with CRYOkwik, and sliced into 10-15 sections. Each section was weighed and assayed for radioactivity. The activity per gram of tissue was relatively constant in the sections, indicating that the radionuclide was distributed fairly uniformly in the testis.

Subcellular Distribution

Following intratesticular injection of the radionuclide, the subcellular distribution was performed 1 day post-injection according to procedures described in Ref. 7. Briefly, the injected testes were removed and the testicular cells isolated promptly to separate cytoplasmic and nuclear fractions. The nuclear fraction was further separated into protein and DNA components. The activity in each fraction was obtained by counting aliquots of these fractions using an appropriate radiation detector. Subcellular distribution of the ^{35}S-cysteamine was also performed using the same procedures.

Irradiation with External X rays

For external irradiation of the testis, an overhead fluoroscopy X ray unit was employed (8). The selective irradiation of mouse testes was accomplished after the animals were anesthetized with sodium pentobarbital (60 mg/kg of body weight) and placed in custom-made lead shields to expose only the testes to the X ray beam. Exposure levels were determined using a Victoreen R meter.

RESULTS

Biological Clearance and Dosimetry

The biological clearance of ^{125}IUdR, H^{125}IPDM, and ^{210}Po-citrate were reported elsewhere (4,5). The biological clearance of intratesticularly injected ^{35}S-MEA yields a similar two-component exponential expression:

$$f = 0.54\, e^{-0.693t/0.43} + 0.46\, e^{-0.693t/40},$$

where f is the fraction of injected activity remaining in the testis, and t is the time (h) post-injection. Using the clearance data for the various radiochemicals, the average absorbed dose to the testis was calculated following MIRD formalism (22). Details of the calculations are given elsewhere (1,5).

Optimal Day for the Assays

The minimum spermhead count for the two iodine compounds and for external X rays was on 29th day (5,8), whereas for ^{210}Po it was on 36th day (4). The optimal day in the presence of radioprotectors was checked in each case and found to be the same. Hence, the spermhead survival assay with and without MEA was performed on these days. The abnormal spermhead assay was performed 9 days later as described in Ref. 6.

Subcellular Distribution of the Radiochemicals

The subcellular distributions of all the radiochemicals, taken from our earlier reports (4-6), are given in Table I. All of the ^{125}IUdR activity was bound to the DNA of the testicular cells. In the case of H^{125}IPDM and H^{131}IPDM, about 30% of the injected activity was localized in the testicular cells, of which more than 95% was found in the cytoplasm of the cells. About 20% of the ^{210}Po-citrate activity was found in the cell nucleus and the remaining 80% in the cytoplasm. In all cases, the distribution of the radionuclides was not influenced by the presence of the radioprotector. The subcellular distribution of ^{35}S-MEA in the testis following i.t. administration is given in Table II.

Spermhead Survival

The mean lethal doses at 37% survival (D_{37}) are 8.5 ± 2.1, 10 ± 1, 68 ± 6, and 61 ± 6 cGy for ^{125}IUdR, ^{210}Po-citrate, H^{125}IPDM, and H^{131}IPDM, respectively (4,5). The D_{37} value for external X irradiation of the testes is 67 ± 3 cGy (8). These results show that the Auger emitter ^{125}I bound to the DNA is at least as effective as the high-LET α particles of ^{210}Po. On the other hand, the cytoplasmically localized H^{125}IPDM is only as lethal as external X rays. The dose response curves are shown in Figs. 1A-1E for these radiochemicals and external X rays in the presence and absence of MEA. The observed D_{37} values in presence of MEA are 26.4 ± 5.6 cGy for ^{210}Po-citrate,

237 ± 48 cGy for $H^{131}IPDM$, 260 ± 32 cGy for $H^{125}IPDM$ (5), 31 ± 6 cGy for $^{125}IUdR$ (5), and 154 ± 53 cGy for X rays.

TABLE I
Summary of Subcellular Distribution Studies[a]

Radiochemical	Subcellular Distributions[b]
120 kVp X rays	-
$H^{125}IPDM$	100% Cy, 0% N, 0% D
$H^{131}IPDM$	100% Cy, 0% N, 0% D
$^{125}IUdR$	0% Cy, 100% N, 100% D
^{210}Po-citrate	80% Cy, 20% N, 45% D
$^{125}IUdR$+MEA	0% Cy, 100% N, 100% D
^{210}Po-citrate+MEA	80% Cy, 20% N, 45% D

[a] The numbers are reproduced from Ref. 6.

[b] % Cy is percentage of activity in cytoplasm, % N is percentage of activity in nucleus and % D is percentage of activity in cell nucleus bound to DNA.

TABLE II
Subcellular Distribution of ^{35}S-Cysteamine in Mouse Testis[a]

%Testis Activity in Cells	% Cellular Activity in Nucleus	% Nuclear Activity in DNA
25	10	53

[a] The data represents the average of two experiments.

Induction of Sperm-shape Abnormalities

Figures 2A and 2B show the fraction of abnormal epididymal sperm as a function of average absorbed dose to the testis for $^{125}IUdR$ and ^{210}Po-citrate, respectively (6). These curves exhibit a linear increase in the abnormal fraction in the low-dose region and saturate at higher doses. This saturation is

A

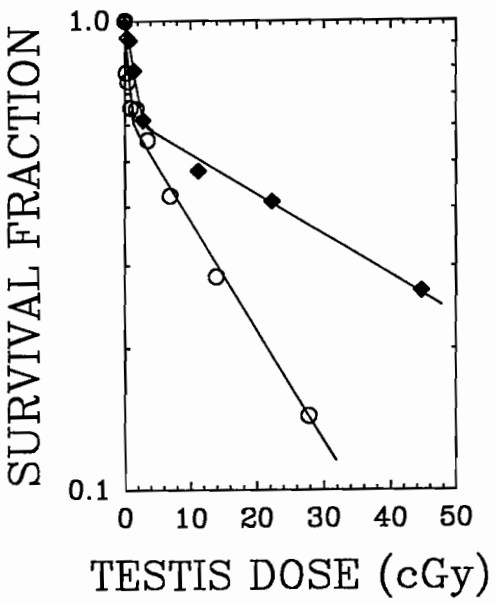
SURVIVAL FRACTION
1.0
0.1
0
10
20
30
40
50
TESTIS DOSE (cGy)

B

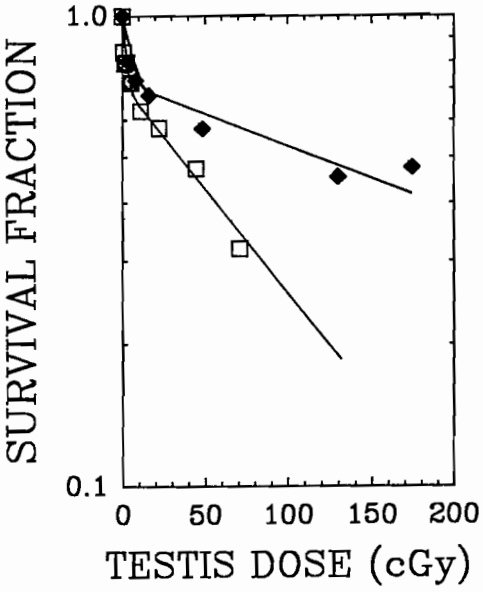
SURVIVAL FRACTION
1.0
0.1
0
50
100
150
200
TESTIS DOSE (cGy)

C

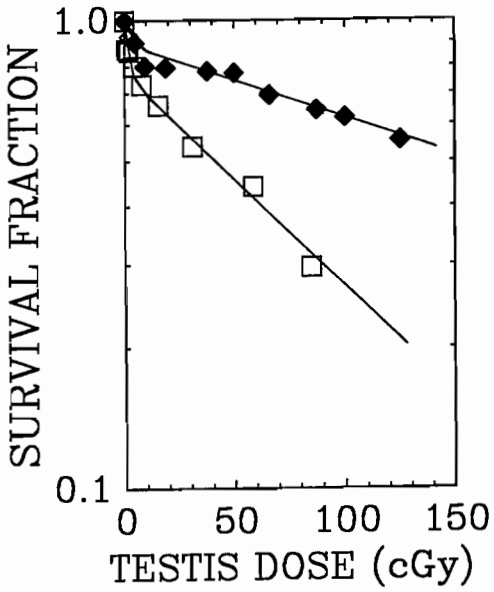
1.0
0.1
SURVIVAL FRACTION
0
50
100
150
TESTIS DOSE (cGy)

D

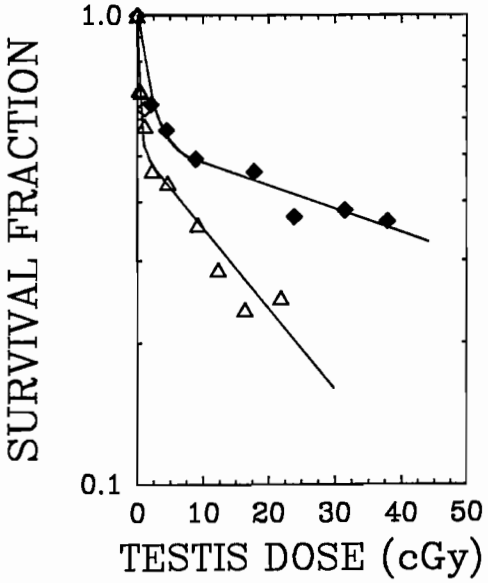
1.0
0.1
SURVIVAL FRACTION
0
10
20
30
40
50
TESTIS DOSE (cGy)

E

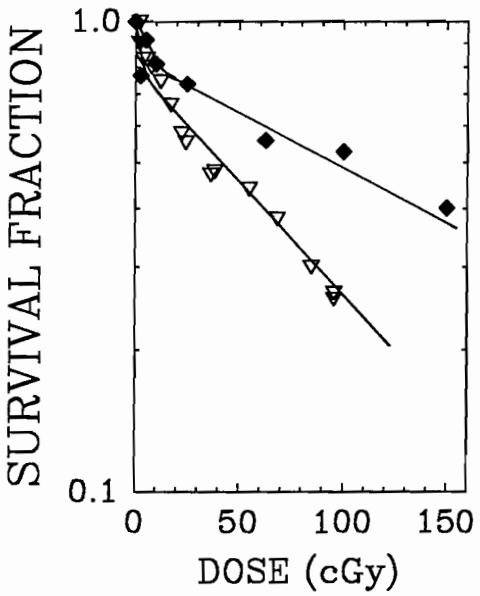

FIG. 1. Spermhead survival as a function of average testicular absorbed dose from intratesticularly administered radiochemicals. A) ^{210}Po-citrate: open circles without MEA and closed diamonds with MEA. B) H^{131}IPDM: open squares without MEA and closed diamonds with MEA. C) H^{125}IPDM: open squares without MEA and closed diamonds with MEA. Data taken from Ref. 5. D) ^{125}IUdR: open triangles without MEA and closed diamonds with MEA. Figure reproduced from Ref. 5. E) X rays: open reverse triangles without MEA and closed diamonds with MEA.

perhaps due to increased spermatogonial cell killing at high doses. However, the slope of the initial portion of the curve provides a sensitive comparison of the relative efficacy of the various types of radiations. Therefore, in each figure, the low-dose region of the curve is displayed as an inset. The initial slopes for ^{125}IUdR with and without MEA are 0.12 ± 0.01 %abnormals/cGy and 1.7 ± 0.1 %abnormals/cGy, respectively (6). For ^{210}Po-citrate, the corresponding initial slopes are 0.7 ± 0.04 %abnormals/cGy and 7.1 ± 0.5 %abnormals/cGy (6).

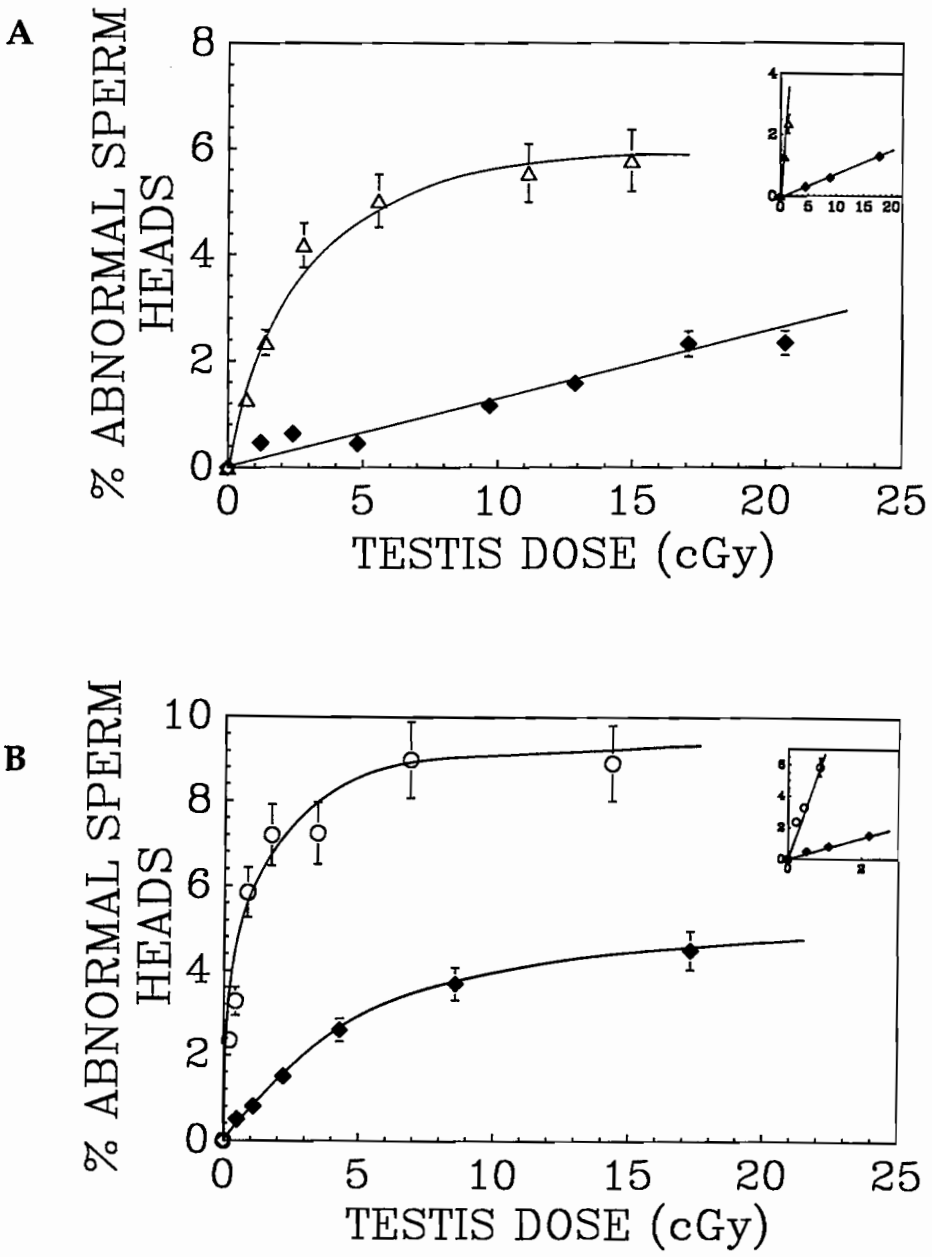

FIG. 2. Fraction of abnormal spermhead versus testicular absorbed dose from the intratesticular injection of radiochemicals. A) ^{125}IUdR: open triangles without MEA and closed diamonds with MEA. B) ^{210}Po-citrate: closed circles without MEA and closed diamonds with MEA. Data in A and B are reproduced from Ref. 6.

DISCUSSION

The radioprotective capacity of a variety of chemicals has been well established in various biological models using acute external beams of radiation. However, with the exception of the recent work by Rao *et al.* (5,6), to the best of our knowledge the protective action of chemicals against the effects of chronic irradiation by tissue incorporated radionuclides or external beams have not been studied. The effectiveness of a radioprotector, usually referred to as the dose modifying factor (DMF), is the ratio of absorbed doses at a chosen biological end point in the presence and absence of the chemical protector. The present spermhead survival studies which utilized the agent HIPDM to cytoplasmically localize ^{125}I (Auger emitter) and ^{131}I (β emitter) yielded DMF values of 3.8 and 3.9, respectively when MEA was used as the radioprotector (Figs. 1B & 1C). For DNA incorporated ^{125}I, we previously reported a DMF value of 3.6 (5). In the case of the α emitter ^{210}Po, a DMF of only 2.6 was observed for spermhead survival (Fig. 1A). This result for ^{210}Po is in good agreement with that of Bird (16) who obtained a similar DMF value for α particles. It is interesting to note that there is no significant difference in the protection offered by MEA for cytoplasmically localized and DNA incorporated ^{125}I. Furthermore, MEA offers equal protection against the low-LET β emitting radiochemical $^{131}IUdR$. This suggests that the high-LET type effects of $^{125}IUdR$ may be largely due to indirect action of radical species as opposed to direct deposition of energy in the critical targets. This suggestion is supported by the recent Monte Carlo calculations of Wright *et al.* (23) and Pomplun *et al.* (24, this volume), which simulate the direct and indirect interactions with DNA resulting from an ^{125}I decay on the DNA.

As indicated above, the data in this work also sheds light on the potential of MEA to protect against chronic versus acute irradiation. For acute exposure with external X rays where the testicular dose is delivered over a few minutes, a DMF of 2.4 was obtained with the spermhead survival assay (Fig. 1E). In contrast, DMF values of 3.9 and 3.8 were obtained for cytoplasmically localized ^{131}I and ^{125}I, respectively. Here, the dose is delivered over a period of several days. This suggests that superior protection is offered against chronic low-LET irradiation from incorporated radionuclides than against acute external beams. It should he noted, however, that the protective effect of MEA may be dependent not only on the dose rate, but also on its concentration in the tissue during the time the dose is delivered. Therefore, it may be necessary to have information regarding the cumulative

concentration (*i.e.* μg-h) of the chemical protector in the organ during the time of exposure, and perhaps its subcellular distribution. In fact, Smoluk *et al.* (25) showed that MEA binds to DNA and suggested that the protective action of chemical may indeed be related to the extent it binds to the DNA. Our subcellular distribution studies with radiolabeled MEA also indicate some binding of MEA to the DNA in the testicular cells. It is essential that further data be collected to investigate the dependence of radioprotection on these parameters.

Using sperm-shape abnormality as the biological end point, we obtained DMF values of 14 and 10 for ^{125}IUdR and ^{210}Po-citrate, respectively (6). These values are significantly higher than those observed for spermhead survival, and point to the dependence of DMF values on the biological end point. Furthermore, the increased protection observed with ^{125}IUdR compared to ^{210}Po α particles supports our earlier conclusion that the biological damage caused by DNA incorporated ^{125}I is largely due to the indirect action of radical species produced in the immediate vicinity of the decay site.

Further studies are underway with other radioprotectors such as vitamin C in order to get a clearer understanding of the mechanism of the Auger effect. The limiting factor in these studies is the high degree of chemotoxicity associated with most protectors. Some compounds, even in small quantities (~ ng), can affect spermatogonial cell survival and therefore are not useful for these studies. For instance, WR compounds may not work in this model because of their severe chemotoxicity to spermatogonial cells. Nevertheless, there are numerous compounds available which may shed light on the mechanism of the Auger effect.

ACKNOWLEDGMENTS

This work was supported in part by USPHS Grant No. CA-32877 (DVR), NJ Cancer Commission Grants 688-009 (RWH) and 689-042 (DVR), and New Jersey Cancer Commission Fellowship Grant 689-080 (VRN).

REFERENCES

1. D.V. RAO, G.F. GOVELITZ, and K.S.R. SASTRY, Radiotoxicity of thallium-201 in mouse testes: Inadequacy of conventional dosimetry. *J. Nucl. Med.* **24**, 145-153 (1983).
2. D.V. RAO, V.B. MYLAVARAPU, K.S.R. SASTRY, and R.W. HOWELL, Internal Auger emitters: Effects on spermatogenesis and oogenesis in mice. In *DNA Damage by Auger Emitters*, (K.F. Baverstock and D.E. Charlton, Eds.) Taylor & Francis, London. pp 15-26, 1988.
3. D.V. RAO, V.R. NARRA, G.F. GOVELITZ, V.K. LANKA, R.W. HOWELL, and K.S.R. SASTRY, In vivo effects of 5.3 MeV alpha particles from Po-210 in mouse testes: Comparison with internal Auger emitters. *Radiat. Prot. Dosim.* **31**, 329-332 (1990).
4. D.V. RAO, V.R. NARRA, R.W. HOWELL, G.F. GOVELITZ, and K.S.R. SASTRY, In-vivo radiotoxicity of DNA-incorporated I-125 compared with that of densely ionising alpha-particles. *The Lancet* Vol **II**, No 8664, 650-653 (1989).
5. D.V. RAO, V.R.NARRA, R.W.HOWELL, and K.S.R. SASTRY, Biological consequence of nuclear versus cytoplasmic decays of I-125: Cysteamine as a radioprotector against Auger cascades in vivo. *Radiat. Res.* **124**, 188-193 (1990).
6. D.V. RAO, V.R. NARRA, R.W. HOWELL, V.K. LANKA, and K.S.R. SASTRY, Induction of spermhead abnormalities by incorporated radionuclides: Dependence on subcellular distribution, type of radiation, dose rate, and presence of radioprotectors. *Radiat. Res.* **125**, 89-97 (1991).
7. D.V. RAO, K.S.R. SASTRY, G.F. GOVELITZ, and H.E. GRIMMOND, In vivo effects of iron-55 and iron-59 on mouse testis: Biophysical dosimetry of Auger electrons. *J. Nucl. Med.* **26**, 1456-1465 (1985).
8. D.V. RAO, K.S.R. SASTRY, H.E. GRIMMOND, R.W. HOWELL, G.F. GOVELITZ, V.K. LANKA, and V.B. MYLAVARAPU, Cytotoxicity of some indium radiopharmaceuticals in mouse testes. *J. Nucl. Med.* **29**, 375-384 (1988).
9. K.G. HOFER, C.R. HARRIS, and J.M. SMITH, Radiotoxicity of intracellular Ga-67, I-125, H-3. Nuclear versus cytoplasmic radiation effects in murine L1210 leukaemia. *Int. J. Radiat. Biol.* **28**, 225-241 (1975).
10. A.I. KASSIS, R.W. HOWELL, K.S.R. SASTRY, and S.J. ADELSTEIN, Positional effects of Auger decays in mammalian cells in culture. In *DNA Damage by Auger Emitters*, (K.F. Baverstock, D.E. Charlton, Eds.) Taylor & Francis, London. pp 1-14, 1988.
11. A.I. KASSIS, F. FAYAD, B.M. KINSEY, K.S.R. SASTRY, R.A.TAUBE, and S.J. ADELSTEIN, Radiotoxicity of I-125 in mammalian cells. *Radiat. Res.* **111**, 305-318 (1987).
12. A.I. KASSIS, K.S.R. SASTRY, and S.J. ADELSTEIN, Kinetics of uptake, retention, and radiotoxicity of I-125 IUdR in mammalian cells: Implications of localized energy deposition by Auger processes. *Radiat. Res.* **109**, 78-89 (1987).
13. R.W. HOWELL, V.R. NARRA, D.V. RAO, and K.S.R. SASTRY, Radiobiological effects of intracellular polonium-210 alpha emissions: A comparison with Auger-emitters. *Radiat. Prot. Dosim.* **31**, 325-328 (1990).
14. R.W. HOWELL, D.V. RAO, D. HOU, V.R. NARRA, and K.S.R. SASTRY, The question of relative biological effectiveness and quality factor for Auger emitters incorporated into proliferating mammalian cells. *Radiat. Res.* **128**, 282-293 (1991).

15. H.M. PATT, E.B. TYREE, R.L. STRAUBE, and D.E. SMITH, Technical papers: Cysteine protection against x-irradiation. *Science* **110**, 213-214 (1949).
16. R.P. BIRD, Cysteamine as a protective agent with high-LET radiations. *Radiat. Res.* **82**, 290-296 (1980).
17. E.F. OAKBERG, Spermatogonial stem-cell renewal in the mouse. *Anat. Rec.* **169**, 515-532 (1971).
18. M.L. MEISTRICH, N.R. HUNTER, N. SUZUKI, P.K. TROSTLE, and H.R. WITHERS, Gradual regeneration of mouse testicular stem cells after exposure to ionizing radiation. *Radiat. Res.* **74**, 349-362 (1978).
19. A.J. WYROBEK, L.A. GORDON, J.G. BURKHART, M.W. FRANCIS, R.W. KAPP, Jr., G. LETZ, H.V. MALLING, J.C. TOPHAM, and M.D. WHORTON, An evaluation of the mouse sperm morphology test and other sperm tests in nonhuman mammals. A report of the U. S. environmental protection agency gene-tox program. *Mutation Res.* **115**, 1-72 (1983).
20. B. LUI, J. CHANG, J.S. SUN, J. BILLINGS, A. STEVES, R. ACKERHALT, M. MOLANAR, and H.F. KUNG, Radioactive iodine exchange reaction of HIPDM: Kinetics and mechanism. *J. Nucl. Med.* **28**, 360-365 (1987).
21 R.S. HARAPANHALLI, V.R. NARRA, R.W. HOWELL, and D.V. RAO, [^{35}S] Cysteamine: Facile Synthesis, and in vivo biokinetics and subcellular distribution. *Nucl. Med. Biol.* In Press (1991).
22. R. LOEVINGER, and M. BERMAN, A revised schema for calculating the absorbed dose from biologically distributed radionuclides. *MIRD Pamphlet No. 1*, revised. Society of Nuclear Medicine, New York, 1976.
23. H.A. WRIGHT, R.N. HAMM, J.E. TURNER, R.W. HOWELL, D.V. RAO, and K.S.R. SASTRY, Calculations of physical and chemical reactions with DNA in aqueous solution from Auger cascades. *Radiat. Prot. Dosim.* **31**, 59-62 (1990).
24. E. POMPLUN, J. BOOZ, and D.E. CHARLTON, A Monte Carlo simulation of Auger cascades. *Radiat. Res.* **111**, 533-552 (1987).
25. G.D. SMOLUK, R.C. FAHEY, and J.F. WARD, Equilibrium dialysis studies of the binding of radioprotector compounds to DNA. *Radiat. Res.* **107**, 194-204 (1986).

DISCUSSION

Yasui, L. S. LeMotte and Little showed a 5 fold increase in DNA damage induction from ^{125}I decay when decays were accumulated in cells without radioprotector (no glycerol). But cell survival does not change when decays are accumulated in the presence or absence of glycerol, suggesting an indirect effect is not a major factor in cell survival. How do you respond to this past data with respect to your results?

Narra, V. R. The experiments of LeMotte and Little were carried out with cultured cells in the frozen state. The efficiency of radical scavenging in the frozen state may be very different than *in vivo* at 37°C. This may explain the difference between our results and those of Lemotte & Little. It also

should be pointed out that radioprotection of cultured cells at 37°C is much more difficult than for spermatogonial cells. Experiments with cultured cells at 37°C necessarily involves prolonged exposure (1 wk) to the protector. Our experience has been that the cytotoxic nature of protectors precludes exposing the cells to concentrations of protectors that are high enough to afford appreciable protection. The testis, on the other hand, seem to be fairly resistant to the chemical toxicity of various radioprotectors.

Martin, R. F. Can you estimate the concentration of cysteamine in the cells at risk?

Narra, V. R. No, we have not directly measured the concentration of cysteamine in the spermatogonial cells, however, we are presently working on techniques which will allow us to accomplish this.

336 Biophysical Aspects of Auger Processes, AAPM Symposium Series No. 8 (1992) 336-351
Eds. RW Howell, VR Narra, KSR Sastry, DV Rao

MICROSCALE SYNTHESIS OF CARBOPLATIN LABELED WITH THE AUGER EMITTER PLATINUM-193m: RADIOTOXICITY VERSUS CHEMOTOXICITY OF THE ANTITUMOR DRUG IN MAMMALIAN CELLS

MICHAEL T. AZURE,[1] KANDULA S.R. SASTRY,[2]
RONALD D. ARCHER,[1] ROGER W. HOWELL,[3] and
DANDAMUDI V. RAO[3]

[1]Department of Chemistry, University of Massachusetts,
Amherst, MA 01003, USA

[2]Department of Physics and Astronomy, University of Massachusetts,
Amherst, MA 01003, USA

[3]Division of Radiation Research, Department of Radiology,
University of Medicine and Dentistry of New Jersey, Newark, NJ 07103, USA

ABSTRACT

The 4.3 d Platinum-193m emits numerous low energy Auger electrons by virtue of its 3-step isomeric decay almost entirely by internal conversion. We have produced this radionuclide by the $^{192}Pt(n,\gamma)^{193m}Pt$ reaction, and synthesized ^{193m}Pt labeled carboplatin, and carboplatin with a stable Pt metal center using a microscale synthetic approach. The clonogenic survival of Chinese hamster V79 cells is investigated following 2-3 h exposure of the cells to various extracellular concentrations of the cold drug as well as the radiolabeled compound. At 37% survival, the extracellular concentration of nonradioactive carboplatin is about 140 μM compared to 35 μM with the radiolabeled analog. These results suggest the potential of ^{193m}Pt-carboplatin in chemo-Auger combination therapy.

INTRODUCTION

Platinum-coordinated compounds have been of much interest as potential chemotherapeutic agents since the serendipitous discovery of the effects of cis-diamminedichloroplatinum(II) (cisplatin) by Rosenberg *et al.* (1) in 1969. Other compounds with transition metals and main group elements have also been investigated (2), but they have not demonstrated the same therapeutic efficacy toward cancer as cisplatin. However, there are problems associated with cisplatin treatment despite its successes, the foremost being renal toxicity and physiological discomfort.

A large number of cisplatin analogs are being investigated at present for their viability as chemotherapeutic agents. One compound which has yielded promising results for a variety of carcinomas is cis-diammine(1,1-cyclobutanedicarboxylato)-platinum(II) or carboplatin (Fig. 1.) The renal toxicity and other associated deleterious physiological phenomena are strongly diminished and clearance of the drug from the body is much faster

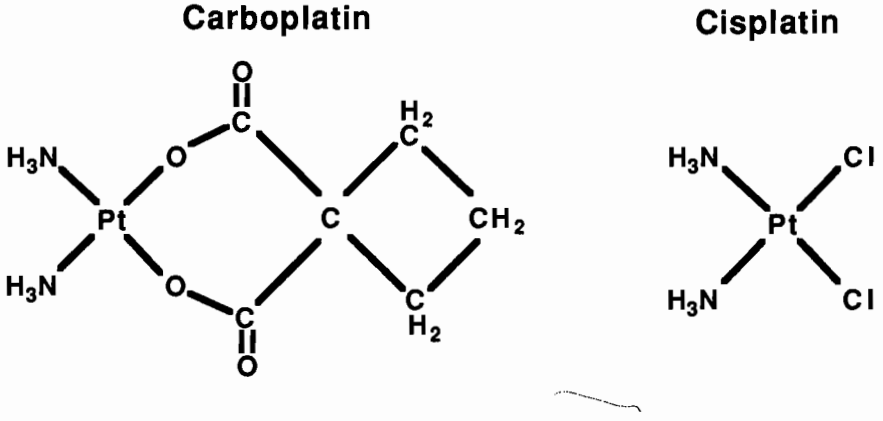

FIG. 1. Carboplatin, an analog of cisplatin. Both species have square planar molecular geometry, the leaving groups are the 1,1-cyclo-butanedicarboxylato in carboplatin and the chlorides in cisplatin.

than for cisplatin (3). The drug dose necessary to produce fifty percent survival in V79 cells is approximately seven times greater for carboplatin

than for cisplatin (4). Because platinum is a heavy metal, platinum-containing compounds are toxic to the necessary and beneficial body cells as well as to the malevolent ones. Such chemical toxicity may be strongly reduced, in principle, by administration of the drug at lower dosages without affecting the therapeutic efficacy, as indicated below.

It is well known that the antitumor action of these drugs (*e.g.* cisplatin, carboplatin) is intimately related to specific binding of the drug molecules to the DNA of the cells. It is also well established that the high radiotoxicity of Auger emitters is manifest upon their binding to the DNA (*e.g.* ^{125}IUdR). Studies *in vitro* and *in vivo* have repeatedly demonstrated the severe cytocidal effects of ^{125}IUdR, a thymidine analog, when incorporated into the DNA of proliferating cells (5,6). These considerations, when combined together, point to the potential of a new class of radiolabeled platinum coordination compounds as chemo-Auger therapeutic agents. The central goal of our research is to synthesize such compounds and investigate their effectiveness in model cell systems. By virtue of their highly internally-converted isomeric-decay modes, the radionuclides ^{193m}Pt and ^{195m}Pt are copious emitters of Auger electrons (7,8). Platinum-193m is of particular value as a metal center in the drug molecules because it can be produced at a high specific activity (see below). The present work is concerned with microscale synthesis of carboplatin labeled with ^{193m}Pt and study of the biological effects in a mammalian cell line in culture.

PRODUCTION OF RADIONUCLIDES

The half-lives of ^{195m}Pt and ^{193m}Pt are 4.02 d and 4.33 d, respectively (9). Both radionuclides can be produced through bombardment with thermal neutrons in a reactor: ^{194}Pt(n,γ)^{195m}Pt, ^{192}Pt(n,γ)^{193m}Pt. The average Auger yields calculated through Monte Carlo methods for the two radionuclides are comparable; 26 and 33 Auger electrons per decay of ^{193m}Pt and ^{195m}Pt, respectively (7). The following considerations indicate the relative merits for the two radionuclides in biomedical applications.

1. Platinum-194 constitutes 32.9% of naturally occurring platinum whereas platinum-192 makes up only 0.78%. Highly enriched ^{192}Pt (57%) is available through Oak Ridge National Laboratory, albeit expensive.

2. The cross sections for the above nuclear reactions are 2 barns (9) for ^{193m}Pt and 0.09 barn for ^{195m}Pt (9). The attainable specific activity of ^{195m}Pt is therefore limited. In contrast, ^{193m}Pt can be produced at specific activities 10-40 times higher than ^{195m}Pt by the (n,γ) reaction.

3. ^{193m}Pt can also be produced through the following nuclear reactions: ^{193}Ir(d,2n)^{193m}Pt and ^{192}Os(α,3n)^{193m}Pt. Accordingly, it may be obtained at a very high specific activity following chemical separation of the target material, since the only platinum in the system is ^{193m}Pt. The cross sections for the iridium-193 and osmium-192 reactions are 0.07 barn (10) and 0.5 barn (11), respectively. The latter of the two reactions is being explored as a possible method of production.

4. ^{195m}Pt is easily produced at a modest cost. The X ray and γ ray yields for the two radionuclides differ greatly, with ^{195m}Pt having the edge in this comparison. ^{195m}Pt has a 0.17 yield (12) for the 98.9 keV γ ray (most pronounced). ^{193m}Pt has a 0.0011 yield (13) for its most pronounced γ ray of 135.5 keV. The Pt K X Ray yields for ^{195m}Pt and ^{193m}Pt are 0.77 and 0.15, respectively (7,8). The high photon yields for ^{195m}Pt make it an excellent candidate for tracer studies. For therapeutic applications, however, the high specific activity of ^{193m}Pt is essential.

MICROSCALE SYNTHESIS OF CARBOPLATIN(^{193m}Pt)

To minimize the chemotoxicity of platinum, it is important to use as small an amount of the metal as possible. We have developed a scheme of synthesis involving only micromolar quantities of platinum. Here we briefly describe the procedures and mechanism of the synthesis.

Five milligrams of ^{192}Pt enriched to approximately 57% were irradiated for one week with thermal neutrons at a flux of about 4×10^{14} neutrons/cm^2-s at the University of Missouri Reactor Facility. The sample was dissolved in aqua regia and shipped from Oak Ridge National Laboratory.

The amount of radioactivity produced ranges between 35-100 mCi, depending upon reactor flux and quantity of target material. Since this is a significant amount of radioactivity, proper safety precautions must be taken. In addition to lead shielding, mirrors are strategically placed to observe the

system. Manipulation of the materials is done through automation, vacuum line or applied mechanics, as necessary.

The first step in the radiosynthesis of carboplatin is the isolation of contaminants (^{199}Au and ^{192}Ir) from nuclear side reactions. Solvent extraction with methylethylketone and precipitation are used, respectively, for removal of these radionuclides. The synthetic scheme most often used by our group is presented in Fig. 2. There are other synthetic avenues being investigated at present, however none have yielded the same quality of the product. In order to increase the yield of the cis isomer over the trans isomer, most synthetic chemists convert the tetrachloroplatinate salt to the tetraiodo complex because of the enhanced trans-directing properties of iodide. However, we do not do this because, during the conversion from the halide complex to the aquo complex through the addition of silver nitrate, the silver halide precipitate occludes much of the platinum. The microscale quantity of platinum requires a minimization of precipitation reactions and transfers.

Purification of the carboplatin is achieved through column separation and ion exchange resins. Analyses are performed with UV-visible spectroscopy and thin layer chromatography.

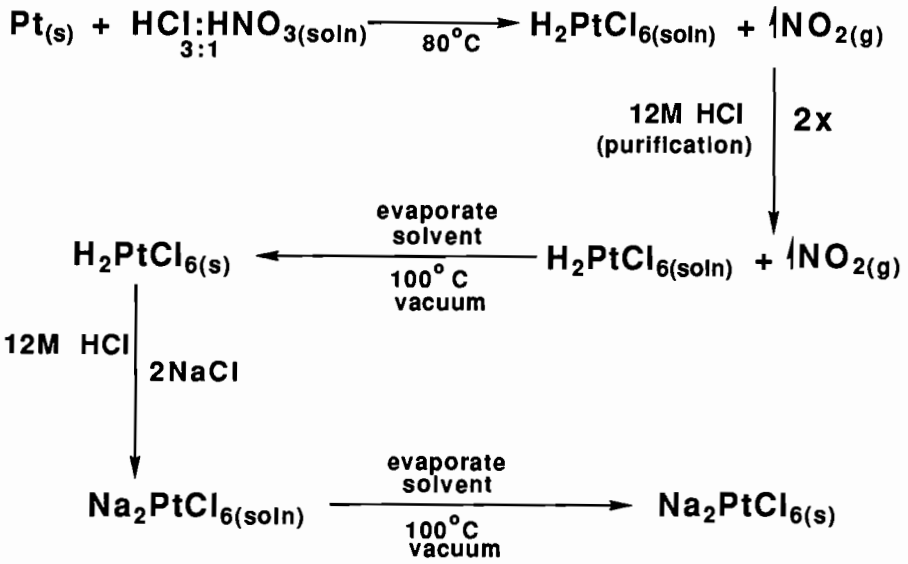

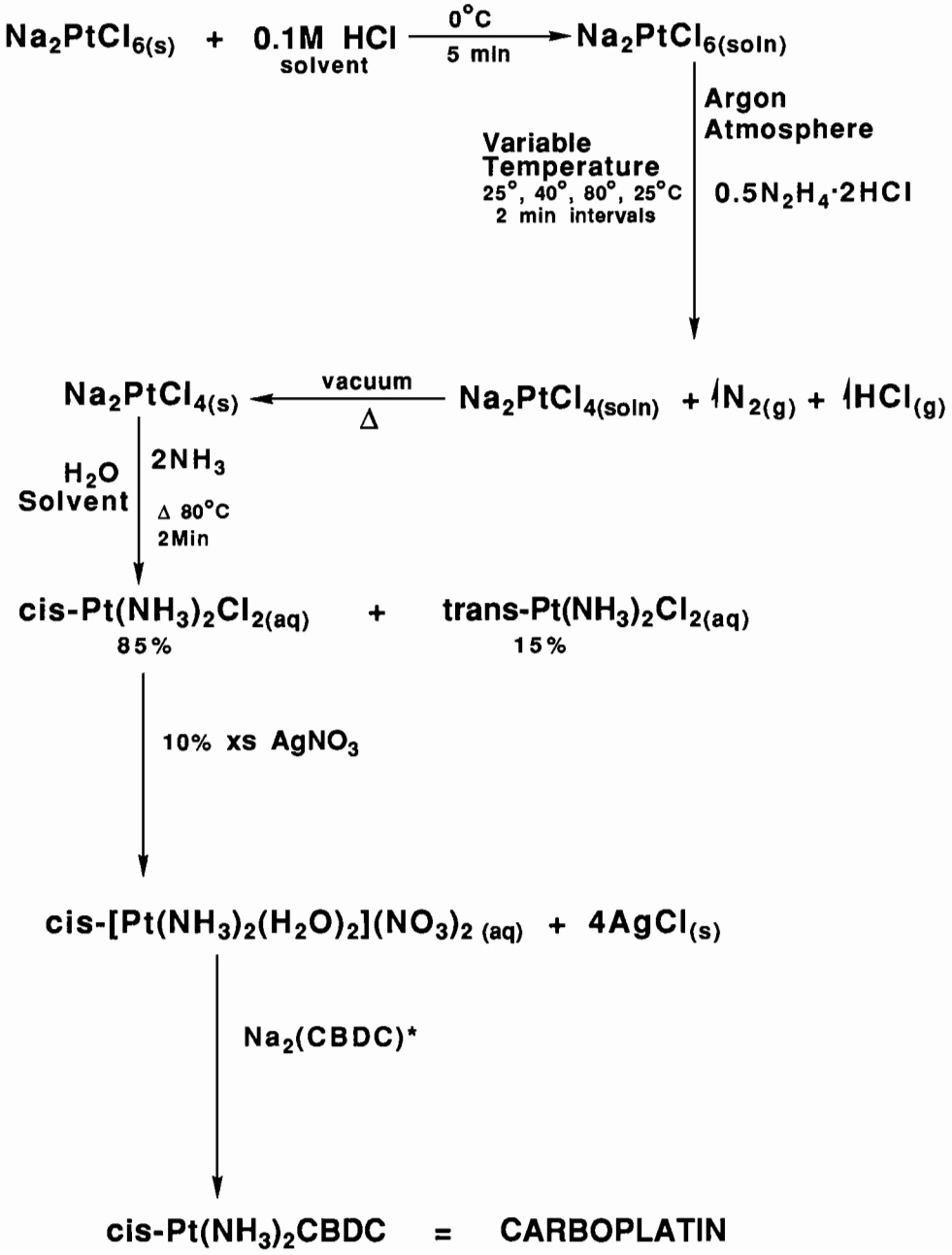

FIG. 2. Schematic of the synthetic mechanism of carboplatin.
*Na_2(CBDC) = sodium cyclocbutanedicarboxylate.

After the carboplatin has been synthesized, the dried product is dissolved in sterile water. The drug concentration and activity are then assessed. Spectrophotometric methods and thin layer chromatography are, once again, used for the chemical analysis and NaI(Tl) and Ge(Li) detectors for the radioanalysis. Thin layer chromatography with photographic paper affixed to the silica gel plates works very well for purity analysis and precludes the use of an indicator.

In order to project the electron spectrum from the nuclear decay, Monte Carlo calculation methods were utilized. Computer simulations of the nuclear and atomic transitions were performed on the Physics VAX at the University of Massachusetts. The average electron spectrum from ^{193m}Pt decay in Fig. 3 includes electrons from internal conversion, Auger, Coster-Kronig and super Coster-Kronig processes (7).

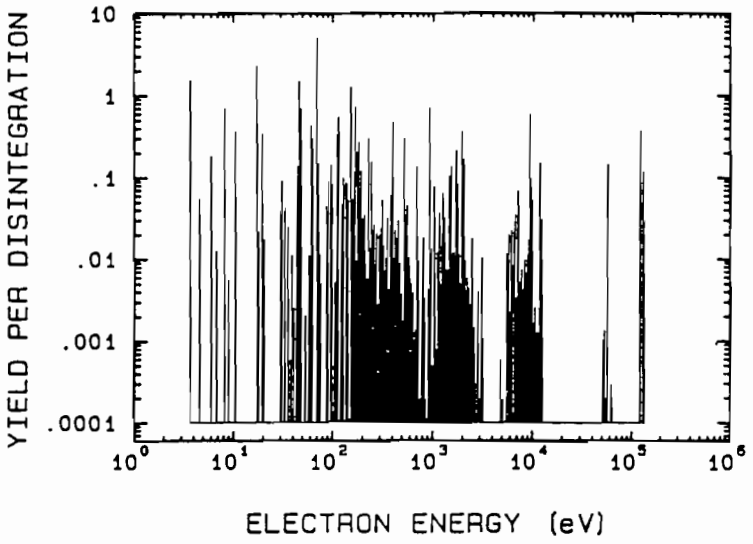

FIG. 3. Monte Carlo simulation of the average electron spectrum in decay of ^{193m}Pt.

BIOLOGICAL STUDIES WITH CARBOPLATIN

Chinese hamster lung fibroblasts (V79 cells) were used in these studies. The advantages of this mammalian cell line as a model for *in vitro* studies have been noted by Kassis *et al.* (14). Clonogenic survival of the cells exposed to the radiolabeled carboplatin or the unlabeled drug was the biological end

point. The kinetics of uptake, post-incubation retention and subcellular distribution of the radiolabeled compound were also studied.

The experimental methods and protocols were essentially the same as developed by Kassis *et al.* (15) The details are also given by Howell (7). The cells were cultured in Gibco (Grand Island, NY) minimum essential medium (MEM) supplemented with 2 mM L-glutamine, 10 mM Hepes buffer, 10% fetal calf serum, 50 units/ml penicillin, 50 μg/ml streptomycin, and 0.1 mM non-essential amino acids. The pH was adjusted to 7.0 with $NaHCO_3$. Medium with calcium (MEMA) was used for survival studies; and MEMB, free of calcium, for uptake and retention studies which require the cells to be mobile. Use of MEMB reduced the probability of cell clumping, and lack of calcium had no effect on cell doubling time or survival (15). Cells in suspension were counted using a Coulter counter and verified with a hemocytometer.

Kinetics of Cellular Uptake

Exponentially growing V79 cells were trypsinized, suspended in MEMB, and conditioned for 4 h at 37°C in an atmosphere of air with 5% CO_2, with the incubation tubes gently shaken on a rocker-roller. The cells (2×10^5 cells/ml) were then treated with radiolabeled carboplatin of various concentrations, and incubated further under the same conditions. Aliquots of the suspension were taken at different times, the cells were washed four times and counted. The microfuge method of Kassis and Adelstein (16) was used to determine the whole cell uptake, the radioactivity being assayed with a Ge(Li) well-detector. The fraction of the total cell uptake when plotted as a function of incubation time (Fig. 4) shows saturation within 2-3 h. Accordingly, cells were incubated with the drug for 2.5 h for all the rest of the experiments.

Cellular Retention

Following 2.5 h of incubation with the radiolabeled carboplatin, the cells were washed four times with MEMB, resuspended in the calcium-free medium and incubated further. At various later times, aliquots of the suspension were taken and the cellular content of radioactivity determined.

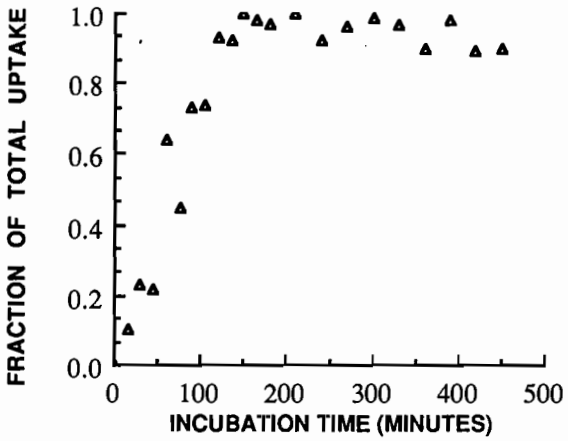

FIG. 4. Kinetics of cellular uptake of radiolabeled carboplatin by V79 cells as a function of time.

Survival Study

Survival studies were performed using carboplatin with radiolabeled and non-radiolabeled platinum metal centers in the same time frame under the same conditions. The cells were trypsinized and conditioned for four hours at 37°C (5% CO_2 atmosphere) in MEMB on a roller at a concentration of 400,000 cells/ml. The cells were diluted to a cell concentration of 200,000/ml with MEMB, treated with radiolabeled or non-radiolabeled carboplatin of various concentrations and incubated for the 2.5 h uptake period under the same incubation conditions. The extracellular concentrations for the radiolabeled carboplatin ranged from 5 to 55 μM. The concentrations for the non-radiolabeled carboplatin varied from 15 to 200 μM. The cells were removed and immediately placed on ice, and were maintained in that condition when not being manipulated. A 0.8 ml aliquot was extracted from each tube containing the radioactive drug, and put aside for the whole cell uptake study. The remaining cell suspension was washed four times with MEMA, and resuspended in MEMA. Serial dilutions were performed on each tube so that final cell concentrations of 20,000/ml; 2000/ml; and 200/ml were obtained. Incubation flasks (25 cm^2) were seeded with 1.0 ml of each of the dilutions and nutrified with 4.0 ml of MEMA. The cells were then incubated for one week under standard conditions to allow for colony formation. The

resulting colonies were washed three times with normal saline, fixed with methanol and stained with crystal violet. The colonies were then counted. The criterion for cell survival was taken to be its ability to form a colony with 50 or more cells (7). The survival fractions were determined in comparison with colonies formed by cells unexposed to the drug. The data thus accrued in the radiolabeled and non-radiolabeled studies are plotted in Fig. 5.

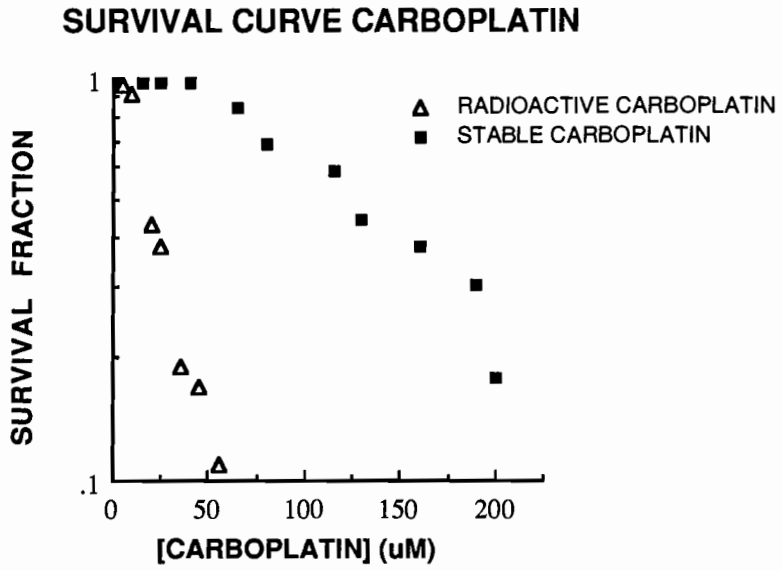

FIG. 5. Survival of V79 cells. The survival fraction is plotted against the extracellular concentration of carboplatin in the incubation medium in studies with the "cold" and radiolabeled compounds.

Whole Cell Uptake

The whole cell uptake studies were carried out using the 0.8 ml aliquot taken from each of the tubes from the survival study. The cell suspension was centrifuged for 5 min at 2000 rpm and 4°C. After centrifugation, 100 µl of the supernatant was removed and layered onto 300 µl of fetal bovine serum (FBS) in a 450 µl centrifuge tube and centrifuged at 15,000 rpm for one minute, frozen in liquid nitrogen, and then the tip was cut off and placed in a borosilicate gamma tube for radioassay. This supernatant fraction was used to correct for the actual activity in the cell pellet. Another 10 µl of the

supernatant from the 2000 rpm centrifugation was spotted onto absorbent paper and placed in a gamma tube to determine the concentration of radioactivity in the medium. The supernatant was decanted (the 2000 rpm sample), the cell pellet was broken up by vortex mixing and then resuspended in MEMA. An 100 µl aliquot of the cell suspension of known cell concentration (measured via Coulter counter) was layered onto 300 µl of fetal bovine serum in a 450 µl centrifuge tube and centrifuged at 15,000 rpm. The same tube-cutting and radioassay procedure was used. The measured radioactivity in the cell pellet was corrected using the values obtained for the supernatant (with no cells). All trials were done in triplicate.

Intracellular Activity Distribution

The intracellular activity distribution study was conducted in a manner similar to the survival study. The cells were processed the same way up to the wash. The contents of the ten culture tubes were combined. The cell concentration was determined using a Coulter counter. The cell suspension was washed two times with cold calcium-free salt solution composed of the following: 0.4 mM KH_2PO_4, 0.4 mM $Na_2HPO_4 \cdot 7H_2O$, 0.74 mM $MgSO_4 \cdot 7H_2O$, 5 mM KCl, and 0.12 M NaCl. The cells were then suspended in 2 ml of cold hypotonic sucrose buffer (0.25 M sucrose, 3 mM $CaCl_2$, 50 mM Tris, pH 7.0) and then placed on ice for five minutes and aliquots were taken for cell counting and radioassay. Disruption of the cell membrane was done by adding 2 ml of sucrose buffer containing 2% Triton X-100 and vortex mixing (17). The cells were placed on ice for an additional five minutes and then vigorously vortexed for thirty seconds. At this point a sample for radioassay was collected. This sample contained cytoplasmic components and whole nuclei. The nuclei were centrifuged at 2000 rpm for 15 min at 4°C. The nuclei formed a pellet at the bottom of the centrifuge tube. The supernatant contained the cytoplasmic fraction. The cytoplasmic fraction was decanted and put on ice for further radioanalysis. The nuclei were washed once with cold sucrose buffer (40 ml) and suspended in 2 ml of the same.

Aliquots of the the suspended cell nuclei were assayed for the content of radioactivity in the whole nucleus. Guanidine-HCl precipitable activity analysis (indicative of the drug bound to the DNA) was done by taking a 5 ml aliquot of the nuclei suspension and adding 10 ml of cold guanidine-HCl (6 M) to it and gently mixing with a glass rod. 15 ml of cold ethanol was added followed by further gentle mixing. The contents of the Erlenmyer flask were transferred to a Gelman Type A-E filter and then the flask, stirring rod and

filter were washed three times with 10 ml cold guanidine-HCl: ethanol solution with each wash being filtered to ensure isolation of all DNA remnants. The filter paper was transferred to a gamma tube for radioassay.

Aliquots of cytoplasmic fractions were radioassayed. The remainder of the fractions were centrifuged at 15,000 rpm for 20 minutes. The supernatant was decanted and the pellet containing the mitochondria was washed once, resuspended in sucrose buffer, and assayed for radioactivity.

RESULTS AND DISCUSSION

In this paper, we have presented the initial results of our studies with carboplatin, an anti-tumor drug, labeled with ^{193m}Pt, a prolific emitter of Auger electrons. Rather than a 50 mg Pt target used traditionally in the ORNL procedures for cisplatin synthesis (^{195m}Pt metal center), we have used only a 5 mg Pt target with 57% enrichment in ^{192}Pt. Our approach to microscale synthesis of the carboplatin complex labeled with ^{193m}Pt, as well as the synthesis of the compound with the stable metal center, gave about a 50% yield. Three alternative mechanisms are also explored, but the same yield has not been achieved. Two of the alternative mechanisms also utilize silver halide precipitation reactions, Ag_2O to separate thiocyanate and Ag_2SO_4 to separate halide components. In microscale synthesis, precipitation reactions create avenues by which significant amounts of the radionuclide can coprecipitate by being occluded in the precipitating moiety, the silver halides in this case. Therefore precipitations are minimized, and the yields are not as high as reported for larger scale operations. The third synthetic scheme uses dimethyl formamide (DMF) as the solvent and removes undesired species through filtration of precipitates, albeit in lower quantity than the other three syntheses. However, DMF is quite toxic and removal from the system creates some problems due to the microscale quantity being carried in the vapor to the upper regions of the reaction glassware. The analyses indicate that the purification processes are satisfactory for the method outlined in this paper.

The biological applications of the drug to the V79 cells yielded some promising results. The uptake kinetics data indicate a saturation after 2-3 hours of the incubation. Howell *et al.* have found similar kinetics of uptake by V79 cells (7,8) for trans-diamminedichloroplatinum(II) or transplatin, radiolabeled with ^{195m}Pt. Preliminary results of the retention study show that

the bulk of the intracellular activity is eliminated in 2-3 days post-incubation. This is comparable to the results of Howell *et al.* with ^{195m}Pt-transplatin (7,8).

Subcellular distribution studies show that about 70% of the activity that penetrated the cell is in the nucleus, and 60% of the latter bound to the DNA. In their studies with ^{195m}Pt-transplatin, Howell *et al.* found that 57% of the intracellular activity was in the cell nucleus, 42% of which was bound to the DNA (7,8).

The survival curves for V79 cells (Fig. 5) exposed to radiolabeled versus non-radiolabeled carboplatin are strikingly different. For the non-radiolabeled carboplatin, the survival curve has a broad shoulder, and the extracellular concentration of the drug in the incubation medium is about 140 μM at 37% cell survival. These results are in excellent agreement with the work of Roberts and Fraval (4) on the chemical toxicity of non-radioactive carboplatin to V79 cells. In contrast, no shoulder is evident with the radiolabeled compound. The mean lethal drug concentration is about 35 μM at which no cell killing occurs with "cold" carboplatin alone. The issue of synergistic effects with ionizing radiation and platinum metal complexes is long standing. While our study does not address this question, we note that Douple and Richmond (18) reported no radiosensitization of V79 cells under oxic conditions for cisplatin and transplatin. Perhaps, the same may be true for carboplatin as well (19).

Although the Pt target for reactor irradiation is enriched in ^{192}Pt to the maximum extent available (57%), production of ^{195m}Pt is inevitable. The average uptake/cell of the radiolabeled compound is approximately the same as for ^{195m}Pt-transplatin (7). According to ORNL, the initial proportion of the activities of ^{193m}Pt to ^{195m}Pt was about 8:1. Quantitative estimates of the activities of the two radionuclides in the cell are essential for cellular dosimetry. No doubt, ^{193m}Pt was predominant in the cell. Its quantification, however, presented an unanticipated difficulty. Although use of the Ge(Li) well-detector facilitated efficient detection of photons, this geometry also resulted in accidental sum peaks of the intense Pt K X rays emitted in the isomeric decays of the radionuclides. The characteristic γ photons, emitted in low yield, were masked by the sum peaks as a consequence. This technical problem is easily resolved by moving the source out of the well, and further studies are planned accordingly.

In spite of the above limitation, the present work is a significant new contribution. Carboplatin is an antineoplastic drug; when radiolabeled with the ^{193m}Pt moiety, its efficacy for cell killing is very high compared to the cold drug. This suggests that ^{193m}Pt labeled carboplatin may prove to be a viable chemo-Auger therapeutic agent that may achieve the same efficiency as the non-radioactive drug but at much lower dosages. Conceptually at least, a similar approach with cisplatin should be possible.

ACKNOWLEDGMENTS

This work is supported by USPHS Grant No. CA-32877 and New Jersey Cancer Commission Grant No. 688-009.

REFERENCES

1. B. ROSENBERG, L. VAN CAMP, J.E. TROSKO, and V.H. MANSOUR, Platinum compounds : A new class of anti- tumor agents. *Nature* (London), **222**, 385 (1969).
2. I. HAIDUC and C. SILVESTRU, Metal compounds in cancer chemotherapy. *Coord. Chem. Rev.* **99**, 253-296 (1990).
3. H. SHARMA, N THATCHER, J. BAER, *et al.*, Blood clearance of radioactively labelled cis-diammine-1,1-cyclobutanedicarboxylate platinum(II) (CBCDA) in cancer patients. *Cancer Chemo. and Pharma.* **11**, 5-7 (1983).
4. J.J. ROBERTS and H.N.A. FRAVAL, The interaction of antitumor platinum compounds with cellular DNA in cultured cells and animal tissues: Relationship to DNA cellular repair processes. *Biochimie* **60**, 869-877 (1978).
5. D.V. RAO, V.R. NARRA, R.W. HOWELL, G.F GOVELITZ, and K.S.R. SASTRY, In vivo radiotoxicity of DNA-incorporated I-125 compared with that of densely ionizing alpha particles. *The Lancet*, II, 650-653 (1989).
6. A.I. KASSIS, S.J. ADELSTEIN, and K.S.R. SASTRY, Kinetics of uptake, retention and radiotoxicity of $^{125}IUdR$ in mammalian cells: Implications of localized energy deposition by Auger processes. *Radiat. Res.* **109**, 78-89 (1987).
7. R.W. HOWELL, Radiobiological effects of Auger electrons in the decay of Pt-195m. *PhD. Dissertation*, University of Massachusetts, Amherst (1987).
8. R.W. HOWELL, K.S.R. SASTRY, A.I. KASSIS, D.V. RAO, S.J. ADELSTEIN, H.A. WRIGHT, R.N. HAMM, and J.E. TURNER, Auger decay of platinum-195m: Track structure in liquid water and high-LET type radiotoxicity of Pt-195m labeled transplatin in mammalian cells. (to be published).
9. C.M. LEDERER, J.M. HOLLANDER, and I. PERLMAN, *Table of Isotopes*, Sixth Edition, Wiley: New York, 116, 1967.
10. G. WILKINSON, Radioactive isotopes of platinum and gold. *Phys. Rev.* **75**, 1019-1029 (1949).

11. K.S.R. SASTRY and E. SPEJEWSKI, Personal Communication (1985).
12. Z. CHUNMEI, *Nuclear Data Sheets for A = 195*, **57**, 49 (1989).
13. V.S. SHIRLEY, *Nuclear Data Sheets for A = 193*, **32**, 593-677 (1981).
14. A.I. KASSIS, R.W. HOWELL, K.S.R. SASTRY, and S.J. ADELSTEIN, Positional effects of Auger decays in mammalian cells in culture. In *DNA Damage by Auger Emitters*, (K.F. Baverstock and D.E. Charlton, Eds.) Taylor and Francis: London, 1-14 , 1988.
15. A.I. KASSIS, K.S.R. SASTRY, and S.J. ADELSTEIN, Intracellular distribution and radiotoxicity of chromium-51 in mammalian cells: Auger electron dosimetry. *J. Nucl. Med.* **26**, 59-67 (1985).
16. A.I. KASSIS and S.J. ADELSTEIN, A rapid and reproducible method for the separation of cells from radioactive media. *J. Nucl. Med.* **21**, 88-90 (1980).
17. W.C. HYMER and E.L. KUFF, Isolation of nuclei from mammalian tissues through the use of Triton-100X. *J. Histochem. Cytochem.* **12**, 359-363 (1964).
18. E.B. DOUPLE and R.C. RICHMOND, A review of interactions between platinum coordination complexes and ionizing radiation: Implications for cancer therapy. In *Cisplatin, Curent Status and New Developements*, (A.W. PRESTAYKO, S.T. CROOKE and S.K. CARTER, Eds.) Academic Press: Orlando, 125-147,1980.
19. J.A. O'HARA, E.B. DOUPLE, and R.C. RICHMOND, Enhancement of radiation induced cell killing by platinum complexes in V79 cells. *Int. J. Radiat. Oncol. Biol. Phys.***12**, 1419-1422 (1986).

DISCUSSION

De Sombre, E.R. Do you have an explanation for the biology of the early uptake plateau? Have you saturated all the available sites?

Azure, M.T. Uptake curves with an early plateau as in this work (Fig. 4) are also observed in other cases (*e.g.* ^{195m}Pt-labeled transplatin (7)) for the same cell line. At the present time we do not fully understand the biological aspects of all possible binding sites. The uptake is concentration dependent, the tighter sites being filled preferentially at lower concentrations of the drug in the incubation medium. The plateau implies saturation of all the relevant sites.

De Sombre, E.R. What was the reason for the choice of carboplatin over cisplatin?

Azure, M.T. Convenience. Both are antineoplastic drugs. Cisplatin is effective at much lower concentrations than carboplatin. The specific activity of ^{193m}Pt available at present is not sufficiently high to delineate the effects of the Auger emitter from the chemical effects of cisplatin alone. Our goal is to examine the efficacy of ^{193m}Pt metal center in platinum antitumor drugs in general. These initial experiments with carboplatin demonstrate the idea. We plan to work with cisplatin with the radiolabel in the future as higher specific activities of the Auger emitter become available.

Kassis, A.I. What is the D_0 in decays/cell?

Howell, R.W. Approximately the same as in the case of ^{195m}Pt-transplatin (7). We encountered some systematic difficulty in quantification.

Sastry, K.S.R. Although ^{193m}Pt is the dominant one, there is also a significant amount of ^{195m}Pt. Use of a well-type Ge(Li) detector resulted in accidental sum peaks of the intense Pt K X rays. This effect masked the weak characteristic γ rays. This problem is easily rectified by placing the source outside the well. We will pursue these aspects further.

Kassis, A.I. Why carboplatin instead of transplatin?

Azure, M.T. Both of these are of interest. Carboplatin has tumorcidal efficacy while transplatin is merely chemotoxic. In these initial studies, we have preferred to work with carboplatin labeled with the Auger emitter.

 Biophysical Aspects of Auger Processes, AAPM Symposium Series No. 8 (1992) 352-371
Eds. RW Howell, VR Narra, KSR Sastry, DV Rao

ESTROGEN RECEPTOR-DIRECTED RADIOTOXICITY WITH AUGER ELECTRON-EMITTING NUCLIDES: E-17α-[^{123}I] IODOVINYL-11β-METHOXYESTRADIOL AND CHO-ER CELLS

EUGENE R. DESOMBRE[1], ALUN HUGHES[1], BABAK SHAFII[1], LIBERTAD PÚY[1], PAOLA C. KUIVANEN[1], ROBERT N. HANSON[3], and PAUL V. HARPER[2]

[1]Ben May Institute, [2]Departments of Surgery and Radiology, University of Chicago, Chicago, IL 60637

[3]Department of Chemistry, College of Pharmacy, Northeastern University, Boston, MA 02115

ABSTRACT

The specific radiotoxicity of the Auger-electron-emitting nuclide, I-123, covalently attached to a steroidal estrogen, E-17α-[^{123}I] iodovinyl-11β-methoxyestradiol, [^{123}I]I-VME2, was studied in Chinese hamster ovary cell lines with or without estrogen receptor (ER) from a stable transfection with ER cDNA. Using the halodestannylation reaction, I-123-labeled estrogens have been synthesized with specific activities approaching the theoretical specific activity of I-123. When incubated for 1 h with suspended cells, [^{123}I]I-VME2 caused a dose-dependent, estrogen-inhibitable radiotoxicity in the cells expressing ER. Little effect was seen in the cells lacking the transfected ER. Autoradiography confirmed the nuclear localization of [^{123}I]I-VME2, but showed a heterogeneous distribution among cells, especially at lower ligand concentrations. Estimates suggest that the mean lethal dose for this ER-directed radiotoxicity is in the range of several hundred decays per cell,

compatible with its use in ER-containing cancers which usually contain thousands of ER per cell.

INTRODUCTION

Endocrine therapies have been used for the treatment of breast cancer for nearly a century (as reviewed in 1). At present there is increased specificity in the application of endocrine therapies due to the knowledge that responding cancers contain estrogen receptors (ER) (2), but not all ER-containing cancers respond. Certain ER-containing cancers, such as ovarian carcinoma, show little response to endocrine therapies (3) and even breast and endometrial cancers, which have higher response rates, often recur despite initial response. Part of the reason for this relates to the nature of current endocrine therapies, which are cytostatic rather than cytotoxic. Thus the treatment causes shrinkage of the tumor, due to the therapy-induced reduced proliferation rate, but does not actually kill the cancer cells.

Basic research over the last several decades has led to a better understanding of the role of steroid receptors in the regulation of growth and differentiated function in a variety of tissues (4). The estrogen receptor, a member of the steroid receptor family of nuclear, DNA binding proteins (5), stimulates growth of a number of normal and neoplastic tissues. After binding estrogen the receptor dimerizes (6) and in this form associates with the specific estrogen response elements in DNA, thereby initiating new or increased RNA synthesis leading to new proteins and cell proliferation. It has been recently recognized that some of the new proteins resulting from the estrogen-receptor interaction in the cell are growth factors (7). In fact, it is believed that constitutive production of these growth factors may be responsible for the estrogen independence of some of the ER-containing, endocrine-unresponsive cancers.

However, for the purposes of our research, the important characteristic of the family of steroid receptors, and particularly estrogen receptors, is their high affinity, non-covalent association with the specific response elements in the DNA. We therefore suggested that, in view of the cytotoxic effects of Auger-electron-emitting nuclides incorporated into DNA (8,9), Auger electrons emitted from DNA-associated, ER-bound radioligands should be effective in causing double-strand DNA breaks, and be specifically radiotoxic for ER positive cells and cancers (10). On the other hand, the evidence for

substantially reduced radiotoxicity for the Auger electron cascade process occurring outside the nucleus (11) would suggest that ER negative cells should be largely insensitive to radiotoxicity with ER-directed ligands bearing Auger-electron-emitting nuclides. Some time ago it was reported that ER-dependent radiotoxicity was observed using 16α-[^{125}I]iodoestradiol with cells in tissue culture (12). However, because of the long half-life of I-125 (60 days), and the short residence time of estrogens in ER-positive cells, it was necessary to freeze the cells for several half-lives to demonstrate the radiotoxicity, shown as reduced plating efficiency as a function of the time the cells were stored frozen. Clearly, with the numbers of estrogen receptors per cell (thousands) and the average residence time of estrogens (hours) it is unlikely that I-125 would be a feasible Auger-electron-emitting nuclide for such ER-directed therapy.

It is curious, therefore that an I-125-labeled antiestrogen, iodotamoxifen, has been reported to show specific radiotoxicity in the ER-containing cell line, MCF-7, without such cell freeze-storage (13,14). Initial studies compared the survival of ER-containing MCF-7 cells with ER-negative V79 cells in culture and showed a significantly greater sensitivity of MCF-7 cells to the radiotoxicity of [^{125}I]iodotamoxifen (13). However, the D_{37} value of 0.5 pCi/cell corresponded to more than 1 million molecules per cell, more than an order of magnitude greater than the ER content of MCF-7 cells, so it was clear that the uptake was not entirely ER-mediated. Furthermore, no data were available comparing the relative radiosensitivity of MCF-7 and V79 cells in general. A second study (14) used ethanol precipitation to assess the amount of [^{125}I]iodotamoxifen associated with protein or DNA. This result is difficult to interpret as the non-covalently ER-bound ligands are usually readily extracted from ER with ethanol, even from whole cells. However, since only a small fraction of the total cell associated I-125 remained after ethanol extraction, the survival curve of MCF-7 cells related to ethanol precipitated [^{125}I]iodotamoxifen was considerably closer to that seen with [^{125}I]iododeoxyuridine, incorporated into DNA. This was encouraging to the authors. However, a recent study (15) showed that a large portion of the radiotoxicity due to [^{125}I] iodotamoxifen could not be inhibited by co-incubation with either unlabeled estradiol (suppressing ER binding) or unlabeled tamoxifen (competing for the so-called antiestrogen sites), although the unlabeled tamoxifen was the more effective inhibitor of the two. Thus it is clear that most of the radiotoxicity of [^{125}I]iodotamoxifen was not mediated through the estrogen receptor, substantially decreasing the potential of this ligand for therapy of ER+ cancers.

To circumvent these problems, we decided to study an ER-binding ligand, 17α-iodovinyl-11β-methoxyestradiol, based on the steroidal estrogen, moxestrol, which has at least an order of magnitude higher affinity for ER than does tamoxifen. In addition, we employed the 13.2 h half-life nuclide, I-123, whose short half-life should allow direct assessment of radiotoxicity in tissue culture using two closely related cell lines. The cells used are Chinese hamster ovary cells (CHO), which are believed to lack ER, and a stable transfectant, CHO-ER (16), of the same cell line expressing ER introduced from ER cDNA of MCF-7 cells. Thus we could compare the same cell with or without ER, and study radiotoxicity in the presence or absence of excess unlabeled estrogen by direct colony assay. However, well into this study we discovered that the ER cDNA introduced in these cells contained a single base change from wild type ER (16,17), resulting in ER with a lower affinity for estrogen. Despite this complication, we can report here the estrogen-receptor-specific radiotoxicity of I-123-labeled estrogen in CHO-ER cells, demonstrating the feasibility of this new approach to therapy of ER-containing cancers with Auger-electron-emitting nuclides.

MATERIALS AND METHODS

Synthesis of E-17α-[^{123}I] iodovinyl-11β-methoxyestradiol, [^{123}I]I-VME2

One hundred μg E-17α-tributylstannylvinyl-11β-methoxyestradiol in 100 μl ethanol was added to the vial containing Na[^{123}I]I in 0.1 N NaOH (supplied by Nordion International, Inc, Kanata, Ontario), followed by 100 μl of a mixture of acetic acid:H_2O_2, 100:1, which had been preincubated at room temperature for 1 h. After mixing, the reaction was allowed to proceed at room temperature for 15 min, the mixture was drawn up into a syringe and its radioactivity determined in a Capintec dosemeter. The mixture was then injected onto a 10 mm by 250 mm Econosil 10 μ C_{18} reverse phase HPLC column, pre-equilibrated with 10% acetonitrile in water. The column was eluted with a 30-min gradient of 10-100% acetonitrile at 3 ml per min, under which conditions the [^{123}I]I-VME2 elutes between 27 and 28 min, while the tin precursor elutes at 37 min. The peak fractions were combined and evaporated to a small volume. Ether and water were added and mixed, the ether removed, and the aqueous portion re-extracted with additional ether which was combined with the first extract. The ether extracts were evaporated under reduced pressure and the [^{123}I]I-VME2 taken up in ethanol. The ethanol was evaporated under a stream of nitrogen at room temperature and

more ethanol added to azeotrope off any water absorbed by the ether. The [^{123}I]I-VME2 was then dissolved in 50% ethanol to maintain sterility.

Determination of Effective Specific Activity of [^{123}I]I-VME2

Six 100-µl portions of a 200,000 x g supernatant of a 1:10 homogenate of immature rat uteri in 10 mM Tris, 10 mM KCl, 1 mM EDTA, pH 7.4 buffer (TKE buffer) were placed in incubation tubes chilled in ice. Unlabeled estradiol (E2, 12.5 µl of 5 µM) was added to two of these tubes, TKE buffer (12.5 µl) was added to 3 other tubes and 12.5 µl of the antiestrogen receptor monoclonal antibody, H222 (18) was added to the final tube. Then 12.5 µl of what would be projected to be 50 nM [^{123}I]I-VME2, based on an anticipated specific activity of ~7.4 MBq/pmol (~200 µCi/pmol), was added to 4 of the tubes (two with buffer, one with H222, one with cold E2). To the other two tubes, 12.5 µl of a 50 nM tritiated estradiol solution (2.2 kBq/pmol, 60 nCi/pmol) was added. Each mixture was incubated for at least 1 h in ice, and added to a pellet of 125 µl of 1% charcoal (Norit A) + 0.1% Dextran T40 in TKE buffer (DCC) in an Eppendorf microtube. The DCC was resuspended with the mixtures, incubated for 10 min in ice to adsorb unbound ligands, and then centrifuged (Beckman microfuge) for 1 min at 13,000 rpm in the cold. One hundred µl aliquots of the DCC supernatants were layered on 10-30% sucrose gradients in either low salt (TKE) or high salt (TKE with 400 mM KCl) buffer. The tubes were placed in a Beckman SW 60 rotor and centrifuged for 15 h at 208,000 x g, 2°C. After sedimentation, the density gradients were fractionated from the bottom by displacement with paraffin oil and collected into glass tubes (I-123) or scintillation vials (H-3) for determination of radioactivity. The radioactivity for I-123 was corrected for decay to the time the gradients were layered or the *in vitro* incubations with cells began. The effective specific activity of [^{123}I]I-VME2 was calculated from the ratio of decay-corrected, cold estradiol inhibited, specifically-bound radioactivity of the 2 radioactive estrogens to the 8S receptor and the known specific activity of [^{3}H] estradiol:

$$\text{Sp.Act.}[^{123}\text{I}]\text{I-VME2} = (60)\left(\frac{\text{8S DPM } [^{123}\text{I}]\text{I-VME2 alone} - \text{8S DPM } [^{123}\text{I}]\text{I-VME2+excess E2}}{\text{8S DPM } [^{3}\text{H}]\text{E2 alone} - \text{8S DPM } [^{3}\text{H}]\text{E2+excess E2}}\right)$$

(using tritiated estradiol of 60 Ci/mmole). The result was confirmed by comparing the specific 8S DPM for [^{123}I]I-VME2 on low salt gradients with the specific DPM of the ER complex with [^{123}I]I-VME2 shifted downfield by the antibody in high salt gradients.

Radiotoxicity of [^{123}I]I-VME2 in CHO and CHO-ER Cells

Normal Chinese hamster ovary cells or those transfected with ER cDNA prepared from MCF-7 cell mRNA (16), growing in T150 flasks, were trypsinized, collected by centrifugation, suspended in medium (16) and the cell number counted with a hemocytometer. The cells were diluted to a concentration of 1.5 to 2 million cells per ml and incubated at 37°C with occasional mixing with various concentrations of [^{123}I]I-VME2 alone or together with an estimated 100-fold excess of unlabeled estradiol in medium. Similar incubations were also carried out with the same concentrations of unlabeled estradiol alone, sodium [^{123}I]iodide or medium alone. After incubation the cells were collected by centrifugation for 5 min at 500 x g at room temperature, washed twice by resuspending in medium and centrifugation, and finally resuspended in 1 ml of medium for cell counting, radioactivity determination, plating and autoradiography. For plating the cells were diluted to densities of 100 to 12,500 cells per 1 to 2 ml and plated in 6-well plates, usually with 6 replicates for each group. The cells were allowed to form colonies for 1 week, at which time the medium was removed, the wells washed with phosphate buffered saline, fixed with Bouin's fixative for 10 min, washed with water, stained with 0.45% crystal violet, washed with water to remove excess stain and air dried. The large colonies, greater than 50 cells per colony, were counted at the densities in which separate, individual colonies could be recognized. Cell survival was expressed as a percentage, based on the ratio of the number of colonies in an experimental group, divided by those in the medium controls. Aliquots of the initial radioactive incubation mixtures, as well as the washes and resuspended washed cells, were assayed to determine the initial concentrations of [^{123}I]I-VME2 in the incubations and the amount of the [^{123}I]I-VME2 retained by the washed cells after incubation. To establish the time-dependent retention of I-VME2 in cells after plating, an experiment was performed with plated cells exposed to [^{125}I]I-VME2. For this purpose CHO-ER cells were plated and, after attachment, exposed to [^{125}I]I-VME2 for 1 h at 25° or 37°C. The radioactive medium was replaced with standard medium, the cells incubated for varying times at 25° or 37°C, the medium removed and the radioactivity still remaining with the cells extracted with ethanol for assay in a γ counter.

Autoradiography

To determine the cellular distribution and subcellular localization of the [^{123}I]I-VME2 in washed CHO or CHO-ER cells following incubation in

suspension culture, 50 µl of the resuspended, washed cells were smeared on emulsion-coated slides. For this purpose ethanol washed slides were coated in a dark room by dipping in a solution of Kodak NTB3 emulsion diluted 1:1 in distilled water at 40°C, dried and stored at 2°C overnight. After distributing the cells on a slide with a glass rod in the dark room, the slide was immediately placed on dry ice and when a group of slides were finished they were transferred to a light-tight box that was stored at -20°C for two days. The images were developed by allowing the slides to warm to room temperature for 30 min, developing for 5 min in Kodak D-19, washing in water and fixing for 5 min in Kodak rapid fix A. The cells were then stained with hematoxylin and eosin, dehydrated, and mounted with Permount.

RESULTS

With limited numbers of ER per cell and a relatively short residence time of estrogens in ER-containing cells *in vivo*, it is important to maximize the number of molecules of the radiolabeled estrogen in each cell to deliver maximum radiotoxicity. It is therefore important to achieve very high specific activities for the I-123-labeled estrogens so that as high a proportion as possible of the estrogen molecules incorporated in each cell contain I-123. Fortunately, the iododestannylation reaction (19) provides an efficient, stereospecific, as well as rapid, method to incorporate I-123 into estrogens. Since even using mCi quantities of I-123 the mass of the iodoestrogen is too small to easily measure, conventional specific activity determinations, based on the ratio of radioactivity to UV absorption, are likely to be crude estimates. However, because of the high affinity of many I-123 labeled estrogens for the estrogen receptor, it is possible to use sedimentation analysis to accurately determine the specific activity by assessing specific binding to ER. As shown in Fig. 1, on low salt gradients [^{123}I]I-VME2 sediments with the 8S form of the receptor (Fig. 1B) at the same location as the standard estrogen, [^{3}H] estradiol (Fig. 1A). The specificity of this association is evident by the displacement of both of these radiolabeled estrogens from the receptor in the presence of excess unlabeled estradiol. The binding of [^{123}I]I-VME2 to ER is further confirmed by the recognition of the [^{123}I]I-VME2-ER complex by the ER antibody, H222 (Fig. 1C). In this case, the [^{123}I]I-VME2 associated with the ER 4S monomer, seen in high salt, sediments further downfield when incubated with H222 antibody. This is indicative of the ternary complex of ER antibody with the ER to which the [^{123}I]I-VME2 is non-covalently bound. By comparing the specifically inhibitable radioactivity of [^{123}I]I-VME2 (18,650,000 decay

corrected DPM) and that of [^{3}H]-estradiol (14,917 net DPM) bound to the 8S receptor, and using the known specific activity of [^{3}H]-estradiol (2.2 kBq/pmol, 60 Ci/mmol), one can calculate that the specific activity of [^{123}I]I-VME2 shown in Fig. 1 is approximately 2.78 MBq/pmole (75,000 Ci/mmole). This is about 31% of the theoretical specific activity of I-123. Recently, we have prepared [^{123}I]I-VME2 at specific activities as high as 8.47 MBq/pmol (229,000 Ci/mmol) and an I-123-labeled iodotriphenylethylene estrogen at essentially the theoretical specific activity of I-123.

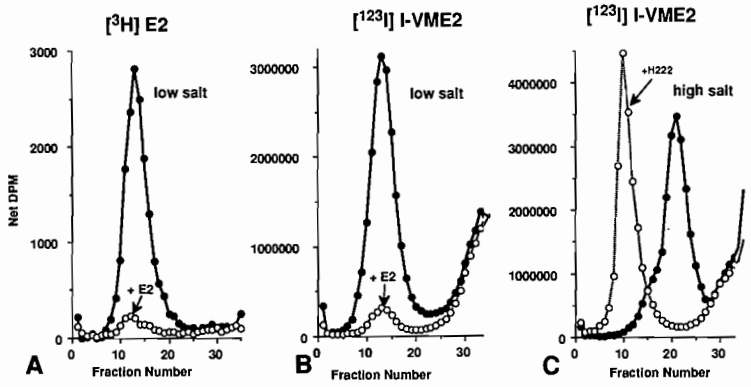

FIG. 1. Sedimentation analysis of [^{123}I]I-VME2. [^{3}H]E2 (A) or [^{123}I]I-VME2 (B,C) was added to aliquots of rat uterine cytosol without (closed circles) or with (A, B, open circles) approximately 100-fold excess of unlabeled E2, or with 1 μg/ml anti-ER antibody H222 (C, open circles). After incubation at 4°C, unlabeled ligands were removed by incubation with DCC, layered on low salt (A, B) or high salt (C) sucrose gradients and centrifuged for 15 h at 208,000 x g, 2°C. Gradients were collected from the bottom.

To show that [^{123}I]I-VME2 is specifically radiotoxic to ER-containing cells we incubated 1.2 nM [^{123}I]I-VME2 with both CHO-ER and CHO cells in suspension culture for one hour at 37°C. After washing, the cells were plated in multiwell dishes for colony assay. In this study we compared cells which had been incubated with: (1) [^{123}I]I-VME2 alone; (2) [^{123}I]I-VME2 in the presence of a 100-fold excess of unlabeled estradiol to inhibit binding of the radioiodoestrogen to ER; (3) unlabeled estradiol itself; and (4) medium alone. As seen in Fig. 2, the [^{123}I]I-VME2 was only radiotoxic to the CHO-ER cells. This concentration of [^{123}I]I-VME2 had little effect on the ER-negative CHO

cells. Furthermore, most, but not all of the radiotoxicity of the [^{123}I]I-VME2 could be prevented in the CHO-ER cells by co-incubation with excess unlabeled estradiol, and under the conditions used, the excess unlabeled estradiol alone had no effect on the survival of the cells. While the incubation with unlabeled estradiol reduced the amount of cell associated radioactivity, about 12% as much radioactivity remained with the washed CHO-ER cells incubated with [^{123}I]I-VME2 in the presence as in the absence of unlabeled E2. This shows that there is a significant amount of non-specific binding of the [^{123}I]I-VME2 to the CHO-ER cells when incubated in suspension culture. Interestingly, a similar amount of non-specific binding of [^{123}I]I-VME2 was seen with CHO cells incubated in the absence of unlabeled estradiol, but this residual [^{123}I]I-VME2 did not cause substantial cell killing (Fig. 2).

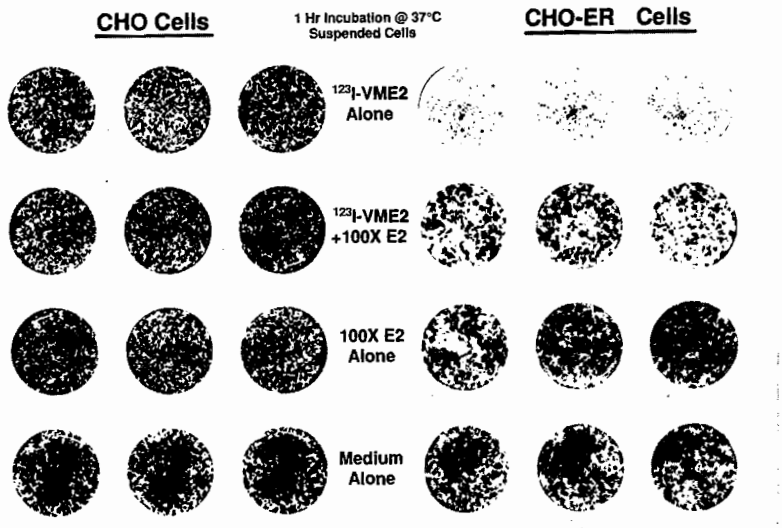

FIG. 2. Radiotoxicity of [^{123}I]I-VME2 in CHO and CHO-ER cells. Suspended cells were incubated with 1.2 nM [^{123}I]I-VME2 alone or along with 100-fold excess of unlabeled E2, the same concentration of estradiol alone or medium for 1 h at 37°C. After washing, the cells were plated in 6-well plates and allowed to form colonies which were fixed and stained with crystal violet.

The results shown in Fig. 2 indicated substantial cell killing, but the number of cells made colony counts of the control wells impossible. Colony assays at lower plating densities indicated that about 7% of the CHO-ER cells survived after incubation with [^{123}I]I-VME2 alone. Assessment of the

distribution of cell labeling by autoradiography, Fig. 3, provided a basis for understanding the radiotoxicity results. As seen in Fig. 3, there was a significant variation in the number of silver grains over various cells, ranging from what looked like thousands of silver grains densely covering some nuclei, to more moderate numbers of grains per cell to grain densities similar to the background. The autoradiograms confirmed the expected concentration of the labeled estrogen in the nuclei of the cells but unexpectedly indicated that between 5 and 10% of the cells had densities of silver grains which were similar to the background. For this experiment we harvested confluent cells. In subsequent experiments using cells harvested at lower cell densities we have seen a more uniformly high degree of cell labeling by autoradiography at the highest concentrations of [^{123}I]I-VME2 used.

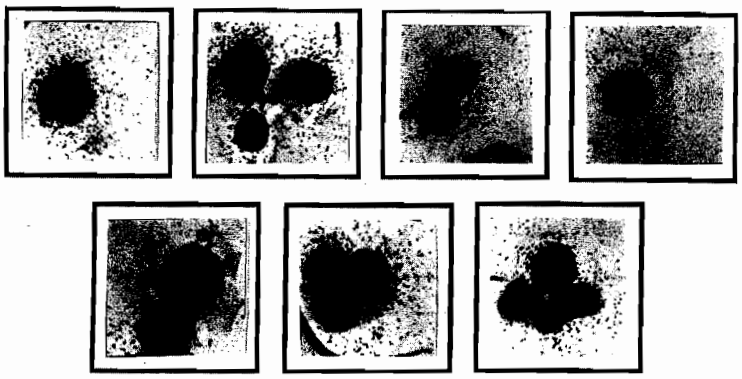

FIG. 3. Autoradiography of CHO-ER cells incubated with [^{123}I]I-VME2. CHO-ER cells incubated for 1 h with 1.2 nM [^{123}I]I-VME2 and washed to remove unbound ligand were spread on emulsion coated slides and processed after 2 days at -20°C. Panels show representative autoradiograms of various cells on the slide.

Further studies have shown that the radiotoxicity of [^{123}I]I-VME2 in CHO-ER cells is dose-dependent (Table I). Consistent with the results shown in Fig. 2, the effect of [^{123}I]I-VME2 on CHO cells was dramatically less than that on CHO-ER cells. In this experiment we found that at high concentrations of [^{123}I]I-VME2 there was some radiotoxicity of [^{123}I]I-VME2 even with the CHO cells (Table I). Clearly, this effect is small compared to the effect in the ER-positive CHO-ER cells. In recent experiments this difference in radiotoxicity of [^{123}I]I-VME2 to CHO-ER and CHO cells at nanomolar concentrations has

corresponded to more than 3 orders of magnitude. Sedimentation analyses on extracts of these CHO cells do not provide any evidence for extractable ER from the CHO cells. However, we can not completely rule out small amounts of a non-extractable estrogen binding component in the nucleus or elsewhere in the cells, although whole-cell assays of specific uptake of estrogens by these cells likewise do not provide definitive evidence for significant amounts of any specific estrogen binding components. In several experiments we have observed a small degree of radiotoxicity of [^{123}I]I-VME2 in CHO cells, which is largely prevented by co-incubation with excess unlabeled estradiol, consistent with a low concentration of an estrogen-specific binding component in the CHO cells. As seen in Table I, even higher concentrations of I-123 as sodium iodide have no radiotoxicity for the cells, indicating that the presence in the medium of similar concentrations of I-123 is not radiotoxic.

The protective effect of unlabeled estradiol is shown in Table II, along with analysis by autoradiography of the density range of silver grains over CHO-ER cells (as a function of concentration of [^{123}I]I-VME2 to which the cells

TABLE I

Radiotoxicity of I-123 Iodide and I-VME2 for CHO and CHO-ER Cells

Cell type	Group[a]	μCi/ml	nM	% Survival
CHO-ER	[^{123}I] I-VME2[b]	137	1.56	0.0 ± 0.0
		27.8	0.315	4.3 ± 1.8
		4.8	0.055	76.1 ± 8.0
		0.83	0.009	102.0 ± 7.3
	[^{123}I] I NaI	189		103.8 ± 11.2
CHO				
	[^{123}I] I-VME2[b]	145	1.64	62.7 ± 7.0
		29.5	0.33	95.6 ± 6.9
		4.96	0.056	108.1 ± 9.7

[a] Suspended cells were incubated 1 h, 37°C with the radioligand, the cells washed and plated in multiwell plates for colony assay.

[b] Specific Activity 3.23 MBq/pmol (88,000 Ci/mmol).

TABLE II
Relationship of Cell Labeling to Radiotoxicity[a]

[^{123}I] I-VME2[b] Concentration	unlabeled E2 conc Survival	Molecules/ Cell	Autoradiography (% of cells) high	mid	low	neg	%
0.69 nM		55,400	100	0	0	0	0.0
0.59 nM	170 nM	10,800	0	0	75	25	49 ± 25
0.20 nM		18,313	80	10	10	0	0.0
0.07 nM		5,000	0	60	30	10	70 ± 19

[a] Suspended CHO-ER cells were incubated for 1 h at 37°C with the [^{123}I] I-VME2, washed, and aliquots assayed for I-123, spread on emulsion coated slides for autoradiography and plated in multiwell plates for colony assay.

[b] Specific activity 8.48 MBq/pmol (229,000 Ci/mmol).

were exposed). At the highest concentration of [^{123}I]I-VME2, 0.69 nM, all the cells showed high density labeling, and the average number of [^{123}I]I-VME2 molecules per cell was about 55,000. When incubation with a similar concentration of [^{123}I]I-VME2 was carried out in the presence of a nearly 300-fold excess of unlabeled estradiol, the number of molecules per cell only dropped by about 80%, but now 25% of the cells showed no grain density above background, and the rest showed only low density labeling. When the concentration of [^{123}I]I-VME2 used was decreased 3-fold, the average number of molecules of [^{123}I]I-VME2 per cell dropped proportionately, but there was also a wider range of silver grain densities over the cells. Despite the change in the autoradiographic pattern, all the cells were significantly above the background level of silver grains and at low plating density all the cells were killed (indicating > 95% cell kill in this experiment). However, when the concentration was again decreased by a factor of 3, and the average number of molecules per cell dropped commensurately, there now were appreciable numbers of cells which were labeled at the low or background level, and about 70% of the cells survived. Thus, there is clearly a concentration dependence of the extent of cell killing due to [^{123}I]I-VME2 and concomitant with decreases in the average number of I-123 labeled estrogens per cell a change in the distribution of autoradiographic grain density over the cells. We have recently studied the fate of [^{125}I]I-VME2 initially taken up by CHO-ER cells and found that, in no doubt largely due to the decreased affinity of the mutated ER of these cells (17), even the [^{125}I]I-VME2 specifically bound is

rapidly lost from the cells at 37°C, with a mean residence time of only about an hour.

DISCUSSION

The high-LET type radiotoxicity associated with the Auger electron cascade process makes such electrons particularly attractive for cancer therapy due to the oxygen independence of their effects and their potential to deliver damage to key cellular components. However, the very short range of the electrons, a consequence of their generally low energy, has limited their applications. Obviously what is desirable is a reasonably specific mechanism to localize the Auger electron emitter in the nucleus of the target cells. The ideal route would be that of incorporation into the DNA, which has been shown to be very potent for causing multiple double-strand breaks in the DNA, and resultant efficient radiotoxicity in cells in culture (8,9). Although many cancers have greater rates of proliferation than many normal tissues, certain normal cells, such as the epithelium of the intestine, also may have very high proliferative rates so that systemic therapy with an Auger electron emitter incorporated simply as a function of the rate of cell proliferation of the tissue could be problematic.

We have been exploring the therapeutic potential of using a nuclear protein to deliver a non-covalently bound ligand with an Auger electron emitter to the vicinity of DNA. This approach is not without pitfalls, as a non-covalent association of the radiolabeled ligand will lead to eventual loss of the ligand from the cells, even assuming that one can concentrate it in the desired cells in the first place. Furthermore, there are few, if any, nuclear proteins believed to be specific to cancer cells. Because of the high concentration of estrogen receptors in some breast, endometrial and ovarian cancers and the recognition that ER are high affinity, DNA-binding proteins, ER-directed therapy with Auger-electron-emitting nuclides seemed to be a reasonable candidate for a trial of such therapy. While significant concentrations of ER are also found in the pituitary and normal tissues of the reproductive tract, the rate of replication in these tissues is lower in general than that of the cancers, and if necessary the reproductive organs could be removed (and often may have been already removed in older patients). In fact the removal of the pituitary was used for therapy of ER positive breast cancers in the past (1). However, before seriously considering such therapy for ER positive cancers in patients, it is important to understand the

characteristics of the potential radiotoxicity *in vitro* and in animal model systems. We therefore set out to determine whether it was possible to specifically kill cells in tissue culture in an ER-dependent manner, and to estimate the number of molecules per cell, or decays per cell, needed for such radiotoxicity. With such information in hand it would be more appropriate to study the uptake and retention of various potential radiolabeled estrogens in patients to determine the mean residence time as a function of route and dose to compare with the number of decays per cell needed, as established in the experimentally simpler *in vitro* studies.

The results here establish that the steroidal estrogen E-17α-[^{123}I]-iodovinyl-11β-methoxyestradiol specifically kills ER-containing cells in culture. Because of the high affinity association of estrogens with ER and the generally slow dissociation of estrogen already bound to ER, one would expect that short incubations of ER+ cells with the I-123-labeled estrogen should be sufficient. In fact, despite the unexpectedly rapid loss of [^{123}I]I-VME2 from the CHO-ER cells, a 1-hour incubation with the radiolabeled estrogen was sufficient to produce very effective cell killing of CHO-ER cells, as determined by colony assay. This radiotoxicity can be very substantially reduced by inclusion of a large excess of unlabeled estradiol in the incubations with the I-123-labeled estrogen, which also specifically reduces the I-123 uptake in ER-containing CHO-ER cells, but not in CHO cells in which the radiotoxicity of this I-123-labeled estrogen is several orders of magnitude lower. While the reasons that a more than 100-fold excess of unlabeled estradiol can not completely protect the ER positive cells from this radiotoxicity are not entirely clear, the large degree of protection clearly confirms the ER-mediation of the killing. In fact it appears that the lack of complete protection may be due to the presence of ER in the CHO-ER and may be specific to tissue culture experiments. After washing the cells, which would substantially reduce the levels of unlabeled estradiol, the non-specifically bound [^{123}I]I-VME2 would be free to exchange with ER-bound, unlabeled estradiol, now present in a smaller excess in the CHO-ER cells. However, in the CHO cells, with little or no ER present, there should be no mechanism for the non-specifically bound [^{123}I]I-VME2 to be directed to sites near the DNA, hence little radiotoxicity. Since the amount of [^{123}I]I-VME2 remaining associated with the washed CHO-ER cells incubated in the presence of excess unlabeled estradiol is 10-20% of that present in the absence of unlabeled estrogen (Table II), significant amounts of [^{123}I]I-VME2 remain associated with the cells. In this regard, it is of interest that as seen in Table II, the number of I-123 molecules per cell in the presence of unlabeled E2 is about double that seen following an

incubation with a lower concentration of [^{123}I]I-VME2 in the absence of unlabeled E2 that gave a 30% cell kill. Second, based on the relative affinities of estradiol and moxestrol (11β-methoxy estradiol), in which the higher affinity of moxestrol is reflected in a slower dissociation rate from ER, if the redistribution results in new occupancy of ER by [^{123}I]I-VME2, it may be preferentially retained by ER.

The results presented here are complicated by the lower affinity ER found to be present, probably as a cloning error, in the CHO-ER cell line. It has been determined that a single base change in the cDNA gives rise to a single amino acid change (glycine 400 to valine) in the ER, resulting in a lower affinity for estradiol (17). The lower affinity most certainly translates to a shorter residence time for estrogens in the cells. Our preliminary results indicate that the retention of I-VME2 at 37°C is substantially less than that at 25°C in CHO-ER cells and the actual average residence time for I-VME2 in these cells at 37°C is less than an hour. This loss could also reflect a greater rate of metabolism of the ligand at the higher temperatures as well as the processing of the receptor but since it is less dramatic with MCF-7 cells which have wild type receptor it is likely that the lower affinity of the CHO-ER receptor is the cause. Because of this rapid loss of bound ligand, our calculations indicate that only 5 to 6% of the I-123 initially bound to the CHO-ER cells will decay while still associated with these cells at 37°C. While this complicates the model, it indicates the substantial potential for even more effective killing of cells which contain the higher affinity, wild type ER. Studies are currently underway in our laboratory with MCF-7 cells containing apparently normal ER. Nevertheless, the comparison of CHO and CHO-ER cells, which should display similar radiosensitivities, helps to establish the ER-dependency of the killing. Such does not appear to be the case for the studies previously reported (13-15) using [^{125}I] iodotamoxifen with MCF-7 cells. In those studies the number of molecules per cell calculated from the cell associated I-125 at the mean lethal number of molecules is about 1.3 million, at least 10-30 times greater than the total number of ER molecules present in the MCF-7 cell. Hence it was likely, based on this data alone, that ER was not required for the effect. Furthermore, as recently shown, a substantial amount of the toxicity could be inhibited by unlabeled antiestrogen, which was not inhibited by cold estrogen, indicative of mediation of the non-ER antiestrogen specific binding sites. Such sites, found in many cells and at substantial concentrations in some normal tissues, would not constitute a good targeting mechanism to approach ER-containing cancers. This is supported by the diverse distribution of radiolabeled antiestrogens in animals. Finally, if one calculates the number

of decays which could occur during the average 6-12 hour residence time of ligands for ER *in vivo*, it becomes clear that using the 60-day half-life nuclide, I-125, with an ER-directed ligand is not a practical *in vivo* approach to therapy based on the Auger electron cascade process.

Our autoradiographic studies suggest that the cellular content of ER in a population of cells may not be uniform. This may reflect changes in ER expression as a function of cell cycle or growth conditions, as suggested by the differences we have observed with cells harvested at different densities, as well as a normal variation of ER content among cells in the same population. When incubated with nanomolar concentrations of radioiodoestrogen, cells harvested at less than 50% confluence show a uniform, high autoradiographic grain density. However, the same cells incubated with lower concentrations of the same iodoestrogen demonstrate more variability in grain density, consistent with a variation in ER content within a uniformly growing population.

Such differences in ER content would be expected to have important implications for therapy, as the uptake and retention of estrogen by a cell will depend on the concentration of the estrogen and of ER. It is generally recognized that there is heterogeneity of ER expression within breast cancers. This can be clearly shown by immunohistochemical staining for ER using specific monoclonal anti ER antibodies (20). Nonetheless, it is found that most ER positive breast cancers initially respond to endocrine therapy despite such heterogeneity of ER distribution. This can be understood in light of evidence for a paracrine mechanism of growth stimulation. There is increasing evidence now for estrogen-dependent production of peptide growth factors in ER-containing breast cancer cells, at least *in vitro* (7). Such products, released by ER+ cells, could stimulate the growth of nearby ER negative cells as well. However, by the mechanism described, if the ER-containing cells were eliminated, any ER negative cells dependent on the growth factors produced by the ER positive cells would be expected to stop proliferating.

Considerable challenges remain to bring estrogen receptor-directed therapy to the clinics. Clearly the delivery of sufficient I-123-labeled estrogen to the ER positive cancer cells, without causing excessive radiotoxicity to the non-cancerous ER positive cells, or nonspecific radiotoxicity to the patient, will be a challenge. Nonetheless, the first critical step is to demonstrate the radiotoxicity of an Auger-emitter/estrogen complex specific to ER-containing

cells, which we have presented here. Based on the results presented in this paper, and the estimated mean retention time of I-VME2 in the CHO-ER cells of less than one hour, it can be calculated that the mean lethal number of decays of I-123 is in the range of 300 decays per cell. Especially with the higher affinity, wild type ER expected to be present in most human cancers, numbers of cancer-cell-bound radioiodoestrogens necessary to localize more than the mean lethal number of the radiolabeled ligands in these cells would seem to be reachable *in vivo*, in view of the many thousands of ER present per cell in some cancers. It is of theoretical significance that the preliminary estimates of mean lethal number of I-123 decays for an I-123-labeled estrogen in these studies is similar in magnitude to the estimates of mean lethal decays of I-123 incorporated into the DNA of V79 cells, *i.e.* 277 decays (21). These results are consistent with an earlier report by Sundell-Bergman and Johanson (22) which indicated that the efficiency of inducing double strand DNA breaks with the thyroid hormone [^{125}I] triiodothyronine, mediated by the T3 receptor, also a member of the steroid receptor superfamily (5), was as high as that due to [^{125}I] iododeoxyuridine incorporated into DNA. This would suggest that the radiolabeled estrogen must indeed be held in close proximity to the DNA by its association with the estrogen receptor. It also suggests that the probable envelopment of the estrogen within the receptor protein does not substantially reduce the DNA-lytic potential of the Auger electrons. Thus the therapeutic challenge will be to deliver the radiolabeled estrogen as specifically as possible to the ER+ cancer, borne by an estrogen which maximizes its cellular retention. Although it would be wonderful to be able to specifically kill all the cancer cells without otherwise harming the patient, current cytotoxic therapies generally have significant side effects. Clearly factors such as the biological half-life of the ligand and its rate of metabolism will also be of importance to the radiotherapeutic potential of such compounds. Furthermore, animal studies will have to clarify that the even small potential of such radiolabeled estrogens to kill ER negative cells *in vitro* will not be a problem *in vivo*. To be able to deliver a therapeutic dose to the cancer with only minimal side effects to the patient would be a contribution to cancer therapy. The next step will be to identify the best ER-binding carrier, based on cell and animal distribution studies, to be able to proceed to tests of the radiotoxicity in tumors in animals and to begin patient studies. However, we feel that the specificity and dosimetry of the reported results in cells in culture provide some cause for optimism for the substantial process that remains before this new type of therapy can be applied in patients.

CONCLUSION

These studies demonstrate that it is possible to prepare very high specific activity I-123-labeled estrogens, approaching the specific activity of I-123, using the stereospecific halodestannylation reaction with commercially available I-123 sodium iodide. They also show that the I-123 Auger electron cascade targeted to the cell nucleus via covalent attachment to an estrogen which has high affinity to the estrogen receptor can effectively and specifically kill ER positive cells in a dose-dependent, estrogen-inhibitable manner following only a short exposure of the cells to the radiolabeled estrogen in suspension culture. Cells lacking ER show little damage by such treatment, and, as expected, even quite substantial amounts of I-123 iodide are without significant effect in the cells. Estimates of the mean lethal number of I-123 decays for the radiolabeled estrogen are in the same range as previous reports of the radiotoxicity of I-123 incorporated into DNA, consistent with the delivery of the I-123 attached to the estrogen in close proximity to DNA.

ACKNOWLEDGMENTS

This research was supported by the Illinois Division of the American Cancer Society (grant 89-45), the National Cancer Institute (CA 49906), Dow Chemical Co, and the Jules J. Reingold Fellowship Fund (to L Púy). We gratefully acknowledge the contribution of CHO-ER cells by G. L. Greene, University of Chicago.

REFERENCES

1. E.R. DESOMBRE, Steroid receptors in breast cancer. In *The Breast* (R.W. MCDIVITT, H.A. OBERMAN, L. OZZELLO, and N. KAUFMAN, Eds.) Williams and Wilkins, Baltimore, 1984, pp 149-184.
2. E.R. DESOMBRE, P.P. CARBONE, E.V. JENSEN, W.L. MCGUIRE, S.A. WELLS, Jr., J.L. WITTLIFF, and M.B. LIPSETT, Steroid receptors in breast cancer. *New Engl. J. Med.* **301**, 1011-1012 (1979).
3. E.R. DESOMBRE, J.A. HOLT, and A.L. HERBST, Steroid receptors in breast, uterine and ovarian malignancy and consideration of their diagnostic and therapeutic usefulness. In *Gynecologic Endocrinology*, 4th Edition (J.B. JOSIMOVICH and J. GOLD, Eds.) Plenum Press, New York, 1987, pp 511-528.
4. E. V. JENSEN, Steroid Hormone Receptors. In *Current Topics in Pathology, Vol 83 Cell Receptors*. (G. SIEFERT, Ed.) Springer-Verlag, Heidelberg, 1991, pp 365-431.
5. R. M. EVANS, The steroid and thyroid hormone receptor superfamily. *Science* **240**, 889-895 (1988).

6. D. A. LANNIGAN and A. C. NOTIDES, Estrogen regulation of transcription. In *Molecular Endocrinology and Steroid Hormone Action* (G. H. SATO and J. L. STEVENS, Eds.) Alan R. Liss, Inc., 1990, pp187-197.
7. R. CLARKE, M. E. LIPPMAN, and R. B. DICKSON, Mechanisms of hormone and cytotoxic drug interactions in the development and treatment of breast cancer. In *Molecular Endocrinology and Steroid Hormone Action* (G. H. SATO and J. L. STEVENS, Eds.) Alan R. Liss, Inc., 1990, pp 243-278.
8. A. I. KASSIS, S. J. ADELSTEIN, and W. D. BLOOMER, Therapeutic implications of Auger-emitting radionuclides. In *Radionuclides in Therapy*, (R. P. SPENCER, R. SEEVERS, and A. FRIEDMAN, Eds.) CRC Press, Boca Raton, FL, 1987, pp 119-134.
9. E.R. DeSOMBRE, P.V. HARPER, A. HUGHES, R.C. MEASE, S. J. GATLEY, O.T. DEJESUS, and J. L SCHWARTZ. Bromine-80m radiotoxicity: Potential for estrogen receptor-directed therapy with Auger electrons. *Cancer Res.* **48**, 5805-5809 (1988).
10. E.R. DeSOMBRE, R.C. MEASE, A. HUGHES, P.V. HARPER, O.T. DEJESUS, and A.M. FRIEDMAN. Bromine-80m-labeled estrogens: Auger-electron emitting, estrogen receptor-directed ligands with potential for therapy of estrogen receptor positive cancers. *Cancer Res.* **48**, 899-906 (1988).
11. A.I. KASSIS, S. J. ADELSTEIN, and W. D. BLOOMER. Therapeutic Implications of Auger-emitting Radionuclides, In *Radionuclides in Therapy* (R. P. SPENCER, R. SEEVERS, and A. FRIEDMAN, Eds.) CRC Press, Boca Raton, FL, 1987, pp 119-134.
12. D. A. BRONZERT, R. B. HOCHBERG, and M. E. LIPPMAN. Specific cytotoxicity of 16a-[^{125}I]iodo-estradiol for estrogen receptor-containing breast cancer cells. *Endocrinology* **110**, 2177-2179 (1982).
13. W. D. BLOOMER, W. H. MCCLAUGHLIN, R. R. WEICHSELBAUM, G. L. TONNESEN, S. HELLMAN, D. E. SEITZ, R. N. HANSON, S. J. ADELSTEIN, A. L. ROSNER, N. A. BURSTEIN, J. J. NOVE, and J. B. LITTLE, Iodine-125-labelled tamoxifen is differentially cytotoxic to cells containing oestrogen receptors. *Int. J. Radiat. Biol.* **38**, 197-202 (1980).
14. W. D. BLOOMER, W. H. MCLAUGHLIN, R. R. WEICHSELBAUM, R. N. HANSON, S. J. ADELSTEIN, and D. E. SEITZ, The role of subcellular localization in assessing the cytotoxicity of iodine-125 labeled iododeoxyuridine, iodotamoxifen and iodoantipyrine. *J. Radioanal. Chem.* **65**, 209-221 (1981).
15. W. H. MCLAUGHLIN, K. M. R. PILLAI, J. P. EDASERY, R. D. BLUMENTHAL, and W. D. BLOOMER, [^{125}I] Iodotamoxifen cytotoxicity in cultured human (MCF-7) breast cancer cells. *J. Steroid Biochem.* **33**, 515-519 (1989).
16. P. J. KUSHNER, E. HORT, J. SHINE, J. D. BAXTER, and G. L. GREENE, Construction of cell lines that express high levels of the human estrogen receptor and are killed by estrogens. *Mol. Endocrinol.* **4** ,1465-1473 (1990).
17. L. TORA, A. MULLICK, D. METZGER, M. PONGLIKITMONGKOL, I. PARK, and P. CHAMBON, The cloned human oestrogen receptor contains a mutation which alters its hormone binding properties. *EMBO J.* **8**, 1981-1986 (1989).
18. G. L. GREENE, Application of immunochemical techniques to the analysis of estrogen receptor structure and function. *Biochem. Actions Horm.* **11**, 207-239 (1984).
19. R. N. HANSON, D. E. SEITZ, and J. C. BOTTARO, E-17a-[^{125}I] Iodovinylestradiol: An estrogen receptor seeking radiopharmaceutical. *J. Nucl. Med.* **23**, 431-486 (1982).
20. E.R. DESOMBRE, S.M. THORPE, C. ROSE, R.M. BLOUGH, K.W. ANDERSEN, B.B. RASMUSSEN, and W.J. KING. Prognostic usefulness of estrogen receptor immunocytochemical assays (ER-ICA) for human breast cancer. *Cancer Res.* **46**, 4256-4264 (1986).
21. G. M. MAKRIGIORGOS, A. I. KASSIS, J. BARANOWSKA-KORTYLEWICZ, K. D. MCELVANY, M. J. WELCH, K. S. R. SASTRY and S. J. ADELSTEIN, Radiotoxicity of 5-[^{123}I]Iodo-2'-deoxyuridine in V79 Cells: A Comparison with 5-[^{125}I]Iodo-2'-deoxyuridine. *Radiat. Res.* **118**, 532-544 (1989).

22. S. SUNDELL-BERGMAN and K. J. JOHANSON, Impaired repair capacity of DNA strand breaks induced by ^{125}I-triiodothyronine in Chinese hamster cells. *Biochem. Biophys. Res. Commun.* **106**, 546-552 (1982).

DISCUSSION

Van den Abbeele, A. D. What is the stability of this compound *in vivo* or in plasma at 37°C?

DeSombre, E. R. The ^{123}I-VME2 does not bind to transport protein in the blood and is rapidly cleared from the body. However, the cleavage of the iodine carbon bond is not a major process as indicated by the relatively low thyroid uptake. This is likely due to the stability of the vinyl carbon-iodine bond.

Harapanhalli, R. S. In the radiolabeling method described by you "halodestannylation" do you see any *cis-trans* isomerizations?

DeSombre, E. R. The halodestannylation reaction is particularly advantageous because it occurs with complete retention of the steric configuration of the precursor tributyl compound. For our purposes, to prepare ligands with short half-life nuclides it is also convenient since it occurs rapidly, often complete in 10-15 min at room temperature.

Johanson, K. J. Have you studied whether the chromosomal damages appear at any specific sites of the chromosomes? What is the range of the number of estrogen receptors per cell in the human body?

DeSombre, E. R. 1) We are interested in studying specific damage of chromosomes as some estrogen regulated genes have been located on specific chromosomes. We have not yet been able to carry out these studies. 2) The numbers of estrogen receptors in breast cancers range from an average of possibly 500 per cell for a low ER positive tumor to more than 10,000 for an ER rich cancer.

Laster, B. H. Have you ever attempted your binding assays at 4°C?

DeSombre, E. R. Not yet.

Martin, R. In the case of the diphenyl compound, how stable is the vinyl iodide *in vivo*?

DeSombre, E. R. We do not have any detailed data on the effect of the somewhat bulky phenyl groups or the stability of the vinyl iodide *in vivo*. Our general impression is that the stability of the triphenyl vinyl iodide is not appreciably different than that of the steroidal vinyl iodides.

 Biophysical Aspects of Auger Processes, AAPM Symposium Series No. 8 (1992) 372-395
Eds. RW Howell, VR Narra, KSR Sastry, DV Rao

DIAGNOSTIC AND THERAPEUTIC APPLICATIONS OF AUGER ELECTRON EMITTING 5-[^{123}I/^{125}I]IODO-2'-DEOXYURIDINE IN CANCER

ANNICK D. VAN DEN ABBEELE,[1] JANINA BARANOWSKA-KORTYLEWICZ,[1] S. JAMES ADELSTEIN,[1] PAULO A. CARVALHO,[1] RONALD F. TUTRONE,[2] JEROME P. RICHIE,[2] PATRICK Y.C. WEN,[3] PETER McL. BLACK,[4] GIULIANO MARIANI,[5] and AMIN I. KASSIS[1]

Departments of [1]Radiology (Division of Nuclear Medicine), [2]Urology, [3]Neurology, [4]Neurosurgery, Harvard Medical School, Boston, MA 02115, USA,

[5]University of Pisa and CNR Institute of Clinical Physiology, Pisa, Italy

ABSTRACT

We have examined the diagnostic and therapeutic potential of the thymidine analog 5-iodo-2'-deoxyuridine (IUdR), radiolabeled with the Auger emitters ^{123}I and ^{125}I, in a variety of animal and human malignancies. The results indicate that intracerebral gliosarcoma in rats could be detected by scintigraphy after a single intratumoral injection of [^{123}I]IUdR and that [^{123}I/^{125}I]IUdR was specifically incorporated into tumor-cell DNA in high concentration and not into actively dividing epithelia of the normal tissues examined, or into bone marrow. We compared the intratumoral route of administration with the intraarterial injection of the radiopharmaceutical and demonstrated that only the intratumoral route achieved optimal target to background ratios. These data suggest that intratumoral administration of

this Auger-electron-emitting carrier may be useful for the diagnosis and treatment of human CNS malignancies, and a clinical trial is underway. In addition, the specificity of targeting of this radiopharmaceutical is being tested in patients with colon adenocarcinoma following direct intratumoral injection during colonoscopy. The results show that [^{125}I]IUdR can be safely administered in these patients and autoradiographic studies of the tumor after surgical resection indicate high tumor to nontumor ratios with [^{125}I]IUdR mainly incorporated into the DNA of tumor cell nuclei. Preliminary studies have also been carried out in animals bearing bladder cancer. Following the direct intravesical administration of [^{123}I/^{125}I]IUdR, highly favorable tumor to normal bladder ratios were demonstrated, and IUdR uptake in early neoplastic transformation of the bladder urothelium was observed. These data strongly suggest the potential for radiolabeled IUdR in the diagnosis and therapy of human tumors when direct intralesional or intracavitary administration of this radiopharmaceutical is feasible.

INTRODUCTION

Our continued interest in the potential diagnostic and therapeutic applications of Auger electron emitters has led us to examine the use of 5-iodo-2'-deoxyuridine (IUdR) radiolabeled with the Auger emitters ^{123}I and ^{125}I ([^{123}I/^{125}I]IUdR) in several animal and human malignancies including glial neoplasms (1), ovarian cancer (2-4), bladder cancer, and colon adenocarcinoma (5). This thymidine analog is specifically incorporated into DNA during the synthetic phase of the cell cycle (6,7) and during the repair of sublethal chromatin damage in the G_1 phase (8). Most of the DNA incorporated IUdR is retained for the life of the cell or its progeny (9-12). In contrast, the unincorporated IUdR is rapidly catabolized to iodouracil and/or dehalogenated (13,14) and its half-life in circulation is very short, less than five minutes in man and seven minutes in mice (11,13). Although this *in vivo* instability might appear to be a negative feature for any radiodiagnostic or radiotherapeutic agent, it may under certain circumstances (*i.e.* intralesional administration) prove to be a positive characteristic, since the rapid systemic degradation and subsequent elimination of the product would result in detoxification. Moreover, none of the major catabolic products are incorporated into nuclear DNA resulting, therefore, in minimal incorporation into the DNA of normal dividing cells distant from the administration site.

The radionuclides iodine-123 and iodine-125 are both prolific emitters of Auger electrons. While relatively innocuous when located outside the nucleus (15-17), they have considerable toxicity following intranuclear localization (12,15-22). They also have demonstrated therapeutic effectiveness *in vivo* in a murine ovarian tumor model following intracavitary administration (2-4). In addition, iodine-123 emits 159 keV γ rays that are favorable for external gamma camera imaging. Since unincorporated IUdR is rapidly catabolized and eliminated, the resulting background activity is low, an ideal situation for imaging purposes. Furthermore, the very high specific activity of this radionuclide (8,510 TBq/mmol (23,24)) will allow acquisition of images even if only a few molecules of IUdR become incorporated. Thus, the diagnostic potential of [^{123}I]IUdR in cancer can also be envisioned.

The rationale behind the potential use of radioiodinated IUdR in the diagnosis and therapy of cancer is based on the following arguments. Since neoplastic tissues are actively dividing, usually more so than normal tissues, the thymidine analog IUdR will become incorporated into these proliferating cells and, radiolabeled with an Auger emitter, it will also be lethal. Based on its short half-life in the circulation, the clinical application of radiolabeled IUdR in cancer requires tumors that are accessible to either intralesional, intracavitary or intraarterial administration in order to (i) bypass the rapid and extensive dehalogenation and degradation, (ii) maximize the uptake by the tumor and (iii) minimize the toxicity to normal dividing tissues.

To test these hypotheses, we selected two animal tumor models and one human malignancy in which site-directed administration of the radiopharmaceutical was feasible. One animal tumor model consisted of intracerebral gliosarcoma in rats in which either the direct intratumoral or the intraarterial route of administration was tested. This model has the additional advantage of consisting of a neoplasm surrounded by essentially nonproliferating tissue. We also examined the potential of radiolabeled IUdR in rats bearing a chemically-induced bladder cancer following the direct intravesical administration of the radiopharmaceutical. Finally, we tested the specificity of targeting and metabolic fate of [^{125}I]IUdR in patients with colon adenocarcinoma after direct intratumoral injection during colonoscopy.

MATERIALS AND METHODS

1. 5-[^{123}I/^{125}I]iodo-2'-deoxyuridine

No carrier added [^{123}I/^{125}I]IUdR was synthesized by a recently developed, single-step process using a mercuro-derivative of 2'-deoxyuridine (23,24). ^{123}I and ^{125}I were supplied by Nordion International Inc. (Vancouver, British Columbia, Canada) and Amersham (Arlington Heights, IL), respectively. The compound was purified on a C18 reverse phase HPLC column.

2. Animal Tumor Models

a. Rat brain tumor model: Exponentially growing, cultured 9L gliosarcoma cells (2×10^4 cells in 10 µl normal saline, [NS]) were injected intracranially (right caudate nucleus) into anesthetized Fisher 344 rats (three-week-old males) using a stereotactic apparatus, as previously described (1). Tumors 0.5 to 5 mm in diameter developed within 2 weeks. Control animals were sham-operated (10 µl of NS). Fifteen to 17 days following tumor or NS inoculation, a mixture of [^{123}I/^{125}I]IUdR was administered either intratumorally (i.t.) or intraarterially (i.a.) and the results obtained by these two routes of administration were compared. The drinking water of all animals was supplemented with potassium iodide (0.1% KI) 48 to 72 h prior to the administration of the radiopharmaceutical. Sixteen tumor-bearing and 8 control animals received a single intracranial injection (10 µl) of a mixture of 5.55 to 14.8 MBq [^{123}I]IUdR (150-400 µCi) and 0.56 to 1.48 MBq [^{125}I]IUdR (15-40 µCi) through the same hole and with the same coordinates used to introduce the tumor or NS inoculum (1). Another group of 4 tumor-bearing and 4 control rats were injected i.a. (100 µl) with a mixture of 14.8 MBq [^{123}I]IUdR (400 µCi) and 2.96 MBq [^{125}I]IUdR (80 µCi). The right common carotid artery (CCA) was accessed using the method described by Bullard *et al.* (25). Briefly, following exposure of the CCA, separation from the vagus nerve, and dissection towards the bifurcation, the external carotid artery was ligated in order to increase drug delivery to the ipsilateral cerebral hemisphere. Radiolabeled IUdR was then administered in a single bolus injection, the opening in the arterial wall closed with fast drying glue (Quick Gel from Duro™), and the wound closed with surgical clips.

b. Rat bladder tumor model: The carcinogen N-methyl-N-nitrosourea (MNU) known to induce transitional cell carcinoma of the bladder (26,27) was instilled directly into the bladder lumen of 4-to-5-week old female Fisher 344 rats (4 animals) via bladder catheterization using a 22-gauge angiocatheter (1.5 mg/0.15 ml saline intravesically, every other week for a total of 3 doses). The drinking water was supplemented with a combination of trimethoprim-sulfamethoxasole, neomycin sulfate and polymixin B formulated as described previously (28). Twelve weeks after the last MNU infusion, the bladder was catheterized and emptied and [^{123}I/^{125}I]IUdR (22.75 MBq [^{123}I]IUdR [615 μCi] and 2.07 MBq [^{125}I]IUdR [56 μCi]) was administered through the catheter in a 200 μl volume and left in place for 2 h. The bladder contents were then withdrawn and the bladder rinsed several times with normal saline (300 μl wash). Nontumor-bearing control rats (4 animals) were injected by the same route with identical amounts of [^{123}I/^{125}I]IUdR. The drinking water of all animals was supplemented with potassium iodide (0.1% KI) from 48 to 72 h prior to the administration of the radiopharmaceutical up to the time of sacrifice.

3. Human Studies

Following approval by the Committee for the Protection of Human Subjects in Research and after informed consent forms were signed, 9 patients with colon adenocarcinoma were injected intratumorally with [^{125}I]IUdR (7-8 MBq [190-216 μCi] in 0.5 ml NS) during endoscopy 24 to 72 h prior to ablative surgery. All patients were asked to take potassium iodide supplements (10 drops of saturated KI solution 3 times a day) for 10 days beginning 48 h prior to the injection of radiolabeled IUdR.

4. Scintigraphy

a. Rat brain tumor model: Planar scintigraphic images were obtained at 1, 14, 24 and 38 h postinjection of [^{123}I/^{125}I]IUdR (GE Starcam gamma camera equipped with a medium energy collimator, anterior views, 128 X 128 matrix, 10 min acquisition, 2.67 magnification). With the intraarterial injection, in addition to the planar images, single photon emission computed tomographic (SPECT) images were also acquired using the ASPECT (annular SPECT) camera (128 X 128 matrix, 120 projections with a 360° rotation of the collimators and 15 s data collection per projection [total acquisition time of 30 min], with coronal, sagittal and rotating three-dimensional displays calculated from reconstructed slices (29)).

b. Rat bladder tumor model: Planar scintigraphic images were obtained with a GE Camstar gamma camera at 2 to 5 h and 14 to 16 h postinjection of [^{123}I/^{125}I]IUdR (gamma camera equipped with a LEAP collimator, anterior views, 128 X 128 matrix, 10 min acquisition, 2.67 and 4.0 magnification). ASPECT images were also acquired as described above.

5. Biodistribution of Radiolabeled IUdR

These studies were conducted in order to quantitate the *in vivo* distribution of the radiopharmaceutical (percent injected dose per gram of tissue, %ID/g) and to derive the tumor to normal tissue ratios.

a. Animal tumor models: In the rat brain tumor model, blood samples were collected from the time of injection up to the time of sacrifice and clearance curves were derived. Following the last imaging session (36-43 h postinjection) the animals were sacrificed and various organs and tissues - tumor and/or right brain, left brain, frontal lobes, bladder, urine, kidney, skin, muscle, stomach, small intestine, large intestine, spleen, liver, heart, lung, right skull, left skull, femoral bone, and thyroid - were dissected, rinsed, blotted dry, weighed, and their radioactive content was determined in a gamma counter (Packard Auto-Gamma 500) along with that of stomach contents, blood, and bone marrow.

In the rat bladder tumor model, biodistribution of radiolabeled IUdR in tumor- and nontumor-bearing rats was determined 18 h after intravesical administration of the radiopharmaceutical. Various organs and tissues of interest - bladder, urine, kidney, uterus, ovaries, skin, muscle, stomach, stomach contents, small intestine, large intestine, spleen, liver, heart, lung, bone, bone marrow, blood and thyroid - were obtained, and processed as described above.

b. Human studies: Following the intratumoral injection of [^{125}I]IUdR, blood and urine samples were collected up to 72 h after injection, and clearance curves were derived. At the time of surgery (24-72 h postinjection), in addition to the tumor, biopsy samples of the following normal tissues were obtained, weighed and their radioactive content determined: colon (both within 1 cm and at 15 cm from the injection site, n=9), abdominal muscle (n=9), omentum (n=4), abdominal fat (n=4), lymph nodes (n=4), liver (n=2), gallbladder (n=2), bile (n=2), and iliac crest (n=1).

Urine samples (pooled from 0-24 h and 24-48 h; n=6) were filtered through 0.2 μm Millipore filters and analyzed on a C18 reverse phase HPLC column. Samples with high radioactivity content (usually the earlier time points) were injected directly on the column after filtration since a small volume (approximately 50 μl) attained the limits of detection. For samples with less radioactivity, the following procedure was applied: filtered urine samples were extracted with a chloroform/tetrahydrofuran (5/1) mixture (4 X 1 ml/ml urine) to remove any IUdR and metabolites soluble in organic solvents. Aliquots from organic and aqueous layers were counted in a gamma counter to follow the distribution of radioactivity. The organic layer was evaporated under a stream of N_2 to a volume of about 100 μl and analyzed on a C18 column. The aqueous layer was treated with chloramine-T (0.1 mg/ml urine) and extracted with methyl ethyl ketone or chloroform (4 X 0.5 ml) to collect oxidized ^{125}I. Aliquots of each fraction were counted. This second organic layer was treated with 10 μl (10 mg/ml) aqueous sodium metabisulfite solution, evaporated to about 100 μl and analyzed.

Plasma samples (1 h, 2 h, 3 h; n=6) were treated in a similar manner. To samples with a high radioactivity content (usually earlier time points postinjection), an equal volume of ethanol was added to precipitate proteins (10 min on ice). Samples were centrifuged at 6000 rpm for 20 min, supernatant aliquots and pellets were counted, and approximately 100 μl of supernatant was injected on the C18 column. In samples with low radioactivity, proteins were precipitated with an equal volume of 20% TCA on ice (20 min), centrifuged as above, and counted. The supernatants were neutralized with either solid $NaHCO_3$ or its saturated solution and then treated as the urine samples described above. HPLC fractions were counted to determine ratios of degradation products. Each sample and each fraction were also run on silica TLC plates using dichloromethane/tetrahydrofuran (4/1) as solvent.

6. Autoradiography

The actual specificity of targeting and the microdistribution of DNA-incorporated [$^{123}I/^{125}I$]IUdR were determined by microautoradiography. The distribution and frequency of grains were assessed over the entire section and compared to the histopathological findings. As a result of the short range of the emitted electrons, the autoradiographic resolution of Auger-electron-emitting isotopes within thin-tissue sections is excellent.

a. Rat brain tumor: At the time of the biodistribution studies, the following tissues were quickly frozen in isopentane and liquid nitrogen: brain, tongue, skin, muscle, esophagus, small intestine, large intestine, spleen, liver, kidney, heart, lung, bladder, stomach, testes, eyes, and lymph node. Bone marrow smears were also obtained. Tissues were sectioned (6 μm sections), transferred onto glass slides and fixed with methanol (-20°C, brain sections; room temperature, bone marrow smears) or Bouin's solution (room temperature, all other tissues). The sections fixed in Bouin's solution were rinsed in ethanol (50% and 70%) and allowed to dry. The tissue sections and bone marrow slides were then coated with NTB2 emulsion (Kodak) and stored desiccated at 4°C in light-tight boxes. After various times of emulsion exposure (up to 7 months), the autoradiographic slides were developed for 3 min in D-19 developer (Kodak) and fixed for 5 min in D-11 fixer (Kodak). Finally, the tissue sections were washed in distilled water, stained with hematoxylin/eosin, dehydrated, cleared, and mounted in Permount. Bone marrow slides were stained with Giemsa stain. Tissue and bone marrow slides were then examined under light microscopy.

b. Rat bladder tumor: After rinsing the bladder with NS, 300 μl of 10% buffered formaldehyde was injected into the bladder and a suture was placed at the neck of the organ. The bladder was excised and placed in a vial containing 10% buffered formalin and subsequently embedded in paraffin. The bladder and the frozen tissues obtained from the biodistribution studies (skin, stomach, small and large intestine, kidney, ureters, uterus and ovaries) were then sectioned (5-7 μm thickness), fixed (except for the bladder sections already fixed *in vivo*) and processed as described above as were the bone marrow smears obtained in these animals.

c. Human studies: To determine the specificity of targeting of [^{125}I]IUdR, microautoradiography was performed at 1 and 2 h postinjection on blood smears and at the time of surgery on semi-thin tissue sections of the tumor and the following normal tissues: colonic mucosa, liver, lymph nodes, fat, and abdominal wall.

RESULTS

1. The Radiopharmaceutical

The radiochemical purity of the product was greater than 99% as determined by TLC and reverse phase HPLC. The specific activities for [^{123}I]IUdR and [^{125}I]IUdR were 8,510 and 81.4 TBq/mmol, respectively. Since the syntheses were carried out under no-carrier-added conditions, *i.e.* without the addition of Na^{127}I, the resulting specific activities are expected to be identical to those of ^{123}I and ^{125}I, respectively.

2. Rat Brain Tumor

a. Intratumoral injection: Scintigraphy was performed 1 to 38 h after [^{123}I]IUdR injection. In the nontumor-bearing rats, activity seen over the brain at 1 h had cleared by 14 h and was not seen at 24 h or 38 h (Fig. 1A). Other areas of intense activity appeared over the stomach and the bladder suggesting excretion of free iodine. Because the drinking water was supplemented with KI, there was no activity in the thyroid. The images obtained in tumor-bearing animals also showed activity in the brain at 1 h; however, as opposed to the controls, activity remained localized in a specific area of the brain in all the tumor-bearing rats at 14 h and at later time points (Fig. 1B). Tumors as small as 0.5 mm in diameter (measured at the time of dissection) were visualized.

The blood clearance curves demonstrated a rapid decrease of ^{123}I activity in both tumor-bearing and control animals with a $T_{1/2}$ of 7 h. As reported previously (1), the biodistribution data indicated that $0.36 \pm 0.14\%$ of the injected dose per gram was seen in the right brain compared to $0.09 \pm 0.015\%$ in the control animals. In some experiments, the tumors were invisible macroscopically and a large proportion of the weighed tumor sample was in fact normal brain tissue. Therefore this %ID/g underestimated the actual tumor uptake. The activity in all other organs and normal tissues was low, as suggested by the scintigraphic studies, with the exception of the bladder, urine, stomach and stomach contents, a reflection of the metabolism of IUdR. The tumor to normal tissue ratios derived from this typical experiment ranged from 8 to 190.

The autoradiographic studies demonstrated that all tumor-bearing animals had significant uptake of radiolabeled IUdR in the tumor bed but not in the surrounding normal brain (Fig. 2A); the brain sections of sham-operated control animals were free of silver grains. Only at late time points (> 5 month exposure) did we observe the presence of silver grains in one or two cuboidal epithelial cells lining the ventricular system (results not shown) of injected animals. Autoradiography of normal tissue sections did not show the presence of silver grains associated with actively dividing normal epithelia such as skin, tongue, small and large intestine. Of particular interest for therapeutic purposes, bone marrow smears were also free of cell-associated silver grains (Fig. 2B).

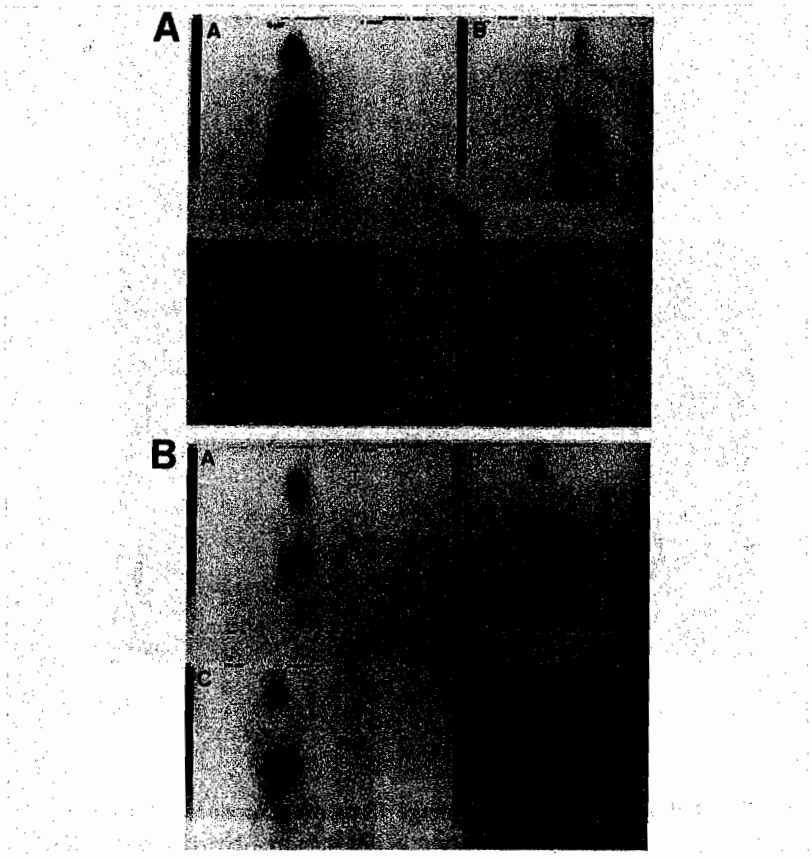

FIG. 1. Scintigraphic images obtained in **(A)** nontumor-bearing rat (sham-operated control) and **(B)** rat bearing 9L gliosarcoma intracranially, 1 h (A), 14 h (B), 24 h (C), and 38 h (D) following intratumoral injection of [^{123}I/^{125}I]IUdR. T, tumor; S, stomach; B, bladder.

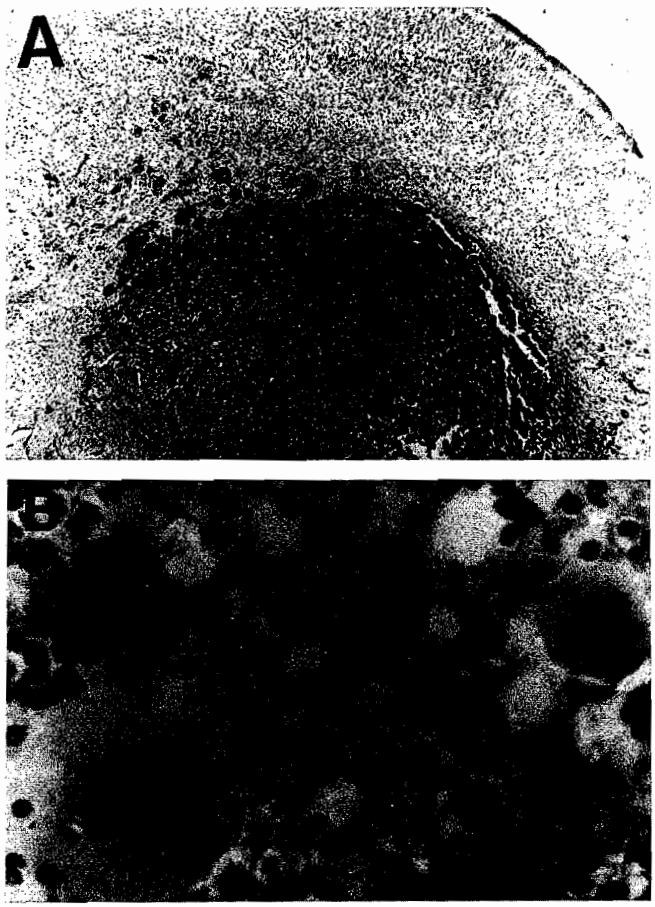

FIG. 2. (A) Autoradiographic image (5 month exposure) of thin (5-6 μm) section obtained from brain of gliosarcoma-bearing rat (X 30) following single intratumoral administration of [^{123}I/^{125}I]IUdR. **(B)** Autoradiographic image of bone marrow smear (X 600, 5 month exposure) of rat following single intratumoral administration of [^{123}I/^{125}I]IUdR.

b. Intraarterial injection: The intracerebral tumors in this group were large (> 0.5 cm), and these animals had signs of increased intracranial pressure, including lethargy and emesis. This circumstance may have compromised the distribution of the radiopharmaceutical and should be considered when interpreting the data.

The results of the imaging studies were similar in the control and experimental groups: (i) areas of intense activity included the right portion of the neck (*i.e.* the injection site), the nose/mouth area, the stomach and the bladder, and (ii) no specific uptake was observed in the brain.

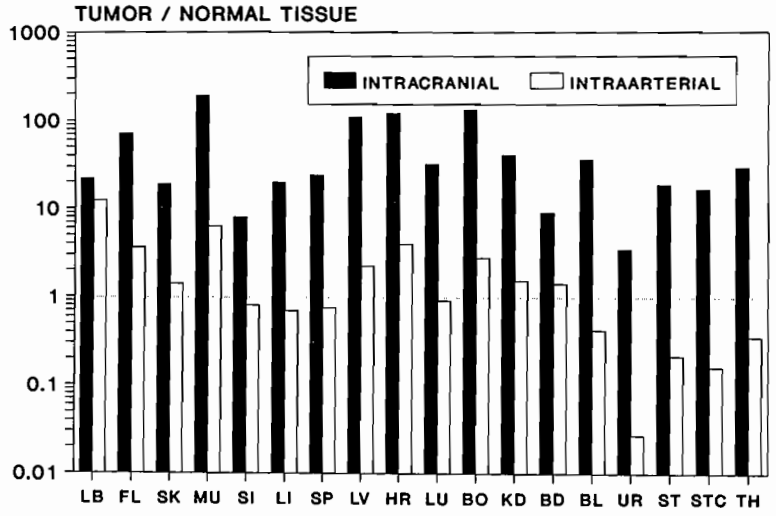

FIG. 3. Tumor to normal tissue ratios obtained from animals bearing intracerebral tumors and injected either intratumorally (closed bars) or intraarterially (open bars) with [^{123}I/^{125}I]IUdR approximately 40 h earlier. LB, left brain (uninjected side); FL, frontal lobes; SK, skin; MU, muscle; SI, small intestine; LI, large intestine; SP, spleen; LV, liver; HR, heart; LU, lung; BO, bone; KD, kidney; BD, blood; BL, bladder; UR, urine; ST, stomach; STC, stomach contents; TH, thyroid.

The biodistribution data indicated that 0.19 ± 0.19% of the %ID/g was seen in the right brain of the tumor-bearing animals compared to 0.0016 ± 0.0004 %ID/g in the sham-operated animals. The activity in all the normal organs or tissues was higher in the experimental group compared to the control and higher than the activity observed in the tissues of animals injected via the intracerebral route. This resulted in target to normal tissue ratios that were less favorable compared with the direct intracerebral injection (Fig. 3), ranging from 0.03 (urine) to 12 (left brain) for the intraarterial injection and 3.4 (urine) to 190 (muscle) for the intracerebral injection. In sharp contrast with what was observed following direct intracranial injection, microautoradiographic studies performed after intraarterial injection did not demonstrate any specificity of uptake by the intracerebral tumor. Furthermore, after intraarterial administration, uptake by normal dividing epithelia was observed in the skin, the tongue, the small and large intestine and the eye.

3. Rat Bladder Tumor

The scintigraphic images performed within 16 h following intravesical administration of the radiopharmaceutical were inconclusive because activity was observed in the bladder region in both tumor-bearing and control animals. This was most likely related to the presence of free iodine and other radiolabeled catabolites in the urine, which is a reflection of the metabolism of radiolabeled IUdR at these early time points after administration. The tumor-bearing animals retained a higher amount of radioactivity compared with the control animals, *i.e.* the systemic distribution of activity was higher in the experimental group.

The biodistribution data indicated, however, a significant difference ($p < 0.05$) in the percent injected dose per gram in the bladder of tumor-bearing animals compared to the control group (0.06 ± 0.03 %ID/g versus 0.0006 ± 0.0004 %ID/g, respectively). As suggested by the imaging studies, the overall distribution of activity among the normal tissues was higher in the tumor-bearing group compared with the control group as reflected by the following values (%ID/g) in various tissues such as blood (0.068 ± 0.044 versus 0.013 ± 0.011), liver (0.035 ± 0.029 versus 0.005 ± 0.005), spleen (0.042 ± 0.035 versus 0.006 ± 0.005), kidney (0.073 ± 0.039 versus 0.008 ± 0.008), small intestine (0.025 ± 0.01 versus 0.004 ± 0.003), and muscle (0.01 ± 0.007 versus 0.002 ± 0.002). At the time of the biodistribution studies it was noted that all the tumor-bearing animals had evidence of bilateral hydronephrosis

(with wide communication between the bladder and the ureters), urinary infection, and lithiasis. These complications, which seldom occur in bladder cancer patients, most probably contributed to the systemic distribution of the radiopharmaceutical. In the control group most of the intravesical inoculum remained within the bladder and permeation to the systemic circulation was very low, limited to normal diffusion (mediated by broad-specificity facilitated-diffusion nucleoside transporters (30)) and/or possible minimal trauma to the bladder wall secondary to the catheterization procedure. In order to obtain a better assessment of the expectations in humans where the delivery of the radiopharmaceutical would be well controlled and confined to the bladder, we expressed the target to nontarget ratios as the quotient of the activity observed in the bladder of the tumor-bearing animals to that of the normal tissues of the control animals (Fig. 4). These ratios are all above 1 ranging from 1.21 (stomach) to 91 (normal bladder) except for the urine and the stomach contents which are the sites of excretion of free iodine.

The autoradiographic studies confirmed the presence of infection/inflammation as well as stones in all the tumor-bearing animals. All animals had low grade papillary tumors with hyperplasia (stage Ta (31)) but no carcinoma *in situ* or squamous metaplasia or invasion. However, even at this early stage of tumor development, the autoradiographic studies demonstrated IUdR uptake in the areas of hyperplasia. Radiopharmaceutical uptake was also observed in normal inflammatory cells in the stroma (results not shown).

4. Human Studies

An average of $0.12 \pm 0.12\%$ of the injected dose was present per gram of tumor (range 0.02-0.38). The approximate amount of [^{125}I]IUdR effectively injected within the tumor was estimated by collecting and measuring the activity contained in the washing fluid used during the colonoscopy. Based on these measurements, the approximate injected dose ranged from 0.4 MBq to 7.4 MBq (11-200 μCi). The tumor to normal tissue (colon [within 1 cm and 15 cm from the tumor site], omentum, abdominal muscle, abdominal fat, liver, gallbladder, bile, lymph nodes, and iliac crest) ratios were very high (mean 873, range 122-2391). Microautoradiography confirmed these high tumor to nontumor ratios and localization of the IUdR mainly in the tumor cell nuclei (Fig. 5). No cell associated activity was observed in the blood smears.

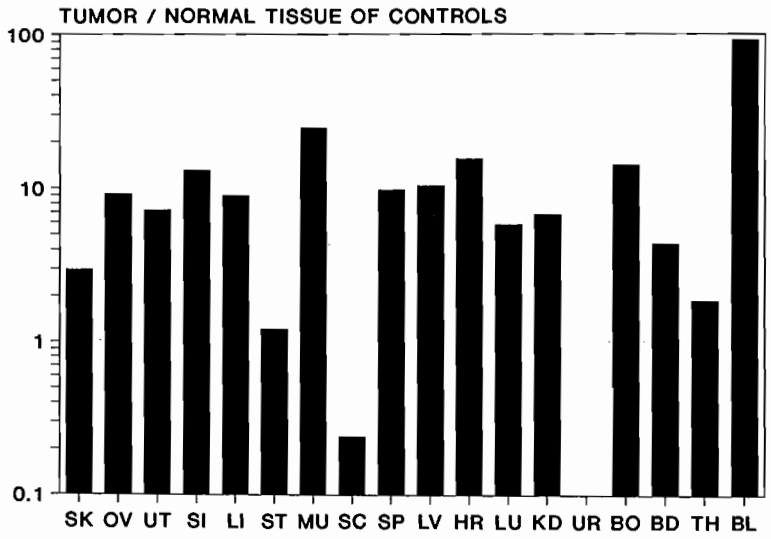

FIG. 4. Tumor to normal tissue ratios obtained from rats bearing bladder tumor and control animals. Results were expressed as the quotient of radioactivity associated with bladder of tumor-bearing animals divided by that associated with normal tissues of control animals. [^{123}I/^{125}I]IUdR had been administered 18 h earlier intravesically in all animals. SK, skin; OV, ovaries; UT, uterus; SI, small intestine; LI, large intestine; ST, stomach; MU, muscle; SC, stomach contents; SP, spleen; LV, liver; KD, kidney; UR, urine; BO, bone; BD, blood; TH, thyroid; BL, bladder.

Neither urine nor plasma samples had any radioactivity associated with the material retained on the filter or the protein precipitate, respectively. Most of the radioactivity injected was present in the urine. The 0-24 h pooled urine collection showed that on average $89 \pm 9.9\%$ was either $^{125}I^-$ or its oxidized form and $8.9 \pm 8.8\%$ was undegraded [^{125}I]IUdR (n=6). In 2 patients, 10.5% and 2.2% of the total activity was found associated with unknown species. In the 24-48 h pooled urine, 100% of the radioactivity was in the form of iodide. Activity in plasma peaked at 1 to 2 h following [^{125}I]IUdR injection and then decreased with a $T_{1/2}$ of 8 h. HPLC analysis indicated that at 1 to 2 h greater than 99.9% of the radioactivity was free iodide. After 3 h, $94.7 \pm 6.7\%$ was $^{125}I^-$ (range 82-100%) and $5.3 \pm 6.7\%$ (range 0-18%) was ^{125}IUdR (n=6).

FIG. 5. Autoradiographic image of thin (5-6 μm) section obtained at surgery from colon of patient with colon adenocarcinoma (300X : 30 d exposure) following single direct intratumoral injection of [^{125}I]IUdR 24 h earlier.

DISCUSSION

5-Iodo-2'-deoxyuridine is a thymidine (TdR) analog in which the 5-methyl group of TdR is replaced by iodine. The van der Waals radius of the 5-methyl group of thymidine is 2.0 Å, while that of the iodine atom is 2.15 Å. This similarity gives a compound that behaves remarkably like TdR (6,7,10,12), resulting in its efficient incorporation into the DNA of dividing cells with a thymidine replacement that can be as high as 50% (32). This substitution occurs only during the DNA synthetic (S) phase of the cell cycle (6,7) and during DNA repair of sublethal chromatin damage (G_1 phase) (8). Since at any particular time a certain fraction of the cells within a tumor undergo DNA synthesis, IUdR will be incorporated, and it could, therefore, become a suitable carrier of diagnostic and/or therapeutic radionuclides for

certain types of cancer. In the case of primary brain tumors, for example, high target to background ratios can be expected for this cell-cycle-phase-dependent agent since these tumors arise within a tissue that is essentially nondividing. This was confirmed in our previous studies when we demonstrated that brain tumors in rats could be visualized following direct intratumoral administration of [^{123}I]IUdR with high sensitivity (all tumors were visualized) and high specificity (uptake was observed in tumor tissue only) even when the tumors were invisible macroscopically (< 0.5 mm) (1). [^{123}I]IUdR with its high specific activity (8,510 TBq/mmol) and its favorable imaging characteristics (159 keV γ rays) could therefore become a useful agent for the diagnosis of residual or progressive tumor and could allow differential diagnosis between active tumor and scar, necrosis and edema. Our research effort is now being extended to a clinical trial in patients with primary brain tumors.

Our studies also emphasize the importance of the route of administration. Bagshawe and co-workers reported mixed results following the intravenous injection of radioiodinated IUdR in patients with various tumors (33-35). These observations can be explained by the well-known, rapid systemic degradation and short half-life in circulation of radiolabeled IUdR (13,14). In addition, nonselective uptake of IUdR into normal dividing cells precluded its effective use as a systemic agent and required the concomitant administration of drugs such as hydroxyurea and 5-fluorouracil in an attempt to improve selective uptake by tumor cells (36). The rationale for optimal delivery of this radiopharmaceutical rests, therefore, on intratumoral, intraarterial or intracavitary administration. These routes can potentially (i) lead to higher concentration of the radiopharmaceutical in the tumor while minimizing systemic distribution of the compound, (ii) bypass the main site of metabolism, *i.e.* the liver, (iii) limit the dilution factor resulting from delivery of the agent into the circulation and permit the delivery of more radioactive IUdR directly to the target, and (iv) allow delivery of a dose at the target that could otherwise be attained only if potentially toxic amounts of the radiopharmaceutical were administered systemically. In view of this, we compared direct intralesional administration of the radiopharmaceutical with intraarterial injection in rats bearing intracerebral gliosarcoma tumors. The data showed clearly that, within the limitations of our tumor model, the intraarterial injection did not meet our goals and led to uptake by the dividing epithelia of normal tissues without specific tumor targeting. Only the intralesional route of administration achieved specific cerebral tumor targeting with minimal normal tissue uptake, *i.e.* optimal target to nontarget

ratios. This is essential with cell-cycle-phase selective drugs not only for imaging purposes but also for therapeutic applications, since normal tissues containing proliferating cells, such as the bone marrow or intestinal mucosa, are frequently dose-limiting in cancer therapy. The *in vivo* instability of radiolabeled IUdR in the systemic circulation with its rapid dehalogenation becomes in this case a distinct advantage, since the direct intralesional administration of the radiopharmaceutical should allow high levels of intact radiolabeled IUdR to reach tumor cells while its short biologic half-life in circulation should limit its incorporation into the DNA of proliferating normal tissues. In addition, IUdR being a low molecular weight compound (MW=354.1), it will diffuse freely throughout the tissue. Since there are no reports of antibody response against this small molecule, it will lend itself to repeated injections.

Our results also indicate the feasibility of scintigraphic visualization of bladder tumors in humans following intravesical administration of [^{123}I]IUdR since (i) our autoradiographic studies have demonstrated uptake at an early stage of tumor development, *i.e.* the hyperplasia/dysplasia stage, (ii) IUdR-incorporated activity should remain associated with the tissue, (iii) unincorporated activity, *i.e.* free iodine or other radiolabeled metabolites in the urine, can be removed by voiding or catheterization and the bladder washed prior to imaging, and (iv) IUdR can also be radiolabeled with ^{131}I, an isotope with a longer half-life than ^{123}I (8 days versus 13.2 h), allowing imaging at a later time point, *i.e.* after the metabolism of IUdR has occurred and the radiolabeled metabolites have been excreted. Experimental [^{131}I]IUdR studies in animals are underway to test this hypothesis. Furthermore, intravesical administration of radiolabeled IUdR in patients with bladder cancer would permit not only direct delivery to the target but also a well controlled delivery system for diagnosis and/or therapy in which (i) tumor cells can be exposed for appropriate time intervals to precise concentrations of radiolabeled IUdR, a situation which is particularly desirable since IUdR uptake is proportional to the exposure period as well as to its extracellular concentration (12,22), and (ii) the possibility of removal of unincorporated IUdR will limit the radiation dose to the patient.

In addition to its scintigraphic potential for the diagnosis of active tumor, IUdR radiolabeled with the Auger electron emitters ^{125}I and ^{123}I has been shown to be highly toxic to various normal and tumor mammalian cell lines *in vitro* (12,15-17,21,22) and has demonstrated therapeutic effects following intraperitoneal injection into mice bearing an ascites tumor of

ovarian origin (2-4). Following the incubation of radiolabeled IUdR with cultured mammalian cells and the intranuclear localization of the radiopharmaceutical, there is an exponential reduction in cell survival with no shoulder on the survival curves, a high relative biological effectiveness (RBE) value of 7 (37), an oxygen enhancement ratio (OER) of 1.4 (21) (significantly smaller than the OER of 3 for X ray exposure), and the production of double strand breaks (38-40). In contrast, the decay of ^{125}I extranuclearly, for example within the cell cytoplasm (15,17,37), affixed to cell plasma membranes (16), or extracellularly (12,17,37) produces no extraordinary lethal effects and these survival curves resemble those observed with X rays, *i.e.* they have a distinct shoulder, shallower slopes, and a low RBE (< 2). Our experience, and that of others, with this and several other Auger electron emitters have reiterated the dependence of Auger-electron-emitting toxicity on the intranuclear DNA localization of the radionuclide (37,41). The radiotherapeutic effectiveness of [^{123}I]IUdR and [^{125}I]IUdR has been demonstrated *in vivo* in an experimental murine ascites tumor model of ovarian origin following intraperitoneal injection. In this instance the intracavitary administration of both radiopharmaceuticals led to rapid uptake by ascites tumor cells but not by normal cells and resulted in significant tumorcidal effect (2-4,42). Furthermore, when radioiodinated IUdR was given in fractionated doses synchronized to the cell cycle of these tumor cells, increases in median survival time were observed as well as some cures (2-4,42). These findings suggest that IUdR radiolabeled with Auger electron emitters may be an efficient therapeutic agent for the treatment of cancers, such as brain and bladder tumors, that are accessible to the direct intralesional or intracavitary delivery of the radiopharmaceutical.

Because of (i) the very short range of the electrons produced (nanometer dimensions) during the decay of these isotopes, (ii) their critical dependence on intranuclear localization for toxic effects, and (iii) the heterogeneous distribution of the radiopharmaceutical within the tissue of interest, classical dosimetry based on the MIRD schema and the ICRU procedures greatly underestimates the actual energy deposited in these cells (37,43-45). Studies are therefore currently being conducted in tumor-bearing animals following the intratumoral injection of the radiopharmaceutical to derive dosimetric estimates at the cellular level in order to define the tumoricidal and optimal therapeutic dose. In order to be therapeutically effective, this Auger-electron-emitting carrier must not only specifically target tumor cells in sufficient concentration to achieve tumoricidal dose, but must also target the entire tumor cell population. Because of its cell-cycle

dependency, this goal may only be attained by appropriate dose fractionation or continuous infusion in order to label all cells as they pass through the S phase of DNA synthesis. This requires knowledge of the intrinsic anatomical and biological characteristics (including cell population kinetics) of tumors in humans. Finally, since such an agent would allow a better understanding of tumor cell biology in individual patients, it might also play a major role in predicting and following response to therapy and thereby become an integral part of the decision-making process in the diagnosis and therapy of a variety of human cancers.

CONCLUSION

Animal and human studies have shown that the direct intratumoral or intracavitary administration of radiolabeled IUdR leads to specific incorporation of the Auger electron emitters ^{123}I and ^{125}I into the DNA of dividing tumor cells and high target to nontarget ratios. [^{123}I/^{125}I]IUdR may therefore allow differential diagnosis between active tumor and scar, necrosis and edema. In addition, being selective for proliferating cells, this radiopharmaceutical may promote a better understanding of the intrinsic characteristics of the tumor and define its degree of aggressiveness as well as its response to various therapeutic modalities. Finally, since [^{123}I]IUdR and [^{125}I]IUdR have strong antineoplastic potential, they could become an integral part of the therapeutic regimen of many human cancers that are accessible to direct intralesional or intracavitary administration.

ACKNOWLEDGMENTS

This work was supported by USPHS grant RO1 CA 15523-16. The authors gratefully acknowledge the valuable technical assistance of Ms. R. A. Aaronson and Mr. R. M. Berman.

REFERENCES

1. A.I. KASSIS, A.D. VAN DEN ABBEELE, P.Y.C. WEN, J. BARANOWSKA-KORTYLEWICZ, R.A. AARONSON, W.C. DeSISTO, L.A. LAMPSON, P. McL. BLACK, and S.J. ADELSTEIN, Specific uptake of the Auger electron-emitting thymidine analogue 5-[^{123}I/^{125}I]iodo-2'-deoxyuridine in rat brain tumors: Diagnostic and therapeutic implications in humans. *Cancer Res.* **50**, 5199-5203 (1990).

2. W.D. BLOOMER and S.J. ADELSTEIN, Antineoplastic effect of iodine-125-labelled iododeoxyuridine. *Int. J. Radiat. Biol.* **27**, 509-511 (1975).
3. W.D. BLOOMER and S.J. ADELSTEIN, 5-^{125}I-iododeoxyuridine as prototype for radionuclide therapy with Auger emitters. *Nature* **265**, 620-621 (1977).
4. J. BARANOWSKA-KORTYLEWICZ, G.M. MAKRIGIORGOS, A.D. VAN DEN ABBEELE, R.M. BERMAN, S.J. ADELSTEIN, and A.I. KASSIS, 5-[^{123}I]iodo-2'-deoxyuridine in the radiotherapy of an early ascites tumor model. *Int. J. Radiat. Oncol. Biol. Phys.* **21**, 1541-1551 (1992).
5. G. MARIANI, A. GUADAGNI, A. CEI, A.D. VAN DEN ABBEELE, G. BEVILACQUA, P. SALVADORI, R. DISTEFANO, J. BARANOWSKA-KORTYLEWICZ, S.J. ADELSTEIN, F. MOSCA, and A.I. KASSIS, Fate of 5-[I-125]iodo-2'deoxyuridine injected intratumorally in patients with colon cancer. *J. Nucl. Med.* **32**, 1082-1083 (1991) (abstract).
6. M.L. EIDINOFF, L. CHEONG, and M.A. RICH, Incorporation of unnatural pyrimidine bases into deoxyribonucleic acid of mammalian cells. *Science* **129**, 1550-1551 (1959).
7. N.R. MORRIS and J.W. CRAMER, DNA synthesis by mammalian cells inhibited in culture by 5-iodo-2'-deoxyuridine. *Mol. Pharmacol.* **2**, 1-9 (1966).
8. G. ILIAKIS and M. NUSSE, Evidence that repair and expression of potentially lethal damage cause the variations in cell survival after X irradiation observed through the cell cycle in Ehrlich ascites tumor cells. *Radiat. Res.* **95**, 87-107 (1983).
9. P. CALABRESI, S.S. CARDOSO, S.C. FINCH, M.M. KLIGERMAN, C.F. VON ESSEN, M.Y. CHU, and A.D. WELCH, Initial clinical studies with 5-iodo-2'-deoxyuridine. *Cancer Res.* **21**, 550-559 (1961).
10. W.L. HUGHES, S.L. COMMERFORD, D. GITLIN, R.C. KREUGER, B. SCHULTZE, V. SHAH, and P. REILLY, Deoxyribonucleic acid metabolism in vivo. I. Cell proliferation and death as measured by incorporation and elimination of iododeoxyuridine. *Fed. Proc.* **23**, 640-648 (1964).
11. S.L. COMMERFORD, Biological stability of IUdR labeled with ^{125}I after incorporation into the DNA of the mouse. *Nature* (London) **206**, 949-950 (1965).
12. A.I. KASSIS, K.S.R. SASTRY, and S.J. ADELSTEIN, Kinetics of uptake, retention, and radiotoxicity of ^{125}IUdR in mammalian cells: Implications of localized energy deposition by Auger processes. *Radiat. Res.* **109**, 78-89 (1987).
13. W.H. PRUSOFF, A review of some aspects of 5-^{125}I-iododeoxyuridine and azauridine. *Cancer Res.* **23**, 1246-1259 (1963).
14. R.W. KLECHER, Jr, J.F. JENKINS, T.J. KINSELLA, R.L. FINE, J.M. STRONG, and J.M. COLLINS, Clinical pharmacology of 5-iodo-2'-deoxyuridine and 5-iodouracil and endogenous pyrimidine modulation. *Clin. Pharmacol. Ther.* **38**, 45-51 (1985).
15. K.G. HOFER, C.R. HARRIS, and J.M. SMITH, Radiotoxicity of intracellular ^{67}Ga, ^{125}I and ^{3}H: Nuclear versus cytoplasmic radiation effects in murine L1210 leukaemia. *Int. J. Radiat. Biol.* **28**, 225-241 (1975).
16. R.L. WARTERS, K.G. HOFER, C.R. HARRIS, and J.M. SMITH, Radionuclide toxicity in cultured mammalian cells: Elucidation of the primary site of radiation damage. *Curr. Top. Radiat. Res. Q.* **12**, 389-407 (1977).
17. A.I. KASSIS, F. FAYAD, B.M. KINSEY, K.S.R. SASTRY, R.A. TAUBE, and S.J. ADELSTEIN, Radiotoxicity of ^{125}I in mammalian cells. *Radiat. Res.* **111**, 305-318 (1987).

18. K.G. HOFER and W.L. HUGHES, Radiotoxicity of intracellular tritium, ^{125}iodine and ^{131}iodine. *Radiat. Res.* **47**, 94-104 (1971).
19. D.D. PORTEOUS, The toxicity of ^{125}IUdR in cultured mouse BP8 tumor cells. *Br. J. Cancer* **25**, 594-597 (1971).
20. E.W. BRADLEY, P.C. CHAN, and S.J. ADELSTEIN, The radiotoxicity of iodine-125 in mammalian cells. I. Effects on the survival curve of radioiodine incorporated into DNA. *Radiat. Res.* **64**, 555-563 (1975).
21. P.C. CHAN, E. LISCO, H. LISCO, and S.J. ADELSTEIN, The radiotoxicity of iodine-125 in mammalian cells. II. A comparative study on cell survival and cytogenic responses to ^{125}IUdR, ^{131}IUdR and ^{3}HTdR. *Radiat. Res.* **67**, 332-343 (1976).
22. G.M. MAKRIGIORGOS, A.I. KASSIS, J. BARANOWSKA-KORTYLEWICZ, K.D. McELVANY, M.J. WELCH, K.S.R. SASTRY, and S.J. ADELSTEIN, Radiotoxicity of 5-[^{123}I]iodo-2'-deoxyuridine in V79 cells: A comparison with 5-[^{125}I]iodo-2'-deoxyuridine. *Radiat. Res.* **118**, 532-544 (1989).
23. J. BARANOWSKA-KORTYLEWICZ, B.M. KINSEY, W.W. LAYNE, and A.I. KASSIS, Radioiododemercuration: A simple synthesis of 5-[$^{123/125/127}$I]iodo-2'-deoxyuridine. *Appl. Radiat. Isot.* **39**, 335-341 (1988).
24. A.I. KASSIS and J. BARANOWSKA-KORTYLEWICZ, Method for making radioiodinated pyrimidine nucleosides or nucleotides. *U.S. Patent* **#4,851,520**, issued 1989; European Patent Pending.
25. D.E. BULLARD, S.C. SARIS, and D.D. BIGNER, Carotid artery injection in 40- to 99-g Fischer rats: Technical note and evaluation of blood flow by various injection techniques. *Neurosurgery* **14**, 406-411 (1984).
26. R.M. HICKS and J.S.J. WAKEFIELD, Rapid induction of bladder cancer in rats with N-methyl-N-nitrosourea. *Chem. Biol. Interact.* **5**, 139 (1972).
27. G.D. STEINBERG, C.B. BRENDLER, T. ICHIKAWA, R.A. SQUIRE, and J.T. ISAACS, Characterization of an N-methyl-N- nitrosourea-induced autochthonous rat bladder cancer model. *Cancer Res.* **50**, 6668-6674 (1990).
28. J.M. HENRY and J.T. ISAACS, Relationship between tumor size and the curability of metastatic prostatic cancer by surgery alone or in combination with adjuvant chemotherapy. *J. Urol.* **139**, 1119-1123 (1988).
29. B.L. HOLMAN, P.A. CARVALHO, R.E. ZIMMERMAN, K.A. JOHNSON, S.S. TUMEH, A.P. SMITH, and S. GENNA, Brain perfusion SPECT using an annular single crystal camera: Initial clinical experience. *J. Nucl. Med.* **31**, 1456-1461 (1990).
30. P.G.W. PLAGEMANN, R.M. WOHLHUETER, and C. WOFFENDIN, Nucleoside and nucleobase transport in animal cells. *Biochim. Biophys. Acta* **947**, 405-443 (1988).
31. W.F. WHITMORE, Jr., Bladder cancer: An overview. *CA Cancer J. Clin.* **38**, 213-223 (1988).
32. W. SZYBALSKI, X-ray sensitization by halopyrimidines. *Cancer Chemother. Rep.* **58**, 539-557 (1974).
33. K.D. BAGSHAWE, Reversed-role chemotherapy for resistant cancer. *Lancet* **2**, 778-780 (1986).
34. K.D. BAGSHAWE, J. BODEN, G.M. BOXER, D.W. BRITTON, A. GREEN, T. PARTRIDGE, B. PEDLEY, S. SHARMA, and P. SOUTHALL, A cytotoxic DNA precursor is taken up selectively by human cancer xenografts. *Br. J. Cancer* **55**, 299-302 (1987).

35. K.D. BAGSHAWE, Radiochemotherapy with ^{125}I-5-iodo-2-deoxyuridine. In *DNA Damage by Auger Emitters* (K.F. Baverstock and D.E. Charlton, Eds.) pp. 51-54. Taylor & Francis, Ltd., London, 1988.
36. P.A. PHILIP, K.D. BAGSHAWE, F. SEARLE, A.J. GREEN, R.H.J. BEGENT, E.S. NEWLANDS, G.J.S. RUSTIN, and T. ADAM, In vivo uptake of ^{131}I-5-iodo-2-deoxyuridine by malignant tumours in man. *Br. J. Cancer* **63**, 134-135 (1991).
37. A.I. KASSIS, G.M. MAKRIGIORGOS, and S.J. ADELSTEIN, Dosimetric considerations and therapeutic potential of Auger electron emitters. In *Frontiers in Nuclear Medicine: Dosimetry of Administered Radionuclides*, Proceedings of symposium, Washington DC, September 1989 (S.J. Adelstein, A.I. Kassis, and R.W. Burt, Eds.) pp. 257-274. American College of Nuclear Physicians, Washington, 1990.
38. R.B. PAINTER, B.R. YOUNG, and H.J. BURKI, Non-repairable strand breaks induced by ^{125}I incorporated into mammalian DNA. *Proc. Natl. Acad. Sci.* USA **71**, 4836-4838 (1974).
39. A. HALPERN and G. STOCKLIN, Chemical and biological consequences of β-decay. Part II. *Radiat. Environ. Biophys.* **14**, 257-274 (1977).
40. S. SUNDELL-BERGMAN and K.J. JOHANSON, Repairable and unrepairable DNA strand breaks induced by decay of ^{3}H and ^{125}I incorporated into DNA of mammalian cells. *Radiat. Environ. Biophys.* **18**, 239-248 (1980).
41. A.I. KASSIS, R.W. HOWELL, K.S.R. SASTRY, and S.J. ADELSTEIN, Positional effects of Auger decays in mammalian cells in culture. In *DNA Damage by Auger Emitters* (K.F. Baverstock and D.E. Charlton, Eds.) pp. 1-13. Taylor & Francis, Ltd., London, 1988.
42. S.J. ADELSTEIN, A.I. KASSIS, J. BARANOWSKA-KORTYLEWICZ, A.D. VAN DEN ABBEELE, G. MARIANI, and S. ITO, Potential for tumor therapy with iodine-125 labeled immunoglobulins. *Nucl. Med. Biol.* **18**, 43-44 (1991).
43. K.S.R. SASTRY and D.V. RAO, Dosimetry of low energy electrons. In *Physics of Nuclear Medicine: Recent Advances*, American Association of Physicists in Medicine, Medical Physics Monograph No. 10 (D.V. Rao, R. Chandra, and M.C. Graham, Eds.) pp. 169-208. American Institute of Physics, New York, 1984.
44. G.M. MAKRIGIORGOS, S. ITO, J. BARANOWSKA-KORTYLEWICZ, D.W. VINTER, A. IQBAL, A.D. VAN DEN ABBEELE, S.J. ADELSTEIN, and A.I. KASSIS, Inhomogeneous deposition of radiopharmaceuticals at the cellular level: Experimental evidence and dosimetric implications. *J. Nucl. Med.* **31**, 1358-1363 (1990).
45. G.M. MAKRIGIORGOS, S.J. ADELSTEIN, and A.I. KASSIS, Cellular radiation dosimetry and its implications for estimation of radiation risks: Illustrative results with technetium-99m labeled microspheres and macroaggregates. *JAMA* **264**, 592-595 (1990).

DISCUSSION

Humm, J. L. The administration of ^{123}IUdR or ^{125}IUdR intratumorally results, as you have shown, in enormous differential uptake in the tumor to nontumor tissues. The advantages of injecting ^{123}IUdR into the CSF for the

treatment of brain malignancies is clear, where the normal brain tissues are a nondividing cell population. But there are severe limitations of the intratumor route, in that the real goal of targeted therapy is the treatment of metastatic disease. It seems to me that the pharmacologic manipulation of cell cycle turnover as investigated by Bagshawe and colleagues is a more promising direction for the general approach of Auger emitters as a therapeutic modality. What are your long term plans for the continuation of this interesting work?

Van den Abbeele, A. D. At the present moment, our interest is confined to important problems in the treatment of brain, bladder and ovarian cancers, for which significant improvements at the primary site are highly desirable. The potential for targeted radionuclide therapy using Auger emitters as well as other radionuclides for microscopic metastatic disease is a challenge for the future.

DeSombre, E. R. If you are injecting intratumorally would not ^{123}I be the Auger emitter of choice (rather than ^{125}IUdR) if a single injection is used?

Van den Abbeele, A. D. A single injection would not be used for therapy since IUdR is a cell-cycle-dependent agent. For diagnosis, only ^{123}IUdR can be used for scintigraphic purposes. For therapy, either continuous infusion or repeated injections would be needed for those radiopharmaceuticals and there are arguments to be made on both sides for use of ^{123}IUdR or ^{125}IUdR although there may be more practical problems with the use of ^{123}IUdR.

Harapanhalli, R. S. What reasons do you ascribe to the fact that actively dividing epithelial cells do not take up IUdR as against the tumor cells in intratumoral injections?

Van den Abbeele, A. D. 1) In the rat brain tumor model, the tumor is surrounded by essentially nonproliferating tissue. 2) In the case of all the tumor models, once IUdR has percolated through the tumor tissue and reach the circulation, its half-life in circulation is very short (on the order of minutes). This can be used as an advantage since it has prevented uptake by distant dividing tissues in our experiments following a single intratumoral injection. 3) Finally, neoplastic tissue is usually more actively dividing than normal tissue thereby increasing the probability of specific targeting.

Schneiderman, M. What was the dose given to your patients?

Van den Abbeele, A. D. The patients with colon adenocarcinoma were injected intratumorally with 190-216 μCi (or 7-8 MBq) of ^{125}IUdR as a single injection during colonoscopy. The patients with primary brain tumors are being injected intratumorally with 5 mCi of ^{123}IUdR during stereotactic biopsy.

 Biophysical Aspects of Auger Processes, AAPM Symposium Series No. 8 (1992) 396-402
Eds. RW Howell, VR Narra, KSR Sastry, DV Rao

COMMENTARY ON THE PANEL DISCUSSION

KEITH F. BAVERSTOCK

WHO European Centre for Environment and Health
Rome, Italy

Auger emitters present at one and the same time a potentially valuable tool in biological and radiobiological research, a prospect of therapeutic application and a possibly serious radiological hazard. The reason for the qualifications on each of these statements is the uncertainty in our knowledge of the mechanisms by which Auger emitters achieve these effects. The process of Auger decay is a complex one involving the release of many electrons, mostly of low energy; a charging up of the residual atom, as a consequence; and, in the case of spontaneous Auger decay, the transmutation of the decaying radionuclide. Most attention has been focussed on the role of the electrons and, to date, little is understood of the consequences of charging. Theoretical calculations taking into account the stochastic nature of the decay predict intense deposition of energy close to (a few nanometers) the source of the event, and pioneering work in the field confirms that, under laboratory conditions, damage in DNA is limited to the region close to the site of decay. But the cell is altogether a more complex entity, and it is certainly a challenge to confirm this finding in DNA in a cellular environment

Nevertheless, the unique properties of Auger emitters are generally regarded as being due to this very highly localized irradiation albeit that some findings are not entirely supportive of this position. However, there is considerable potential for experimental work in this area as the following discussion indicates. Although the subject is still in the early stages of development, for example, fundamental dosimetric issues can still cause

disputes (see below), it has developed considerably since the last meeting in this series four years ago.

There has been a long running debate in radiobiology in general over whether radiation effects on DNA are due to direct absorption of ionizing energy or mediated indirectly by radiation induced free radicals. Humm (Boston) sought to clarify the concepts, direct and indirect, in the context of Auger effects. Martin (Melbourne) had spoken of direct excitation followed by energy migration, Pomplun (Jülich) had spoken of ionizations within the bound water of DNA. Hofer (Talahassee) had suggested that the extent of indirect effect was measured by oxygen enhancement ratio. Adelstein (Boston) agreed that careful definitions were important. Watery radicals generated close to the DNA probably had no 'choice' but to react with it and therefore could not be classified as 'indirect' on the basis that scavengers can intervene to prevent indirect effects. However, some molecules, such as cysteamine, were able to 'repair' damage by hydrogen donation in addition to scavenging the radicals. This restitution effect need have nothing to do with 'indirect' effect. In simple molecular systems it was possible to distinguish these different effects but in cells this was not possible. Experiments with ^{125}I incorporated at specific sites in the DNA held some promise of resolving these issues especially with a strong model building input.

Sastry (Amherst) urged the retention of the conventional definitions rather than trying to redefine the terms in relation to the effects of Auger emitters. Phenomena such as oxygen effect were a product of the subsequent chemistry and as such not relevant. Halpern (Jülich) pointed out that microdosimetric models of DNA damage based on events initiated over time scales of 10^{-16} s by Auger electron tracks had to relate to measurements made on vastly greater time scales. He wondered about the relevance of such extrapolations, as the microdosimetry is essentially concerned with the physics of energy deposition, but the chemistry eventually responsible for the biological damage that occurs much later.

Clearly this debate is far from resolved and recent work with Auger emitters has highlighted new aspects. For example, the confirmation by Martin of his earlier experiments so successfully explained by 'direct' effect, the fascinating results of Yasui (DeKalb) who finds no evidence for DNA protein cross-linking in cells with Auger emitters located in the nucleus in contrast to X irradiation, the results of Rao and colleagues (Newark) who showed a protective effect of cysteamine *in vivo* and the results of Hofer

(Talahassee) indicating a low-LET like survival curve in cells pulse labeled and harvested for freezing and ^{125}I decay accumulation shortly after labeling as opposed to a high-LET like response at later times. These results seem to highlight the essential complexity of the cell in relation to *in vitro* systems. In my view we have to build models of predictive power based on these mechanisms and design experiments to test the predictions.

A second contentious issue is that of the induced Auger cascade in cold elements and the related issue of the sensitization of radiation effects in DNA containing cold bromine or iodine. This first effect we shall refer to as enhancement and it results from stimulating a cold atom with radiation at or above the absorption energies of inner shell electrons, so called edges. The second effect we shall refer to as sensitization and is due to the extra radiosensitivity that is observed when halides are incorporated into DNA. One question is, do 'edge' effects give radiobiological enhancement? Some experimenters, notably Hieda (Rikkyo), Kobayashi (Tsukuba) and Maezawa (Tokai), claim they do, producing experimental evidence from relatively simple molecules while some theoreticians, notably Humm (Boston), predict only very tiny enhancements. Earlier in the meeting Hieda (Rikkyo) and Halpern (Jülich) disputed different methods of converting exposure to dose in the experiments in which solutions of DNA concentrated in a buffer are irradiated with low energy X rays. Hieda used the combined f-factors for DNA and buffer, while Halpern (Jülich) used only the f-factors for the DNA with no account taken of the buffer. It seems that these two approaches lead, respectively, to somewhat over- or underestimated values of the electron dose to the DNA. The issue of which approach gave the better approximation was unresolved at the meeting. Goodhead (Chilton) maintained that if the dosimetry, including geometric considerations, was clearly defined there should be no room for dispute. It seems strange that there should be dispute over the fundamentals of dosimetry in spite of the obvious complexity of the physics involved.

A somewhat curious result was that reported by Laster (Upton) in which iodine-(cold) gave an enhancement in cell killing with radiations above the appropriate edge but bromine did not. Laster (Upton) was confident this was not a problem of dosimetry and suggested that the effect might be due to saturation since the bromine replacement was three times higher than that for iodine. Humm (Boston) pointed out that because the energy of the K edge for bromine is much lower than that for iodine and the photoelectric cross section is sharply dependent upon energy, the much more numerous

'background atoms', *e.g.* oxygen, would tend to mask the effects from bromine more than those from iodine. Halpern (Jülich) drew attention to the greater extent of charge build up in the case of iodine - a problem that remains open. Laster (Upton) added, in support of the suggestion that a saturation effect was being observed, that the radiosensitization effect of iodine at 10% replacement was about the same (a factor 2.2) as that for bromine at about 60% replacement. Schneiderman (Omaha) noted that no account was taken of the differences in growth of cells with bromodeoxyuridine. This modified their response even without exposure to radiation.

Goodhead (Chilton) questioned the validity of an explanation based upon a saturation effect. This could only arise if allowance had not been made for attenuation of the primary beam as it passed through the sample *i.e.* it would be the consequence of incomplete dosimetry.

Clearly experiments of this kind have many complexities and variables which need careful control and there is a need to design experiments to distinguish between the 'edge' effects and those of radiosensitization. It is important to understand the mechanisms involved because of the potential therapeutic benefit, yet experiments are difficult to compare because of differences in percent replacement, sample geometry *etc.* Such problems might be overcome if theoreticians were to try to predict the most advantageous conditions under which to resolve the contributions of edge effect and radiosensitization. Halpern (Jülich) suggested utilizing L5178Y s/s murine lymphoma cells since the sensitization by BrUdR is very small.

Martin (Melbourne) asked how the double strand break yields from Auger enhancement for iodine and bromine compared. Humm (Boston) said that for iodine it was 0.8 DSB/photoelectric interaction and for bromine 0.4. He warned of the importance, in this instance, of distinguishing between dose and fluence. Below the edge the photoelectric cross-section is 20 times smaller than above it. So to get the same number of interactions 20 times greater fluence is required.

Kobayashi (Tsukuba) pointed out that to convert exposure to dose one is required to know the relevant volume. Considering the cell nucleus as a target, the conversion factor above the edge would be only a few percent larger than below the edge of phosphorous.

Rao (Newark) drew attention to the results of experiments of Kassis (Boston) with ^{125}I, ^{123}I, and ^{77}Br in which the effects of these widely different sized Auger cascades produced about the same effect in terms of dose to the nucleus. Each of these emitters should cause different levels of local strand break damage; yet this does not seem to influence the biological effect. Sastry (Amherst) agreed that dose to the nucleus did seem, in these circumstances, to have meaning. Hofer (Talahassee) had described results from experiments in which synchronized cells at the beginning of S phase were pulse labeled with ^{125}I and then allowed different times of development into S phase before being frozen to allow ^{125}I decay to occur. Samples frozen shortly after pulse labeling produced low-LET like survival curves whereas cells frozen five hours after labeling show characteristic high-LET curves. He proposed that the high-LET effect resulted from the irradiation of something more than the DNA - perhaps some superstructural element in chromatin. Clearly, much remains to be explained. The highly innovative nature of Hofer's (Talahassee) experiments demonstrates as clearly as anything that to believe the current dogma can be stifling. It would at least seem that any assumption that the effects of Auger emitters were entirely explained in terms of damage within two DNA diameters of the decay site was a gross over simplification.

Halpern (Jülich) questioned the accuracy of radiobiological data to permit the kinds of model construction involving complex numerical analysis. He drew particular attention to the implied accuracy in the figure of 17.5 eV for the formation of a single strand break in DNA. Pomplun (Jülich) agreed insofar as there are a lot of phenomena which could not have yet been considered in the models due to the lack of appropriate, and what is most important, coherent data. Adelstein (Boston) noted two results which suggested that there was a finer relationship between strand breaks and survival. One of these was the experiments of Hofer (Talahassee) referred to above, the other work by Makrigiorgos (Boston) that showed that the ratios of D_o to double strand break yields for incorporated ^{123}I and ^{125}I were not the same. Clearly here was a disparity that current modelling devoted to explaining effects entirely in terms of locally induced strand break yields could not resolve, particularly since the results from these experiments were robust. This was an area of experimental biology where the theoretical basis was relatively quantitative.

What emerges is a clear need for interaction between experimentalists and theoreticians but one should not assume that the theory will not need substantial revision in the future. There seem to be relatively few examples of

theory leading the subject. As suggested above, it would be nice to see some purely theoretically based predictions that can be meaningfully tested. There are still fundamental differences of theoretical approach which was made evident in a short exchange between Sastry (Amherst) and Pomplun (Jülich) concerning the validity of the 'frozen orbital' approach for calculating electron energy spectra. This ended with a plea from both Sastry (Amherst) and Pomplun (Jülich) for a clear identification of the limitations of any calculation and a careful definition of terms.

Auger emitters are increasingly used diagnostically in nuclear medicine and as such present a radiological hazard. How should they be catered for in radiological protection? Johanson (Uppsala) noted that the ICRP had first proposed to use a value of $Q = 5$ for Auger emitters but in the final recommendations had dropped the idea. When iodine-125 was brought close to the DNA, as in the case of transfer by thyroid hormone, the effect was definitely akin to high-LET. Perhaps the assumption made by ICRP was that only a small fraction of the iodine became bound in this way.

Howell (Newark) warned that using Q alone would not be enough - something similar to a distribution factor (like N previously employed by the ICRP but now dropped) would be required to take account of subcellular distribution of the nuclides. The important factor in determining the effectiveness of an Auger emitter was chemical form because it seemed that many Auger emitters resulted in the same biological effectiveness if they were identically distributed within the cell. Kassis (Boston) agreed that was largely a matter of the identity of the pharmaceutical and not the isotope.

Adelstein (Boston) drew attention to two observations, one published in 1982 by Commerford *et al.* , suggesting that if the Auger emitter is in the nucleus it did not matter where. This result might suggest that the highly localized nature of the Auger decay did not necessarily indicate that damage was similarly localized. Clearly, in the light of some of the results discussed at this meeting, this question should be re-addressed. The second, a more recent result by the Harvard group seems to indicate dramatic transformation frequencies at doses which barely affect cell survival. These two results have important implications both for radiological protection and fundamental understanding of radiobiology.

From this short discussion it is clear that questions continue to arise in this field which, although being explored by relatively few workers, is no

doubt one of the more vigorous and innovative areas of radiobiology. The geographical separation of workers makes collaboration somewhat difficult but there does seem to be a need for more coherence in both theoretical and experimental approaches. The radiological protection implications deserve much more attention by the granting bodies given the importance of Auger emitters in nuclear medicine, but there can be no doubt that Auger emitters are an increasingly important tool in exploring biology in general and may well find important applications in therapy.

Biophysical Aspects of Auger Processes, AAPM Symposium Series No. 8 (1992) 403-412
Eds. RW Howell, VR Narra, KSR Sastry, DV Rao

CLOSING ADDRESS: BIOPHYSICAL ASPECTS OF AUGER PROCESSES

KURT G. HOFER

Institute of Molecular Biophysics
Florida State University, Tallahassee, FL 32306

I would like to begin my closing remarks by thanking the organizers of this meeting. Anybody who has ever organized an international symposium knows that this is not an easy task. The Program Committee composed of Dandamudi Rao, Kandula Sastry, and Roger Howell, and the Local Organizing Committee composed of Kandula Sastry, Roger Howell, Venkat Narra, and Michael Azure have done an outstanding job in organizing this meeting and they deserve our appreciation and a round of applause.

When I was invited to present this talk, I received precise instructions from Dandamudi Rao. He told me that my closing address should start with a comprehensive review of 20 years of radiobiological research on Auger emitters, followed by a thorough analysis of the 24 papers presented at this Symposium, and ending with overall conclusions on the current status and future prospects of the field. These were clear and explicit instructions, but when it came to preparing the talk, I started to ask myself what could possibly have prompted me to undertake such a task. It must have been an attack of egomania because it surely takes the ego of a battleship to believe that one can do what can not actually be done.

But perhaps a healthy dose of self-confidence is essential for doing scientific research. Being a scientist can be an awfully humbling experience. Nine times out of ten, when we conceive of an absolutely brilliant idea, it turns out to be wrong. That was definitely the case when I started to work on

Auger emitters in 1966. At that time I was doing cell kinetics work on cancers and I was looking for a radionuclide that could be incorporated into the DNA of cells, but would cause only minimal cell damage. So, naturally, I selected ^{125}I. With the benefit of hindsight, this obviously qualifies as one of those humbling experiences that test our self-confidence.

At about the same time Ludwig Feinendegen in Jülich also began to work with ^{125}I. I have no doubt that Feinendegen had more foresight than I and that he knew what he was doing. But with or without foresight, we both found that ^{125}I incorporated into the DNA was immensely toxic to mammalian cells. This work was soon confirmed and extended by Krisch, Adelstein, Ahnstrom, Burki, Painter, Charlton, Booz, Halpern, Warters, and other early Auger enthusiasts. But the biggest boost to the field came in 1975 when Feinendegen organized the famous Jülich meeting on Radionuclides in Biology and Medicine. This meeting brought together all the early workers on Auger emitters and recruited scores of new ones to the field.

By the late 197O's certain firm conclusions about the Auger effect started to emerge. At the risk of oversimplification, I should like to summarize in a few sentences what was known at that time.

We were aware, of course, that Auger emitters decay by electron capture and emission of a burst of Auger electrons; some of these high-energy electrons, but most of them low-energy electrons with a very short range in biological material. It was recognized from the start that emission of such a dense shower of electrons would result in a highly charged daughter atom and in a high density of electron irradiation in the immediate vicinity of the decaying radionuclide. Microdosimetry calculations from several different laboratories confirmed this conclusion, but left open the question whether the cytotoxic effects of Auger emitters were caused by high local concentrations of radiation energy or by charge effects, or possibly by a combination of both.

Regardless of the exact mechanism of action, it was obvious that incorporation of Auger emitters into radiosensitive biological structures was bound to cause extensive local damage. For example, it was demonstrated quite early that ^{125}I decays at the DNA were very efficient in inducing DNA double-strand breaks, mutations, malignant transformations, chromosome aberrations, and other types of highly localized damage in the cell genome.

At the cellular level, the effects of Auger emitters were found to depend largely on the intracellular location of the radionuclides. When incorporated into DNA, ^{125}I caused high-LET-like radiotoxic effects that exceeded those of DNA-associated ^{3}H by a factor of 15 to 25, even though the ratio of intranuclear energy deposition was calculated to be only about 2 to 4. Conversely, Auger emitters decaying outside the cell nucleus in the plasma membrane, lysosomes, mitochondria, or the general cytoplasm proved surprisingly nontoxic to mammalian cells. For example, in one experiment it took about 60 ^{125}I decays/cell at the DNA to cause 50% cell death, but when ^{125}I was attached to the plasma membrane almost 20,000 decays/cell were required to produce the same effect. Even with this massive number of decays, cell death was not caused by damage to the plasma membrane, but by overlap irradiation of the cell nucleus.

So the early work on cells quite clearly demonstrated that radiation death in mammalian cells results from damage to the cell nucleus; cytoplasmic or membrane contributions, if any, had to be minimal. By implication, these findings refuted the enzyme release hypothesis and other hypotheses that attempted to explain radiation death in terms of cytoplasmic or membrane effects rather than nuclear damage.

These studies also had important implications for medical applications of Auger emitters. It was clear that Auger emitters can be very toxic or very non-toxic, depending on where they end up within cells. The obvious conclusion was that for diagnostic applications of Auger emitters, where it is desired to keep cellular damage as low as possible, radiopharmaceuticals should remain localized outside the cell or at least outside the cell nucleus. Conversely, if Auger emitters were to be used for therapeutic applications such as radionuclide therapy of cancers, it would be necessary to find radiopharmaceuticals that can selectively, or at least preferentially, introduce Auger emitters into the nuclei of cancer cells.

So in retrospect, what we knew about Auger emitters by 1980 made a neat and appealing package. But scientists never leave well enough alone. They keep experimenting and probing until inevitably they unearth facts that no longer fit the tidy picture. Some of the more recent work, including the findings presented four years ago at the International Workshop on DNA Damage by Auger Emitters, were summarized in the opening remarks by Jim Adelstein. Without repeating Jim Adelstein's review, it is apparent that some of the research trends he identified are now coming to fruition. This is

particularly true for the growing importance of work with artificially induced Auger cascades in non-radioactive elements.

The induction of artificial Auger cascades essentially involves the use of monoenergetic X ray photons with energies either just above, or just below the K shell absorption peak of the chosen target atom. There are advantages and disadvantages to this approach. An advantage is that Auger effects can be studied on atoms for which there are no suitable Auger emitting radionuclides. Also, this method permits evaluation of the consequences of Auger showers without needing to consider the effects of atomic transmutation and other complications associated with Auger emitters. A disadvantage is the fact that large doses of external radiation must be used and it is sometimes difficult to discern the effects of the Auger cascades against the background of damage from the incident photons.

Of the 7 reports on the effects of photon-induced Auger cascades presented at this Symposium, all but one dealt with molecular aspects of radiation damage. Kobayashi (National Laboratory for High Energy Physics, Tsukuba, Japan) described the effect of K edge irradiation on cystathionine, a sulfur-containing amino acid. He reported that Auger cascades in sulfur induced very effective cleavage of chemical bonds right next to the sulfur atom, but for more distant bonds the rate of cleavage was the same with different photon energies. Takakura (International Christian University, Tokyo, Japan) examined the effects of Auger cascades originating from phosphorus atoms in adenosine-triphosphate and found that at K edge photon energies there was a 3.9-fold enhancement of adenosine-diphosphate formation, a 3.4-fold enhancement for adenosine-monophosphate, and a 1.5-fold enhancement for adenine formation. Furusawa (Tokai University School of Medicine, Japan), also working at phosphorus K edge energies, noted that Auger cascades originating at the phosphate backbone of DNA caused significant enhancement of bacteriophage inactivation.

Halpern (Kernforschungsanlage Jülich, Germany) measured DNA single-strand breaks (SSB's) and double-strand breaks (DSB's) in partially brominated plasmid DNA and observed no effects on SSB and only a minor increase in DSB from photon absorption at the K edge of bromine. He attributed the relatively small contribution of the Auger effect to the fact that the electron flux originating in light atoms outweighs that from bromine. Also working with halogenated pyrimidines were several other investigators, Nikjoo (Medical Research Council, Chilton, U.K.), Johanson (Swedish

University of Agricultural Sciences, Uppsala, Sweden), Laster (Brookhaven National Laboratories, Upton, NY, USA), and Charlton (Concordia University, Montreal, Canada). A common theme in these studies was that both bromodeoxyuridine and iododeoxyuridine incorporation into DNA enhanced the effects of ionizing radiations, with iodine producing substantially larger Auger effects than bromine.

However, these papers also point out some of the difficulties encountered in this type of work, in particular the problem of distinguishing between different mechanisms that contribute to the overall sensitization effect. Nikjoo, presenting the paper submitted by Charlton, mentioned three potential mechanisms of halogen action: (a) production of Auger electrons; (b) creation of highly reactive uracil radicals by interaction of hydrated electrons with halogenated pyrimidines; and (c) reduced damage repair in halogen-containing DNA. So we are left with the conclusion that work with photon-induced Auger cascades is very promising, but the interpretation of the results can sometimes be difficult.

Turning now to work with Auger emitting radionuclides, we again find that molecular work is becoming increasingly prominent. Haydock (Mayo Foundation, Rochester, MN, USA) studied the effects of ^{111}In decay on human carbonic anhydrase I and found that chemical transmutation from indium to cadmium was responsible for the relaxation effects (degree of molecular wobbling), but actual breaking of chemical bonds around the site of decay was caused by energy from Auger electrons.

All the rest of the molecular work dealt with the effects of Auger emitting radionuclides on DNA. Martin (Peter MacCallum Cancer Institute, Melbourne, Australia) confirmed previous evidence that the yield of DNA DSB at the site of ^{125}I decay approaches 1 DSB/decay. This finding does not support earlier work by Linz and Stöcklin (*Radiat. Res.* **101**: 262, 1985) that suggested long-range migration of excitation energy away from the site of decay. Baverstock (Medical Research Council, Chilton, U.K.) also doubts the existence of energy transfer because experiments on ^{125}I-labeled plasmid DNA do not provide any evidence for long-range energy migration in DNA. Baverstock had previously proposed solitons as a potential means of long-range propagation of excitation energy (*Nature* **332**: 312, 1988), but his experimental data did not confirm this hypothesis.

Pomplun (Forschungszentrum Jülich, Germany) presented two papers on DNA damage from Auger emitters, one using ^{123}I, the other ^{125}I. In the ^{123}I paper Pomplun examines a fundamental problem, namely the fact that after two decades of research on Auger emitters we still cannot be completely certain about the number and energies of Auger electrons emitted during electron capture decay. This has obvious implications for microdosimetry calculations. Pomplun's work also deals with another important subject matter, the relative contributions of direct and indirect effects in causing DNA damage by Auger emitters. Until recently it was assumed that essentially all the cytotoxic effects of DNA-associated Auger emitters were the result of direct effects. However, Pomplun's work, in conjunction with previous studies by Rao *et al.* (*Radiat. Res.* **124**: 188, 1990), suggests that both direct and indirect effects contribute to radiation damage by Auger emitters.

This concludes our discussion on molecular effects. Among the cellular studies there is one paper by Nagasawa (Harvard School of Public Health, Boston, MA, USA) that deals with mutation induction by ^{125}I. She reports that mutation induction at the well-studied HPRT locus varies as a function of cell cycle position, both for external X irradiation and for cells labeled with ^{3}H-TdR or ^{125}IUdR during different stages of the S phase. For all three types of exposures, mutation induction at the HPRT locus is most effective for early-S phase cells. However, X rays and radionuclides do differ in the type of mutations induced. For X rays general deletion mutants predominate, whereas for radionuclides mostly partial deletions are observed.

Turning to cellular cytotoxicity studies, DeSombre (University of Chicago, Chicago, IL, USA) describes an interesting system where estrogens are labeled with ^{123}I and used to treat estrogen receptor positive and negative cells. For this system to work the author developed an elegant method for synthesizing high specific activity ^{123}I-labeled estrogens and he finds that ER-positive cells such as CHO cells transfected with estrogen receptors are very efficiently killed in this manner, whereas ER-negative CHO cells do not respond.

Ludwikow (Swedish University of Agricultural Sciences, Uppsala, Sweden) employed ^{125}I-labeled triiodothyronine (the active form of the thyroid hormone) as a means of delivering ^{125}I to the cell nucleus. Using the production of micronuclei as an index for radiation damage, she found that although ^{125}I-triiodothyronine did preferentially accumulate in the cell nucleus of GC cells, ^{125}IUdR was about 9 times more efficient in producing cell

damage than ^{125}I-triiodothyronine. Another novel system for labeling cells with Auger emitters was described by Azure (University of Massachusetts, Amherst, MA, USA). He employed a carboplatin compound that is normally used as a chemotherapeutic agent in cancer therapy and developed a method to label this compound with the Auger emitter ^{193m}Pt. He found that this compound was efficiently incorporated into the cell nucleus of V79 cells and caused greatly enhanced cell death as compared to the cytocidal effects produced by equimolar concentrations of carboplatin containing non-radioactive platinum.

The remaining two papers in the cellular series were presented by a former student of mine, Linda Yasui, and myself. Yasui (Northern Illinois University, DeKalb, IL, USA) examined various types of DNA damage in frozen ^{125}I-labeled cells. She compared different models for the induction of DNA DSB and came to the conclusion that in contrast to the relatively clean DSB produced by X rays, ^{125}I decays produce DNA DSB composed of a whole cluster of lesions. But surprisingly, ^{125}I decay does not seem to result in the formation of DNA-protein crosslinks that are usually seen when cells are exposed to external radiations. It would appear, therefore, that this type of DNA lesion cannot play a major role in cell death. In my own paper I presented evidence that DNA-associated ^{125}I does not invariably act as a high-LET radiation source for cell killing. High-LET-type killing was seen only when decay accumulation was delayed for a few hours after cell labeling. We interpret our data as indicating that radiation death in mammalian cells may be caused by damage to higher-order structures in the cell nucleus.

In the last 5 papers we encounter a number of interesting biomedical applications of Auger emitters. Van den Abbeele (Harvard Medical School, Boston, MA, USA) describes an experimental system where ^{123}IUdR and ^{125}IUdR are used as potential diagnostic and therapeutic agents in rats and humans. After intracerebral injection of the two compounds, the radionuclides were specifically incorporated into the DNA of gliosarcoma cells and similar experiments on bladder cancer also produced positive results. The specificity of targeting was confirmed in preliminary studies on patients with colon adenocarcinoma, so it appears that radioactive IUdR may hold promise as a future diagnostic and therapeutic agent for at least some forms of cancer.

In another whole-body study, Strand (University of Lund, Lund, Sweden) examined the tissue distribution of various ^{111}In-labeled compounds

(chloride, oxine, tropolone, antibodies) in rats and found increased uptake and prolonged retention of ^{111}In in kidney, spleen, liver, bone marrow, lymph nodes, and in the testis. Within these tissues the radioactivity was preferentially incorporated into specific cell types such as macrophages in the testis. But in my opinion, the key point was the finding that ^{111}In becomes localized in the cell nucleus of certain cells. Grafström (University of Lund, Lund, Sweden), working with ^{110}In and ^{111}In demonstrated a pronounced decline in spermhead counts performed 7 weeks after administration of the radionuclides. The damage was particularly acute with X ray exposures, but both ^{110}In and ^{111}In also produced severe damage. This should raise serious questions about radiation risks from the widespread use of In-labeled compounds in diagnostic nuclear medicine.

Howell (University of Medicine and Dentistry of New Jersey, Newark, NJ, USA) examines some of the risks and problems associated with Auger emitters and α emitters by comparing the relative biological effectiveness of Auger emitters under *in vitro* and *in vivo* conditions. As expected, he finds this to be a difficult problem because the results are critically dependent on a variety of factors such as type and dose rate of the reference radiation, method of dose calculation, site of decay, and the nature of the biological end point studied. Obviously, this is an important area of research and additional data are needed.

Finally, in the last paper of the Symposium, Narra (University of Medicine and Dentistry of New Jersey, Newark, NJ, USA) revisits the question as to whether or not the cytotoxic effects of Auger emitters can be counteracted by treatment with chemical radioprotectors such as cysteamine. Using spermhead counts as the assay system, he finds that cysteamine provides protection against both α emitters and Auger emitters, but the degree of protection is much higher for Auger emitters. He suggests that the Auger effect may be largely due to indirect action from radicals which certainly is radically different from what at least I would have predicted.

This concludes my review of the unusually interesting papers presented at this Symposium and brings me to the final part of my remarks, my predictions for the future. But before you reach for your pencils to write down all the sage advice, please remember my record as prognosticator and how I came to work with ^{125}I in the first place. Not everybody can be as gifted in handing out advice as Conrad Hilton, the legendary founder of Hilton Hotels. When asked what words of wisdom he had for the world he replied,

"whenever you take a shower, always put the curtain inside the tub." This is phenomenally good advice, especially if you happen to be the owner of a hotel chain where half of the guest fail to follow this important rule.

I have nothing of such moment to contribute today, but a few modest thoughts might be worth mentioning. One emerging trend in our field is the increasing emphasis on medical applications of Auger emitters, both in diagnostic and in therapeutic nuclear medicine. For many years large numbers of different Auger emitters have been used for diagnostic applications and the situation is further complicated by the fact that these radionuclides are administered in a great variety of chemical configurations. So the problem of assessing risks is by no means trivial and will require considerable additional experimental and theoretical work. At the same time, Auger emitters hold great promise in radionuclide therapy of cancers if (and that is still a very big IF) suitable methods for selective or at least preferential radionuclide delivery to cancer cells can be developed. As pointed out by Feinendegen, "molecular surgery" by Auger emitters could one day provide a means of realizing Paul Ehrlich's dream of a "magic bullet" in cancer therapy.

Equally important will be the continuation and expansion of basic molecular and cellular studies on the Auger effect. Radiation exposure of cells induces mutations, division delay, malignant transformation, premature aging, and outright cell death. The mechanisms and targets for these effects are still not known and should be further analyzed with Auger emitters. For example, based on work with ^{125}IUdR incorporated into DNA, Schneiderman *et al.* (*Radiat. Res.* **116**: 283, 1988) concluded that the primary target for division delay may not be the DNA, but a so far unidentified non-DNA target located at or near the nuclear envelope. Whether or not this structure contributes to radiation-induced cell death or other types of cellular radiation damage remains unknown.

Cancer induction is another example where work with Auger emitters might answer fundamental questions. It is generally agreed that malignant transformation is a two-stage process consisting of an initiation phase and a promotion phase. Initiation is believed to result from damage to DNA, but promotion is almost certainly an epigenetic process that somehow permits or induces the expression of malignant properties in initiated cells. Radiation acts both as an initiator and promotor, so work with Auger emitters incorporated into different subcellular locations might permit us to more

clearly distinguish between these two phenomena and perhaps also to identify the so far unknown target for promotion.

Radiation is also known to accelerate the process of aging both in cells and in whole organisms. Again, in spite of numerous conflicting hypotheses, virtually nothing is known about the molecular and cellular mechanisms responsible for aging. As far as I am aware, no aging work has been performed with Auger emitters and I would not be surprised if studies along these lines were to produce novel insights into aging processes.

These are only a few examples of potential future directions and I am sure that everyone in this audience could add additional possibilities. All these applications depend on the unique decay and dose distribution characteristics of Auger emitters which permit differential radiation exposures of subcellular and even submolecular sites. In many ways, the difference between Auger emitters and external radiations is analogous to the difference between smart bombs and conventional bombs. Auger emitters act like smart bombs that destroy individual components of the system, with only minor collateral damage to distant sites. In contrast, exposure to external radiation is comparable to large-area carpet bombing that indiscriminately damages the system as a whole. Dave Charlton, who dislikes modern warfare, prefers a classical military analogy and compares the Auger effect to a Trojan horse. As long as the horse remains outside of Troy it is harmless, but when brought into the city the consequences can be fatal.

Whether you regard Auger emitters as smart bombs or Trojan horses, there can be no doubt that they offer the potential for unique contributions to our understanding of radiation action. Louis Pasteur once wrote that "all things remain hidden, obscure, and undebatable as long as the cause of the phenomena be unknown, but everything becomes clear when this cause be known". Judging from the work presented at this Symposium we can be fairly confident that when we meet again in 1995 in Sweden, some of the causes that are now obscure will be clear, and Auger emitters will have played an important role in illuminating these causes.

AUTHOR INDEX

SUBJECT INDEX